REGOLITH GEOCHEMISTRY AND EPR: CHARACTERIZATION OF GOLD MINERALIZATION IN DEEPLY WEATHERED TERRAINS, AUSTRALIA

by

Xu Li

School of Earth Sciences

Submitted in fulfilment of the requirements for the degree of
Doctor of Philosophy

UNIVERSITY OF TASMANIA

March 1999

This thesis is dedicated to a significant person from my past
Prof. Xie Xuejing
and two important people in my life today
Glenn and Kevin
With sincere appreciation and thanks for their role in helping build my future.

This thesis contains no material which has been accepted for the award of any other higher degree or graduate diploma in any tertiary institution and, to the best of the author's knowledge and belief, the thesis contains no material previously published or written by another person, except where due reference is made in the text of the thesis.

Xu Li
8 September 1998

This thesis may be made available for loan and limited copying in accordance with the Copyright Act 1968.

ABSTRACT

Thick, commonly lateritic regoliths are widespread in inter-tropical regions of the world, and present a challenges to current exploration techniques. The particular problem in Australian is the widespread deep and varied regolith, frequently with a complex geological history dating back to mid-Permian time. Within this long period, several episodes of deep weathering and selective chemical solution, transport and precipitation, differential erosion, and deposition of sediment, so that the primary features of primary ore deposits are considerably modified and deeply concealed. The lateritic and saprolitic Au associated with subsurface depletion is one of the most common results of the deep weathering.

With these problems in mind, an integrated paramagnetic/lithogeochemical technique has been developed in the exploration for gold in heavily weathered terrain. This technique is based on the degree of impurity in quartz associated with ore deposits and measured by electron paramagnetic resonance (EPR) powder spectroscopy and chemical analysis of the quartz rich acid insoluble residue of the regolith.

Electron paramagnetic resonance spectroscopy, which measures microwave absorption by unpaired electrons in a magnetic field, is a new concept in mineral exploration as quartz samples from mineralized zones often have strong EPR signals due to lattice imperfections. Quartz associated with mineralization has stronger electron paramagnetism than the barren quartz, whilst the EPR signals of residual quartz, including secondary chalcedony with inclusion of primary quartz, are not strongly affected by weathering.

The acid treatment consists of sequential treatment of regolith samples with hot aqua regia, nitric acid and sulphuric acid, dissolving residual sulphides, iron, manganese and aluminium oxides and hydroxides, carbonates, phosphates, sulphates and clay minerals. The remaining acid insoluble residue consists of quartz with some residue sericite, rutile and traces of other resistate minerals.

Three areas with a well described regolith profile and known bulk geochemistry

were selected: the Mystery Zone, Mt Percy, at Kalgoorlie, the Rand Pit, Reedy Mine near Meekatharra in Western Australia, and Jim's Find in the Tanami Desert of Northern Territory. The depth of weathering in these areas varies between rock types, but generally below surface 60-90 m. As strong acid digestion, most of the weathering products have been removed from the reglith samples and this acid insoluble residue reflects the primary signature.

In the acid insoluble residue, quartz associated with mineralization has an EPR spectra typical of lattice imperfections. Case studies of the Mystery Zone, Mt. Percy, the Rand Pit, Reedy Mine and the Jim's Find, Tanami have pronounced EPR signals at the surface above the mineralized zones as well as in Au depletion zones and in the wall rock alteration halos. The distribution of EPR 326.5±5 mT is in accordance with the distribution of certain trace elements, such as Al, K, Rb, W, V, Ga and Ge in all three working areas. In addition, wall rock alteration patterns are commonly expressed by strong $[AlO_4]^o$ centers in the EPR spectra, accompanied by increased K and Rb concentrations, and high Rb/K and Rb/Al ratios. In contrast, the intensity of EPR 326.5±100 mT resembles the element distribution of Fe, Mn, Zn and Ni indicating that EPR 326.5±5 mT weakly reflects the distribution of alteration.

In the acid insoluble residue, the chemical expression of sericitic wall rock is Al, K Rb, V, Ga and W enrichment, high Rb/K ratios in surface material above mineralization, and high Rb/Al ratios in wall rocks. Aluminium, K, Rb, Ga, V, and W related to sericitic alteration in the acid insoluble residue, are commonly good indicators of Au mineralization through the regolith. In the Mystery Zone, Rand Pit and Jim's Find, Al, Cr, Ga, K, Rb, V, W, Rb/K and Rb/Al consistently define the location of Au mineralization. The composite halos Al x K x Rb, Ga+Ge and As+W+Mo also enhance the mineralization halo, with these cumulative indices more useful than the single low-level elements of Ge, As and Mo. Sodium, Ca and Sr depletion is caused by plagioclase destruction. Titanium, Zr, Nb, and possibly V, have a strong correlation to lithological variation and are surface enriched in resistate minerals. However, the acid insoluble residue of near surface material likely reflects secondary dispersion patterns of Ca, Sr, Cr, Cl and S presumably due to extrapment of submicroscopic inclusions.

Similar results may be obtained for these and other potential pathfinder elements, like As, Sb, Bi and Cu, by total geochemical analysis of whole rock pulps. However,

not all Au deposits have an associated suite of pathfinder elements, whilst research presented in this thesis suggests that there is always an EPR signal and high Al, K, Rb, V, Ga and W chemical expression in the acid insoluble residue.

ACKNOWLEDGEMENTS

First and foremost, my thanks go to Dr J.C. van Moort, who not only supervised my work, but spent many extra hours in reading, advising, discussing, correcting, re-reading, editing and administrating. His valuable financial support during this study from 1995 to 1997 was also much appreciated. Without his initiation of this PhD study, and encouragement and cooperation throughout, this thesis would not have been completed.

Sincere thanks also, to Dr P. McGoldrick, for his help and supervision in the final stages of this thesis. His valuable comments and assistance in relation to microscopy observation and text corrections, was most appreciated. He also provided considerable moral support, which helped reduce my stress levels.

This project was supported by various funding bodies: a four year Australian Overseas Postgraduate Research Scholarship award; the Australian Institute of Nuclear Science and Engineering (AINSE project 1995-1997 – "Chemical composition and paramagnetic defects of quartz"); an ARC/Pasminco Exploration Collaborative grant (three year living allowance scholarship from 1995 to 1997); and support from the CRC LEME.

The author has benefited from interaction with various staff of: the School of Earth Sciences, University of Tasmania; Physics Department, Monash University in Melbourne; and the Australian Nuclear Science and Technology Organization (ANSTO) in Sydney.

Many thanks also to Drs C.R.M.. Butt and I.D.M. Robertson of CRC LEME in Western Australia, not only for access to samples from Mystery Zone and Rand Pit, but also for the many discussions and revision of reports and publications related to my study and this thesis. Thanks especially for their reading, editing and anthropomorphizing of my thesis and explaining the inexplicable. Their comments on this thesis have been extremely valuable.

Thanks to Dr. D. R. Hutton at the Physics Department of Monash University, who read and improved the chapters and sections related to EPR.

Thanks to Dr. G.M. Bailey from ANSTO for his assistance on PIXE/PIGE work and technical support of the chemical analyses part of the thesis. Thanks also to P. Johnson and W. Kyu of ANSTO for their assistance in PIXE/PIGE work.

Also appreciated is the assistance of R. Song at the Chemistry Department at Denver University for assistance in EPR analyses and accommodation in Monash during this study. To J. Wang at the Physics School of Sydney University and X. Shen at the Applied Geology Department of University of New South Wales, I give thanks for help with the PIXE/PIGE analyses in Sydney and field work in Cobar, NSW.

Thanks to the School of Earth Sciences administrative staff J. Pongratz, N. Hlaing, and C. Higgins. June provided considerable help regarding computer usage and thesis presentation and Chris gave invaluable moral and administrative support, which has enabled me to overcome work pressure stress and save a tremendous amount of time. This has enabled me to concentrate on the theses and complete it in time. Thanks for your sincere friendship, support and encouragement. Thanks also to the School technical staff P. Cornish and P. Robinson.

To my fellow postgraduates R. Sharpe, P. Winefield and Yu Zhongshou, many thanks for your support and encouragement. Thanks very much to T. Webster, K. Reid and C. Gifkins for their revision of the thesis both technically and grammatically. Their comments were very much appreciated. Special thanks to Robina for her selfless assistance during the last stages, especially for her detailed revision of the manuscript. Special thanks also to D. Rawlings for the accommodation support towards the end.

Thanks to G. Sheldon of Newmont Gold Mining for many discussions about this work and various problems related to exploration geochemistry and the chance to increase my knowledge on different gold deposits in China.

Thanks to Prof. Xie Xuejing of the Institute of Geophysical and Geochemical Exploration (IGGE) of PRC. He introduced me to the field of exploration geochemistry, and my thesis benefited from his valuable input during many resourceful

discussions. Thanks also to Liu Dawen of IGGE for many useful discussions and guidance on the interpretation of geochemical data.

Thanks also to my friends Wai Ching Ng, Dr. Liu Lanzhen and Li Jinlin for their genuine help and encouragement, also to Dr. D. Liu of Physics Department of University of Tasmania for many beneficial discussions about statistical data treatment. To Y. Huang who helped in various ways with this thesis and provided some nice dinners to keep me going.

To my mum and sister, who have always encouraged me in my educational pursuits, I owe a debt of gratitude too large to sum up in a few words.

Finally, I would like to thank my wife Wang Fang for her selfless assistance in sample preparation, EPR and XRD analyses and my lovely son Xu Yuan, who gave me strength to overcome the difficulties experienced while producing and completing this thesis. Thank you.

CONTENTS

LIST OF FIGURES

LIST OF TABLES

LIST OF APPENDICES

Chapter 1

INTRODUCTION

In Australia and other parts of the world, deep regolith is widely distributed and consists of weathered bedrock, often with an overlying cover of transported overburden. The presence of a regolith presents numerous exploration problems as it affects geological, geophysical and geochemical mapping and exploration techniques. A challenge for exploration geochemists is to overcome these weathering effects, and to test and develop techniques on weathered materials that yield the correct information on related mineralization.

An orientation program over three buried gold deposits in the heavily weathered terrain of Western Australia (W.A.) and the Northern Territory (N.T.) was undertaken by the author to evaluate sample treatment prior to chemical analysis. This treatment consists of removing weathering products as far as possible by acid leaching and using the remaining acid insoluble residue as the sample medium. The residue was analyzed chemically and by electron paramagnetic resonance, and the results are compared to those of conventional bulk rock analyses.

This thesis presents data from the Mystery Zone at Mt. Percy, Rand Pit at Reedy Mine, Western Australia, and Jim's Find in the Tanami, Northern Territory including analytical techniques and data interpretation. The development and characterisation of regolith geochemistry and electron paramagnetism are described, and discussed in terms of their implications for gold exploration.

1.1 SELECTION OF THE STUDY AREAS

Australia is the third largest gold producer in the world. Much of its production comes from deeply weathered terrains, mostly in Western Australia and the Northern Territory. One of the largest gold producing areas is the Yilgarn Craton in Western Australia, which contains many Au deposits of multimillion-ounce size. The Granites–Tanami region of the Northern Territory has reserves of about 5 million ounces (Register of Australian Mining 1997/98).

The orientation areas tested in this study possessed most of the following characteristics: reasonably constrained geology and geochemistry; near economic gold grades with associated trace elements; the pediment cover consisting of gravelly soil; and deep regolith profiles. Three buried gold deposits with related mineralization: Jim's Find in the Northern Territory, the Mystery Zone and Rand Pit in Western Australia, were eventually selected as the targets for this study (Figure 1-1). All these areas have been studied in some detail by the Australian Cooperative Research Centre for Landscape Evolution and Mineral Exploration (CRC LEME) (Butt, 1991; Robertson, 1990; Stott, 1994).

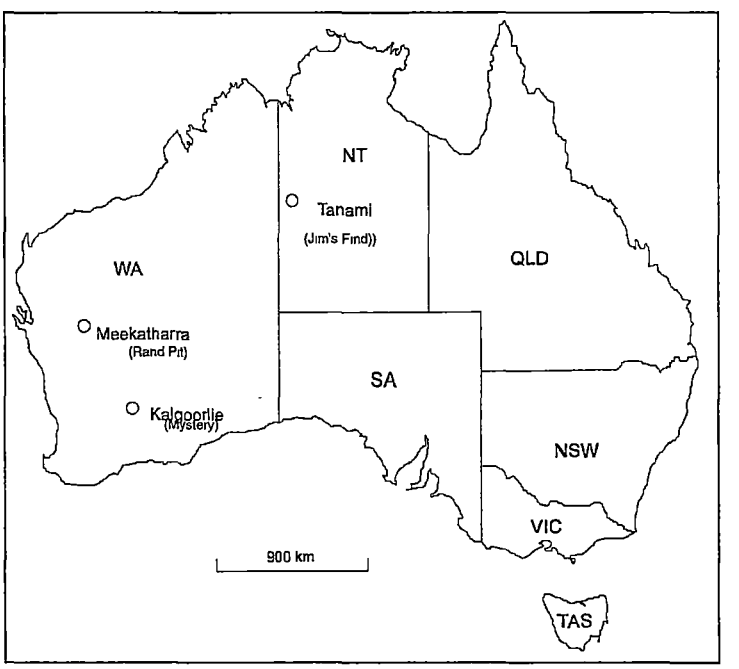

Figure 1-1. Location of study areas

1.1.1 Mystery Zone, Mt. Percy, W.A.

The Mystery Zone of the Mt. Percy Mine is about 2 km northeast of the centre of Kalgoorlie, Western Australia at 30°44'S, 121°28'E. It lies at the northern end of the Kalgoorlie–Kambalda greenstone belt, within the Kalgoorlie gold district (Figure 1-2 [A, C]). Early mining in the area took place mainly from 1893 to 1910, during which time some 70,000 tons of ore were extracted from narrow, relatively low-grade ore bodies, using shallow shafts. Most of the surface of the leases was dry blown (Sauter et al., 1988).

Recent exploration commenced in 1977 by Occidental Minerals, followed by Windsor Resources with mining of the southern end of the Mystery Zone initiated in 1987. Presently the mine is owned and operated by Gold Mines of Kalgoorlie Ltd (50%) and Homestake Mining Corporation (50%). A resource totalling 10.73 Mt at 1.6 g/t yielding 568,000 oz. of gold was given at June 1996, with 2,356 oz. of gold mined by March 1997 (Register of Australian Mining 1997/98).

1.1.2 Rand Pit, Reedy Mine, W.A.

Rand Pit is a gold resource within the Reedy Gold Mine, which is located 600 km NNE of Perth and 65 km SSW of Meekathara in the Murchison mineral field, Western Australia at 27°07'12"S and 118°16'11"E (Figure 1-2 [A, B]). Mining activity at Reedy has occurred intermittently since the discovery of gold by Tom Reedy in 1901. In 1982, Metana Minerals N.L. (Metana) carried out extensive exploration and ore reserves drilling over the Reedy area. Open cut mining commenced at the Rand Pit in 1984. Currently three open pits and an underground operation are worked by Gold Mines of Australia Ltd to produce 540,000 t of ore per year, from which 53,776 oz. of gold are recovered. A proven and probable open cut reserve of 944,000 t at 3.5 g/t and an underground reserve of 439,000 t at 4.8 g/t gold were outlined by June 1996.

1.1.3 Jim's Find, Tanami Mine, N.T.

Jim's Find is a new gold deposit near the Tanami Mine and is located in the remote central west of the Northern Territory. Jim's Find lies approximately 850 km south of Darwin, 600 km NW of Alice Springs and 400 km SE of Halls Creek, on the edge of the Tanami Desert (19°59'S and 120°E), and at the junction of the Alice Springs/Halls Creek road and track to Lajamanu (Figure 1-3). The Tanami Mine lies some 23 km NNE of Jim's Find, whilst the Granites Mine is situated 100 km to the SSE (Eupene et al., 1989). Jim's Find is owned and operated by Acacia Resources and Otter with a reserve of 4.77 Mt at 3.3 g/t of gold at the end of 1996.

Construction of the haul road to the Jim's Find area was underway in early 1997, with production from the pits scheduled to begin in 1998. This area was to become the largest ore producer in the Tanami region, and Jim's Main within the Jim's Find area was expected to be the largest of the Tanami pits.

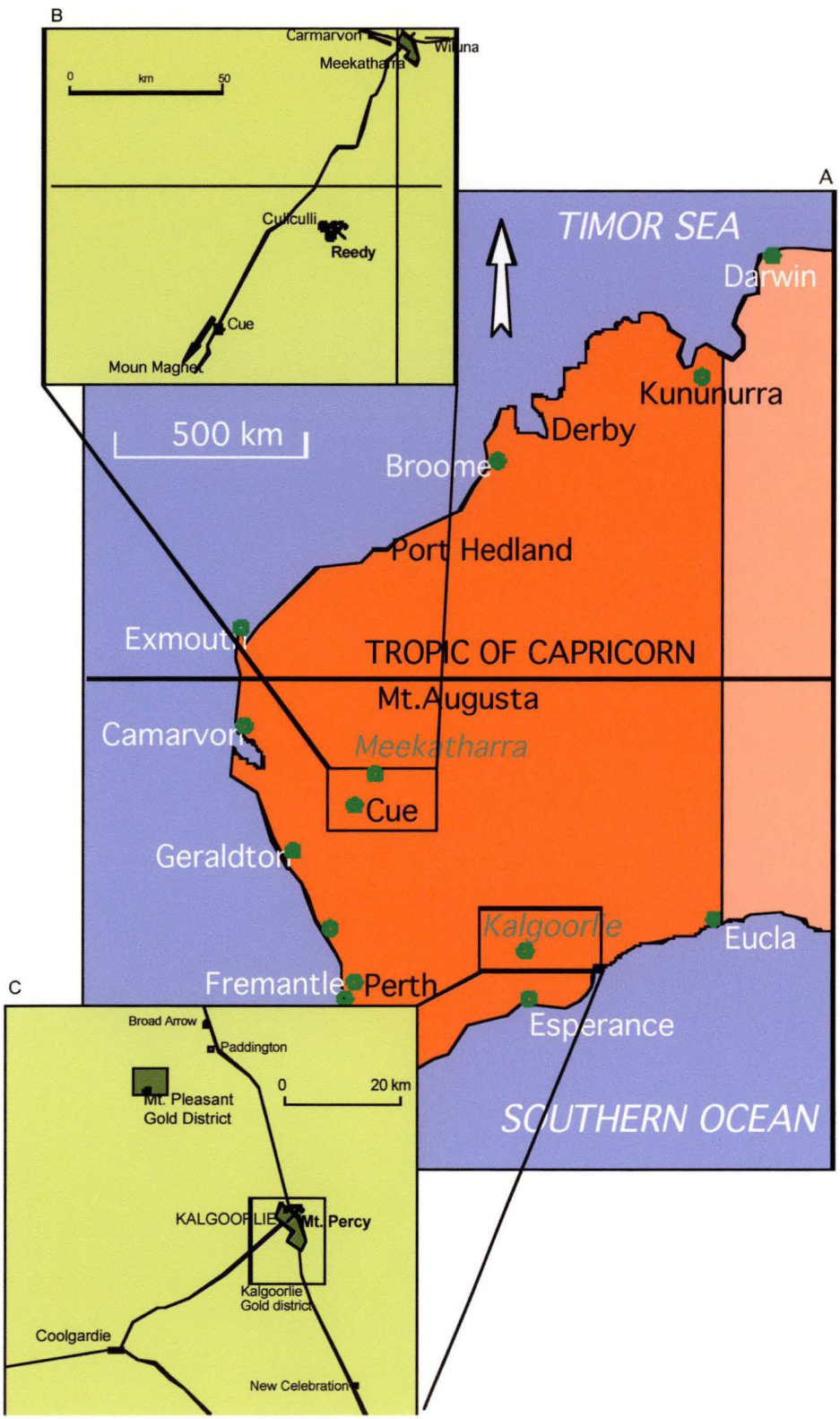

Figure 1-2. Location map of Mt. Percy and Reedy Mines in Western Australia

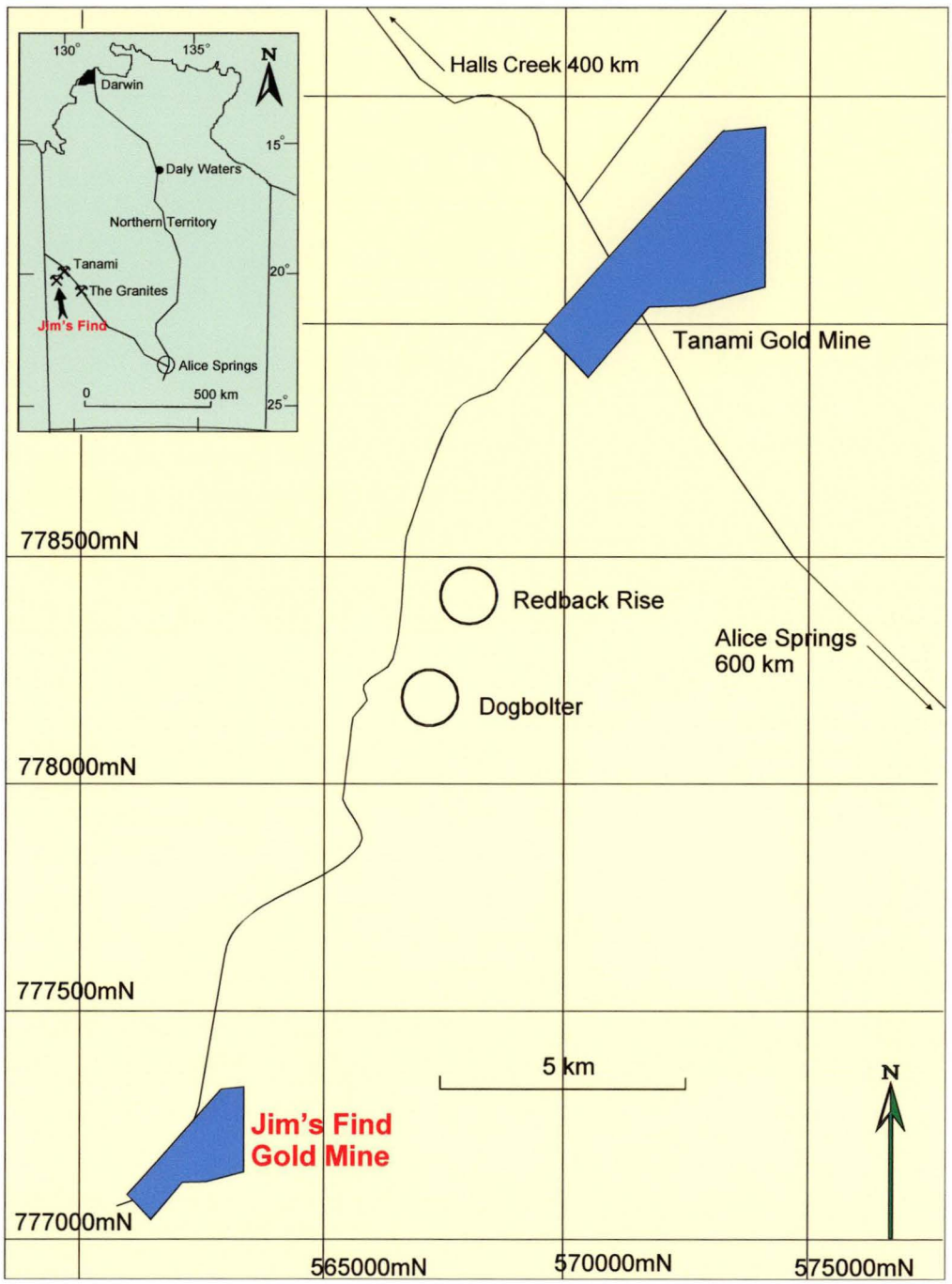

Figure 1-3. Location map of Jim's Find area showing the Jim's Find and Tanami mines and other significant prospects (circled).

1.2 EXPLORATION PROBLEMS IN WEATHERED TERRAIN

The steady growth in Australian gold production over the last 15 years was founded on large scale mining of the low grade margins to known deposits. These resources are becoming exhausted, and nearly all of the prospects of this type have now been tested. Currently exploration is targetting buried gold deposits under deep regolith. In Australia, a particular problem is the widespread deep and varied regolith profile, which has a complex history dating back more than 200 million years to mid-Permian time. Within this long regolith history, multiple episodes of deep weathering and selective chemical solution, transport and precipitation, differential erosion and deposition of sediment are likely, such that the ore deposit features are deeply concealed and considerably modified.

The deep regolith is typified by an extreme diversity of materials. These materials vary in grain diameter from silt to boulders, in texture from massive to well-bedded, in composition from nearly pure silica sand to nearly 30% hydrated iron oxides, in colour from white to black, and ranging from loose and free-running to strongly lithified or cemented. The regolith may also contain a wide variety of chemical deposits, of which silcrete and calcrete are the best known (ALS, 1995).

The thickness of the regolith, which encompasses weathered residuum and continental sediments overlying basement rocks, varies from a few metres to over 150 m (Butt et al., 1997). Thickness variations depend on the edge of the land surface, tectonic activity, climate, climatic history and the nature of the bedrock. The precise depth and nature of components within the regolith is generally impossible to predict from surface observations.

To further complicate the picture, it is now realized that the present arid climate of inland Australia is not typical of its post-Permian history, with much of the regolith formed under warm, humid and wet climatic conditions (Clarke, 1994; Robertson and Butt, 1997) over a period of 100 million years. Consequently, the present regolith and landforms are acumulative expression of the cumulative effects of this long weathering history. Accordingly, the petrophysical, morphological, mineralogical and geochemical characteristics of the regolith are often profoundly different to the rocks from which they were derived.

It is very difficult to distinguish between similar regolith materials which originated by different processes. In the case of a clay-rich layer, it may be of transported origin, and carried to the site by the agencies of wind or water; be formed by deep chemical weathering which yielded a very thick saprolite zone; or produced by lateritic weathering. Each process generates a similar looking material with a different chemical composition and geochemical behavior. All of these give rise to numerous exploration problems.

In summary, there are no general rules for the deep regolith, except that it can exhibit almost infinite variation. A residual soil of predictable geochemical behavior, one of the preferred materials for regional sampling programs, is either not available or cannot be definitely identified by simple tests. Additionally, because of the arid climate of much of Australia, active stream sediment sampling cannot always be used. All of these factors cause tremendous difficulties when interpreting mineral exploration data in regloith terrains. Butt et al. (1997) summarized the problems that hinder the effective application of regolith sampling. These include:

1. profound mineralogical, chemical and physical alteration of bedrock and associated mineralization, so that distinctions between even broad lithological classes is difficult;
2. strong leaching of ore-related elements (e.g. Cu, Au, Zn), particularly from upper horizons of the regolith, resulting in subtle surface expression of mineralization.
3. the development of spurious secondary concentrations of target elements in weathered, unmineralized rocks;
4. lateral changes in the nature of the regolith, due to depth variations and truncation of earlier, pre-existing profiles by the present erosional surface;
5. the presence of a transported overburden cover, which may itself have been weathered after deposition;
6. the super-imposition, often in a single profile, of the effects of weathering under different environmental conditions.

Effective geochemical exploration can only be achieved by the recognition of these problems, and by the selection of sampling and data interpretation techniques appropriate to the target being sought.

1.3 OBJECTIVES OF THE STUDY

This project was designed to develop an exploration method which could decrease or eliminate the effects of weathering on data interpretation. The project concentrates on details of the three deposits mentioned above, because the open pits and drill holes provide profiles through which the geochemical and paramagnetism dispersion from gold mineralization in near complete lateritic regolith can be investigated. Further to this, comparison was made between the results obtained from conventional techniques and the acid insoluble residue analysis developed in this study. This thesis specifically focuses on the use of the acid insoluble residue of regolith and rock as a sample medium for gold exploration. The residue consists essentially of quartz and is relatively free of secondary minerals. Its composition is weakly affected, if at all, by the degree of weathering of the regolith. Compositional and paramagnetic variations of this material are used to characterize differences in primary mineralized and non-mineralized areas. The analytical methods used are proton induced X-ray emission (PIXE) and proton induced g-ray spectroscopy (PIGE) plus electron paramagnetic resonance spectroscopy (EPR).

Samples used in regolith geochemical exploration are normally composed of a variety of minerals in unpredictable proportions. The bulk composition of the samples may vary markedly in accordance with the original composition of the material, transportation, weathering processes and secondary dispersion.

The enrichment of elements in some specific mineral phases during weathering may be overcome by selective sampling, e.g. of pisoliths (Smith and Perdrix, 1983), lag (Robertson, 1996), pedogenic carbonate (Lintern and Butt, 1993) or selective extraction techniques (Hall and Bonhan-Carter, 1998) such as enzyme leach. The Bulk Leach Extractable Gold (BLEG) technique, sometimes called BCL for Bulk Cyanide Leach, was originally developed to cope with the low concentration levels and the "nugget" effect in drainage surveys for gold, and is essentially comparable with results for "total" (hot aqua regia digestion) on soil or lags (Mazzucchelli, 1997). However, studies of geochemical dispersion haloes for example, especially in transported ferruginous lag, are difficult to interpret because the provenance of many different types of lag is not well understood. (Spry and McQueen, 1997). The present study stresses the alternative path of trying to retrieve the original composition of the silicate matrices of the rock by dissolution of secondary minerals through strong acid

leaching. The acid insoluble residue of rocks consists essentially of silicates, usually with a high proportion of quartz. As it is not easy to remove all secondary minerals from regolith material, the first year of this study was dedicated to developing methods to obtain an acid insoluble silicate concentrated as pure as possible.

The conventional methods to remove carbonates and Fe and Mn oxides from soils and sediments use hydrochloric acid (Russell and van Moort, 1987), treatment with nitric acid (van Moort et al., 1995), or even sequential treatment with hot hydrochloric and nitric acid. Such treatment also removes Al oxides and hydroxides, phosphates, residual sulphides and most sulphates. The remaining clays and other minerals such as alunite, can be removed by hot sulphuric acid digestion and subsequent thorough rinsing. Remaining magnetic minerals may be extracted by use of a hand held magnet. Nonetheless, constant vigilance is still required as some minerals, such as talc, are completely acid insoluble, whereas gibbsite and, to a minor degree boehmite and many resistate minerals such as spinels and garnets are acid soluble. Valuable references to the response of individual mineral species to acid treatment can be found in Dana and Ford (1966) and Duba and Rejl (1990), and a discussion of the poor efficiency of extraction techniques to determine so-called "total compositions" of regolith materials can be found in Gedeon and Butt (1977).

1.4 OUTLINE OF THE STUDY

This study involved open pit and drill core samples. One hundred and ninety-two open pit samples from Mystery Zone were used for chemical analysis (Chapter 5) and 167 samples for EPR analyses (Chapter 6). In Rand Pit, 90 open pit samples were used for PIXE/PIGE analyses (Chapter 8) and 93 for EPR analyses (Chapter 9). One hundred and thirty-seven drill core samples from Jim's Find Prospect were used for PIXE/PIGE analyses (Chapter 11) and 67 samples for EPR analyses (Chapter 12).

1.4.1 Sample preparation

The bulk composition of the samples and the host mineral of the metal sought vary markedly in accordance with the complexity of the geology, various weathering and erosion processes, as well as secondary dispersion processes. Commonly, many identifying characteristics of the mineralization become obscured and can be confused with other weathering products. The distribution of primary and secondary

mineralization is dependent upon the effectiveness of the method in removing the particular weathering products from the weathered samples. To overcome problems of the interfering concentration of certain elements at different sites in the profile, a new sample treatment method was introduced.

In order to solve the problems of weathering effects, all samples were treated with hot aqua regia + HNO_3 + H_2SO_4. Aqua regia and HNO_3 were used to dissolve carbonates, silicates, iron hydroxides and sulphides and sulphates, whilst H_2SO_4 was used to dissolve clay minerals, such as kaolinite.

The acid insoluble residue of the rock and regolith pulps consists essentially of silicates, particularly quartz, minor sericite and talc, traces of alkali feldspar and resistate minerals such as zircon and titania polymorphs. It is rare to encounter more than traces of other silicates as they have either already been destroyed by weathering (Loughnan, 1969), degraded or removed by the acid treatment (Nand and van Moort, 1995).

1.4.2 Chemical analysis

Most regolith geochemistry is based on bulk rock geochemistry (Smith et al., 1979), as applied to the three respective study areas which are the subject of this thesis. The total composition is usually based on an acid extraction supposed to represent the "total composition" (Gedeon and Butt, 1977), or more rarely on a total composition determined by physical methods like X-ray fluoresence (XRF) or, after digestion with hydrofluoric acid by inductively coupled plasma mass spectrometry (ICP-MS). Selective extractions, pioneered by soil scientist have now become an essential part of geochemical exploration (Gatehouse et al. 1977; Hall and Bonham-Carter, 1998). Alternatively it is also possible to sample specific regolith components, like pisoliths (Smith and Perdrix, 1983) or the goethite and hematite of hand picked ferruginous material (Wright et al., 1998). In this study the specific regolith component in the acid insoluble residue is essentially quartz. The chemical analyses of these materials have been carried out by proton probe analyses, although it could equally have been done by a combination of other methods like XRF plus INAA or ICP-MS.

1.4.3 Exploration regolith geochemistry techniques

In this thesis, all geochemical investigations were based on the chemical composition of the acid insoluble residue, analyzed by simultaneous PIXE and PIGE methods. These methods are described in Chapter 3. A new concept of sample medium, the hot acid insoluble residue method was used. After samples were treated with strong acid, they were considered 'clean' and assumed that the original rock-forming and mineralization information was preserved. Indicator elements, such as W, Mo, Ga, Pb, Rb, Al and K, exhibit a closer relation to gold mineralization than the total (by XRF) and acid soluble (AAS or ICP-OES/MS) concentrations which are often used in exploration geochemistry. The results of PIXE/PIGE, XRF and INAA were also compared.

1.4.4 Electron paramagnetic resonance (EPR) spectroscopy

The acid insoluble residues were also analyzed by electron paramagnetic resonance (EPR), a method infrequently used in gold exploration. This study develops an integrated geochemical and paramagnetic exploration technique in the search for gold deposits in weathered terrain. The EPR method is based on a measurement of unpaired electrons and provides, in practice, a measurement of lattice defects of quartz and other minerals. Minerals in the mineralized area contain numerous atoms out of place and various substitution and interstitial impurities (including ore constituents and other elements). Consequently this causes a considerable amount of lattice defects and gives paramagnetism (van Moort, 1986). In this study, EPR response of regolith residue was used to characterize the weathered profile in relation to gold mineralization and to distinguish different lithology units. Three major EPR spectra, observed respectively at magnetic flux density sweeps 326.5 ± 5 mT, 326.5 ± 100 mT and 326.5 ± 250 mT, were measured. The principles and instrumentation of EPR are given in Chapter 3.

Chapter 2

APPROACH OF THE STUDY

In Australia, most gold exploration concentrates on seeking gold ore deposits under or in a deep regolith. Some of the earlier gold search programs in deep regolith were simple, with only two stages — acquisition of a favourable greenstone belt or prospective shear zone, followed by drilling the target zone using a closely spaced array of rotary air blast drill holes (ALS, 1995). As our understanding of regolith geology becomes more comprehensive, exploration strategies and stages are increasing in number and complexity. Exploration geochemistry is crucial if we are to understand the regolith.

Geochemical methods for exploring regolith deposits have been progressively developed and effectively applied over the last two decades since the pioneering work of Mazzucchelli and James (1966), who used As as a pathfinder element for gold exploration in laterite covered terrain in Western Australia. In the early eighties, multi-element secondary dispersion halos came into use to define massive sulphide mineralization in deeply weathered terrain (Smith et al., 1979; Smith and Perdrix, 1983; Zeegers et al., 1981). It is only within the last ten years that exploration procedures based on these concepts have been applied regularly, and even then only in restricted areas (Butt, 1995; Roquin et al., 1990). Current research is directed to standardizing regolith terminology, optimizing sampling procedure, increasing the knowledge of geochemical anomalies, weathering and dispersion processes, and the synthesis of regolith/landform evolution. The application of any kind of exploration method in a regolith area must understand the regolith and weathering processes to be able to search for buried gold deposits in lateritic profile.

2.1 REGOLITH DEFINITION

The regolith is the layer of disintegrated and decomposed rock fragments, including soil, just above the solid rock of the Earth's crust. Because of its increasing use in geological sampling, it has been discussed and defined by many authors (Whitten, 1972; Blake, 1979; Twidale, 1990; Charman, 1992; Taylor, 1997) since the 1970s. A powerful and comprehensive description was provided by Woodall (1995), who calls the veneer of sediment, transported soil and deeply leached bedrock which

covers many of the auriferous rocks in Western Australia and more than half of Australia's land surface, the 'mantle of concealment'. The approximate boundaries of the mantle of concealment is shown in Figure 2-1. Australia's regolith can be extremely thick, well over 100 m in some places, especially on the older cratonised areas of Western Australia, the Northern Territory and South Australia. This thick layer of material has great influence over mining in Australia because it can hide important ore bodies and, when disturbed, is easily removed by wind and water erosion.

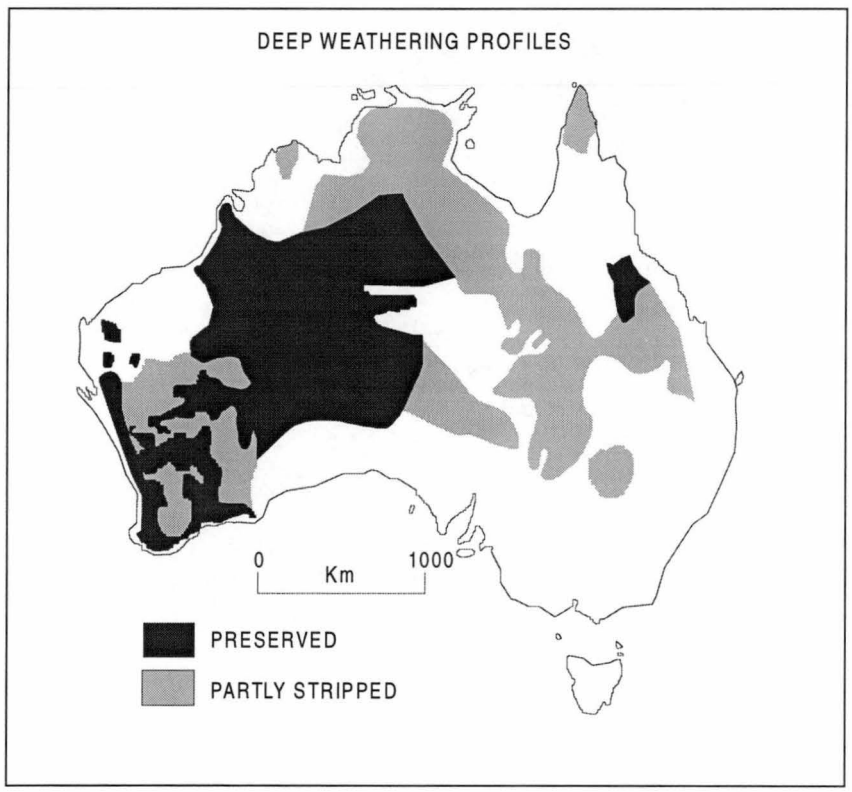

Figure 2-1. Weathering zones of concealment in Australia (from Mackenzie and Woodall, 1978)

2.2 REGOLITH MODEL CLASSIFICATION

Understanding the relationship of regolith and landform is very important. With this understanding, different landforms and geochemical behaviour may be identified so that effective and efficient sampling methods can be chosen. Complete and accurate data interpretation can be married with the knowledge of regolith and landscape evolution, weathering and dispersion processes. Regolith studies in the 1990s developed a classification of its elements, using techniques comparable to soil science in the 1950s (USDA Soil Classification). The thrust of this movement comes from Australia, where an abundance of deep, well preserved and ancient regolith exists. A valuable atlas of weathered rocks with accompanying chemical profile was recently produced by Robertson and Butt (1997).

Conceptual and methodological models that represent data and interpretation for particular generalized situations provide the most convenient method of summarizing information relevant to geochemical exploration (Bradshaw, 1975). Although geological, geomorphologic and environmental conditions are different for each location, so that the geochemical response to mineralization is unique in many respects, similarities in dispersion characteristics are nevertheless present over extensive regions. Geochemical dispersion and exploration models attempt to synthesize these characteristics in order to elucidate the nature and origin of the surface expressions of mineralization. The genetic links between the various weathering profiles define three principal series of geochemical exploration models in Australia (Butt and Smith, 1980; Smith, 1990):

- *Model A*: the (pre-existing) lateritic profile is mostly preserved, so that the ferruginous duricrust is outcropping or sub-outcropping;
- *Model B*: as a result of erosion, the pre-existing lateritic profile is truncated below the duricrust horizon;
- *Model C*: the pre-existing lateritic profile has been entirely eroded, and soil profiles are the product of weathering under more recent climates.

Each of these models correspond to facets and landforms defined and classified according to the degree of stripping of an etchplain, their relationship to the deep weathering profile, the presence of transported overburden and the relief. In turn, three factors describe the geochemical parameters of a land surface.

1. A description of the status of the original profile, as mostly preserved, partly truncated, or fully truncated (Model A, B or C).
2. The amount of recent alteration, classified as minor (0), low (1), moderate (2) or strong (3).
3. The presence of recent (chemical) accumulation, cementation or neoformation, recorded as none [0], aluminum oxides (Al), aluminum silicates (AS), calcium and magnesium carbonates as calcrete (Ca), gypsum (Gy), iron oxides (Fe), silica or silcrete (Si), or transported material [3].

Butt and Zeegers (1992) quoted B 1 Ca [3] as an example, that denotes a truncated profile, with some recent alteration, pedogenic calcrete, and transported overburden. The detail presentation of these models within the general landscape is given on Figure 2-2 and could be used on a world-wide basis for the description of weathering profiles.

2.3 APPLICATION OF THE GEOCHEMICAL MODELS

Within the three study areas, the Mystery Zone and Jim's Find are dominated by the A-type dispersion model, and dominantly consist of areas of outcropping lateritic cuirase (A 0 0 [0]) and duricrust covered by a thin residual or semi-residual soil (A 0 0 [1] or A 0 0 [2]). The Rand Pit is largely controlled by B-type model due to saprolite outcrops, but the section in this study is still akin to an A-type model.

The dispersion of elements mostly proceeds from a combination of hydromorphic (H) and detrital (M) processes, both past and present, related to the formation or evolution of the lateritic profile. In the saprolite, whether kaolinitic or smectitic, many of the target elements (e.g., Cu, Pb, Mo, As) are not strongly leached and anomalies are mostly residual. However, hydromorphic processes disperse some elements (e.g. Zn). The size of the dispersion halo widens in the mottled zone, and reaches its greatest extent in the duricrust. The formation of duricrust involves intense chemical alteration and it is probable that at least part of the Fe accumulated in it has been transported for some distance. Some of the trace elements may have behaved similarly, resulting in a large dispersion halo. Compared to bedrock, the concentrations observed in this halo may be similar (e.g. Pb, W, Sb), enriched (e.g. Mo, As, Au) or more or less depleted (e.g. Cu, Zn, Au), depending upon the stability of the host minerals and the chemical characteristics of the elements concerned.

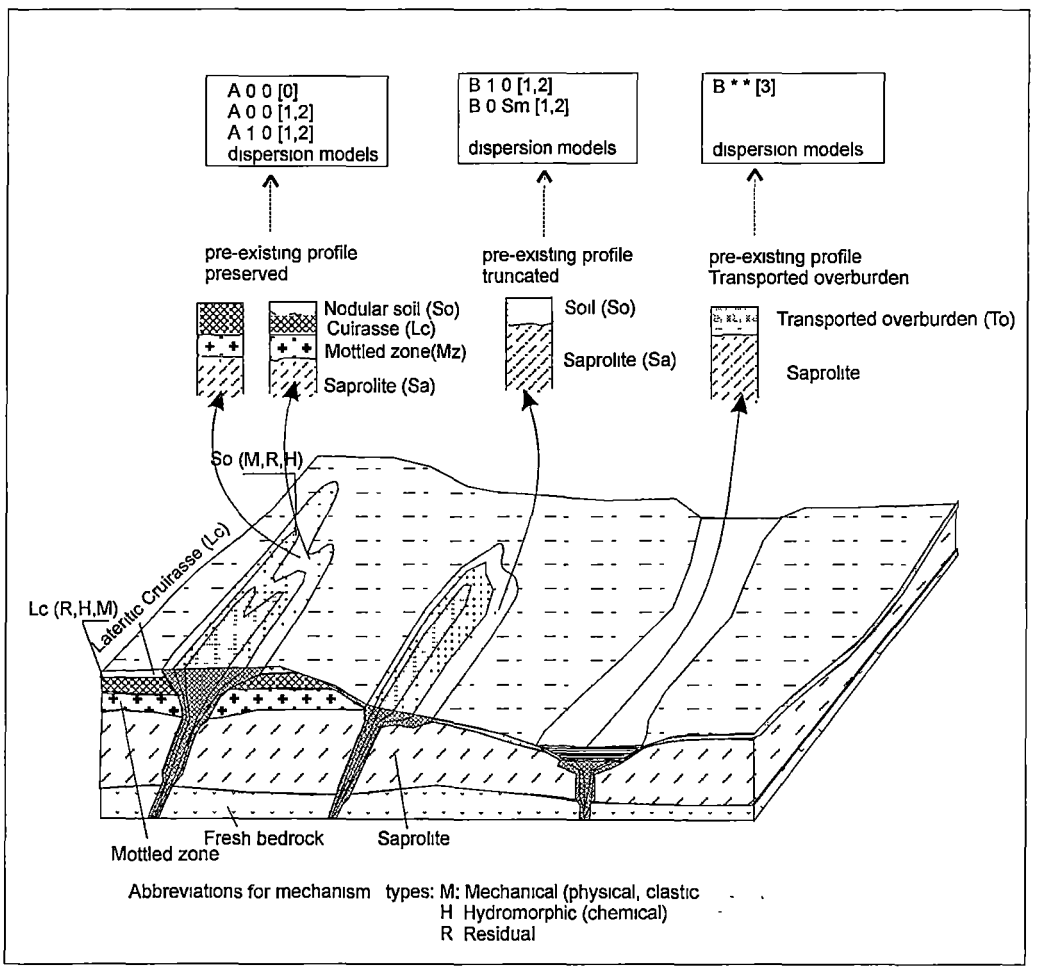

Figure 2-2. Idealized disperson models in preserved or truncated lateritic profiles. Model codes (see text) refer to the presence of lateritic regolith as A preserved; B partially truncated; C absent. Surface: [0] outcrop; [1] residual soil; [2] semi-residual soil; [3] transported overburden (from Butt and Zeegers, 1992).

2.4 GOLD MINERALIZATION IN REGOLITH PROFILE

Applied research into exploration technology suitable for ore search in regolith has largely been focused on the search for gold deposits. Economic or near-economic supergene concentrations of gold may occur in the lateritic and saprolitic zone of deeply weathered regolith in most climatic zones (Gray et al., 1992). Most of the deposits found to date have been in soft and easily mined host materials, with dimensions and shape suitable for open pit mining, and in which the gold is present as a cyanide soluble form, providing high recovery in a simple carbon pulp processing plant.

The natures of many of the processes of weathering and erosion that are important in geochemical dispersion in the regolith are determined by climate. The enrichment of gold is significantly different between areas that have remained relatively humid and those that have been subjected to aridity. For example, the recognition of Au enrichment in regolith over low grade mineralization in the Orogen of eastern Australia (McQueen, 1996), but high grade in the Eastern Goldfields in Western Australia. Lateritic weathering is typically associated with seasonal tropical (savanna) climates but, in many terrains, climates have changed quite profoundly since lateritization. This change in the dominant weathering processes is reflected in the mineralogy and geochemistry of the regolith (Freyssinet et al., 1990). The three study areas, the Mystery Zone, Rand Pit and Jim's Find, not only have many of the dominant geochemical characteristics of the regolith related to the development of the lateritic profile under humid conditions of higher water-tables, but also have others related to more arid environments with lower water-tables. The features produced by these later events modify the pre-existing lateritic profile and tend to be reflected by the more minor components of the regolith.

Lateritic gold mineralizations are more or less flat-lying enrichment zones contiguous with the ferruginous and mottled zones of the lateritic profile. This economic enrichment is largely restricted to regions in Australia having Mediterranean and arid climates (Glasson, 1988). Saprolitic mineralization occurs deeper in the profile, either confined to the source unit or laterally dispersed into the weathered wall rocks, commonly as one or more sub-horizontal zones. The Au is dominantly secondary and of high fineness, but residual primary grains become more abundant deeper in

the profile. Saprolitic enrichments are known and mined only from arid (or once arid) environments (Fletcher, 1985; Ivey, 1987; Lawrance, 1988).

In arid areas, lateritic and saprolitic deposits may both be present where profiles are complete, and are commonly separated by a 5–20 m thick zone that is barren of Au (Gray et al., 1992), though not necessarily of other ore-related elements. Lateral dispersion of Au is evident towards the top of the lateritic profile, particularly in the ferruginous and mottled horizons (Freyssinet et al., 1989; Michel, 1987). Although Au may be dissolved and mobilized during weathering, the repeated strong leaching of the upper saprolite leads to the formation of a depletion zone between the lateritic and saprolitic deposits. Freyssinet and Itard (1997) calculated the gold mass balance in Mt. Percy. The results indicated that about 35% of the initial gold stock is leached close to the weathering front. The leaching process increases progressively from the base to the top of the saprolite to reach a net loss of –67% at a 10 m depth. Consequently, the gold loss is less important between 20 and 35 m depth and the loss changes from –48% to –30%. This depth corresponds to a large lateral dispersion halo of Fe and As associated with scattered secondary gold reprecipitation (Butt, 1995). Where the profile is truncated, any lateritic enrichment will have been destroyed. Nevertheless, an absolute accumulation of fine gold occurs in the mottled zone as a consequence of secondary gold precipitation (Freyssinet, 1993).

The nature of the surface expression of Au mineralization in lateritically weathered terrain depends very strongly upon the climatic and erosion history. The most critical factors are the degree of truncation of any lateritic profile, the effects of post-lateritic weathering, including that occurring at present, and the type of overburden. In the pre-existing lateritic profile (A-type model), the surface expression of mineralization in all morphoclimatic zones reflects the concentration and dispersion of Au in the ferruginous horizons. Anomalies in the mottled zone, duricrust and residual soil tend to be laterally extensive relative to the size of the primary mineralization. The gold contents of residual soils are greatly reduced relative to those of the immediately underlying horizons, even when these represent a significant resource. Nevertheless, they remain anomalous and represent a satisfactory sample.

The low Au contents of soils and upper lateritic horizons are considered to be due to leaching during lateritization and, after uplift or climatic change, by the formation

of soils from lateritic material. Gold has probably been mobilized as organic complexes. In some arid regions, there is evidence that Au dispersion is affected by the precipitation of pedogenic calcrete (Lintern and Butt, 1993) and that surface leaching may be partly offset by the concentration of Au in carbonates (Smith and Anand, 1992). Deeper in the profile, Au is severely leached from the upper part of the saprolite (depleted zone) but may be concentrated at depth. It is predominantly secondary and may show some dispersion into wall rocks, though its lateral extent is far less than in the ferruginous horizons. These contrasting characteristics are due to differences in the dominant mechanisms of Au mobilization.

2.5 IMPACT OF DEVELOPMENTS IN ANALYTICAL CHEMISTRY

The intensive exploration for Au in the past decade has demonstrated that an appreciation of the influence of weathering on dispersion, combined with careful sampling and analysis, can result in the successful discovery of significant new deposits. With the knowledge of weathering profile and sampling procedure, the analytical methods have an important role.

Developments in analytical chemistry have greatly impacted upon geochemical exploration. For several decades up to the 1970s, fire assay was the principal method for Au analysis. However it was relatively expensive and with its lower limit of detection (LLD) of about 0.1 ppm Au, generally insufficient for geochemical exploration. The graphite-furnace atomic absorption spectroscopy (AAS) technique was widely adopted throughout the word during the 1980s, providing analyses of Au to ppb levels. Starting in the mid-1970s, X-ray fluorescence (XRF) has been applied to trace element exploration geochemistry and provided reliable analysis of the total proportions of many elements to ppm levels. This provided important stimulation and progress for multi-element geochemistry, capitalizing on the elements associated with gold mineralization, even if it could not be used to effectively analyze gold. In the 1980s, inductively coupled plasma torch, optical emission spectrometry (ICP-OES) and instrumental neutron activation analysis (INAA) came into commercial use. In particular, INAA was established as a routine analytical technique for multi-element analysis including Au with detection limits as low as 1–5 ppb. Presently, inductively coupled plasma mass spectrometry (ICP-MS) is well on the way to reliable routine use, but there are few reports on its successful analysis for gold in rocks.

Despite the development of high sensitivity multi-element analytical methods, most exploration has continued to rely solely on analysis for Au, depending on its low background abundance and the ability to detect widespread dispersion haloes due to the general stability of the element in the weathering environment. Such reliance on Au alone has reinforced the requirement for the use of large sample weights. This study used insoluble residue as sample medium and PIXE/PIGE analytical techniques that have a wide analytical range and concentrated on multi-element analysis, which may be valuable in defining larger element anomalies other than Au, hence requiring lower sampling densities. Consequently, the method can be used to confirm anomalies and localize alteration zones and their sources in regions where Au has been chemically dispersed. However, not all Au mineralization has a reliable suite of pathfinder elements. For example, some elements, such as As, Cu, Pb and Zn, have been accepted as a group of good pathfinder elements in exploration geochemistry (Smith and Perdrix, 1982). However, in the earlier bulk geochemistry research work in the Rand Pit and Mystery Zone of Western Australia, only As and Cu worked well, but not Pb in Rand Pit (Robertson et al., 1990). In contrast, As and Pb were used to outline gold mineralization at Mt. Percy, but Cu and Zn were not useful (Butt, 1991). In order to overcome these geochemical problems the additional EPR method was applied and tested.

2.6 SUMMARY

Thick, commonly lateritic regolith is widespread from inter-tropical to sub-tropic regions of the world, and presents particular challenges in the exploration for Au. The regolith formed under humid, warm to tropical conditions and, although it may have been modified by later climatic changes, many chemical and mineralogical characteristics are preserved. These include the geochemical expressions of concealed mineralization. Cost-effective geochemical exploration in such areas requires the application of techniques appropriate to past and present regolith processes, and also to the stage of exploration, optimizing with respect to understanding fundamental factors such as analytical and anomaly recognition techniques. This study approaches the impact of deep weathering on gold exploration through application of an integrated analytical PIXE/PIGE and EPR method to meet the challenge of exploring in areas affected by tropical weathering.

Chapter 3

ANALYTICAL TECHNIQUES

This chapter addresses sample preparation and the subsequent analysis of the acid insoluble residue by proton probe and electron paramagnetic resonance spectroscopy. The PIXE/PIGE and EPR sample preparation, principles of the analytical method, the precision, accuracy and detection limit of PIXE/PIGE as well as suitability of the method are introduced and discussed.

3.1 INTRODUCTION

In exploration geochemistry, analytical methods commonly applied are a deter-mination of the concentration of an element or elements after partial digestion with hot acid, e.g. HNO_3, HCl, aqua regia, or aqua regia/perchloric mixture, and total digestion with a mixture of $HF/HNO_3/HClO_4$ by atomic absorption spectrophotometry (AAS), indutively coupled plasma optical emission spectroscopy (ICP-OES) or inductively coupled plasma mass spectroscopy (ICP-MS). X-ray fluorescence (XRF) has been widely used in many countries not only because of its non-destructive sample preparation, but also its cost-effectiveness, good precision and a detection limit of a few ppm for most trace elements, which normally satisfies the demands of exploration geochemistry (Levinson, 1974; Rose et al., 1979; Govett, 1983; Xu, 1987).

A totally different concept of sample medium for geochemical analysis was introduced in this thesis to study the regolith Au deposits in this work. Both chemical and EPR analyses were made on the residual powder samples after hot aqua regia + HNO_3 + H_2SO_4 treatment. This treatment effectively removes weathering products, such as oxides, carbonates and sulphides. Acid insoluble concentrations of elements in the regolith were used to determine the distribution patterns of elements and recognize the wall rock alteration related to Au mineralization. The solid residue was analyzed for 28 elements by simultaneous PIXE and PIGE analytical methods and for three sweep widths of EPR.

A total of 440 chip samples of the regolith and drill core from Mystery Zone, Rand Pit and Jim's Find were involved in this study. Four hundred and twenty-six samples were used for the regolith geochemistry and 327 samples were involved in the electron

paramagnetic resonance (EPR) study. A total of 28 elements (F, Na, Al, Si, S, Cl, K, Ca, Ti, V, Cr, Mn, Fe, Co, Ni, Cu, Zn, Ga, Ge, As, Rb, Sr, Y, Zr, Nb, Pb, U and Th) were analyzed by PIXE/PIGE methods at the Lucas Heights Research Laboratories of the Australian Nuclear Science and Technology Organization (ANSTO) in Sydney. As some elements occur frequently below the minimum detection limit, the following twenty elements, F, Na, Al, K, Ca, Ti, V, Cr, Mn, Fe, Ni, Cu, Zn, Ga, Rb, Sr, Y, Zr, Nb and Pb, were used consistently in the three study areas. Arsenic was also used in each of the Mystery Zone and Jim's Find. The compositions of some elements from the acid insoluble residue were compared with INAA and XRF data obtained from Stott (1994), Butt (1991) and Robertson et al. (1990). The EPR sweep widths (EPR 326.5 ± 5 mT, EPR 326.5 ± 100 mT and 326.5 ± 250 mT) were recorded at the Central Science Laboratory (CSL) of the University of Tasmania.

3.2 SAMPLE PREPARATION

This work is an extension of previous regolith studies and the samples were chosen from the existing collections. The Rand Pit and Mystery Zone samples come from studies carried out by CRC LEME, CSIRO (Butt, 1991; Robertson et al., 1990). The Jim's Find samples are based on Stott (1994).. Samples were also collected from the open pits and drill core in the working areas. A summary of the characteristics of these drill holes and open pits is given in Chapters 4, 7 and 10 respectively.

3.2.1 Sample treatment

The 1–2 kg open pit samples from Rand Pit and Mt Percy (Robertson et al., 1990; Butt, 1991) were extracted and pulped to nominal < 75 µm. The 2–4 kg drill cores from Jim's Find were pulverized in a manganese steel mill to less than 120 µm, and in a second attempt to <75 µm. Samples of 2 grams were weighed into a 20 x 150 mm glass test tube and subsequently treated with hot aqua regia, concentrated HNO_3 and H_2SO_4 in a aluminum block on a thermostatically controlled electric hot plate. The volume of the each acid used is 15 ml. A maximum temperature of 80°C was maintained over a 12-hour period for each acid treatment. After treatment, each sample was washed three times with distilled water and dried at 90°C in an electric oven overnight. Samples were then removed into small acrylic sample bottles and were ready for the EPR measuring and making pills for PIXE/PIGE analyses. The yield of acid insolugble material varies normaly from 10% to 70% with the different nature of regolith.

This analytical procedure is designed to destroy carbonates, Fe, Mn, Al oxides and hydroxides, sulphides, and other weathering products such as kaolinite and other clay minerals.

3.2.2 Variations in acid insoluble residue with grain size

Considering the <75 μm and <125 μm (including the particles smaller than 75μm) fraction size used in the Mystery Zone, Rand Pit and Jim's Find, the effect of the acid treatment on the residue concentration in relation to the grain size of the crushed sample has been examined for the Jim's Find material. Very similar trace and major element contents were obtained for the aqua regia + HNO_3 + H_2SO_4 digestion, except for fluorine, and are considered to indicate sample homogeneity (Figure 3-1). Due to the insolubility, F shows the largest antithetic variation with grain size, being 2 to 4 times higher in the fine fraction than in the coarse fraction. In general, Al is 5–10% lower in the coarse fraction than in the fine fraction. Other elements remain constant with different grain sizes.

Higher F in the fine fraction is probably due to the abundance of mica present in the fine samples, as micas are the main source of F (Rose, 1979). Fluorine is not a key element in this study, the 125 μm size of the sample chosen should satisfy the exploration purpose without missing any information. In this study, the mica, such as biotite, was presumed to mostly occur in the fine fraction because the dominant minerals in the coarse fraction are clay minerals. This is supported by higher aluminium in the coarse fraction due to more abundant clay minerals. The clay minerals within the fine fraction are much easier to wash than in the coarse fraction.

3.2.3 Residue description

This acid treatment processes and removes all weathering products. After the acid treatment, some samples still remained light brown, black and dark brown in color. This suggests some significant minerals, which could not be cleaned out are still in the residue. Samples with different colours were selected for XRD analysis, using a Philip PW 1050 diffractometer with 40 kV and 20 mA at the Chemistry Department of the University of Tasmania. Cu Kα radiation was used. For qualitative analysis, each sample was scanned over the range 5–60° 2θ at a speed of 1° 2θ/min. Estimations were made

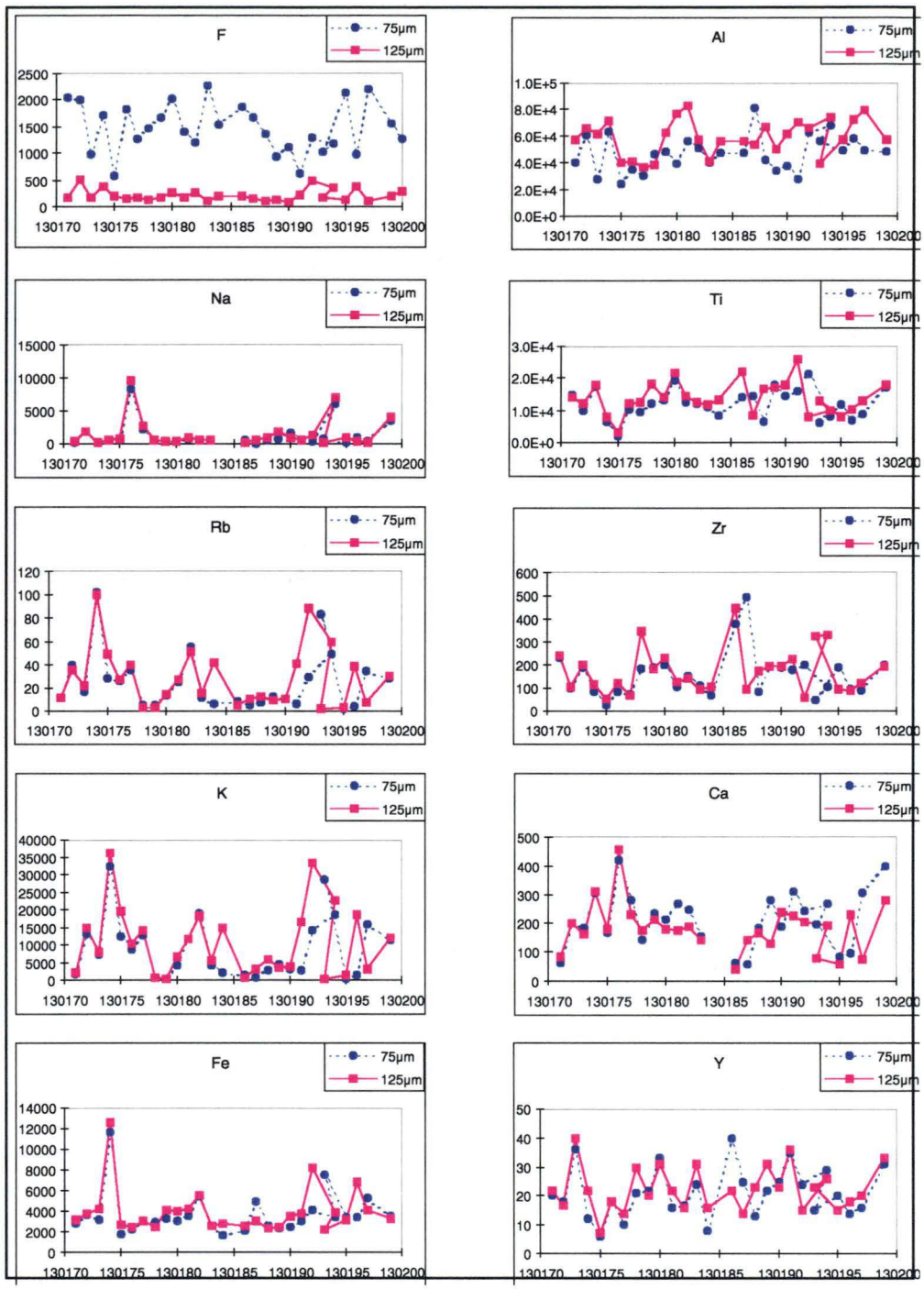

Figure 3-1. Variation in the acid insoluble residue of regolith, Jim's Find, with grain size (X axis represents the sample number, Y-axis represents the concentration in ppm)

using the height above background of a selected XRD peak for each minerals. The results are reported in Table 3-1. Figure 3-2 gives the typical XRD spectra of some samples from this study. The acid insoluble residue from Jim's Find consists essentially of quartz, accompanied with some sericite, feldspar and some resistant minerals like rutile, whilst the acid insoluble residue from Rand Pit and Mt Percy consists mainly

Table 3-1. The physical character and XRD results of regolith acid insoluble residue

Area	Sample	Residue descript	XRD characters
Mystery Zone	MW0173	light brown	Quartz
Mt. Percy	MW0537	light green	Quartz
WA	MW0549	white	Quartz
	MW1288	light green	Quartz, muscovite
	MW1290	white	Quartz, muscovite
	MW1294	white	Quartz, muscovite
	MW1307	white	Quartz, muscovite
	MW1572	light green	Quartz, muscovite
	MW1588	white	Quartz, talc
	MW1793	white	Quartz, feldspar, talc
Rand Pit	RE1	white	Quartz, feldspar, talc, amphibole
Reedy Mine	RE2	white	Quartz, talc, feldspar, amphibole
WA	RE6	white	Quartz, feldspar
	RE7	white	Quartz, feldspar, talc
	RE15	white	Quartz, talc, amphibole
	RE17	white	Quartz, talc, amphibole
	RE19	light gray	Quartz, talc, feldspar, amphibole
	RE22	white	Quartz, talc, amphibole
	RE51	light gray	Quartz, feldspar, talc, amphibole
	RE59	light green	Quartz, feldspar, talc, kaolinite
	RE61	white	Quartz, feldspar, talc, amphibole
	RE66	white	Quartz
	RE100	light green	Quartz, feldspar, talc, amphibole
Jim's Find	130186	white	Quartz, muscovite, rutile
Tanami	130187	white	Quartz, muscovite, kaolinite, rutile
NT	130188	light gray	Quartz, rutile, dickite, muscovite
	130192	light gray	Quartz, rutile, muscovite, dicdite
	130193	light gray	Quartz, muscovite, feldspar, rutile
	130194	light gray	Quartz, muscovite

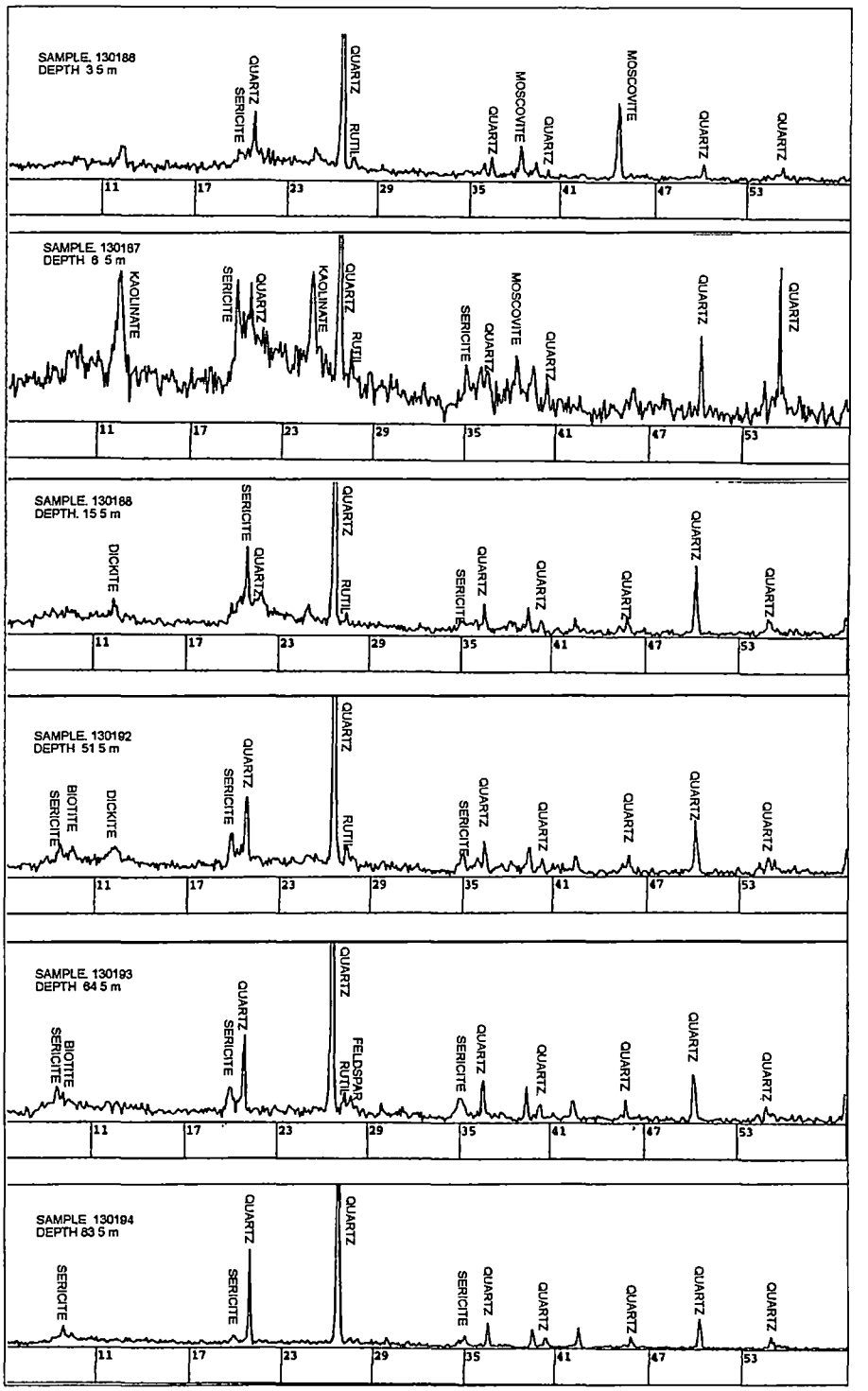

Figure 3-2. X-ray diffraction data of drill core JRC 030 from Section 10150N, Jim's Find, Tanami, N.T.

of quartz accompanied with minor talc, amphibole, muscovite and feldspar.

3.3 PIXE/PIGE ANALYSIS

3.3.1 Introduction

The application of Proton Induced X-ray Emission (PIXE) to geological problems began in the mid-1970s; the earliest studies were those of Horowitz and Grodzins (1975) and Kullerud et al. (1979). The first industrial and commercial application in geology was attempted by Carlsonn and Adeselsson (1980). Since then, PIXE has had increasing application to a variety of geological problems, particularly as data-reduction techniques have improved and progressed (Annegarn, 1984; Carlsson, 1984; Brissaud, 1986; Brissaud, 1987; Bird and William, 1989; van Moort et al., 1990; Miono, 1992; Sie, 1993; Halden, 1995). Most of these studies represent microprobe analysis. The present study uses this method for the determination of the acid insoluble residue chemical composition (Xu, 1996; Xu and van Moort, 1997a; Xu and van Moort, 1998a).

Proton beams also provide a variety of other analytical techniques applicable to mineralogical and geochemical analysis. One of them is used in this study, i.e. Proton Induced γ-ray Emission (PIGE). The PIGE technique was first applied to geological problems in the late 1980s. It is often used as a single technique by detection of MeV ion bombardment, or simultaneously accompanies PIXE for determination of light bulk elements (Boni et al., 1988). Anderson et al. (1989) used PIGE to determine compositions of unopened fluid inclusions and Tulhoat et al. (1993) showed concentrations of Li, B, F and Na can be measured in spodumene, tourmaline and lepidolite to detection limits in the 60–100 ppm range.

Although PIXE/PIGE provides some exciting new insights into the major and trace elements of geological materials, its use has been somewhat restricted because firstly it requires a particle accelerator, that is currently available in few laboratories, and secondly other advanced analytical methods are rapidly developing. These latter include laser ablation microanalysis combined with inductively coupled plasma techniques, with atomic emission spectrometry (ICP-AES) and mass spectrometry (ICP-MS) detection systems. X-ray spectrometry (XRF), atomic absorption spectrometer (AAS) and instrumental neutron activation analysis (INAA) are even more widely used. However, more recent review papers (e.g. Annegarn and Bauman 1990, MacArthur and Ma,

1991) have taken an increasing geological perspective because more and more problems can be solved using trace element analysis of minerals by the PIXE/PIGE method.

Currently, PIXE/PIGE is a mature analytical technique that is gaining increased application to a variety of mineralogical and geochemical problems (Camanske et al., 1992; Halden et al., 1995; Xu, 1996) because of its advantage as a readily quantified, standardless, non-destructive, in situ multi-element analytical technique with high (ppm) sensitivity, reliability and precision. The technique was chosen for this study because of the above-stated reasons together with its speed and the wide range of elements (including Li, F and Na) which can be determined simultaneously. Although similar results may also be obtained by XRF spectrometry, PIXE/PIGE can provide lower detection limits for some useful elements (e.g. Na, Ca and Ga).

3.3.2 Principles of the methods

The high energy protons produced from a accelerator or other sources are directed to a target and cause a variety of interactions, as illustrated in Figure 3-3. Using semi-conductor detectors, X-rays and γ-rays can be measured independently or simultaneously. A typical experimental arrangement of the techniques is shown in Figure 3-4. The more theoretical aspects of the methods are discussed in Bird and Williams (1989).

3.3.2.1 Proton induced X-ray emission (PIXE)

When an incident high speed proton interacts with a target atom, an electron may be ejected from an inner shell (K, L, etc.). This vacancy is then filled with an electron from an outer shell and in doing so the excess energy is emitted as a characteristic prompt X-ray (Figure 3-5). The energy of the X-rays emitted is characteristic to the parent atom and the number of the X-rays is proportional to the concentration of the parent element. A Si(Li) detector is used for X-ray measurement and a computer and related software are used to deal with the spectra and transfer the X-ray intensity (Figure 3-6) to corresponding elemental concentrations.

3.3.2.2 Proton induced gamma ray emission (PIGE)

When a sample is irradiated by high energy protons, characteristic γ-rays are produced for certain elements in the sample, as a result of the incoming particle reacting with

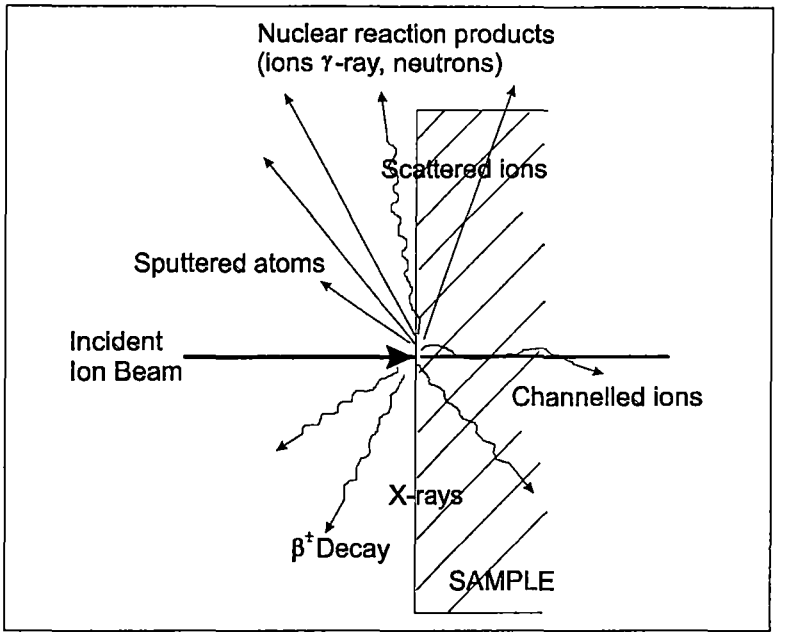

Figure 3-3. Ion Beam interaction (after Bird el al., 1983)

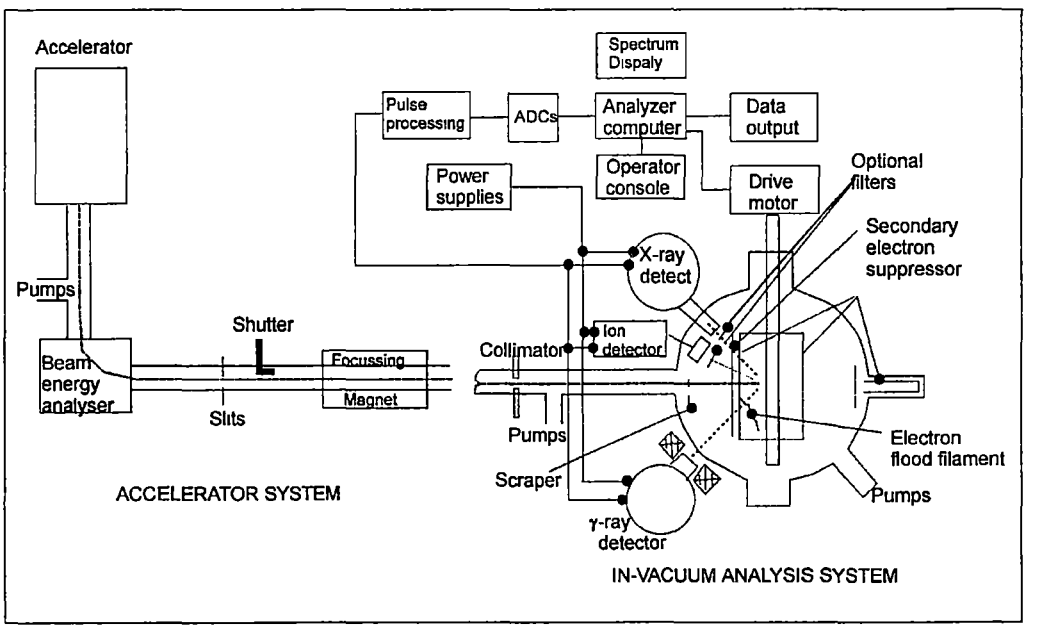

Figure 3-4. A schematic layout of the ion beam analysis facility used in this study (after Bird and Williams, 1989)

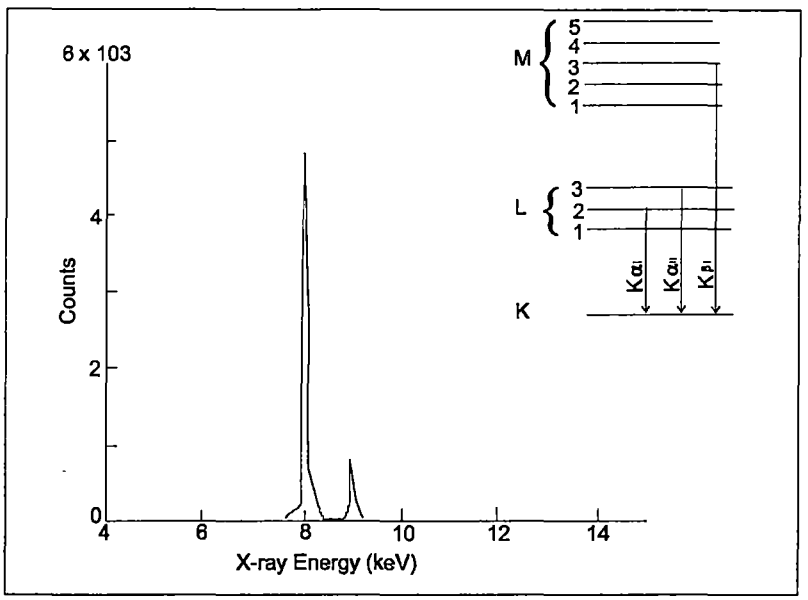

Figure 3-5. The K-ray spectrum for Cu showing K_α and K_β peaks together with the corresponding energy level transitions

the nucleus of the atom. A typical PIGE spectrum is shown in Figure 3-7. The PIGE technique is often used as a complement to PIXE for an accurate quantification in thick geological samples by determining the bulk composition. PIGE requires a Ge(Li) detector instead of the Si(Li) detector used in energy-dispersion PIXE and depending on the design of the specimen chamber, nuclear reactions may be detected concurrently with PIXE. Mathematical models are fitted to the observed PIGE spectrum and optimized to convert the measured γ-ray yields into elemental concentrations (Clayton, 1986).

3.3.3 Analysis procedure

In this work, PIXE/PIGE analysis were carried out at the Physics Division of Lucas Heights, Australian Nuclear Science and Technology Organization (ANSTO) in Sydney, where an automated facility for bulk sample analysis by PIXE/PIGE has been developed on one of the beam lines of the 3 MeV Van de Graaff positive ion accelerator. Up to 60 samples can be loaded on a target stick for analysis in a vacuum chamber, where they are bombarded in sequence with the high energy protons. These protons are collimated by a graphite aperture before entering the target chamber.

A Si (Li) detector and a Ge (Li) detector, for measurements of X-rays and γ-rays

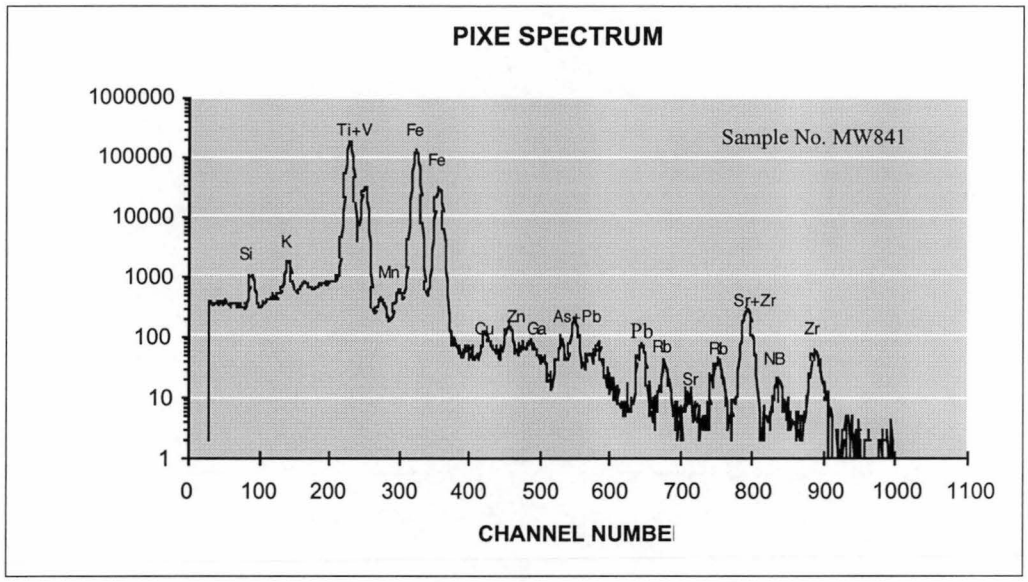

Figure 3-6. A spectrum of a PIXE analysis of acid cleaned regolith powder (MW841), Mt Percy). The peaks, from the left to right, are as follows: SiK_{α}, KK_{α}, FeK_{α}, FeK_{β}, NiK_{α}, CuK_{α} YK_{α}, ZrK_{α}, YK_{β} and ZrK_{β}.

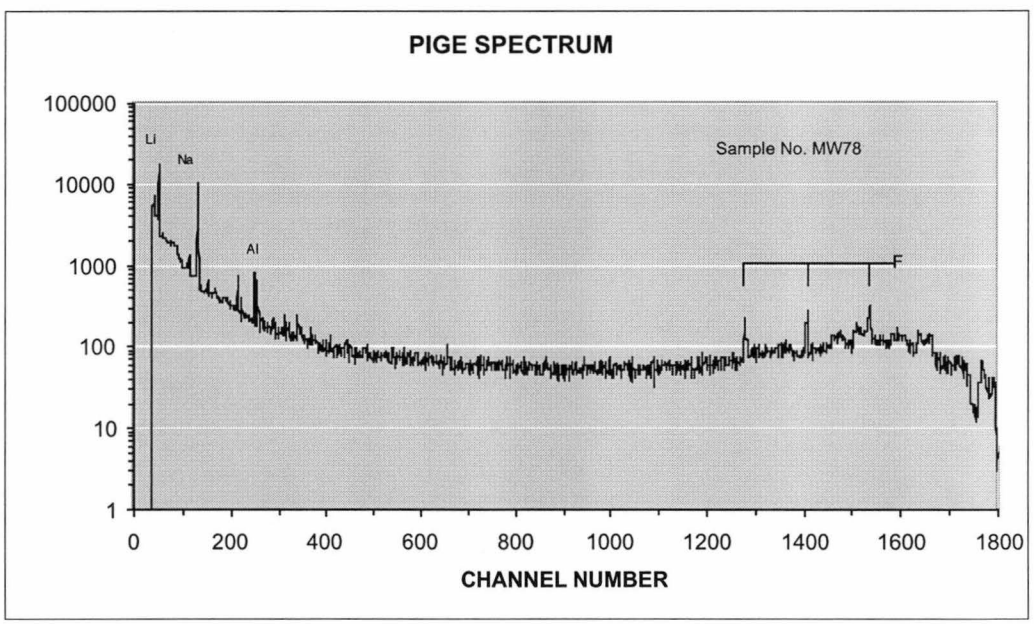

Figure 3-7. A PIGE spectrum obtained from a pressed pill containing 20% C of the standard sample in this study. The γ-ray peaks are well separated.

respectively, are placed around the target chamber (Figure 3-4). A software package called PIXAN developed by Clayton (1986) was used during the analyses to identify the peak areas associated with each element and convert them to a concentration and with associated minimum detection limits (MDL). For each bulk sample analysis, elements with a concentration less than the relevant MDL, had a zero elemental concentration ascribed to them.

3.3.3.1. Sample preparation

A 400 mg acid insoluble regolith residue was mechanically mixed in an acrylic vial for ten minutes with 100 mg of spectrographically pure graphite together with an acrylic ball. Following this, the sample was poured into a 12 mm diameter aluminum cup, smoothed and covered with a cleaned disc of hard acrylic plastic melinex in order to prevent contamination. The cup was pressed at a pressure of 5 t with a Beckman 16 tonne press. All the standard and duplicate samples and graphite blanks were prepared using the same technique for the quality control purpose. After pressing, the acrylic cover was removed and the sample stored in a small plastic bag, ready for measurement by PIXE/PIGE.

3.3.3.2 Instrument setting

The proton energy used was 2.5 MeV protons with a beam current of about 300 nA. The aperture was set at 1.5 mm with a 3.3 mm steeple. The beam spot size was 1.5 mm and run times were adjusted so that the total charge collected was 100 mC. Since this study was concerned with X-ray with energies above 3 keV, a Mylar pinhole filter was placed between the target and the Si (Li) detector with a 26 mm Be window. The filter consisted of a 50 mm Mylar slice attached to the perspex with a 0.8 mm hole. This shielded and reduced the count rate in the detector from low energy X-rays and reduced the electronic dead time to a manageable level.

Gamma rays were measured with a large 30cc Ge(Li) detector placed close to the target at an angle of 45° to the incoming proton beam. The light elements Li, F, Na,

Al and Mg are measured using nuclear reactions, which are chosen to give a high yield of gamma rays for protons at an energy of 2.5 MeV. These measurements can be made simultaneously with the PIXE X-ray analysis. The reactions used, and the gamma rays of interest are as follows:

Li from Li7(p,p'γ)	Ey = 478 keV,
F from F19(p,p'γ)	Ey =197 keV
Na from Na23(p,γ)	Ey = 440 keV
Al from Al27(p,p'γ)	Ey = 1.014 MeV
Mg from Mg24(p,p'γ)	Ey = 585 keV

An energy scale of 4 keV per channel is used so that for a 2000 channel spectrum used in the gamma ray analysis the energy range of 0–8 Mev is used. This allows detection of 6–8 MeV γ-rays from F and Li.

The following elements were analyzed by PIXE using their Kα emission lines: S, Cl, K, Ca, Ti, V, Cr, Mn, Fe, Co, Ni, Cu, Zn, Ga, Ge, As, Br, Rb, Sr, Y, Zr and Mo. The Lα emission lines were used for heavier elements Ba, La, W, Pb, Th and U because the Si (Li) detectors are more sensitive to the Lα emission. The PIGE method was used to extend the PIXE data sets into light element analysis, Li, F, Na, Mg and Al. In the analyses (Appendices 1, 3 and 5), La, Li, Se, Br and Bi are not given due to their very low, erratic levels and a poorly constrained minimum detection limit.

3.3.4 Precision, accuracy and detection limit

Tables 3-2 and 3-3 give examples of reproducibility for a NBS standard sample SRM278 (obsidian), analyzed at fifteen times, and two regolith samples randomly taken from this study measured four times in a one-year period at a consistent instrument setting. Statistically well defined single peaks indicate the precision of the spectrum evaluation, expressed as deviation in relative percentages from the mean values of five replicate standards and four sample measurements, is very good. Deviations ranged from as low as 1% to 20%. The precision of Ni and Cu from standard SRM278 are from 20 to 21%, which is much higher than other elements and the regolith samples. This is attributed to values near or below the detection limits in these elements. Simiarly, due to poor detection limits, some other elements such as Li and Ba in Table 3-2 are not shown in Table 3-3.

Table 3-2 Precision of elements determined in NBS standard sample SRM278 obsidian (n=15)

Element	X(ppm)	S	RSD	Element	X(ppm)	S	RSD
Li	20	2.34	11.7	Ni	7	1.41	20.2
F	313	12.19	3.66	Cu	6	1.26	21.08
Na	287722	492	1.71	Zn	39	1.21	3.13
Mg	<1500	0		Ga	16	1.38	8.89
Al	59427	1097	1.85	Rb	101	5.15	5.05
Si	264920	6216	2.35	Sr	51	6.22	12.32
K	25911	302	1.17	Y	32	4.68	14.86
Ca	5407	302	1.17	Zr	245	15.1	6.17
Ti	1205	28.07	2.33	Nb	15	1.76	12.14
Mn	320	4.68	1.46	Ba	311	92.14	29.64
Fe	11518	190	1.65	Pb	12	2.66	21.65

X= Arithmetic mean
S = Standard deviation
RSD = Relative standard deviation

Table 3-3 Precision of elements determined in regolith samples of this study (n=4)

	Sample No. 130172			Sample No. 130180		
Element	X(ppm)	S	RSD	X(ppm)	S	RSD
F	513	6.2	1.22	269	2.8	1.02
Na	1682	9.17	0.58	354	18.1	5.11
Al	66561	1017	1.53	74352	231	0.31
Si	251173	456	0.18	250265	6108	2.44
K	13864	36.9	0.27	6265	287.78	4.59
Ca	196.5	22.3	11.35	182	15.3	8.79
Ti	11556	175.9	1.52	21131	223	1.06
V	440	11.3	2.57	509	12	2.35
Cr	30.75	5.6	18.28	0	0	
Mn	16.25	0.5	3.08	9	1.4	15.71
Fe	3610	11.9	0.33	3761	157	4.18
Co	28.25	2.5	8.85	24.5	1.3	5.27
Ni	7.5	0.6	7.7	5.54	0.6	10.5
Cu	4.7	0.5	10.45	12	0.8	10.5
Zn	5	0		1.3	14.53	
Ga	13.5	0.6	4.28	11.7	1.7	14.53
As	4.75	1	20.16	11	28	25.71
Rb	38.5	0.6	1.5	15	0.8	5.44
Sr	13.5	1.3	9.56	8	1.4	17.68
Y	17.2	1.7	9.9	32.75	3.6	10.97
Zr	106	1	0.9	238	6.1	2.57
Nb	8.25	0.5	6.06	13.75	1	6.96
W	54.2	2.5	4.61	21.7	1	4.4
Pb	3.5	0.6	16.5	2.25	1.3	55.92

X= Arithmetic mean
S = Standard deviation
RSD = Relative standard deviation

Table 3-4. Analytical accuracy of this study.

Major elements (%)		Na%	Al%	Si%	K%	Ca%	Fe%	Mn*	Ti*
	Recommended[a]	3.13	13.4	72.83	5	1.55	2.14	463	1720
GSR1	Determined[b]	3.18	13.41	72.96	5.1	1.55	2.15	461	1712
	Accuracy[c,%]	1.59	0.07	0.18	2	0	0.47	0.43	0.47
	Recommended[a]	3.86	16.17	60.62	1.89	5.2	4.9	604	3090
GSR2	Determined[b]	3.88	16.21	60.99	1.87	5.24	4.92	625	3114
	Accuracy[c,%]	1.44	0.26	0.61	1.02	0.7	0.46	3.39	0.76
	Recommended[a]	2.88	5.99	28.5	2.58	0.59	1.16	335	1092
SRM278	Determined[b]	2.89	5.96	27.48	2.68	0.56	1.15	325	1247
	Accuracy[c,%]	0.47	0.5	3.63	3.58	6.24	0.79	3.13	14.22

Trace elements (ppm)		Ni	Cu	Zn	Rb	Sr	Y	Zr	Pb
	Recommended[a]	2.3	3.2	28	466	106	62	167	31
GSR1	Determined[b]	1.5	3.5	26.5	460	110	62.2	171	31.3
	Accuracy[c,%]	34.78	9.37	5.36	1.39	3.77	0.4	2.25	0.81
	Recommended[a]	17	55	71	38	790	9.3	99	11.3
GSR2	Determined[b]	15.8	50	73.5	35.8	788	8	96.8	10.8
	Accuracy[c,%]	7.35	10	3.52	3.38	0.25	11.11	2.27	16.67
	Recommended[a]	3	5	36	96	47	—	236	14
SRM278	Determined[b]	—	12	38	102	48.3	27	229	11.75
	Accuracy[c,%]	—	—	5.56	5.99	2.66	—	2.86	16.07

Trace elements (ppm)		As	W	Ga	Ge	Mo
	Recommended[a]	2	3.2	17.25	2	3.5
GSR1	Determined[b]	1	3.5	19	0.5	1.25
	Accuracy[c,%]	50	9.37	9.2	75	64
	Recommended[a]	2	0.47	18	0	0.54
GSR2	Determined[b]	0.25	0.54	18	0	0.25
	Accuracy[c,%]	87.5	14.89	0	—	29
	Recommended[a]	4	0	3.5	0.00-1-	19.3
SRM278	Determined[b]	—	—	—	—	—
	Accuracy[c,%]	—	—	—	—	—

a: Recommend values (GSR1 and GSR2 come from Xie and Yan (1989), SRM 278
b: Determined values come from arithmetic mean of four determinations in this study
c: Accuracy as given is the percentage deviation of the arithmetic mean of a set of four values from the recommended data [(b-a)x100/a]
*: Mn and Ti are presented in ppm

The accuracy of PIXE is not only dependent upon the beam irradation procedure, but also the X-ray line intensity ratios used in fitting overlapping spectra of interfering elements. A problem encountered in the analysis of regolith samples was the overlap of Ti, V and Cr Kα with Ba Lα lines. Moreover, the characteristics of analyzed targets may severely affect the analytical accuracy. After careful sample preparation and matrix calibration, Table 3-4 clearly illustrates high accuracy for the analysis of the major components down to 0.59% mass content, including those of magnitude for neighbouring elements. For most major and minor elements, the accuracy ranges from 0.4–5%. For the elements Ni, Cu, Zn and Pb, the accuracy is poor when element concentrations approach the detection limit. For example, Ni accuracy in sample GSR1 is low (<34%) because of its low abundance. Nonetheless, for most elements in lateritic samples, elements are above their PIXE detection limit. Their geochemical dispersion in lateritic soils was described by Davies and Bloxam (1979) and the results in this thesis (Table 3-5) clearly indicate that they can be accurately analyzed by PIXE, even in the most weathered profile. The results are comparable to routine XRF analysis in exploration geochemistry (Xu, 1989a, b).

The precision and accuracy for Mg is very poor due to the small nuclear cross section for protons on Mg, giving a low yield of gamma rays. The minimum detectable level for Mg in this study is about 1000 ppm. Specifically Mg is measured by the proton inelastic scattering reaction $^{24}Mg(p,p'\gamma)^{24}Mg$, giving γ-rays of energy 585 keV. Other Mg reactions with protons either have lower γ-ray yields or gamma rays which are also produced from Al and cannot be used. Also for protons with energies from 1 to 3 MeV, the highest yields are from Li, B, F, Na and Al. At energies above 3 MeV, the γ-ray yield from medium and heavy elements begin to compete with the light elements. Mg can be determined at 4 MeV (Bird and Williams, 1989). This study does not use Mg as an important indicator element.

Detection limits, which are a function of the charge used (and therefore the total accumulated counts), can be lowered using longer count-times. With a 2.5 MeV proton beam, beam currents of 150–200 nA and duration of analyses of 4–5 minutes, this study identified detection limits for most elements to vary from 2 to 30 ppm. However, some light elements (e.g. Cl and Si) are less constrained with detection limits of 100–

Table 3-5 Distribution parameters for selected trace elements Ni, Cu, Zn and Pb in lateritic soils (from Davies and Bloxam, 1979)

Element	N	Range	Median	Threshold
Ni	134	20-287	80	208
Cu	95	1-65	19	46
Zn	92	13-103	43	88
Pb	63	20-287	49	86

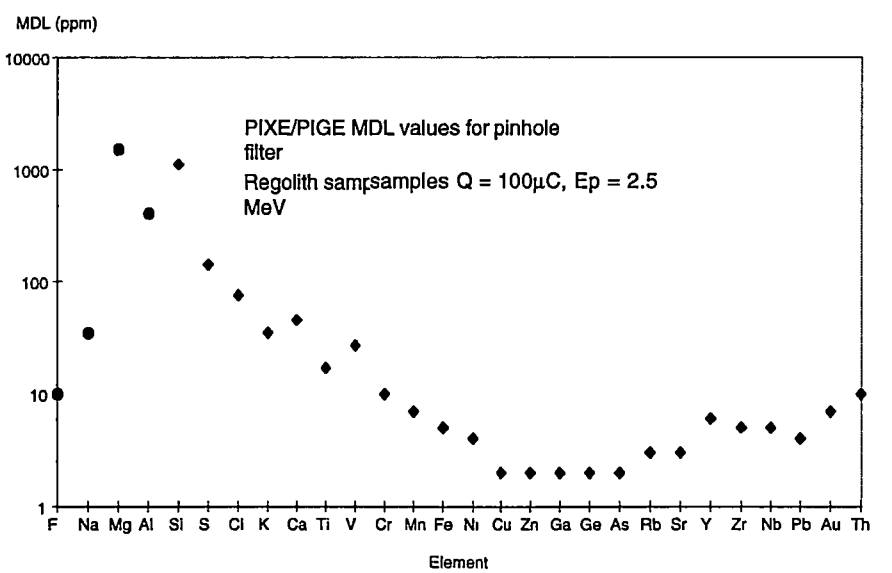

Figure 3-8. Minimum detection limits in this study

1000 ppm, as illustrated in Figure 3-8. The detection limits for other elements not listed here can be evaluated according to Figure 3-8.

3.3.5 Comparison of PIXE/PIGE to XRF and INAA

This study set out to determine the usefulness of PIXE/PIGE analyses on powder samples after acid digestion and to compare the analytical results with results generated by conventional techniques, in order to elucidate its use as a general purpose Au exploration tool/technique.

Figures 3-9 and 3-10 illustrate the binary relation between the analytical results obtained from PIXE/PIGE analyses on the residual powder sample after hot aqua regia + HNO_3 + H_2SO_4 digestion to those from XRF and INAA on the basis of bulk rock. The analyses were performed on the same samples. Samples were chosen from Rand Pit, Reedy Mine because of available XRF and INAA results (Robertson et al., 1990). The major elements of XRF data are presented in oxide format. Moderate to strong positive correlation is observed between K_2O and K, Al_2O_3 and Al, Na_2O and Na, TiO_2 and Ti, and Rb and Sr (Figure 3-9). However, CaO and Ca, and W have a much weaker correlation between the two different analytical methods (Figure 3-9). That is because these elements in the majority of regolith powder samples are not soluble or only slightly soluble under hot acid treatment. This also indicates the acid treatment method eliminates the weathering products without damaging the original rock forming minerals.

Most samples retain the very low Ca values in the acid insoluble residue, implying higher Ca contents in bulk geochemistry likely as carbonates. Some Al and Rb are very high in XRF data but near zero in PIXE/PIGE data and cannot be used to a interpret bulk geochemistry, but these low values of Al and Rb in acid insoluble residue could be predicted that are barren or non-alteration related. Fe, Mn, Pb, Zn V, Cu, Cr, Zr (Figure 3-10) and other elements do not have a significant correlation as they occur largely as weathering products, such as iron and manganese oxides and hydroxides and absorbed elements easily soluble in an acid environment. This indicates that the acid insoluble residue yields better constraints on rock forming minerals, thereby reducing the geochemical effect of weathering. A detailed discussion on the distribution patterns of elements obtained from XRF, INAA and PIXE/PIGE in each of the three study

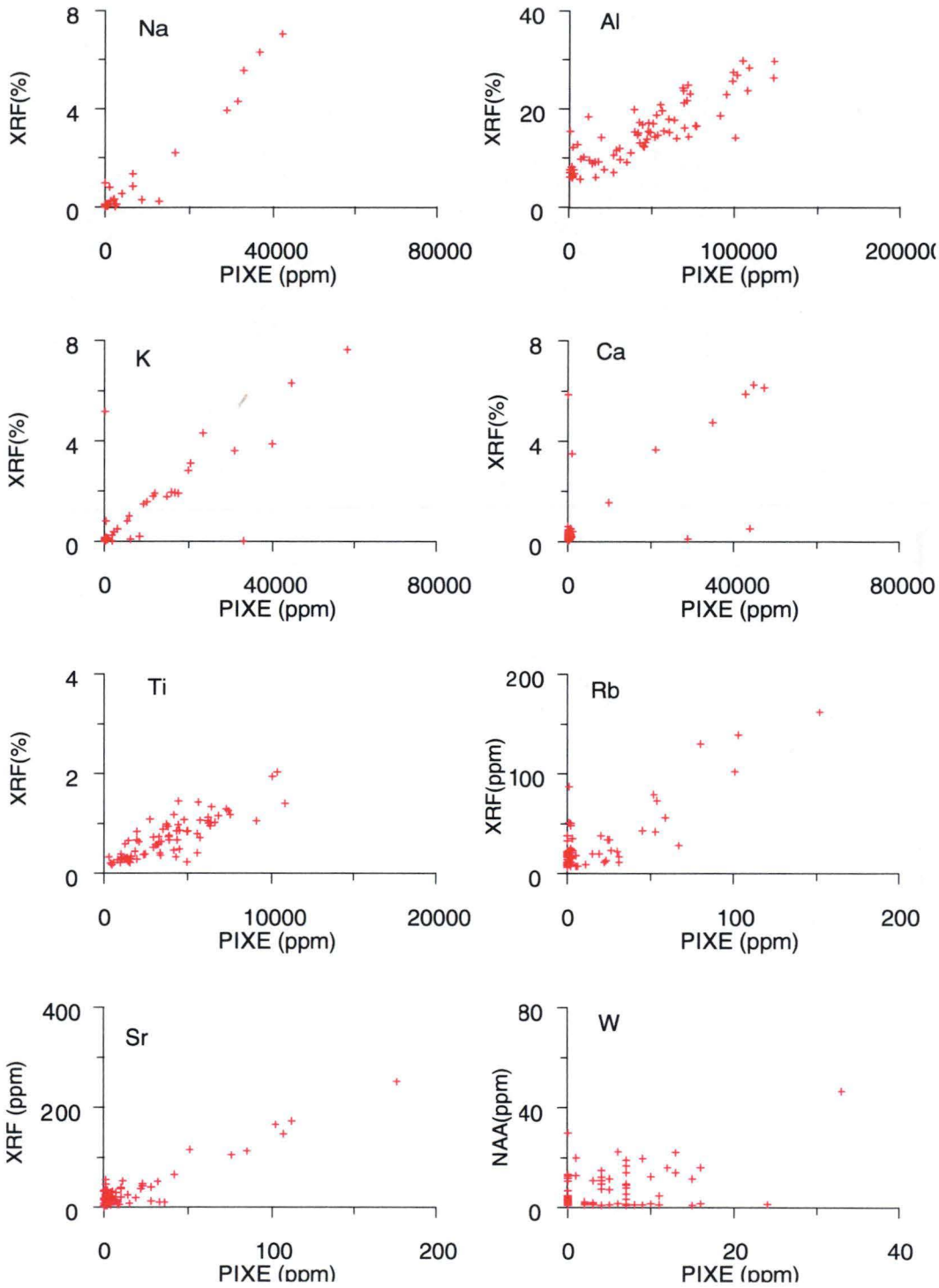

Figure 3-9. Binary plots showing the relation between concentrations of elements analyzed by XRF (bulk rock), INAA (buck rock) and those by PIXE/PIGE (acid insoluble residue). Samples are from Rand Pit, Reedy Mine (n=76)

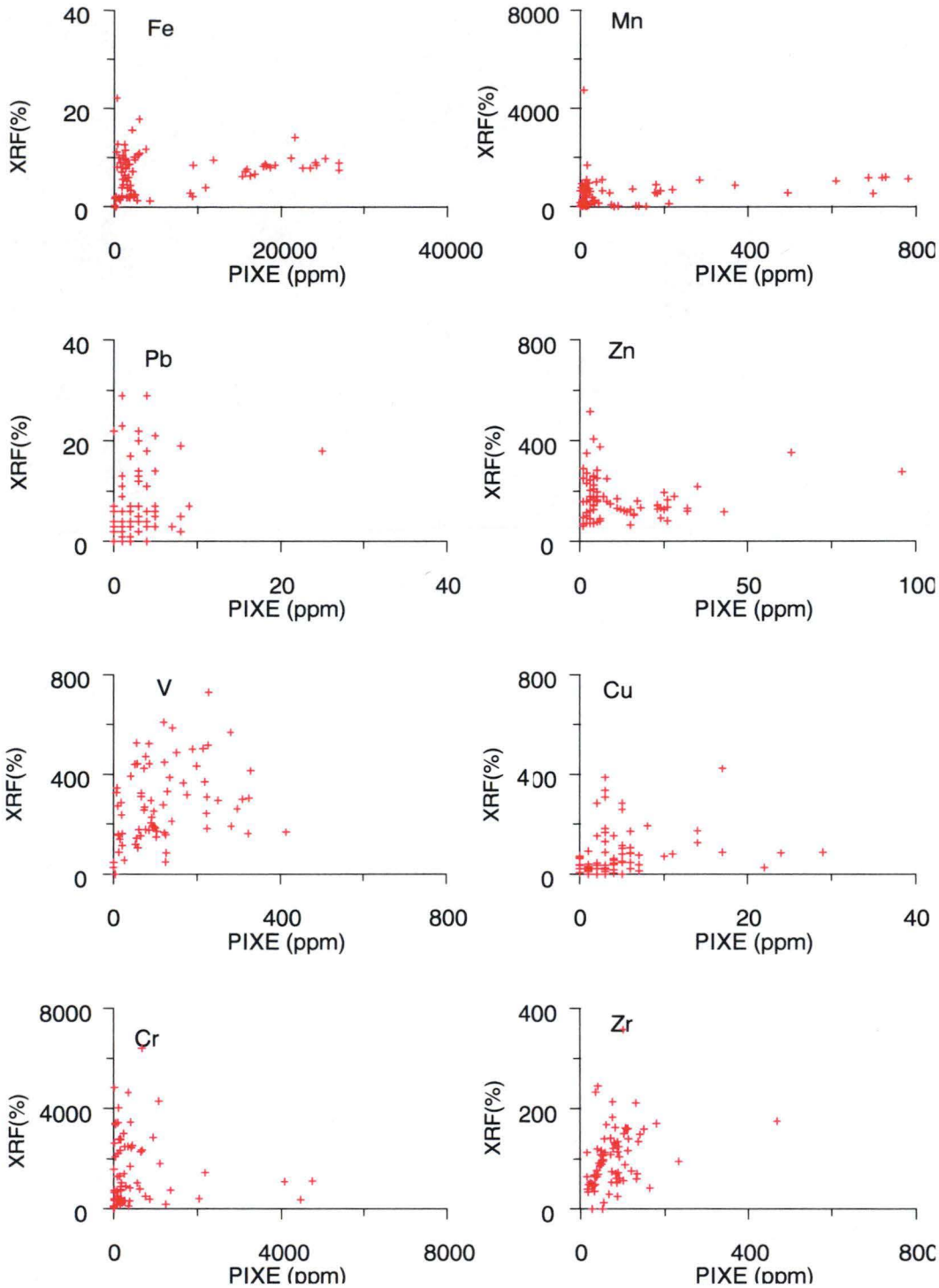

Figure 3-10. Binary plots showing the relation between concentrations of elements (Fe, Mn, V, Cu, Cr and Zr) analyzed by XRF (total content) and those by PIXE/PIGE (acid insoluble residue). Samples are from Rand Pit, Reedy Mine (n=76)

areas is presented in Chapters 5, 8 and 11.

The detection limits for the INAA analyses used in this study are consistent with those of thermal NAA, i.e. using thermal neutrons for activation. The detection limits for Ag, Au, Ba, Co, Cr, Fe, K, La, Na, Sb, Sc, Th, W and Zr are for thermal neutron activation, followed by a count at about seven days after activation. The NAA method is remarkably sensitive for the elements Au and As, whilst the PIGE analyses are remarkably sensitive for F and Na. The PIXE analyses, which is energy dispersive, provides data in the ppm range with detection limits coming close those of wavelength dispersive XRF and better than energy dispersive XRF. The minimum concentrations detectable in this work depends on the pinhole filter used, and ranges from a few ppm for elements with intermediate atomic numbers such as Cu and Zn, to a few hundred ppm for heavier elements such as Sn, where the efficiency for Kα rays is diminished. Elements heavier than Ba can be detected through their Lα lines. Elements analyzed by this method together with detection limits for the INAA and XRF techniques are given in Table 3-6.

In summary, the accuracy, precision and detection limit of the PIXE/PIGE method can satisfy most purposes in exploration geochemistry. Using an acid insoluble residue sample medium, an added simultaneous multi-element capability is achieved, which is potentially beneficial for Au exploration.

3.4 EPR

3.4.1 Introduction

Paramagnetism is largely due to the electron spin of unpaired electrons. Paramagnetism becomes important in a strong external magnetic field and is used extensively in mineral separation techniques. The magnetic susceptibility of paramagnetic material is positive and small, being in the order of $x10^{-4}$–10^{-6} emu/cm^3. Such a magnetic susceptibility is too small to be detected by field magnetometers and too small to be measured by commercially available susceptibility meters, such as a Gouy balance. Most silicates minerals are paramagnetic, however pure quartz is diamagnetic unless impure, in which case it becomes paramagnetic (Pilbrow, 1990).

As the instrumentation is lacking to effectively measure the magnetic susceptibility of paramagnetic materials, in place electron paramagnetic resonance may be used. This

Table 3-6. Typical detection limits for INAA, PIXE/PIGE and XRF on most geological materials (in ppm unless otherwise stated)

Element	INAA[a]	PIXE/PIGE[b]	XRF[c]
Ag	5	80	2
Au	5ppb	7	3
Al	—	400	190
As	1	3	2
Ba	100	50	30
Ca	10000	45	190
Cl	—	75	20
Co	1	3	20
Cr	5	13	10
Cu	—	2	4
Fe	200	5	1000
Ga	—	2	5
Ge	—	2	3
K	2000	35	100
La	1	600	10
Mg	—	1500	190
Mn	—	8	190
Na	100	40	250
Nb	—	5	4
Ni	50	4	5
P	—	40	50
Pb	—	4	5
Rb	30	3	5
S	—	140	50
Sc	0.1	40	2
Si	—	1100	1900
Sn	100	100	5
Sr	500	3	10
Th	0.5	10	10
Ti	—	17	190
V	2	13	5
Y	1	4	10
Zn	50	2	5
Zr	500	5	10

a: Becquerel Laboratories, Lucas Heights, NSW, Australia (data for detection limits are after a seven day decay, except Sr, V and Y are counted earlier.
b: This study conducted at Physics Division, ANSTO, Lucas Heights, NSW, Australia
c: Xu, (1987) and CSIRO, Wembly, W.A., Australia

method measures the resonance of unpaired electrons between the parallel and antiparallel states at specific values of a strong magnet whilst a high frequency microwave radiation of constant frequency is applied.

The absorption of microwave radiation at specific values of the magnetic field intensity and microwave frequency is specific for many materials. There are many practical applications of this EPR technique to science including biology, zoology and medical sciences, chemistry, environmental sciences, physics and material science (Rudowicz, 1997). EPR has also been used in geology for dating and to determine transition metals in various minerals (Goldfarb, 1981; Calas, 1988; Petrov et al., 1989; Burns and Flockhart, 1990; Petrov et al., 1993; Ikeya, 1994). It also has considerable application in the characterization of quartz (Weil, 1984; Scherbakova et al., 1985; van Moort, 1986). Nelson et al. (1982) used the EPR method to characterize the carbonaceous and oxidized Carlin-type Au ore in Nevada, USA. van Moort and Russell (1987) found that auriferous quartz can be characterized by simple room temperature EPR. Subsequently, auriferous jasperoids (van Moort et al., 1995), siliceous wall rock of VHMS deposits (Pwa, 1995), and wall rock of auriferous deposits (Stott et al., 1997) were found to have enhanced EPR signals close to mineralization.

This study evaluates the use of EPR to the regolith in order to characterize any wall rock alteration close to Au mineralization. It also qualifies the difference of EPR signatures between different lithological units and increases our knowledge of EPR properties and its relationship to Au mineralization in the regolith, providing a potential exploration tool for Au and other commodities within and Below the regolith (Xu and van Moort, 1997b; Xu et al., 1997; Xu and van Moort, 1998b).

In this section, the relationship between the EPR spectra and the chemical composition of rock powders from near surface, open pit and drill core samples for each area will be discussed. This is followed by discussion on the distribution of EPR intensities and formulation of an EPR index applicable to Au mineralization.

3.4.2 Principle of the method

EPR spectroscopy is a form of spectroscopy concerned with microwave-induced transitions between magnetic energy levels of electrons having a net spin and orbital

angular momentum (IUPAC, 1989). The technique is therefore based on the alignment of magnetic moments by an externally applied magnetic field and their reorientation by the absorption of incoming electromagnetic radiation.

Since EPR requires the presence of unpaired electrons, its application is restricted to paramagnetic materials. Among these geological materials, quartz is the most studied mineral, because of its technological and widespread geological importance. Pure quartz, neglecting surface effects, does not contain unpaired electrons and consequently has no EPR signal. Near ore bodies, however, quartz often contains numerous atoms out of place due to various substitutional and interstitial impurities (including ore constituents). This results in considerable lattice defects and yields paramagnetism.

EPR can be measured in an electron spin resonance spectrometer at specific levels of a strong, applied magnetic field, while a microwave radiation of constant frequency and intensity is simultaneously applied. The resonance for specific intensities of a swept magnetic field is measured as the first derivative of the absorption of the applied microwave energy. The relation between the frequency (υ), and the value of the magnetic field vector (B), can be expressed in a simplified form as:

$$h\upsilon = g\beta B_{res}$$

Where h is Planck's constant (6.63×10^{-34} J.s.)

υ the microwave frequency (Hz, expressed as s^{-1})

g the spectroscopic splitting factor

β the Bohr magneton (9.27×10^{-24} $J.T^{-1}$)

B_{res} the magnetic flux density at resonance (expressed in Tesla, 1 mT = 10 Gauss)

Detailed descriptions of the theory of EPR can be found in Pilbrow (1990). Its application to geology is given in Calas (1988) and the EPR spectroscopy of quartz discussed in Weil (1984). The technique has the advantage of easy operation, low cost

and simple data interpretation. It is also fast, with spectrum measurements generated in a few minutes.

3.4.3 Instrumentation

An EPR spectrometer consists of four major conponents:

1. A microwave bridge and sample resonator (sample cavity);
2. An electromagnet and power supply with field control and field sweep;
3. Some form of data acquisition which is normally a detector and signal pre-amplifier followed by phase-sensitive detection (PSD) at the magnetic field modulation frequency, a computer and/or recorder display and elementary noise filtering;
4. Computer acquisition and data processing.

Figure 3-11 gives a schematic layout of a typical EPR spectrometer. It has a microwave source, usually a klystron, connected to a reference arm type homodyne bridge. Power

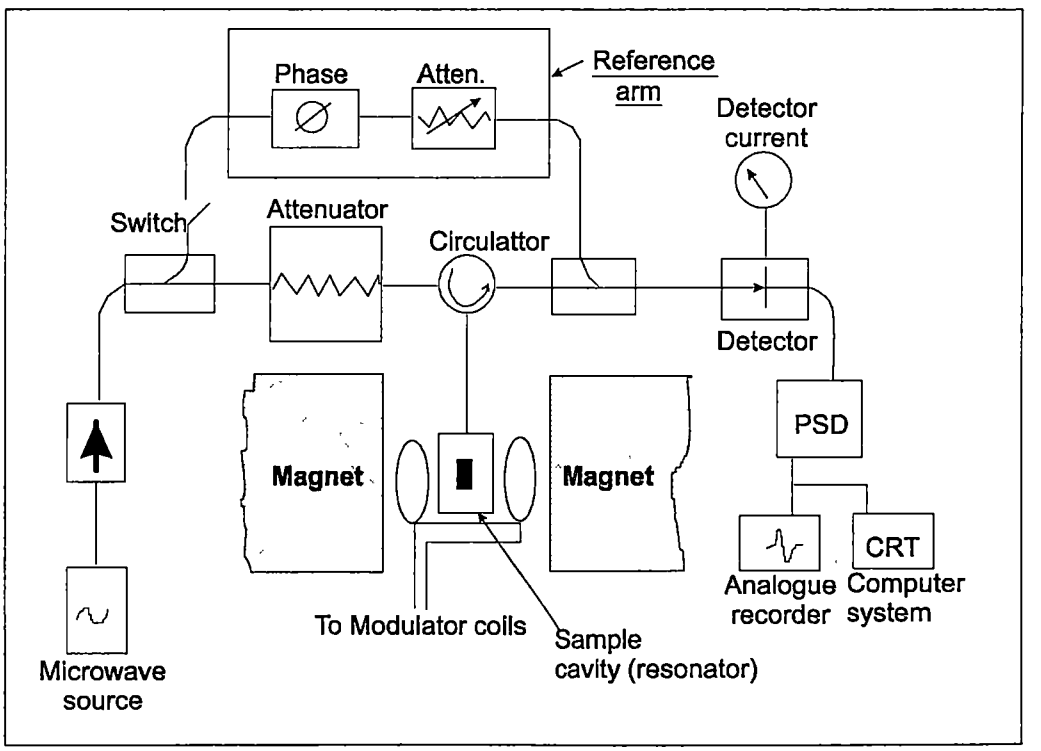

Figure 3-11. Block diagram of a representative modern homodyne EPR spectrometer (after Pilbrow, 1990)

travels to the sample resonator via a precision attenuator and a microwave circulator.

This study used an analogue JEOL JES FE3X EPR spectrometer at the Central Science Laboratory of the University of Tasmania and a Varian E12 EPR spectrometer at the Physics Department of Monash University. Both spectrometers were used under the X-band and with magnetic sweeps centred as a value of 326.5 mT. The radiation passes through the wave guide and into a resonance cavity where the sample is loaded. The cavity system is located in the centre of a strong homogeneous magnetic field between two larger electromagnets. The cavity includes components that hold the sample and that direct and control the microwave beam to and from the sample. The intensity of the outcoming microwave radiation from the resonance cavity is measured by means of a circulator and a detector. The EPR signal is determined as the first derivative of the absorption of microwave energy returning from the sample against the intensity of the magnetic field.

3.4.4 Sample preparation and instrument setting

The preparation of the EPR regolith samples was identical to that of the samples analyzed by PIXE/PIGE and is described in section 3.1. During the course of this

Table 3-7. Instrument settings for EPR analyses at the University of Tasmania

Instrument Items	Parameters
Field Center (Field Set)	326.5
Width (Scan Range)	±5 mT, ±100 mT and ±250 mT
Microwave Power	100 mW
Temperature	Room Temperature
Modulation Width (Modulation amplitude)	2 x 0.1 mT
Modulation Frequency	100 kHz
Amplitude (Receiver gain)	2.5 x100
Response (Time constant)	0.3 seconds
Microwave Frequency	9.17 GHz
Sweep Time (Scan time)	4 minutes/scan
Sample Mass	100 mg

study, two discrete sets of analyses were completed. The first set was to determine the suitability of EPR as an exploration tool in weathered terrains and was conducted at the University of Tasmania. The second set aimed to optimize the instrumental setting for future exploring and was carried out at the Physics Department of Monash University due to more advanced instrumentation available. Table 3-7 gives the first set of instrument settings used at the University of Tasmania. The instrument settings of the second set of experiments conducted at Monash University is nearly identical to those listed in Table 3-7.

3.4.5 General description of EPR spectra

An EPR spectrum of a single radical species is defined by six parameters, which are:

1. Integrated intensity of the components of the EPR signal (e.g. measured as absorption peak height) which is proportional to the total number of unpaired spins in the centres;
2. g-value of the resonance describing the position of an absorption line which characterizes the free electrons;
3. The line shape or width which is the reciprocal of the time that the resonant electron spins are in the higher energy state;
4. Stability or decay of the paramagnetic centre (e.g. Ge centres in silicates after irradiation);
5. Electron splitting when more than one electron is present;
6. The hyperfine structure normally related to nuclear magnetic moments in organic radicals or observed after irradiation (e.g. Al in SiO_2 lattice).

This project aims to determine a possible relationship between EPR response and elements associated with Au. Decay of paramagnetic centres (after artificial interaction), electron splitting and hyperfine structure can only be determined by careful observation, usually on oriented specimens in a series of observations at controlled timing at cryogenic temperature. Such special investigations are beyond the scope of this study.

The regolith samples and quartz concentrates used in this study consist of finely ground powder derived from splits of large samples. Consequently no large crystals of quartz or other silicate minerals could be obtained. At room temperature, there are three main parameters which could define a powder EPR spectrum.

1. The intensity of a specific signal component often measured as the peak height: the distance between the turning points of the first derivative signal (Figures 3-12, 3-13).
2. The effective g value, calculated from a position half way between the turning points (Figure 3-14).
3. The shape or width, and distance on the field sweep axis between the two turning points of the signal measured in mT (Figure 3-12).

The signals observed in this study are similar to those obtained on quartz powders from the Beaconsfield auriferous quartz reef, Tasmania (cf. Figures 3-14 and 3-15) (Russell, 1995).

The first derivatives of natural quartz EPR spectra are often complex. A range of centres have been identified from the quartz EPR spectra as the results of lattice defects (Weil, 1984), which are:

- electron donors replacing Si (e.g. Al or rarely Ga);
- electron acceptors (e.g. Ge, Ti and Fe);
- compensating ions (e.g. H^+, Li^+, Na^+);
- defects caused by irradiation (e.g. broken bonds).

A more detailed discussion of these electron-hole and defect centres (Petrov et al., 1989; Ikaya, 1995) is beyond this study. Only the relevant centres and type of impurities are given.

3.4.5.1 The major signal located between g = 2.0127 and g = 1.9969

A pronounced room temperature EPR signal at g = 2 was described by (McMorris, 1970) from dozens of extracts of igneous, sedimentary and metamorphic quartz and one alpha active obsidian. McMorris (1970) attributed the EPR signal to α-radiation without substantiation. A similar centre can also be observed in some silica glasses (Schnadt and Räuber, 1971), flint (Garrison et al., 1981), volcanic rocks (Shimakowa et al., 1984) and vein quartz (van Moort, 1987; van Moort and Russell, 1987; van Moort and Barth, 1992). The signal often shows hyperfine splitting due to the presence of aluminum after irradiation and immediate EPR analysis at <100 K. This indicates that there is a relationship between the signal and the presence of Al in the sample.

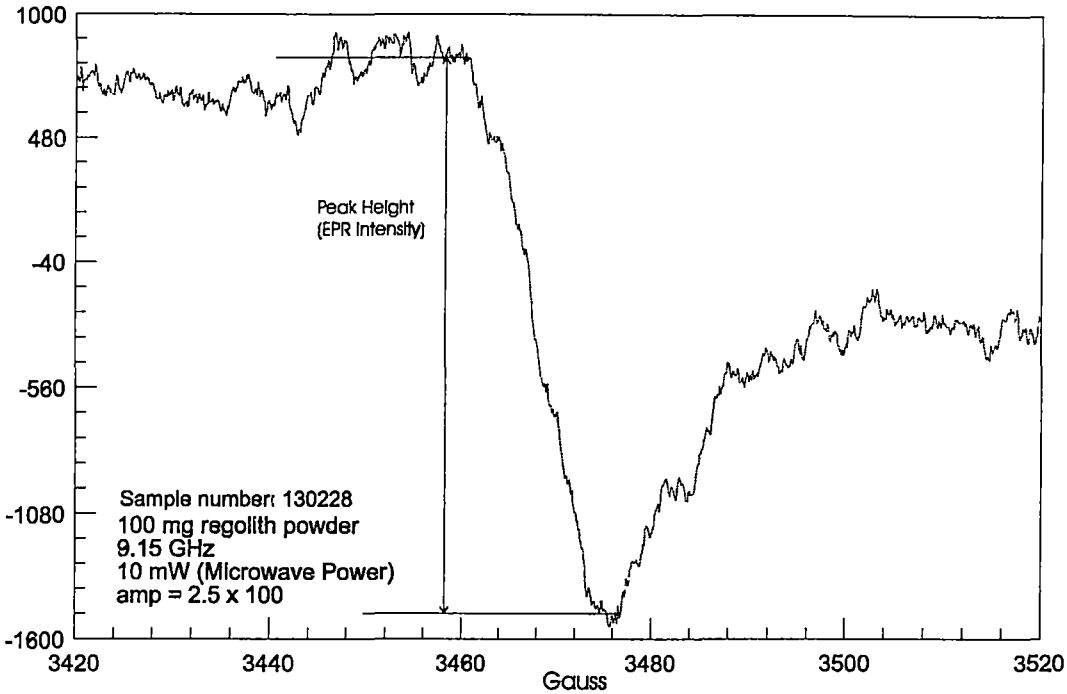

Figure 3-12. EPR spectrum measured at magnetic flux density sweeps 347.6±50G showing the peak height (EPR intensity) and width (Sample from Jim's Find)

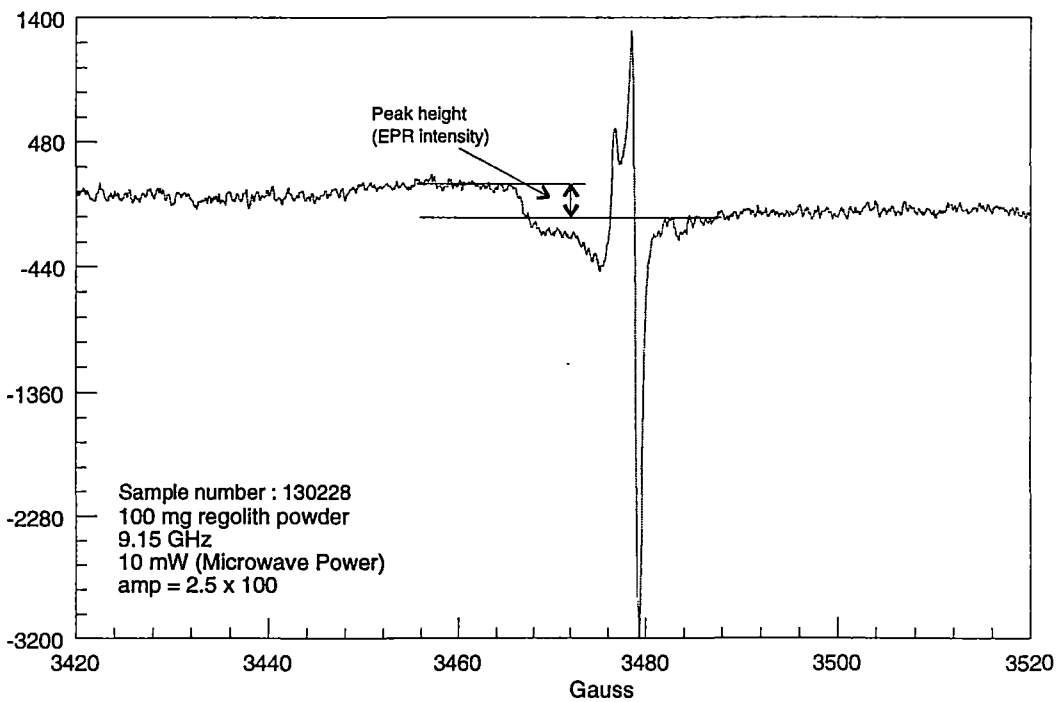

Figure 3-13. EPR spectrum measured at magnetic flux density sweeps 347.6±1000G showing the peak height (EPR intensity) and width (Sample from Jim's Find)

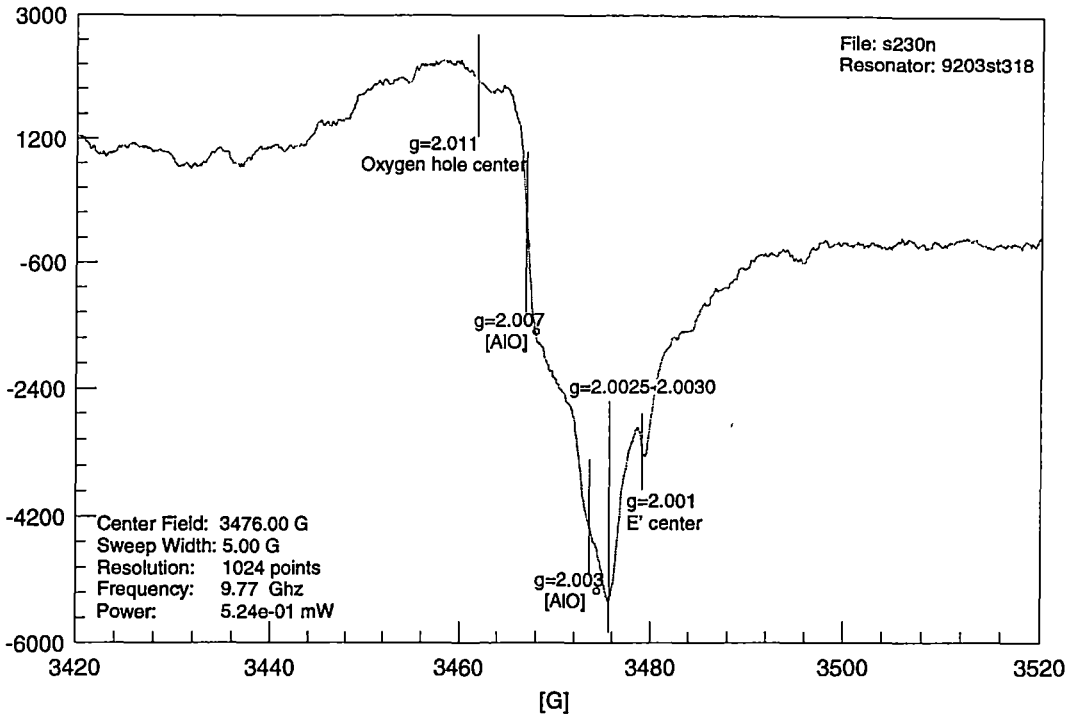

Figure 3-14. EPR spectra of Jim's find sample (130230) measured at magnetic flux density sweeps 347.6±50 G showing different g values

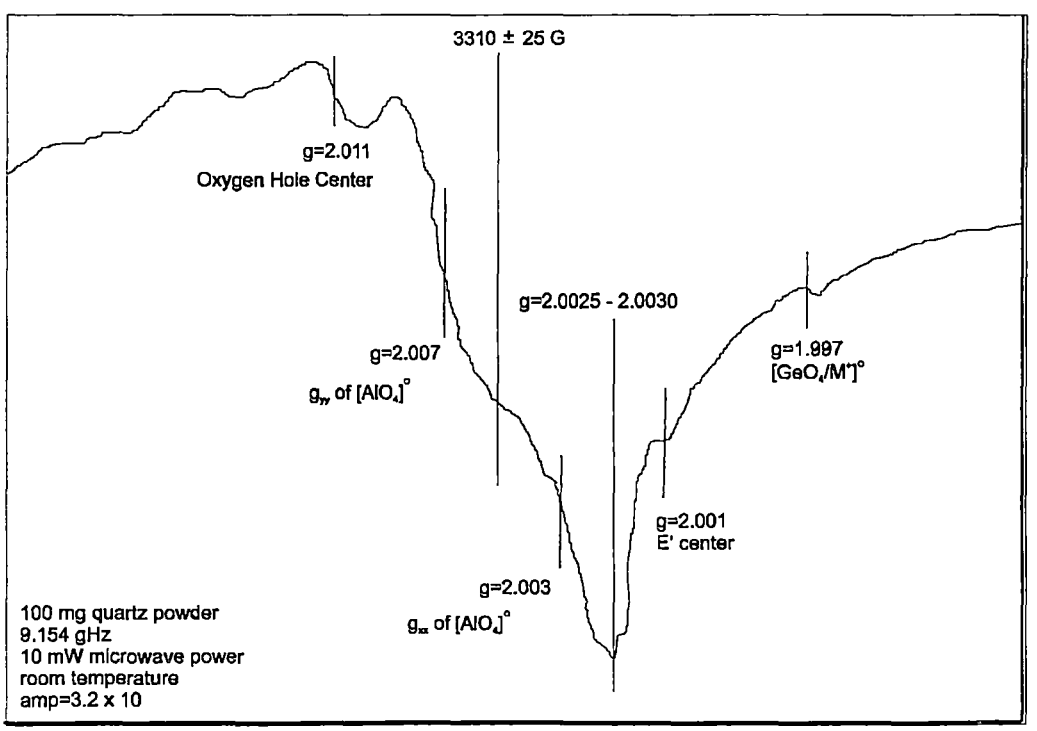

Figure 3-15. EPR spectra of quartz (from Russell, 1995)

This centre is called the Al-O centre by Matyash et al. (1982). The signal consists of two adjacent first derivatives, one with a crossover at g=2.007 and the other with a crossover at g=2.003 (Figure 3-14). Russian scientists have used this centre widely for dating and mineralogy studies. These crossovers are comparable to $[AlO_4]^\circ$ (Griffiths et al., 1984; Weil, 1984).

The g = 2 signal is prominent in the room temperature EPR spectra of the regolith powders in each of the three study areas. It is important in distinguishing Au mineralization from unmineralized powders/rocks.

3.4.5.2 Oxygen hole centre

The oxygen hole centre is caused by the presence of non-bridging oxygen (Griscom, 1980). A detailed discussion on the non-bridging oxygen centre is provided by Maschmeyer and Lehmann (1983). Van Moort (1989) also noted the oxygen hole centre in quartz due to natural or artificial radiation at g = 2.011. Some samples have a clear oxygen hole centre (Figure 3-15) and this defect centre was not used in this study.

3.4.5.3 E' centre

The E' centre is a prominent defect structure in the SiO_2 lattice and can be identified at g = 2.001 (Yip and Fowler,1975). If a bridging oxygen is removed form the lattice, an electron can be trapped in the vacancy.

3.4.5.4 Manganese centre

Mn^{2+} ions have a characteristic hyperfine sextet, which if well developed, is located on a very broad EPR signal at g = 2 (Robins et al., 1981; Ikeya et al., 1986; van Moort and Russell, 1987). The centres are common in the spectra of regolith samples from Rand Pit and Mt Percy of Western Australia examined in this study, but not in Jim's Find of Northern Territory. This suggests that the Mn^{2+} is associated with mafic rocks which host the Au mineralization in the Western Australian research areas.

3.4.6 EPR intensity

The EPR intensities were measured on the first derivative EPR spectra on analogue charts recorded at standard instrument settings (Table 3-5). The magnetic flux density sweeps, 326.5 ± 5 mT, 326.5 ± 100 mT and 326.5 ± 250 mT were applied (Figures 3-12 and 3-13). The first measurement shows details of the central portion of the second and third measurement. The peak height was measured in centimeters on the standard analogue charts. Although relative, these values are reproducible. A high microwave power was chosen to enhance the strong central signal and to suppress the E' signal through saturation. More detailed accounts of EPR powder spectra in the weathered regolith profiles are given in Chapters 6, 9 and 12.

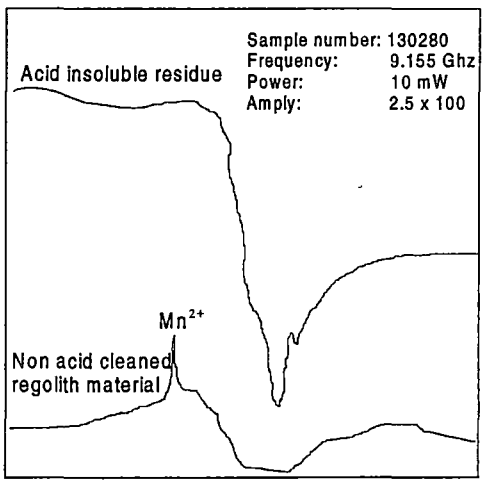

Figure 3-16 Comparison of EPR spectra between an acid cleaned sample and a raw powdered sample. Note that the acid insoluble residue spectrum is stronger and has more detail than the spectrum of the uncleaned regolith material.

3.4.7 EPR variation of raw material

EPR spectra of non-acid treatment samples were also determined. However, these spectra differ from clean samples (Figure 3-16) due to unremoved impurities in raw samples. A strong Mn^{2+} resonance line is observed in the EPR spectrum of non-acid treated samples, but no large central absorption signal is identified in these samples and a positive correlation with Au contents is lacking. The change of line shape between raw and acid treated samples is the result of a magnetic scatter field arising from magnetic

order among the Mn^{2+} ions smearing out the Al^{3+} narrow line spectrum.

3.5 SUMMARY

A new sample medium, acid insoluble residue, for geochemical and EPR analyses for Au exploration is introduced. The residues from a hot aqua regia + HNO_3 + H_2SO_4 digest of powdered samples consist mainly of quartz, accompanied by lesser feldspar, mica, kaolinite and amphibole. Acid treatment reduced the effects of weathering, but retained the original rock forming and alteration features of the samples. It is therefore possible to use treated samples to distinguish between mineralized and barren zones in weathered terrains. The concentration of elements was analyzed by PIXE/PIGE to determine the element distribution patterns. EPR was also applied together with PIXE/PIGE to offer an alternative simple and fast way to evaluate prospective areas.

PIXE and PIGE are used to analyze geochemical samples for a wide range of major and trace elements on the acid insoluble residues, often down to ppm levels. The analyses are simultaneous, multi-element and nondestructive. This exercise has demonstrated that these ion beam techniques have excellent precision (0.4 - 3%) and accuracy (± 0.3 – 6%) for F, Na, Al, Si, K, Ca and Fe. The precision and accuracy of Ti, Mn, Rb and Sr are 3 - 5% and ± 20% respectively. Elements with poor precision and accuracy were either present in concentrations at, or below the minimum detection limit (i.e. Ni, Cu), and generated spurious results (i.e. Zn, Pb). These latter four elements were not significant in the acid insoluble residue used in this study.

It is clear that the PIXE/PIGE techniques are useful tools in aiding the understanding of weathering and element dispersion related to Au mineralization. From a geochemical perspective, the PIXE/PIGE is the direct proton analogue of the electron microprobe and for anyone familiar with energy-dispersion electron microprobe analysis (EPMA) or energy dispersion X-ray spectrometer (EDXRF), the transition to PIXE/PIGE analysis is straightforward.

Feasibility studies on the use of EPR as a mineralization discrimination criterion in weathering profiles are pursued in this study. The principles and procedures of EPR, applied to characterizing the mineralization, belong to a new field of exploration geochemistry. Unpaired electrons produced in quartz and other ore components have

accumulated during ore formation. EPR detects these perturbations and the additive intensity method reveals subtle mineralization features. A significant EPR signal can be observed in acid leach residues for auriferous samples in 326.5 ± 5 mT magnetic flux density sweeps. The characters of magnetic sweeps 326.5 ± 100 mT and 326.5 ± 250 mT are generally similar, and often correspond with the 326.5 ± 5 mT sweeps. In contrast, samples unrelated to Au do not contain unpaired electrons and no alignment of electrons occurs under the magnetic field. The EPR method has the added advantage of seldom requiring destructive chemical preparation.

In conclusion, the acid treatment of samples is essential. The application of EPR spectra to non-acid treated samples does not distinguish the presence of Au mineralization.

Chapter 4

MYSTERY ZONE, MT PERCY, W.A.

4.1 INTRODUCTION

The Mount Percy gold mine is about 600 km east of Perth and 2 km north of the Kalgoorlie township, Western Australia, (latitude 30° 44'S, longitude 12° 28'E). The Mystery Zone consists of the Union Club, Sir John and Lucknow deposits.

The only major publication on the Mt. Percy area was by Feldtmann (1916) who conducted a petrological study and gave detailed descriptions of the individual mines. Petrological studies and classification of the major rock types by McLaren and Thompson (1913) formed a basis for subsequent work, but concentrated on the Golden Mile. Gustafson and Miller (1937) produced a revised map for the north end of Mt. Percy, based on the re-interpretation of major geological structures. The stratigraphy and structure of the Kalgoorlie region was revised by Woodall (1965), based on an improved petrological classification of the rock sequence. Butt (1991) studied the dispersion of gold and over 40 other elements in the lateritic regolith of Mt. Percy and discussed the distribution patterns of these elements extensively in terms of landform evolution and their significance to exploration.

The Mount Percy gold mine is essentially a soft rock mining operation with economic exploitation made possible by the oxidation of the mineralized zones to depths of 50–70 m below surface. In the Mystery Zone, ore grade mineralization occurs in porphyritic rocks and is locally well developed adjacent to mineralized porphyries in the fuchsite-carbonate altered rock.

Early mining at Mt. Percy took place mainly from 1893 to 1910 and during this time some 70,000 tonnes of ore at 9.0 g/t Au was extracted from narrow, relatively low-grade ore bodies, using shallow shafts, excluding the Hannan' s North mine production (Bettanay and Churchward, 1974). Most of the surface of the area was dry blown.

Modern exploration in the area started in 1977 by Occidental Minerals (later Australian Occidental Pty Ltd). Windsor Resources NL acquired the Minerals Division

of Australian Occidental Pty Ltd in December 1984. The decision to proceed with the mining operation was made in January 1985 and the first gold bar was poured in October 1985. Currently the operation is carried out by Gold Mines of Kalgoorlie Ltd (50%) and Homestake Mining Corporation (50%).

4.2 ENVIRONMENTAL FEATURES

4.2.1 Climate

The Kalgoorlie region may be described as a plateau of erosion with no river systems and the present weathering is typical of arid regions. The physiography of the region is undoubtedly largely controlled by climate. The region is too far inland to be affected by moist sea winds. The climate of the region is semi-arid with hot summers and cool to mild winters. Average diurnal temperature ranges measured at Kalgoorlie are greatest in January to February (34–18° C) and least in July (16–5° C). Rainfall averages 250 mm per annum with the wettest period between May and August. Evaporation greatly exceeds precipitation for most of the year, and in the northeastern part of the Boorabbin 1:250 000 sheet, evaporation averages 2200 mm per annum (Hunter, 1993). Erosion in an area with so little moisture must be a very slow process.

4.2.2 Topography and vegetation

Mt. Percy is situated in a relatively high part of the landscape, in a region with only a few tens of metres of relief. Structural variation in the rocks is minor, whilst slow acting agencies of erosion result in little topographic diversity. The hills generally consist of igneous intrusions, and silicified zones and reefs, due to their greater resistance to erosion, have prominent relief, and often traverse the country for many kilometers. Interbedded sheared conglomerates also form prominent hills, 30 m or more in height, and may at times be seen rising from the edge of a "clay pan". The elevation of the whole area is probably due to the armouring effect of the lateritic duricrust, here developed most strongly over the Hannan' s Lake Serpentinite discussed below (Butt, 1991).

The success of floral species is strongly controlled by soil type (Hunter, 1993). Sand heath and tamma scrub form on leached sands, shallow lateritic soils and degraded granitic outcrops (Hunter, 1993). "Rock Pavement Vegetation" consisting of lichen and moss occurs on outcrops of granitoid rock with aquatic plants in pools, and shrubs in crevices and the occasional soil patches. On leached, granitic eluvial and

alluvial soils, mallee and sclerophyll flora form open to closed eucalypt shrub or woodland with a variable, low shrub ground layer. Communities of salt-tolerant halophytes (e.g. saltbush, and samphire) occupy areas bordering playas.

4.2.3 Hydrology

The area falls within the Rebecca and Roe Palaeodrainages which are infilled with sediments of Eocene age (Smyth and Button, 1989; Kern and Commander, 1993). The basal Wollubar Sandstone is the main aquifer in the Roe Palaeodrainage, and there is a similar sandstone in the Rebecca Palaeodrainage (Commander et al., 1994). The basal sandstone is overlain and hydraulically confined by the Perkolilli Shale in the Roe Palaeodrainage, and by a similar sequence in the Rebecca Palaeodrainage. These Tertiary formations are concealed by a variety of Quaternary sediments and by discontinuous belts of terminal playas (salt lakes) occupying the present-day broad valleys.

The groundwater in the palaeochannels is saline or hypersaline. The groundwater is predominantly sodium chloride type, but saturation is reached only locally and seasonally at the surface of the salt lakes (Commander et al., 1992). A marked increase in the groundwater salinity of the palaeochannels, which takes place beneath the salt lakes, indicates that the salt lakes concentrate the salts in the groundwater through evaporation. There is a slow groundwater outflow through the palaeochannels which, in the Roe Palaeodrainage, represents around 0.003% of the rainfall on the catchment area (Commander et al., 1994).

4.2.4 Weathering history and regolith landform

Much of the Yilgarn Craton has been exposed to subaerial conditions since the mid-Proterozoic, although Permian glaciation removed much of the earlier topography and surficial material. Climatic conditions (summarized in Table 4-1) influenced development of the regolith and the behaviour of gold within it. Two episodes were of particular importance:

- Warm, humid conditions in the Cretaceous to mid-Miocene gave rise to lateritic profiles, commonly more than 40 m thick; and
- A drier climate since the Miocene, coupled with minor uplift of continental margins coincided with a lowering of the water table and slower erosion and

Table 4-1. Periods of exposure to sub-arial weathering in Western Australia (from Butt, 1988)

Period	Age (my)	Climate
Late Proterozoic		Glaciation
Early Permian	280-270	Glaciation
Mesozoic	230-65	Temperate to warm; humid
Palaeocene to mid-Miocene	65-15	Sub-tropical to tropical;humid: probably seasonal (savanna)
Mid-Miocene to Pliocene	15-1.8	Sub-tropical; aridity increasing: cooler after 2.5 my
Quaternary	1.8-0	Temperate to warm; semi-arid to arid

(25 000–13 000 yr peak aridity, glacial maximum)

chemical reactions. Subsequent erosion has caused partial truncation of the weathering profile.

Weathering has affected all rocks to a minimum depth of 50 m, destroying many primary features. The complete weathering profile is shown in Figure 4-1. Most rocks are weathered to clays and iron oxides with detrital quartz and carbonate constituents (Johnson et al., 1990). For example, the porphyritic rocks are typically bleached to a white or pale yellow colour in the oxide zone, and have a friable texture. As a consequence, an almost complete lateritic regolith, 50–70 m thick, is present over most of the area. The duricrust is strongly developed overlying talc chlorite carbonate altered rocks and the Golden Mile Dolerite. These form the highest points at the south end of the Mystery Pit and Mt. Percy, upon which the Mt. Percy water-tank is situated. The regolith is the host to secondary gold mineralization within both lateritic duricrust and saprolite (Butt, 1991).

Little outcrop occurs in the study area, which is generally covered by laterite, up to 10 m thick. The weathering zone ranges from 50 m to about 75 m depth. The Mystery Zone open pit shows the deeply weathered terrainat Mt. Percy and whole regolith profile (Figure 4-1).

4.3 REGIONAL GEOLOGY

The Mt. Percy mining region lies within the Norseman–Wiluna belt (Gee et al., 1981) of the Eastern Goldfields Province in the Archaean Yilgarn Craton (Figure 4-2). The geology of the Yilgarn Craton is described by Gee (1975) and Gee et al. (1981), and descriptions of the Eastern Goldfields geology are given by Archibald et al. (1981), Barley and Groves (1988) and Swager et al. (1990).

4.3.1. Structure

The distribution of supracrustal sequences in the Norseman-Wiluna Belt is controlled by north to NNW trending fault systems and lineaments (Figure 4-2) (Travis et al., 1971). The internal structure of the belt is generally synformal, although homoclinal or antiformal structures dominate some structural domains.

Regional deformation involved oblique compression with an early phase of subhorizontal deformation involving recumbent folds and thrusts (Platt et al., 1978; Archibald, 1987). This was followed by upright folding and faulting with an oblique- or strike-slip component (Eisenlohr, 1987; Mueller and Harris, 1987). In the area between Kalgoorlie and Norseman, movement was from the SSE with concave-upwards, low-angle reverse faults linking oblique-and strike-slip faults (Clark et al., 1986). The three-dimensional fault pattern is responsible for present-day outcrop patterns and the regional distribution of granitoids and greenstones (Barley and Groves, 1988). The resulting NNE trending linearity, expressed by granitoid-greenstone contacts, chains of granitoid plutons, major fault systems and tectonic or magnetic lineaments is a distinctive feature of the Norseman–Wiluna Belt.

The structure of the Kalgoorlie area is characterized by steeply dipping isoclinal folds and associated strike faulting (Travis et al., 1971). The dominant structure at the north end is the Kalgoorlie Anticline; a NNW trending, south plunging, isoclinal fold (Figure 4-3), truncated on its western limb by the strike parallel Golden Mile fault with west block down displacement (Figure 4-4). Movement along the fault has brought the Hannan Lake Serpentinite in contact with the younger Black Flag Beds to the west. Lithological boundaries trend parallel to the fold axis of the anticline, about north 25° west. The fold is bounded on the east and west by pronounced northwest trending lineaments which represent a set of major converging faults. Oblique faults throughout the north end are north-trending, west dipping with west block north displacements ranging from 150 m to 1500 m.

4.3.2 Stratigraphy

The Norseman-Wiluna belt is characterized by widespread komatiitic volcanism and the absence of banded iron formations, which distinguish it from adjacent greenstone

Figure 4-1. Complete regolith profile is illustrated by the Mystery Zone Open Pit, Mt. Percy

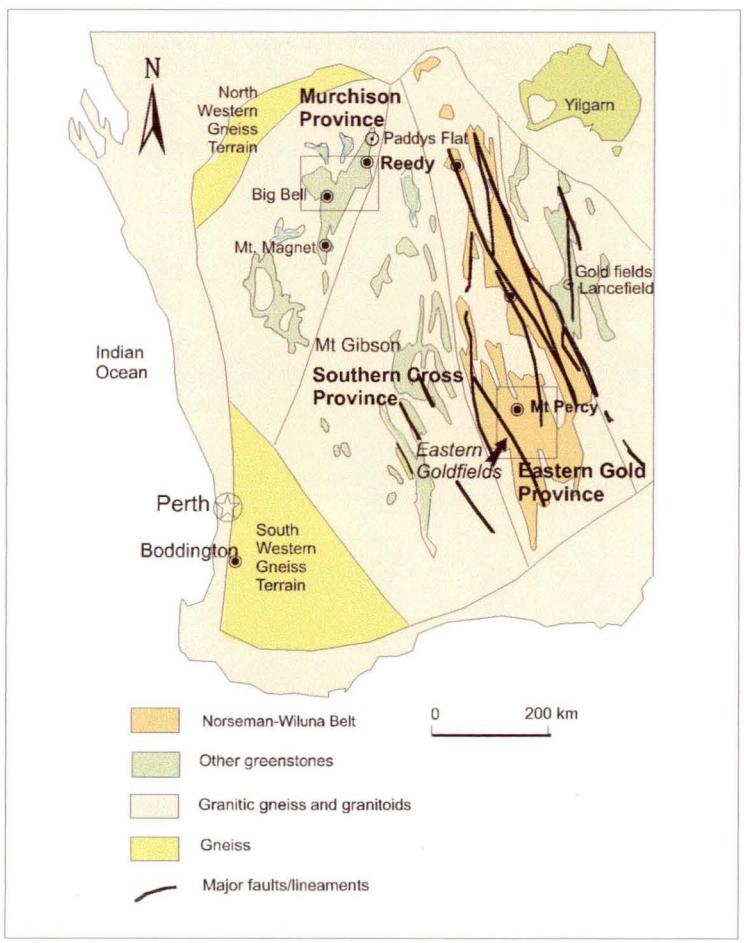

Figure 4-2. Geological map of the Yilgarn Craton and Eastern Goldfields province

belts of the northeast Eastern Goldfields Province and the Southern Cross Province. Although the boundaries of the Norseman-Wiluna Belt are imprecisely defined, the belt is commonly interpreted to be a fault-bounded, graben-like structure within an extensive and more stable, shallow basin (Gee et al., 1981). Supracrustal rocks in this 'graben' and adjoining area have been referred to as rift-phase greenstone and platform-phase greenstone respectively.

The stratigraphic succession at Kalgoorlie consists of metamorphosed ultramafic to mafic volcanic units, mafic sills and a thick overlying sequence of shales, graywackes, sandstones and minor mafic volcanic rocks (Woodall, 1965). These geological aspects are summarized in Table 4-2.

The Hannans Lake Serpentinite is the oldest rock unit of the Kalgoorlie succession and forms the core of the Kalgoorlie Anticline. It is a massive, fine-grained serpentinite, typically altered to dark green talc-carbonate and chlorite-carbonate rocks, and to pale green fuchsite-carbonate rock adjacent to intrusive porphyries.

Overlying the Hannans Lake Serpentinite, and locally gradational with it, is the Devon Consols Basalt, comprising both mafic and ultramafic rock types. It exhibits well-developed variolitic textures and pillow structures and is variably chloritized and albitized. Carbonate and sericitic alteration predominate in bleached zones where quartz veining and pyritization are common.

At the north end of the Sir John area (Figure 4-4) a doleritic intrusive of unknown extent occurs near the lower contact of the Devon Consols Basalt.

The Kapai Slate is a thin but consistent marker horizon, that consists of black shales, slates and cherts. It defines the basal contact of the Williamstown Dolerite and contains varying amounts of pyrite with minor chalcopyrite, pyrrhotite and sphalerite. The Williamstown Dolerite is a differentiated sill which overlies the Kapai Slate to which it has locally transgressive contacts. Inliers of Kapai Slate and Paringa Basalt rarely occur near the lower and upper dolerite contacts, respectively. Within the Williamson Dolerite differentiation trends are from an ultramafic hornblendite at the base to an upper mafic metaquartz dolerite.

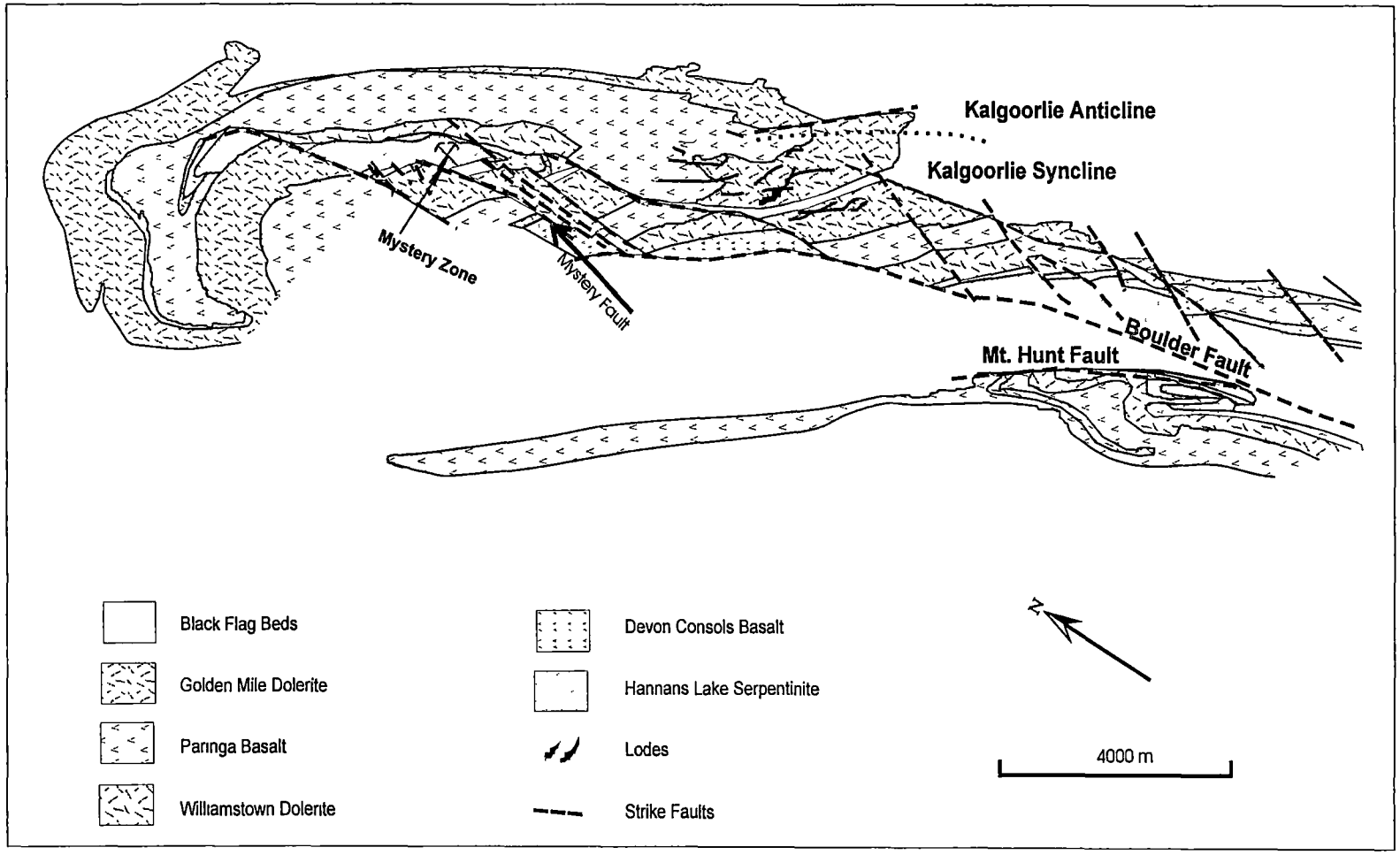

Figure 4-3. Geology showing the main structure at the north end of the Kalgoorlie goldfield (after Travis et. al., 1971)

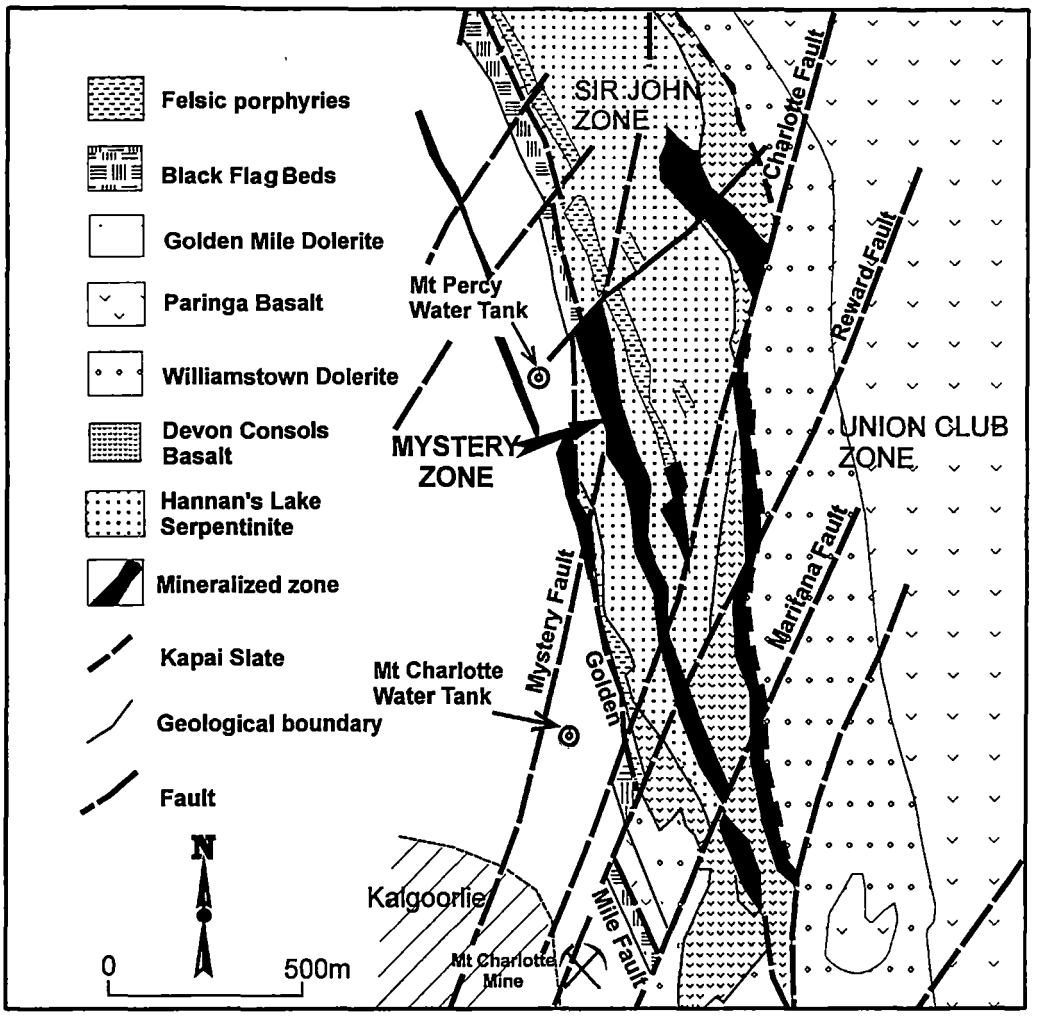

Figure 4-4. Location map of Mystery Zone showing the principal faults (after Sauter et al., 1988)

The stratigraphically younger Paringa Basalt and Golden Mile Dolerite occur to the west of mineralization at Mystery, whilst the Golden Mile Dolerite and a thin slice of Black Flag Beds occur to the west (Sund et al., 1984).

4.3.3. Gold mineralization within the Kalgoorlie area

Two main types of mineralization are defined in the area:

- The first type of mineralization occurs at the Mystery Zone, and comprises variably mineralized and altered quartz-albite porphyries emplaced within talc-carbonate altered Hannans Lake Serpentinite. Intense fuchsite, pyrite and carbonate alteration of the serpentinite occur adjacent to the porphyry bodies. Gold mineralization is

carbonate altered rock. Several sets of vein orientations are present, some of which have sulphide alteration haloes and bleaching due to breakdown of adjacent mafic minerals.

- The second style of mineralization is defined approximately 300 m to the east of the Mystery Zone and occurs within altered Devon Consols Basalt, Kapai Slate and to a lesser extent the Williamstown Dolerite (i.e. the Sir John, Union Club and Lucknow deposits). The ore zone has a total strike length of approximately 1.8 km but is segmented into three ore bodies due to later faulting. Gold mineralization is associated with pyrite and quartz veins within both the Devon Consols Basalt and the highly pyritic, black shale and cherts of the Kapai Slate. The ore bodies are best developed adjacent to the cross-cutting faults and within drag fold structures adjacent to the Kapai Slate (Johnson et al., 1990; Sund et al., 1984).

This study focuses on the first type of mineralization occurring in the Mystery Zone

Table 4-2. Stratigraphic succession at Kalgoorlie area (after Clout et al., 1988; Travis et al., 1971; Woodall, 1965)

Rock Unit	Thickness	Dominant lithology
Black Flag Beds	3000?	Felsic to intermediate pyroclastics, flows and intrusives with associated sulphidic black shale and graywacke.
Golden Mile Dolerite	up to 800	Differentiated quartz-gabbro sill; tholeiitic composition.
Paringa Basalt	300-900	Tholeiitic to magnesian basalts, pillowed to massive, with minor interflow sediments.
Williamstown Dolerite	150-300	Sill of quartz-gabbro in upper half and ultramafic hornblendite in lower half.
Kapai Slate	1.5-3	Graphitic shale.
Devon Consols Basalt	60-150	Magnesian basalts in upper half to komatiitic basalts in lower half. Minor interflow sediments.
Hannans Lake Serpentinite	300-900	Massive serpentinized peridotites, picrite basalts and olivine basalts.

This study focuses on the first type of mineralization occurring in the Mystery Zone at Mt. Percy.

4.4. LOCAL GEOLOGY

The Mount Percy gold deposits are located at the north end of the Kalgoorlie field, on the eastern limb of the Kalgoorlie Anticline.

4.4.1. Structural setting

Intense fracturing and shear structures between the major strike and cross-cutting fault systems have created structural environments for the introduction of mineralizing fluids. Gold mineralization is best developed adjacent to north trending, west dipping faults that have apparent dextral displacements (Sund et al., 1984). The major faults, from south to north, are the Maritana, Reward, Charlotte, Mystery and an unnamed fault further north and northwest. Gold in the Mystery Zone ore body is largely controlled by the Mystery Fault and two splay faults at the northern end of the Mystery Zone (Figure 4-4).

All rock units including the porphyries are folded. The folds are interpreted as drag folds about flat-pitching east–west axes and these axes are favourable locations for gold mineralization (Sund et al., 1984).

4.4.2 Host rocks

The Mystery ore body consists of mineralized porphyry with adjacent fuchsite-carbonate alteration within the Hannans Lake Serpentinite. The porphyry has intruded along planes of weakness parallel to the regional strike. The zone is approximately 725 m long and up to 40 m wide. Although numerous and similar porphyry lenses are recognized within the Hannans Lake Serpentinite, and to a lesser extent the Devon Consols Basalt, not all appear to contain significant Au grades. The steeply dipping porphyritic intrusions have intense metasomatic alteration haloes with variable extent into the enclosing rocks (Figure 4-5).

4.4.2.1 Hannans Lake Serpentinite

The Hannans Lake Serpentinite is the oldest unit in the mine sequence and is a serpentinized dunite. Regional metamorphism has resulted in talc, chlorite and

carbonate assemblages. Adjacent to intrusive porphyries, bleached haloes occur, with a gradation from a dark grey-green talc-chlorite-carbonate altered rock to a light grey carbonate-quartz-mica rock altered with proximity to porphyry. Chlorite, forms up to 7% of the talc-chlorite-carbonate derivative, but is generally absent in bleached rocks. Adjacent to porphyry intrusions the serpentinite is commonly altered to a bright green fuchsite-carbonate-quartz rock (Sund et al., 1984).

4.4.2.2 Intrusive porphyries

A number of porphyries were intruded into the Hannans Lake Serpentinite and have a wide variation in the proportions of carbonate and sericite alteration. The porphyries are generally pale grey rocks of quartz latitic composition, consisting predominantly of varying proportions of oligoclase, orthoclase and quartz phenocrysts (Sund et al., 1984). Intense metasomatic alteration of the enclosing rocks is attributed to porphyry intrusion with fuchsite-carbonate alteration in adjacent rock. Carbonate alteration is extensive and feldspars are frequently altered to sericite. Rarely, where less altered, the porphyries are dark greyish brown to pink containing well preserved feldspar and amphibole phenocrysts (Johnston, 1990).

Quartz and quartz-carbonate veins, may contain tourmaline and occur throughout the Mystery Zone porphyry. These veins are generally less than 1 cm wide and are sometimes enveloped by sulphide alteration haloes that consist of a fine-grained grey dusting of pyrite in the porphyry wallrock.

4.4.2.3 Fuchsite-carbonate rock

The fuchsite-carbonate alteration zone is best developed in the south of the Mystery Zone where the porphyry is less well-developed, as a series of narrow slivers within the 40-m wide fuchsite alteration zone. Fuchsite-carbonate rocks are frequently mylonitized with fuchsite concentrated in veins and often associated with sulphides (predominantly pyrite) and some leucoxene. Carbonate (predominantly ankerite) constitutes in excess of 60% of the rock. Chlorite is generally associated with sulphides and some tourmaline occurs locally. Although quartz and quartz-carbonate veins are dominant in the fuchsite alteration zone, they are often irregular and discontinuous (Sund et al., 1984).

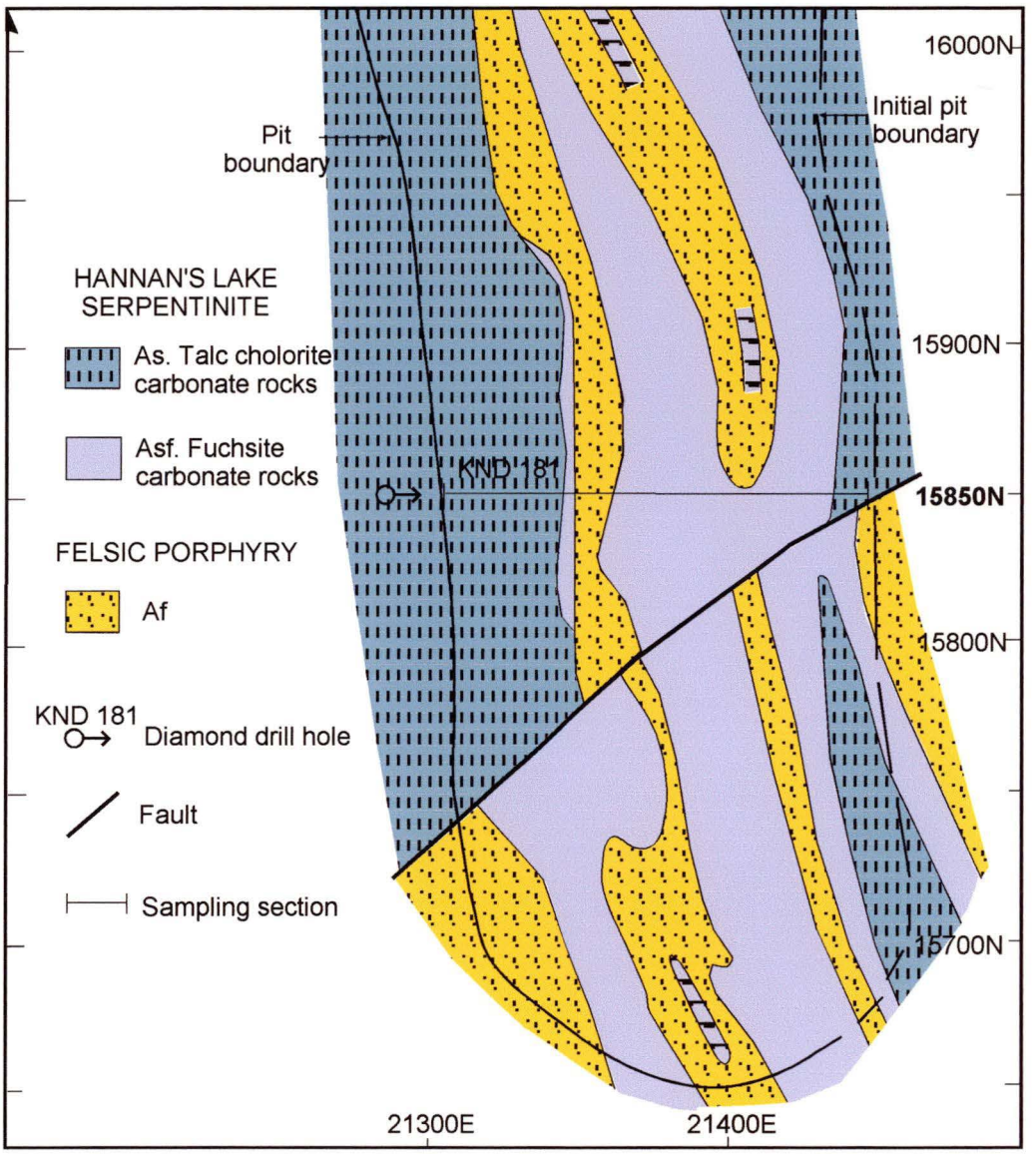

Figure 4-5. Geology of the southern end of the Mystery Zone, Mt. Percy (from Butt, 1991), projected to 400 m RL, indicating the section selected for study

4.4.3. Mineralization

In the Mystery Zone, primary gold mineralization occurs throughout the porphyries as a series of narrow steeply dipping ore lenses (Barley, 1984) (Figure 4-6). Mineralization in the fuchsite-carbonate rock is locally well developed adjacent to these mineralized porphyries (Butt, 1998). Sulphides, predominantly pyrite, are disseminated through the porphyry as fine euhedral grains and form up to 8% modal. Sulphide mineralization in the fuchsite alteration zone is variable and most intense (up to 10% of the rock) in the highly sheared or mylonitized zones (Haycraft et al., 1984). Sulphides are commonly concentrated in fuchsite-rich veins, as well as adjacent to discontinuous quartz-carbonate veins. Pyrite is the most common sulphide and is abundant in the porphyries (Sund et al., 1984).

As gold mineralization is associated with sulphides along fractured zones, particularly at the porphyry intrusive margins (Barton, 1987), Au is usually found in strongly carbonate altered and pyritic shear zones. At the northern end of the Mystery Zone, a cross-cutting fault offsets the mineralized porphyry and marks the limit of economic mineralization. The Au occurs as very fine free gold and is associated with pyrite. Minor chalcopyrite and sphalerite are associated with the pyrite, and silver and nickel tellurides have also been identified (Sund, 1984).

Weathering and oxidation have had a significant influence on the distribution of gold. In the Mystery Zone, gold occurs in the laterite profile, which is up to 10 m thick. Below the laterite zone, leaching has removed much of the gold over a thickness of 5–15 m, particularly within the porphyries.

4.5. SAMPLE COLLECTION

The objective of the sampling program was to obtain a representative suite of samples to define the vertical and lateral variation in geochemical elements and EPR signatures of their acid insoluble residue through the regolith overlying gold mineralization. Two sections across the mineralized zone, 15850N and 15900N were studied earlier by Butt (1991). The selection of samples was based on features evident from exploration and diamond drilling. Pit samples were taken by ripping shallow trenches across strike by bulldozer and hand-collecting and compositing the spoil over 1 m horizontal intervals.

In this study, 192 regolith samples from section 15850N were selected for PIXE/PIGE analysis, and 167 samples from the same section were chosen for EPR determination. The locations of these samples together with the geology and regolith profiles are given in Figure 4-7.

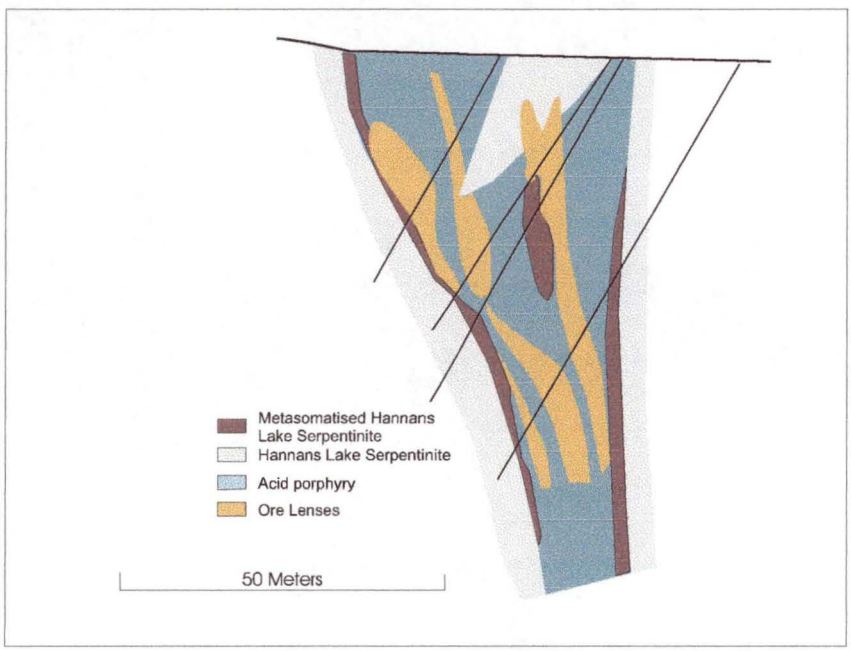

Figure 4-6. Narrow steeply dipping ore lenses at Mystery Zone, Mt. Percy, W.A.(from Barley, 1988)

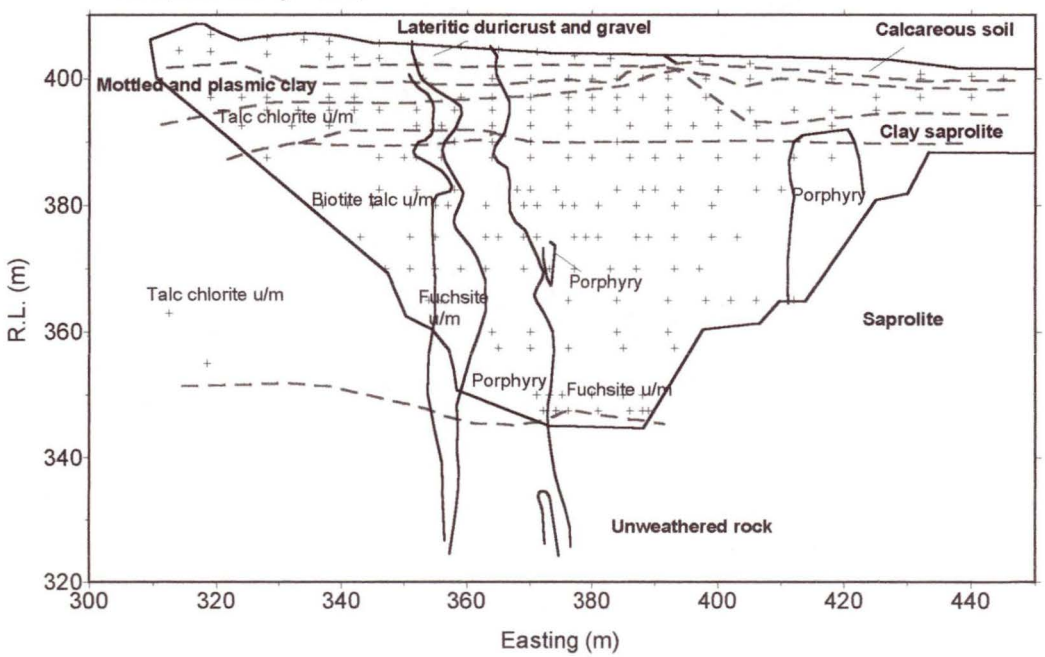

Figure 4-7. Logged and interpreted geology of Section 15850, Mystery Zone (after Butt, 1991), with the sample locations (+)

Chapter 5

GEOCHEMISTRY AT MYSTERY ZONE

The element distributions at Mystery Zone, Mt. Percy are shown as contour maps in this chapter. Plotting intervals were selected on the basis of the principal populations evident in the histograms and cumulative frequency graphs of the whole data set of acid insoluble residues shown on Figures 5-1 to 5-4. Contour maps were generated using Surfer v.6.04 with a simple linear kriging method. Elements having similar geochemical affinities are described together. Comparative statistical data for each group of elements in the main regolith horizons over the principal lithological units are given in Appendix 1.

5.1 REGOLITH GEOCHEMISTRY

Primary Au mineralization at Mt. Percy is overlain by an almost complete lateritic profile. A typical well preserved lateritic profile commonly consists of four principal superposed units, which from the base up, are parent rock, saprolite, mottled zone, and duricrust (Fressinet and Itard, 1997). The depth of weathering is from 50–70 m. The principal regolith units present on Section 15850N across the Mystery Zone are shown on Figure 4-6 and on the element distribution plots presented in the following section. The mineralogical changes within the profiles over the principal lithologies are shown on Figure 5-5. The regolith is the host to secondary gold mineralization within both the lateritic duricrust and the saprolite.

5.1.1 Saprolite

Despite the initial weathering and any subsequent modification, saprolite is characterized by the preservation of rock fabrics. In the upper part of this horizon, most of the primary minerals have been weathered to kaolinite and goethite; only quartz and resistant minerals (zircon, tourmaline, chromite, etc.) remain unaffected (Fressinet and Itard, 1997). At Mt. Percy, saprolite is overlain by upper horizons which consist of mottled zone, plasmic clay and lateritic duricrust. The saprolite is approximately 40–50 m in thickness.

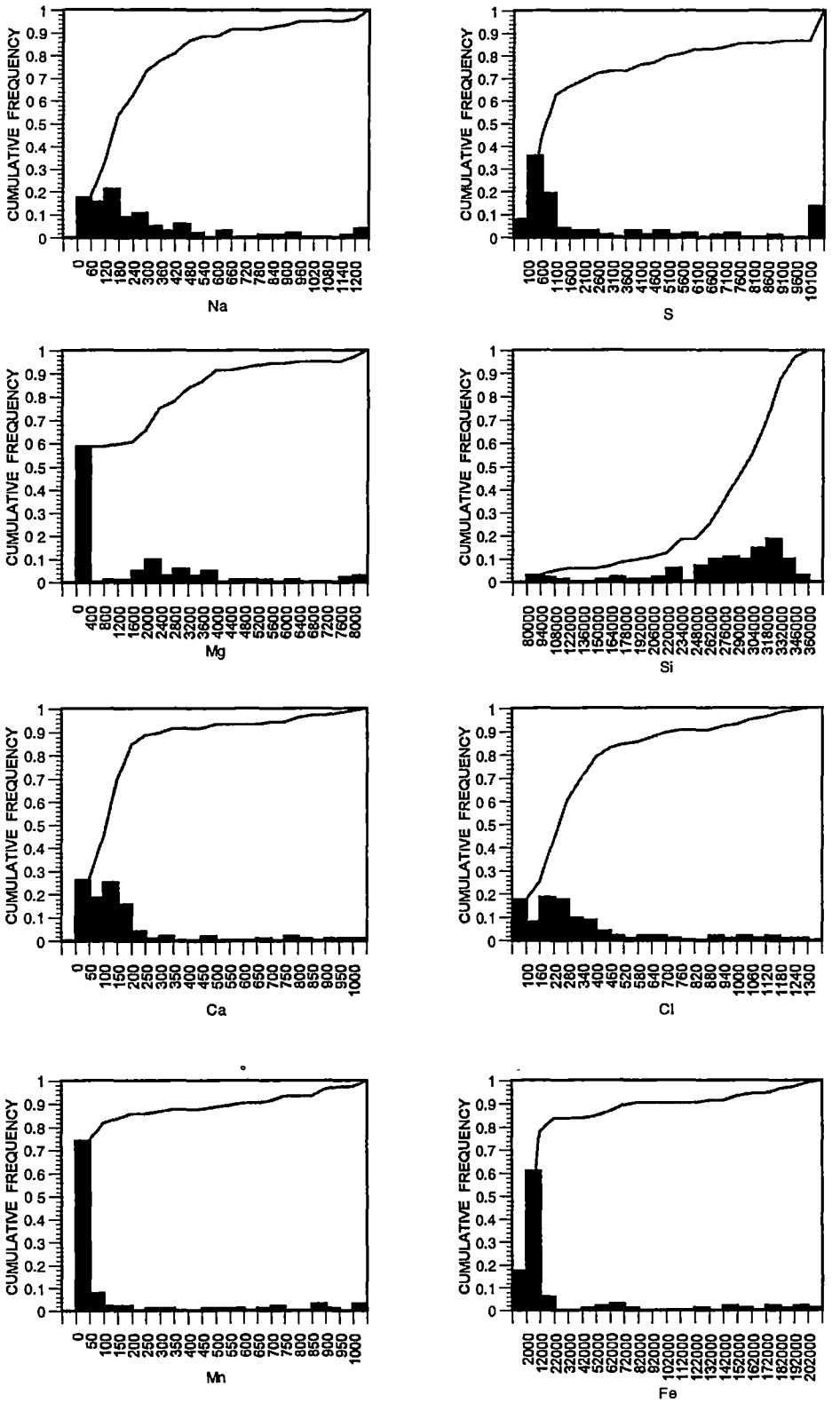

Figure 5-1. The histograms and cumulative frequency plots of Na, S, Mg, Si, Ca, Cl, Mn and Fe in ppm of the acid insolube residue.

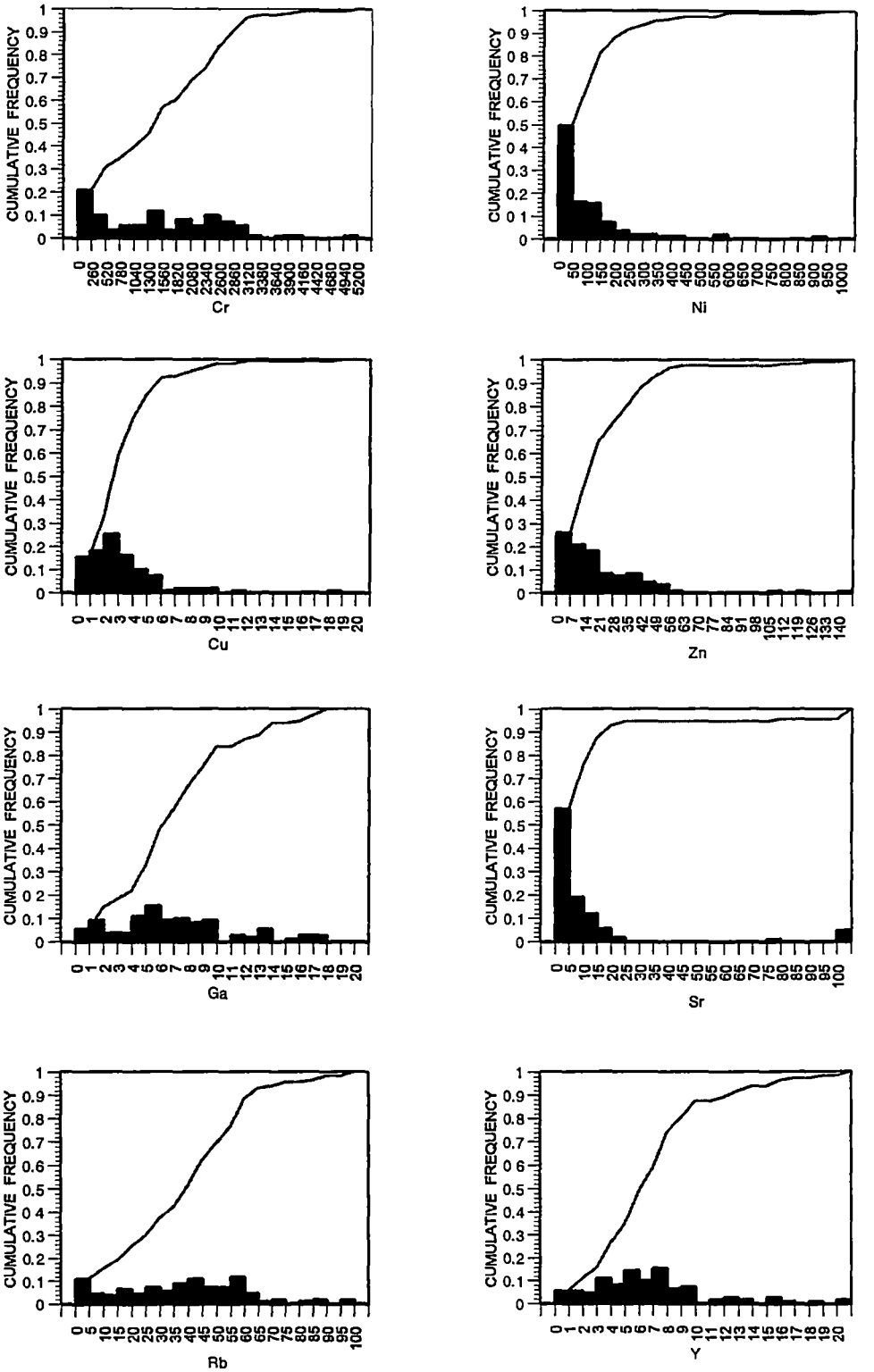

Figure 5-2. The histograms and cumulative frequency plots of Cr, Ni, Cu, Zn, Ga, Sr, Rb and Y in ppm of the acid insoluble residue.

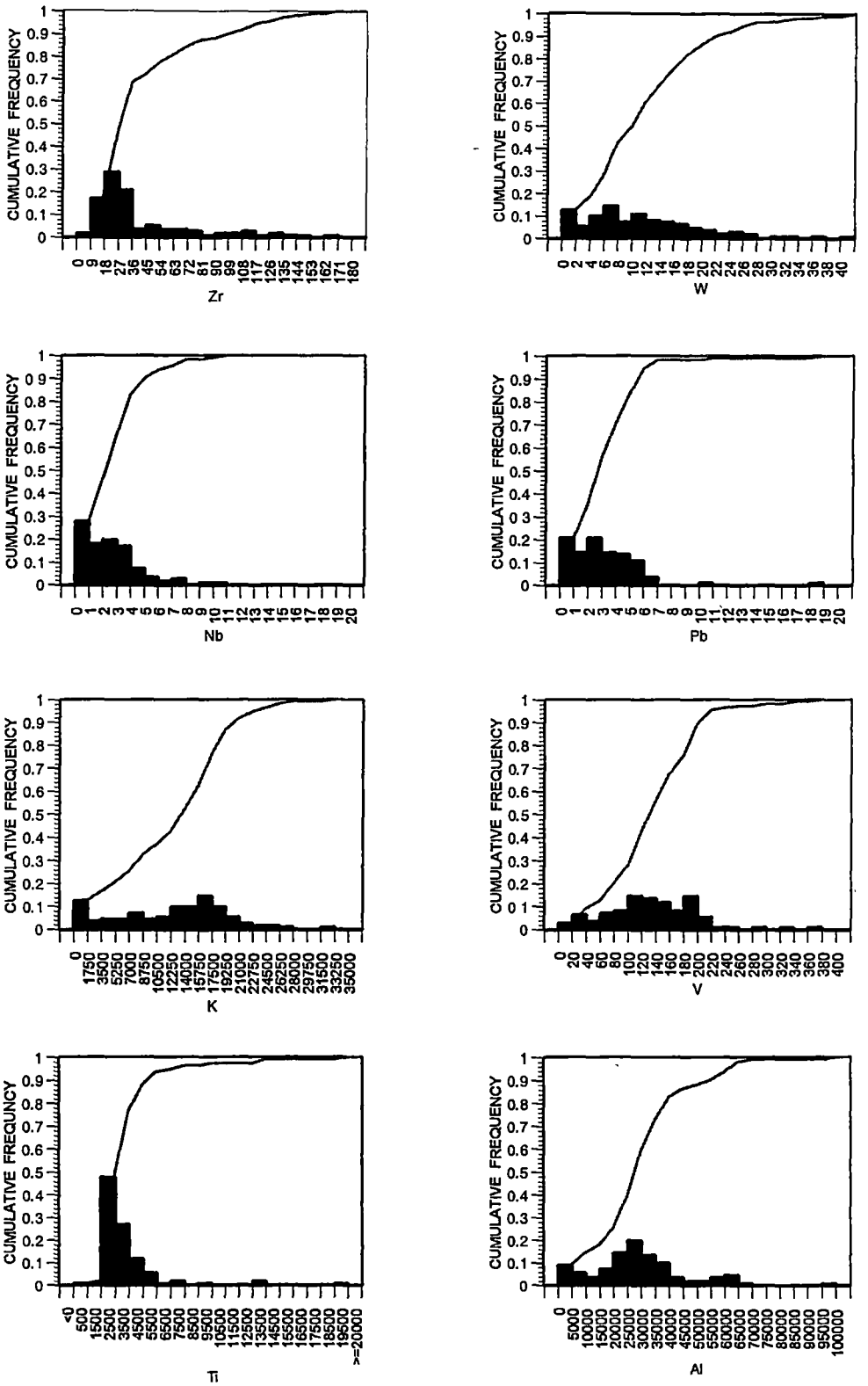

Figure 5-3. The histograms and cumulative frequency plots of Zr, W, Nb, Pb, K, V, Ti and Al in ppm of the acid insoluble residue.

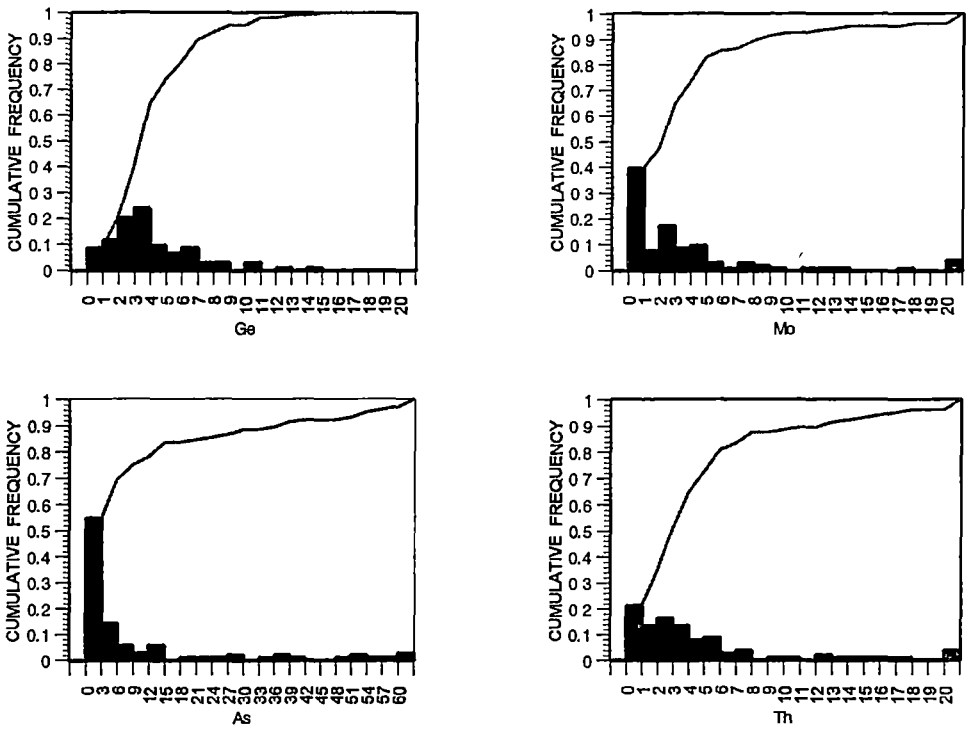

Figure 5-4. The histograms and cumulative frequency plots of Ge, Mo, As and Th in ppm of the acid insoluble resdiue.

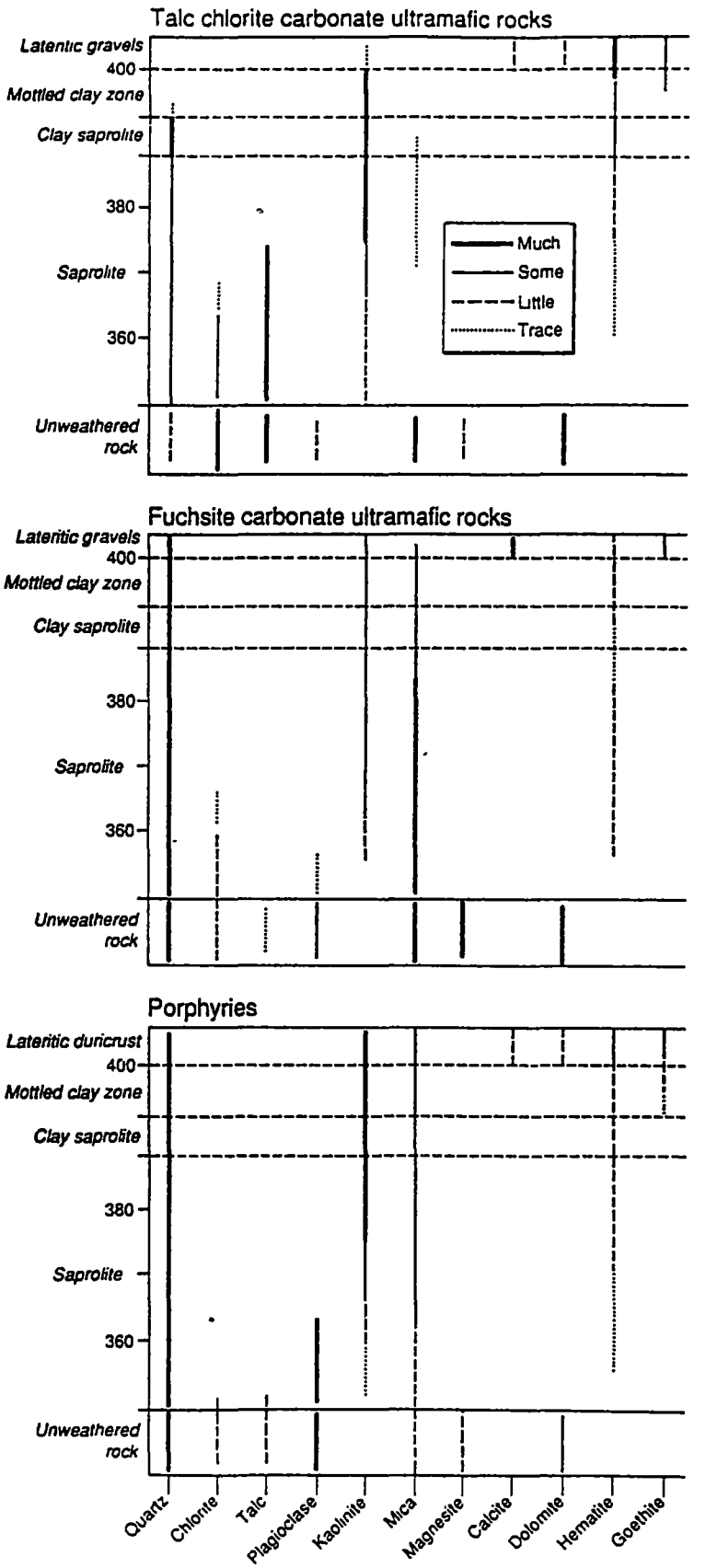

Figure 5-5. Mineralogy of the main regolith horizons over the three principal lithological units (from Butt, 1991)

5.1.2 Mottled and plasmic clay zone

The plasmic horizon, defined as massive clays or silty clays commonly with a mesoscopically homogeneous plasmic fabric, are developed over quartz-poor rocks (Robertson and Butt, 1997). This zone is transitional between the saprolite and the lateritic duricrust and gravels. It consists of pale green-grey clay and silty clays, strongly colored by secondary iron oxides (Butt, 1991). In the plasmic clays, the iron oxides are present as diffuse impregnations throughout the matrix, whereas in the mottled clay, they occur as secondary structures such as pisoliths and highly irregular nodules and aggregates. The thickness of the zone varies from 4–8 m.

5.1.3 Lateritic duricrust and gravels

The lateritic duricrust exists above the clay saprolite and its thickness may change by a few metres. It varies from about 5 m over the talc-chlorite altered ultramafic rocks to less than 1 m thick over some porphyries and fuchsitic altered ultramafic rocks. The lateritic materials are pisolitic, nodular or weakly cemented as duricrusts and friable gravels elsewhere. Nodules, nodule coatings and channel fillings of calcrete are common in the lateritic horizon, particularly in the upper, more friable material where it is gradational to soil. Some lateritic materials over fuchsitic ultramafic rocks are also silicified.

5.1.4 Calcareous soil

A thin cover of red-brown loamy soil, containing abundant lateritic nodules and pisoliths, was present over the profile. The soil is calcareous with fine grained calcium carbonate dispersed in the matrix and also present as calcrete nodules, fracture fillings, rhizomorphs and coatings. It varies in thickness from about 1 to 2 m.

5.2 Au DISTRIBUTION

The distribution of gold determined by INAA in the regolith is shown in Figure 5-6 (Butt, 1991). The Au distribution is typically patchy, despite the close sampling interval used in the study. This pattern likely reflects heterogeneity in the occurrence of both primary gold and secondary gold, as well as the variable presence of coarse particulate gold. The principal features of the distribution patterns are as follows.

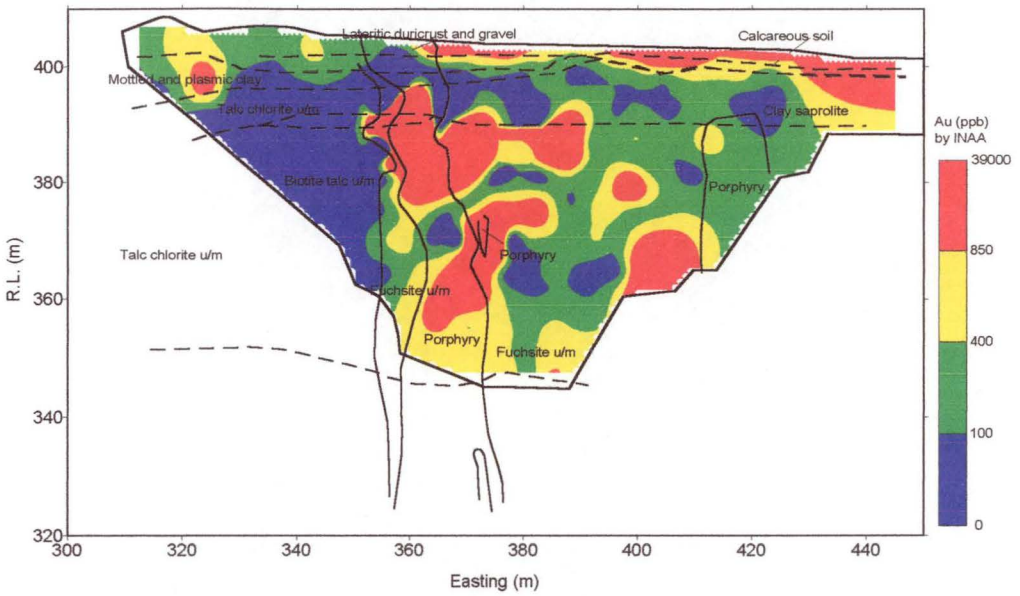

Figure 5-6. Au distribution at 15850N, Mystery Zone, Mt. Percy, illustrating surface enrichment, depletion in the lateritic duricrust and enrichment in the saprolite (after Butt, 1991)

1. Primary and saprolitic Au mineralization is indicated by a widespread zone of gold enrichment close to the surface, within the lateritic duricrust and the overlying soil. This supergene enrichment occurs to the east of the porphyry intrusion and is comprised of Au (i) associated with Fe oxides and presumably accumulated during lateritic weathering and (ii) associated with pedogenic carbonates and accumulated during more recent arid phases. The samples with the highest gold contents are generally the most calcareous. The Fe oxides and the calcrete are very finely divided so that complete separation was not possible. However, it appears that Au does not consistently favour either component, which suggests that the concentration is related to the environment rather than to a specific mineral host. These results are consistent with findings elsewhere in the southern Yilgarn Block; namely that pedogenic calcrete horizons are an important site for Au enrichment (Lintern, 1989). It is not known whether this Au enrichment was primary or secondary.
2. A leached and depleted zone (mostly < 100 ppb Au), 5–10 m thick is present just beneath the lateritic duricrust and gravels (below about 2–4 m). This zone corresponds approximately to the upper, clay-rich zones of the regolith (i.e. the mottled and plasmic zones and some upper saprolite). It also coincides with a zone of Br concentration. Sporadic samples rich in Au indicate the quartz veins hosted Au that was protected from weathering processes.

3. Possible supergene Au enrichment is present in the saprolite zone, which is about 20 m thick at about RL 390 m. The distribution suggests some homogenization and dispersion within the weathered porphyry and fuchsitic ultramafic rocks.

Gedeon and Butt (1990) studied the form, structure and geochemistry of particulate gold in the lateritic regolith of the Mystery Zone and concluded secondary Au enrichment based on its morphology and composition.

5.3 ACID INSOLUBLE RESIDUE GEOCHEMISTRY

The samples chosen from different lithologies and location of the profile were examined by transmitted light on a petrographic microscope as powders on glass lides after a drops of eugenol had been introduced. When necessary, oblique reflected light was used.

Information gathered by both lighting methods, one showing surface colour and fabric and the other showing birefringence and other optical properties, detailed mineralogy and fabric, are complementary.

The mineralogy of representative samples was also determined by X-ray powder diffractometry at the University of Tasmania. The XRD methodology has been stated in Section 3.2.3, Chapter 3.

In the Mystery Zone, mineralogical components determined by the petrographic microscopy and XRD indicate that the samples consist mainly of angular quartz, microscrystalline quartz aggregates, dirty opal partly as overgrowths on quartz nuclei, opal fragments, some secondary silica mainly chalcedony, some rutile and mica (Figure 5-7a).

For further checking, environmental scanning electron microscopy (ESEM) at the Central Science Laboratory was used. The samples are carbon coated polished thin sections of grains in epoxy resin. Figure 5-7b shows typical residual material observed by ESEM. The samples are essentially fragments of clear primary quartz, sometimes with sericite inside, and exceptionally free sericite. There is some chalcedony with kaolinite inclusions . Some rutile and in one case gibbsite was observed in secondary chalcedony. Often there are large amounts of sericite together with primary quartz

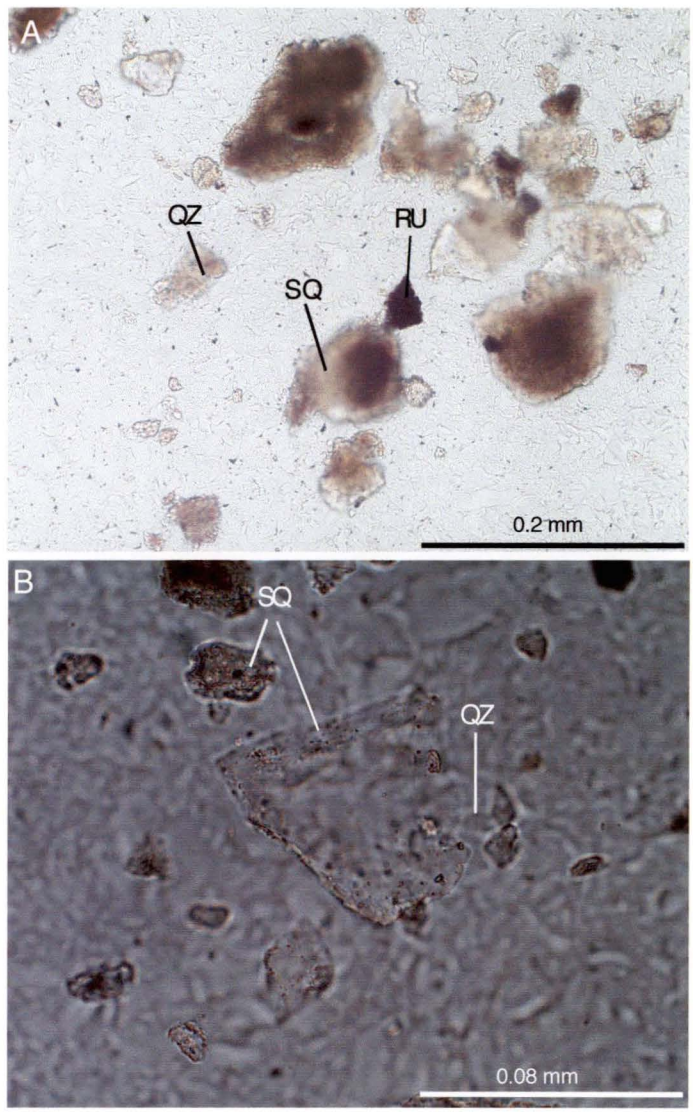

Figure 5-7. Photographs of transmitted light microscope
A: MW41 small proportion of clear quartz fragments (QZ), but mainly dirty opal(SQ), partly as overgrowth on quartz nuclei, also opal fragments and some rutile (RU)
B: MW270 small proportion of clear quartz fragments (QZ), but mainly secondary quartz (SQ), some secondary quartz overgrowth on primary quartz

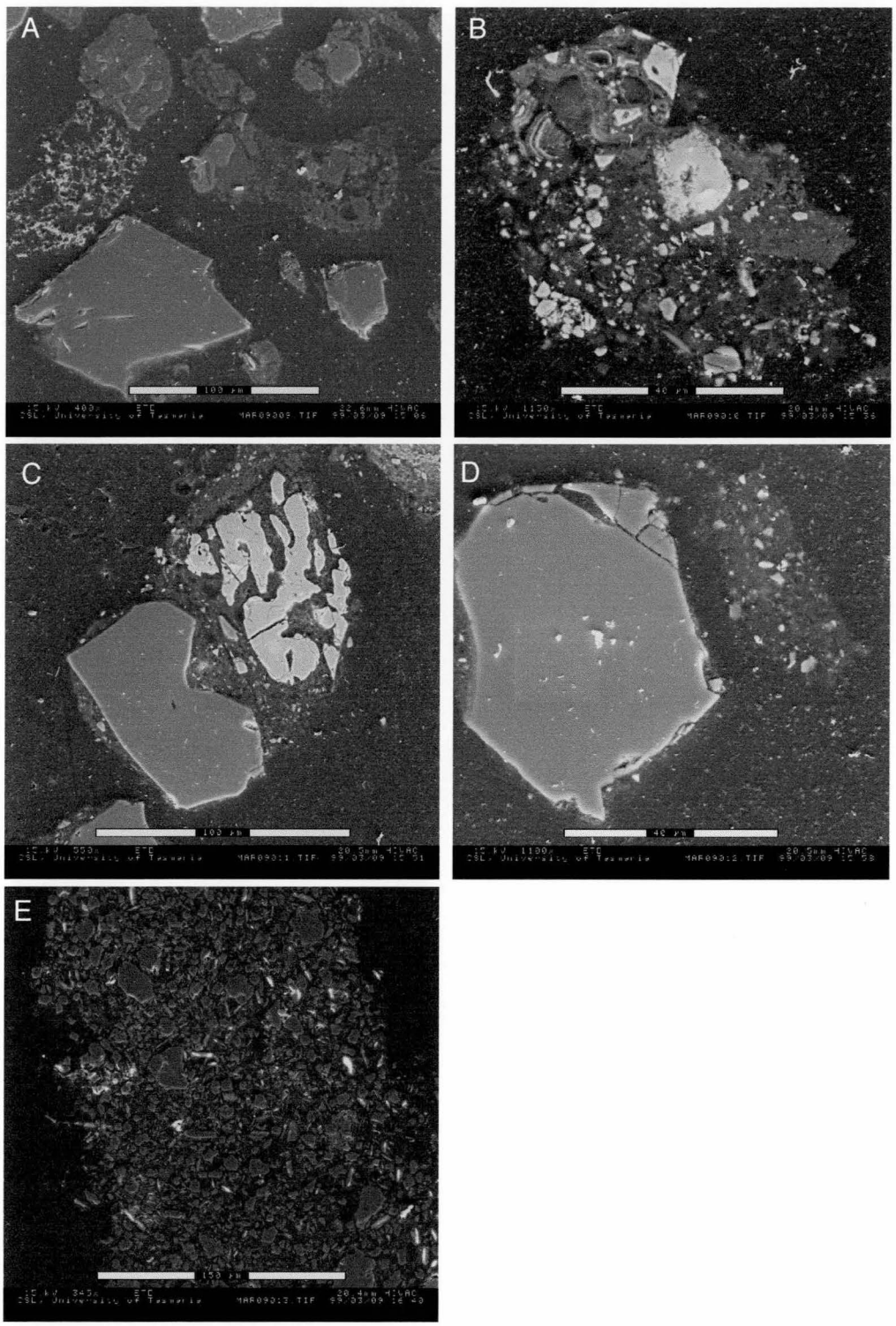

Figure 5-7b: ESEM micrographies
A: MW41fragments of clear primary quartz, secondary chalcedony with and without inclusions of primary quartz and one grain with some kaolinite in secondary quartz
B: MW270 composite grain of small primary quartz fragments and some gibbsite and rutile in secondary chalcedony
C: MW184 large corroded rutile together with a chunk of primary quartz in secondary chalcedony
D: MW184 primary quartz and a secondary chalcedony fragment with quartz and rutile inclusion
E: MW1611 large amount of sericite and primary quartz as a dense packing in secondary chalcedony

as a dense packing in secondary chalcedony. Higher in the profile, considerable amounts of secondary chalcedony occur with varying amounts of angular primary quartz, kaolinite and rare rutile inclusions.

The grouping of elements, as used by Butt (1991), will be followed in this discussion in order to facilitate comparison with the existing literature. The element distributions along section 15850N are shown as contour maps presented separately after the element description. Contour intervals were selected on the basis of the principle population evident in the acid insoluble residue data given in Figures 5-1 to 5-4.

The distribution pattern of Au was compared with that of other elements analyzed in this study, A strong correlation was observed between the distribution of their concentrations with those on the gold plots. A persistent spatial relationship exists between the concentrations on compared plots across the three section lines. These relationships are taken to indicate a certain affinity between the gold and the compared elements. Further investigation is necessary to determine whether the correlation results from a primary genetic relationship, whether they represent an artifact of the weathering environment or whether they are pure coincidental.

The elements identified as having a close relationship with Au throughout the regolith are described together and this section presents their distribution patterns. The explanation and discussion of these distributions is given in the following section. The principal features of the distribution patterns of the elements identified as having affinities with gold mineralization across section 15850N at Mystery Zone, Mt. Percy are as follows.

5.3.1 Major elements (Al and Fe)

Aluminium and Fe form the one of major constituents of the acid residual products and result from deep seated, prolonged chemical weathering. Due to closure, the abundance and distributions of these elements is commonly interdependent.

Aluminium: Aluminium has a range of 0–97079 ppm in the acid insoluble residue of the regolith and the distribution contour map is given in Figure 5-8. Aluminium

is leached from the lateritic duricrust and gravel, as well as the calcareous soil (< 2%). An anomalous concentration of Al enriched samples (5–7%) is noted to the west of 360E between R.L. 380 to 390 m, which occurs in the mottled and plasmic clay, overlying the talc-chlorite ultramafic rocks. Generally Al is depleted above the upper saprolite. The Al concentrations at depth are largely controlled by the occurrence of feldspar in porphyritic rocks and the presence of fuchsite altered ultramafics. Aluminum has low values in unaltered biotite, talc altered ultramafic rocks, where Al is less than 1 ppm.

Iron: Iron has a range of 59–219416 ppm and is strongly enriched at the two sides of long section 10150N (Figure 5-9). At the west sides of the profile in the lateritic duricrust and mottled zone, higher Fe contents occur near the surface. The lower Fe content of the porphyry (<0.4%) and talc chlorite altered ultramafic (< 0.2%) compared with that of fuchsite ultramafic rocks in the saprolite zone (> 0.3%) exhibits an iron distribution characteristic of different lithological units. The distribution of Fe is similar to the distribution of Mn.

5.3.2 Alkaline earth elements (Ca and Sr)

Calcium: Because of dissolution by acid, the Ca concentration is significantly low and variable. Ca ranges from 0 to 1119 ppm and its distribution contour map is

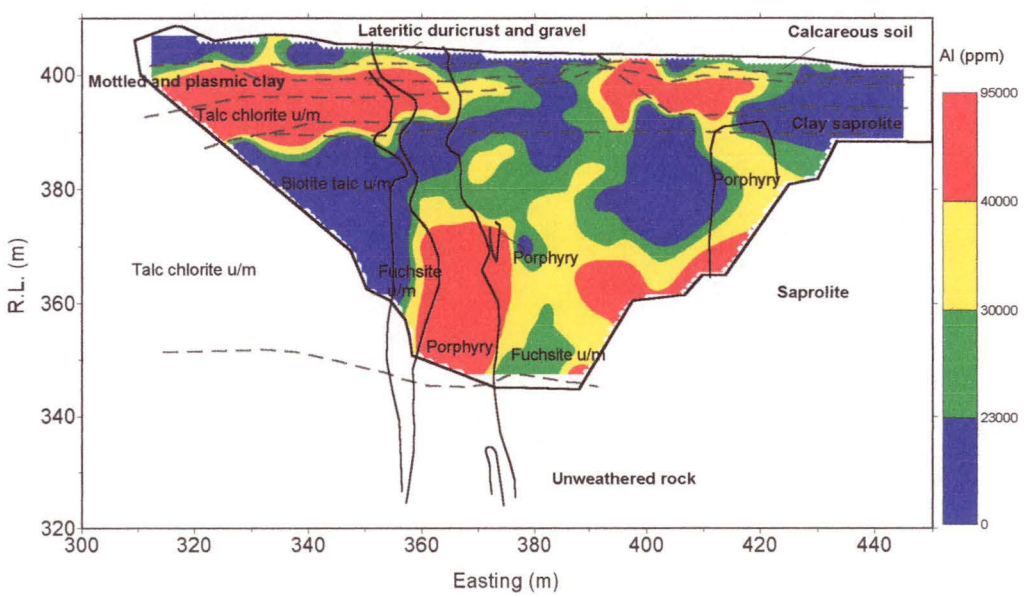

Figure 5-8. Al distribution in the acid insoluble residue at 15850N, Mystery Zone, Mt. Percy

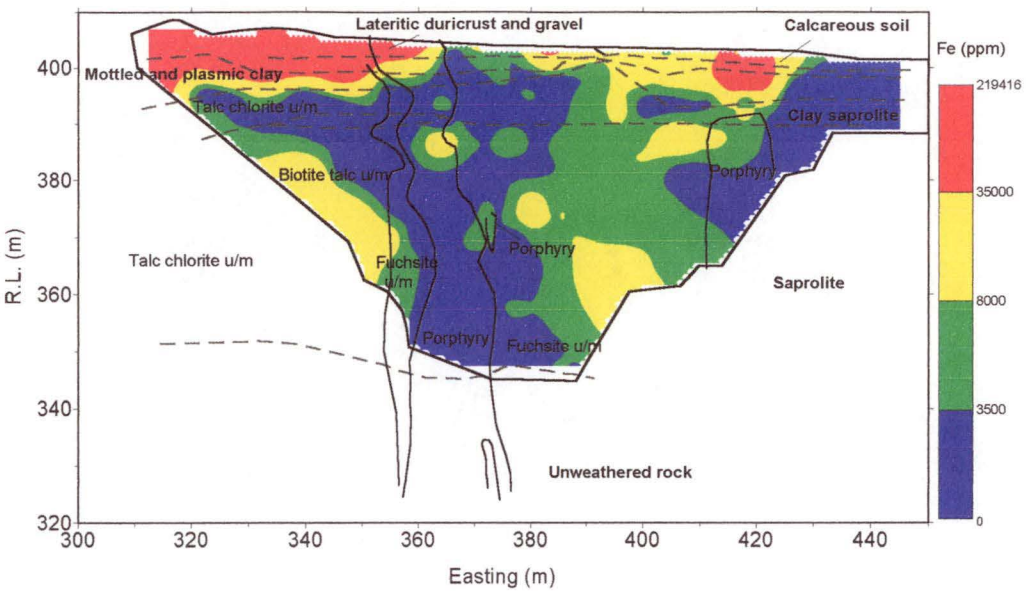

Figure 5-9. Fe distribution in the acid insoluble residue at 15850 N, Mystery Zone, Mt. Percy, W.A.

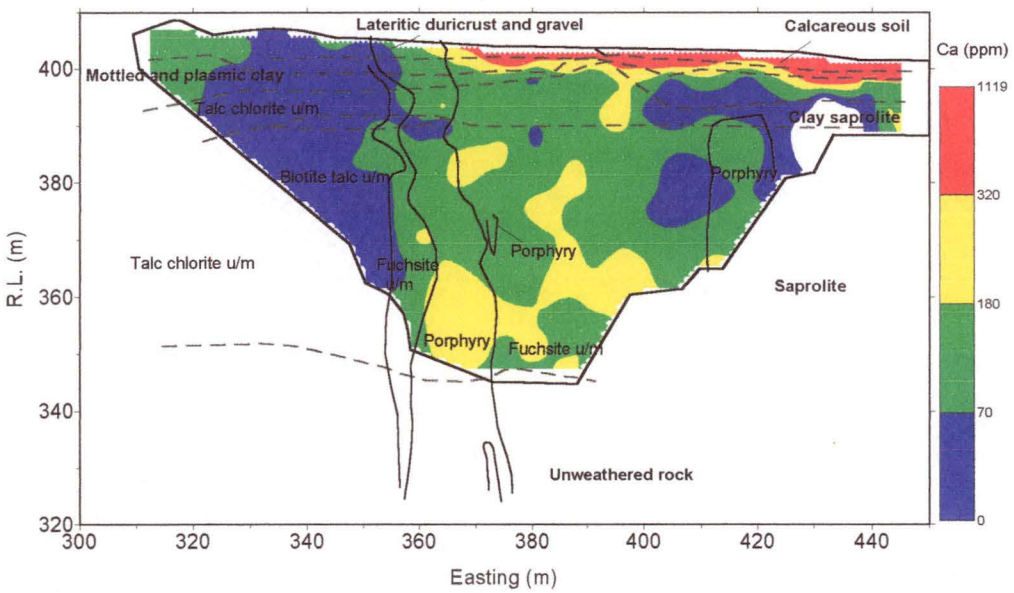

Figure 5-10. Ca distribution in the acid insoluble residue at 15850 N, Mystery Zone, Mt. Percy, W.A.

given in Figure 5-10. A strong Ca enrichment (>320 ppm) in the acid insoluble residue occurs directly above the mottled and plasmic clay zone, particularly in the fuchsite ultramafic rocks. Calcium has the lowest values in the talc-chlorite and biotite-talc ultramafic rocks which are below 70 ppm. The average content of Ca in porphyry and fuchsite ultramafic rocks is two times greater than that of talc altered ultramafic rocks. The depletion process is not understood. Visible variations in the Ca content occur in the middle part of the saprolite from R.L. 350 to 370, where host rock is fuchsite altered ultramafic.

Strontium: The concentration of Sr ranges from 0 to 245 ppm (Figure 5-11). Sr is enriched near the surface in the lateritic duricrust and calcareous soil zone, with levels greater than 15 ppm. The behavior of Sr below the lateritic duricrust and gravel, as well as the calcareous soil at the Mystery Zone is different from Ca but similar to the bulk geochemistry of regolith, except for its occurrence in the porphyry intrusive. The ultramafic rocks of the profile in the mottled and saprolite zone are strongly depleted in Sr, which is below 5 ppm. However, Sr levels are much higher in the porphyry where the average concentration of Sr is greater than 10 ppm.

5.3.3 Alkali metals (Na, K and Rb)

Sodium: Sodium ranges from 0 to 37395 ppm and its distribution contour map is given in Figure 5-12. Similar to Sr, Na is enriched near the surface in the lateritic duricrust and calcareous soil zone. Sodium concentrations in the ultramafic rocks are normally less than 0.02%. The distribution of Na in the regolith profile also has a significant enrichment at the lower part of the saprolite zone, which is larger than 1% and over ten times that of Na in the upper part of the profile, except for the porphyry. Sodium is higher in these porphyries than in the ultramafic rocks with an average concentration more than 0.03%. Based on these values, there is no obvious leaching effect in the talc dominated ultramafic rocks. In general, the concentration of Na is low in these geological units.

Potassium: Potassium distribution is controlled by the presence of micas and to a lesser extent potash feldspar. It varies from 23 to 34328 ppm in the regolith profile, with most values larger than 0.1% (Figure 5-13). The distribution of K has two different patterns. The concentration of K in the talc dominated ultramafic rocks is only a few hundred ppm, whereas K is enriched in the saprolite horizon hosted by

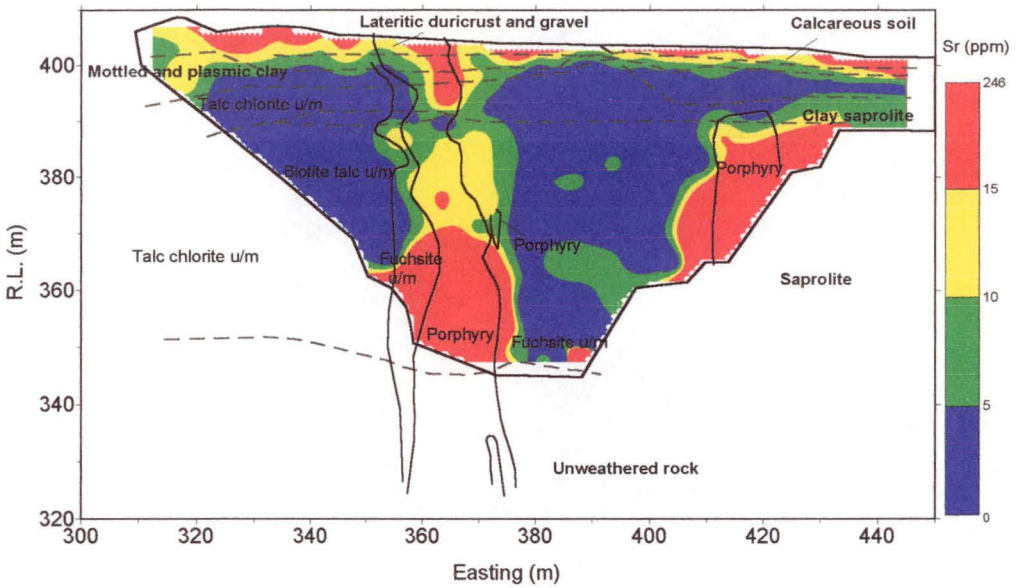

Figure 5-11. Sr distribution in the acid insoluble residue at 15850N, Mystery Zone, Mt. Percy, W.A.

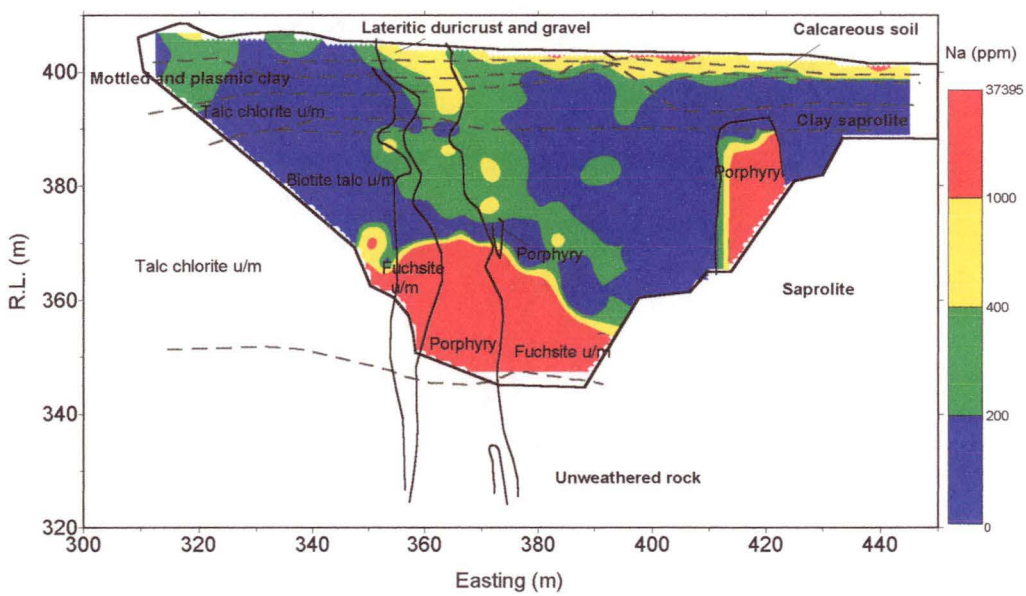

Figure 5-12. Na distribution in the acid insoluble residue at 15850N, Mystery Zone, Mt. Percy, W.A.

porphyries and fuchsitic ultramafic rocks. The average concentration of K in these rocks is above 1%, which is over ten times that in talc altered ultramafic rocks.

Rubidium: The Rb distribution is similar to K, and is also largely controlled by mica. It ranges from 0 to 148 ppm and the distribution contour map is given in Figure 5-14. The high values of Rb (>35 ppm) in acid insoluble residue occur in the fuchsite altered ultramafic rocks. The concentration of Rb in the talc dominated ultramafic rocks is less than 9 ppm. In the calcareous soil and underneath clay saprolite zones, Rb concentration is also low and tends to decrease towards the surface (normally only a few ppm). There is a minor leaching effect in the lateritic duricrust.

5.3.4 Base and transition metals (Cu, Pb, Zn, Ni and Mn)

Copper: Copper has a range of 0 to 26 ppm (Figure 5-15). Copper is high in the talc-chlorite and biotite-talc ultramafics, the porphyries and the mottled and plasmic clay. A zone with values greater than 6 ppm Cu occurs in the mottled zone, whilst even higher values occur in the talc-chlorite ultramafic rocks. The average value of Cu in biotite ultramafic rocks is low (<3 ppm). Overall, the low concentration of Cu in the fuchsite ultramafic rocks is typical for the whole regolith profile, starting from the surface and down to the bottom of the saprolite, except for occasional sporadic high values near the surface and/or in the saprolite.

Lead: The Pb abundance in the acid insoluble residue of the regolith profile of the study area is generally low (0–51 ppm) and is illustrated in Figure 5-16 with an erratic distribution pattern. Lead enrichment occurs in the lateritic duricrust and calcareous soil. Very low values (<3 ppm) also occur in the saprolite horizon, except for a few samples in the porphyries.

Zinc: Zinc has a range of 0–205 ppm and the distribution contour map is given in Figure 5-17. Even when the concentration of zinc is reasonably high, the distribution pattern in the regolith is erratic. There is a depletion trend throughout the profile, particularly in the talc dominated ultramafic rocks. The concentration of Zn in the porphyry intrusion is low, and generally less than 10 ppm. Zinc is, however, enriched in the fuchsite altered ultramafic rocks compared to other parts of the profile. A depleted zone also occurs between R.L. 382 and 370 m.

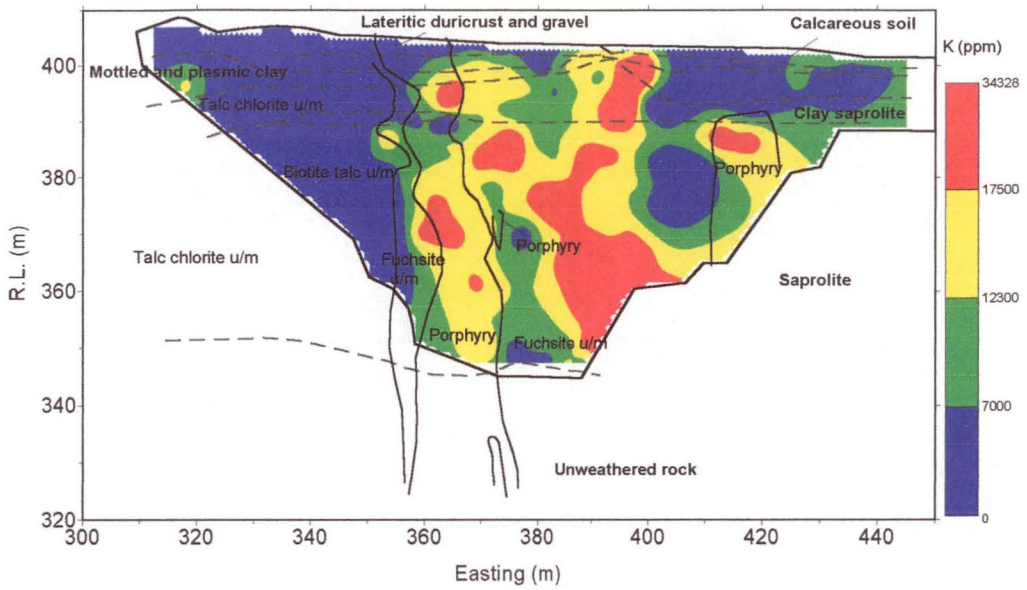

Figure 5-13. K distribution in the acid insoluble residue at 15850N, Mystery Zone, Mt. Percy, W.A.

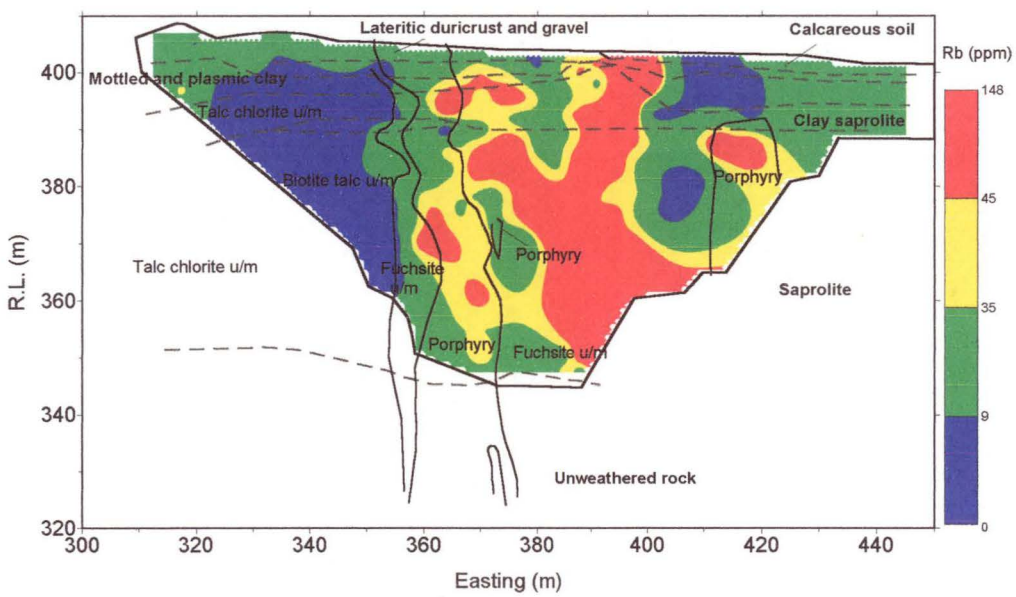

Figure 5-14. Rb distribution in the acid insoluble residue at 15850N, Mystery Zone, Mt. Percy, W.A.

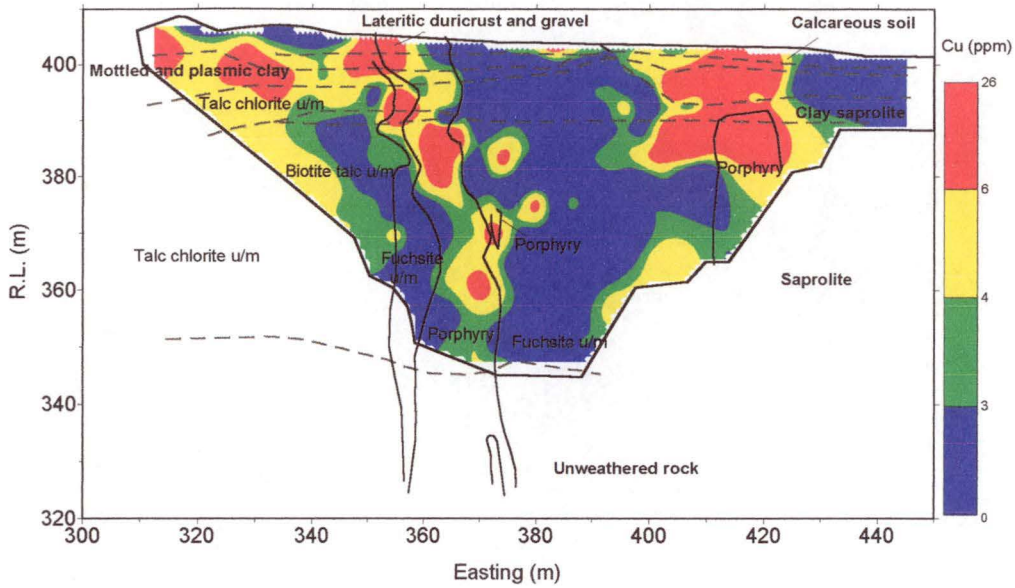

Figure 5-15. Cu distribution in the acid insoluble residue at 15850N, Mystery Zone, Mt. Percy, W.A.

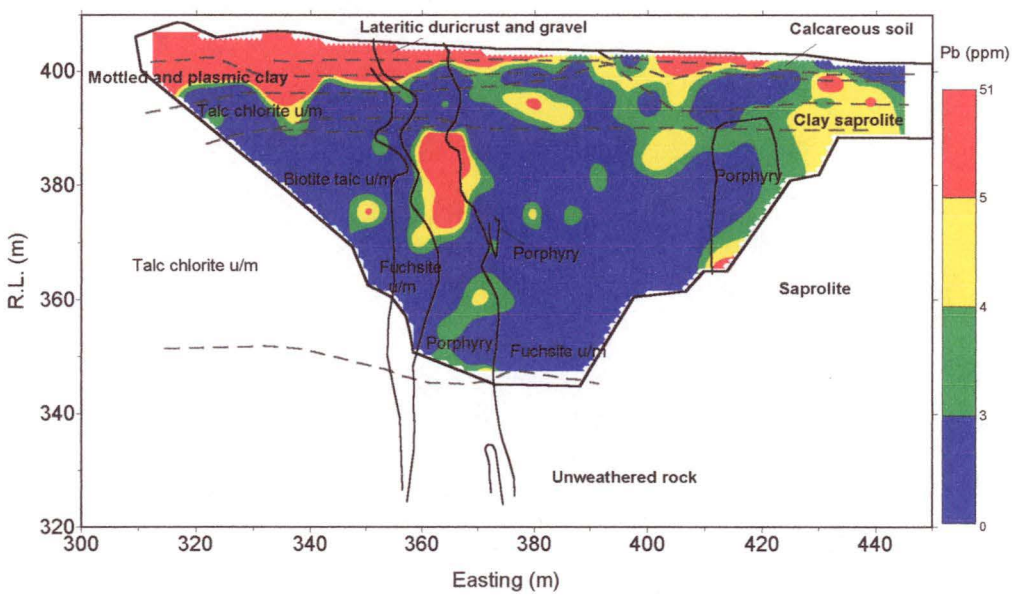

Figure 5-16. Pb distribution in the acid insoluble residue at 15850N, Mystery Zone, Mt. Percy, W.A.

Nickel: Nickel has a similar distribution to Zn and varies from 3 to 916 ppm (Figure 5-18). The highest Ni content occurs in the ultramafic units. This high distribution extends into the upper part of the regolith profile, including the mottled and lateritic duricrust zones, with values ranging from 50 ppm, but most values are greater than 100 ppm. Ni in the porphyry intrusions is very low, generally less than 50 ppm.

Manganese: Manganese ranges from 0 to 1148 ppm. The most significant Mn concentrations occur in the lateritic duricrust with values greater than 500 ppm. There is no marked leaching zone above the mottled zone. Generally, Mn is very low in the saprolite (<20 ppm), except for some sporadic values around 50 ppm. The distribution of Mn (Figure 5-19) is similar to that of Pb (Figure 5-16), implying that both elements are hosted by the same minerals or that Pb- and Mn-bearing minerals have the same distributions.

5.3.5 Lithophile transition elements: (Cr, Ti and V)

Chromium: Chromium ranges from 0 to 5099 ppm and the distribution contour map is given in Figure 5-20. In the acid insoluble residue, Cr is enriched in the fuchsite altered ultramafic rocks, with an average concentration larger than 1000 ppm. This enrichment extends through the whole regolith profile, from the surface to the base of the saprolite. In contrast, the concentration of Cr is lower in the porphyry and talc dominated ultramafic rocks with an average of less than 550 ppm; which is significantly lower than Cr values in the fuchsitic ultramafic rocks.

Titanium: Titanium values range from 235–272337 ppm in the regolith profile and its distribution contour map is given in Figure 5-21. The Ti content steadily increases upwards through the profile, with strong enrichment in the mottled zone, lateritic duricrust and calcareous soil horizon, containing values over 5000 ppm. The concentration of Ti is, however, depleted in the saprolite zone, except for a few sporadic high samples distributed in the profile. The average concentration of Ti in the saprolite is less than 3000 ppm.

Vanadium: Vanadium is clearly surface enriched. The V content of the regolith has a range of 0–2717 ppm and is illustrated in Figure 5-22. In the talc dominated ultramafic rocks units, V is concentrated in the mottled and lateritic duricrust and

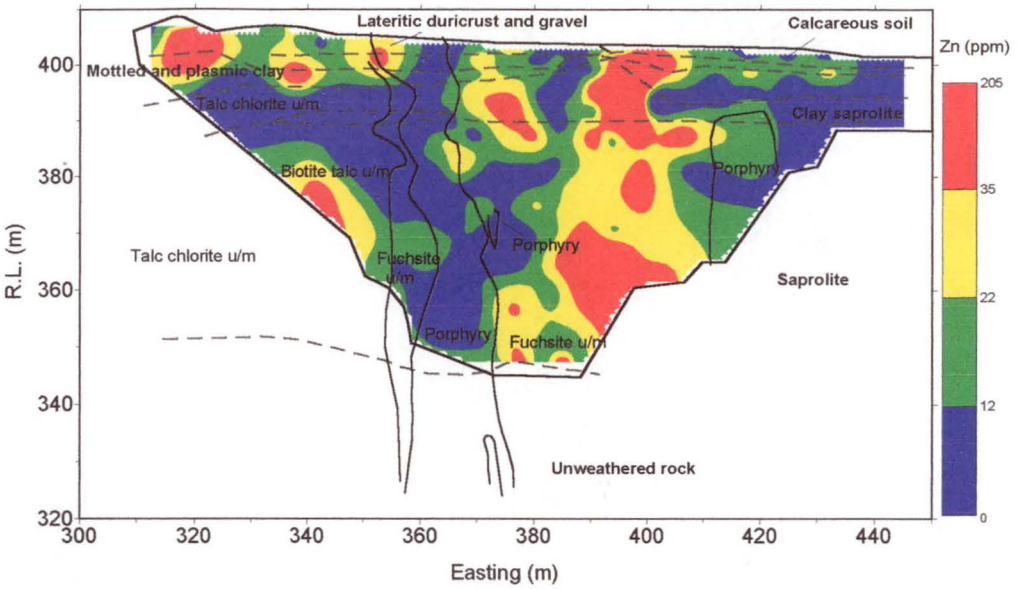

Figure 5-17. Zn distribution in the acid insoluble residue at 15850N, Mystery Zone, Mt. Percy, W.A.

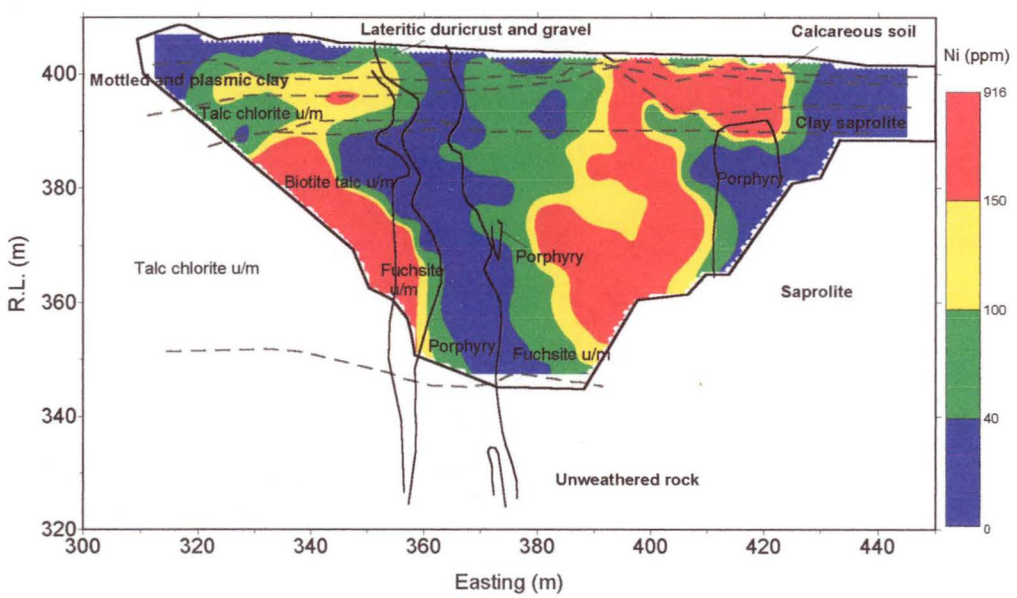

Figure 5-18. Ni distribution in the acid insoluble residue at 15850N, Mystery Zone, Mt. Percy, W.A.

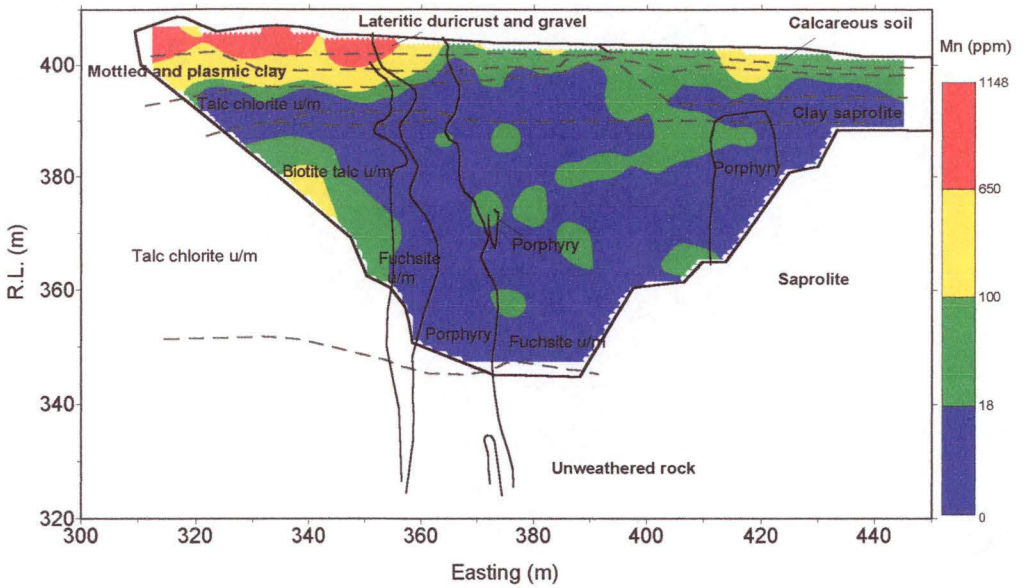

Figure 5-19. Mn distribution in the acid insoluble residue at 15850N, Mystery Zone, Mt. Percy, W.A.

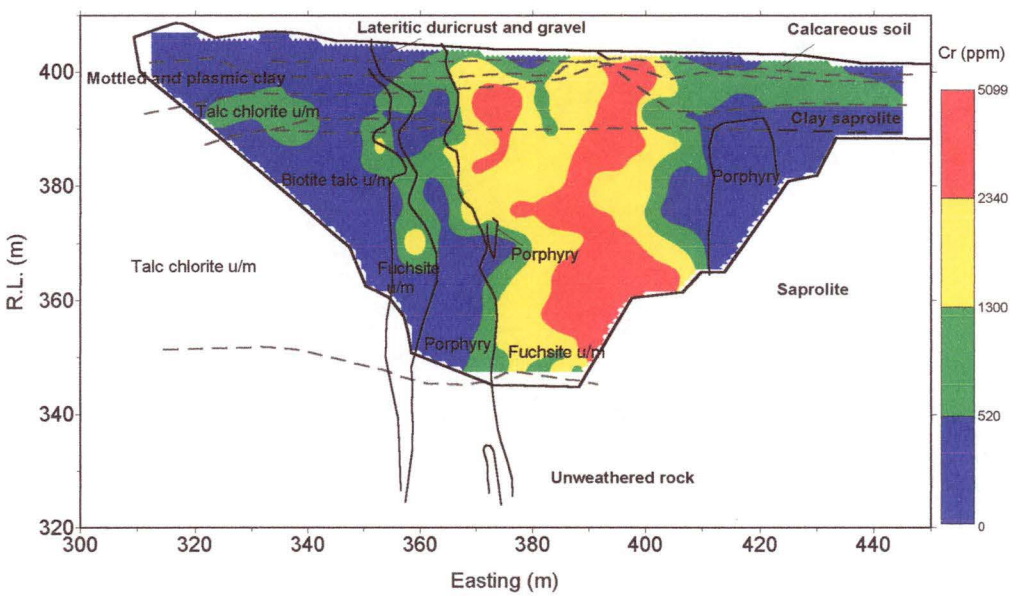

Figure 5-20. Cr distribution in the acid insoluble residue at 15850N, Mystery Zone, Mt. Percy, W.A.

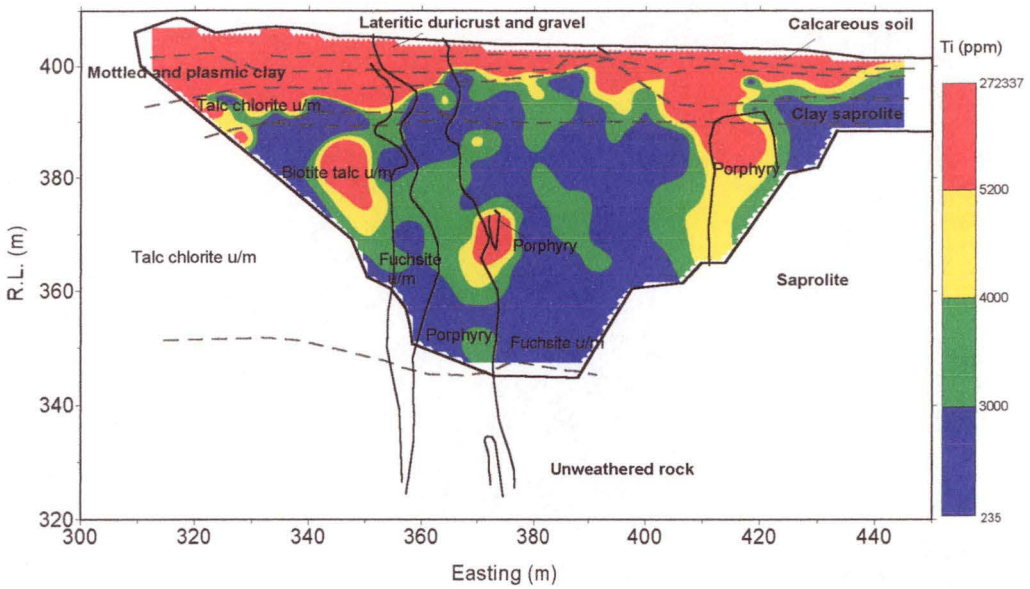

Figure 5-21. Ti distribution in the acid insoluble residue at 15850N, Mystery Zone, Mt. Percy, W.A.

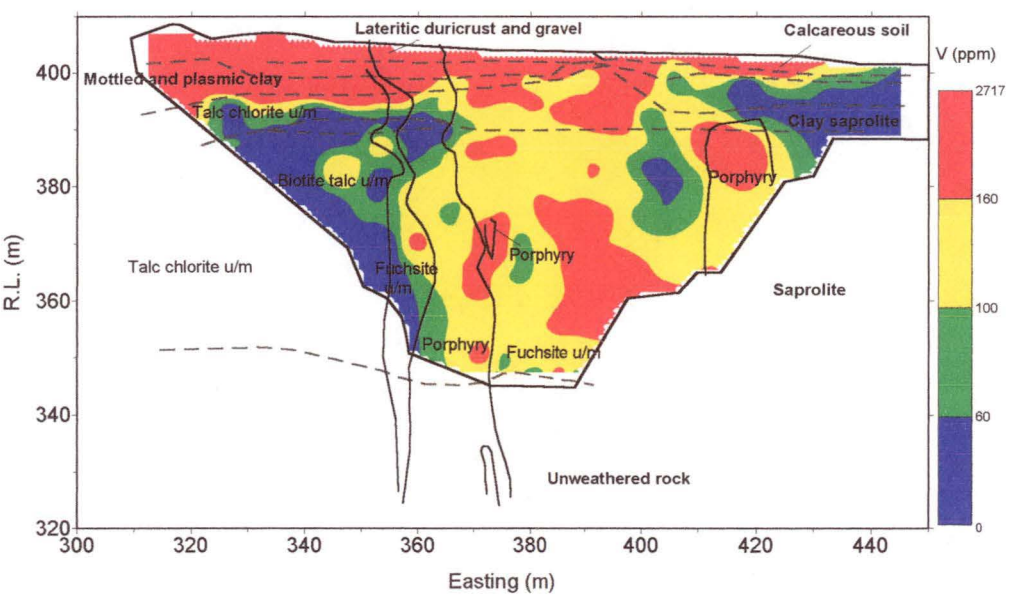

Figure 5-22. V distribution in the acid insoluble residue at 15850N, Mystery Zone, Mt. Percy, W.A.

strongly depleted in the saprolite horizon. In contrast, within the porphyry and fuchsite altered ultramafic rocks there is only minor depletion in the upper saprolite horizon between R.L. 380 and 390 m. Below R.L. 380 m, the concentrations of V (>160 ppm) are not continuous. Nevertheless, significant V (>60 ppm) constantly occurs in the porphyries and fuchsitic ultramafic rocks under the lower part of the mottled zone.

5.3.6 Immobile elements: (Zr, Nb and Th)

The elements Zr, Nb and Th, generally exhibit little chemical mobility in the weathering environment. Zr, Nb and Th are all members of the second and third transition series and have similar chemical characteristics. Zircon is probably the principal host mineral for each of these elements and hence the stability of zircon determines their distribution and dispersion in the regolith (Butt, 1991).

Zirconium: Zirconium varies from 7 to 1262 ppm and increases upwards through the regolith. The distribution contour map is given in Figure 5-23. Two clear enrichment zones of Zr occur in the regolith profile; one in ultramafic units of the profile where Zr is strongly concentrated in the top of the profile, and the other in the talc dominated rocks. In the latter, Zr is concentrated near the surface (>110 ppm) and low values occur at the border of saprolite and talc-chlorite ultramafic rocks. The lower Zr is more upwardly continuous in the fuchsite altered ultramafic rocks to the bottom of the mottled and plasmic clay zone. The average concentration of Zr is below 35 ppm in the saprolite zone. In contrast, Zr depletion is less intense in the porphyry. The concentration of Zr in the saprolite is less than in its overlying weathered covering (40–120 ppm), but it is still significantly greater than that observed in the ultramafic rocks. The Zr distribution is similar to the distribution of Ti (Figure 5-20).

Niobium: Niobium concentrations in the regolith vary from 0 to 84 ppm. The distribution contour map is given in Figure 5-24. Its distribution in the upper part of the profile is similar to that of Zr (cf. Figure 5-23). The Nb values are elevated between R.L. 405 and 415 m in the lateritic duricrust and mottled zone above the talc dominated horizon. In the fuchsite ultramafic rocks, this Nb enrichment zone is thin and about a few metres wide with Nb depleted almost throughout the whole profile. There is little difference between the Nb concentrations of the porphyry

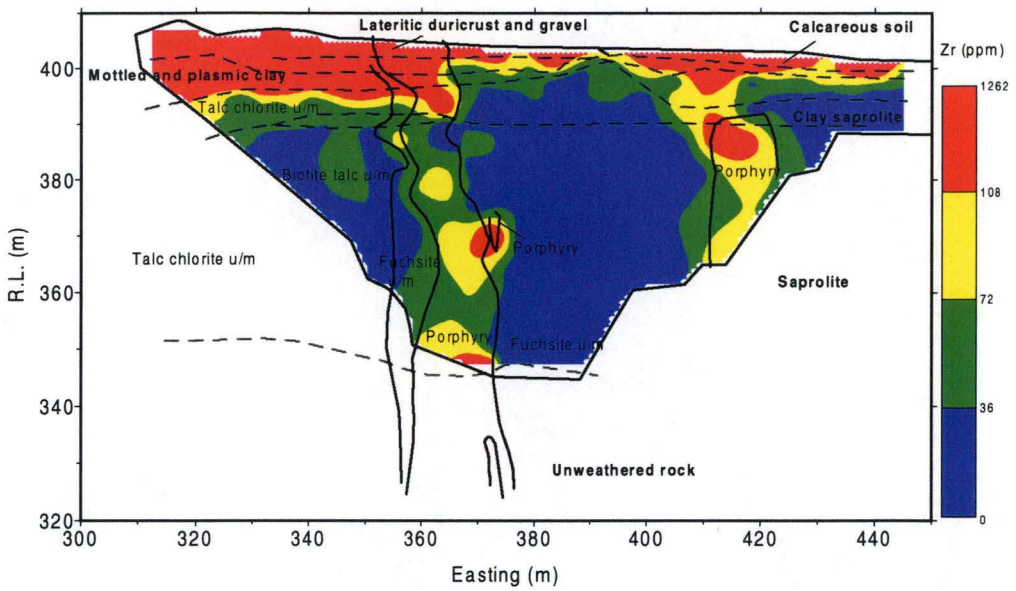

Figure 5-23. Zr distribution in the acid insoluble residue at 15850N, Mystery Zone, Mt. Percy, W.A.

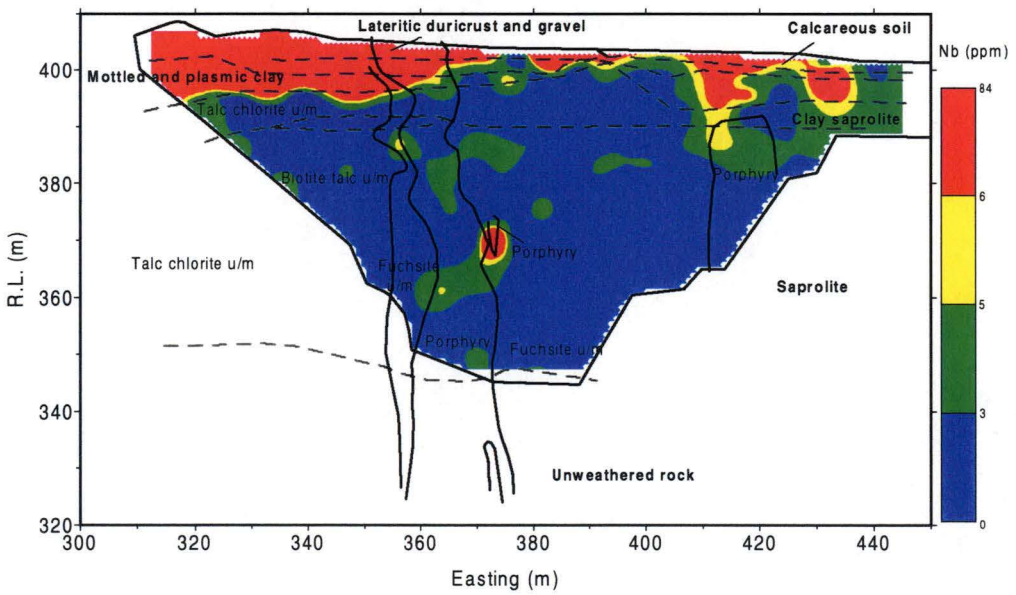

Figure 5-24. Nb distribution in the acid insoluble residue at 15850N, Mystery Zone, Mt. Percy, W.A.

intrusion and the ultramafic rocks which are low, except for a few sporadic higher values.

Thorium: Significant accumulations of Th are also noted in the lateritic duricrust and mottled zone. Its content in the profile varies from 0 to 25 ppm and its distribution is given in Figure 5-25. Because Th concentrations in the saprolite and saprock are close to the detection limit, the distribution pattern may be spurious, and consequently, Th will not be discussed further.

5.3.7 Other elements: (As, S, W, Ga, Mo, F, Y and Cl)

Arsenic: Arsenic has a range of 0 to 70 ppm and the distribution contour map is given in Figure 5-26. The As content of the acid insoluble residue appears to indicate that As is concentrated in the top 10–15 m of the profile. Arsenic is more enriched in the lateritic gravel and mottled clay zones, particularly above the talc-chlorite altered ultramafic rocks (>30 ppm). The concentration of As in clay saprolite and the saprolite zones is generally low (<3 ppm).

Sulphur: Sulphur in the mineralized porphyries and fuchsitic ultramafic rocks is present mainly in pyrite, with some arsenopyrite, chalcopyrite and galena as accessory minerals. The values in the acid insoluble residue vary from 28 to 55741 ppm. The S distribution contour map is given in Figure 5-27. The concentration of S in the lateritic gravel and mottled clay zones is quite low, at less than a few hundred ppm, except for a few scattered samples with values around 1000 ppm. Deeper in the profile S values are high, averaging over 3000 ppm.

Tungsten: Tungsten varies from 0 to 192 ppm in the regolith profile and its distribution contour map is given in Figure 5-28. Tungsten is consistently enriched throughout the primary mineralization, in and related to the porphyry intrusion and fuchsitic ultramafic rocks, with concentrations of 10–40 ppm over the porphyries and 5–20 ppm in the fuchsitic ultramafic rocks. Comparatively lower values of <2 ppm occur in the unmineralized talc-chlorite altered ultramafic rocks. Tungsten is however enriched in the upper part of talc-chlorite ultramafic rocks, lateritic gravel (>50 ppm) and mottled clay zones (6–20 ppm).

Gallium: The content of Ga varies from 0 to 28 ppm. The distribution contour map

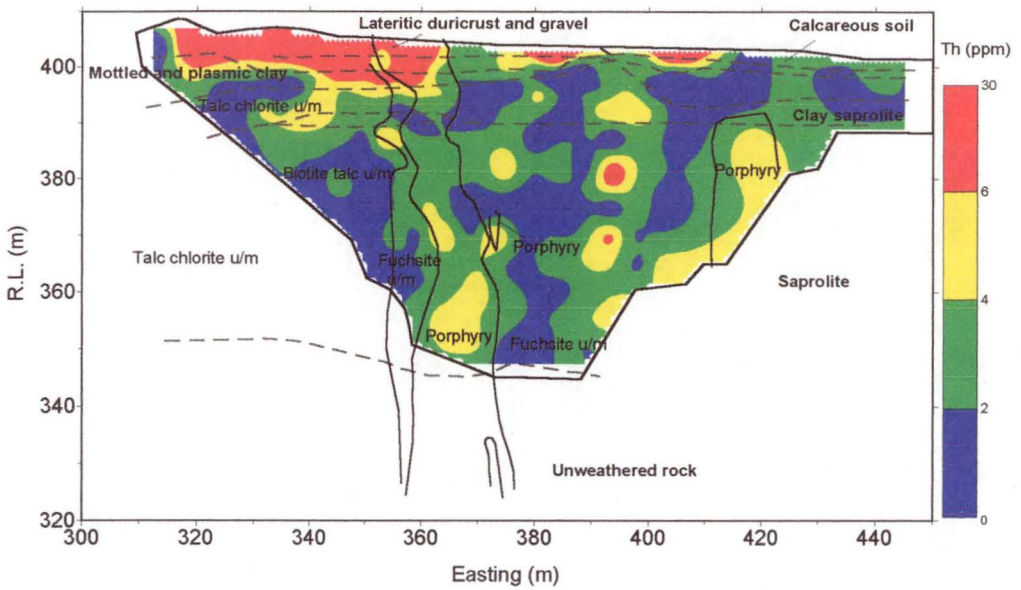

Figure 5-25. Th distribution in the acid insoluble residue at 15850N, Mystery Zone, Mt. Percy, W.A.

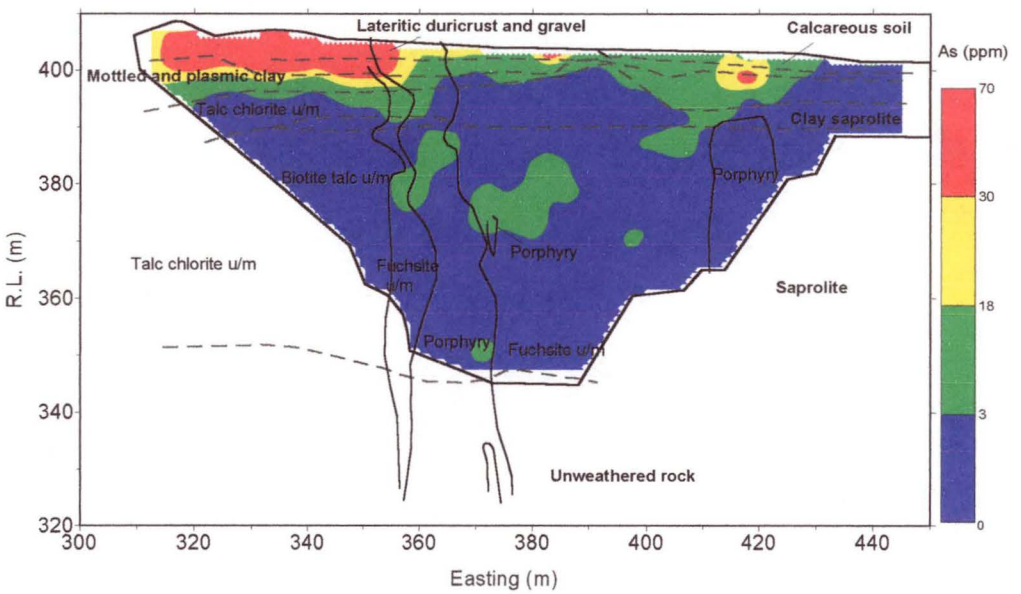

Figure 5-26. As distribution in the acid insoluble residue at 15850N, Mystery Zone, Mt. Percy, W.A.

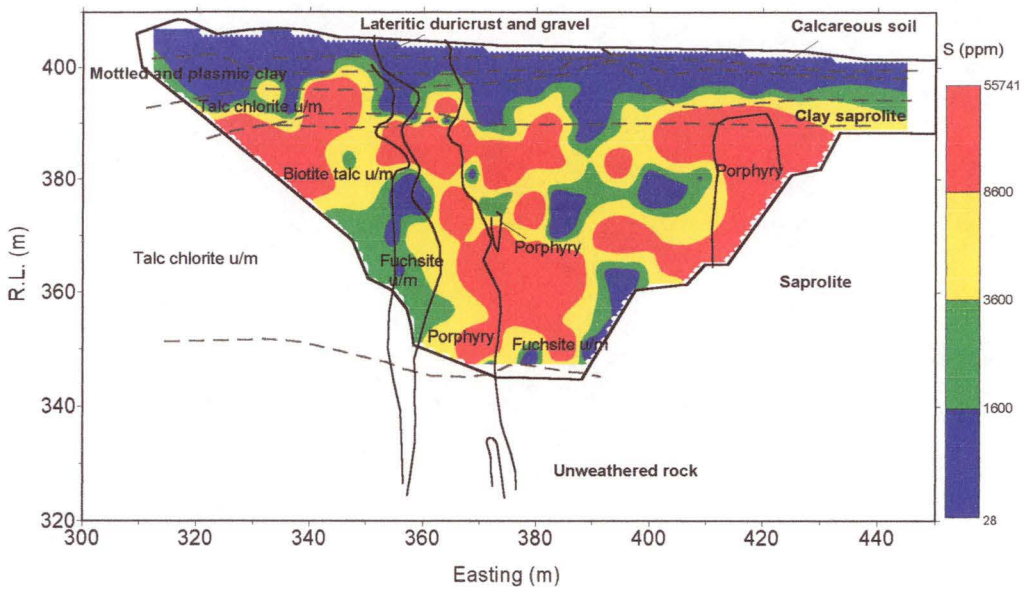

Figure 5-27. S distribution in the acid insoluble residue at 15850N, Mystery Zone, Mt. Percy, W.A.

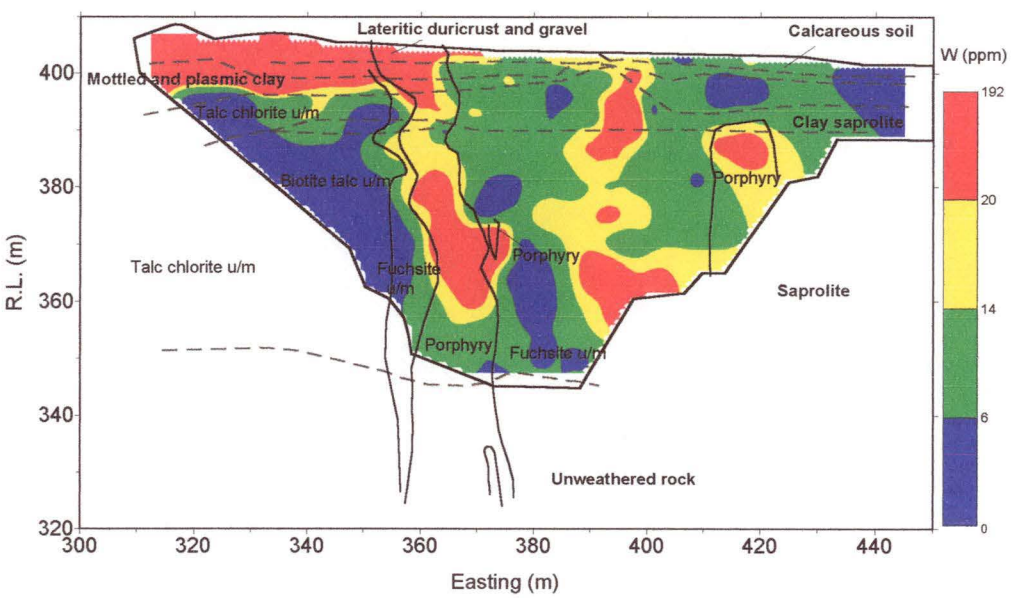

Figure 5-28. W distribution in the acid insoluble residue at 15850N, Mystery Zone, Mt. Percy, W.A.

is given in Figure 5-29. Its distribution is similar to W (Figure 5-28) in the regolith, except that the upper part of the talc-chlorite altered ultramafic rocks has low Ga values (in the lower part of the saprolite profile it is less than 4 ppm). The highest Ga values occur in the porphyries (7–17 ppm). The concentration of Ga is commonly between 4 to 11 ppm in the fuchsitic ultramafic rocks. Generally, high Ga occurs in the middle to lower saprolite and saprock horizon. A leaching effect (strong depletion) is evident in the lateritic residuum zone. The distribution of Ga is heterogeneous, suggestive of weak dispersion associated with weathering.

Molybdenum: Molybdenum has a range of 0 to 30 ppm and its distribution contour map is given in Figure 5-30. Mo enrichment occurs in the lateritic gravel and mottled clay zones. Molybdenum values from deeper in the profile are low. Because most Mo in the acid insoluble residue is close to the detection limit, the element can not be used as a key pathfinder element in the Mystery Zone.

Fluorine: The concentration of F ranges from 102 to 3823 ppm and its distribution contour map is given in Figure 5-31. The concentration of F is elevated (over 1000 ppm) above the mottled clay zone. The concentration decreases heterogeneously from the clay saprolite to the upper part of the saprolite (R.L. 390 –370 m). Below the R.L. 370, the concentration of F is uniformly low. Values of F less than 600 ppm occur in the lower saprolite.

Yttrium: The distribution of Y in the regolith is rather patchy. It ranges from 0 to 131 ppm. The distribution contour map is given in Figure 5-32. Yttrium enrichment mainly occurs in the talc dominated ultramafic rocks, where the concentration in lateritic gravel ranges from 50 to 130 ppm and values vary from 5 to 36 ppm in the lower part of the profile. Some enrichment occurs in the lateritic and mottled clay zone of the porphyry and fuchsitic altered ultramafic rocks, but the concentration is lower than that observed in the talc ultramafic rocks at 5–30 ppm. The lowest abundance in Y is identified in the clay saprolite and saprolite zones overlying the porphyry and fuchsitic ultramafic rocks units, where it is generally less than 10 ppm.

Chlorine: Chlorine varies from 0 to 1276 ppm and its distribution contour map is given in Figure 5-33. Cl is enriched in the lateritic duricrust and gravel overlying the talc chlorite rocks (>1000 ppm). Elsewhere in the profile, Cl enrichment is similar

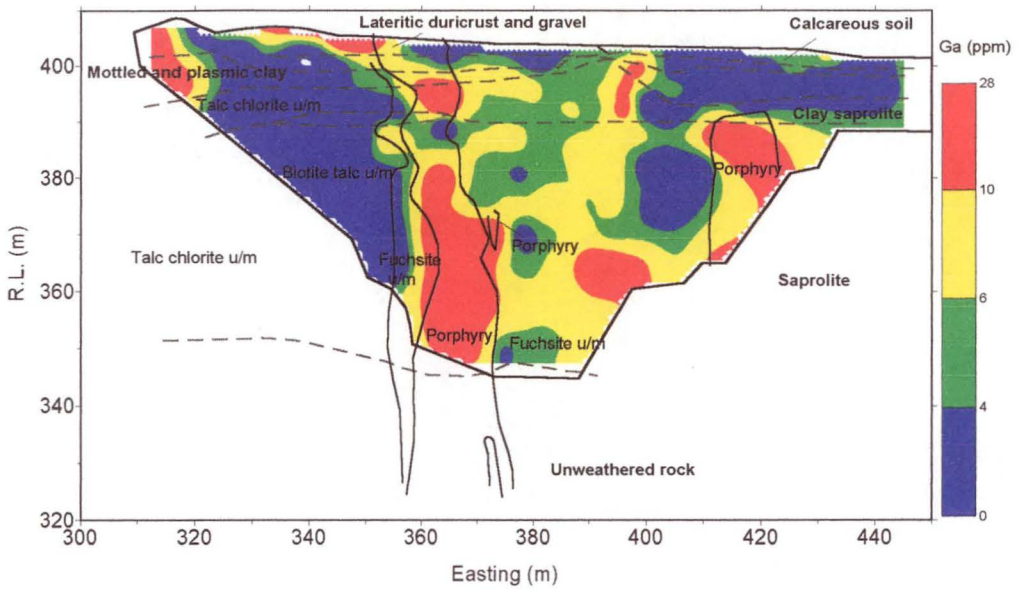

Figure 5-29. Ga distribution in the acid insoluble residue at 15850N, Mystery Zone, Mt. Percy, W.A.

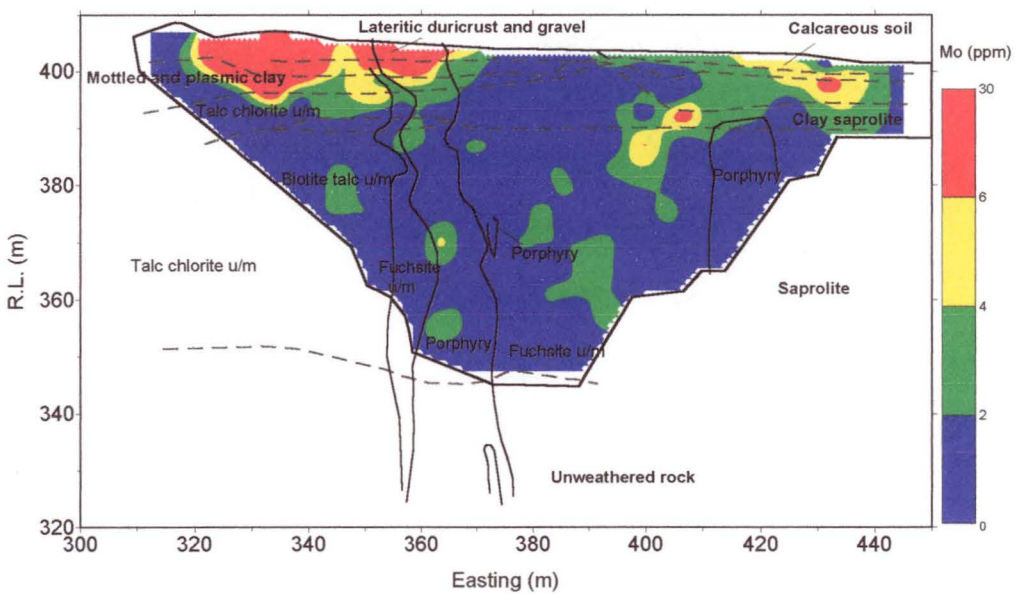

Figure 5-30. Mo distribution in the acid insoluble residue at 15850N, Mystery Zone, Mt. Percy, W.A.

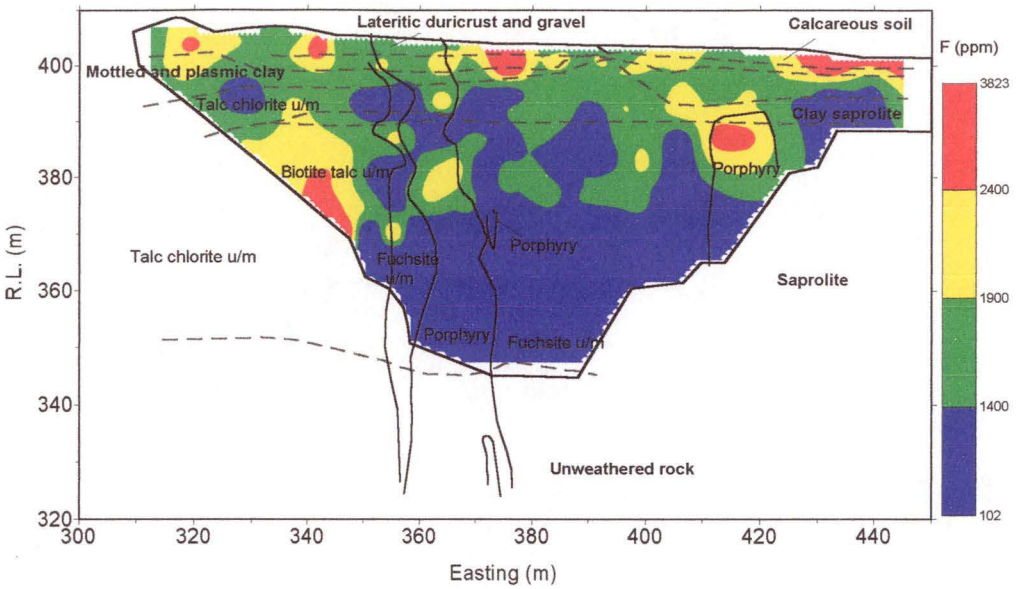

Figure 5-31. F distribution in the acid insoluble residue at 15850N, Mystery Zone, Mt. Percy, W.A.

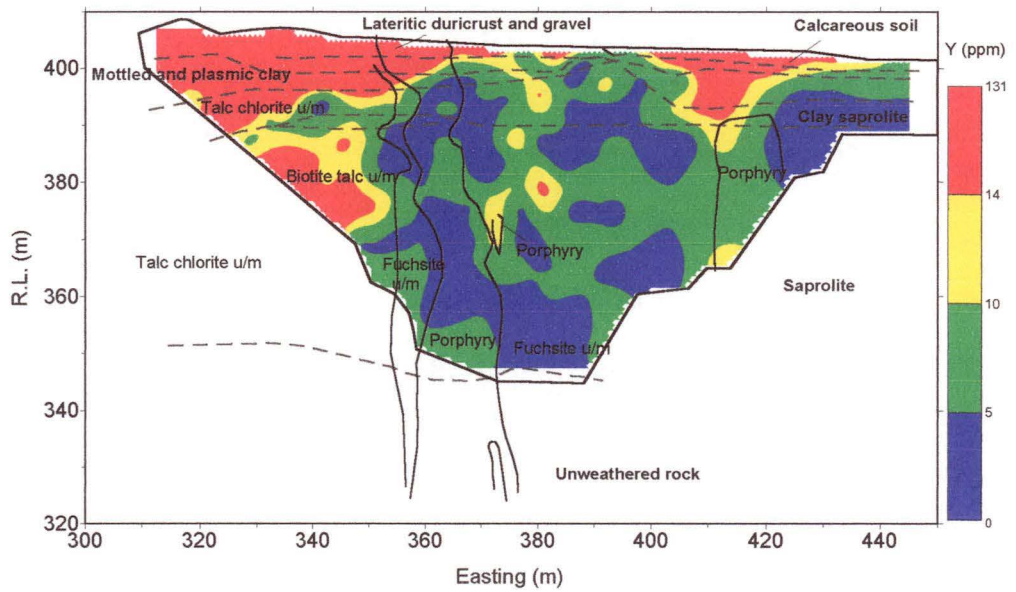

Figure 5-32. Y distribution in the acid insoluble residue at 15850N, Mystery Zone, Mt. Percy, W.A.

to F (Figure 5-31). In the lower part of saprolite, Cl concentration is generally less than 100 ppm.

Germanium: Germanium content in the acid insoluble residue of the regolith is very low. It varies from 0 to 20 ppm and the distribution contour map is given in Figure 5-34. The average concentration of Ge is less than 2 ppm in the porphyries. There are some moderate concentrations greater than 6 ppm in the lateritic duricrust, soil and mottled clay zones. The high Ge occurs near the surface of the fuchsitic ultramafic rocks and continues into the lower part of the profile to the bottom of the saprolite zones.

5.4 ELEMENT DISTRIBUTION

The element distribution of weathering products has long been one of the most reliable guides for mineral exploration in areas of deep weathering and residual cover (Smith and Anand, 1990). However, because weathering tends to obscure the original chemistry, mineralogy and texture, confusion is common between the weathering products of ore and those of ordinary rocks. The elemental composition of the acid insoluble residue has been used to see if the weathering effects can be reduced, and if expressions of primary mineralization, dispersion and wall rock alteration can be distinguished in the secondary weathering environment. This section provides a discussion of the element distributions of the acid insoluble residue detailed in section 5.3.

5.4.1 Statistical methods

The geochemical data of the acid insoluble residue generated in this study were treated by two statistical methods: factor analysis and cluster analysis. These two statistical methods were developed primarily as a tool in humanity studies (psychological data), but are currently extensively applied to geology (Davis, 1973). Factor and cluster analysis represent a group of techniques that are used to resolve the intercorrelations within a set of variables. Their application to this study is

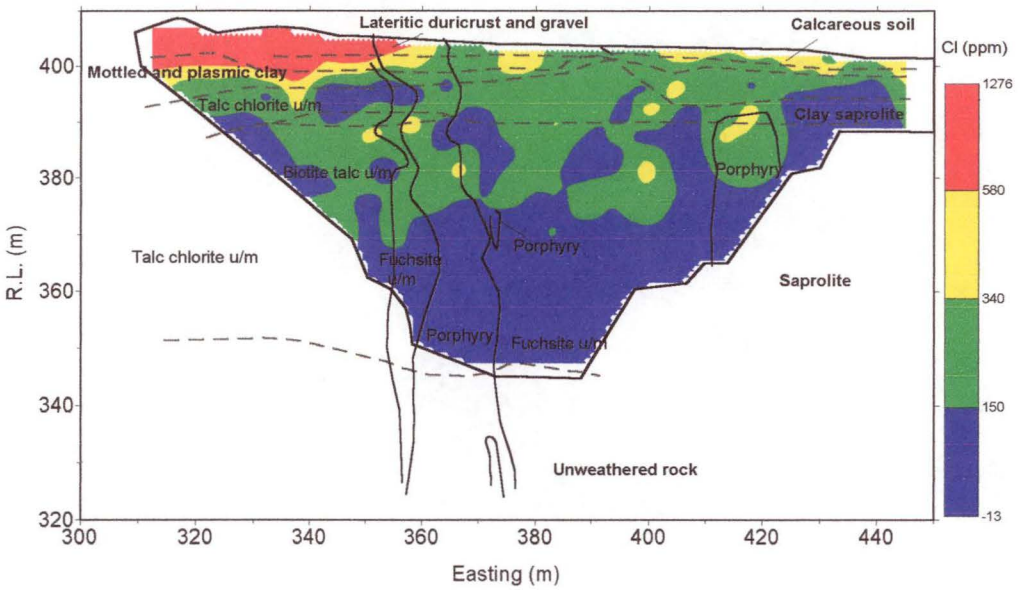

Figure 5-33. Cl distribution in the acid insoluble residue at 15850N, Mystery Zone, Mt. Percy, W.A.

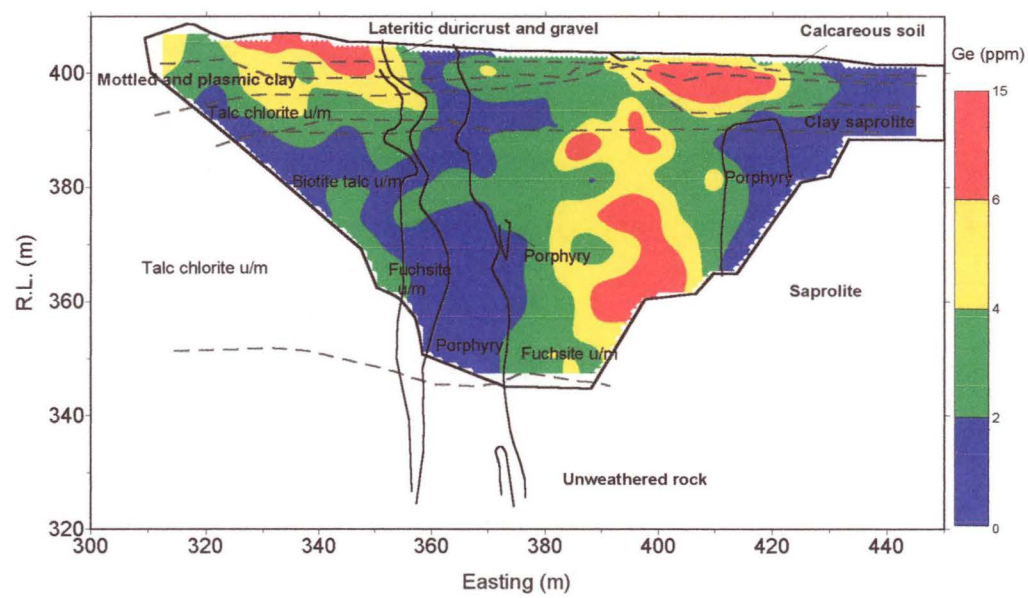

Figure 5-34. Ge distribution in the acid insoluble residue at 15850N, Mystery Zone, Mt. Percy, W.A.

under the consideration that a number of geological processes that played a role in the development of the regolith which probably affected a range of elements, and conversely, each element was affected by a number of different processes. It is clear that the variation of many elements within the regolith is complex, being the sum of the effects of a number of different processes. Factoring and/or clustering is an efficient way of displaying the complex relationships between many variables and cluster analysis can be used to resolve some of this complexity.

One hundred and ninety-two samples were taken from the acid insoluble residue of the Mystery Zone for analysis. The means and standard deviation of the raw and $\log_{10}$ transformed data are given in Table 5-1. The variances of all elements are high: Mo has the smallest variance with a variation coefficient of 38% for the untransformed data. Therefore, all the statistical methods described below have been applied to $\log_{10}$ transformed data.

Table 5-2 contains the Spearman correlation matrix derived from the $\log_{10}$ transformed data of the 192 samples. The factor analysis is given in Table 5-3. Following Guttman (1956), Kaiser (1960) recommended that factors with eigenvalues less than 1.0 are insignificant. However, the Mystery Zone data differ from typical psychological data in that (1) a much smaller number of variables were factored, (2) the data are probably more precise, and (3) the weaker factors can be interpreted with greater certainty.

In this context, the result of the factor analysis indicates that factor 1 accounts for most of the variation in the elements As, Fe, Mn, Mo, Nb, Pb, Sr, Th, Ti, V, W, Y and Zr. These elements in the Mystery Zone are considered residually enriched during weathering (e.g. Zr as primary zircon), or precipitated and absolutely enriched in the profile like Fe. This is supported by their enrichment in the upper part of the profile. Factor 1 shows strong opposition between Cr which is mostly located in the fuchsite facies and the elements accumulated in the ferruginized horizons of the top profile. Factor 2 consists of Al, Au, Ca, Ga, K, Na, Rb, Sr, V, W and Zn. This group of elements reflects the sericite and carbonate alteration associated with the gold mineralization. Factor 3 consists of Cr, Fe, Mn, Ni and Zn which represent the distribution of remaining ferromagnesian minerals, such as amphibole, biotite and fuchsitic alteration. Factor 4 represents probably residual Al-oxides (association Al-Ga-Cr). Not all the common factors can be interpreted (Cameron, 1968). These

Table 5-1. Statistical data, Mystery Zone, Mt Percy, W.A. (n=192, data based analysis of acid insoluble residue)

Element	X	S	V	XL	SL	VL
Au*	758.31	3307.6	4.36	2.14	0.84	0.39
F	1367.73	769.18	0.56	3.02	0.36	0.12
Na	1955.7	5869.13	3	2.35	0.89	0.38
Al	30240.78	20507.11	0.68	4.3	0.61	0.14
K	9622.55	8163.43	0.85	3.56	0.84	0.24
Ca	150.53	161.72	1.07	1.98	0.49	0.25
Ti	18116.47	49733.23	2.75	3.72	0.5	0.13
V	271.54	489.7	1.8	2.12	0.49	0.23
Cr	1187.91	1094.17	0.92	2.65	0.92	0.35
Mn	77.46	207.11	2.67	1.2	0.69	0.58
Fe	15488.45	38877.57	2.51	3.68	0.55	0.15
Ni	108.19	140.65	1.3	1.76	0.49	0.28
Cu	3.67	3.51	0.96	0.43	0.34	0.79
Zn	21.61	24.8	1.15	1.12	0.46	0.41
Ga	5.88	4.44	0.76	0.63	0.37	0.59
As	6.27	12.84	2.05	0.37	0.51	1.38
Rb	30.44	24.85	0.82	1.23	0.59	0.48
Sr	12.06	29.5	2.45	0.67	0.53	0.79
Y	13.37	21.71	1.62	0.85	0.45	0.53
Zr	109.86	215.59	1.96	1.67	0.49	0.29
Nb	6.16	13.17	2.14	0.4	0.47	1.18
Mo	2.63	1	0.38	0.23	0.33	1.43
W	17.38	27.05	1.56	0.96	0.49	0.51
Pb	4.18	5.92	1.42	0.4	0.39	0.98
Th	3.54	3.96	1.12	0.38	0.35	0.92

X=arithmetic average, S=standard devistion, V=S/X
XL=X based at log10 transformed data, which is same as SL and VL
Au(ppb) data listed as being in bulk sample

Table 5-2. Spearman correlation matrix of acid insoluble residue, Mystery Zone, Mt Percy, W.A. (Data are logarithm based 10, n=192)

	Au	F	Na	Al	K	Ca	Ti	V	Cr	Mn	Fe	Ni	Cu	Zn	Ga	As	Rb	Sr	Y	Zr	Nb	Mo	W	Pb	Th
Au	1																								
F	-0 11	1.00																							
Na	0.49	-0.45	1.00																						
Al	0.11	-0.05	0.33	1.00																					
K	0.43	-0.17	0.52	0.45	1.00																				
Ca	0.47	0.01	0.52	0 30	0.65	1.00																			
Ti	-0.02	0.37	-0.10	0.13	-0.48	-0.11	1.00																		
V	0.23	0.19	0.20	0.46	0.10	0.25	0.75	1.00																	
Cr	0.00	-0.18	0.06	0.27	0.59	0.29	-0.74	-0.34	1.00																
Mn	0.11	0.22	-0 08	-0.04	-0.42	-0.03	0.72	0.45	-0.59	1.00															
Fe	0.03	0.20	-0.06	0.11	-0.33	0.02	0.71	0.54	-0.46	0.77	1.00														
Ni	-0 20	-0.06	-0.31	0.02	-0.12	-0.15	-0.17	-0.21	0.38	0.11	0.34	1.00													
Cu	0.00	0.18	-0.17	0.09	-0 21	-0.17	0.15	-0.04	-0.17	0.30	0.29	0.17	1.00												
Zn	0.21	-0.09	0.16	0.05	0.20	0.30	0.03	0.20	0.14	0.32	0.46	0.45	0.00	1.00											
Ga	0.33	-0.11	0.43	0.58	0.64	0.41	-0.02	0.41	0.14	-0.04	0.09	-0.10	-0.04	0.23	1.00										
As	0 15	0 28	-0.03	0.06	-0.30	-0.03	0.74	0.55	-0.51	0.63	0.62	-0.10	0.28	0.06	-0 04	1.00									
Rb	0.49	-0.10	0.53	0.43	0.88	0.68	-0.17	0.36	0.33	-0.12	0.03	-0.08	-0.20	0.35	0.73	-0.06	1.00								
Sr	0.42	-0.07	0.67	0.29	0.33	0.51	0.25	0.38	-0.29	0.19	0.07	-0.53	-0.03	0.01	0.44	0.22	0.44	1.00							
Y	-0.19	0.38	-0.25	0.02	-0.54	-0.21	0.79	0.47	-0.60	0.57	0.58	-0 06	0.13	-0.06	-0.18	0.60	-0.30	0.11	1.00						
Zr	0.05	0.45	-0.02	0.18	-0.36	-0.05	0.90	0.65	-0.74	0.61	0.54	-0.32	0.24	-0.09	0.09	0.67	-0.12	0.41	0.71	1.00					
Nb	0.11	0.30	0.01	0.06	-0.37	-0.07	0.84	0.59	-0.69	0.63	0.62	-0.21	0.22	0.04	0.03	0.67	-0.08	0.32	0.66	0.80	1.00				
Mo	0.04	0.24	-0.09	0.02	-0 28	-0.09	0.60	0.46	-0.46	0.49	0.45	-0.07	0 07	0.07	-0.05	0.50	-0.06	0.17	0.50	0.57	0 58	1.00			
W	0 38	0 18	0.18	0.28	0.20	0.17	0.49	0.66	-0.34	0.33	0.42	-0.19	0.06	0.27	0.50	0.42	0.45	0.32	0.21	0.50	0.47	0.41	1.00		
Pb	0.10	0.27	0.06	0.07	-0.18	0.06	0.62	0.52	-0.49	0.45	0.47	-0.21	0.10	0.14	0.10	0.47	0.06	0.31	0.46	0.56	0.53	0 38	0.46	1.00	
Th	0 16	0.17	0.12	0.10	-0.04	0.13	0.49	0.49	-0.40	0.33	0.35	-0.22	-0.03	0.09	0.20	0.34	0.16	0.37	0.30	0.50	0.42	0.36	0.49	0 38	1.00

Table 5-3. Factor score coefficient matrix, Mystery Zone (data based on acid insoluble residue)

Factor	1	2	3	4	5	6
Al	0.112	0.555	0.16	0.511	0.404	-0.315
As	0.788	-0.035	0.072	-0.05	0.13	0.108
Au	0.104	0.613	-0.046	-0.371	0.019	0.37
Ca	-0.04	0.752	0.048	-0.081	-0.105	0.29
Cr	-0.762	0.26	0.344	0.263	-0.017	0.03
Cu	0.237	-0.196	0.25	0.047	0.713	0.43
F	0.386	-0.203	0.024	0.527	-0.243	0.597
Fe	0.749	-0.02	0.542	-0.145	0.044	-0.074
Ga	0.072	0.783	0.119	0.25	0.129	-0.143
K	-0.394	0.85	0.051	0.185	-0.042	0.116
Mn	0.772	-0.108	0.3	-0.291	0.085	0.074
Mo	0.671	-0.062	0.023	-0.003	-0.191	-0.077
Na	-0.03	0.734	-0.227	-0.4	0.228	-0.186
Nb	0.873	-0.027	-0.075	-0.048	0.071	-0.001
Ni	-0.191	-0.244	0.868	-0.02	0.041	-0.108
Pb	0.681	0.111	-0.04	-0.02	-0.125	0.05
Rb	-0.061	0.906	0.165	0.094	-0.135	0.073
Sr	0.357	0.638	-0.425	-0.206	0.193	0.036
Th	0.566	0.244	-0.121	-0.003	-0.278	-0.06
Ti	0.957	-0.106	-0.026	0.069	-0.011	-0.118
V	0.733	0.433	0.068	0.225	-0.103	-0.208
W	0.594	0.48	0.092	0.13	-0.174	0.025
Y	0.769	-0.307	-0.017	0.13	-0.003	-0.126
Zn	0.109	0.313	0.721	-0.35	-0.225	0.01
Zr	0.91	-0.014	-0.197	0.159	0.105	0.035

first three factors (1, 2, and 3) are the key factors in this Mystery Zone study.

Similar results were obtained by cluster analysis. The cluster analysis was carried out by dividing the data into two groups; the first group are samples from upper level of the profile above RL 390, which consist of clay saprolite, mottled plasmic clay zone and lateritic duricrust and gravel, as well as calcareous soil; the second is from the lower levels within the saprolite zone below RL 390 m. In the shallow profile group, the first cluster (Figure 5-35) comprises the elements Al, Ni, Cr, Cu, Zn, Ga, Na, Ca, Au, F, K and Rb which are essentially related to differential wall rock alteration. The second cluster consists of Sr, W, Ti, V, Mn, Fe, As, Y, Zr, Nb, Pb, Th and Ge and are interpreted to comprise elements in weatherable minerals such as feldspar. This second cluster therefore represents weathering intensity supported by their enrichment in the uppermost part of the shallow profile. In the deeper profile of the saprolite

deeper profile of the saprolite zone, there are three clusters (Figure 5-36). The first cluster consists of Na, Rb, Au, Th, K, Ca, Zn, As, W, Al, V, Cr, Ga and Cu. These elements are enriched in the saprolite zone, which hosts the gold mineralization and related wall rock alteration. The second cluster consists of Pb, Zr, F, Sr, Y, Ti and Nb, which are depleted in the saprolite zone. The third cluster consists of Mn, Fe and Ni, which are partly enriched in the talc-chlorite and fuchsite altered ultramafic rocks. This is considered to be related to the distribution of ferromagnesian minerals in the profile (i.e. amphibole and biotite).

The following interpretation is based on the factor and cluster analyses detailed above. The data has been divided into groups which are ore/alteration and lithology related.

5.4.2 Element groups and geochemical zonation

The geochemical behavior of most elements varies with depth, with a natural geochemical subdivision of the profile into deep and shallow zones. The boundary between the two zones is variable, but generally lies at about 10–20 m below the surface and roughly corresponds to the deeper zone of saprolite and shallow zone of lateritic duricrust and clay materials. In the deep part of the profile, the distributions of most elements are ore- or lithology-related. Elements in the shallow zone have been affected by intense weathering with some elements enriched, some depleted and a few having remained relatively stable. A few elements (e.g. Al and Fe) have scattered and erratic enrichment and depletion characteristics. A small number of these elements, those that have been shown to be ore related at depth, have retained their usefulness as pathfinder elements in the shallow part of the profile.

5.4.3 Deep profile: Ore/alteration related elements

The extent of the primary dispersion of Au and other ore related elements in the wallrocks could not be determined confidently without a detailed study of the fresh rocks below the Mystery Zone, which is beyond the scope of this study. The geochemistry of the fresh bulk rock was discussed by Butt (1991). Nevertheless, the acid insoluble geochemistry broadly defined the elements that were ore related in the acid insoluble residue, so that they can be used as a guide during gold exploration.

Figure 5-35. Cluster analysis of acid insoluble residue data from the upper part of Mystery Zone

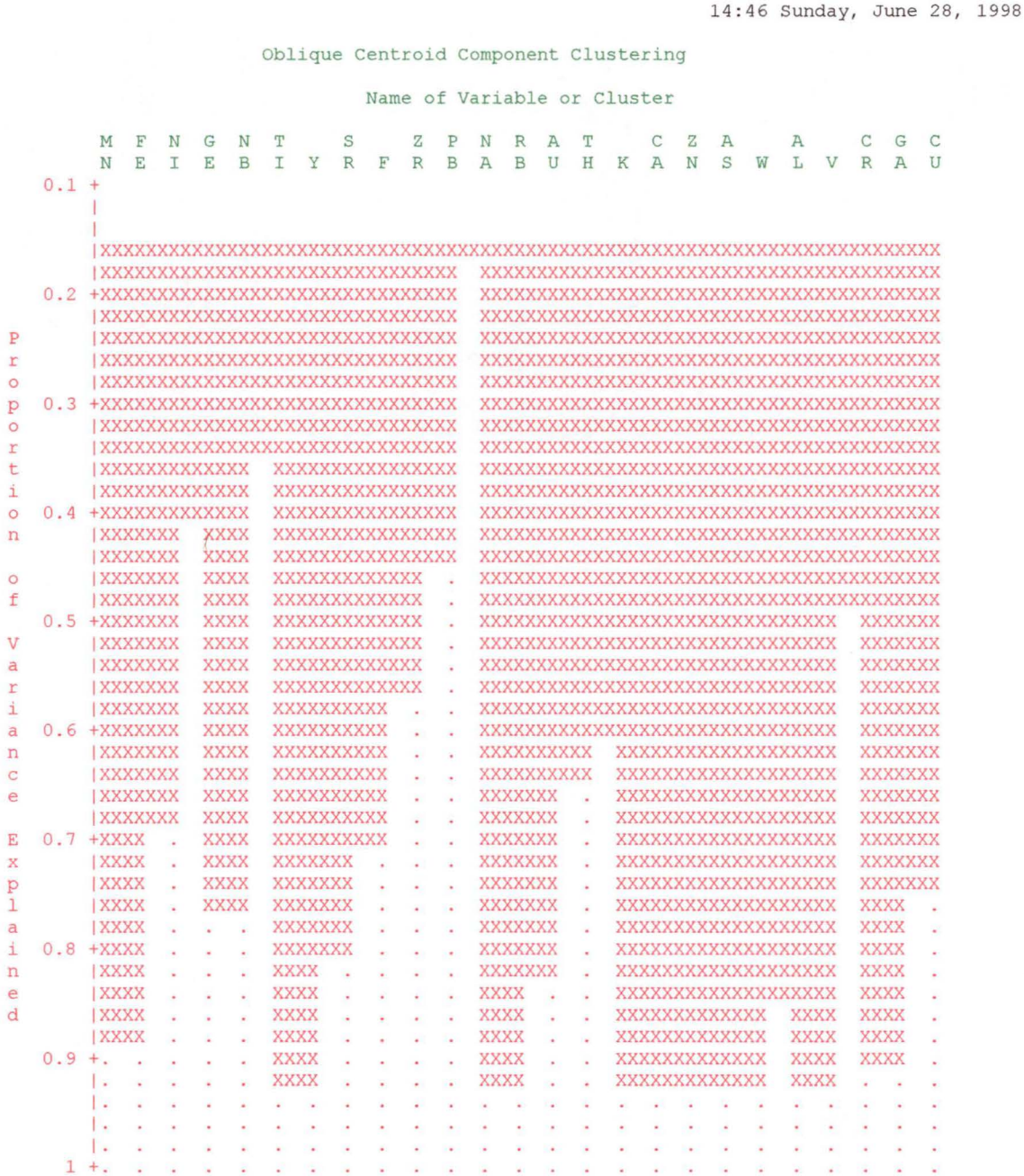

Figure 5-36. Cluster analysis of acid insoluble residue data from the upper part of Mystery zone

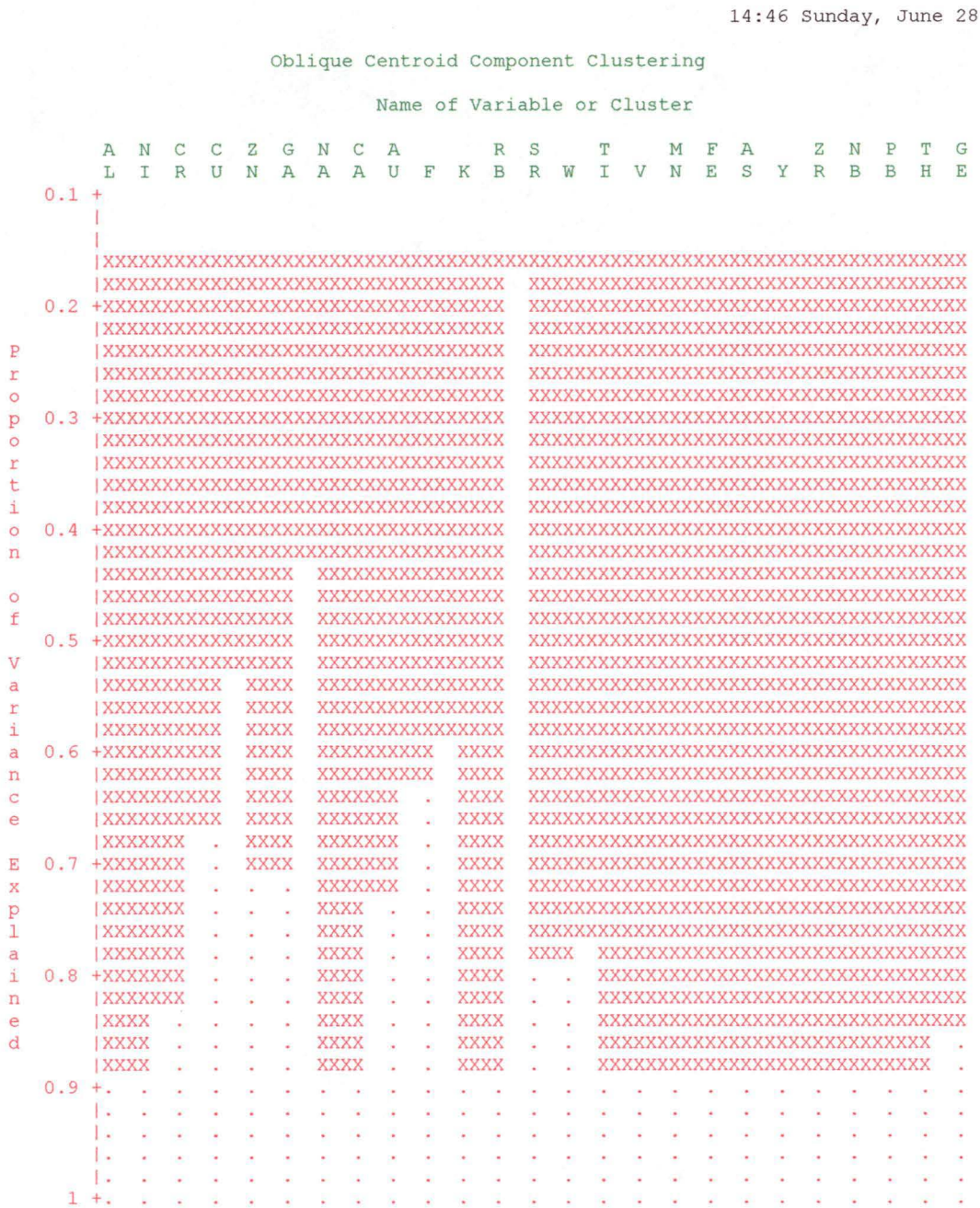

Gold, which defines the mineralization, is present throughout the saprolite in abundances broadly similar to those observed in fresh rock (Butt, 1998). Some Au concentration and possible lateral dispersion, particularly in the clay saprolite, enhances the weathered expression of the primary Au mineralization. The distributions of the other ore-associated elements mentioned in the statistical section above, generally have good consistency in the saprolite, due to similar mobilization trends during weathering. Concentrations of Al, Rb, K, Zn, W, Ga, V and Ca in acid insoluble residue are enriched in the mineralized porphyries and fuchsitic altered ultramafic rocks, whilst high Cr concentrations occur in the fuchsitic altered ultramafic rocks, and a Cu concentration occurs over the porphyries and talc-chlorite ultramafic rocks.

Aluminium is present in alumino-silicate minerals (e.g. mica, feldspar, etc.) in the acid insoluble residue. The 5–6% content of Al in the deeper part of the porphyries is slightly lower than that expected in fresh porphyries (Johannsen, 1958). This result differs from the results obtained by Butt (1991), who noted that strong kaolinization in the mid and lower saprolite was accompanied by strong enrichment in Al (up to 11%) in the porphyries. The acid insoluble residue of the fuchsitic ultramafic contains 3–4 % Al, in contrast to the biotite talc ultramafics (<1%). Unexpectedly, substantial Al concentrations occur in the subsurface, particularly above the ultramafics. These enrichments may be due to some residual kaolinite trapped in secondary quartz.

High K contents (1–2%) are present in the porphyries and fuchsite altered ultramafics. According to the microscope observation, the K distribution is mainly controlled by the presence of muscovite as an alteration product in the porphyries and fuchsite as an alteration product in the ultramafics rather than the contribution by feldspar. A further influence is likely remnants of primary potash feldspars in the porphyries. The K halo is more extensive than the Au dispersion. No bulk rock K data are available for section 15850N, however Butt (1991) found a similar distribution pattern in section 15900N with the exception that the K "anomaly" does reach the surface.

The Rb distribution is similar to K and is largely controlled by the occurrence of micas, and probably feldspar in the porphyries. Its distribution pattern is essentially

the same as that of the bulk geochemistry, indicating that the weathering does not significantly affect the character of Rb. High Rb concentrations occur in porphyries and in particular fuchsitic ultramafic rocks. The Rb distribution extends vertically into the lateritic gravel, representing an increase in the abundance of muscovite. The surface expression of Rb is more pronounced than that of K.

The ratios of Rb/K and Rb/Al also used in this study and because of their different concentrations, these ratios are multiplied by 10^3 terms. The Rb/K ratio has high values near the surface where the secondary Au is enriched (Figure 5-37). Highly anomalous values occur over the regolith profile of the altered fuchsitic ultramafic rocks, from lateritic duricrust to the bottom of the saprolite, and define the muscovite alteration zone. In contrast, the ratios in the porphyries and unaltered fuchsitic ultramafic rocks are generally low. There are only a few places which are an exception, probably due to the inhomogeneity of the samples. The high Rb/K values in biotite-talc ultramafic rocks, indicate the occurrence of Rb in biotite and implies that biotite could not be leached out in the concentrated sulphuric acid treatment. Rb is associated with K most likely because of the differentiation systematics where Rb is expected to be concentrated relative to K in the "felsic" fraction. However, during weathering, K^+ is either depleted in the formation of soil K minerals (such as illite), absorbed on other clays, or removed by fluid migration. These fractions of K have been removed from the analyzed residue by strong acid digestion. The acid insoluble K is likely derived from some K-mineral related to the alteration. The Rb concentration was related to K only when illite came from weathered micas and feldspars. Reynolds (1963) reported that sedimentary rocks that contain detrital feldspars or micas will show K/Rb ratios that are inherited from the source rocks. As such, the ratio of Rb and K can probably be used to predict the abundance of sericite and/or K-feldspars in the lower profile.

The Rb/Al ratio is high in the lateritic duricrust and in both the porphyries and ultramafic rocks (Figure 5-38), and may be a good indicator of Au mineralization. The average of Rb/Al values in the non-mineralized mottled clay zone down to the saprolite in talc-chlorite and talc altered ultramafic rocks is lower ($<0.4 \times 10^{-3}$) compared with that of the mineralized zone in the porphyries and fuchsitic ultramafic rocks, where it is at least three times greater. The mechanics of the Rb and Al ratio was given in section 5-5. At Mt. Percy, Rb/Al ratio can be used to outline not only

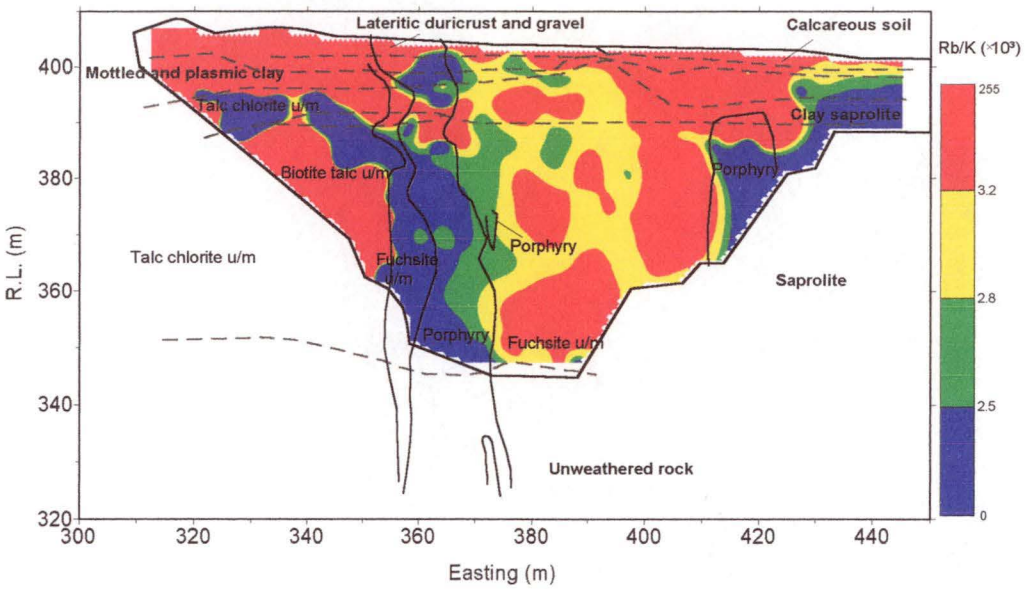

Figure 5-37. Rb/K distribution in the acid insoluble residue at 15850N, Mystery Zone, Mt. Percy, W.A.

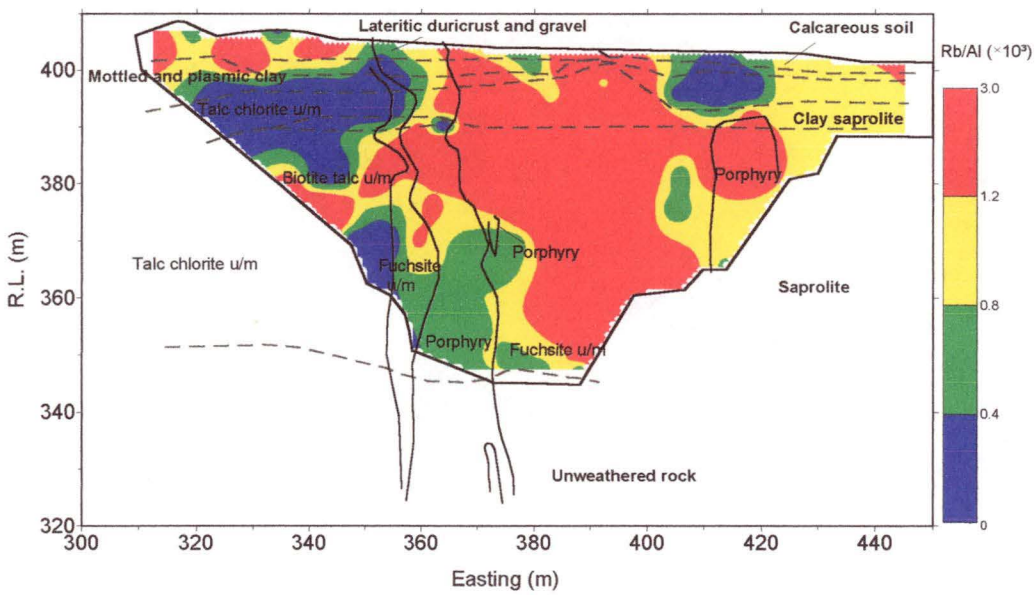

Figure 5-38. Rb/Al distribution in the acid insoluble residue at 15850N, Mystery Zone, Mt. Percy, W.A.

the mineralization at depth, but also the surface enrichment, presumably because of the presence of a Rb rock muscovite (van Moort et al., 1995).

Copper is probably hosted in ferromagnesian silicate minerals as it shows a strong positive correlation with Fe and Mn. The high concentrations of Cu in porphyries have an irregular distribution. The Cu content in fuchsitic ultramafic rocks is very low. It is less than 3 ppm over the entire regolith profile, except for a few scattered higher values (9–10 ppm Cu). Some extremely high Cu concentrations occur above the clay saprolite zone from 410E to 430E and relate to the underlying porphyry unit. In general Cu appears to be concentrated in the surface material above the porphyries. In the talc dominated ultramafic rocks, the distribution pattern indicates that it is weakly leached from the lateritic duricrust, with a patchy distribution in the clay-rich mottled zone. It is not clear why Cu is absent from the fuchsitic ultramafic rocks.

Zinc has a slightly upward increasing trend across the weathering profile and there is a strong correlation with Fe and Mn, particularly near surface. There is a Zn depletion zone from the clay saprolite to the upper part of the saprolite in talc-chlorite ultramafic rocks, and from the middle to the upper part of the saprolite in fuchsitic altered ultramafic rocks. The concentration of Zn in porphyries is relatively low (<20 ppm) and remains constant throughout the regolith profile. The distribution of Zn is rather erratic. The distributions of Zn and Cu are independent of each other, so they do not share a common host mineral with similar secondary dispersion characteristics.

The distribution of W in the acid insoluble residue is similar to that of the bulk geochemistry, having a somewhat more restricted occurrence to the ore zones and immediate surroundings. Tungsten is consistently enriched throughout the primary mineralization with concentrations of 11–40 ppm over the porphyries and values between 5–27 ppm in the fuchsitic altered ultramafic rocks, compared to < 2 ppm in the unmineralized talc-chlorite ultramafic rocks. The W distribution is also similar to the Mn and Fe surface enrichments, suggesting some dispersion during weathering. Such dispersion is clear in the upper part of the profile over the talc-chlorite altered ultramafic rocks, which contain over 100 ppm W in the lateritic duricrust and 6–20 ppm in the mottled clay zone from the contact with the fuchsitic rocks and the porphyry. The continuation of a W trend throughout the regolith potentially results

from the occurrence of the W as residual scheelite (Butt, 1991). Tungsten is potentially the best indicator element for Au.

Gallium distribution in the acid insoluble residue is similar to the that of Al and W, indicating Ga is either concentrated in feldspars, amphiboles and micas, substituting for Al or hosted by the same mineral as W. Ga contents are high in the aluminous porphyritic rocks (usually greater than 10 ppm). Its content in the fuchsitic altered ultramafic is 4–10 ppm beneath the lateritic duricrust, compared to < 2 ppm in the talc altered ultramafic rocks. This distribution suggests that Ga is associated with muscovite-alteration related to the fuchsitic rocks and porphyries. Its low concentration in the talc ultramafic rocks indicates that it originally occurred in chlorite as a substitution for Al, with the chlorite destroyed in the acid treatment. Figure 5-39 illustrates the correlation between Ga and Al, as well as Ga and K, reflecting the close coherence of Ga with Al and K in most geochemical processes. This implies Ga can be used to outline the alteration related to the gold mineralization together with Al and K. This use of the acid insoluble residue as a sample medium is significant as Ga cannot be used as an indicator element for Au in bulk rock geochemistry. Figure 5-40 gives the Ga distribution in the bulk geochemistry (Butt, 1991). Ga concentrations in the bulk rock chemical data gradually increase upwards, with a marked enrichment in the clay-rich horizons, especially in the talc-chlorite ultramafic rocks.

The V distribution in the deeper part of the cross section is similar to that of Al, K, Rb, Ga and W. The V halo is distinct and correlates with the fuchsite ultramafic rocks and porphyries in the deeper profile indicating mica alteration. This character differs significantly from the bulk geochemistry. Butt (1991) stated that V is consistent in all geological units and presumed V to be hosted by the same minerals as Ti. In the acid insoluble residue of the deeper profile, V is mainly contributed to by V in muscovite, indicating its relationship with muscovite alteration.

The Cr distribution in lateritic regolith is strongly influenced by its host mineral in unweathered rocks. In many ultramafic rocks, Cr is hosted by chromite, which is generally resistant to weathering. At Mt. Percy, however, chromite is uncommon and its distribution in bulk chemistry and acid insoluble residue is very different. In bulk geochemistry, Cr is present in ultramafic rocks and independent of the degree

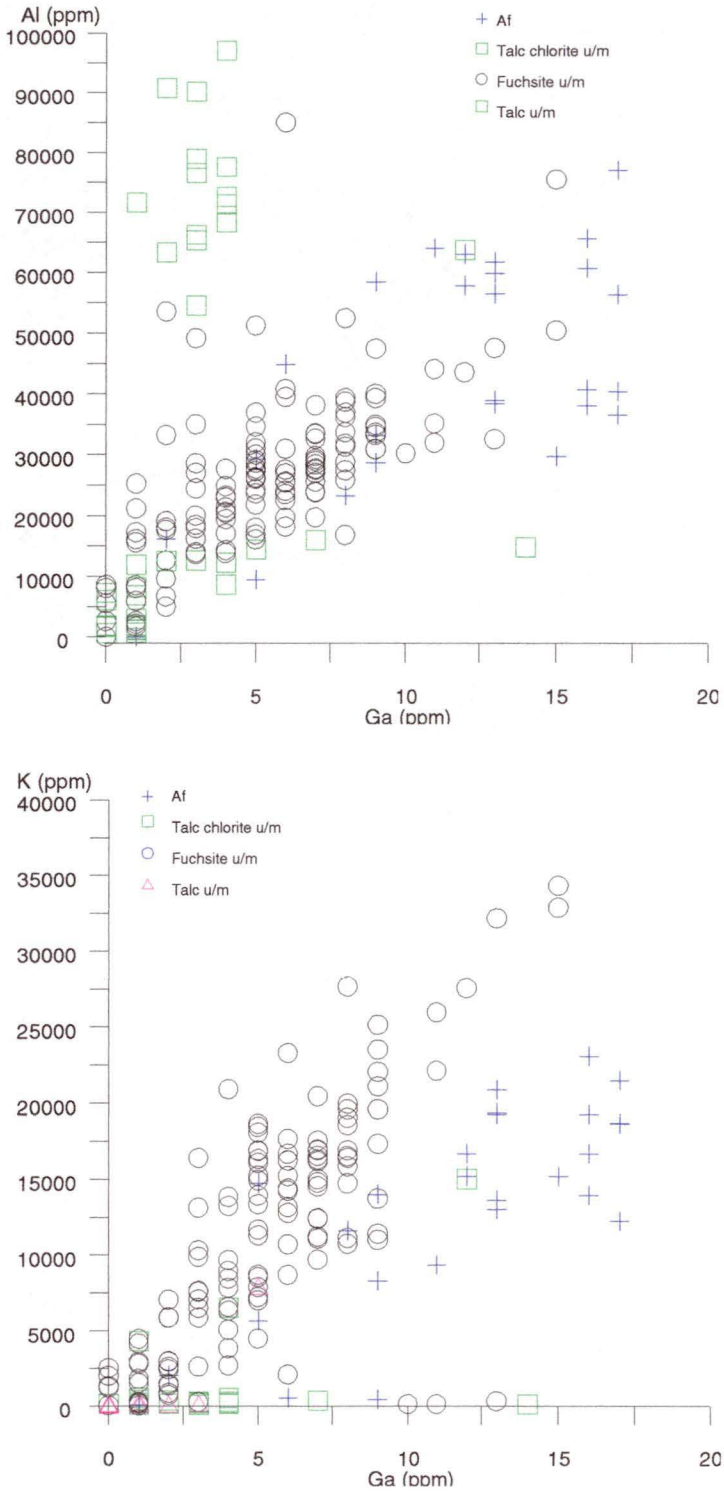

Figure 5-39. Scatter diagrams illustrating the correlation between Ga and Al, Ga and K of the acid insoluble residue in the regolith profile at Mystery Zone, Mt. Percy, W.A.

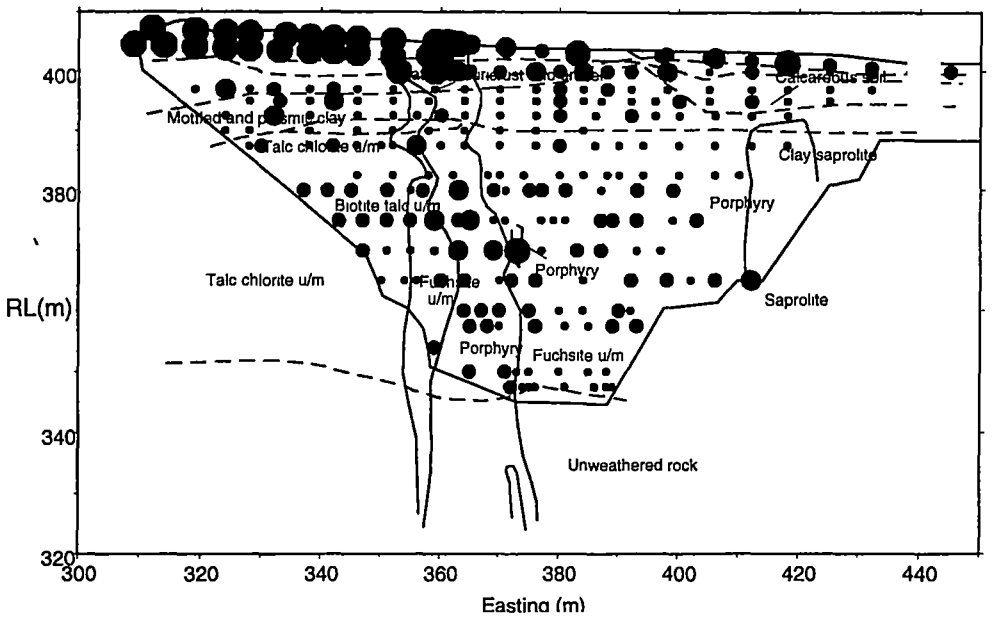

Figure 5-40. Ga distribution in bulk geochemistry at 15850N, Mystery Zone, Mt. Percy, W.A (after Butt, 1991).

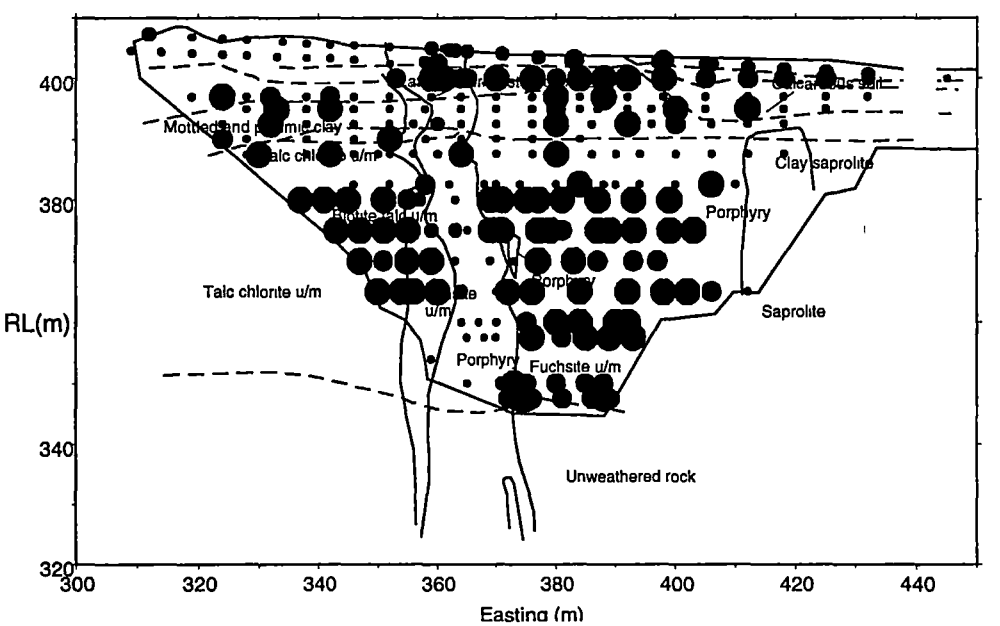

Figure 5-41. Cr distribution in bulk geochemistry at 15850N, Mystery Zone, Mt. Percy, W.A. (after Butt, 1991)

of weathering, although some depletion can be observed in the lateritic gravels above the talc-chlorite altered ultramafics (Figure 5-41).

Butt (1991) explained that Cr is present in ferromagnesian minerals, principally chlorite in talc dominated ultramafic rocks. While chlorite and talc are less abundant in the fuchsitic ultramafic rocks, but the fuchsite itself is a host to some Cr. In this study, because chlorite is slightly soluble in HCl and easily soluble in H_2SO_4 (Tröger, 1979), its abundance is reduced to a few hundred ppm in the talc-chlorite and biotite-chlorite altered ultramafic rocks, with levels of a few ppm in the mottled clay and clay saprolite. Because muscovite is insoluble in these acids, the Cr distribution of the residue does not increase toward the upper part of the profile, like that of the bulk geochemistry, but is enriched vertically from the bottom of the regolith profile up to the surface. This Cr pattern is best explained as reflecting the fuchsitic (chromian muscovite) alteration which is related to mineralization. It is not certain whether fuchsite is the principal Cr host mineral in the unweathered rocks, but residual fuchsite is significant in the clay-rich and ferruginous upper horizons of the regolith, where a close correlation between the Cr and K contents ($r = 0.83$, Figure 5-42) exists. Both Cr and K have enrichment in fuchsite ultramafic rocks.

Within the fuchsite altered ultramafic rocks and porphyries, the average concentration of V is much higher (149 ppm) than that of talc altered ultramafic rocks (49 ppm). This reflects V muscovite in the fuchsitic ultramafic rocks. The high concentration of V in fuchsitic ultramafic and porphyries can provide indications of gold mineralization related muscovite alteration (van Moort et al., 1995).

Na in the bulk rock geochemistry is only present in significant concentration in the fresh rocks underneath the regolith and in the lower parts of the porphyries and fuchsitic ultramafics. The same distribution pattern is observed in the acid insoluble residue and is related to weathering processes. Sodium is less mobile than calcium as sodium feldspars are more resistant to weathering than calcium-rich feldspar which host Ca. Surprisingly, Na is enriched near surface, particularly in the calcareous soils. This enrichment pattern is possibly governed by inclusions in secondary chalcedony.

The data of Butt (1991) indicated that Ca is depleted throughout the regolith, except

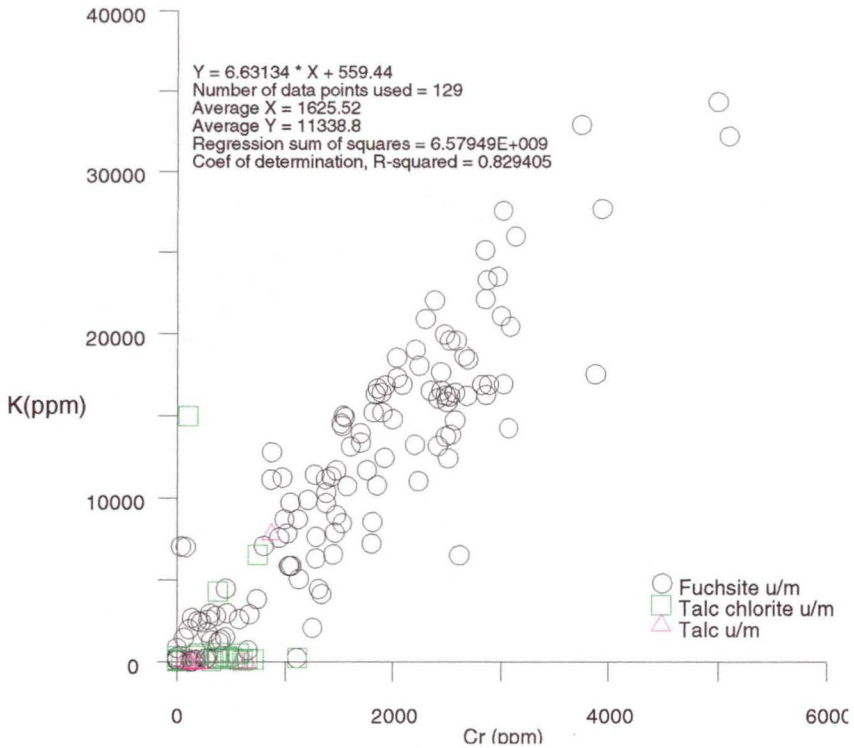

Figure 5-42. Plot illustrating the correlation between K and Cr of the acid insoluble residue in the ultramafic rocks

in a thin surface veneer of calcareous soils and part of the lateritic duricrust. The regolith Ca values are low, particularly in the porphyries. In the acid insoluble residue, the porphyries and fuchsite altered ultramafics have the higher Ca enrichment. There is a positive correlation between the contents of the Ca and Au. Presumably the Ca is locked into the muscovite, or is alternatively trapped in carbonate inclusions.

Primary mineralization at Mt. Percy is associated with the fuchsite-carbonate alteration of the ultramafic rocks and the porphyries which intrude them. The alteration zone is typically pyritic (Butt, 1991), and in addition to Au, is characterized by high abundances of S, W, Ga and Ge in the acid insoluble residue. There is, however, no close correlation between Au and these elements within the alteration zone itself.

The distribution of Mo is simple because of its low and relatively constant background concentrations in the regolith and its general immobility under earth surface conditions. It is only enriched in the lateritic duricrust and mottled clay zone with a heterogeneous distribution. It is not evident what mineral hosts Mo.

The distribution of Sr in the acid insoluble residue is similar to that of the bulk

geochemistry. In the regolith, Sr is strongly leached even from the lowest horizon of the regolith overlying ultramafic rocks. Concentrations of less than 5 ppm Sr occur throughout the saprolite to mottled zones overlying ultramafic units. Over the porphyries, however, Sr is retained at concentrations of over 100 ppm in the lower saprolite, and reduced from 11–20 ppm upwards. The distribution of Sr corresponds to the presence of albite (Butt, 1991), which is relatively resistant to weathering. Strontium is strongly enriched in the calcareous soils, lateritic duricrust and gravel, with similar patterns to Ca and Na. This is probably the result of carbonate inclusions in secondary chalcedony.

5.4.4 Deep profile: Lithology-related elements

The elements As, F, Fe, Mn, V, W, Ti, Zr, Nb and Y classified in factor 2 are immobile and/or lithology related. Some of them, such as Ti, Zr, Nb and Y are clearly related to lithology and immobile in the acid insoluble residue, indicating that resistate and heavy minerals not only survive the extensive chemical leaching in deeply weathered terrains (Andrew and McQueen, 1994), but also remain in the residue even after strong acid treatment. Their enrichment is not related to surface enrichment of zircon and titania polymorphs.

Titanium has a steady increase upwards through the profile both in acid insoluble residue and bulk chemistry, because it has restricted mobility during weathering and tends to accumulate residually in the regolith. The Ti content of the talc chlorite ultramafic (mean 5.1% Ti) is much higher than that of other rocks, viz. 1.5% Ti in the porphyries, 1.3% in the fuchsite ultramafic rocks and only 0.6% in talc ultramafic rocks. Ti is strongly concentrated in the lateritic duricrusts with a number of samples containing over 20% Ti. In the bulk geochemistry, Ti is strongly concentrated relative to Zr so that lithological discrimination based on Ti-Zr plots is not possible (Butt, 1991). In this study, the ratio of Ti/Zr remains relatively constant in different geological units, even under conditions of intense chemical weathering, except for the talc-carbonate altered ultramafic rocks. Table 5-4 shows the average Ti, Zr and V in the geological units at Mystery Zone. The Ti-Zr geochemistry of acid insoluble residue broadly reflects the different lithologies (Figure 5-43). In Figure 5-43, talc dominated ultramafic, fuchsite carbonate ultramafic rocks and porphyry are also distinguished on the basis of their Ti-Zr contents.

Although the cluster analysis shows that V in deep profile is wall rock alteration

related, the concentration of V also exhibits a good correlation with Mn, Ti, Zr, Nb, Y and Fe. This means it has the ability to discriminate different lithologies. Within the mottled clay zone and lateritic duricrust, V has a very similar distribution to Ti, with both elements concentrated relative to Zr, particularly over the talc-chlorite altered ultramafic rocks. This indicates that the V resides in titanomagnetite, which is often resistant and can carry over thousands ppm of vanadium. It is evident from the pairs of V and Ti within the regolith (Figure 5-44) that the acid insoluble residue Ti and V have a possibility to be used to classify different lithologies, like Ti and Zr (Figure 5-43).

The distribution of Zr and Nb is similar, except for the enrichment of Zr in porphyries.

Table 5-4. Average values of Ti, Zr and V in different geological units

Unit	Ti	Zr	V
Porphyry (Af)	14991	166	291
Talc-chlorite carbonate ultramafic (As)	50993	226	529
Fuchsite-carbonate ultramafic rocks (Asf)	13120	81	231
Talc-carbonate ultramafic rocks (Ast)	6364	40	82

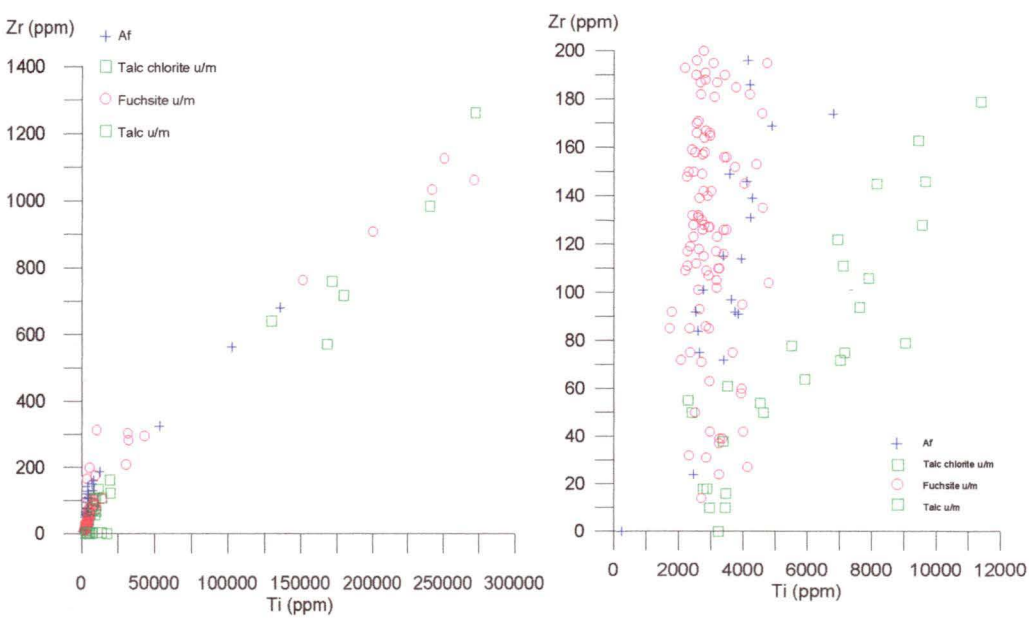

Figure 5-43. Ti-Zr plots illustrating their close correlation and concentration in the regolith and reasonable discrimination between difference lithologies

Both elements increase upwards through the regolith, are elevated over the ultramafic rocks, and are enriched in the lateritic duricrusts and soils, with even greater enrichment in the mottled and plasmic clay zone over the talc-chlorite ultramafic rocks. The location of porphyries is readily defined from the distribution of Zr in the saprolite. Geological discrimination is, however, not clear in the clay-rich zone from the talc-chlorite ultramafic rocks. Although the concentrations of Zr and V correlate well (r = 0.96, Figure 5-45), the discrimination between different lithologies is poorer than that of Ti vs Zr and Ti vs V. Despite this, the plots of Zr vs K broadly distinguish the different ultramafic rocks (Figure 5-46) due to the abundance of K in fuchsitic rocks. Because of the poor detection limit of Th by PIXE, its distribution is not discussed in detail.

One of the most significant features about the distribution of the elements mentioned above, is their accumulation in the lateritic duricrust, particularly within talc-chlorite altered rocks. The elements all have a positive correlation with Fe, Mn, V and W (Table 5-5) and the highest concentrations of both sets of elements are present in the massive hard protective shell (cuirass) on these rocks in the studied section. Butt (1991) explained this to be the result of the trace element alteration composition of the felsic lithologies. The porphyries are indeed the probable source of the immobile elements, which form a residual accumulation.

Yttrium is very much like Ti. It is more concentrated in the talc and talc-chlorite

Table 5-5. The Spearman correlation table among the immobile elements and some other elements (n=192)

	Zr	Nb	Th	Y	Ti	V	W	Mn	Fe
Zr	1								
Nb	0.97	1							
Th	0.73	0.73	1						
Y	0.95	0.95	0.7	1					
Ti	0.98	0.97	0.7	0.96	1				
V	0.95	0.94	0.74	0.91	0.96	1			
W	0.91	0.89	0.51	0.86	0.92	0.88	1		
Mn	0.92	0.92	0.62	0.82	0.94	0.93	0.82	1	
Fe	0.85	0.89	0.66	0.79	0.88	0.89	0.79	0.9	1

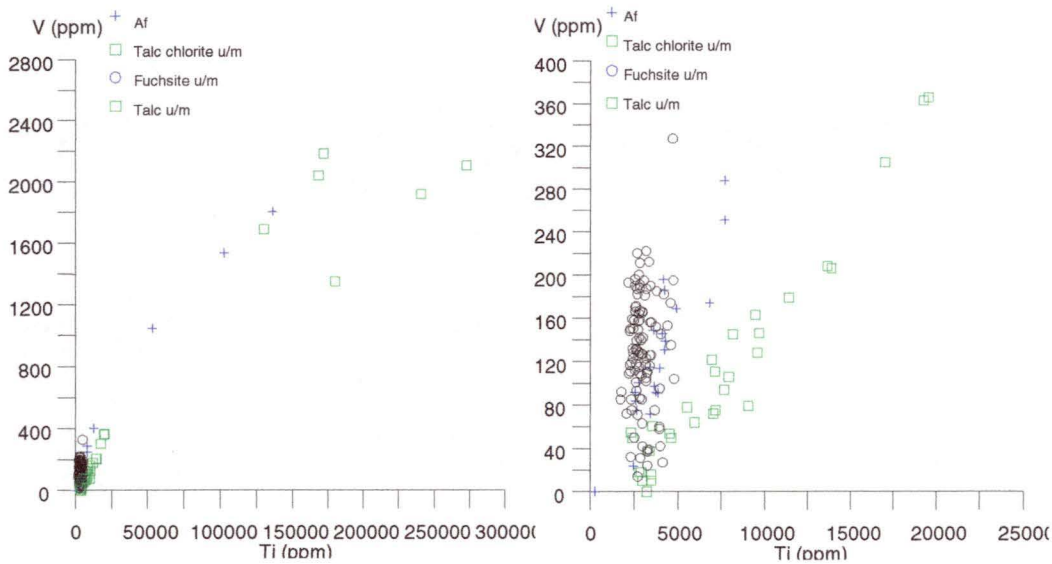

Figure 5-44. Ti-V plots illustrating their close correlation and concentration in the regolith and the discriminaiton between different lithologies

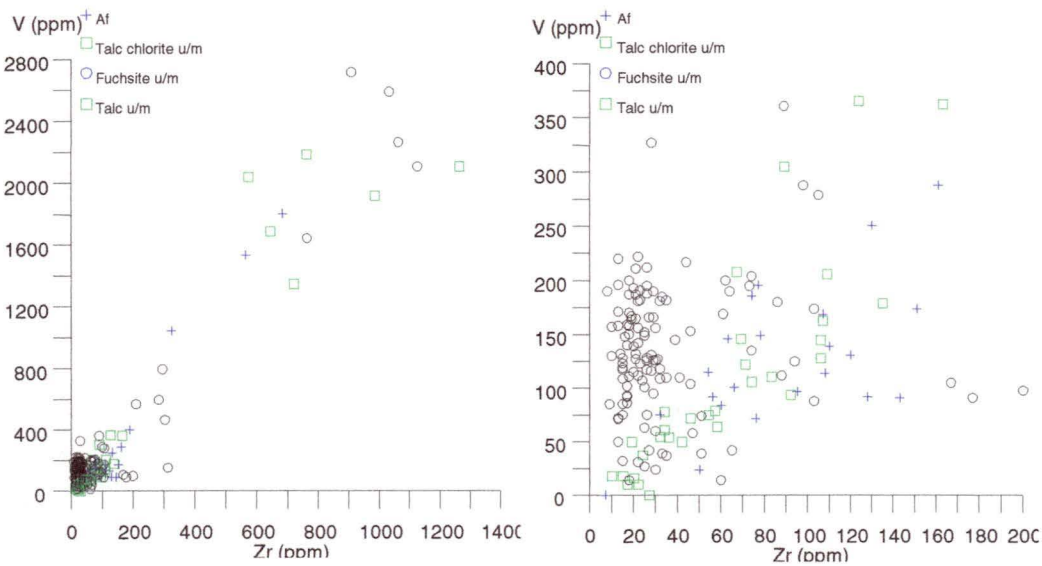

Figure 5-45. Zr-V plots of the acid inoluble residue illustrating their close correlation and concentration in the regolith and the poor discrimination between different lithologies

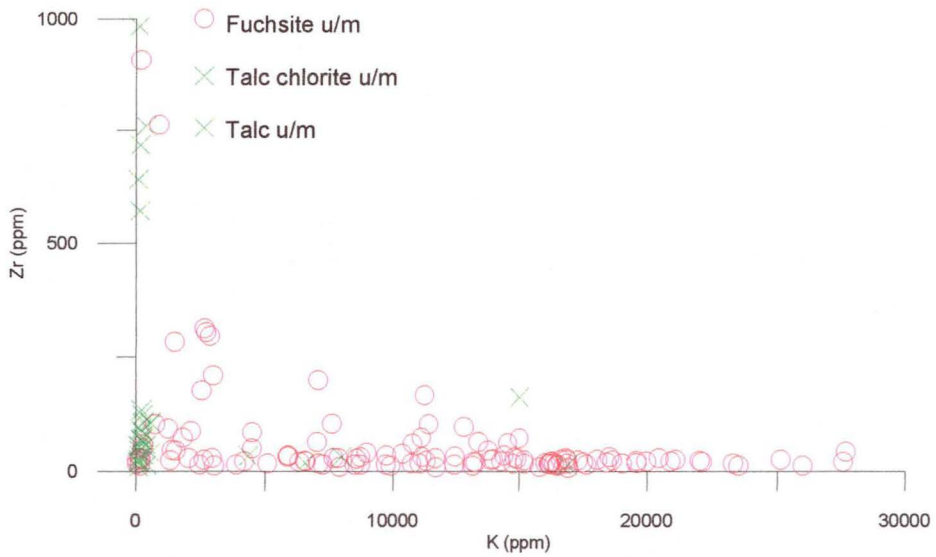

Figure 5-46. Zr-K plots illustrating the discrimination between fuchsite ultramafic rocks and talc dominated ultramafic rocks

ultramafic rocks, particularly over the mottled clay and lateritic duricrust. It is probably hosted in rutile, but is also a component of biotite, amphibole and other ferromagnesian minerals (Wedepohl, 1978). The discrimination between the different ultramafic rocks is maintained in the saprolite below R.L. 390. The distribution of Y in the porphyries and fuchsitic ultramafic rocks is sporadic, likely caused by lesser dispersion due to the heavier character of rare earth elements. The behaviour of the Y in lateritic environments is not well understood. Nevertheless, the enrichment of Y in the acid insoluble residue of biotite-talc altered ultramafic rocks gives evidence that it is not immobile during weathering.

The Pb abundance is very low in the regolith, especially after acid treatment, and is generally less than 3 ppm. Some scattered high values (from 5 ppm to 12 ppm) occur in the profile. Unlike the bulk chemistry, Pb is strongly concentrated in the lateritic duricrust and mottled clay zone, particularly over the talc-chlorite altered ultramafic rocks. Its distribution correlates well with Ti, V, Mn, Fe and As, indicating its related immobile character.

In the bulk chemical analyses, Fe is higher in the biotite-talc ultramafics and in some fuchsitic ultramafics. It is enriched in the near surface over all lithologies except over the fuchsite ultramafics. The same patterns are present in the acid insoluble residues of the porphyries (0.1–0.3% Fe), biotite-talc ultramafics (0.3–2%), fuchsite ultramafic

(0.3–2) and in the lateritic duricrust and gravel, mottled zone plasmic clay (0.8–8%), above the porphyries and in the calcareous soils (0.8–21%). There is a high positive correlation between Fe and Mn in the surface material, probably caused by the coexistence of Fe and Mn oxide-hydroxide inclusions in secondary chalcedony.

The distribution of Mn in the acid insoluble residue has an apposing trend to the bulk geochemistry. Manganese is similar to the patterns of Fe in the regolith profile. Above the mottled clay zone, Mn has higher concentrations in talc-chlorite ultramafic rocks and porphyry than in fuchsitic ultramafic rocks. Manganese is strongly depleted in the clay saprolite to saprolite with a few slightly high scattered concentrations in the saprolite. The similarity between the distributions of Mn and Fe implies that both metals are hosted by the same primary minerals (i.e., ferromagnesian minerals) occurring initially as diffuse stains of secondary Fe oxides and subsequently as discrete segregations. They are released together on weathering.

Ni is a typical transition element associated with primary ferromagnesian minerals like olivine and augite, or serpentine derived from these. It substitutes readily for Mg. Not surprisingly, the talc-chlorite, talc-biotitic and fuchsite altered ultramafics all have elevated Ni contents in comparison to the porphyries. Nickel correlates well with Cu and Zn, as it substitutes for ferrous iron. Surprisingly Ni is not depleted in the acid insoluble residue at the top of the regolith, except near surface. It is assumed that the Ni occurs as nickeliferous inclusions substituting in chalcedony (Frondel, 1962).

5.4.5 Shallow profile: Pathfinder elements

There is a widespread zone of Au enrichment close to the surface, within the lateritic duricrust and the overlying soil. A leached and depleted zone (mostly <100 ppb) Au), 5–10 m thick is present just beneath the lateritic duricrust and gravels (below about 2–4 m). Sporadic concentrations of Au indicate the occurrence of quartz veins, in which Au has been protected from weathering. The position of the underlying primary mineralization cannot be predicted from the supergene Au distribution.

Arsenic near the surface has two different enrichment areas. One is above the deep

Au mineralization and As values range from 3–30 ppm. This enrichment is proximal to the primary Au mineralization. The As enrichment zone at the west side of the profile is greater than 30 ppm, which is larger than that observed on the eastern side. The reason for this is not clear. Although the distribution of As in the shallow part of the profile is erratic, high As (3–30 ppm) is found overlying Au mineralized zones.

Vanadium is anomalous in the upper 10–20 m of the profile. Although there is a lack of continuity between V anomalies in the porphyry and the upper part of the saprolite, this distribution pattern suggests that V is a good pathfinder element near the surface.

Tungsten has a broad enrichment (>6 ppm) and is locally enriched to more than 20 ppm. Some apparent strong W concentrations continue from the surface down into the mineralized porphyries and fuchsite ultramafic rocks. It is also a useful pathfinder at shallow to moderate depth.

Gallium near the surface has background abundances (1–4 ppm) in the upper part of the porphyries and fuchsitic altered ultramafic rocks, suggestive of extensive leaching, despite a weak anomaly (>6 ppm) above the deeper Au mineralization. At a depth of 15 m (below RL 400), Ga appears to be weakly enriched (4–10 ppm), though, again, most of these enrichments (6–18 ppm) are near the mineralization. At the western side of the profile, Ga also reflects the Au surface enrichment. As a result, Ga is considered a good pathfinder element, particularly below depths of about 10 m.

Chromium has a local enrichment (>500 ppm) in the upper part of the fuchsitic ultramafic rock, which extends into the deeper Au mineralization, but it is depleted in the porphyries. This enrichment may be due to the fuchsitic alteration which although associated with Au mineralization is not related to the primary mineralization itself.

Zinc occurs in moderate concentrations (>12 ppm) around the mineralization, except in porphyries and a similar distribution is observed in the upper 10 m of the profile. As Zn has a few scattered high values in the unmineralized biotite-talc ultramafic rocks, it may have some potential as a pathfinder element.

Rubidium, together with Al and K, appears to be weakly to moderately enriched in a horizon in the upper 15 m of the profile, but Al (<2%) is depleted in most of the upper 5–10 m of the profile. Higher K (<0.7%) only occurs in the porphyries and fuchsite ultramafic rocks with the mineralization underneath. These three elements are good indicators of alteration associated with Au mineralization.

All the Ge concentrations are at or above the 2 ppm detection limit. They are similar to those of Ga, with the exception of low values in the porphyries (<2 ppm). Although there is some locally erratic enrichment (6–15 ppm) in the upper 10–20 m of the profile, the data from this study does not clearly indicate the use of Ge as a near surface pathfinder, due to its low abundance in porphyries and generally widespread low concentrations. Unlike the bulk geochemistry, high Ge concentration in the regolith is associated with the fuchsitic altered ultramafic rocks and persists into the lateritic duricrust or calcareous soil. Ge is also enriched in the lateritic gravel and mottled zone over the talc-chlorite alteration zone, probably due to similar reasons as those for Ga. In general the content of Ge is very low.

5.4.6 Shallow profile: Enriched elements

The upper part of the profile is generally enriched in the major elements Fe and Al, except for some minor Al depletion in the top 5 m. The upper part of the profile in the acid insoluble residue also shows enrichment in Zr, Ti, Nb, Th, Na, Sr, Ca and V. Zirconium, Ti and Nb are more concentrated in the top 5 to 15 m of the profile, presumably in resistate minerals. The behavior of Th in lateritic environments is not well understood (Butt, 1991). Because the concentration factor and distribution pattern is similar between Zr and Ti, their concentrations in resistate minerals must control their contribution. Sodium, Sr and Ca represent carbonate inclusions in secondary chert. Vanadium is surface enriched like Zr and Ti, but also occurs at depth in the porphyries and fuchsite altered ultramafics. The surface enrichment of V is probably caused by accumulation of titanium oxides and the V-rich muscovite associated with the mineralization.

Considerable, but localized, surface enrichment of Mn, As, Pb, Mo and Fe occurs mainly in the mottled and plasmic clay and overlying duricrust. These concentrations are an expression of Fe-Mn minerals incompletely removed by the acid treatment.

5.5 MULTI-ELEMENT INDICES DISTRIBUTION

It has been discussed extensively by Beus and Grigorian (1977) that well constrained geochemical halos can be identified around ore bodies if a group of indicator elements are combined. As the concentration of some useful indicator elements in the acid insoluble residue are low at Mt. Percy, combinations of these elements can be used to reduce the analytical errors and contribute significantly to the reliability of their interpretation. Considering that some elements are below the detection limit and have a zero value concentration, the additive composite method has been generally used to avoid multiplication by zero when determining a multiplicative composite index. Although an arbitrary half detection limit could be used instead of zero values in the multiplication, the additive method is preferred in this study due to the considerably lower contents of some potentially interesting elements such as As, Ge and Mo. In contrast, the multiplication of Al, K and Rb can be applied as they have satisfactory sensitivities to the analytical technique. The multiplicative halo method is less time consuming compared to the additive method because it eliminates the necessity of determining the background contents of each indicator element and normalizing the values of their concentration in all the chosen samples.

Figure 5-47 shows the multiplicative halo of Al x K x Rb. The highest index values occur in the alteration zone from the bottom to the surface of the profile. The effect of the secondary surface enrichment of Au mineralization is removed. Al x K x Rb can be used to precisely define the alteration zone in the vertical section without losing any surface information from the acid insoluble residue. Although the grouping is probably biased towards Al because minor variations in Al will swamp much greater percentage variation in K and Rb, the high Al x K x Rb values outline the sericite alteration zone better than the individual element, which in turn defines the Au mineralization

Figure 5-48 shows the additive halos of Ga+Ge. It is easy to see that the additive halo is larger and more pronounced than either of the individual halos of these elements. The halo exhibits vertical zonality in the saprolite, defining the Au mineralization zone. In the upper portion of the cross section, the halo of Ga+Ge has a broad distribution and tends to indicate near surface Au enrichment.

Figure 5-49 illustrates the additive halo of As+W+Mo. The distribution pattern of As+W+Mo is similar to that of Ga+Ge, but is more pronounced above the clay saprolite zone. The additive values of As+W+Mo yield a wide anomalous zone around the Au mineralization, whereas the halos of each of the individual elements are weaker and seldom extend beyond the metalliferous zone.

Figure 5-50 illustrates the additive halos of As+W+Mo+Ga+Ge. It is even more pronounced than the former two additive halos. The anomaly occupies the whole regolith profile of the porphyries and the ultramafic where the primary Au mineralization occurs, and extends to the top of talc-chlorite altered ultramafic, in the zone of secondary Au enrichment.

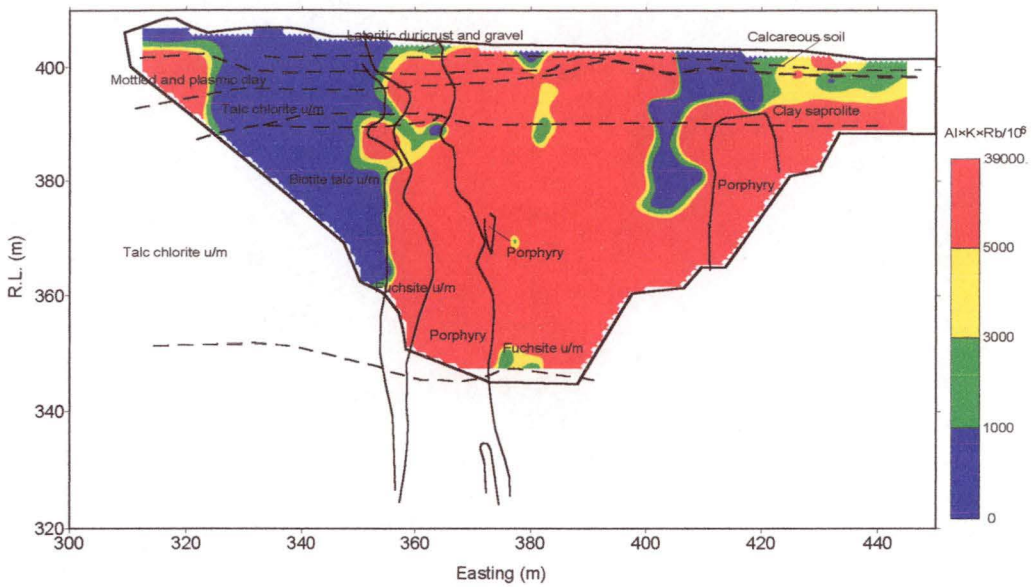

Figure 5-47. Al x K x Rb distribution of the acid insoluble residue at 15850N, Mystery Zone, Mt. Percy, WA.

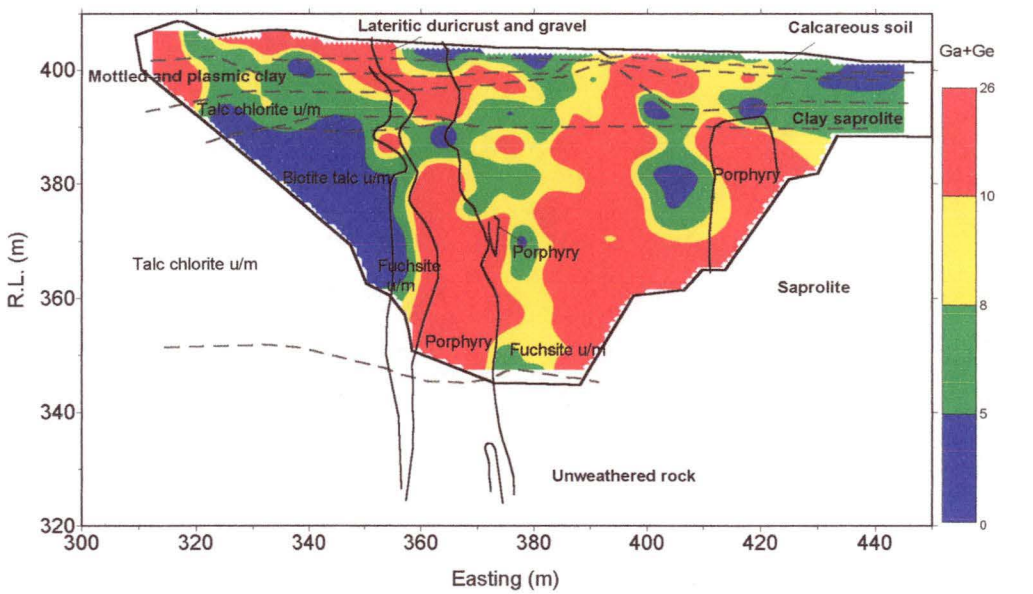

Figure 5-48. Ga+Ge distribution of the acid insoluble residue at 15850N, Mystery Zone, Mt. Percy, WA.

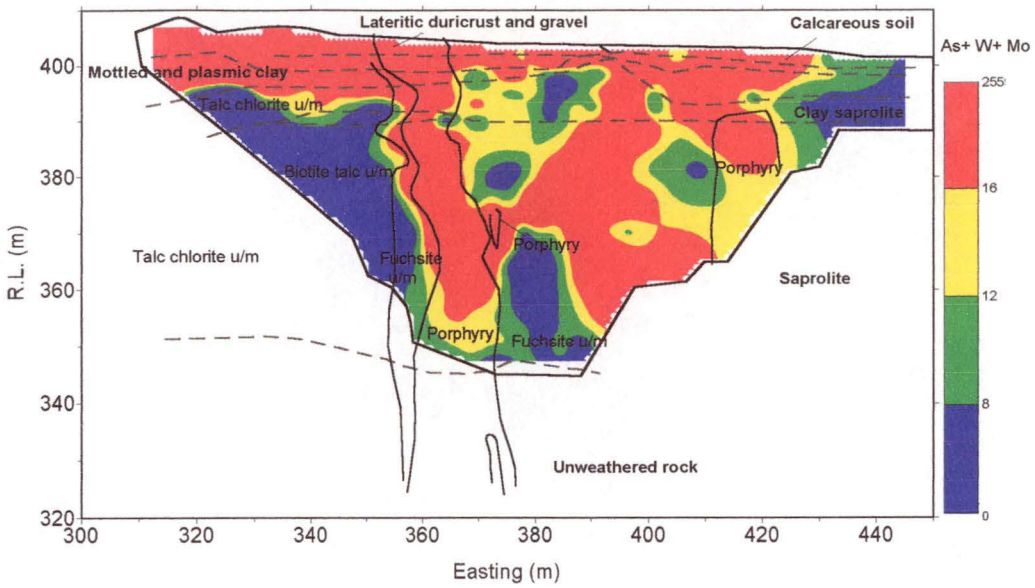

Figure 5-49. As+W+Mo distribution of the acid insoluble residue at 15850N, Mystery Zone, Mt. Percy, WA.

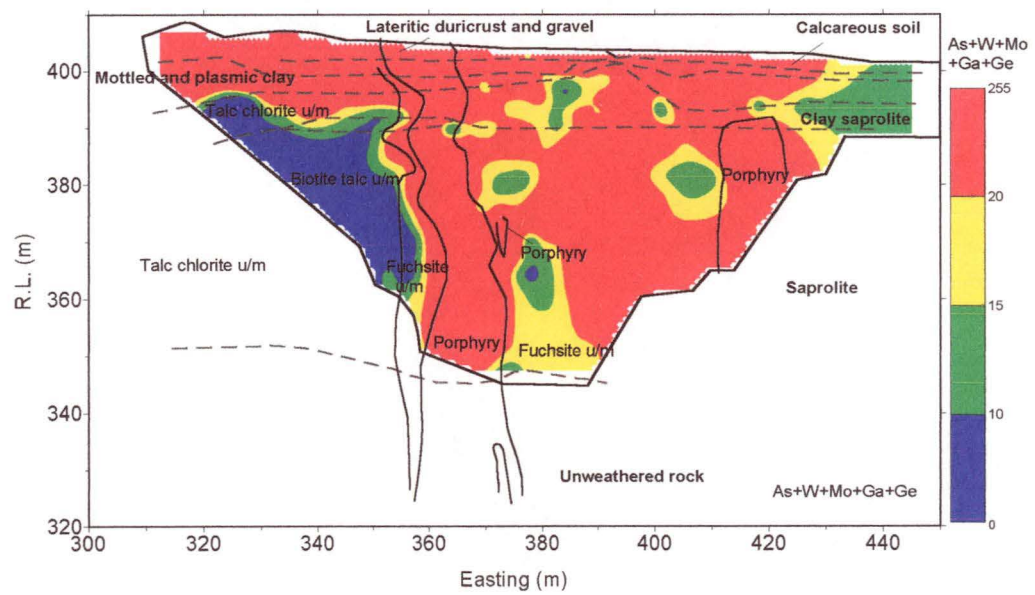

Figure 5-50. As+W+Mo+Ga+Ge distribution of the acid insoluble residue at 15850N, Mystery Zone, Mt. Percy, WA.

Chapter 6

EPR CHARACTERIZATION AT MYSTERY ZONE

6.1 INTRODUCTION

The use of EPR in gold exploration has been extensively discussed in Chapter 3 and recent publications (van Moort et al. 1995; Xu et al., 1997; Xu and van Moort, 1997; van Moort and Russell, 1997; van Moort et al., 1998). In this chapter, the results of EPR measurements on acid insoluble residue for the Mystery Zone are presented together with their relation to Au and trace elements. The acid insoluble residue investigated consists essentially of quartz, with minor muscovite and talc.

6.2 EPR DISTRIBUTION

The EPR distributions of the intensities of the X-band signals over the ±5 and ± 100 mT sweeps are presented as contour maps in this chapter. The plotting intervals were selected on the basis of the principal population evident in the histograms and cumulative frequency graphs of the whole data set (Figure 6-1).

Comparative statistical data for each EPR signal in the main regolith horizon over the principal lithological units are given in Tables 6-1 to 6-3.

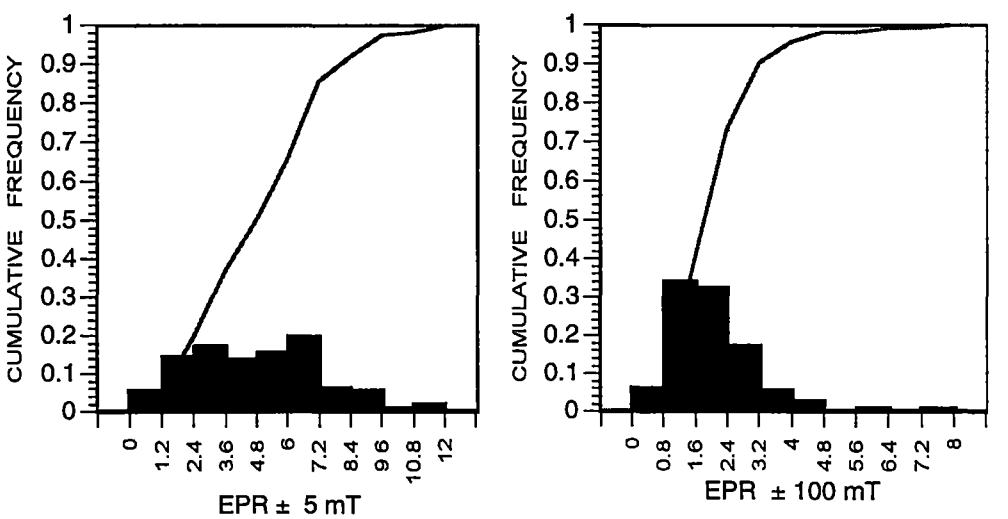

Figure 6-1. EPR histograms and cumulative frequency plots of acid insoluble residue at Mystery Zone, Mt. Percy, W.A.

The distribution of EPR signals at the Mystery Zone, Mt. Percy, is typically patchy, even at the close sampling intervals used in the study. Their distribution is, however, similar to the Au distribution. This patchiness presumably reflects differences in the impurities of the primary quartz as well as admixtures of secondary quartz.

6.3 EPR ± 5 mT

Comparative statistical data for EPR 326.5±5 mT in the main regolith over the principal lithological units are given in Table 6-1. At Mt. Percy, the pronounced EPR signals at magnetic flux density sweeps of 326.5 ± 5 mT (measured at the standard instrument setting) in porphyries and fuchsitic ultramafic rocks are on average larger than the average of the signals in talc dominated ultramafic rocks. The signal intensities in the porphyries range from 0 to 10.6 cm, and in fuchsitic ultramafic rock from 0 to 10.8 cm, and the character of EPR spectra in these rocks is generally the same. Although the average intensity of EPR 326.5 ± 5 mT is significant, the distribution map is rather patchy (Figure 6-2) because of the considerable scatter in the data.

The high EPR intensities in the quartz residue from the porphyries and fuchsitic ultramafic rocks extend from the bottom of the profile into the upper portion of the cross section. Unfortunately samples from the lateritic duricrust and calcareous soil horizon were not available for the EPR study because insufficient material was left. Judging by the strong EPR signal intensity in the clay saprolite and mottled clay zone, it is presumed to extend to the surface. There is a strong indication that EPR of the acid insoluble residue samples is not affected by weathering processes.

Table 6-1. Comparative statistics, EPR 326.5±5 mT (n=sample number, x=arithmetic mean, s=standard deviation)

	Lithology					Regolith					
Unit	Af	As	Asf	Ast	Ak	C	Lk	M	Mc	S	Sc
n	25	19	112	11	2	9	6	4	11	98	36
x	5.2	0.06	4.05	1.25	0	2.86	0.48	1.38	3.53	3.84	4.14
s	2.36	0.28	2.78	2.52		3.39	1.18	2.75	2.62	2.76	3.31

Af: Porphyry
C: Plasmic clay
As: Talc chlorite u/m
Asf: Fuchsite u/m
Ast: Talc u/m
Ak: Calcareous soil
C: Plasmic clay
Lk: Calc laterite
M: Mottled zone
Mc: Mottled clay
S: Saprolite
Sc: Clay saprolite

In contrast, the EPR intensity and distribution of the acid insoluble residue in the non-mineralized talc-chlorite and talc altered ultramafic rocks are totally different. Generally no EPR signal could be measured in the acid insoluble residue of the talc-chlorite ultramafic unit, as the spectra are flat, especially far away from the geological boundary with the fuchsite altered ultramafic unit. There is no significant difference in modal EPR intensity (0–2 cm) in the regolith of the talc-chlorite-carbonate ultramafic rocks (Xu Li and van Moort, 1997). A minor signal was observed in a few samples from talc ultramafic rocks, but most of them are without any distinct signal.

6.4 EPR ± 100 mT

Comparative statistical data for EPR 326.5 ± 100 mT in the main regolith over the principal lithological units are given in Table 6-2. The EPR intensity measured at magnetic flux density sweep 326.5 ± 100 mT follows the variation trend of EPR 326.5 ± 5 mT (Figure 6-3). In the porphyries, it varies from 0 to 3.5 cm, most of them greater than 2 cm. The distribution of strong signals is not continuous like that of the EPR ± 5 mT signal. In fuchsite altered ultramafic rocks, the intensity changes from 0 to 5.6 cm, with most over 1 cm. The intense distribution area is smaller, but reflects a patchy occurrence of primary Au mineralization with a higher background. Although the signal in the EPR ±100 mT sweep ranges from 0 to 1.5 cm in talc-chlorite altered ultramafic rocks, it usually consists of a flat spectrum in which no intensity can be measured. Four samples in the talc altered ultramafic rocks have significant signals. Because of the limited sample number used in the talc ultramafic rocks, it is not clear if the EPR ± 100 mT signal can be used to distinguish between talc-chlorite and talc (biotite) altered ultramafic rocks.

Table 6-2. Comparative statistics, EPR 326.5±100 mT (n=number of sample, x=arithmethic mean, s=standard deviation)

	Lithology					Regolith					
Unit	Af	As	Asf	Ast	Ak	C	Lk	M	Mc	S	Sc
n	25	19	112	11	2	9	6	4	11	98	36
x	1.9	0.17	1.6	1.6	0	1.07	0.2	1.17	1.2	1.79	1.26
s	1.09	0.43	1.12	2.47		1.17	0.49	0.87	0.86	1.33	1.14

Af: Porphyry
C: Plasmic clay
As: Talc chlorite u/m
Asf: Fuchsite u/m
Ast: Talc u/m
Ak: Calcareous soil
C: Plasmic clay
Lk: Calc laterite
M: Mottled zone
Mc: Mottled clay
S: Saprolite
Sc: Clay saprolite

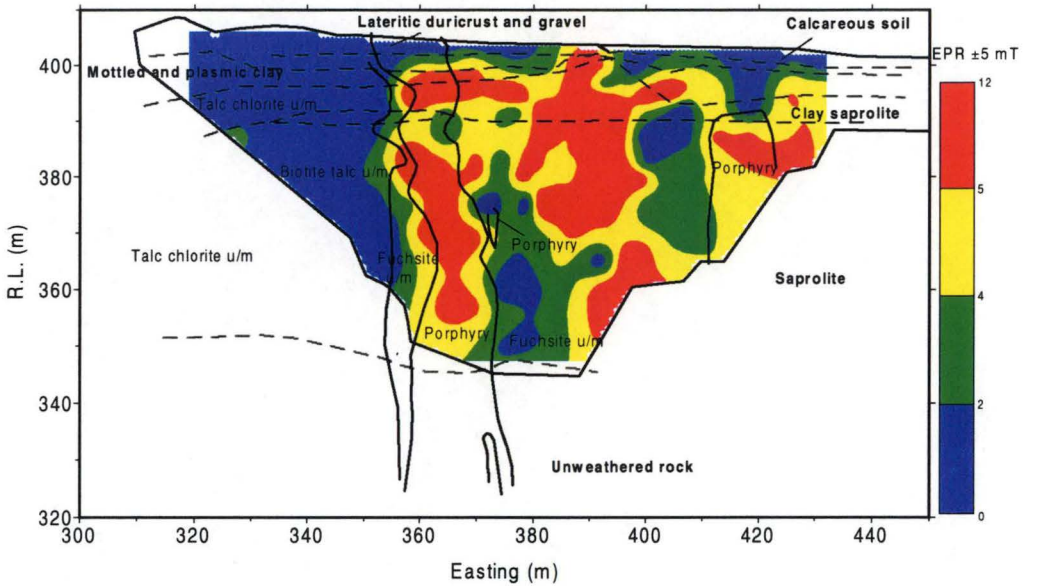

Figure 6-2. Distribution of EPR 326.5±5 mT of acid insoluble residue at Mystery Zone, Mt. Percy, W.A.

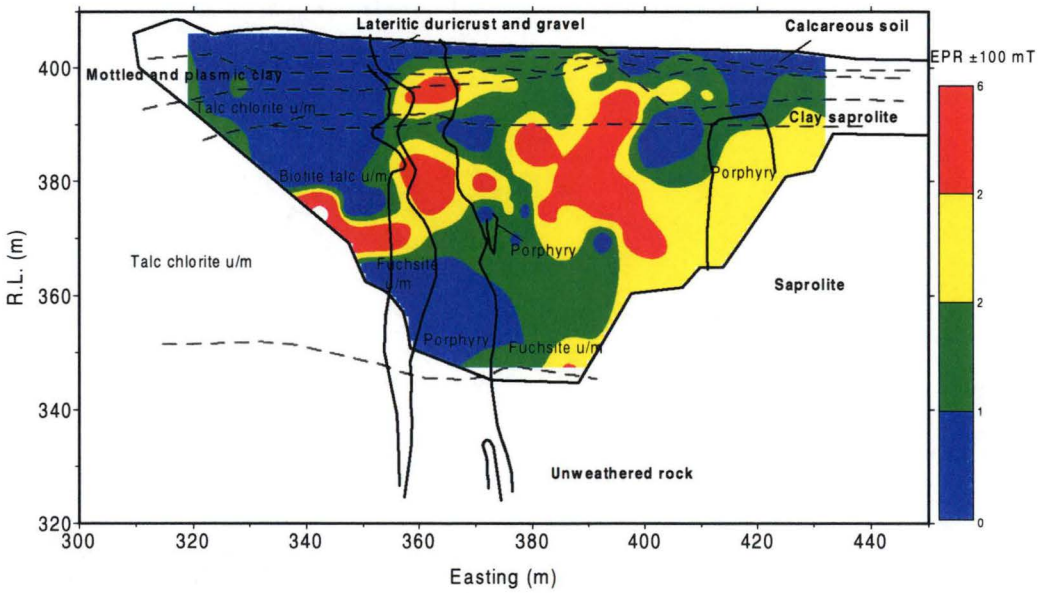

Figure 6-3. Distribution of EPR 326.5±100 mT of acid insoluble residue at Mystery Zone, Mt. Percy, W.A.

As near-surface samples were not available for EPR measurements, the near-surface expression of EPR ± 100 mT was not observed.

6.5 EPR 326.5±250 mT

Comparative statistical data for EPR 326.5±250 mT in the main regolith over the principal lithological units are given in Table 6-3. The EPR 326 ± 250 mT spectra are the same as the signals of EPR ± 100 mT; its distribution is identical to that of ± 100 mT (Figure 6-4) (see section 6.4, above).

6.6 THE RELATIONSHIP BETWEEN EPR AND Au

Comparing the distribution patterns of Au (Figure 5-5) and EPR, it can be seen that both EPR 326.5±5 mT and 326.5±100 mT reflect the primary Au mineralization zone within the porphyries and fuchsite altered ultramafic rocks. The EPR features relate to primary Au mineralization and extend to the surface. The near surface secondary enrichment of Au is not observed in EPR, except directly above the primary mineralization (cf. Figures 5-6 and 6-2). This implies that the EPR expression is only related to primary quartz and perhaps a secondary response derivation, associated with the primary gold mineralization at depth.

Figure 6-5 gives the distribution chart of EPR ± 5 mT and Au at the Mystery zone. Because the Au contents vary from a few ppb to almost 50 ppm, it has an extremely high standard deviation, and therefore the logarithm of the Au concentration is used. The samples are ordered in numerical order. Figure 6-5 clearly illustrates a

Table 6-3. Comparative statistics, EPR 326.5±250 mT (n=number of sample, x=arithmetic mean, S=standard deviation)

	Lithology					Regolith					
Unit	Af	As	Asf	Ast	Ak	C	Lk	M	Mc	S	Sc
n	25	19	112	11	2	9	6	4	11	98	36
x	1.96	0.18	1.63	1.63	0	1.1	0.23	1.27	1.31	1.79	1.25
s	1.07	0.45	1.13	2.48	0	1.09	0.57	0.95	0.94	1.36	1.1

Af: Porphyry
C: Plasmic clay
As: Talc chlorite u/m
Asf: Fuchsite u/m
Ast: Talc u/m
Ak: Calcareous soil
C: Plasmic clay
Lk: Calc laterite
M: Mottled zone
Mc: Mottled clay
S: Saprolite
Sc: Clay saprolite

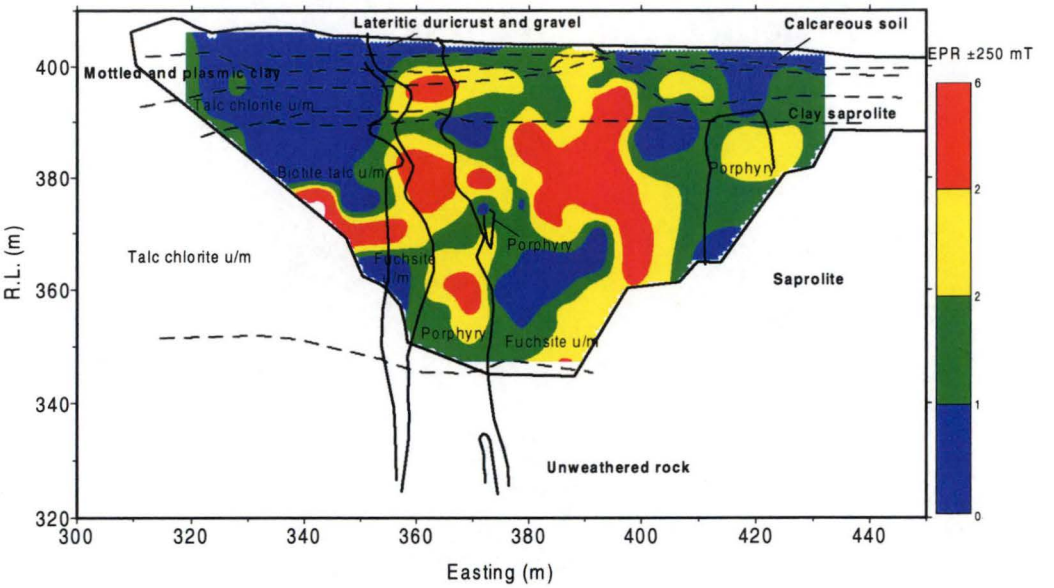

Figure 6-4. Distribution of EPR 326.5±250 mT of acid insoluble residue at Mystery Zone, Mt. Percy, *W.A.*

positive correlation between the EPR ± 5 mT signal and the log Au content of the samples. The EPR ± 5 mT signal mainly represents the occurrences of primary quartz and it show better results than other EPR signal, such as EPR ± 100 mT and ± 250 mT, because EPR ± 5 mT reflects the signal at the resonance centre rather than broad ± 100 mT and ± 250 mT showing the Mn^{2+} and other noisy signals (Russell, 1995)

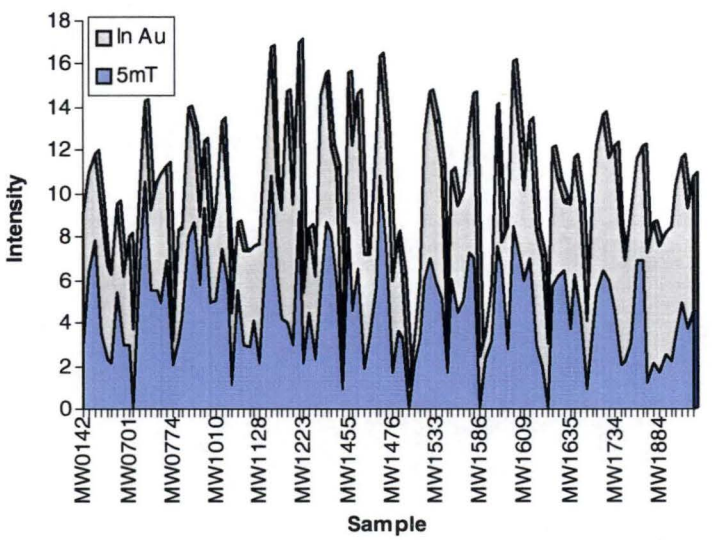

Figure 6-5. Cumulative frequency distribution of EPR 326.5±5 mT of acid insoluble residue and Au (bulk geochemistry) at Mystery Zone, Mt. Percy, W.A.

6.7 THE RELATIONSHIP BETWEEN EPR AND TRACE ELEMENTS

A study on the relation between the intensity of the EPR signal at 326.5 ± 5 mT and trace element concentration of quartz associated with mineralization has been conducted by Russell (1995) and Russell and van Moort (1997). The study was carried out on 307 quartz spot samples from veins from the Beaconsfield Gold Mine, Tasmania. The material was selected for purity and in free of sericite and feldspar. The samples were cleaned with hot fuming nitric acid to remove possible iron and manganese oxides and hydroxides, carbonates and any sulphide minerals. There is a strong correlation between the trace element contents of this material and EPR. It is contributed by the primary quartz which contains electron donors, electron acceptors Fe, Ti, and Ge and the compensating ions H^+, Li^+ and Na^+, to which K^+ may be added. More detailed description on the relationship between EPR and trace elements provided by McMorris (1970), Griscom (1980), Russell (1995) and Russell and van Moort (1997).

The Spearman rank correlation coefficients between EPR and concentration of some elements are given in Table 6-4. The elements are divided into two groups: one element is related to wall-rock alteration including Al, K, Ca, Cr, Ga, Rb, W, Zn, Na and Sr; the second is related to weathering resistant mineral elements (Ti, V, Y, Zr, Nb, As, Th, Fe, Mn and Pb).

Because the secondary quartz contains lots of inclusions, which do not yield significant EPR response, the EPR signal is mostly produced by the primary quartz. It is clearly that K-alteration is associated with quartz in the mineralized ultramafic environment at the Mystery Zone. Thus, EPR signal which is produced by primary quartz may show some positive correlations with the elements associated with primary quartz in the mineralized facies. Generally, the relationship between the alteration related elements (Table 6-4) and EPR intensity measured at magnetic flux density sweeps 326.5 ± 5 mT and 326.5 ± 100 mT exhibit positive weak to high correlation in the various rock units, but the correlation between immobile elements and EPR are negative. Although some correlation coefficients are low, they are statistically significant due to the number of samples. Figure 6-6 shows the distribution of critical probability levels of Spearman's coefficient of correlation. It can be seen that coefficients 0.4 and 0.2 represent the 95% confidence intervals and these are

Table 6-4. Spearman rank correlation coefficients between EPR intensities and some elements (samples base on acid insoluble residue)

Unit	EPR	Alteration/Mineralization related									
		Al	K	Ca	Cr	Ga	Rb	W	Zn	Na	Sr
	±5 mT	0.02	0.66	0.45	-0.08	0.45	0.59	-0.09	-0.28	0.12	0.14
Af	±100 mT	-0.03	0.57	0.45	-0.01	0.41	0.5	-0.03	-0.33	0.13	0.11
(n=25)	±250 mT	-0.01	0.6	0.43	-0.01	0.43	0.53	0.04	-0.33	0.09	0.05
	±5 mT	-0.29	0.33	0.31	0.31	-0.01	0.2	-0.1	-0.17	0.02	-0.07
As	±100 mT	-0.1	0.6	0.52	0.21	0.19	0.4	-0.18	-0.12	0.12	0.1
(n=19)	±250 mT	-0.1	0.65	0.55	0.18	0.23	0.44	-0.18	-0.09	0.15	0.12
	±5 mT	0.22	0.39	-0.02	0.41	0.35	0.34	0.13	0.07	-0.2	-0.14
Asf	±100 mT	0.15	0.33	-0.07	0.34	0.28	0.28	0.2	0.3	-0.15	-0.18
(n=112)	±250 mT	0.11	0.28	-0.08	0.29	0.21	0.22	0.14	0.21	-0.13	-0.19
	±5 mT	-0.03	0.89	0.05	0.49	0.68	0.82	0.71	-0.52	0.55	0.72
Ast	±100 mT	-0.22	0.1	-0.24	0.39	-0.07	0.3	-0.05	0.23	0.34	0.31
(n=11)	±250 mT	-0.22	0.11	-0.26	0.39	-0.06	0.32	-0.04	0.21	0.33	0.32

Unit	EPR	Weathering resistance related									
		Ti	V	Y	Zr	Nb	As	Th	Fe	Mn	Pb
	±5 mT	-0.51	-0.46	-0.42	-0.44	-0.4	-0.59	-0.45	-0.34	-0.49	0.1
Af	±100 mT	-0.36	-0.32	-0.37	-0.31	-0.17	-0.4	-0.44	-0.37	-0.36	0.07
(n=25)	±250 mT	-0.36	-0.3	-0.37	-0.29	-0.15	-0.42	-0.32	-0.38	-0.37	0.09
	±5 mT	-0.12	-0.14	-0.21	-0.16	-0.12	-0.11	-0.21	-0.1	-0.1	-0.08
As	±100 mT	-0.16	-0.15	-0.24	-0.17	-0.11	-0.11	-0.11	-0.15	-0.14	-0.16
(n=19)	±250 mT	-0.16	-0.15	-0.25	-0.17	-0.11	-0.1	-0.12	-0.15	-0.14	-0.16
	±5 mT	-0.23	-0.11	-0.31	-0.27	-0.23	-0.36	-0.25	-0.24	-0.31	-0.17
Asf	±100 mT	-0.22	-0.15	-0.31	-0.28	-0.24	-0.32	-0.24	-0.17	-0.24	-0.29
(n=112)	±250 mT	-0.22	-0.16	-0.29	-0.27	-0.24	-0.3	-0.26	-0.19	-0.25	-0.25
	±5 mT	-0.22	-0.05	-0.49	-0.08	0.06	0.25	-0.1	-0.54	-0.48	-0.18
Ast	±100 mT	-0.37	-0.37	0.08	-0.49	0.01	-0.05	-0.23	0.43	0.34	-0.23
(n=11)	±250 mT	-0.38	-0.37	0.07	-0.49	0.02	-0.04	-0.23	0.41	0.33	-0.23

Af: Porphyry As: Talc chlorite u/m
Asf: Fuchsite u/m Ast: Talc u/m

significant with the sample numbers 25 and 100 respectively. In Table 6-4, most of coefficients are larger than an absolute value 0.2. This indicates that EPR correlates well with these elements.

In the matrix of the alteration/mineralization element group, the EPR intensity measured at magnetic flux density sweeps 326.5 ± 5 mT in all lithological units have moderate to high correlation coefficients with Al, K, Rb and Ga (Figures 6-7, 6-8). This indicates that Au mineralization is associated with the muscovite alteration and in which Ga substitutes for Al. Aluminum correlates well with EPR in fuchsite altered ultramafic rocks, but is weak in porphyries. In contrast, this group of elements have a negative relationship in talc-chlorite and talc altered ultramafic rocks implying their unaltered character. There are moderate positive correlations between

EPR ±5 mT and Ca in porphyries and talc-chlorite ultramafic units. The positive correlation with Cr and Sr occurs in all lithological units except the porphyries. A negative correlation occurs between EPR ± 5 mT and Ca and Sr, which are depleted in the wall rock alteration zone. Such a relationship indicates that the EPR response in the rock is related to the wall rock alteration. For other elements, the correlation is weakly negative in most units broadly reflecting their immobile character.

The relationship between EPR and weathering resistant mineral related elements Ti, V, Y, Zr Nb, As, Th, Fe, Mn and Pb show moderate to highly negative correlation. This indicates that the enrichment of resistant minerals are not related to Au mineralization related.

The relationship between EPR intensity measured at magnetic flux density sweeps 326.5 ± 100 mT and the elements from alteration and weathering resistant mineral have similar results to that of EPR 326.5 ± 5 mT, often with minor enhancement or depletion. The relationship between EPR 326.5 ± 100 mT and the group of mineralization related elements (Table 6-4) is not always the same. A weak to moderate correlation with Cu and Zn occurs, except for the similar correlation to Ga and Rb like EPR 326.5 ± 5 mT.

Between EPR intensity measured in 326.5±250 mT sweeps and the two elements groups the correlation exactly follows EPR 326.5±100 mT.

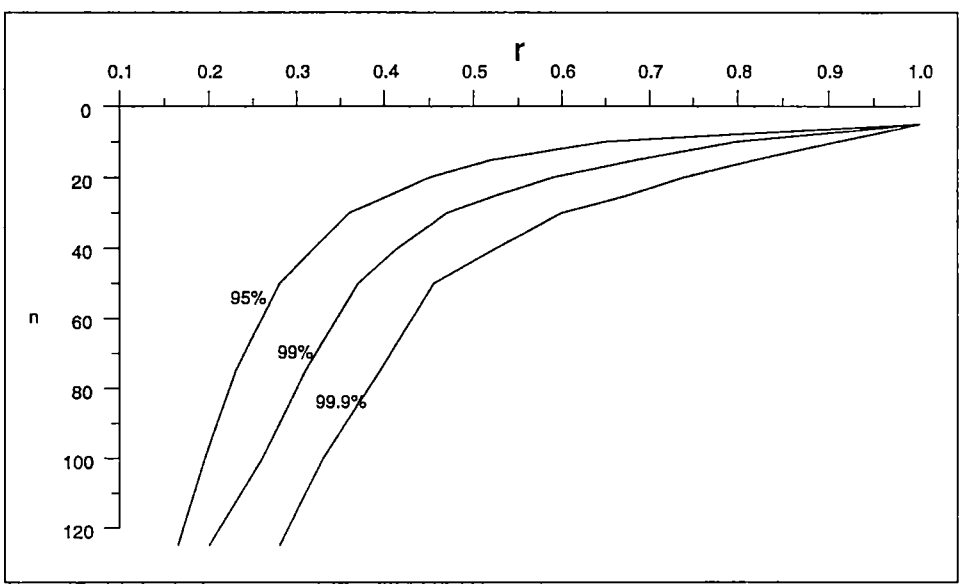

Figure 6-6. Distribution of critical probability levels of Spearman's coefficient of correlation (n=number of samples, r=coefficient)

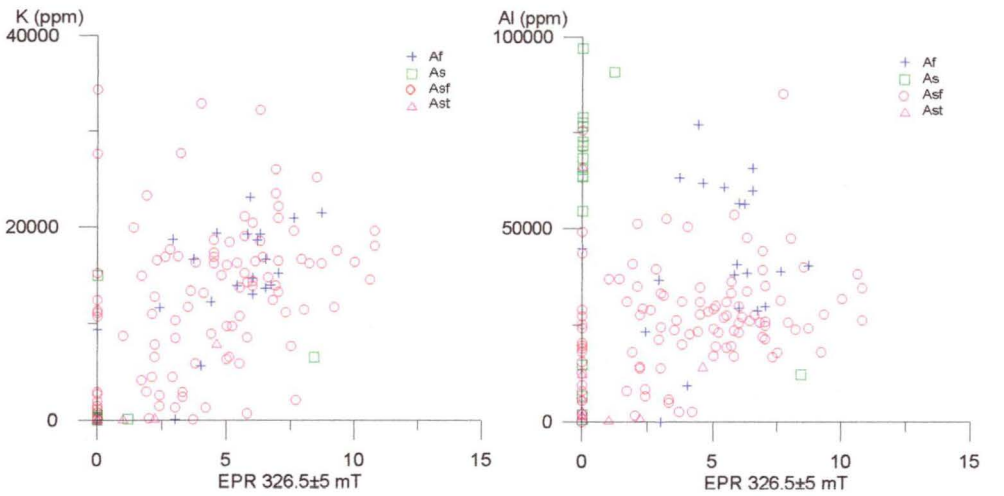

Figure 6-7. The binary plots of EPR vz. K and Al of the acid insoluble residue showing the positive relationship between EPR and alteration

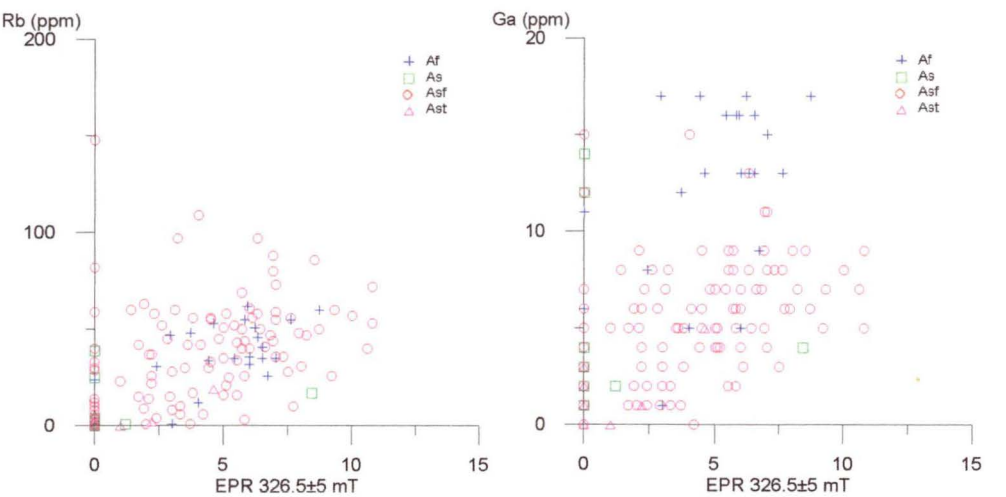

Figure 6-8. The binary plots of EPR vz. Rb and Ga of the acid insoluble residue showing the positive relationship between EPR and alteration

Chapter 7

RAND PIT, REEDY MINE, W.A.

7.1 INTRODUCTION

The Reedy Gold Mine lies 50 km to the northeast of Cue and 4.3 km southeast of Cullculli near Meekatharra, Western Australia. The mine consists of five gold deposits, North Rand, Rand, North Triton, Triton and South Emu. The Rand Pit is located at 118°60'11"E and 27°07'12"S.

After the discovery of gold by prospector Tom Reedy in 1901, four deposits (North Emu, South Emu, Rand and North Rand) were worked intermittently for approximately 30 years. The majority of early work on the North Emu and South Emu orebodies was carried out by the Mararoa G.M. Co. N.L. In 1933, Triton Gold Mines NL was formed to take over part of the operation from Western Gold, who had explored the North Rand and South Emu orebodies extensively and had developed a new shaft at the North Emu lode. In 1982, Metana Minerals N.L. (Metana) purchased the two leases covering the South Emu mine, and have acquired tenements covering the entire Reedy lode system and areas of possible strike extensions to the north and south. Since 1982, Metana has carried out extensive exploration and ore reserve drilling over the Reedy area. The decision to commence mining was made in 1983, after delineation of approximately 1.5 Mt of ore grading 4.0 g/t gold which was accessible to open pit mining. Potential exists for underground mining of both the South Emu and North Rand lodes after the present open pit reserves are exhausted (Henderson and Hill, 1990).

7.2 ENVIRONMENT FEATURES

Ferruginous regolith materials are abundant and widespread in the landscapes of the Yilgarn Craton of Western Australia. Many of these materials preserve geochemical dispersion patterns from concealed mineral deposits (Bettanay and Churchward, 1974).

7.2.1 Climate

The project area is semi-arid with an average rainfall of 215 mm. Most of the rain falls around March and is derived from convective storms, with subsidiary rainfall centered around January and May. The months September through to November are largely dry. The mean maximum temperature reaches 38°C in December to January with a mean minimum of 7°C in June and July, with marked diurnal and seasonal temperature fluctuations. Evaporation greatly exceeds precipitation with annual evaporation rates of 2280–2790 mm and this becomes extreme in summer (Bettanay and Churchward, 1974).

7.2.2 Topography and vegetation

The Rand pit of the Reedy gold mine lies on a stony, erosional plain, which forms part of a low divide between minor drainage systems of the Austin and Annean playa lakes. These plains have been developed by the erosion of the deeply weathered Great Plateau of WA. They consist of low, broad, gently-sloping, flat-topped interfluves, interspersed with narrow, linear, drainage floors. There are a few stony rises and low hills which expose weathered, generally ferruginized, Archaean greenstones and a few patches of lateritic duricrust. The area is drained by a dendritic system of seasonal streams occupying broad, shallow channels, filled with polymictic gravel (Robertson et al., 1990). The flora is dominated by mulga (Acacia) bush and annual grasses (Beard, 1976).

Deeply-weathered country rocks form the basement to a dominantly fine, gravelly, ferruginous alluvium, up to 2 m thick, much of which has been silicified to Wiluna Hardpan (Bettanay and Churchward, 1974). There are rare coatings of fine-grained carbonate along horizontal partings in the hardpan. Overlying the hardpan are shallow, stony to very friable, fine, sandy, red to brown, clay loams, <0.5 m thick, with an acid pH. These contain gravels which, at the surface, form a ferruginous lag. Some of these lag materials are of lateritic origin, others are ferruginized lithorelics of the parent rock.

The geomorphology near the mine suggests extensive stripping of the upper parts of the regolith, which is considered to have mantled this landscape since Tertiary times. The ferruginous, gravelly, alluvial cover forms a very thin veneer at the south end of

the Rand Pit, commonly a meter or less thick, with a few small channels set in it. The mottled zone is poorly developed and appears to have been extensively stripped. The thin layer of hardpan alluvial cover continues along the eastern wall of the pit but, here, the mottled zone thickens considerably. A wedge of highly ferruginized lateritic material lies between the saprolitic mottle zone and the hardpan alluvial cover.

Parts of this saprolite zone are polymictic and seem to be transported but most is monomictic. It is probably an alluvial material, representing nodular fragments of the mottled zone, from which the intervening clays have been washed, leading to a breccia of collapsed fragments. The underlying surface of the saprolite is very irregular in places, showing low relief, deep cavities and even a large 'boulder' resting on the saprolite 'surface', surrounded by lateritic 'overburden'. This brecciated lateritic material is a significant Au resource.

7.2.3 Weathering history and regolith landform

The rocks of the mine sequence have been deeply weathered but the depth of weathering varies between rock types. Weathering depths range from 30–40 m in the South Emu area to 70–80 m at the North Rand deposit (Figure 7-1). The lode, basalts and dolerites are more intensely weathered than the chlorite and actinolite schist and massive intrusive porphyries.

7.3 REGIONAL GEOLOGY

The Reedy Mine is situated on the eastern edge of the Meekatharra–Mt. Magnet greenstone belt which forms part of the Murchison Province of the Yilgarn Block (Figure 4-1). Mafic rocks and intrusive rocks are the main components and, in contrast with the Eastern Goldfields Province, ultramafic rocks are only a minor component. Most clastic sedimentary rocks are derived from adjacent felsic volcanic centres (Ayres, 1983). Granitoids intrude the lower portion of the greenstone succession.

The spatial association of gold deposits with major faults and shear zones appears to be a more or less universal feature of Archaean granite greenstone terrains (Watkins and Hickman, 1990a). Regionally the volcano-sedimentary sequence has been folded into a series of anticlines and synclines. It is considered that the major crustal fractures have acted as conduits for gold bearing hydrothermal fluids. The major faults and shear zones of the region are shown on Figure 7-2. Some authors (Partington, 1987;

Figure 7-1. The south face of the Rand Pit showing the topgraphic and weathering profile

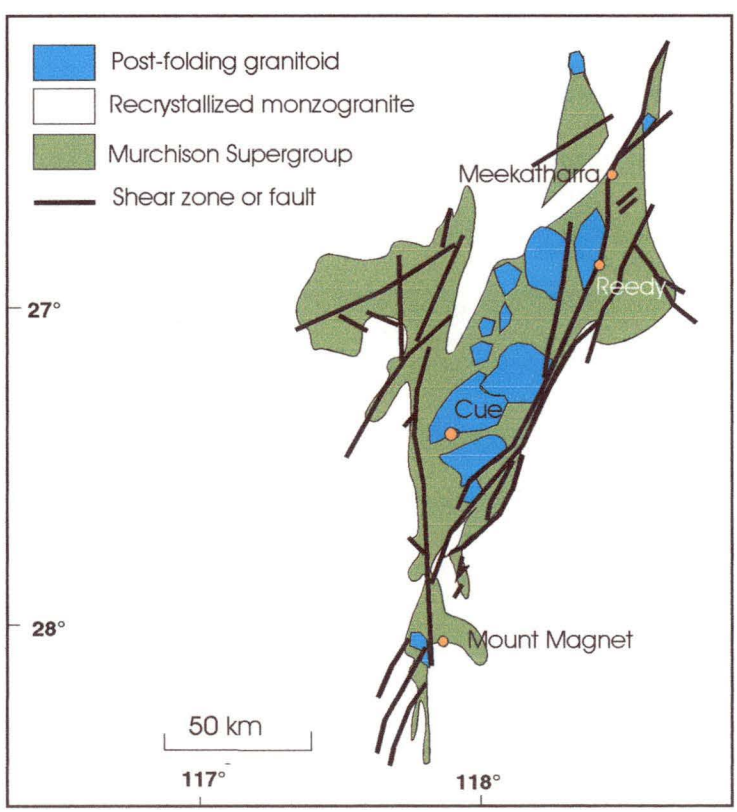

Figure 7-2. Simplified regional geology map showing the major shear zone and faults (after Watkins and Hickman, 1990a)

Vearnicombe et al., 1988) have claimed that the major faults and shear zones of the Yilgarn Craton are barren, and that gold mineralization is located in subsidiary brittle ductile and brittle shears, faults and tensional fractures, 1–10 km away. However, in the Murchison region important mining areas, including Reedy, Cue and meekatharra, are within major shear zones (Watkins and Hickman, 1990a)

Gold mineralization is widespread in the region, unlike the Eastern Goldfields where an area of about 3 km^2 at Kalgoorlie has accounted for most of that region's total gold production. On a regional scale, economic gold mineralization is concentrated in a limited range of geological environments, and almost all the gold deposits are in greenstone belts and most of them are located on the area's major faults and shear zones (Watkins and Hickman, 1988).

The majority of gold deposits in the Murchison Province are clearly epigenetic in origin. Three main types of epigenetic gold deposits can be recognized and are listed as follows (Watkins and Hickman, 1990a): (1) basalt- and, less commonly, dolerite-hosted quartz-vein deposits; (2) ultramafic schist- and, less commonly, mafic schist-hosted shear-zone deposits; and (3) BIF- and chert-hosted deposits. Type 2 dominates in the Meekatharra–Reedy domain. In this type of gold mineralization; ultramafic-hosted epigenetic gold deposits occur in wide (0.5 to 1 km), regionally extensive and pervasively sheared zones. Mafic rocks may form a minor component. All major ultramafic hosted deposits are in the Meekatharra–Reedy area.

7.4 LOCAL GEOLOGY

The stratigraphy in the immediate vicinity of the mines, from west to east, consists of interlaminated mafic schists and banded iron formation, followed by interlayered chlorite, tremolite and talc schists, post-tectonic porphyry pods and layers of carbonaceous schists of the ore zone. Passing into all these are metadolerites (Figure 7-3). All the rocks are schistose, with one strong schistosity and, in places, a kinking in the rocks suggests a second schistosity. Although no definitive lava flow structures were found, some features, suggesting flattened and deformed pillow structures were seen on the lower-mid bench at the southeast corner of the Rand Pit. Although these could also be interpreted as intersecting fractures, a pillow structure origin is preferred. These rocks comprise high-Mg and tholeiitic basalts and ultramafic and mafic sheet intrusions with felsic volcanics and volcanogenic sediments. The depositional environment has been interpreted as a submarine sequence of mafic

and ultramafic volcanics with argillaceous and chemical interflow sediments. Henderson and Hill (1988) considered that dolerite intrusion occurred prior to folding but some of the doleritic rocks could equally well have been thick flows (Robertson et al., 1990). Intrusion of granitoid porphyries, which are located close to the Au-bearing lodes, occurred after folding, possibly during granite emplacement and during or prior to major shearing.

The mineralized shear zone at Reedy lies on the eastern limb of a southerly plunging syncline, in which the known deposits occur as a series of discontinuous, linear lodes over a strike length of 3.5 km. The individual lodes strike at approximately 350° and dip steeply west, although dip reversals are not uncommon, particularly in areas of faulting and folding.

7.4.1 Host rocks

The host rock is talc-chlorite-carbonate-albite schist, tremolite-chlorite schist, pyritic metadolerite, and quartz-veined, pyritic porphyry (Watkins and Hickman, 1990b). The depositional environment has been interpreted as an originally flat lying submarine sequence of mafic and ultramafic volcanics with argillaceous and chemical interflow sediments (Henderson and Hill, 1990). Quartz-feldspar porphyry intrusions are common, and locally there are high gold grades at the margins of these intrusions, where pyrite, arsenopyrite, fuchsite (chrome mica) and sericite are well developed (Watkins and Hickman, 1990a). The schistose units surrounding the lodes are composed of extensively altered rocks, including talc-chlorite, talc-carbonate and talc tremolite. Major accessory minerals include quartz, albite, graphite and calcite, with minor serpentine, fuchsite and pyrite. Pillow basalts are evident in the footwall sequence of the Rand Pit. The quartz-albite-muscovite porphyry occurring both within the lodes and the footwall sequence is the other main intrusive rock type.

7.4.2 Alteration

The main types of alteration are K-metasomatism, silicification, chloritization, and carbonation (Watkins and Hickman, 1990b). Chlorite alteration is strongly developed within the hanging wall mafic schists and is more pronounced close to the lode zone. It is commonly accompanied by potassium alteration and carbonate veining. The footwall ultramafics in immediate contact with the lode in the North Rand,

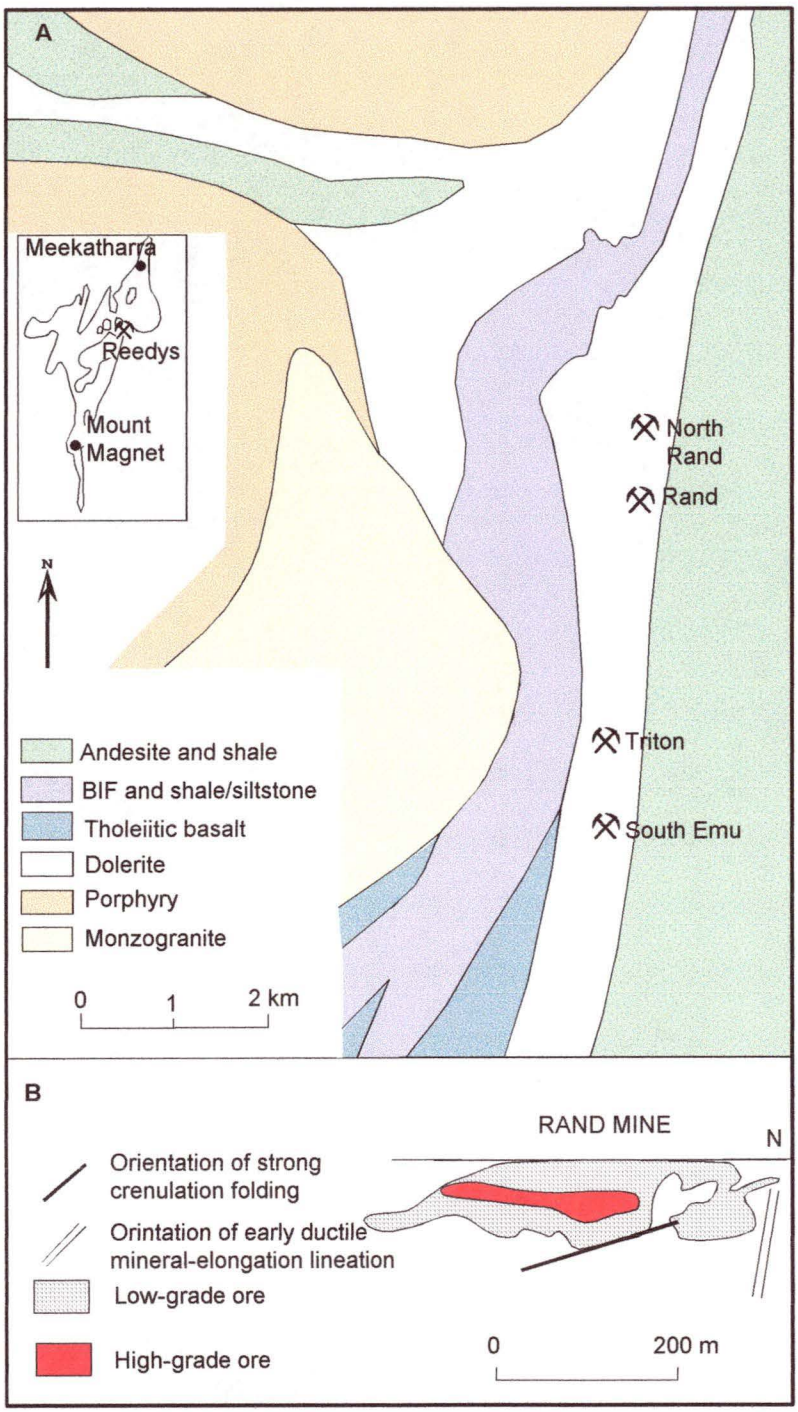

Figure 7-3. Geology of the Rand Pit, Reedy Mine: A Plan and B long section (after Watkins and Hickman, 1990)

Rand and North Triton deposits are dominated by variable proportions of talc and chlorite, with serpentinization evident in some areas. Carbonate is also present, and chrome alteration is indicated by the occasional occurrence of fuchsite. Chlorite and carbonate, resulting from the alteration of actinolite, with saussuritized feldspar, are present in the footwall dolerite and basalts (Henderson and Hill, 1990). Consequently, the dominant silicification, sulphidization, potassium and sericitization within the lode zone caused a biotite and quartz rich assemblage with companion calcite, chlorite, muscovite and albite.

7.4.3 Structure controls

Gold mineralization at Reedy is structurally controlled and occurs along the sheared contact of dolerite, basalt, ultramafic schist, quartz-feldspar porphyry and shale (Figure 7-2). The main structural controls are confinement within a narrow schistose zone and the overall southerly plunge of the mineralization. Because the plunge is subparallel to the strong mineral lineation developed within the lodes and adjacent host rocks, Henderson and Hill (1990) stated that west block moved upwards accompanied by dextral shearing. In terms of gold production and known ore reserves the western zone is economically the most important by far (Watkins and Hickman, 1990b). The higher concentrations of gold occur within high shear zones indicating the shearing intensity has a major influence on mineralization,

Post-mineralization faulting is evident in the Rand and South Emu pits. Subhorizontal faults with both sinistral and dextral movement displace the lodes by up to 2 m. Larger subvertically dipping faults trending 320° to 340° transect the lodes and show horizontal displacement up to 10 m (Henderson and Hill, 1990).

7.4.4 Mineralization

There are three distinct mineralized lode horizons within the north trending regional shear zone in the Reedy area. They lie along a considerable but discontinuous strike length of 3.5 km and dip steeply west on the eastern limb of a southerly plunging syncline. Watkins et al. (1987) classified the mineralization as a shear zone and quartz vein type within mafic/ultramafic rock and associated with porphyry. The main lode is a pyritic quartz-biotite-carbonate-albite schist (Watkins and Hickman, 1990b). Accessory minerals include sericite, chlorite and pyrrhotite. In some areas, particularly in the Rand lode, high grade gold mineralization occurs in a strongly sheared and

kaolinized, pyrite rich quartz-feldspar unit. Mineral banding and lineation are well developed in the lode, and sulphide concentrations are common along joint planes crosscutting the schistosity.

Mineralization is essentially auriferous pyrite with accessory, non-auriferous pyrrhotite. Most of the gold associated with pyrite is submicroscopic and generally less than 20 mm. Some very coarse gold is found on the margins of quartz veins and some very rich specimen gold has been obtained from the base of the Rand Pit. Gold mineralization within the lode is not uniform. Numerous zones of high and low grades ore occur across strike, and are reasonably continuous along both strike and dip. The main factors affecting these grade variations are pyrite concentration and the intensity of shearing. Background gold concentration within the host rocks is much less than the 0.5 g/t cut off grade used to delineate ore during mining.

The Reedy lode system is confined within a wide regional shear situated between two relatively brittle rock units, a banded iron formation to the west, and an intrusive dolerite in close proximity to the lodes to the east. The shear zone appears to be the main controlling factor in the economic concentration of gold mineralization, but whether the mineralizing fluids were derived from the surrounding volcaniclastic pile by remobilization during metamorphism, or were late stage fluids associated with granite and porphyry intrusions, is unresolved. Campbell (1953) regarded the lode as a metasedimentary horizon and this is not inconsistent with the view of Watkins and Hickman (1990) as these lodes are structurally related to a competency contrast during folding near the contact of a dolerite intrusive body, with localized shear zones developing along this interface, within which the concentration of gold occurred.

Low-grade laterite-hosted gold mineralization is also locally developed near the shear zone.

7.5 SAMPLE COLLECTION

The south face of the Rand Pit shows a sequence of near vertical, alternating, mafic and ultramafic rocks with interspersed felsic pods and bands of quartz-mica rocks and black shales. The whole profile has been metamorphosed to amphibolite facies.

It is very hard to discriminate between mafic and ultramafic rocks, even where the rocks are almost fresh near the bottom of the pit. The best distinction can be made on the presence or absence of talc as a major component. On the upper-mid and upper benches (467–480 m R.L.) the colors become less distinctive due to intense weathering and ferruginization. Between the upper bench (480 m R.L.) and the surface, the color differences are largely swamped by Fe oxide staining.

Representative samples of 1–2 kg were collected from approximately horizontal traverses about one meter above the floor of the pit (then at approx., 417 m R.L.) and one meter above each of four benches cut in the south face of the pit, one comprising the main access ramp (Robertson et al., 1990). The whole face was photographed and the locations of the sample points were re-plotted from the detailed photography. To this plot was added the geological information gathered while sampling and the geology of the complete face was then elucidated. The mica schists tend to be auriferous and are referred to as the S1 and S3 ore shoots, the principal mafic bands are referred to as M1 and M3 and the ultramafic bands as Um2 and Um6. The porphyry intrusions are referred to as P1 , P2 and P3 (Figure 7-4).

As the original sampling pattern employed at Rand Pit was designed to investigate weathering processes rather than to carry out a dispersion study, there are no surface samples available for this study. A total of 89 samples were chemically analyzed at Rand Pit for this study.

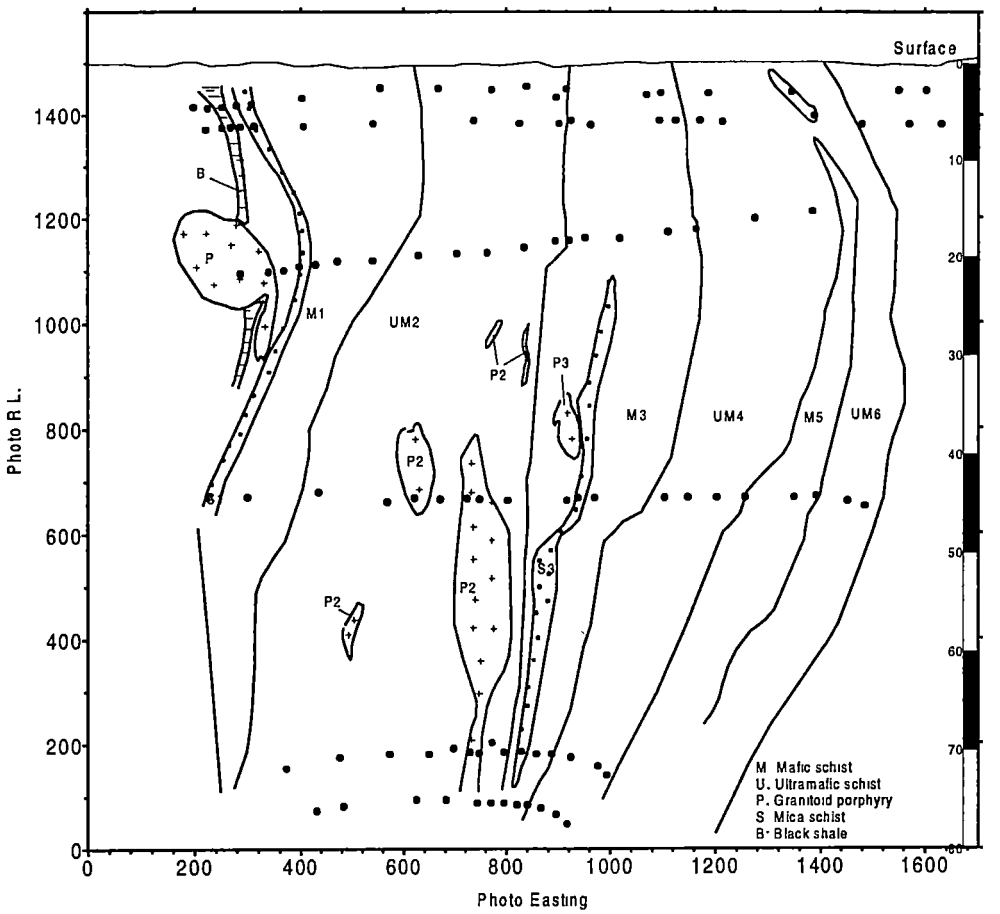

Figure 7-4. The diagram of sample location at Rand Pit, Reedy Mine, W.A. (after Robertson et al., 1990)

Chapter 8

GEOCHEMISTRY AT RAND PIT

Acid insoluble geochemistry maps of the south face of Rand Pit have been included for 25 elements, where elements have been analyzed by PIXE/PIGE. For five elements (Cu, Pb, W, Mo and Th) an appreciable proportion of the data are below the detection limit, so interpretation should be considered with care. The As, Ge, Br and U data, though reported for completeness in Appendix 3 were also not plotted because of their low occurrences. In addition, plots of element abundances against photo R.L. have been constructed separately for each rock type to demonstrate both the variance within each rock type and the effects of weathering (Appendix 3).

The element distributions at Rand Pit, Reedy Mine are shown as contour maps in this chapter. The plotting intervals were selected somewhat subjectively by using the principal populations evident in the histograms and cumulative frequency graphs of the whole data set shown on Figures 8-1 to 8-4. Elements having similar geochemical affinities are described together. Comparative statistical data for each group of elements in the main regolith over the principal lithological units are given in Table 8-1.

8.1 REGOLITH GEOCHEMISTRY

The regolith profile at Rand Pit has been intensively studied by the Australian Cooperative Research Centre for Landscape Evolution and Mineral Exploration (CRC LEME). This section gives a brief summary of the main regolith zones according to Robertson and his colleagues at CRC LEME (Robertson, 1990; Robertson and Butt, 1997).

In the study area, weathering and oxidation are quite intense in the mine sequence rocks. The regolith has been stripped to the base of the mottled zone and the depth of weathering varies between rock types, but is generally to about 70–80 m. The south face of the Rand Pit has exposed granitoid porphyry pods set in interstratified mafic, ultramafic and mica schists (Figure 7-3). Even the freshest samples show signs of Fe staining along cleavages and parts of quartz veins have been fretted out. The boundary between fresh rock and saprock is the weathering front but the accurate

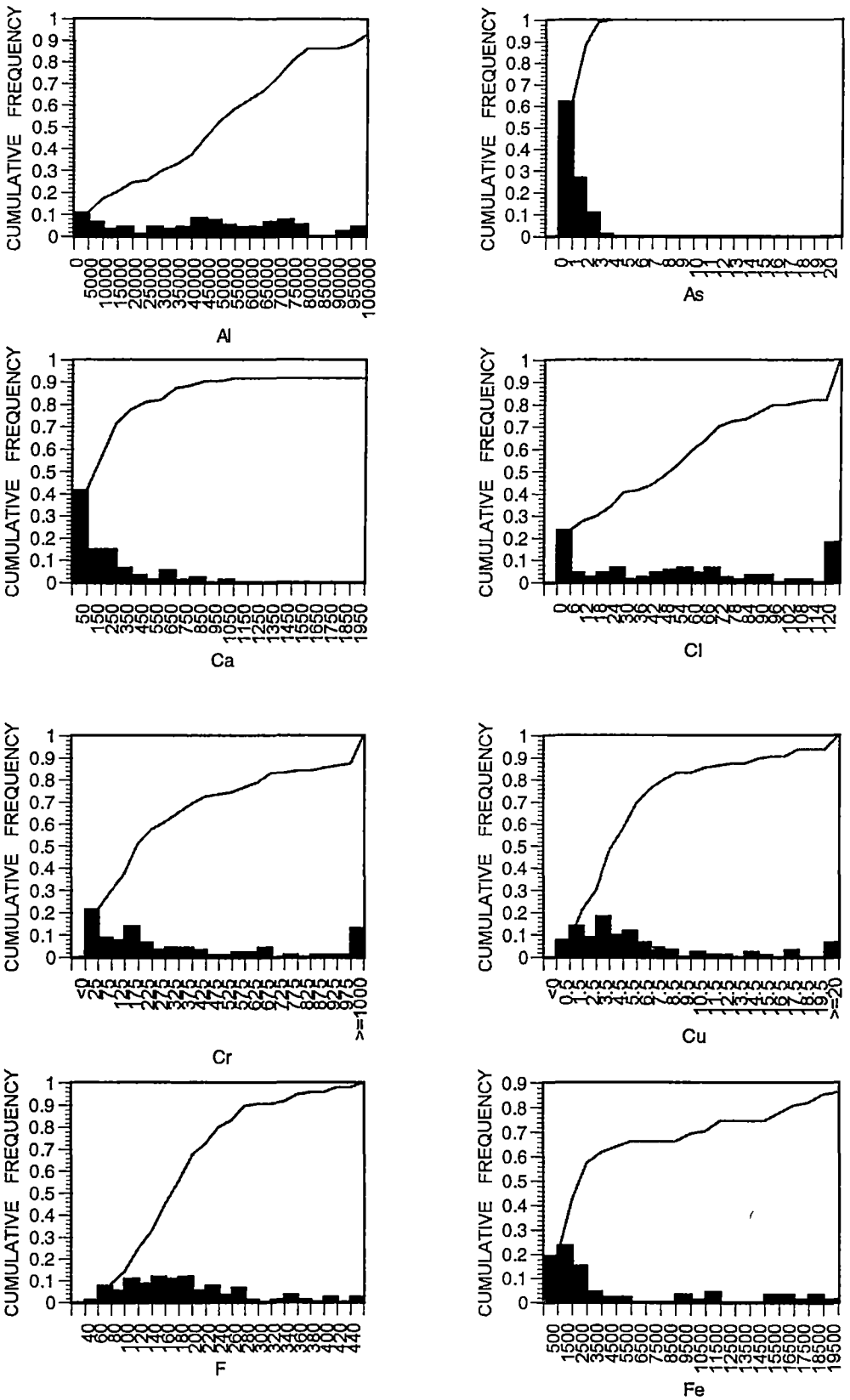

Figure 8-1. The histograms and cumulative frequency plots of Al, As, Ca, Cl, Cr, Cu, F and Fe in ppm of the acid insoluble residue

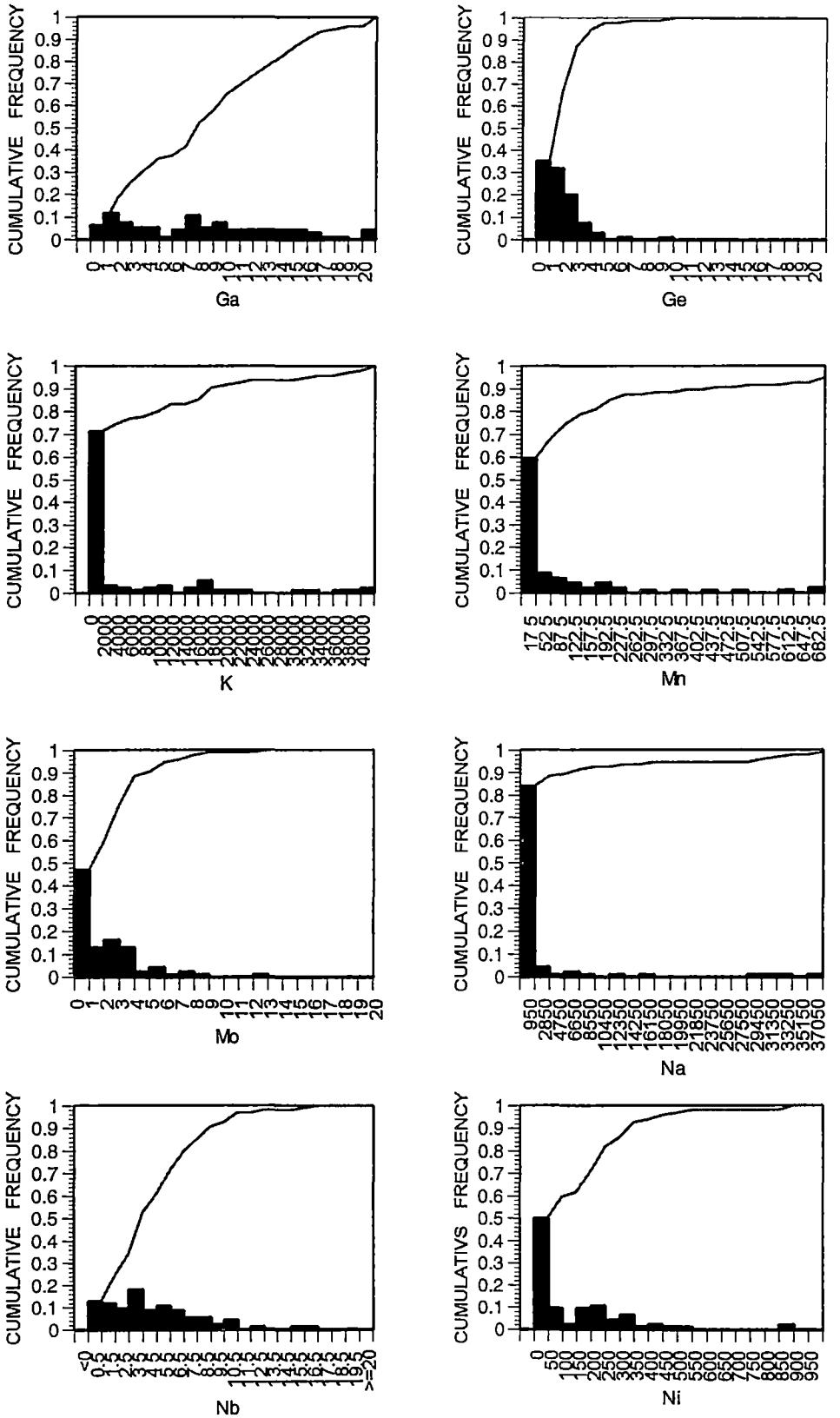

Figure 8-2. The histograms and cumulative frequency plots of Ga, Ge, K, Mn, Mo, Na, Nb and Ni in ppm of the acid insoluble residue

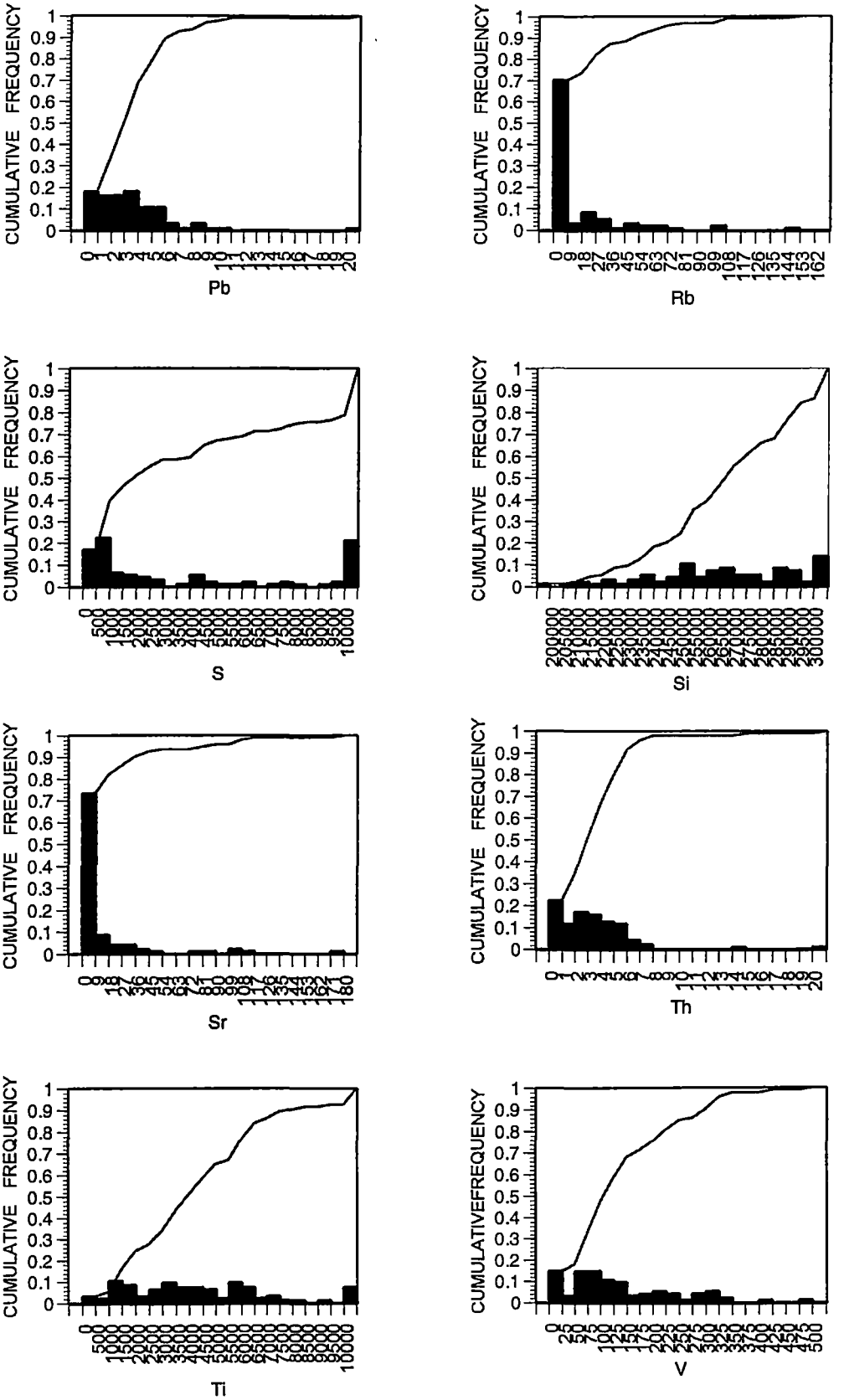

Figure 8-3. The histograms and cumulative frequency plots of Pb, Rb, S, Si, Sr, Th, Ti and V in ppm of the acid insoluble residue

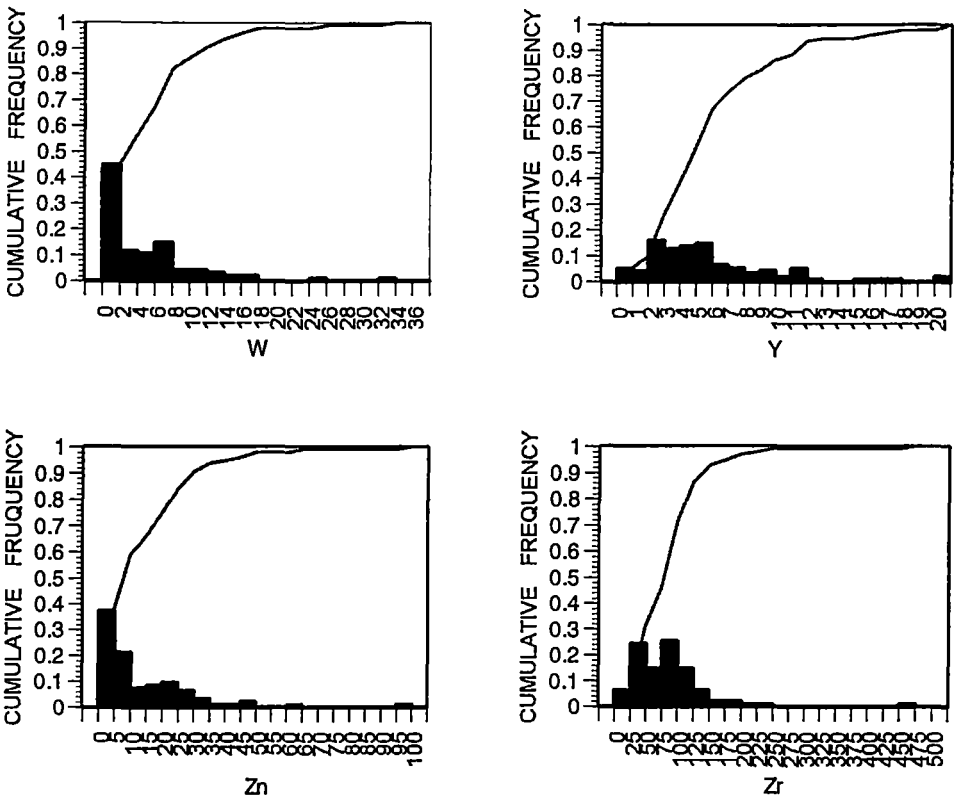

Figure 8-4. The histograms and cumulative frequency plots of W, Y, Zn and Zr in ppm of the acid insoluble residue

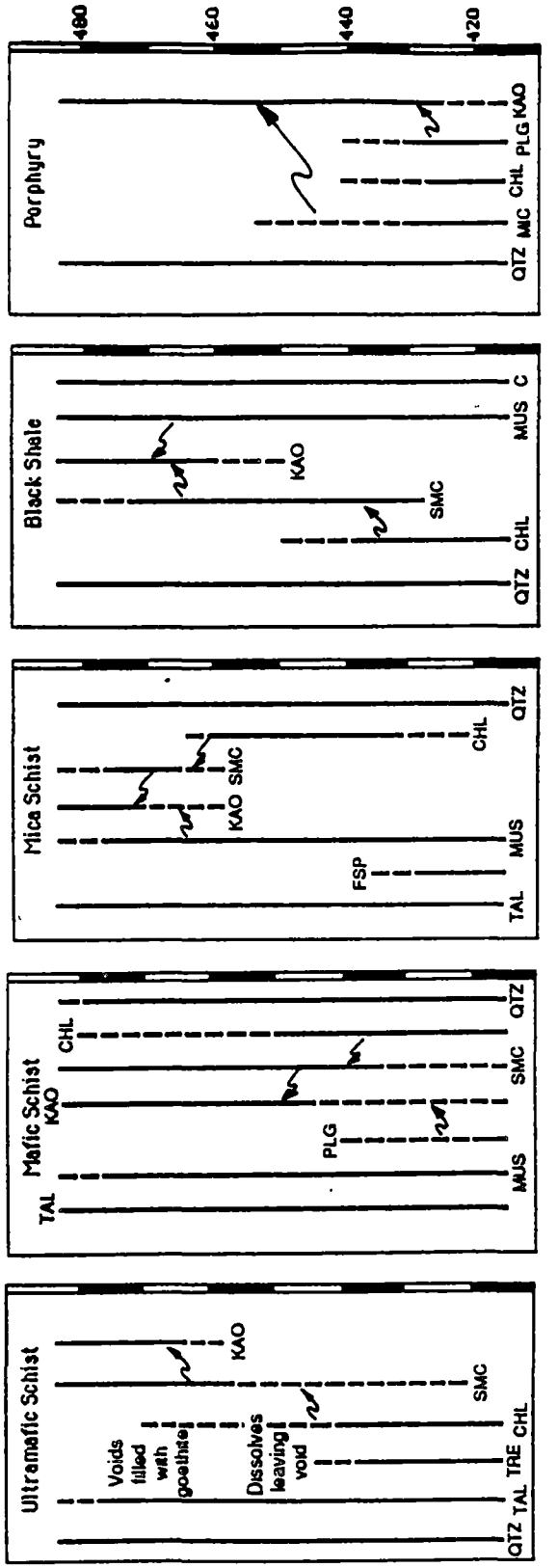

Figure 8-5. Distribution of minerals in each rock type with depth in regolith (CHL=Chlorite; KAO=Kaolinite; MIC=Microcline; MUS=Muscovite; PLG=Plagioclase; QTZ=Quartz; SMC=Smecitite; TAL=Talc; TRE=Tremolite); (from Robertson et al., 1990)

location of this boundary can, in many instances, be severely limited by scale. At the top of the profile, weathering is intense and a zone of low bulk density (<2.0) forms a layer 10–20 m thick. In addition to this overall deeply weathered layer, a few narrow, nearly vertical zones of low specific gravity, 10 m wide, extend to 50 m. These narrow zones in part surround zones enriched in Au (>100 ppm) which previously may have been pyritic. The decay of pyrite and the resultant acid conditions would promote localized deep weathering. The mineralogical changes within the profiles over the principal lithologies are shown on Figure 8-5.

8.1.1 Saprock

The onset of weathering occurs at about 70 m and is indicated by white or cream turbidity in the albite that has been partly altered to very fine-grained kaolinite. Only slightly higher, the albite is almost completely kaolinized. Some pyrite and goethite has stained the rock more extensively. The cleavage is followed by sinuous quartz lenses.

8.1.2 Saprolite

Complete kaolinization of plagioclase and oxidation of sulphides marks the base of the saprolite and this is accompanied by widespread to patchy goethite staining along quartz vein. Chlorite is partly altered to smectite at 50 m depth, alteration is completed at 30 m depth. Some of the smectite has altered to kaolinite, but the schistose fabric remains. Near the top of the saprolite, the primary fabric is partly obliterated, quartz grains in vein quartz become separated, solution cavities and channel ways occur and the saprolite grades into the pedolith above.

Some saprolites have a well preserved schistose fabric, whereas others, which contain sinuous quartz patches, consist of very fine-grained, low birefringence kaolinite, some talc and a kaolinite-smectite mixture that has a slightly higher birefringence than kaolinite alone. This mixed phase occurs as patches with a sworled fabric. Most of these rocks are saprolitic, though some pedolithic fabrics occur on a small scale.

The saprolite at 10 m depth generally consists of a very fine- to relatively coarse-grained, schistose mat of kaolinite and talc, with some muscovite and smectite after a chloritic cleavage, and fine-grained granular quartz. There are also numerous solution

channels and vesicles, some of which are infilled with fragments of saprolite, set in a matrix of clay. Saprolitc fabrics are preserved in these rocks as residual schistosities, now consisting of clays and quartz, but pedolithic fabrics become increasingly important.

8.1.3 Plasmic zone

At 30 m depth, the mafic rocks consist of a schistose fabric of talc, chlorite and quartz, which has become reorganized progressively by recrystallization of kaolinite. This reorganization causes loss of the original rock fabric and marks the transition from saprolith to pedolith. The restructured plasmic materials close to the surface (2–10 m) become increasingly more closely cut by small channelways and voids, many of which are lined with kaolinite and completely or partly infilled with mixed kaolinite and smectite.

The mottled zone has not been sampled and will not be discussed here.

8.2 Au DISTRIBUTION

The distribution of gold determined by INAA in total geochemistry, which defines the mineralization in the regolith is shown in Figure 8-6. Gold is concentrated in and around two sub-economic ore shoots on the south face of the Rand Pit that roughly conform to the S1 and S3 mica schist zones. There is a zone of lateral Au dispersion with Au abundances of >10 ppb that in many places reaches >30 ppb in the top 5-15 m of the profile. Strongly anomalous Au only extends to the surface over the S3 ore shoot, where one sample contained over 120 ppb. Two samples over the S1 ore shoot contained over 300 ppb at 5 m depth but they are all overlain by samples assaying <60 ppb. This pattern suggests a zone of weak Au enrichment (>100 ppb) at about 5-10 m, overlain by a zone of Au depletion (<50 ppb).

Most of the gold in the regolith is presumed to be secondary, on the basis of its morphology and composition (Freyssinet et al., 1990; Gedeon and Butt, 1990).

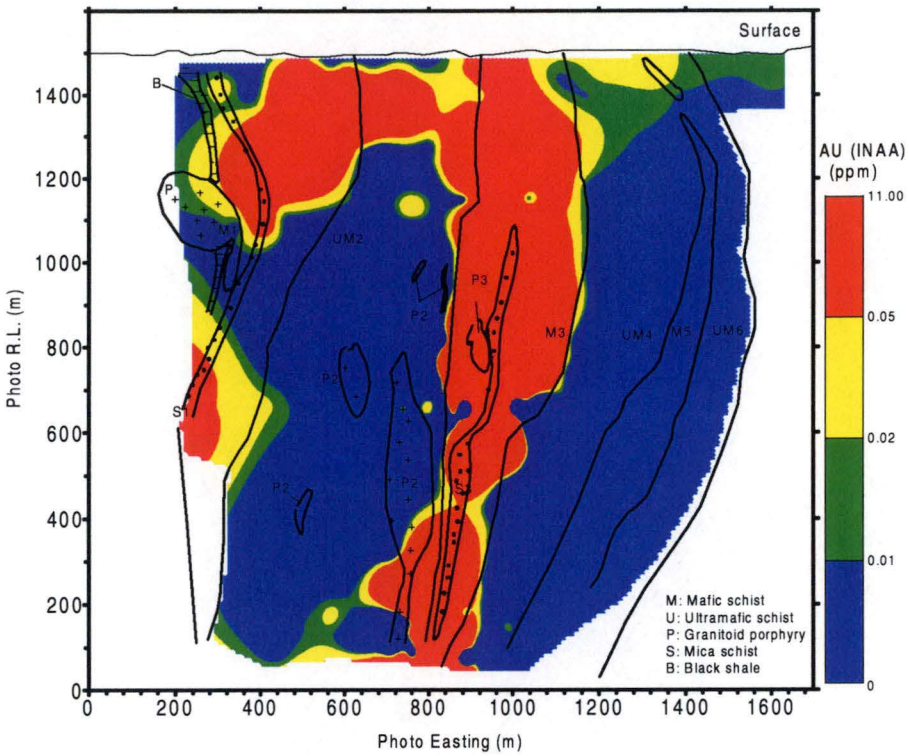

Figure 8-6. Au (INAA) distribution of bulk geochemistry at Rand Pit, Reedy Mine, W.A.

8.3 ACID INSOLUBLE RESIDUE GEOCHEMISTRY

The mineralogy study of the acid insoluble residue at Rand Pit suggests the main minerals are angular quartz fragments and larger microcrystalline quartz with some inclusions, such as sericite inclusion. Secondary silica (e.g. chalcedony), is often observed. The minor minerals are mainly muscovite and zircon; some residual kaolinite may be present. Figure 8-7a and 8-7b show the typical observation of the acid insoluble residue at Rand Pit by optical microscopy and environmental electron scanning microscopy (ESEM) respectively.

The element distributions at the south face of Rand Pit are shown as contour maps after the element description. The contour intervals were selected on the basis of the principal population evident in the histograms and cumulative frequency graphs of the whole data set shown on Figures 8-1 to Figure 8-4.

Comparing the distribution pattern of gold with other elements, a strong correlation could be observed in the distribution of their concentrations, or there exists a persistent spatial relationship between the concentrations on compared plots across the section. These relationships are taken to indicate a certain affinity between the gold and the

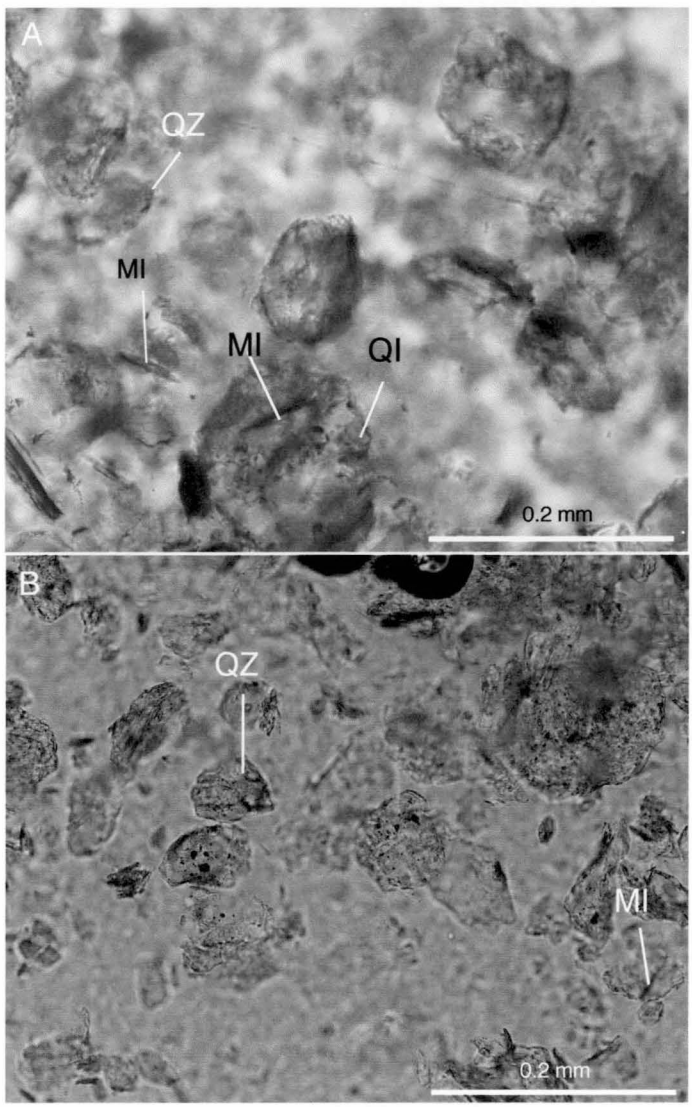

Figure 8-7a: Photographys of transmitted light microscopy
A: RE70 angular quartz fragments(QZ) and larger microcrystalline chalcedony aggregates with inclusion(QI) as well as some mica (MI)
B: RE23 angular fragment of crystal quartz (QZ), some larger chalcedony aggregates with inclusion and some mica (MI)

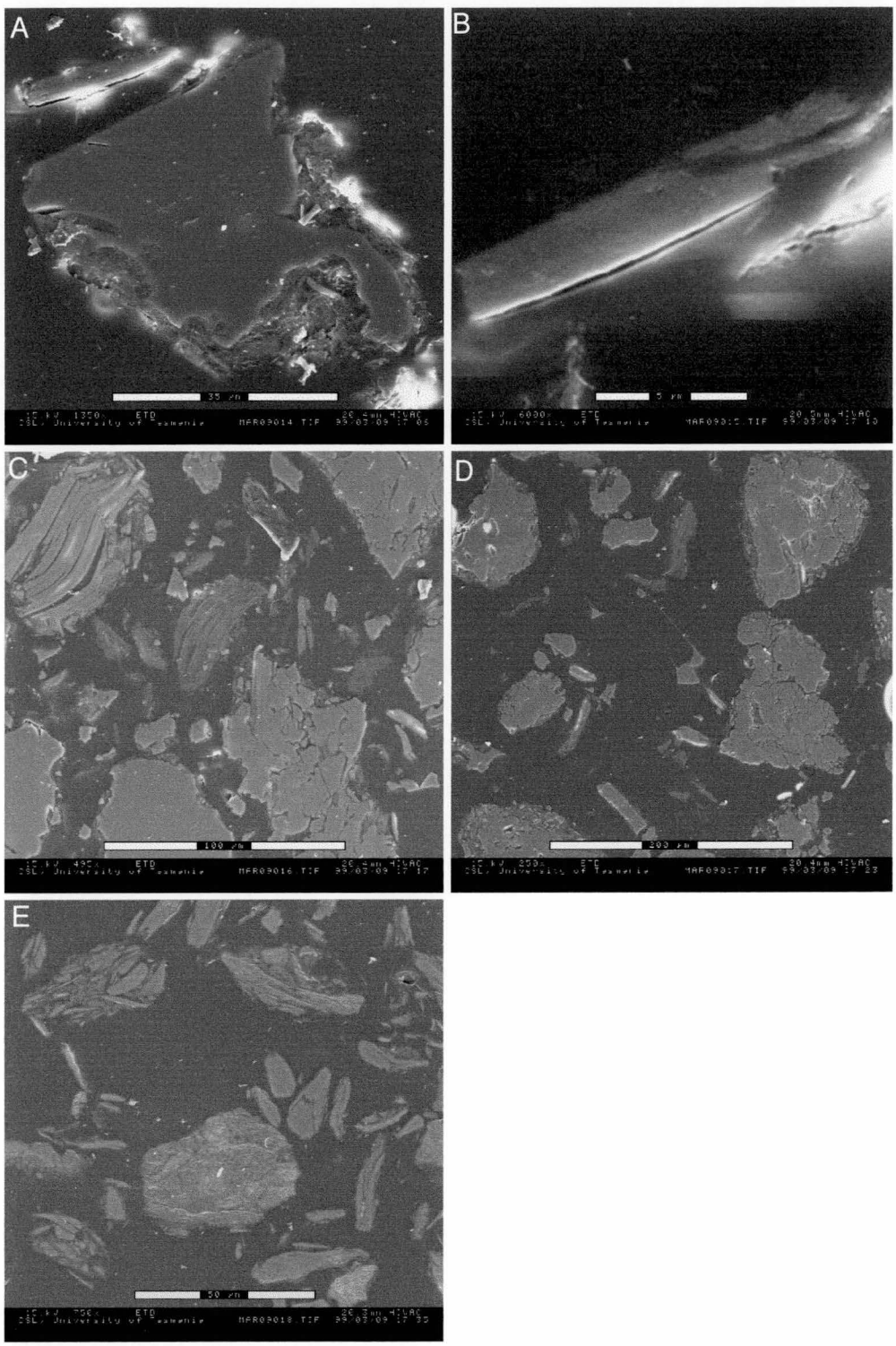

Figure 8-7b: ESEM microcopys
A: RE70 corroded primary quartz with kaolinite surround; small talc needle
B: RE70 talc needle
C: RE23 Mg- rich sericite and cracked primary quartz
D: RE23 cracked primary quartz and Mg-rich sericite
E: RE101 kaolinite with high silica content

compared elements. But further investigation is necessary to determine whether the correlation results from a primary genetic relationship, as an artifact of the weathering environment or is a coincidental relationship.

The elements identified as showing affinities with the Au mineralization are described together. The principal feature of the elemental distribution patterns across the south face of Rand Pit, Reedy Mine are as follows.

8.3.1 Major elements (Al, Fe)

Aluminium and Fe are the common major constituents of residual products resulting from prolonged chemical weathering.

Aluminium: It has a range of 400 to 123841 ppm in the acid insoluble residue of the regolith. The distribution contour map is shown in Figure 8-8. Aluminium has low values in the three ultramafic rocks units (< 2%). The lowest value occurs in these units, which is only 0.04% ppm. Higher values occur in the porphyries, the black shale and the mica schists (> 4%). The highest individual and average values of Al occur in the mica schist, which are respectively 12.3% and 6.0%, compared to 9.9% and 0.4% of Al in the ultramafic rocks. Surface enrichment of Al occurs above photo R.L. 1000, especially above the porphyries (up to 12% Al); the surface enrichment above the ultramafics is limited to 7% Al.

Iron: It has a range of 30 ppm to 3.1% and is high (with the average value >1%) in the ultramafic units. The distribution contour map is shown in Figure 8-9. The lower Fe content of the porphyry, mica schist and mafic units (< 0.2%) compared to that of black shale within ultramafic rocks (>0.2%) and mafic schist (> 2.1%) shows that the characteristics of Fe distribution varies with the differences in geology.

8.3.1.2 Alkaline earth elements (Ca and Sr)

Calcium: Calcium has a range of 16 to 4.7%. The distribution contour map is shown in Figure 8-10. A near surface enrichment (>180 ppm) in calcium in the acid insoluble residue is noted to occur directly above the photo R.L. 1200. More visible changes in the calcium content occur in the middle part of the profile. Ca is depleted from photo R.L. 1200 to 700, which is 15-42 m under the surface and shows its highest

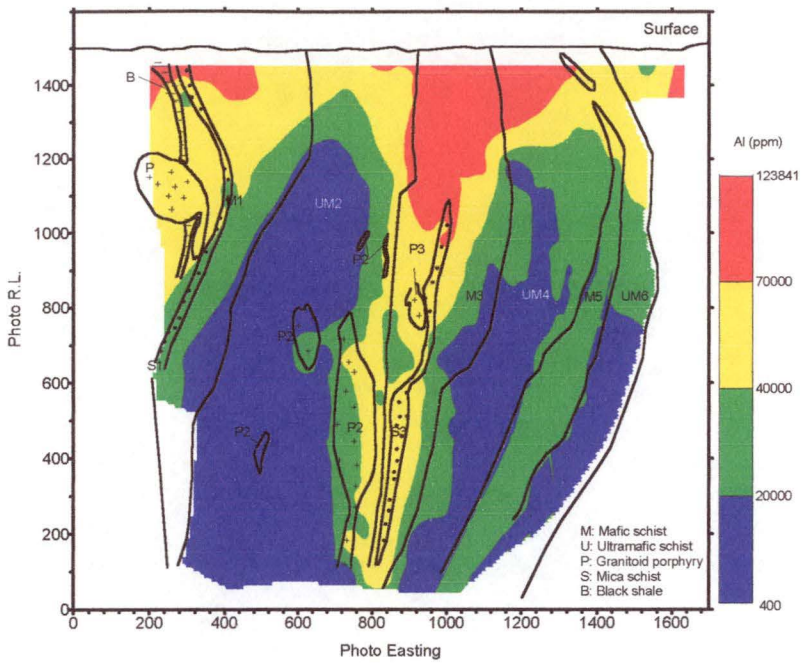

Figure 8-8. Al distribution of acid insoluble residue at Rand Pit, Reedy Mine, W.A.

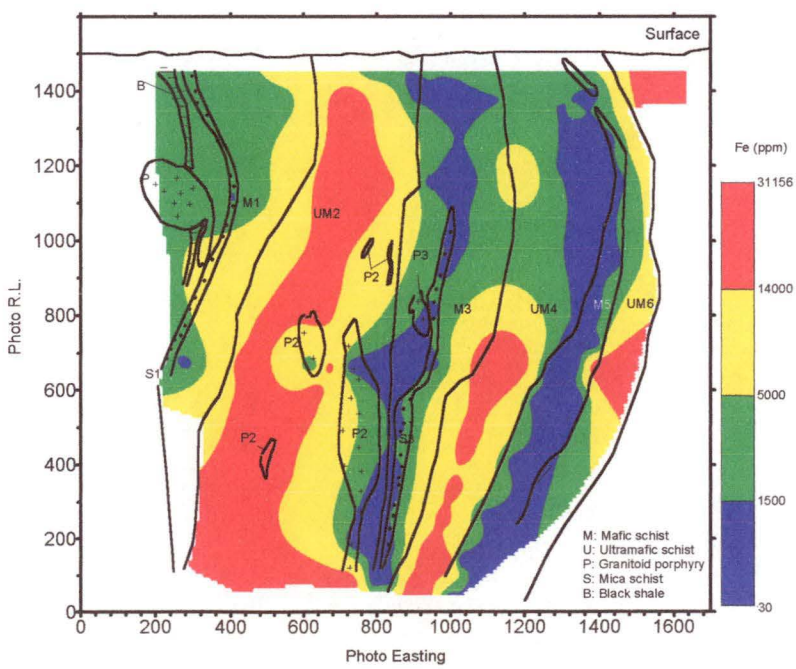

Figure 8-9. Fe distribution of acid insoluble residue at Rand Pit, Reedy Mine, W.A.

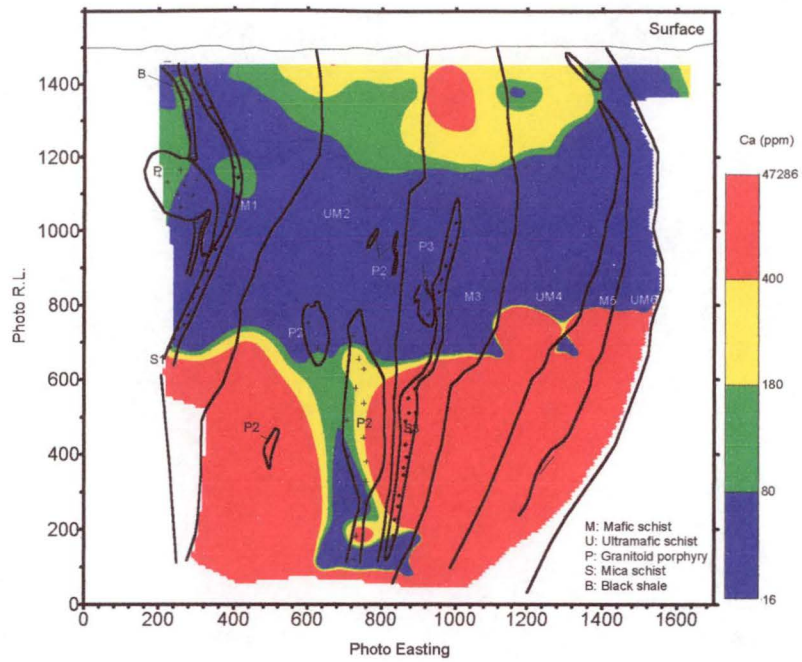

Figure 8-10. Ca distribution of acid insoluble residue at Rand Pit, Reedy Mine, W.A.

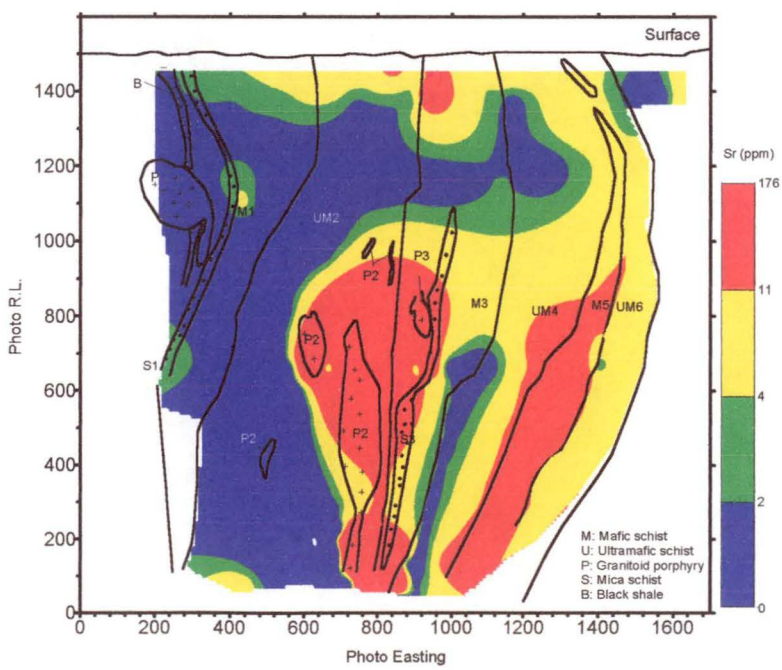

Figure 8-11. Sr distribution of acid insoluble residue at Rand Pit, Reedy Mine, W.A.

values in the lower part of the profile, except at the location of the porphyry intrusion. Ca has extreme values in the ultramafic rocks. The average content of Ca in porphyries (average 433 ppm) is two times greater than that of black shale, mica schist and mafic schist rocks (200-233 ppm), compared to 1.9% in the ultramafic rock.

Strontium: The concentration of Sr changes from 0 to 176 ppm. The distribution contour map is shown in Figure 8-11. Sr shows minor enrichment near the surface in the lateritic zone (>4 ppm). The behavior of strontium below the surface in Rand Pit does not follow that of calcium like the bulk regolith geochemistry, except for the same characters of its occurrence in the porphyry intrusion. Very low values occur in the ultramafic rocks below 2 ppm in the west of the profile, but Sr is 6 ppm on average over the whole of the ultramafic rocks, compared to 9-14 ppm in other units except porphyries. It is much higher in the porphyries where average concentration in Sr is 89 ppm, with a maximum of 176 ppm.

8.3.3 Alkali metals (Na, K and Rb)

Sodium: Sodium ranges from 0 to 42221 ppm. The distribution contour map is shown in Figure 8-12. Leaching occurs through most of the weathering profile. Sodium concentrations in the ultramafic rocks are normally less than 0.02%. The

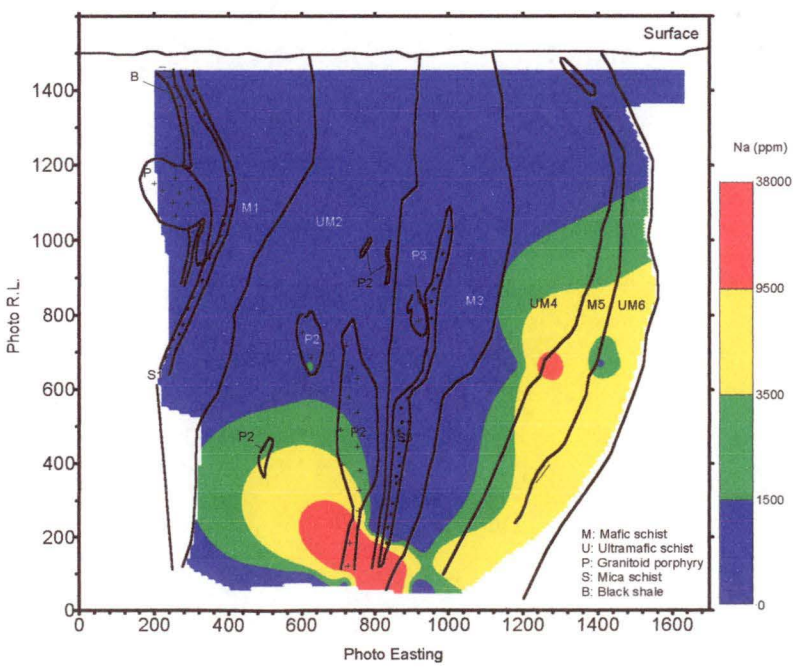

Figure 8-12. Na distribution of acid insoluble residue at Rand Pit, Reedy Mine, W.A.

distribution of Na in the regolith profile shows the highest value at the lower part of the saprolite zone, which is greater than 1% and over ten times that of Na in the upper part of the profile. Generally the concentration in Na is similar in black shale and mica schist with the average content of 200–300 ppm, which is rather low in these geological units. There is some similarity between the Na and Ca distribution patterns at depth.

Potassium: Potassium varies from 5 to 58217 ppm in the regolith profile, with most values greater than 1000 ppm. The distribution contour map is shown in Figure 8-13. The concentration of potassium in the ultramafic rocks is very low, from 5 to 1882 ppm with the average 226 ppm. Potassium is enriched in the mafic schist, especially in the black shale (average 1.7%) and mica schist (average 2.0%). Potassium concentration in porphyry is also very high, with the highest value 5.8%, but its average value is similar to that of mica schist (2.0%). The K distribution appears to be largely mica and feldspar related because of their existence in acid insoluble residue.

Rubidium: Rubidium ranges from 0 to 152 ppm and its distribution closely follows that of K and is largely controlled by micas and feldspars. The distribution contour map is shown in Figure 8-14. A pronounced occurrence of Rb is located in the porphyry intrusions, with an average of 51 ppm. The concentration of Rb in the ultramafic rocks has the lowest values of less than 6 ppm.

8.3.4 Base and transition metals (Cu, Pb, Zn, Ni and Mn)

Copper: Copper has a range of 0 to 48 ppm. The distribution contour map is shown in Figure 8-15. The concentration in copper is changed significantly in the regolith profile. It shows a zone of greater than 7 ppm Cu in the zone near the surface and is essentially less than 2 ppm at lower levels. Copper is more concentrated in black shale and mafic schist, where the average value in greater than 5.4 ppm, which is almost two times than that of porphyry, mica schist and ultramafic rocks.

Lead: Lead normally between 0 and 10 ppm with occasional values up to 25 ppm. The distribution contour map is shown in Figure 8-16. The distribution of Pb in the profile indicates higher values occur mainly in the mafic schist associated with black shale and mica schist. Very low values (<3 ppm) occur in the ultramafic schist, on average less than 1 ppm, though a few higher values up to 10 ppm are sporadically

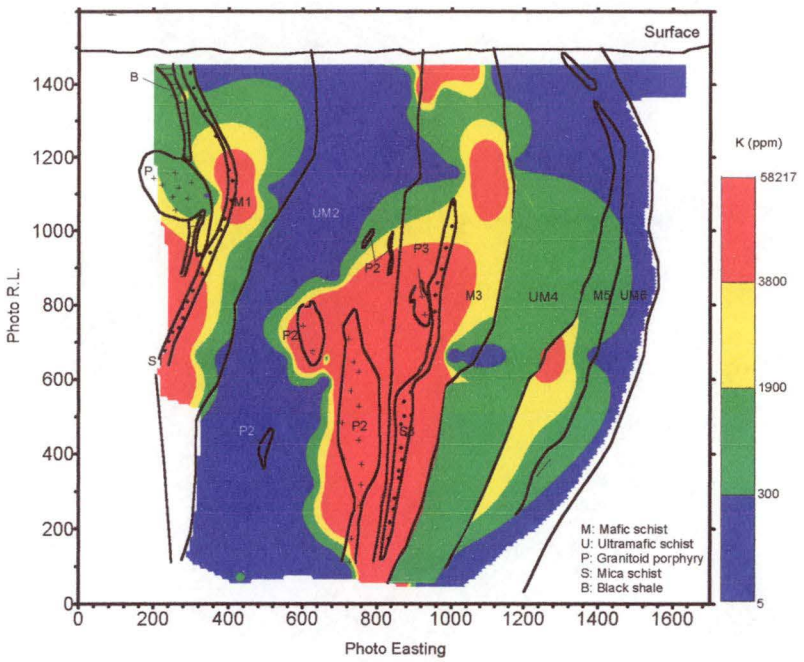

Figure 8-13. K distribution of acid insoluble residue at Rand Pit, Reedy Mine, W.A.

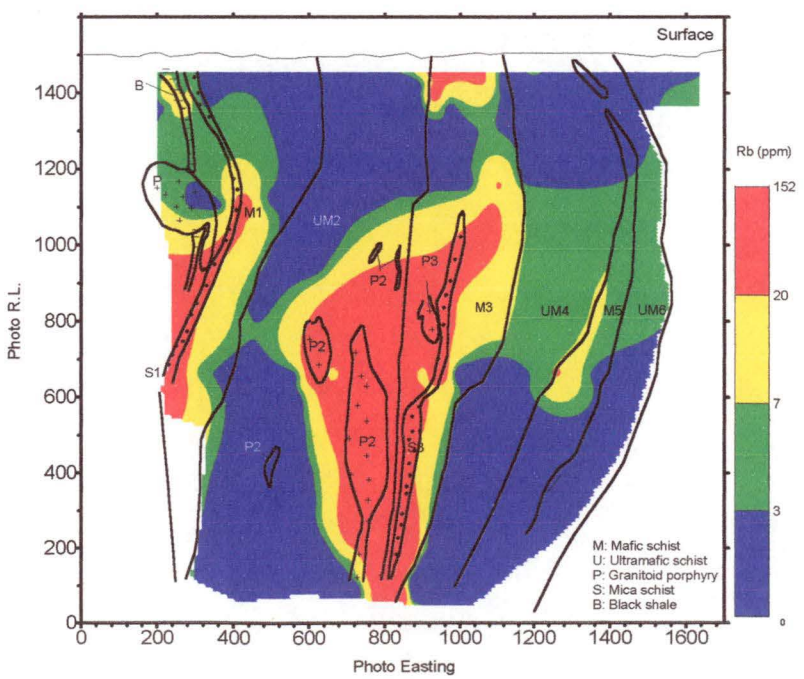

Figure 8-14. Rb distribution of acid insoluble residue at Rand Pit, Reedy Mine, W.A.

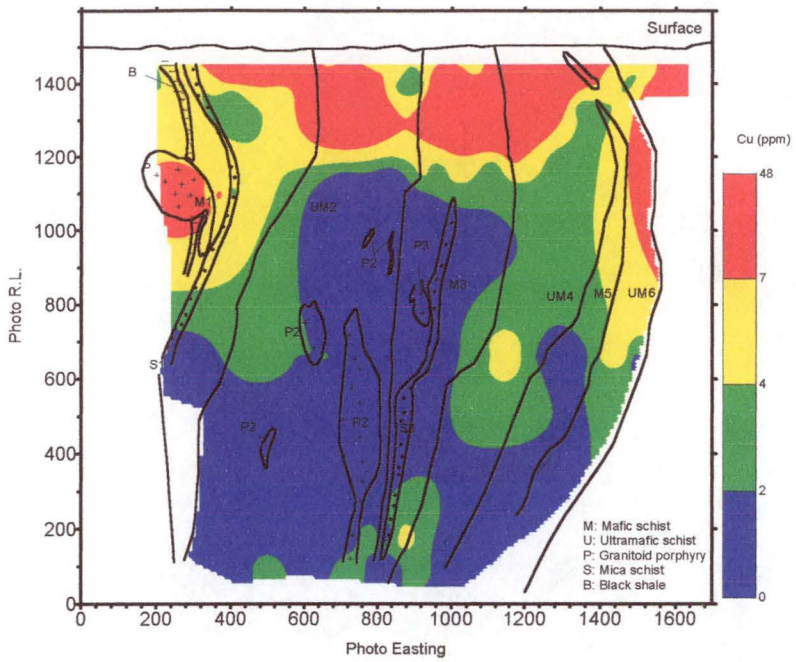

Figure 8-15. Cu distribution of acid insoluble residue at Rand Pit, Reedy Mine, W.A.

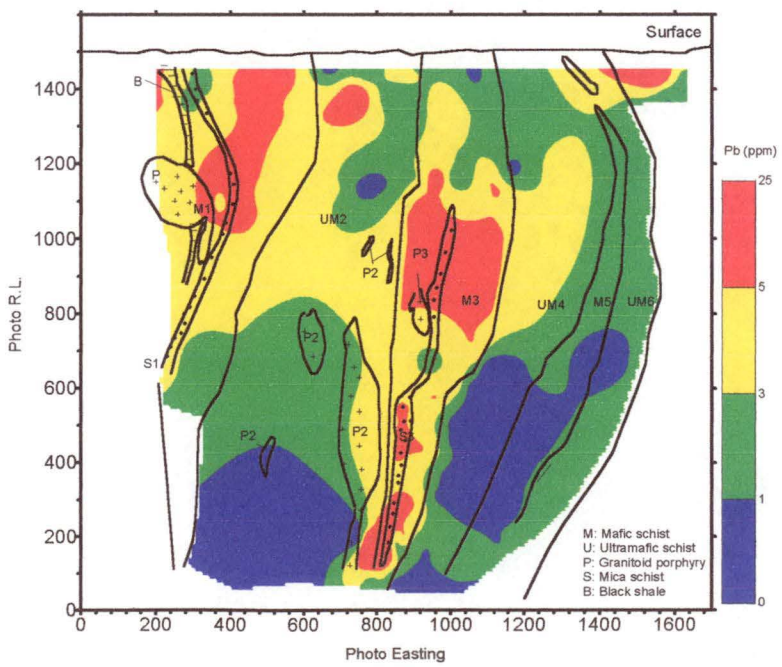

Figure 8-16. Pb distribution of acid insoluble residue at Rand Pit, Reedy Mine, W.A.

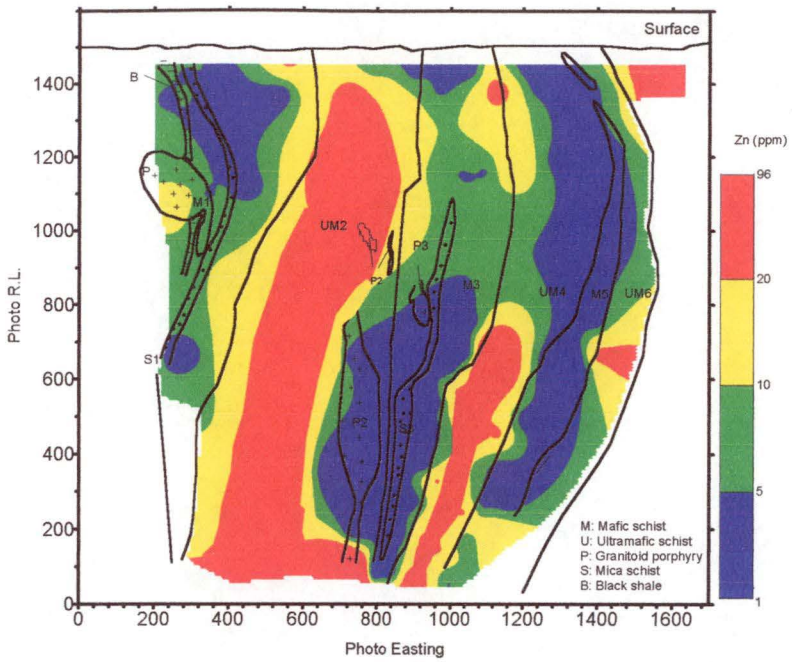

Figure 8-17. Zn distribution of acid insoluble residue at Rand Pit, Reedy Mine, W.A.

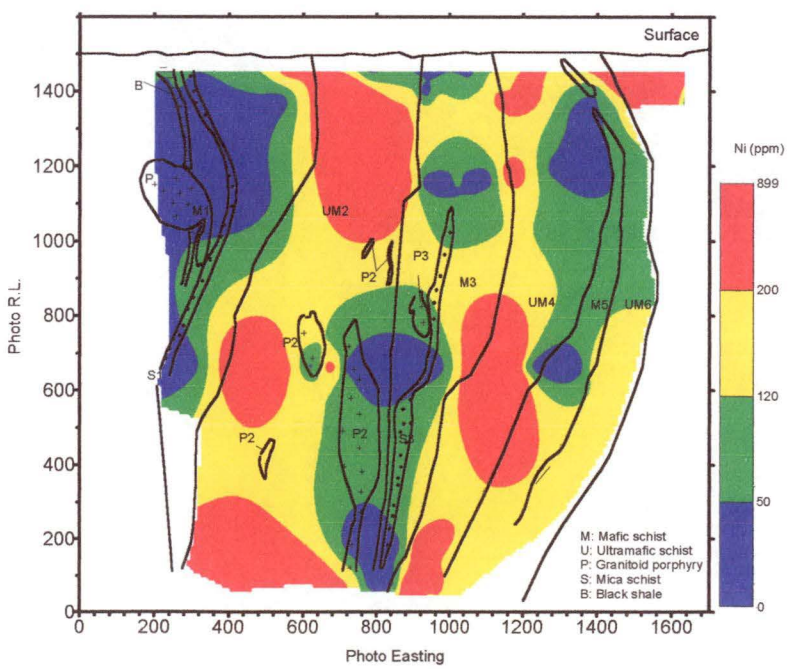

Figure 8-18. Ni distribution of acid insoluble residue at Rand Pit, Reedy Mine, W.A.

distributed within the ultramafic rocks. The enrichment of Pb in porphyries varies between from 0 to 25 ppm.

Zinc: Zinc has a range of 0 to 96 ppm. The distribution contour map is shown in Figure 8-17. Zinc is more concentrated in the ultramafic schist and varies from 3 to 96 ppm with an average concentration of 25 ppm. In contrast, it is rather low in other rocks, particularly in porphyries, where it is on average less than 4 ppm. The distribution of zinc in black shale, mafic schist and mica schist is very similar with an average concentration of 5 to 6 ppm.

Nickel: Nickel has a similar distribution pattern as zinc, with values ranging from 0 to 899 ppm. The distribution contour map is shown in Figure 8-18. The highest Ni values occur in the ultramafic schist. This high concentration extends into the upper part of the regolith profile with values up to 899 ppm. The average concentration is 277 ppm in ultramafic schist, which is much greater than in the other geological units, where it is less 10 ppm in porphyries and mica schist, and 20-50 ppm in black schist and mica schist.

Manganese: The manganese content of the regolith is very low. It ranges from 0 to 1071 ppm. The distribution contour map is shown in Figure 8-19. Manganese has very similar distribution pattern to that of Zn and Ni. There is neither marked nor enrichment leaching effect of Mn near the surface. Higher values occur deeper in the profile in ultramafic rocks, especially below the photo R.L. 600, where the Mn content is greater than 200 ppm. The average concentration of Mn content in ultramafic rocks is 430 ppm, which is far greater than that of other rocks (12–30 ppm).

8.3.5 Lithophile transition elements: (Cr, Ti and V)

Chromium: Chromium ranges from 0 to 4748 ppm. The distribution contour map is shown in Figure 8-20. In the acid insoluble residue, the most concentrated Cr occurs in the ultramafic rocks with the highest concentration greater than 4000 ppm. A near surface enrichment zone exists above the photo R.L. 700 m, about 40 m below the surface. In contrast, the concentration of chromium in the rocks near the ore shoots is very low (< 80 ppm), far less than the average concentration in these

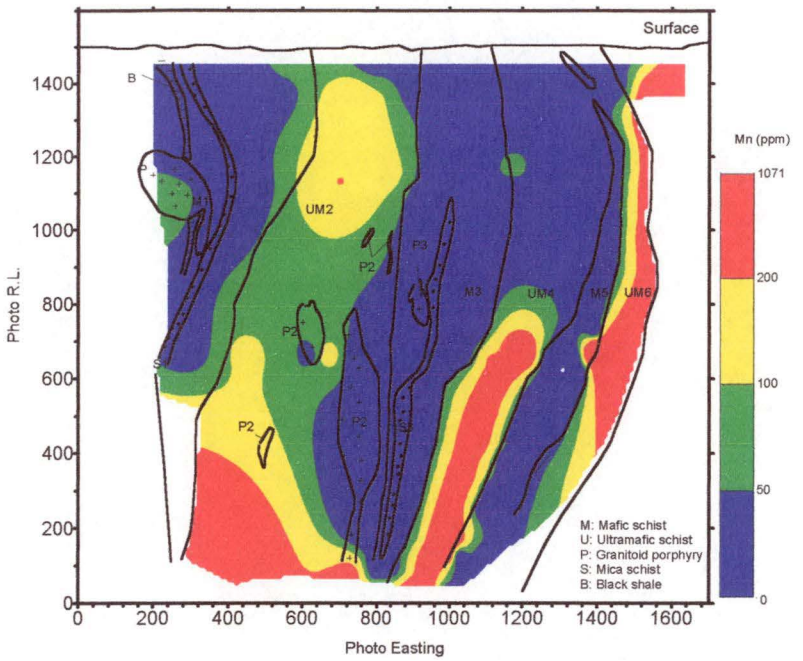

Figure 8-19. Mn distribution of acid insoluble residue at Rand Pit, Reedy Mine, W.A.

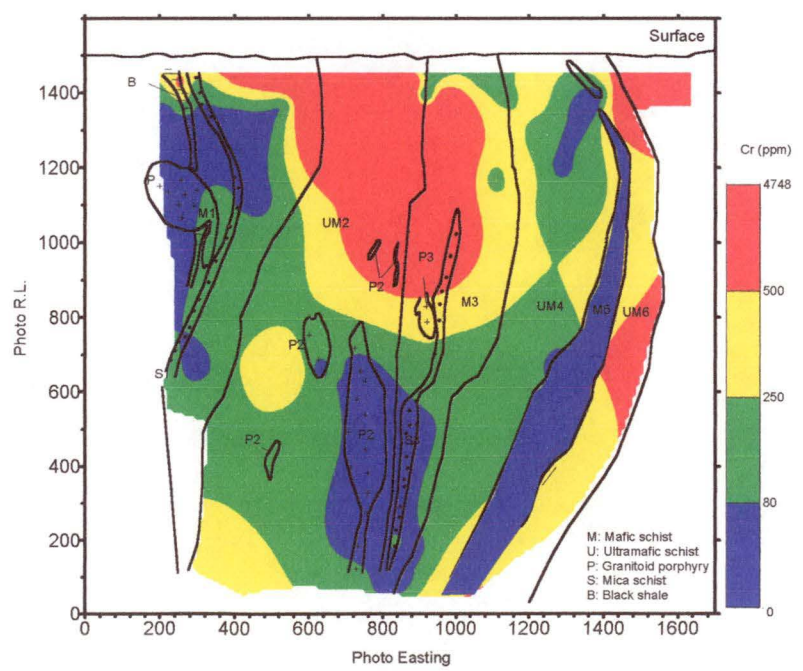

Figure 8-20. Cr distribution of acid insoluble residue at Rand Pit, Reedy Mine, W.A.

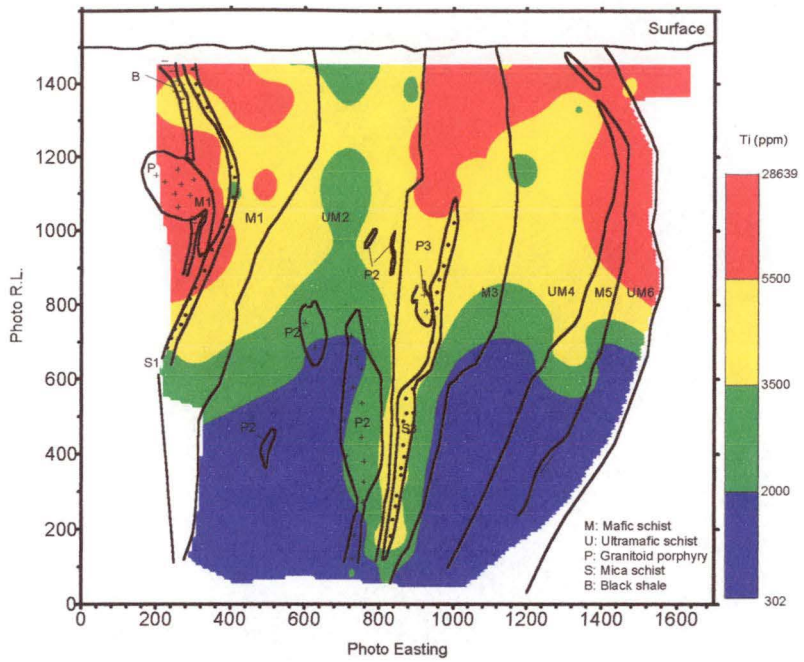

Figure 8-21. Ti distribution of acid insoluble residue at Rand Pit, Reedy Mine, W.A.

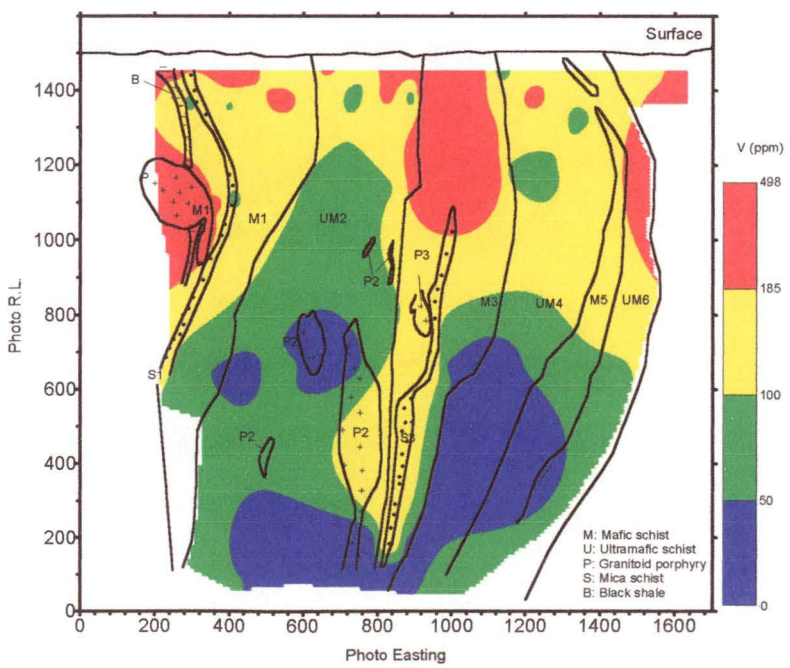

Figure 8-22. V distribution of acid insoluble residue at Rand Pit, Reedy Mine, W.A.

rocks. Chromium concentrations are also reasonably high in the mafic schist.

Titanium: Titanium ranges from 302 ppm to 28639 ppm in the regolith profile. The distribution contour map is shown in Figure 8-21. The content of Ti steadily increases upward and is strongly enriched in the upper zone of the profile with a value over 3500 ppm. It is more concentrated in the upper part of mafic schists (>5500 ppm). The concentration of Ti is lower under the photo R.L. 600 m, except in the mineralization zone of the mafic schist, where Ti is still higher than 2000 ppm. This value is greater than that of average concentration of ultramafic schist, very much like Al.

Vanadium: The vanadium content of the regolith has a range of 0–498 ppm. The distribution contour map is shown in Figure 8-22. Generally speaking, its distribution is similar to that of Ti. It is more enriched above the photo R.L. 800 m and shows lower values below. The enrichment zone is mainly within the mafic schist units. The average concentration in black shale and mafic schist is about 155 ppm which is three times than that of ultramafic rocks and porphyries while V is more concentrated in the mica schist (average 187 ppm).

8.3.6 Immobile elements: (Zr, Nb and Th)

These elements generally exhibit little chemical mobility in the weathering environment and all show strong surface enrichment in resistate minerals. The elements Zr, Nb and Th are all members of the second and third transition series and have very similar chemical characteristics. Zircon is probably the principal host mineral for each of these elements and hence the stability of zircon determines their distribution and dispersion in the regolith (Butt, 1991).

Zirconium: Zirconium varies from 15 to 469 ppm and increases upward through the regolith. The distribution contour map is shown in Figure 8-23. There are two very clear distribution zones of Zr in the regolith profile, and in ultramafic rock units of the profile have the lowest values. In the mafic schist rocks, the Zr is concentrated near the surface (>110 ppm) and above about photo R.L. 1100, 20 m below the surface. The average concentration of Zr is less than 21 ppm in the ultramafic schist with the lowest value 15 ppm. In contrast, Zr is more concentrated

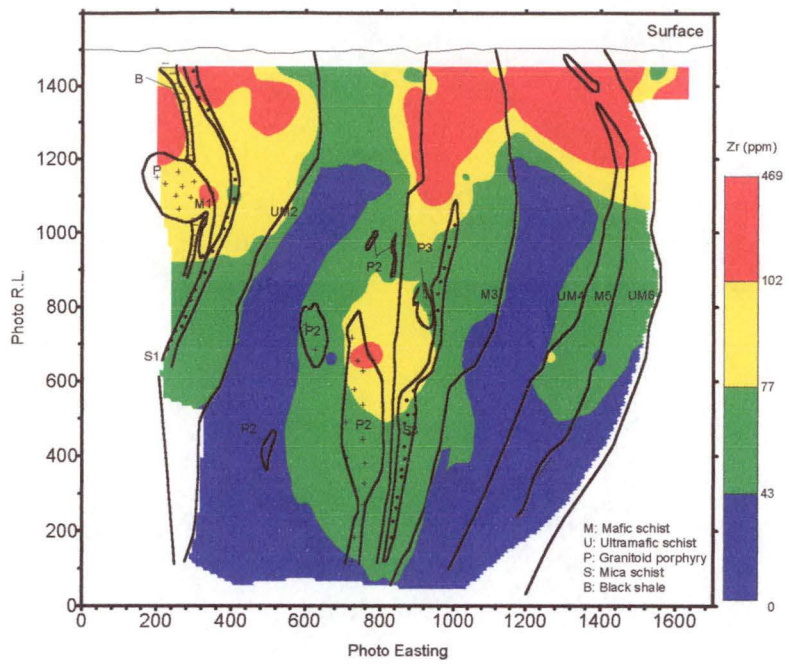

Figure 8-23. Zr distribution of acid insoluble residue at Rand Pit, Reedy Mine, W.A.

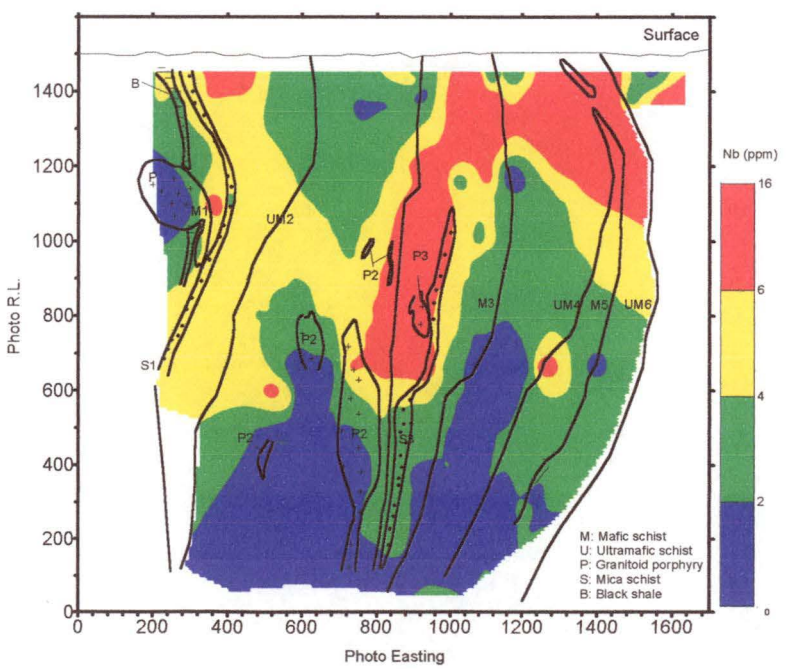

Figure 8-24. Nb distribution of acid insoluble residue at Rand Pit, Reedy Mine, W.A.

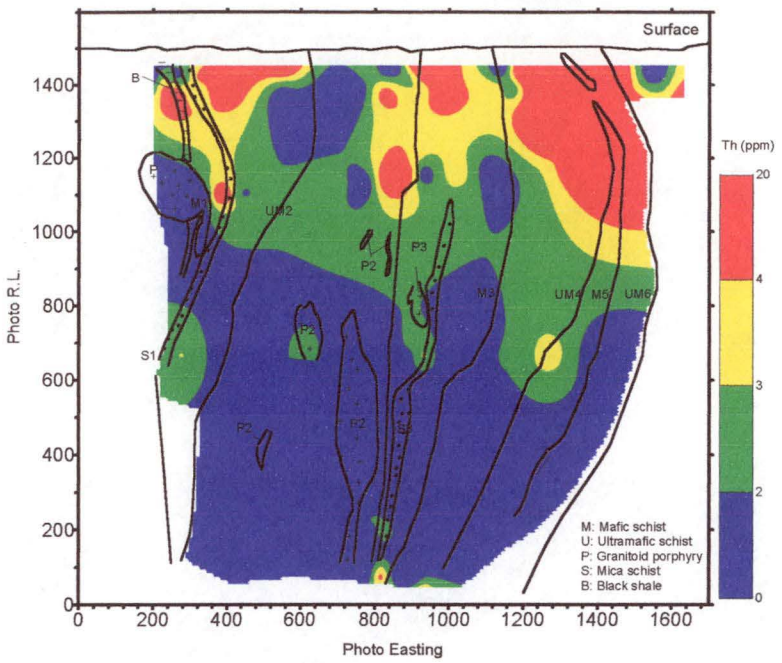

Figure 8-25. Th distribution of acid insoluble residue at Rand Pit, Reedy Mine, W.A.

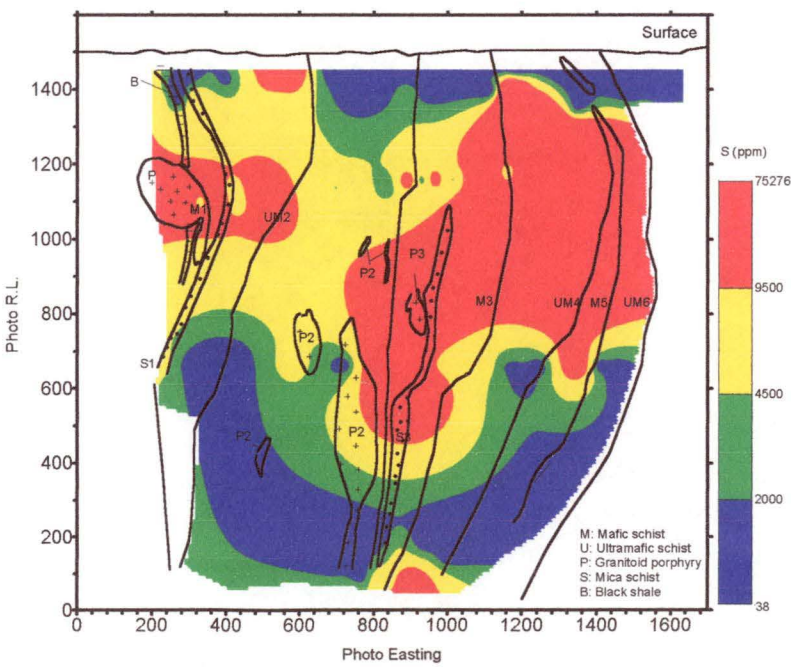

Figure 8-26. S distribution of acid insoluble residue at Rand Pit, Reedy Mine, W.A.

in mafic schist, especially in black shale where the average Zr concentration is 97 and 112 ppm respectively. The concentration of Zr in the porphyries and mica schist is very similar with an average concentration of about 70 ppm.

Niobium: Niobium concentration in the regolith ranges from 0 to 16 ppm. The distribution contour map is shown in Figure 8-24. Its distribution in the upper part of the profile is very similar to that of Zr. Niobium is enriched from the middle to upper part of the profile in ultramafic schist. Compared with the concentration of zirconium, Nb has the lower values both in ultramafic schist and porphyries. The average content is close to 1 ppm.

Thorium: Significant accumulations of thorium are also noted in the upper zone of the profile. Its content in the profile varies from 0 to 20 ppm. The distribution contour map is shown in Figure 8-25. Compared to the average value of 1 ppm in the ultramafic schist, Th is higher in mafic schist and black shale, which is 3 and 6 ppm respectively. In porphyries and mica schist, its level is close to that of ultramafic schist. Because Th concentrations are quite low and close to the detection limit, the element will not be discussed in the following section.

8.3.7 Elements associated with mineralization: (As, S, W, Ga, Mo, F, Y and Cl)

Arsenic: Arsenic has a range of 0 to 3 ppm. The As content of the acid treated residue is very low in Rand Pit, Reedy Mine. As average concentration is below 1 ppm in all of geologic units, which is below the detection limit of PIXE, the contour map has not been given here and the element will not be discussed in this study.

Sulphur: Sulphur in the acid insoluble residue ranges from 38 to 75276 ppm. The distribution contour map is shown in Figure 8-26. Zones of high S values, with an average concentration over 4500 ppm, are between photo R.L. 1300 and 600 in the saprolite horizon. In contrast, the concentration of sulphur in the near surface zones is quite low, at only a few hundred ppm, except for a few samples. Sulphur is also enriched near the ore shoot at the bottom of the mica schist and black shale.

Tungsten: Tungsten varies from 0 to 33 ppm in the regolith profile. The distribution contour map is shown in Figure 8-27. Tungsten is consistently enriched throughout

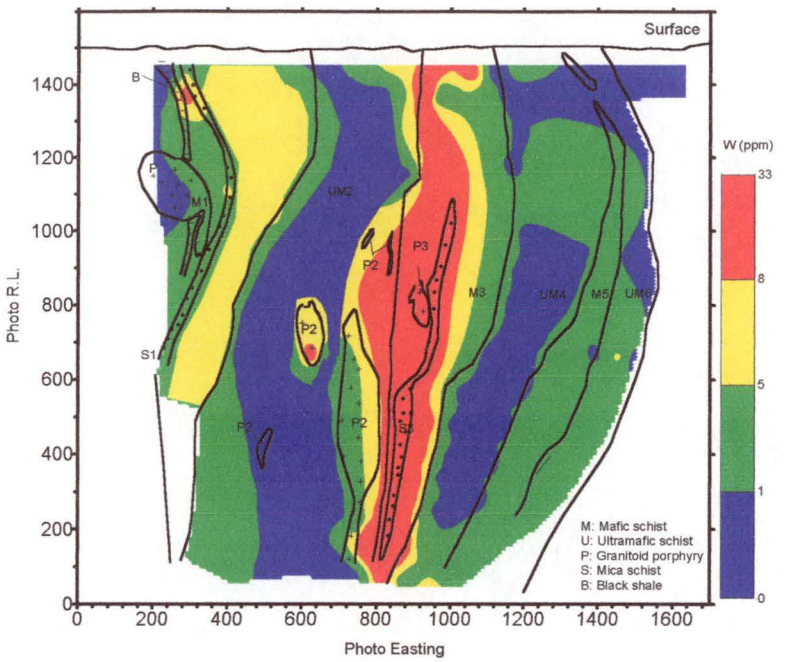

Figure 8-27. W distribution of acid insoluble residue at Rand Pit, Reedy Mine, W.A.

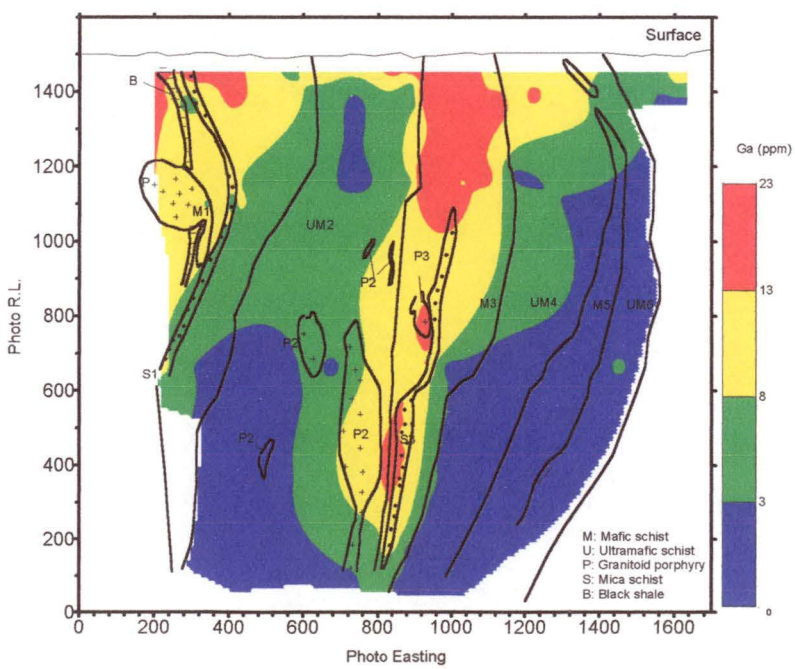

Figure 8-28. Ga distribution of acid insoluble residue at Rand Pit, Reedy Mine, W.A.

the main primary mineralization in M3, which is mainly related to the porphyry intrusion, and the mica and mafic schist. Average concentrations of greater than 10 ppm occur in the porphyries and mica schist, compared to less than 2 ppm in the unmineralized ultramafic rocks.

Gallium: The content of Ga varies from 0 to 23 ppm. The distribution contour map is shown in Figure 8-28. Its distribution is generally similar to that of W and Al in the regolith, but is concentrated in M1 and M3 where the primary mineralization occurred. The highest Ga concentrations (6–21 ppm) occur in the mafic rocks, porphyries, mica schists and black shale. The average concentration of Ga is normally greater than 10 ppm in mineralization related rocks, compared to less than 5 ppm in ultramafic rocks. Generally, high Ga occurs above the Photo RL 700, which is the middle to upper saprolite horizon.

Germanium: Germanium in the acid insoluble residue is very low. Although it ranges from 0 to 6 ppm, it is generally less than 2 ppm. The spatial distribution is not plotted here.

Molybdenum: Molybdenum has a range of 0 to 12 ppm, but is generally less than 2 ppm. The distribution contour map is shown in Figure 8-29. It shows some similarity with W, Ga and Al. Because levels of enrichment in the acid insoluble residue are close to the detection limit, Mo will not be used as a key element in Rand Pit.

Fluorine: The concentration of F changes from 56 to 642 ppm. The distribution contour map is shown in Figure 8-30. The concentration of F is more enriched in the ultramafic and mica schist (average concentration about 200 ppm) than in mafic schist and porphyry intrusion (average concentration from 110 to 140 ppm). There is no depletion or enrichment to be observed in the profile.

Yttrium: The distribution of yttrium in the regolith is rather simple. It ranges from 0 to 27 ppm. The distribution contour map is shown in Figure 8-31. The high values of Y mainly occur in the mafic schist of the upper part of the profile. Some high values occur in the ultramafic rocks, but the average concentration is lower than that of mafic rocks (5 ppm) and most of them lower than 3 ppm. The lowest

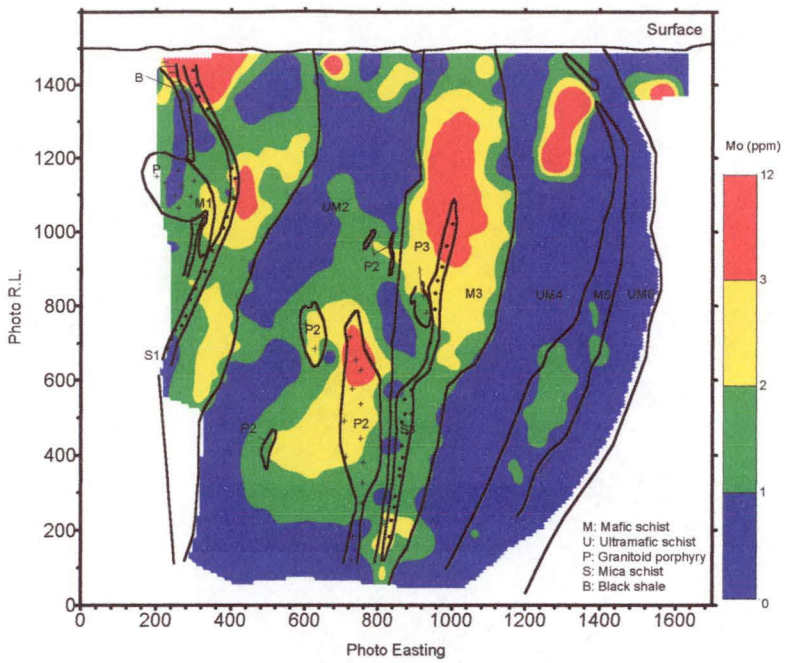

Figure 8-29. Mo distribution of acid insoluble residue at Rand Pit, Reedy Mine, W.A.

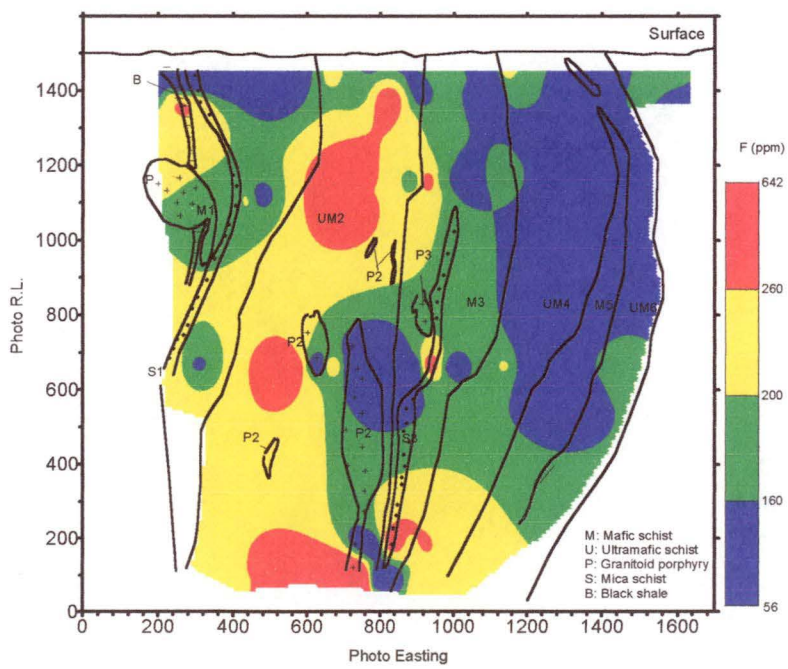

Figure 8-30. F distribution of acid insoluble residue at Rand Pit, Reedy Mine, W.A.

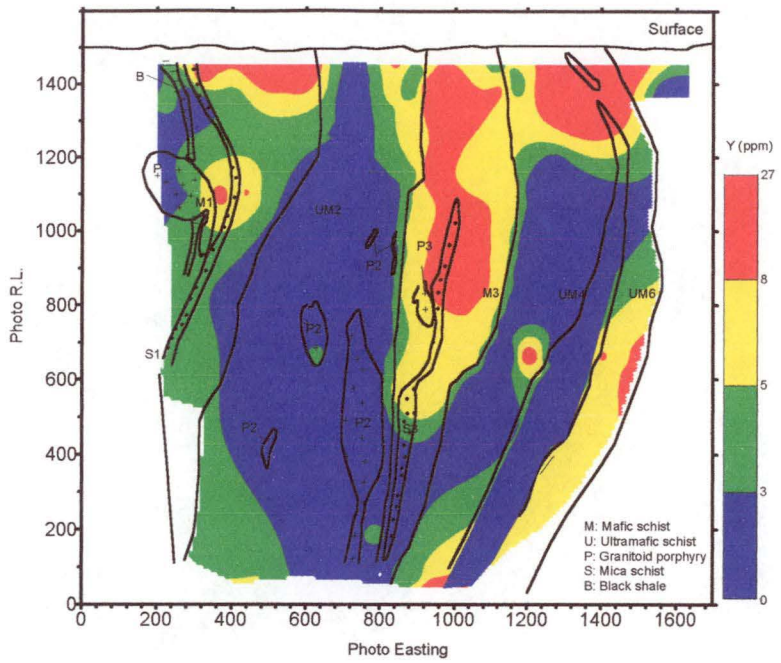

Figure 8-31. Y distribution of acid insoluble residue at Rand Pit, Reedy Mine, W.A.

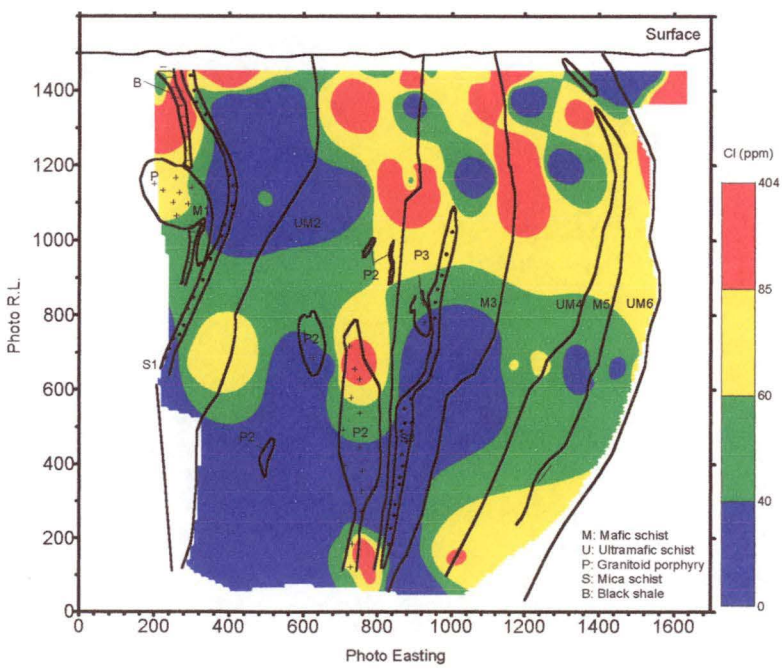

Figure 8-32. Cl distribution of acid insoluble residue at Rand Pit, Reedy Mine, W.A.

abundance of Y is found in porphyry intrusion, where Y ranges from 0 to 4 ppm.

Chlorine: Chlorine varies from 0 to 404 ppm. The distribution contour map is shown in Figure 8-32. Although the concentration of chlorine is not continuous, it is more concentrated above photo R.L. 800, perhaps expressing surface enrichment. Comparatively, the average concentration of chlorine is higher in porphyries and mafic schist, which are 87 and 68 ppm respectively. The lowest values are found in mica schist, which in only about a few tens of ppm.

8.4 DISCUSSION OF ELEMENT DISTRIBUTION

The geochemical behavior of acid insoluble residue of most elements varies with depth and lithology. This section provides the statistical results of 22 elements (i.e. Na, Al, F, K, Ca, Ti, V, Cr, Mn, Fe, Ni, Cu, Zn, Ga, Rb, Sr, Y, Zr, Nb, W and Pb; Au (INAA) of bulk geochemistry was also included). These elements chosen is based on the previous work mentioned in Chapter 5. They are mostly either alteration or lithology related. According to the results of factor and cluster analyses, a discussion is given on the element distribution of the acid insoluble residue detailed in section 8.3.

8.4.1 Statistics results

The 89 acid insoluble residue samples have been used in the statistical analysis. Due to the possible genetic link between alteration and mineralization, and in order to characterize the larger-scale alteration related to mineralization, attention was focused in this study on: (i) the variation in the intensity of geochemical alteration associated with the sericitization; and (ii) the chemical addition and depletion associated with alteration and mobilization. Factor and cluster analyses were chosen as appropriate statistical techniques to attain these objectives. Most researchers who use clustering methods experiment with a variety of similarity measures and clustering techniques, and choose the combination that yields the most satisfactory results with their data. The great benefit of cluster analysis is that it provides a way to classify objects (or say elements as different variables here) that is relatively simple and direct, and it presents the results in a manner that is both familiar and easily understood (Davis, 1973).

Arsenic, Ge and Mo were excluded from the factor and cluster analyses due to the high proportion of analytical results below detection limits. Prior to the factor and

Table 8-1. Spearman correlation mattrix of Rand Pit, Reedy Mine, W.A. (data was logarithm based 10, n=89)

	Au	F	Na	Al	K	Ca	Ti	V	Cr	Mn	Fe	Ni	Cu	Zn	Ga	Rb	Sr	Y	Zr
Au	1 00	0 07	0.11	0 34	0.34	-0 07	0 17	0 08	-0.13	-0 35	-0 37	-0 47	-0 15	-0 38	0 33	0.36	0 25	0.15	-0 18
F	0 07	1.00	-0.07	-0.38	-0.12	-0 03	-0.15	0 03	0.40	0 39	0.43	0 26	-0.11	0 47	-0 20	-0.09	-0 33	-0.17	-0 36
Na	0 11	-0 07	1.00	-0 20	0.61	0 56	-0.48	-0 56	-0.58	0.10	-0.28	-0 37	-0.45	-0 24	-0.31	0 58	0 69	-0 18	-0 36
Al	0 34	-0 38	-0 20	1 00	0 22	-0 27	0.68	0.50	-0 02	-0.57	-0 50	-0 39	0 32	-0.51	0 84	0 27	0.23	0 28	0 78
K	0 34	-0.12	0.61	0.22	1.00	0.19	-0.16	-0 27	-0 67	-0.30	-0 56	-0.78	-0 42	-0.62	0 19	0 92	0 61	-0 10	0 05
Ca	-0 07	-0 03	0.56	-0 27	0.19	1 00	-0.47	-0 17	-0.08	0 37	0 12	0.00	-0 21	0.05	-0.36	0.12	0.48	0 23	-0 33
Ti	0 17	-0 15	-0.48	0.68	-0 16	-0 47	1.00	0 77	0.26	-0.23	0 01	-0.01	0 53	-0.09	0.56	-0 05	-0.24	0 21	0 67
V	0 08	0 03	-0 56	0 50	-0 27	-0.17	0 77	1.00	0 57	-0.01	0 28	0.20	0.43	0 08	0.46	-0.23	-0 36	0.40	0 53
Cr	-0 13	0 40	-0.58	-0.02	-0 67	-0 08	0 26	0 57	1 00	0 39	0 67	0.71	0 38	0 63	0 03	-0.61	-0 56	0 22	-0.05
Mn	-0 35	0 39	0.10	-0.57	-0 30	0.37	-0 23	-0 01	0 39	1.00	0 81	0.55	-0 03	0 75	-0 64	-0.21	-0 15	-0 11	-0 56
Fe	-0 37	0 43	-0 28	-0 50	-0 56	0.12	0.01	0 28	0 67	0.81	1 00	0.78	0.21	0.82	-0 51	-0.52	-0 52	-0 01	-0 40
Ni	-0 47	0 26	-0 37	-0.39	-0.78	0 00	-0.01	0 20	0 71	0.55	0.78	1.00	0.40	0.82	-0 35	-0.75	-0 51	0 04	-0 27
Cu	-0 15	-0 11	-0 45	0.32	-0 42	-0 21	0.53	0.43	0 38	-0.03	0 21	0 40	1 00	0 27	0.30	-0 32	-0.22	0 20	0 36
Zn	-0 38	0 47	-0 24	-0 51	-0 62	0.05	-0 09	0.08	0.63	0 75	0.82	0 82	0 27	1.00	-0.46	-0.54	-0 48	-0 05	-0 46
Ga	0 33	-0 20	-0 31	0 84	0 19	-0.36	0 56	0.46	0 03	-0.64	-0 51	-0 35	0 30	-0 46	1.00	0.21	0 09	0 35	0 76
Rb	0 36	-0.09	0 58	0 27	0 92	0 12	-0 05	-0 23	-0.61	-0 21	-0 52	-0 75	-0 32	-0 54	0 21	1.00	0 62	-0 14	0 06
Sr	0.25	-0.33	0 69	0 23	0 61	0.48	-0 24	-0.36	-0 56	-0 15	-0 52	-0 51	-0.22	-0.48	0.09	0.62	1 00	0 00	0 01
Y	0 15	-0.17	-0 18	0 28	-0 10	0 23	0 21	0.40	0 22	-0.11	-0 01	0 04	0 20	-0 05	0.35	-0 14	0 00	1.00	0 39
Zr	0 18	-0 36	-0 36	0.78	0 05	-0 33	0.67	0 53	-0 05	-0.56	-0 40	-0 27	0 36	-0 46	0.76	0 06	0 01	0 39	1.00
Nb	0 16	-0 13	-0 35	0 53	-0.08	-0 29	0 59	0 58	0.16	-0 31	-0.15	-0 17	0 21	-0.27	0 50	0.01	-0.17	0.30	0 71
W	0.47	-0 11	0 25	0 22	0 52	0 07	-0 03	-0 05	-0 40	-0 43	-0 57	-0 60	-0 31	-0 54	0 30	0 48	0.36	0 06	0 12
Pb	0 29	-0 16	-0.19	0.39	0.10	-0 26	0 41	0.33	-0 03	-0.25	-0 16	-0 27	0.17	-0 21	0 37	0.12	-0.06	0 18	0 32

cluster analyses, logarithm base 10 transformation were carried out for all elements in order to improve the symmetry of the frequency distribution.

Table 8-1 summarizes the Spearman correlation coefficient derived from the $\log_{10}$ transformed data of the 89 samples. It can be seen Au correlates well with Al, K, Ga, Rb, Sr, W and Pb implying they are mineralization or alteration related elements. Compared to the correlation table of bulk geochemical data calculated by Robertson et al. (1990) with 92 samples, the coefficients of these elements derived from the acid insoluble residue are more significant even if there are less samples involved in this study. Another group of elements, Zr, Ti, V, Y, Nb, are generally immobile and show a weak positive correlation with Au that is related to lithology. A moderate to strong negative correlation occurs between Au and Fe, Mn, Ni and Zn. In bulk geochemistry, the relationship between Au and Fe, Mn, Ni and Zn is also negative, but the level of correlation is much less. It can be concluded that the acid insoluble residue at Rand Pit is a better sample medium than in bulk geochemistry to define

Table 8-2. Factor score coefficient matrix, Rand Pit, Reedy Mine, W.A.

	Factor 1	Factor 2	Factor 3	Factor 4	Factor 5
Al	0.63	0.64	0.14	-0.08	0.16
Au	0.51	0.08	0.16	0.53	-0.23
Ca	-0.06	-0.52	0.73	-0.22	-0.14
Cr	-0.68	0.5	0.24	0.22	-0.13
Cu	-0.22	0.62	0.09	-0.3	0.29
F	-0.44	-0.11	0.02	0.72	-0.04
Fe	-0.89	0.07	0.24	0.16	0.17
Ga	0.58	0.66	0.04	0.04	-0.06
K	0.75	-0.43	0.14	0.21	0.24
Mn	-0.73	-0.3	0.38	0.14	0.29
Na	0.34	-0.77	0.3	-0.06	0.19
Nb	0.28	0.68	0.1	0.07	-0.01
Ni	-0.89	0.19	0.06	-0.17	-0.01
Pb	0.3	0.42	0.02	0.21	0.22
Rb	0.72	-0.36	0.17	0.26	0.38
Sr	0.6	-0.46	0.38	-0.24	0.16
Ti	0.16	0.83	0.07	0.1	0.33
V	-0.08	0.81	0.36	0.19	0.07
W	0.65	-0.15	0.06	0.29	-0.34
Y	0.09	0.4	0.6	-0.17	-0.47
Zn	-0.9	0.01	0.12	0.11	0.13
Zr	0.5	0.74	0.05	-0.2	0.01

geochemical characteristics.

From the principal component function, factor scores were obtained for a total of 22 elements (Table 8-2). They represent variation in different geological and geochemical functions.

Interpreted in this context, the result of the analysis for factor 1 indicates that Al, Au, Ga, K, Rb, Sr, W, Pb, Na and Zr are relatively enriched in the more altered rock portions, i.e. mafic rocks including the porphyry intrusions and alteration within the mafic rocks compared to the less altered ultramafic rocks. The less altered portions, on the other hand, are relatively more enriched in Cr, Fe, Mn, Ni and Zn. In factor 2, results suggest immobility of Al, Cr, Ga, Nb, Ti, Pb, V and Zr and their surface enrichment during the alteration and weathering.

The cluster analysis results are given in Table 8-3. The cluster 2 consists of Au, Na, Al, K, Ga, Rb, Sr, W and Pb, and is very similar to factor 1. The elements reflect the

Table 8-3. Oblique principal component cluster analysis

	Cluster 1	Cluster 2	Cluster 3
Al	0.86	0.24	-0.56
Au	-0.08	0.19	-0.11
Ca	-0.27	-0.15	0.92
Cr	0.1	-0.05	-0.24
Cu	0.45	-0.26	-0.12
F	-0.14	-0.42	0.19
Fe	-0.53	-0.64	0.88
Ga	0.85	0.22	-0.51
K	-0.07	0.76	-0.24
Mn	-0.42	-0.36	0.99
Na	-0.27	0.57	-0.08
Nb	0.75	0.04	-0.33
Ni	-0.35	-0.69	0.44
Pb	0.19	0.38	-0.26
Rb	-0.07	0.78	-0.25
Sr	-0.2	0.73	-0.14
Ti	0.91	0.01	-0.45
V	0.85	-0.05	-0.24
W	0.16	0.65	-0.27
Y	0.66	-0.03	0.09
Zn	-0.39	-0.65	0.5
Zr	0.76	0.09	-0.39

different alteration process related to mineralization. In contrast, elements Cr, Mn, Ni, Cu and Zn with the most negative component probably indicate ferromagnesian oxides (i.e. chromite) and asbolane ($Mn[O,OH]_2.[Co,Ni,Ca]_x.OH_2x/nH_2O$), or other manganese oxides like coronadite ($Pb, H_2O)Mn_2O_{10}$ occurring in the ultramafic rocks. The first cluster consists of Al, Cu, Ga, Ti, Ga, Pb, V and Zr. The data express the immobility of these elements during the alteration and weathering. The third cluster Ca, F, Fe, Mn, Ni and Zn reflects the ferromagnesian minerals. Fluorine may sit into biotite or muscovite. Reasons for inclusion of Ca in this group are not clear.

Application of the factor and cluster analyses using the acid insoluble residue data together with the Spearman correlation matrix, indicate that a possible alteration halo can be monitored by the group of elements: Au, Al, K, Ga, Rb, Sr, Pb and W, and probably also Na, V, Ti and Zr. The elements Al, Ti, V, Cr, Ga, Y, Zr, Nb and Pb, are not only immobile during metamorphism and weathering, but also did not undergo remobilization related to alteration of mafic rocks at Rand Pit, Reedy Mine. The elements Fe, Mn, Ni and Zn are related to ferromagnesian minerals.

8.4.2 General feature of elemental distribution

In Chapter 5, attention was given mostly to the specific features of irregularities in gold distribution and their link to hydrothermal alteration. Interrelationships of gold and regolith trace elements were introduced, but did not show universality.

Endogenic halos of such elements as Pb, Zn, Cu, As, Sb etc. in gold deposits have been studied by many workers. Certain elements of this group have been utilized in prospecting for gold ores. However, the necessity arises for an examination of these elements to determine if they are suitable for a deeply weathered profile, and also to compare gold halos with those of other "ore" element in the light of the regolith profile.

The author has at his disposal data on the distribution of trace elements in the regolith of all three regolith deposits mentioned in Chapter 1. It is thought, however, that it will be sufficient to use the Rand Pit, Reedy Mine as an example to show the interrelationships of gold with these elements and to see if the conclusion derived in Chapter 5 on Mt. Percy can be widely used.

8.4.3 Alteration/primary mineralization related elements

Although the concentration of many elements in the fresh ore zone is much lower in Rand Pit than in the Mystery Zone mentioned in Chapter 5, a similar group of elements can be recognized through the statistical analysis and geochemistry distribution patterns by use of acid insoluble residues. Unlike the bulk geochemistry, the Au associated elements in these two areas are different. In Mt Percy, mineralization/alteration is indicated by high concentration of W, Sb, As and K in the surface horizons and As, Sb, W, S and K (Butt, 1991). In contrast, Bi, U, K, Ba, Rb and the REE reflect the association of Au with mica schist, and Sn, W, Ag, Mo and Se also show weak correlation with Au, in Rand Pit (Robertson et al., 1990).

Gold, the best indicator for the primary mineralization, was plotted in the section on the south face of the Rand Pit. The anomalies in the mafic units (M1 and M3) occur where mica schists S1 and S3 cut across them. It shows a wider distribution at the upper part of the regolith, but is narrow along the envelope of M3 towards the bottom of the profile.

Distribution patterns similar to that of gold, can be seen for Al, Rb, K, Pb, W and Ga, and to a certain extent V, which can thus be considered to be mineralization related elements. All show significant correlation with Au, unlike other, so called, ore associated elements such as Zn, Cu and Sb. The elements As and Mo may be ore related but their concentrations are too close to the detection limit to be certain. This is to be expected where elements may be concentrated sporadically in a vein system (Robertson et al., 1990). Other elements, such as V, Ti and Zr, also show similar distribution to gold, but there is lack of continuity near the ore shoots. It is considered they are most likely related to lithology.

In the bulk geochemical data, Al is generally enriched in the upper part of the profile. The acid insoluble residue shows a similar Al distribution. Both the mafic and the ultramafic units show relative enrichments in Al in the upper part of the profile. The contours with larger than 0.4% Al occur in the upper 5–15 m of the profile. The extent of this surface enrichment is smaller than that of bulk geochemistry, in which higher Al occurs in the upper 10–20 m of the profile. Robertson et al. (1990) suggested that this may be due to deposition of kaolinite leached from the previously overlying (now stripped) duricrust and redeposited in the upper saprolite.

The enrichment of Al at the upper profile is the result of intense leaching of alkali and the alkaline earth elements that followed the destruction of feldspars, chlorites and amphiboles and the formation of the clay during lateritic weathering. Because the solubility of the weathering products in acids, the surface enrichment of Al in the acid insoluble residue remains a surprise, which can only be explained by entrapment of kaolinite and some residual muscovite in secondary quartz. Aluminium deeper in the porphyries and schist represent feldspar and muscovite, as discussed earlier.

Potassium and Rb have similar distribution patterns, where at Rand Pit, both of them show relatively vertical zonality from the bottom of the mica schist and mafic rocks. Their high concentration (K > 0.38% and Rb > 20 ppm) in the felsic rocks and mica schists is related to their concentrations in potash feldspar and micas. Some high K and Rb concentrations near the surface imply that mica persists and is enriched at the top of the profile. At depth, their concentrations are related to their K-feldspar host minerals.

The anomalous distribution of K and Rb in the acid insoluble residue is much clearer than in bulk geochemistry showing the alteration related to mineralization because the residue may represent their occurrence in micas. In bulk geochemistry, both K and Rb show only relatively limited areas of high concentration.

The W distribution in acid insoluble residue is very similar to that of bulk geochemistry and correlates well with the gold concentration and needs not to be discussed further. The overall pattern suggests some limited dispersion of W in the mineralization related units. Tungsten distribution is generally homogenous, indicating some dispersion during weathering. Tungsten is of great value as a near surface pathfinder for gold at Rand Pit.

The Ga distribution in acid insoluble residue is similar to that of bulk geochemistry, and very much like the Al distribution. Figure 8-33 shows the correlation between Ga and Al. The Ga/Al ratio from acid insoluble residue is relatively constant for all lithologies, whereas Ga is enriched in the black shale and mica schist from bulk chemistry analysis (Figure 8-34). Although the distribution of Ga in the lower part

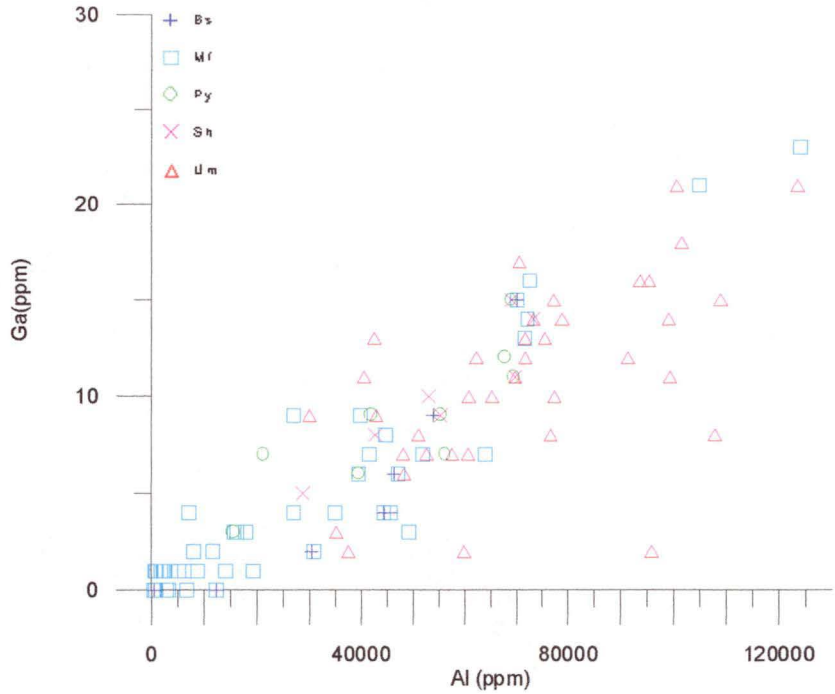

Figure 8-33. Al-K plots of acid insoluble residue illustrateing their close correlation

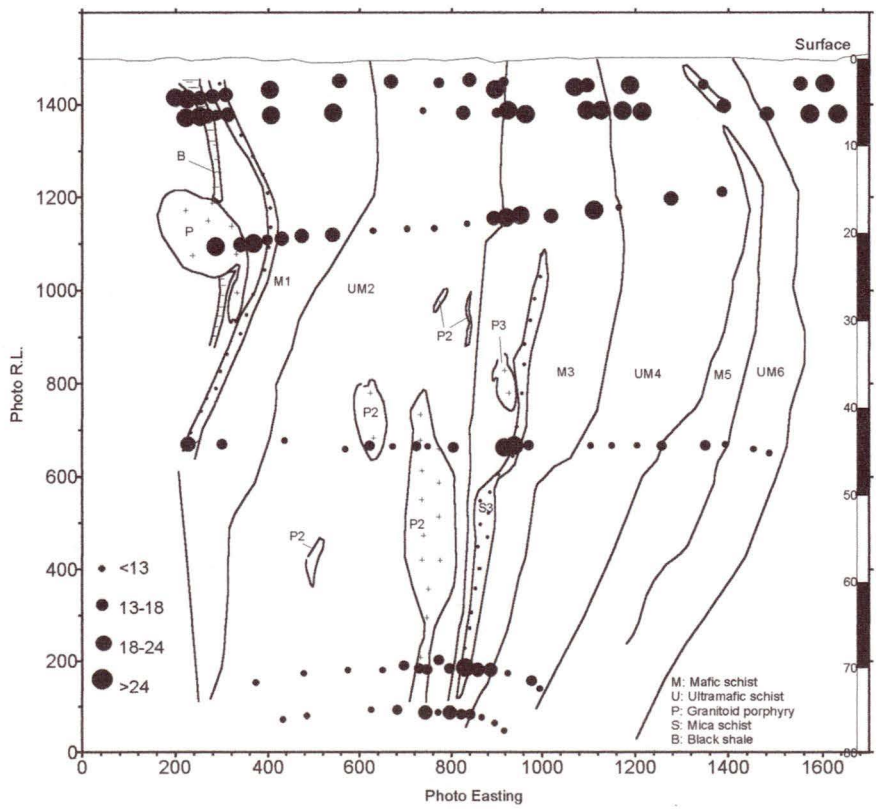

Figure 8-34. Ga (ppm) distribution of bulk geochemistry at Rand Pit, Reedy Mine, W.A.(aftre Robertson et al., 1990)

of the profile is erratic, the highest concentrations (13–23 ppm) are found over the mineralized zones, indicating Ga is either concentrated by substituting for Al particularly in feldspars, some amphiboles and micas or is hosted by the same mineral as W. The former assumption is preferred, because the Ga content is greater in the more aluminous porphyritic rocks (generally > 10 ppm). But its content in the fuchsitic ultramafic rocks is greater below the lateritic duricrust, where it ranges from 4–10 ppm, compared to that of talc ultramafic rocks where Ga is less than 2 ppm. It reflects the relationship of Ga to muscovite alteration in the fuchsitic rocks and porphyries. Its decrease in talc ultramafic rocks indicates it was originally related to chlorite where it substitutes for Al, but it was erased because of acid effects. This explains the general tendency of Ga to be dispersed through the whole regolith profile in bulk geochemistry, rather than its distribution which is related to muscovite alteration in the fuchsitic ultramafic rocks. Gallium in bulk chemical exploration (Figure 8-34) is less reliable as a surface indicator element than it is as an acid insoluble residue.

Figure 8-35 and 8-36 show the bulk geochemistry K and Ca distribution. Comparing with the acid insoluble geochemistry, it can been seen that the good correlation between the two methods exists at the bottom of the profile. The poor the correlation, the near the laterite horizon. It indicates that the acid insoluble residue geochemistry gives better accuracy of the primary geochemical signal than the analysis of bulk geochemistry.

Although Pb abundance is very low in the profile, especially after acid treatment, its distribution can still be clearly outlined around the ore shoots where it reaches the surface in M1. It is more widely distributed within the mafic rocks where mineralization occurs. There is no obvious depletion in the top of the profile.

Arsenic in the acid insoluble residue of the regolith at Rand Pit is low. After strong acid attack, the concentration of arsenic is less (<3 ppm) and most of the As data lie close to or below the PIXE detection limit (1–2 ppm). It is not a useful pathfinder at Rand Pit, and neither is As in the bulk chemistry of particular use because its halo is too broad.

Although much of the Mo data lie close to or below the PIXE detection limit, Mo

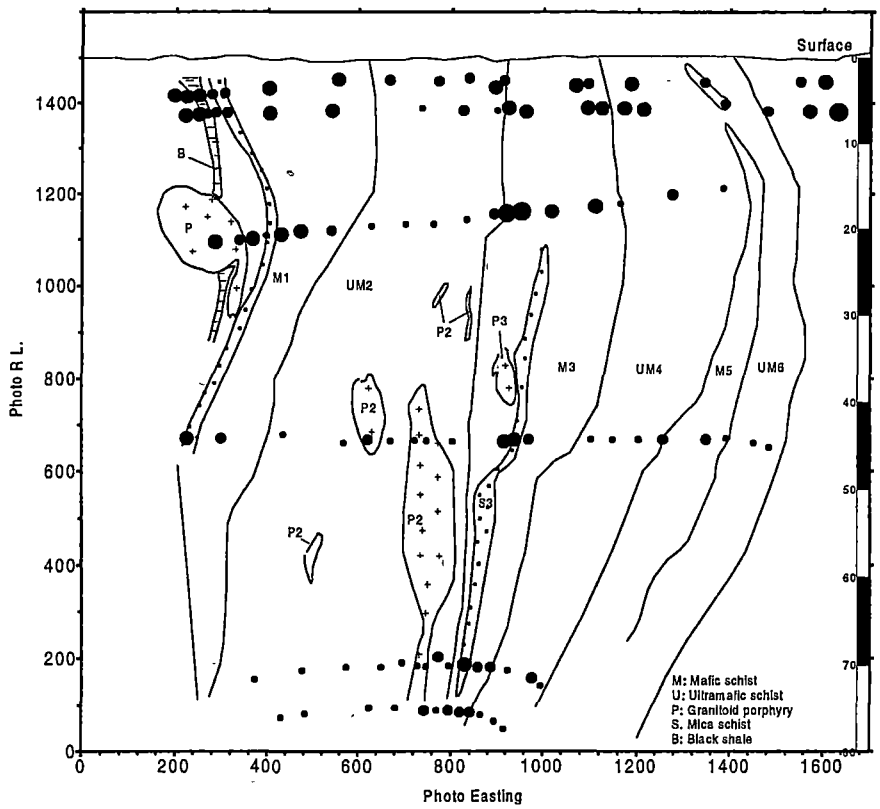

Figure 8-35. K (%) distribution of bulk geochemistry at Rand Pit, Reedy Mine, W.A. (aftre Robertson et al., 1990)

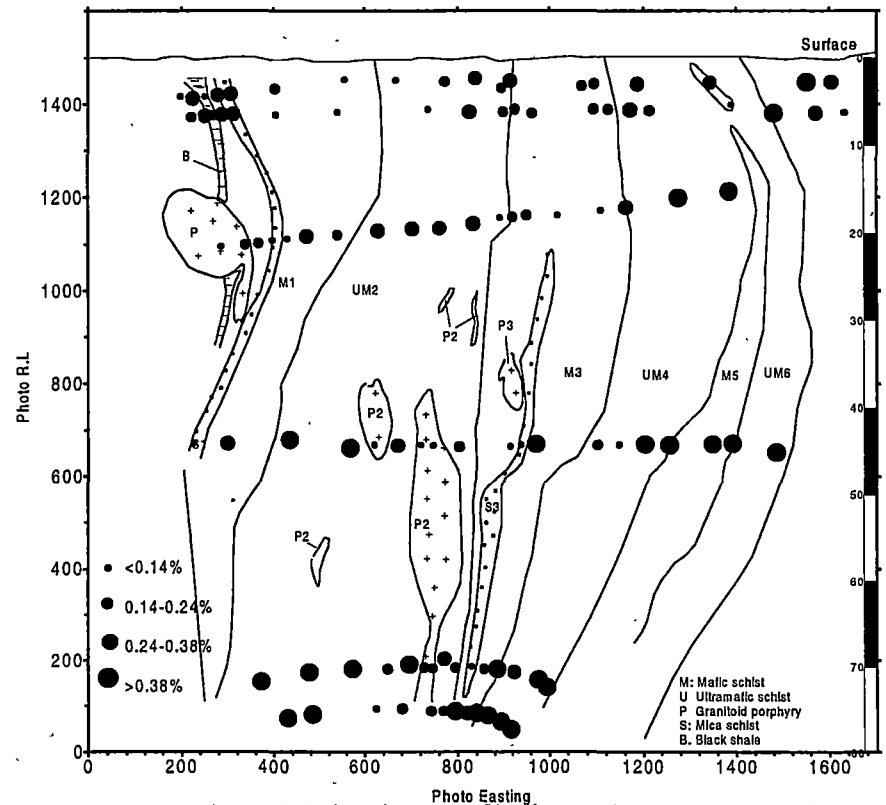

Figure 8-36. Ca (%) distribution of bulk geochemistry at Rand Pit, Reedy Mine, W.A. (aftre Robertson et al., 1990)

still seems to be weakly enriched (>2 ppm) locally in the upper part of the profile. Even though Mo seems to be related to the primary Au mineralization, the erratic nature of its anomalies in the upper part of the profile and enrichment in the porphyry pods suggests that Mo would not be a good pathfinder. Perhaps Mo analysis by a more sensitive analytical method (ICP/MS) would provide a clearer picture.

Although Na and Sr are statistically included in the alteration related group, there is no spatial correlation with gold mineralization. Na is probably the most strongly depleted. Plagioclase feldspar has been weathered completely very deep in the profile. Strontium in the acid insoluble residue is similar to that of bulk geochemistry. It characterizes the porphyry pods, the mafic rocks and, to a minor extent, entrapment in secondary chalcedony near the surface.

8.4.4 Lithology Related Elements

Elements, such as Al, Cr, Ga, Nb, Ti, V, Nb, Zr classified in cluster 2, are clearly related to lithology.

Aluminium and Ga differentiate the mafic and mica schist units and the porphyry pods from the ultramafic rocks. The Ga/Al ratio is relatively constant for the mafic and ultramafic rocks and the granitoid porphyries but Ga is enriched in the sedimentary rocks (black shale and mica schist) relative to Al. (Figure 8-33). Gallium and Al correlate with Ti, V, Cu, Rb, Sr, Zr, W and Pb.

Chromium shows a distinct concentration difference between the mafic and ultramafic units, especially in the lower part of the profile. The mobility of Cr on weathering depends upon its mineralogical form in the fresh rock. Chromites tend to survive weathering and the Cr in them accumulates as a residual elements (Robertson et al., 1990). Because Cr^{3+} closely resembles Al^{3+} and Fe^{3+} in its chemical properties and ionic size, it will behave similarly to these ions during weathering processes, and will be finally concentrated in clays. Under progressive oxidation, Cr in pyroxenes, amphiboles, micas and ilmenite is generally released as the soluble Cr^{2-} ion, which tends to be concentrated in residual weathering products (Shriaki, 1978). In laterites overlying ultramafic rocks, Cr is often concentrated up to several percent of Cr_2O_3 (Hotz, 1964). In the top profile of mafic units M1 and M3 (including mica schist), Cr is extremely concentrated (>500 ppm) even after the acid treatment

and most of clay minerals have been moved away, probably due to weathering of silicate-hosted Cr in ultramafic rocks. Two explanations may be feasible, the Cr is locked as chromite in secondary chalcedony or alternatively the element is locked in chrome bearing talc.

Titanium increases more steadily upwards through the profile in acid insoluble residue than in bulk geochemistry. Titanium in unaltered rock is present in ilmenite, sphene, rutile, biotite and amphibole (Robertson et al., 1990). On weathering it converts to stable anatase or may be taken up by clays (Correns, 1978) and Fe oxides. At Rand Pit acid insoluble Ti seems to be an alteration related element and a useful indicator for separating some lithologies. This element is at distinctly higher concentrations (average 5168 ppm) in the mafic and mica units. Some part of the upper profile show Ti enrichment, particularly those overlying the ultramafic rocks of UM4 and UM6. This is possibly due to residual concentration during weathering.

Vanadium is dispersed in the upper 15–40 m of the profile. High V values (>100 ppm) overlie both ore shoots and are also present as a dispersion to the east of the S3 ore shoot in the top 30 m of the profile. Its distribution pattern is very similar to Ti probably indicating they are hosted by the same minerals, e.g. titano magnetite. Within the mafic schist, the average concentration of V (188 ppm) is much higher

Table 8-4. Average values of Ti, Zr AND V in different geological units

Units	Ti	Zr	V
Black shale	3989	113	156
Mafic schist	5168	97	154
Porphry pods	2941	69	60
Mica schists	4809	71	188
Ultramafic schist	1063	21	53

than in the ultramafic rocks. It is probably due to the vanadian muscovite related muscovite alteration. But there is a lack of continuity between V anomalies in the uppermost part of the S3 zone and those at the ore shoots, which suggests either that the V is not related to the primary Au or that the V has been depleted at the bottom of the profile. One should be very cautious when using V as a pathfinder in Rand Pit.

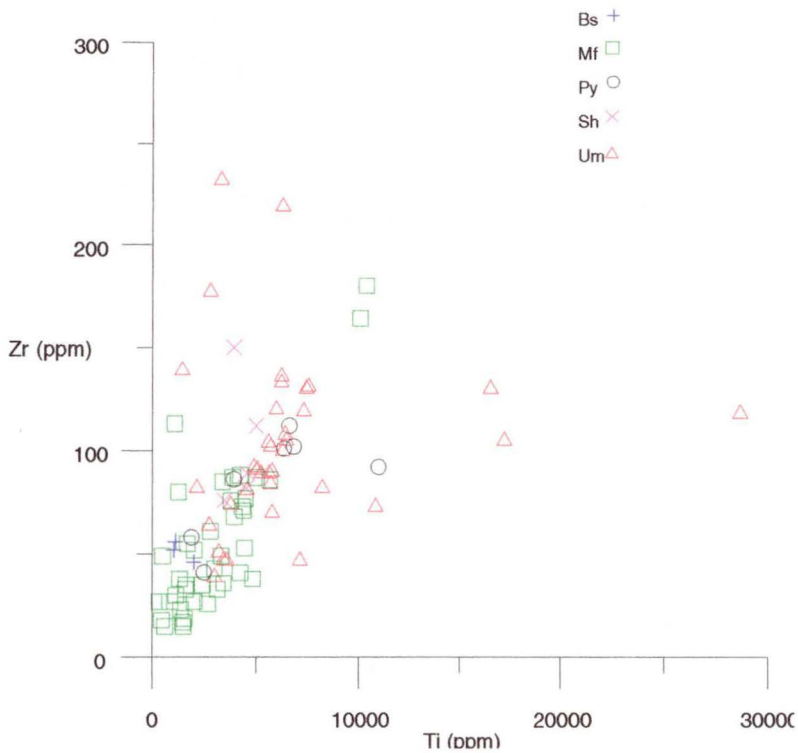

Figure 8-37. Ti-Zr plots illustrating their close correlation and concentration in the regolith and the poor discrimination between different lithologies

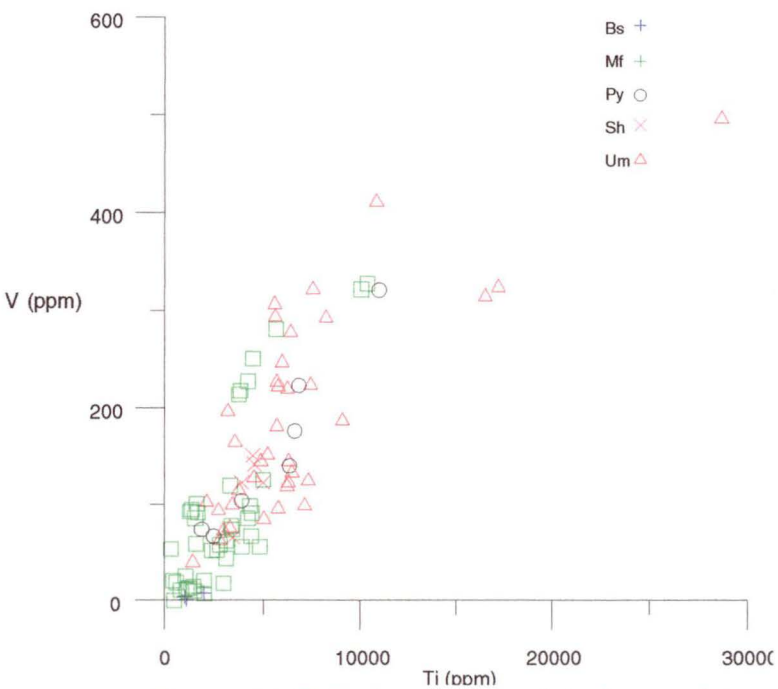

Figure 8-38. Ti-V plots illustrating their close correlation and concentration in the regolith and the poor discrimination between different lithologies

The lithological discrimination based on Ti-Zr plots is shown in Figure 8-37. It illustrates their close correlation in the regolith and the poor discrimination between different lithologies. Table 8-4 shows the average Ti, Zr and V in different geological units. The Ti and V plots (Figure 8-38) show very poor discrimination between different lithologies.

The higher Zr concentration (>65 ppm) in the mafic and mica schists persists through the entire profile. A significant, residual increase in the Zr content of the mafic and ultramafic rocks occurs in the top 10-15 m of the profile. The Nb distribution is very similar to that of Zr.

8.4.5 Ferromanganese related elements

The third cluster (Table 8-3) shows a group of associated ferromanganese elements, F, Fe, Mn, Ni and Zn. They are mostly concentrated in the ultramafic rocks, and are related to the occurrence of primary ferromanganese minerals such as tremolite and their alteration products such as manganese oxides.

Iron distribution is simpler in the acid insoluble residue than in the bulk geochemistry where it is locally enriched at the base of the mottled zone.

Nickel is abundant in the ultramafic rocks, and has very similar distribution patterns to that of Zn. It is strongly depleted in the mafic units around the ore shoots due to destruction of ferromagnesian minerals during hydrothermal wall rock alteration. Nickel therefore shows a strong negative correlation with Au. The distribution of Ni in the weathering process was studied by Turekian (1978), who found that Ni was controlled by the iron-manganese association. The surface and near surface expression of Ni has been strengthened to reflect the alteration, and/or silicate distribution. This can not be observed from the bulk geochemistry in which Ni is depleted near the surface, as Ni is rarely mobilized during weathering.

Zinc occurs in low concentrations (1–10 ppm) around the ore shoots and mineralization related mafic rocks and is generally depleted (<5 ppm) in the top a few meters of the profile. In contrast, it is strongly enriched (10–96 ppm) in ultramafic schist, even near the surface.

The distribution of Mn in the acid insoluble residue follow the pattern of Fe, Zn and Ni, but shows stronger depletion (<50 ppm) in the upper part of the profile overlying the mafic and, to a lesser extent, the ultramafic rocks. This indicates Mn is hosted by the same primary minerals as that of Fe.

The distribution of F shows a random orientation pattern, in spite of the numerically positive correlation with the other elements of cluster 3.

8.4.6 Shallow profile: Enriched elements

There is a zone of lateral Au dispersion with Au abundances of >10 ppb that in many places reaches >50 ppb. Strongly anomalous Au extends to the surface over the S1 and S3 ore shoots. This pattern suggests a zone of weak Au enrichment (>50 ppb) at about 10 meters, overlain by a zone of Au depletion (<10 ppb). In the acid insoluble residue, Al, Sr, Cu, Ti V, Y, Ga, Rb, K, W, Mo, Ca and Sr, are associated with the secondary enrichment. These elements are those of the first cluster, associated with mineralization plus Y, Mn, Ca and Sr, and to a certain extent Cu.

Aluminium and Ga are enriched at the surface, especially along the ore shoots in mafic rocks. Both could be very good pathfinder elements for gold in Rand Pit, Reedy Mine.

Rubidium and K are also enriched at the surface, but exhibit much smaller halos than those of Al and Ga. The Rb and K halos exist only above the ore shoots, and these surface enrichments reflect underlying gold mineralization.

Tungsten has similar distribution character to that of Rb and K near the surface. The limited dispersion of W in the upper horizon of the profile suggests that it is related to the underlying mineralization from its distribution above ore shoots. Tungsten is therefore a good pathfinder element.

Copper is anomalous in the upper 10–15 m of the profile, but has been depleted throughout the entire profile below 15–30 m. That explains the uncertainty of depletion zone between 15 to 30m. There is a lack of continuity between Cu anomalies in the upper part of the S3 zone and those at the surface in bulk geochemistry.

Robertson suggested either that the Cu is not related to the primary Au or that the Cu has been depleted from this zone. According to this study, from Cu in acid insoluble residue, it is depleted in the whole lower part of the profile, thus suggesting that the element is not ore-related.

Titanium, Zr and V have similar distribution pattern near the surface. They are enriched in the shallow part of the profile, and are particularly concentrated in the mafic rocks above the mineralization, and represent resistate minerals.

Yttrium is also enriched near the surface, but its distribution is erratic. Yttrium is more concentrated in the mafic rocks than in ultramafic rocks. Although Y is relatively abundant in the rocks surrounding the S1 and S3 ore shoots, it is strongly depleted at different levels overlying these ore shoots. The distribution of Y in the porphyries is rather low indicating a lower dispersion because it is a heavier rare element. The behavior of the Y in lateritic environment is not well understood. Burkov and Podporina (1967) reported a significant decrease in the lighter lanthanides, including Y, in the kaolinite zone overlying granitic rocks. They ascribed this decrease to leaching and lanthanide mobility under acid conditions.

Lead surface enrichment only occurs in M1. There is minor depletion in other units. It can be used as a subsurface pathfinder element. Although Mo has some surface expression related to its greater enrichment within mineralization related mafic and mica schists, they are too close the detection limit. Thus it may possible be a useful surface indicator, but it must be interpreted with some caution.

The distribution of the alkali earth elements, Ca and Sr, is somewhat similar in the upper part of the profile. Both of them are relatively enriched above photo R.L. 1200, and show a clear depletion zone from 15 m below the surface to 30 m, between photo R.L. 1200 to 700.

Strontium is concentrated across the uppermost part of the profile but seems to have been leached at depths between 10 and 25 m, except in the eastern part of the profile in ultramafic rocks. The depletion in Sr (< 2 ppm) is probably linked to feldspar breakdown which is thought to be a gradational process with plagioclase breakdown occurring deep in the profile and progressively greater K-feldspar degradation higher

up.

Calcium is more mobile than Sr. The depletion zone of Ca (<80 ppm) is much wider than that of strontium, which is about 30 m In bulk geochemistry, this depletion zone could not be observed due to their occurrence in carbonates and other clay minerals. Ca is more concentrated below the photo R.L. 700 (>400 ppm). This enrichment zone in the lower part of the profile indicates the less weathering effecting on feldspar and other main rock-forming components

The surface expression of Sr and Ca enrichment is mostly a result of their mobility. It indicates that they are very readily taken up by near-surface carbonates and also absorbed by clays. Although most of these carbonates and clay minerals have been washed out by strong acid treatment, the residue may still contain traces of these components and some feldspars which contributes to the difference between the surface expression and depletion zone.

8.5 MULTI-ELEMENT INDICES DISTRIBUTION

As has been discussed in section 5.5, well defined geochemical halos can be revealed around ore bodies a group of indicator elements are combined. In Randy Pit, Reedy Mine, the additive multiple elements have been used. Because the concentrations of some good indicator elements are very low in the acid insoluble residue, their distributions are sometimes erratic because of the instrumental drift or fluctuations of instrumental reading. With the additive method, these factors are reduced in varying degrees, e.g. Ge is too low to interpret its distribution in Rand Pit. By adding Ga and Ge, the distribution pattern revealing gold mineralization is enhanced.

Figure 8-39 shows the additive halos of Ga+Ge. Its distribution conforms to the mineralization halos. It is larger and more pronounced than any of their mono-element halos. The halos exhibit vertical zonality and break through to the surface in the saprolite showing the mineralization zone. In the upper portion of the cross section, the halos of Ga+Ge show a broad and a distinct tendency to indicate the gold enrichment near the surface.

Figure 8-40 shows the additive halos of W+Mo+Ga. It is the generally same as that of Ga+Ge, but its more pronounced above the clay saprolite zone. The additive

values of W+Mo+Ga present a very large anomalous zone around the gold mineralization and the primary halos break through to the surface, whereas the halos of each individual element are weaker and seldom beyond the metalliferous zone. However, this does not mean there is no relationship between these individual elements and gold. These small and weak halos are probably caused by the low sensitivity of the analytical methods used to detect these elements, where, in particular the element abundance is lower in acid insoluble residue than in bulk geochemistry.

Figure 8-41 and 8-42 show the additive halos of Cu+Pb+V and As+W+Mo. They are very pronounced compared to the former two additive items. The anomaly of Cu+Pb+V occupies in the whole regolith profile of the porphyries and the ultramafic rocks where the primary mineralization occurs, and penetrates to the surface. Because of the surface expression is so widespread caution must be exercised: perhaps Cu+Pb+V is elevated throughout the surface of the entire area, irrespective of mineralization. As+W+Mo is very similar to Ga+Ge and W+Mo+Ga and could be very useful as pathfinder indices.

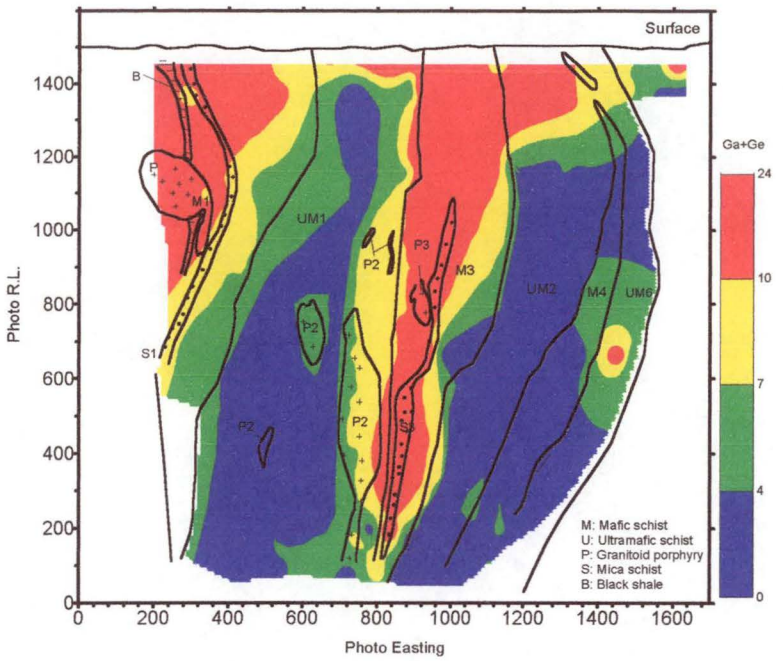

Figure 8-39. Ga+Ge distribution of acid insoluble residue at Rand Pit, Reedy Mine, W.A.

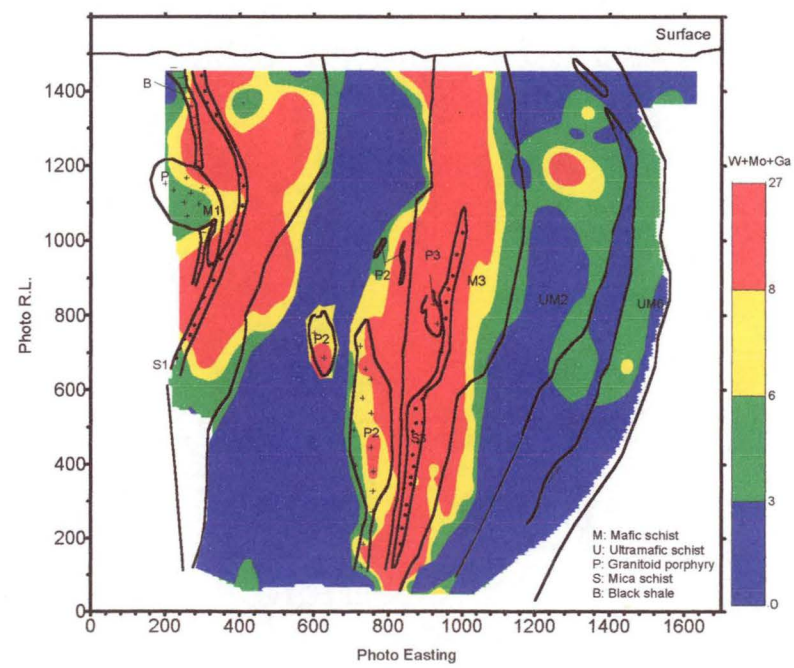

Figure 8-40. W+Mo+Ga distribution of acid insoluble residue at Rand Pit, Reedy Mine, W.A

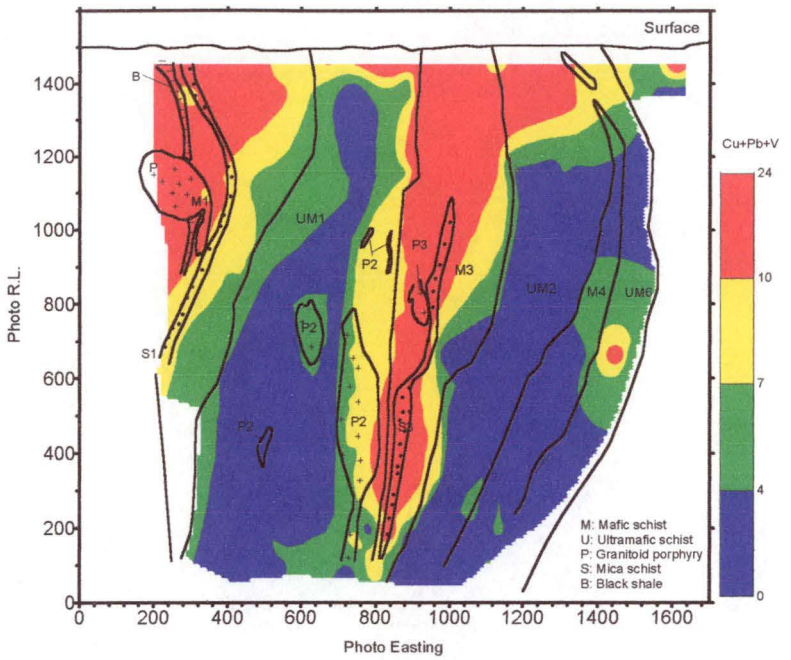

Figure 8-41. Cu+Pb+V distribution of acid insoluble residue at Rand Pit, Reedy Mine, W.A.

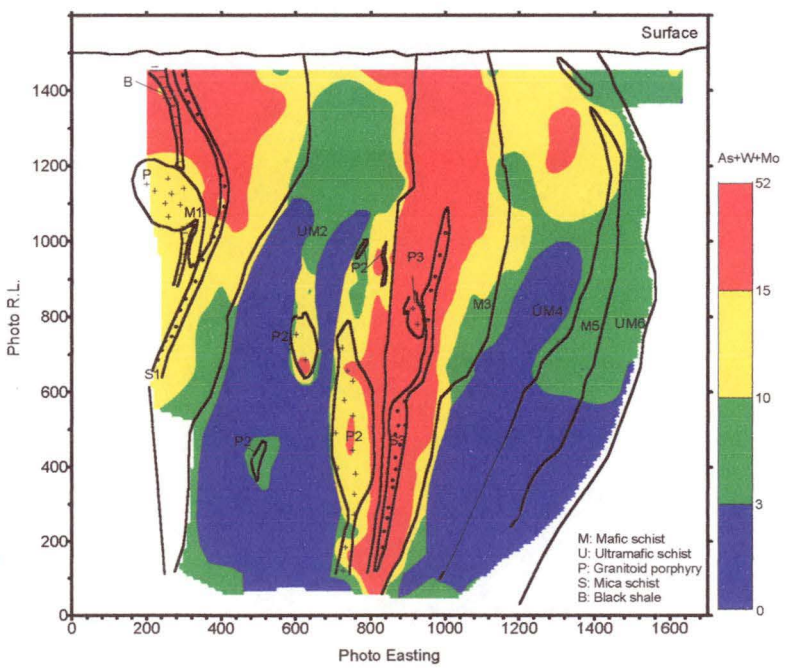

Figure 8-42. As+W+Mo distribution of acid insoluble residue at Rand Pit, Reedy Mine, W.A.

Chapter 9

EPR CHARACTERIZATION AT RAND PIT

9.1 EPR DISTRIBUTION

The EPR distributions together with geology at Rand Pit are plotted as contour maps in this chapter. The plotting intervals were selected on the basis of the principal population evident in the histograms and cumulative frequency graphs of the whole data set shown on Figure 9-1.

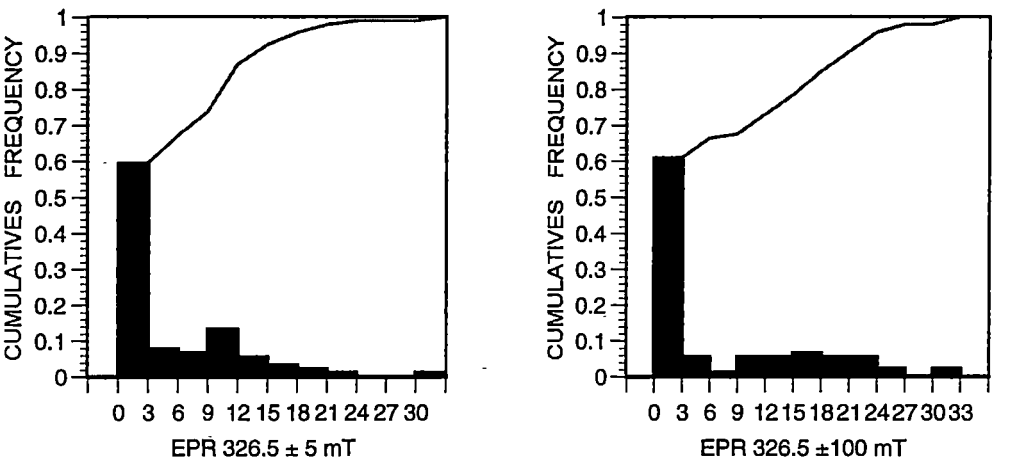

Figure 9-1. EPR histograms and cumulative frequency plots of acid insoluble residue at Rand Pit, Reedy Mine, W.A.

9.2 EPR 326.5 ± 5 mT

Comparative statistical data for EPR 326.5 ± 5 mT in the main regolith over the principal lithologies is given in Table 9-1.

At Rand Pit, the EPR signals measured at magnetic flux density sweep 326.5±5 mT are more pronounced in black shale (BS), mica schists (Sh) and mafic rocks (Mf). The intensity ranges from 0 to 23.5 with the average greater than 5. In contrast, the EPR 326.5 ± 5 mT signal is much smaller in the ultramafic rocks (Um). Although it ranges from 0 to 36 and the average value is 2.4, it is generally less than 1, with no EPR signal detectable in many of the samples and a few extreme values increase the

Table 9-1. Comparative statistics, EPR 326.5±5 mT (n = number of samples, x = arithmetic mean, s = standard deviation)

Units	Xmin	Xmax	n	x	s
Bs	0	11	4	5.25	6.08
Mf	0	23.5	39	7.5	6.44
Py	0	2.2	7	1.18	0.97
Sh	0	12.6	5	6.2	4.7
Um	0	36	37	2.4	6.7

Bs=Black shale Mf= Mafic schist Py=Porphyry Sh=Mica schist Um=Ultramafic schist

average value. The average EPR intensity in mafic units is two times greater than that of ultramafic units even allowing for the occasional high values in ultramafic rocks. These few high values of EPR signal occur near the surface next to mafic schist. They are probably due to the redistribution of some primary quartz.

The distribution pattern of the EPR intensity in the ±5 mT sweep is related to gold mineralization (Figure 9-2). The contour map shows that EPR ±5 mT values near the surface along the mafic schists are quite high (greater than 5 cm as measured under standard conditions). Two anomaly zones extend down to about 30 m below the surface in black shale and mica schist within the mafic schist. Below this level, the EPR intensities remain high to the base of the ore shoots. Most of EPR 326.5 ± 5 mT signals in the ultramafic rocks have zero values, except for some high measurements at the surface in UM4 near the M3, but this near surface anomaly only lasts a few metres. It is likely to be caused by the mechanical redistribution of the primary quartz near the surface. Generally speaking the EPR signature in ultramafic schists indicates that there is no mineralization. In contrast, the EPR 326.5±5 mT intensity signature is pronounced in black shale, mica schist and mafic rocks, where the gold mineralization occurs. The distribution pattern coincides well with the mineralization zone, including the mineralization related porphyry intrusive. Although EPR ±5 mT is not significant in porphyries, it still can be easily distinguished from its surrounding ultramafic rocks.

Thus EPR ±5 mT is one of the best mineralization indicators, particularly near the surface.

9.3 EPR 326.5± 100 mT

Comparative statistical data for EPR 326.5±100 mT in the main regolith over the principal lithological are given in Table 9-2.

The intensity of the EPR intensity measured at magnetic flux density sweep 326.5 ± 100 mT follows the Mystery Zone, Mt. Percy studies mentioned in the Chapter 6. In mafic rocks, it varies from 0 to 15 cm with the average value 1.77, but most of them are less than 1 cm. Its behavior in black shale and mica schist is similar to that of mafic rocks, but without any exceeding 5 cm. In porphyries, the average intensity is higher than those of black shale, mica schist and mafic units, but it still rather low compared to that of ultramafic rocks. The most pronounced EPR 326.5 ± 100 mT intensity signal occurred in ultramafic schists. These vary from 0 to 32 cm with the average 13.8 cm which is far more than those of other lithologies if mineralization is related.

From the distribution pattern of EPR 326.5 ± 100 mT intensity, a negative anomaly could be distinguished around the mineralization zone in the ultramafic rocks and it is possible to use it to distinguish different lithologies.

Table 9-2. Comparative statistics, EPR 326.5 ± 100 mT (n = number of samples, x = arithmetic mean, s = standard deviation)

Units	Xmin	Xmax	n	x	s
Bs	0	2.6	4	1.45	1.07
Mf	0	15	39	1.77	2.33
Py	0.3	11.5	7	3.5	4.68
Sh	1.2	3.2	5	2	0.83
Um	0	32	37	13.8	9.12

Bs=Black shale Mf= Mafic schist Py=Porphyry Sh=Mica schist Um=Ultramafic schist

9.4 EPR 326.5±250 mT

Comparative statistical data for EPR 326.5 ± 250 mT in the main regolith over the different lithological units are given in Table 9-3.

The signature of EPR intensity measured at magnetic flux density sweep 326.5 ± 250 mT follows that of EPR 326.5 ± 100 mT. Their distribution patterns are also almost identical.

Table 9-3. Comparative statistics, EPR 326.5±250 mT (n = number of samples, x = arithmetic mean, s= standard deviation)

Units	Xmin	Xmax	n	x	s
BS	0	2.6	4	1.45	1.27
Mf	0	15	39	1.77	2.28
Py	0.3	13.25	7	4.5	6.9
Sh	0	2.3	5	2	0.86
Um	0	29	37	13.2	8.44

Bs=Black shale Mf= Mafic schist Py=Porphyry Sh=Mica schist Um=Ultramafic schist

9.5 THE RELATIONSHIP BETWEEN EPR AND Au

Comparing the distribution pattern of gold (Figure 8-6) and EPR, it can be seen that the distribution of EPR 326.5 ± 5 mT intensities (Figure 9-2) is related to mineralization. It reflects the primary mineralization zone occurring in black shale and mica schist where situated in the mafic rocks. These primary alteration related EPR features remain preserved at the upper part of the profile. EPR, however, does not outline zones of secondary gold enrichment away from the vertical projection of primary gold mineralization.

The positive correlation between Au contents and EPR 326.5±5 mT spectrum is related to mineralised quartz which shows specific Au mineralisation properties. Concenquently, EPR 326.5±5 mT can be used as a very good surface indicator in the search for gold mineralization in geological setting similar to those at Rand Pit, Reedy Mine.

9.6 THE RELATIONSHIP BETWEEN EPR AND TRACE ELEMENTS

Spearman rank correlations between EPR and concentration of some elements are given in Table 9-4. Only the samples from porphyry, mica schist, mafic and ultramafic rocks have been used for the calculation because of the limited sample numbers in the black shales. EPR 326.5 ± 250 data have not been included because of their similarity to those of EPR 326.5 ± 100 mT.

The relation between EPR intensity measured at magnetic flux density sweeps 326.5 ± 5 mT and the alteration and/or mineralization related elements exhibit weak to moderate correlation in mafic and ultramafic rock units. As with the study at Mt.

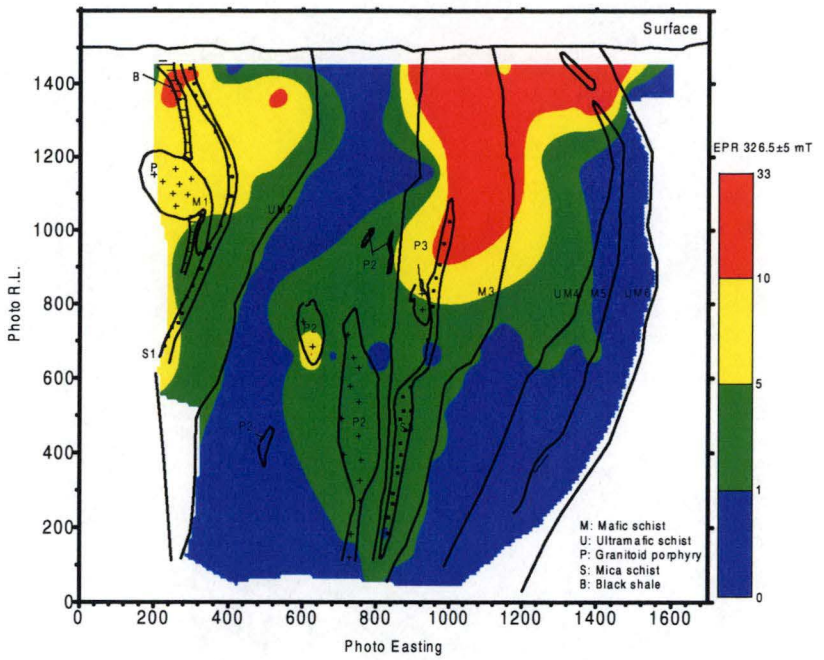

Figure 9-2. Distribution of EPR 326.5±5 mT of acid insoluble residue at Rend Pit, Reedy Mine, W.A.

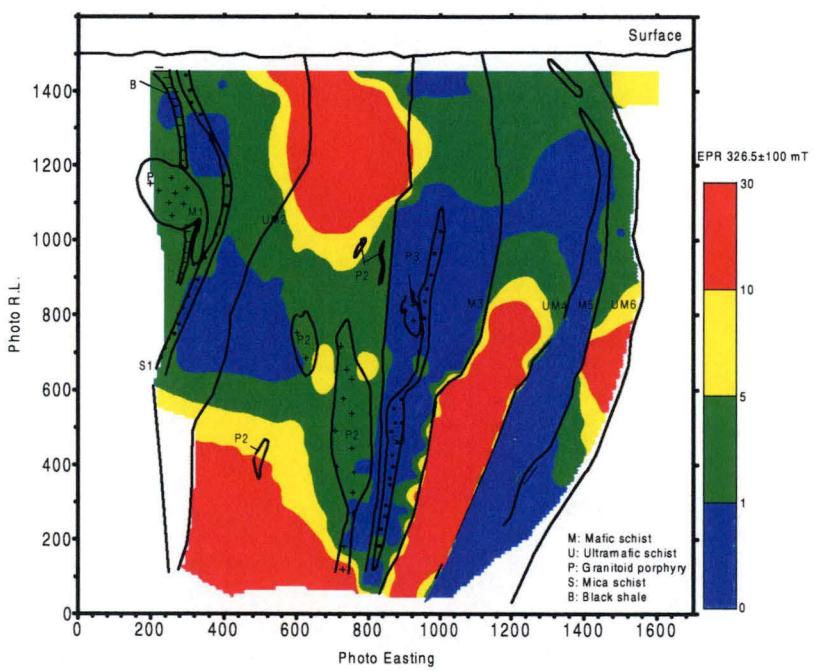

Figure 9-3. Distribution of EPR 326.5±100 mT of acid insoluble residue at Rend Pit, Reedy Mine, W.A.

Table 9-4. Spearman rank correlation coefficients between EPR intensities and some elements (n=93)

		Alteration/Mineralization related						
Unit	EPR	Al	K	Rb	Ga	Sr	W	Au
Py	±5 mT	-0.35	0.12	0.13	-0.03	-0.55	0.03	-0.25
(n=7)	±100 mT	-0.23	0.61	0.61	-0.61	-0.44	0.74	0.54
Sh	±5 mT	0.53	-0.2	-0.25	0.51	-0.08	0.24	-0.91
(n=7)	±100 mT	-0.25	0.52	0.58	-0.2	0.38	-0.07	0.76
Mf	±5 mT	0.5	-0.18	-0.13	0.37	-0.27	-0.15	-0.29
(n=28)	±100 mT	0.38	-0.14	-0.22	0.44	-0.37	0.08	-0.12
Um	±5 mT	0.47	-0.07	-0.01	0.41	-0.01	-0.1	0.11
(n=34)	±100 mT	-0.6	0.05	-0.05	-0.65	0.06	-0.08	-0.14

		Weathering related					
Unit	EPR	V	Y	Zr	Nb	Cr	Ti
Py	±5 mT	0.01	0.48	0.4	0.28	-0.04	-0.1
(n=7)	±100 mT	0.94	0.39	-0.03	0.38	0.06	0.83
Sh	±5 mT	0.51	0.76	0.09	-0.35	-0.2	0.63
(n=7)	±100 mT	-0.24	-0.76	-0.1	0.3	0.56	-0.46
Mf	±5 mT	0.4	0.1	0.23	-0.04	-0.05	0.17
(n=28)	±100 mT	0.46	0.29	0.42	0.47	0.07	0.52
Um	±5 mT	0.33	0.66	0.89	0.74	-0.22	0.67
(n=34)	±100 mT	-0.37	-0.28	-0.49	-0.45	0.25	-0.58

		Ferromanganese related					
Unit	EPR	Mn	Fe	Ni	Cu	Zn	Ti
Py	±5 mT	0.07	0.4	0.75	0.07	0.29	-0.1
(n=7)	±100 mT	0.91	0.81	0.05	0.29	0.56	0.83
Sh	±5 mT	-0.3	0.5	0.32	0.7	0.83	0.63
(n=7)	±100 mT	0.65	-0.53	-0.41	-0.84	-0.73	-0.46
Mf	±5 mT	-0.26	-0.28	0.06	0.44	-0.15	0.17
(n=28)	±100 mT	-0.24	-0.17	-0.28	-0.02	-0.14	0.52
Um	±5 mT	-0.31	-0.49	-0.26	0.31	-0.33	0.67
(n=34)	±100 mT	0.56	0.69	0.32	-0.24	0.64	-0.58

Py=Porphyry Sh=Mica schist Mf= Mafic schist Um=Ultramafic schist

Percy, EPR 326.5 mT and trace elements Al, K, Rb, Ga, W and Pb have moderate to high correlation coefficients indicating a close relationship between the muscovite alteration and gold mineralization in mica schist and mafic rocks. A strong positive relationship exists between EPR and weathering resistant mineral related elements Ti, V, Y, Zr and Nb in mica schist than in mafic rocks. This is possibly due to the presence of zircon coming from older basalts. The recognition of zircon from different provenance by EPR are discussed in Yim (1997). Older zircon has a more pronounced

EPR signal. Higher levels in the mica schist and black shale probably mean these minerals are more stable during sedimentary rock formation and acted as accompanying elements together with the gold mineralization. In the ultramafic rocks, EPR 326.5 ± 5 mT shows moderate to strong positive relationship with these lithologically related elements, but a very weak negative relationship with the group of alteration related elements. EPR 326.55 mT does not show a strong correlation relationship with the mineralization related elements in porphyries offering some evidence that probably the porphyry intrusive pods are not related to mineralization.

In contrast, the relationship between EPR intensity measured at magnetic flux density sweeps 326.5 ± 100 mT and the trace elements is quite different. EPR 326.5 ± 100 mT positively correlate very well with K, Rb and Sr in the mica schists showing the correlation between EPR 326.5 ± 100 mT and albite and muscovite alteration. Its higher correlation with the resistant elements in mafic rocks, such as, Ti, V, Zr, Nb and Y, reflects its resistant feature under the weathering process in Reedy Mine area. There is also a moderate correlation between EPR 326.5±100 mT and some mineralization related elements, such as Al, Ga and As in the mica schists and mafic rocks. However, this correlation between EPR.326.5 ± 100 mT and mineralization related elements is weaker than that for EPR 326.5 ± 5 mT. In the ultramafic rocks, the intensities of EPR 326.5±100 mT show high positive relation with Mn, Fe, Ni and Zn, which represent ferromanganese minerals. In contrast, it shows stronger negative relationship with the group of mineralization related elements. EPR326.5 ± 100 mT and ferromagnesian mineral related elements in black shale and ultramafic show moderate negative correlation whereas they show positive correlation in porphyries and ultramafic rocks.

EPR intensity measured in 326.5 ± 250 mT sweeps exactly follows that of EPR 326.5 ± 100 mT.

Figures 9-4 and 9-5 plot EPR 326.5 ± 5 mT and ±100 mT against. Al, Ga, Cu, V, Ti and Zr showing the relation between EPR signature and these elements. Generally speaking, EPR 326.5 ± 5 mT is more significant in mafic rocks. In contrast, EPR 326.5 ± 100 mT signals are stronger in ultramafic units. This implies that the EPR 326.5 ± 5 mT is mainly primary quartz related, while EPR 326.5 ± 100 mT is controlled by ferromanganese minerals. The relationship between EPR and chemical

analysis reveals that EPR 326.5±5 mT shows moderate to high positive linear correlation with Al, Ga, V, Ti and Zr, but EPR 326.5 ± 100 mT do not show this high correlation.

It is interesting to note that although there is a positive correlation between the intensities of the EPR 326.5 ± 5 mT signal and the spatial distribution of Au in the profile, there is no positive correlation between the EPR intensities and the spatial Au contents in the rocks. This confirms the conclusion of Russell and van Moort (1997) for an auriferous reef: EPR is not a substitute for Au assay; it provides only an indicator that Au may be present. The same authors also stressed that it is extremely unlikely to find remnants of Au in the absence of a strong EPR signal.

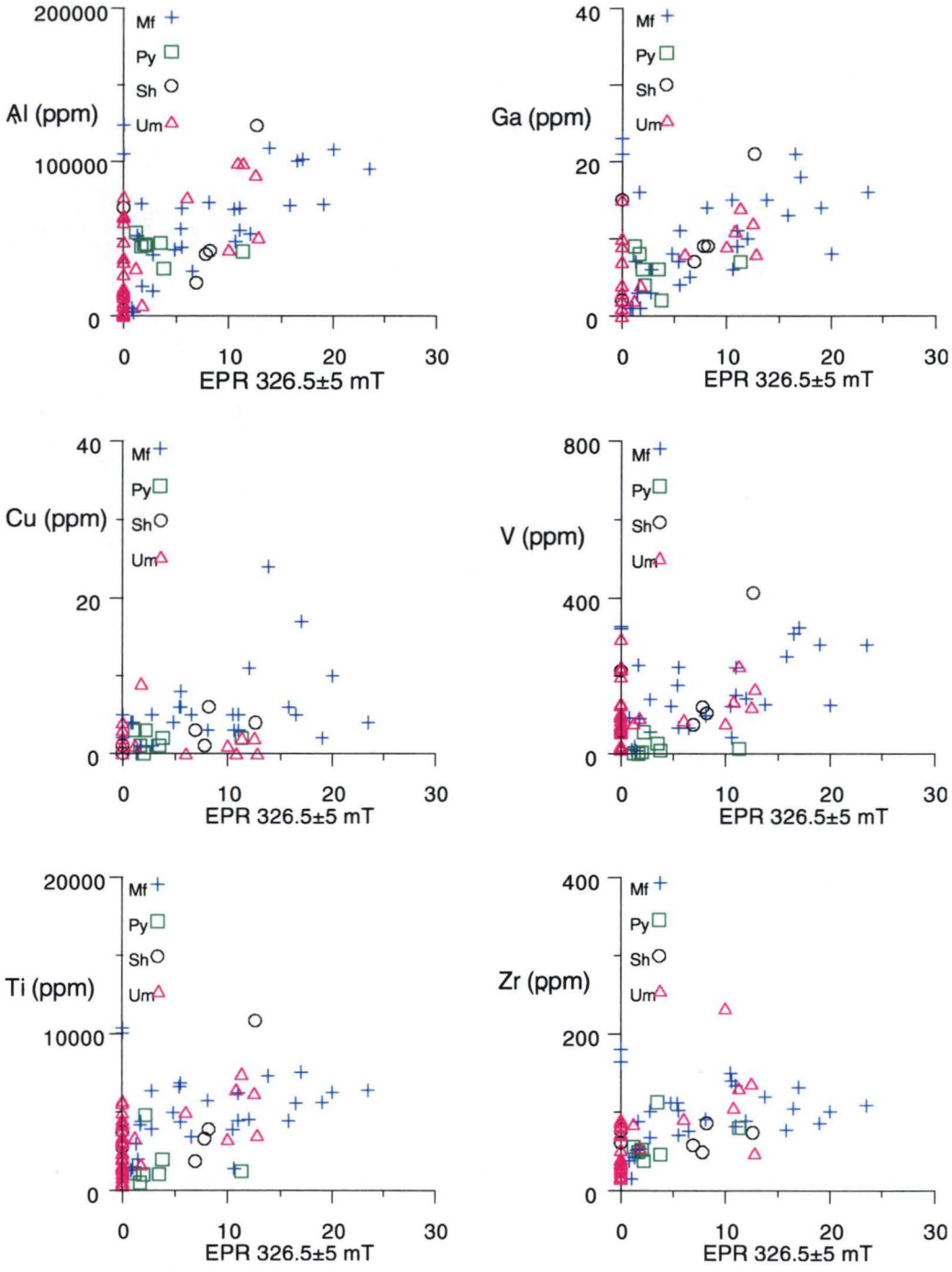

Figure 9-4. The binary plots of EPR 326.5±5 mT vs Al, Ga, Cu, V, Ti and Zr in the acid insoluble residue showing their moderate to high positive relationship

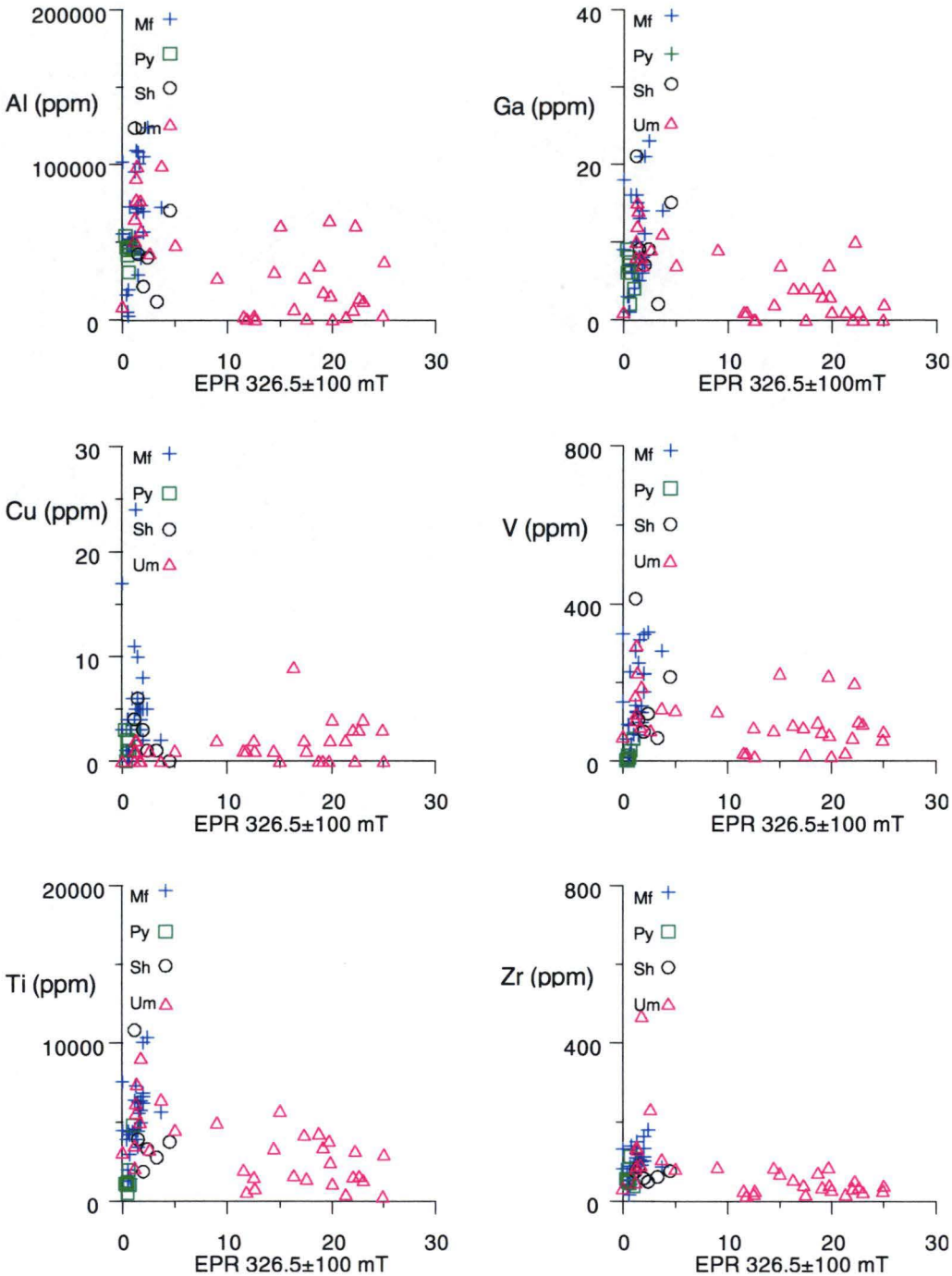

Figure 9-5. The binary plots of EPR 326.5±100 mT vz. Al, Ga, Cu, V, Ti and Zr in the acid insoluble residue

Chapter 10

JIM'S FIND PROSPECT, TANAMI, N.T.

10.1 INTRODUCTION

Jim's Find is along strike from the Tanami Gold Mine (Figure 1-3). Gold was originally discovered at Tanami in 1900, and the Tanami Gold Mine has been worked intermittently since then. Large-scale open cut mining commenced in 1987 and finished in January 1994. During this time, approximately seven million tonnes of ore were mined at an average grade of 2.1 g/t Au. New prospects/deposits, such as Dogbolter, in the area south of the original mine site are currently being evaluated and are expected to increase the total resource to over 1,000,000 ounces of gold.

Jim's Find was discovered by Centre Desert Joint Venture (CDJV). Originally CDJV involved regional scale mapping and surface line sampling between March 1989 and September 1990 and identified main gold in soil anomalies reflecting sub-surface regolith hosted mineralization at the Redback Rise and Dogbolter prospects (Koerber et al., 1992). Continued regional evaluation led to the delineation of the Jims Find Prospect in 1991 (Stott, 1994). It lies some 23 km SSW of the Tanami Mine. Detailed soil sampling, and first pass and infill Rotary Air Blast (RAB) drilling across the CDJV 197.1 km of 200 m spaced cross lines, the Jim's Find Grid (JFG), delineated three prominent anomalous gold zones: the Jims North, Jims Track and Jims South Anomalies. The largest and southern most of the identified gold in soil anomalies was renamed and regridded as the Jims South. This study of the Jim's Find was concentrating on the Jim's South

.

In this chapter, the regional environmental feature, weathering process, regional geology and mineralization are presented.

10.2 ENVIRONMENT FEATURES

The geomorphology of central Australia consists of an only slightly eroded flat laterized and silicified plain developed during the Tertiary age. Understanding environmental change will assist the establishment of regolith stratigraphy and weathering history, and provide regolith–landform control for geochemical interpretation.

10.2.1 Climate

The project area is located on the south western edge of the Tanami Desert, and has a semi-arid tropical climate. Rainfall recorded at Rabbit Flat, the closest Meteorological Station to the Jim's Find area, for the past 19 years varied between a low of 109 mm and a high of 817 mm and had a average 453 mm. Approximately 79% of the average rainfall was noted between November and March (Domahidy, 1990). Temperatures vary seasonally and diurnally with summer maximum temperatures reaching 45°C and winter temperatures to below zero. High temperatures and the presence of dry winds (prevailing from the East) combine to cause high evaporation rates. The average annual evaporation rate determined by evaporation at Rabbit Flat over a nineteen-year interval, is 3750 mm. This represents over seven times the average annual rain fall.

10.2.2 Topography and vegetation

The topography of the project area reflects the semi-arid nature of the central Australian desert. It is generally flat-lying with subtle regional terraces and numerous low and ridges. The soil is generally sandy with varying amounts of surface gravel. The extremes of temperature and the dryness restrict the natural growth of plants to well separated individuals, which are specially adapted to existing in drought prone environments. Vegetation is sparse with spinifex grass dominant. Saltbush and low acacia bushes, and a few eucalypts are scattered over the project area

10.2.3 Hydrogeology

Ground water features in the southern tenement areas were summarized by Stott (1994) according to a hydro geological map of the Granites–Tanami mining region and accompanying explanatory notes released by the Power and Water Authority, NT.

Major aquifer potential across the Tanami Mining sheet is recognized within Cainozoic palaeodrainages. Aquifers include both sedimentary and chemical deposits. Ground water has also been intersected during drilling of lower Proterozoic basement rocks. This water is reported to be contained within fracture controlled aquifers.

Ground water was intersected within Mt. Charles Beds during open pit development on the Tanami Mine Lease. Seepage was noted at about 65 m below the surface.

Limited drilling into Gardiner sandstone units in the Tanami region has yielded only minimal water seepage. Water was also found to be lacking along the unconformable basal contact between Gardiner Sandstone and Mt. Charles Beds. Of the water recovered from the Mt. Charles Beds, two analyses are available. Tentative interpretations by Domahidy (1990) suggest that the ground water is brackish to saline. Chemically the water is distinctive with low bicarbonate and high sulphate concentration.

10.2.4 Weathering history and regolith landform

As water is a most important contributor to rock breakdown in the weathering process, weathering at JFP under a semi-arid climate is very slow. The regolith stratigraphies and the regolith-landform regime distribution at JFP have been studied, and up to four major steps of weathering history have been documented (Stott, 1994).

- Deep chemical weathering under humid climatic conditions to form a lateritic regolith profile.
- Erosion of lateritic profile with a topography broadly similar to that of today under arid climatic conditions. This is evident from the location of relict screes against the JFP ridgelines. This break in the lateritization was accompanied by profile leaching to allow formation of the collapsed saprolite zone.
- A period of renewed lateritization (i.e. relapse to conditions conducive for chemical weathering. That is a return to humid climatic conditions, possibly intermittent with more arid conditions) that allowed for the iron cementation of near surface components.
- Renewed erosion under more persistent arid climates.

Figure 10-1 shows the landform of Jim's Find

10.3 REGIONAL GEOLOGY

Due to poor exposure and deep weathering, the regional geology of the Granites-Tanami Inlier is poorly understood compared to other Proterozoic inliers throughout northern Australia (Figure 10-2). The main references for the regional geology of the area is the Bureau of Mineral Resources 1:250,000 map publication for "Tanami" and "The Granites" by Blake et al. (1979). This section summarizes the tectonic setting of Australia in the Proterozoic, and details previous interpretations of the province-scale regional geology of the Granites–Tanami Inlier.

Figure 10-1. The topography map at Jim's Find, Tanami Desert, N.T.

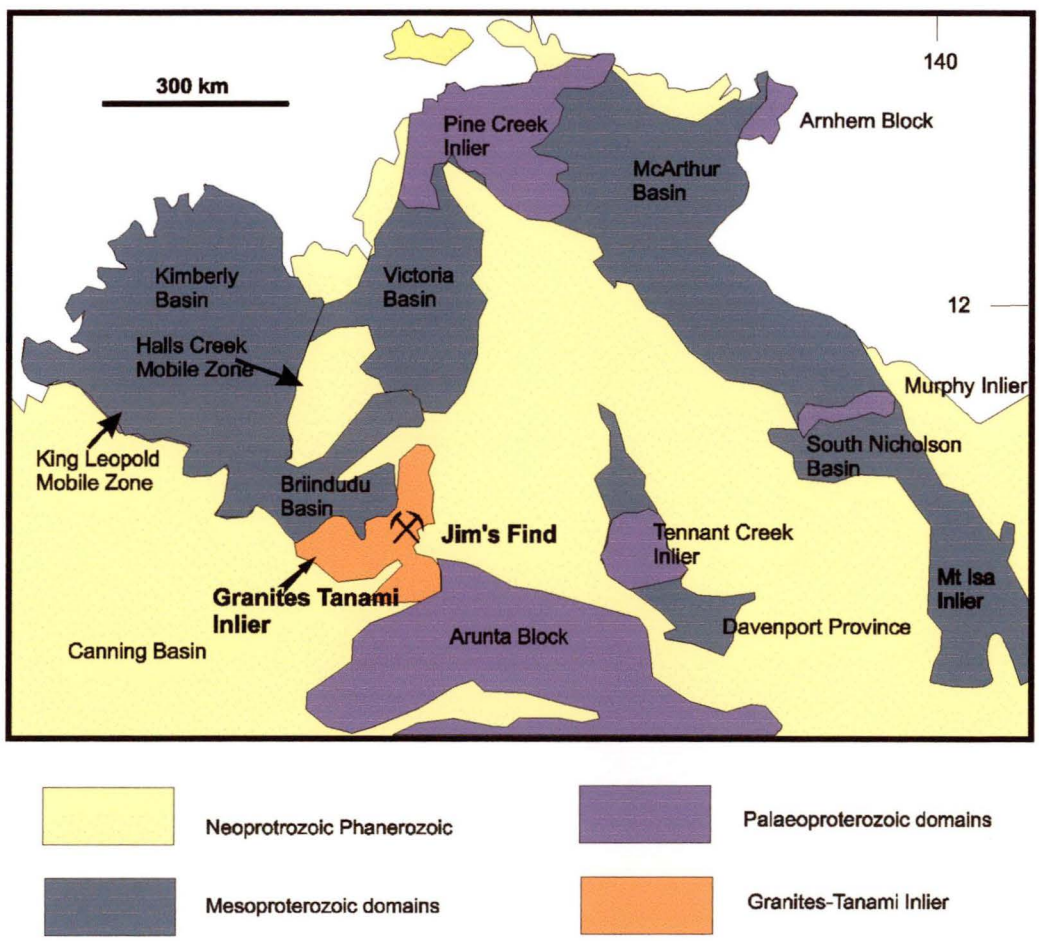

Figure 10-2. The major Proterozoic inliers of Northern Australia (from Plumb et al., 1990)

10.3.1 Tectonic framework

During the last decade the prevailing view of Australia Proterozoic tectonics was that proposed by Etheridge et al. (1987). They suggested that by the Early Proterozoic Australia was essentially cratonised, and vertical accretion was the primary mode of crustal formation. Consequently, the Proterozoic was largely characterized by intracontinental tectonics, as evidenced by a series of similar tectono-stratigraphic histories of the Palaeoproterozoic inliers that outcrop across the northern and central parts of Australia. In Northern Territory, those Lower Proterozoic Inliers were named as the Granites–Tanami, Pine Creek, Tennant Creek and Arunta Inliers. These inliers represent the limited surface expression of the broad North Australian Orogenic Province. This province has wide spread deformation and low grade metamorphism which are attributed to the ensialic Barramundi Orogeny (Etheridge et al., 1987). This major orogenic event affected most of Northern Australia between 1880 to 1850 Ma (Page, 1985). The Barramundi Orogeny terminated basin formation and was accompanied by the emplacement of an extensive and uniform suite of I-type granites and volcanic. The period immediately following the Barramudi Orogeny is inferred to have been a further period of crustal extension and basin formation. These younger basins directly overlie the Barramundi Sequence and can be distinguished by basal units which contain abundant volcanics and quartz-rich clastics that grade upwards into finer clastics, carbonates and evaporites (Rutland, 1990).

Mid Proterozoic basins of the north Australian Platform Cover found blanketing basement rocks in the Northern Territory belong to the Victoria River, the Birrindudu and the NW half of the McArthur Basins.

10.3.2 Regional stratigraphy of the Granites–Tanami district

The oldest exposed rocks are Early Proterozoic sediments and volcanics, which host the Granites mineralization (Nicholson, 1990). These rocks have been isoclinally folded and cleaved and subjected to greenschist facies regional metamorphism in and episode dated at about 1960 Ma. Blake et al. (1979) divided the Tanami Complex into five separate units — the Mt. Charles, Killi-Killi, Mongra, Helena Creek and Nanny Goat Creek Beds, with only the Mt. Charles Beds present within the Tanami mineralization area (Figure 10-3). This unit is characterized by its relative abundance of fine grained siliceous metasediments and a minor volcanic component (Plumb,

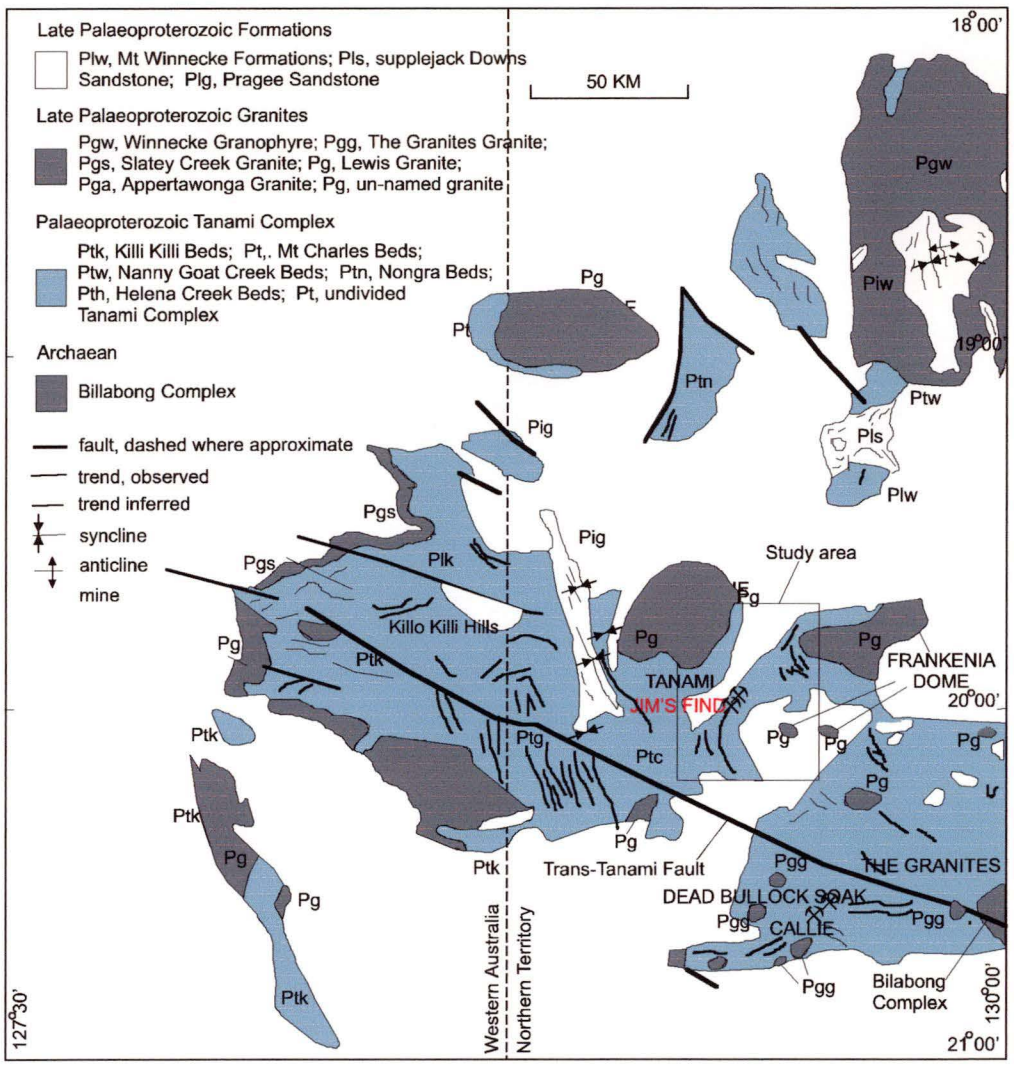

Figure 10-3. Map of the Granites - Tanami Inlier illustrating the regional geology and distribution of varous units of the Tanami Complex and location of the major granites (after Black et al., 1991)

1990). Lithological units include fine- to medium-grained greywacke, phyllite, laminated and banded cherts, basalt and minor felsic volcanic rocks. As with all units of the Tanami Complex, rocks commonly show steep to near vertical dips, tight folding and widespread fault disruption.

Granites emplacement has been localized within large domal structures throughout the Granites–Tanami Inlier (Figure 10-3). Their age ranges from Archaean to Palaeoproterozoic (Page et al., 1995; Page et al., 1996), although due to poor exposure, only a limited number of age determinations have been obtained. Two groups of felsic intrusives can be defined:

- The Winnecke Granophyre which intrudes Proterozoic formations in the North East of the Block with a U-Pb age of between 1815-1830 Ma; and a later unnamed post-orogenic suite that which is 1790–1800 Ma (Page and Sun, 1994). Rock types present include pink to gray granophyre that is commonly porphyritic and consists of K-feldspar, plagioclase, quartz and biotite phenocrysts within micrographic groundmass. Other rock types include non-porphyritic adamellite and acid porphyries. Major element chemistry is K and Rb rich.
- The later suite is thought of as less extensive outcrops which mark intrusives across the remainder of the Block to include the Granites Granite, Saley Creek and Lewis Granites. These intrusives differ from first group by higher Na_2O and lower K_2O values (Blake et al. 1979).

A brief description of the stratigraphy summarized from Eupene (1988) is as follows: Early Proterozoic clastic sediments of the Pargee Sandstone and Supplejack Downs Sandstone and interbedded acid volcanic rocks and clastic sediments of the Mount Winnecke formation overlie the Tanami complex. Middle Proterozoic sediments of the Birrindudu Group overlie the earlier Proterozoic rocks. These have been later moderately folded and domed.

During Adelaidean and Cambrian times, sediments of the Wade Creek Sandstone, Redcliff Point Group, Duerdin Group, Edward Albert Group and the Wiso Basin were deposited. Basalts and sediments of the Antrim Plateau Volcanics were also deposited.

During Devonian time, the sediments of the Lucas Formation and the Pedestal,

Angus Hill, and Chuall Beds were deposited while the Larranganni Beds and Hazlet Beds were probably deposited during the Mesozoic age.

10.3.3 Gold mineralization within the Granites–Tanami mining region

Economic mineralization recovered from the Granites–Tanami Mining Region has, to data been restricted to gold. Recovery of this commodity has been solely from Mt. Charles Beds. Some minor occurrences of copper, uranium and rare elements have been reported (Blake et al., 1979).

There are two main kinds of gold mineralization present in the Tanami and Granite areas. The Tanami area consists of sheeted quartz-carbonate veins within interbedded sedimentary and basaltic packages, in which gold exists within clusters (ore shoots) of quartz-carbonate veins associated with envelopes of sericite-pyrite alteration. Mineralization is preferentially hosted by basalt and greywacke. Oxidized ore, which comprises all presently know reserves, extends to a maximum depth of 60 m. Altered mineralized basalt is typically yellow or orange in color, contrasting with the generally unmineralized pink or purple regolithic basalt. Residual laterite overlies the mineralization in places, but it is not consistently mineralized. Silicification occurs throughout the mine area to a depth of 2–10 m. Gold is enriched in a number of horizontal layers within the oxidized zone, which are marked by increased grade and/or thickening of the ore shoots. In the Granites Gold Mine, gold occurs further as strata bound disseminated within the host unit (Ireland, 1988).

The host unit, is interpreted as a mixed facies BIF which has been metamorphosed to amphibolite grade conditions (Mayer, 1990). The gold is of high purity, and generally medium-grained (i.e. visible in drill core) (Ireland, 1989). The host unit is gold anomalous throughout, but the better mineralization occurs as tabular bodies and lenses, sometimes as multiple zones stacked in parallel associated with thickenings of the host unit. It is uncertain whether these concentrations are original depositional features or whether they have been produced by subsequent remobilization.

10.4 LOCAL GEOLOGY

In this section, the mine-scale stratigraphy, sedimentology and mineralization are presented.

10.4.1 Geology of the Jim's Find Prospect

The Jim's Find Prospect lies on a NW/SE anticlinal structure at the southern end of corridor between two large granite domes, Coomarie and Frankenia (Figure 10-4). The corridor consists of folded and faulted rocks, interbedded pillow basalt and mudstone with rare greywacke and chert (Nicholson, 1990).

Of the five informal sedimentary units of Tanami Complex only the Charles Beds have been recognized in the Jim's Find area (Figure 10-5). These comprise a sequence of fine to medium grained greywacke, phyllite, banded iron formation, chert, basalt and minor felsic volcanic rock. Exposure is confined to isolated low, rounded hills, with less than ten percent outcrop. Lack of exposure restricts the identification of lithological boundaries between the ridgelines.

Rock type identification from Rotary Air Blast (RAB) and Reverse Circulation (RC) drilling into the regolith has historically proved to be difficult due to mesofabric destruction in the drill spoil. Accurate stratigraphic information for Jim's find is thus constrained to areas where diamond drill holes have been collared. Basaltic volcanics with intercalated fine grained lithic metasediments, massive basalts, black pyritic carbonaceous shale and dacite porphyry have been identified (Koerber et al., 1992; Ruxton, 1994; Stott, 1994).

10.4.2 Mineralization at Jim's Find Prospect

The gold mineralization in this section is summarized from the available literature on the Jim's Find Prospect, much of which has been reported by Ruxton (1994).

The first type of mineralization is the core mineralization, in which gold is considered to be primary, having remained unaffected by any weathering process. The distribution of this gold in the regolith is related to an inferred primary structural control on the ore body. A brittle fault trends N–S with a moderate to steep westerly dip. Core mineralization extends into the fresh rock.

The second style is peripheral mineralization, in which gold has been redistributed during weathering. This gold occurs as sub-horizontal layers that show strong spatial

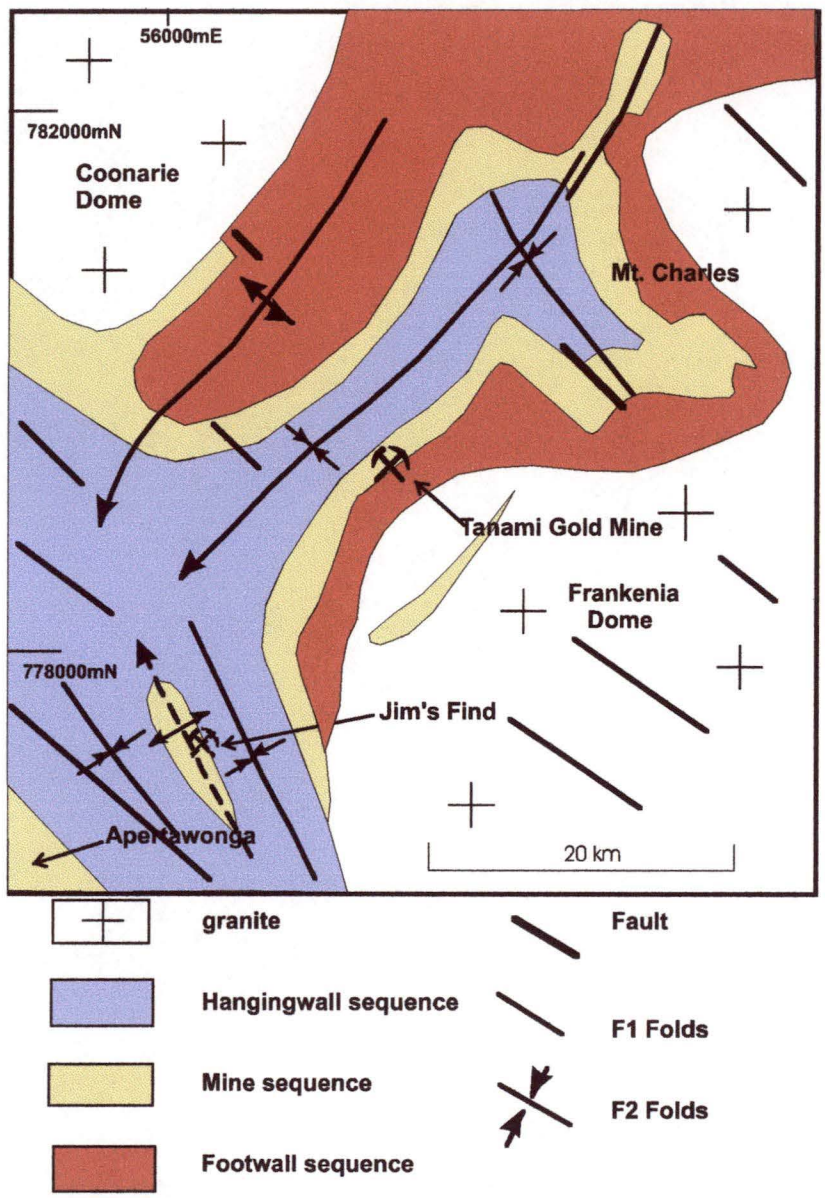

Figure 10-4. Geological interpretation of the detailed study area (after Blake, 1979, and Tunks, 1996)

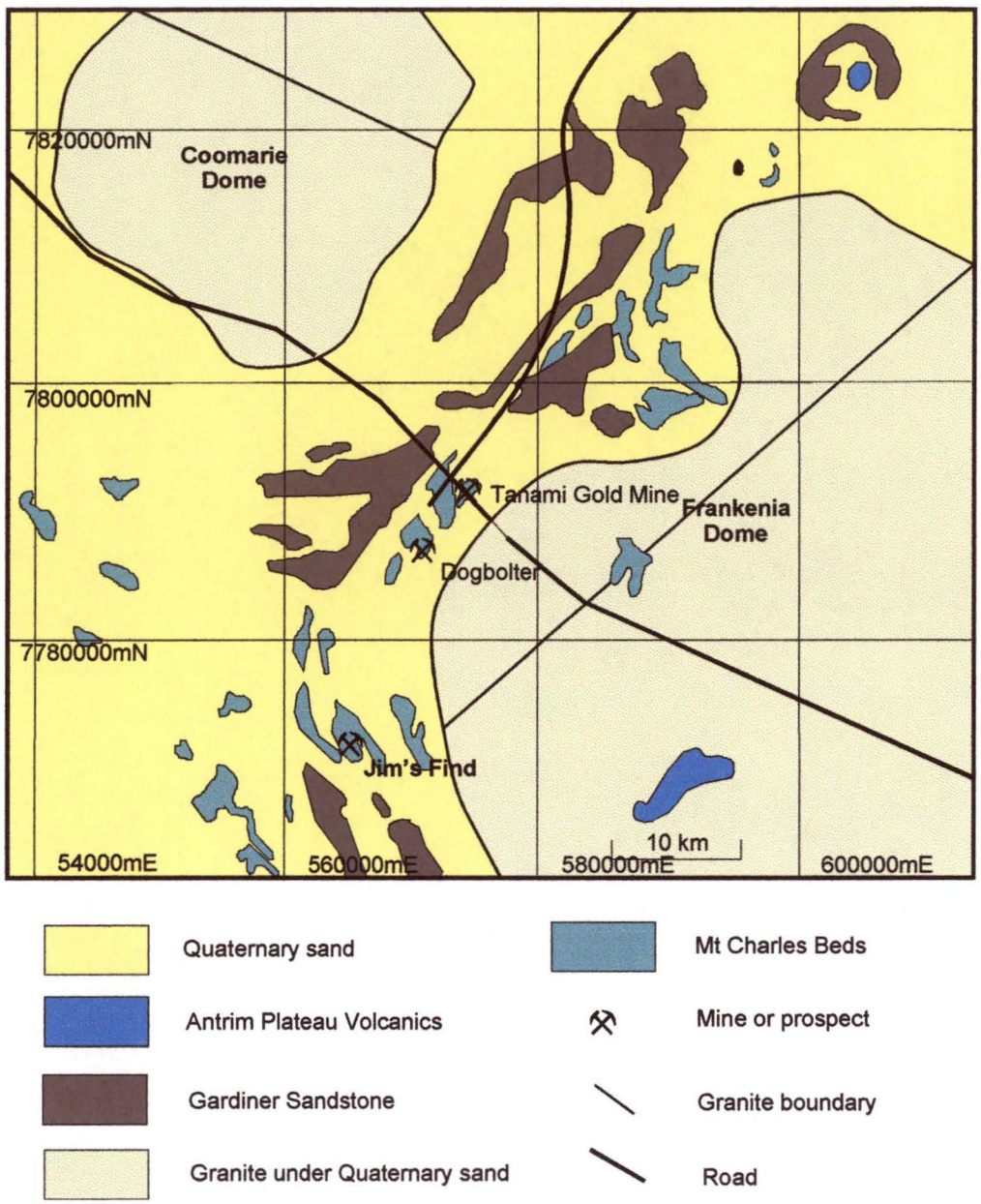

Figure 10-5. The distribution of Mt Charles Beds at the Jim's Find

associations around the core mineralization. Lower grades are reported for peripheral mineralization than those reported for ores from the core zone.

Mineralized zones within fresh bedrock are characterized by chlorite-sericite-pyrite ± leucoxene ± albite ± chalcopyrite alteration. Within the regolith, mineralization characteristically occurs in zone of brecciated and sheared quartz, sericite-clay chlorite altered rocks with limonite after pyrite.

10.5 SAMPLE COLLECTION

The original objective of the sampling program by Stott (1994) at the Jim's Find Prospect was to obtain information on element distributions throughout the lateritic regolith. This study will use the same samples. The aim is to further check if the acid insoluble residue can better define the regolith geochemical character and can be widely used to determine the behavior of the mineralization system, including the gold related pathfinder elements and associated wall rock alteration assemblages, as well as their EPR characteristics. Samples were taken from drill holes along three section lines across the anomaly: 10150N, 10250N and 10400N (Figure 10-6). Line 10150N was chosen to allow investigation of near surface depletion of gold and the presence of any immobile pathfinder element. Lines 10250N and 10400N were chosen as they offered well constrained mineralized zones.

A total of 137 samples from three sections were used for PIXE/PIGE comprising 74 samples in section 10150N, 25 samples in 10250N and 38 samples in 10400N. Only 67 samples from section 10150N were used for EPR analyses. Collar locations of the drill holes from which the samples were taken are given in Figure 10-5. The sampling point together with the regolith profile at the longer section 10150N is shown in Figure 10-6.

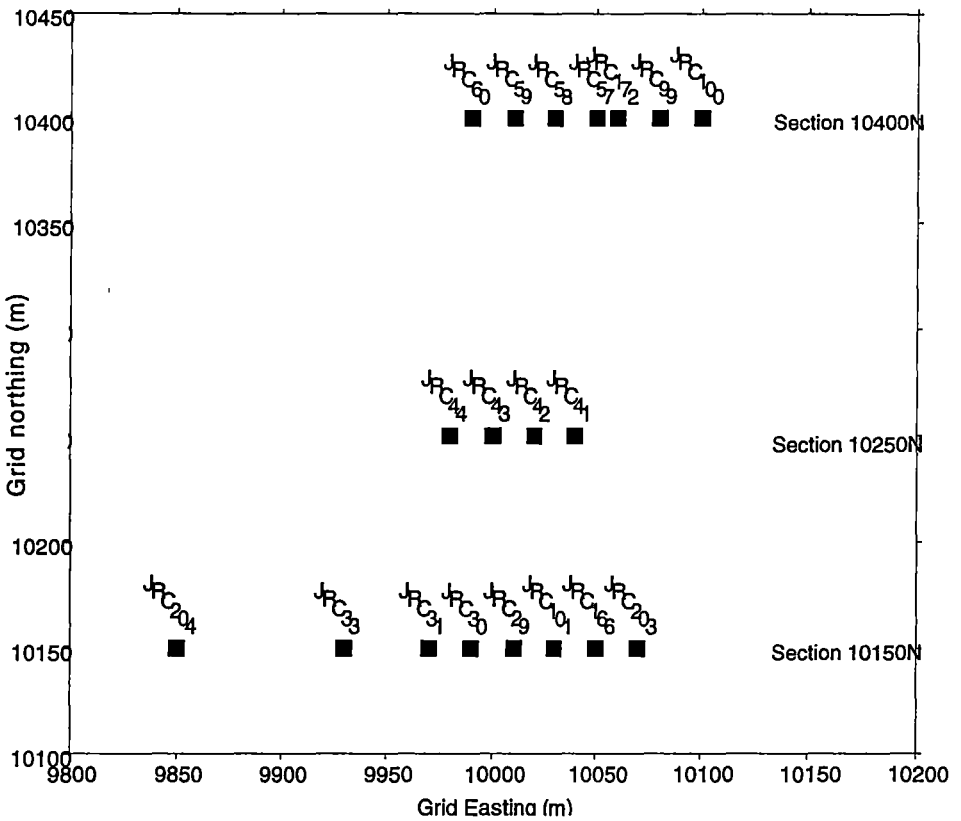

Figure 10-5. The location of reverse circulation (JRC) drill holes used for Jim's Find sampling program

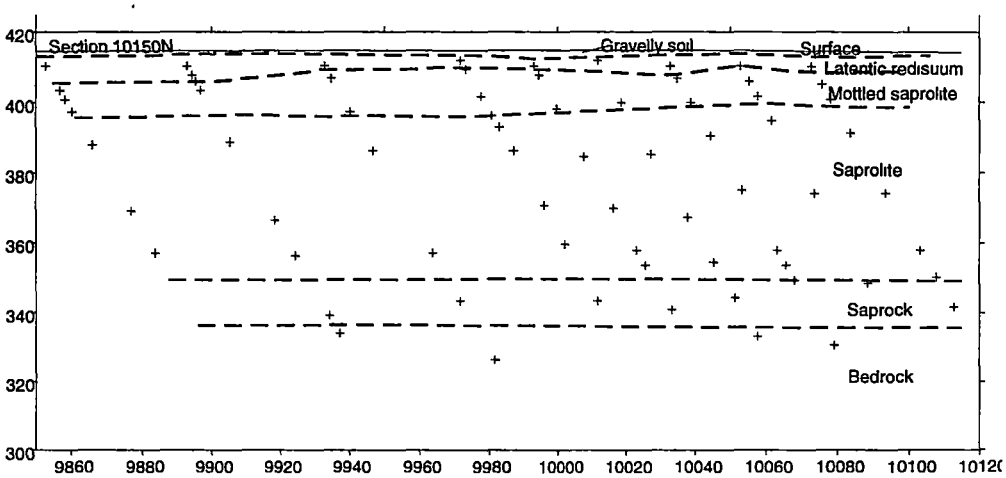

Figure 10-6. The sample location at 10150N, Jim's Find, N.T. showing the regolith profile

Chapter 11

GEOCHEMISTRY AT JIM'S FIND PROSPECT

Traditional gold panning as an exploration technique did not prosper in the Tanami due to the shortage of water. Instead modern exploration of surface sample uses conventional fire assay, or more commonly aqua regia soluble Au that is analyzed by graphite furnace atomic absorption (AA) after methyl isobutyl ketone (MIBK) extraction. These determinations may be complimented by AA analyses of As. Material from surface trenching, diamond and the more common percussion drilling is increasingly assessed by neutron activation analyses (NAA) and ion coupled plasma (ICP) for Au and its pathfinders As, Sb and W.

Multi-element analysis of regolith material has been used for a considerable time to assist with the interpretation of vestiges of original lithology in the regolith (Hallberg, 1984). More recently the CSIRO–Australian Mineral Industry Research Association project "Exploration for concealed gold deposits, Yilgarn Block, Western Australia" has been using whole rock samples to characterize enrichment and depletion pattern of over 40 elements in the regolith (Butt, 1991; Robertson et al., 1990). The analysis of this material was carried out by a combination of techniques including XRF, AA, INAA, etc.

Because of the often dispersed nature of gold occurring within the regolith, several special projects were set up in order to obtain better understanding of the nature and genesis of the lateritic regolith, as well as the supergene Au deposits within the regolith. The purpose of these projects is to provide a data base that can be applied during Au exploration in and beneath the regolith. The most recent of these studies is on Jim's Find Prospect, an exploration area immediately south of Tanami Mine (Stott, 1994).

This chapter provides documentation of the geochemical dispersion patterns for various major and trace element components of acid insoluble residue throughout the complete lateritic regolith profile preserved in the Jim's Find Prospect. Furthermore, it aims to check the chemical and mineralogical changes that occur during weathering. Sample preparation and analytical methods have been described in Chapter 3.

11.1 REGOLITH GEOCHEMISTRY

Primary mineralization at Jim's Find is overlain by an almost complete lateritic profile. The depth of weathering is from 70–90 m. The principal regolith units present on the three sections across the Jim's Find Prospect are shown on Figures 12-6 and on the element distribution plots (Figures 11-8 to 11-34).

11.1.1 Saprock

This 20 m thick zone is transitional between the saprolite and the bedrock marked by the weathering front. Below this front, primary minerals are stable. Above it, primary minerals are unstable and become increasingly less stable up through the weathering profile. In percussion drill chips, the base of the saprock horizon is most clearly marked by the breakdown of the disseminated sulphides within the bedrock units.

11.1.2 Saprolite

The saprolite forms a broad lower zone of deep weathering profile, which is about 40–50 m thick. In this zone, micro fabrics are retained in the weathered rocks during the isovolumetric replacement of primary minerals by aggregates of clays, oxides and oxy-hydroxides. The saprolite becomes softer and increasingly clay-rich towards the surface and, as a result of settling, consolidation and the development of iron oxide segregation, the rock fabrics are destroyed and it merges with the plasmic and mottled clays at about 15 m depth. The saprolite is the most commonly sampled material in prospect evaluation, usually obtained by drilling.

11.1.3 Mottled saprolite

This zone is transitional between the saprolite and the lateritic duricrust and gravels. Butt and Zeegers (1992) define this zone as the presence of localized spots or blotches of iron oxides and oxyhydroxides. It consists of pale grey-yellow red clay with iron-rich blotches. The blotches vary from irregularly shaped to subrounded. Small subrounded mottles may be regarded as incipient nodules.

11.1.4 Lateritic residuum and gravelly soil

These are present as an almost continuous horizon at the upper part of the regolith. The lateritic materials are found to occur as pisolitic, nodular gravel component, or indurated surface crust. The maximum drill hole depth shows these materials are around 10 meters in thickness. Normally it is about 5 m.

11.2 Au DISTRIBUTION

Data analysis for the following interpretations on the Au distribution and the comparison with other elements, is by neutron activation analysis (NAA), conducted by Becquerel Laboratories Pty Ltd. at Lucas Heights, New South Wales on powders prepared by the CSIRO in Perth (Stott, 1994). The experimental detection limit for NAA is 5 ppb Au. The high detection limit of Au by PIXE (5 ppm) is too high to be of practical use.

The general dispersion model of gold from auriferous quartz during regolith evolution has been discussed in Chapter 2. Because metallic gold is almost inert under the physical-chemical conditions prevailing in most weathering environments, it generally behaves as an immobile elements and secondary dispersion is predominantly by physical mechanisms. Mechanical dispersion affects Au held in resistant mineral grains (Butt, 1997). This resistance to weathering is largely responsible for the economic concentration of Au as residual deposits in lateritic terrain (Gray et al., 1992).

Distribution patterns for Au concentration within the laterite profile at the Jim's Find prospect are shown across the three sections, 10150N, 10250N and 10400N in Figures 11-1, 11-2 and 11-3 respectively. Gold distribution patterns across sections 10250N and 10400N, define constrained subvertical to vertical mineralized zones. The trend of these zones is visibly persistent throughout the entire regolith profile. The mineralized zone is here after defined as the linear vertical to subvertical zone mapped out by high gold grade in the lower saprolite zone and presumably reflecting the trend and location of the hypogene orebody.

The principle features of the distribution patterns of gold across three sections, as revealed by the element distribution plots, are as follows:

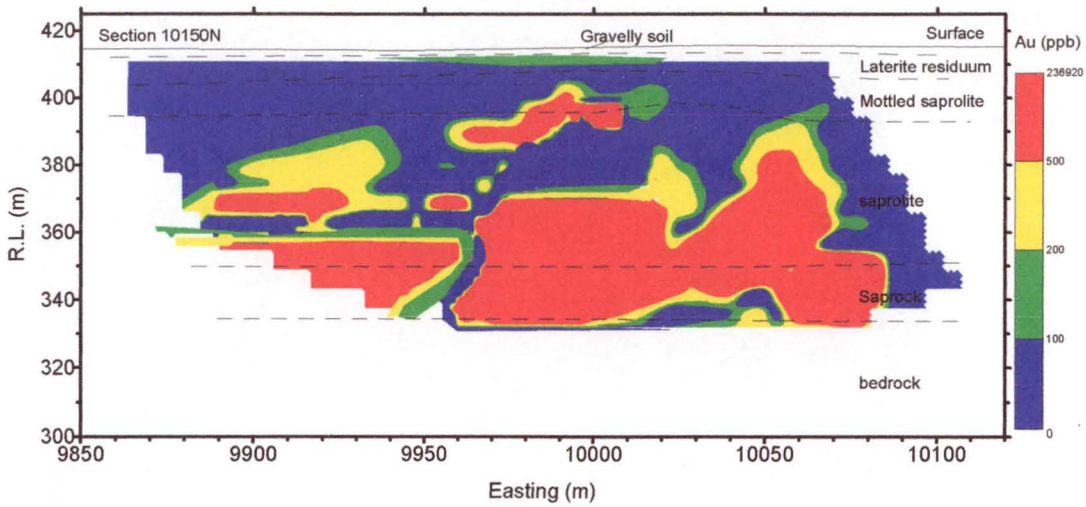

Figure 11-1. Au distribution of bulk geochemistry at 10150N in Jim's Find, N.T.

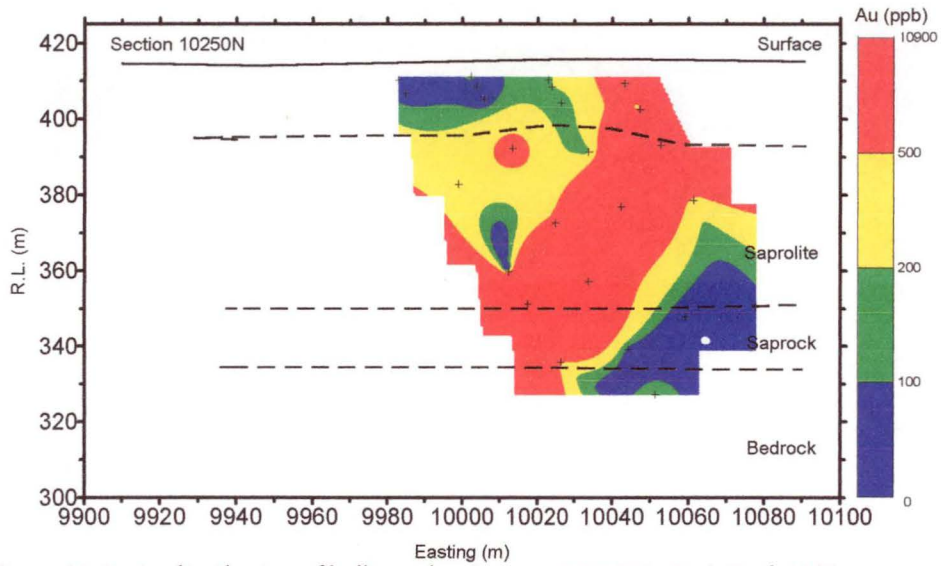

Figure 11-2. Au distribution of bulk geochemistry at 10250N in Jim's Find, N.T.

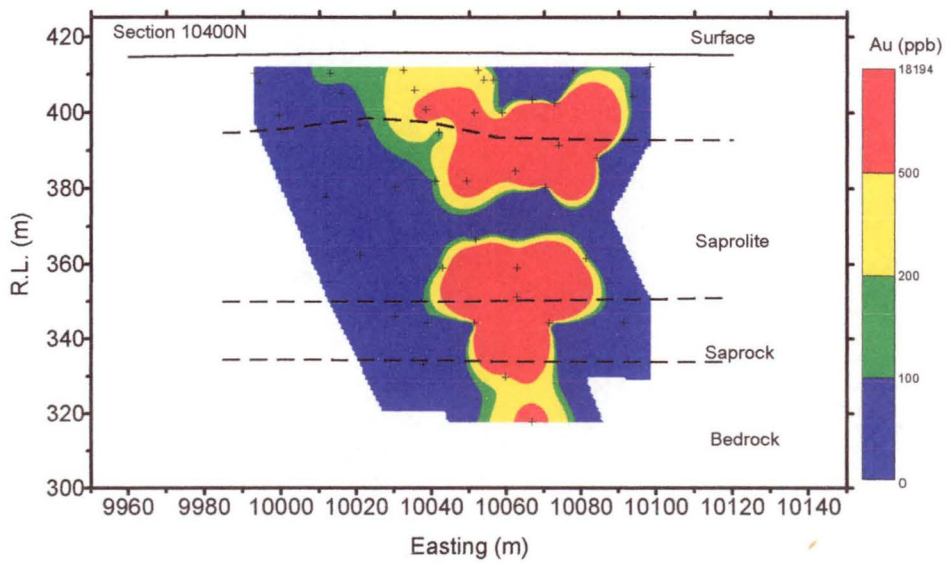

Figure 11-3. Au distribution of bulk geochemistry at 10400N in Jim's Find, N.T.

1. Lateritic supergene gold. A pronounced zone of gold enrichment has developed about the surface or near surface continuation of the identified subvertical to vertical hypogene mineralization zone. This near surface mineralization is found on sections 10150N and 10400N. In section 10400N it reaches the surface. Zones of Au enrichment exhibit flat flying to broadly concave shapes continuous with both the upper most mottled saprolite and saprolite. Sometime anomalous Au concentrationextends to the overlying lateritic gravelly soil horizon. This mineralization is known as the lateritic supergene gold enrichment.
2. Depleted zone. In the section 10150N and 10400N, the central core zone of the near surface lateritic supergene enrichment is underlain by a zone, along the trend of the hypogene ore, along which the concentrations of gold are depleted relative to both underlying and overlying concentrations. This zone of depletion, which is approximately 10-15 m thick, occurs in the mottled saprolite around R.L. 410 m. The zone is marked by concentration of gold mostly less than 100 ppb. There is also another depletion zone in the saprolite around R.L. 370 m.
3. Saprolitic supergene gold. Inspection of sections 10150N and 10400N reveals the presence of two discrete zones of saprolitic supergene gold enrichment around the hypogene trend. This upper supergene horizon sits in the saprock and lower part of the saprolite about an RL of 353 m. The depth corresponds with the depth of the water table as reported from the Tanami Mine.

11.3 ACID INSOLUBLE RESIDUE GEOCHEMISTRY

Section 10150N covers a greater area and has the potential to provide more information regarding lateral element dispersion than the two other smaller sections 10250N and 10400N. Because they are too short, the acid insoluble residue chemistry will focus on the longer section 10150N. The element distributions at 10150N are shown as separate contour maps after each element description. The distribution maps of the other two sections 10250N and 10400N are attached in Appendices 7 and 8. The contour intervals used were selected on the basis of the principal population evident in the histograms and cumulative frequency graphs from the whole data set shown on Figures 11-4 to Figure 11-7.

For some elements, a strong positive correlation is observed between their concentration distribution and with those of the gold plots, while for other elements a persistent spatial relationship exists. These relationships indicate a certain affinity

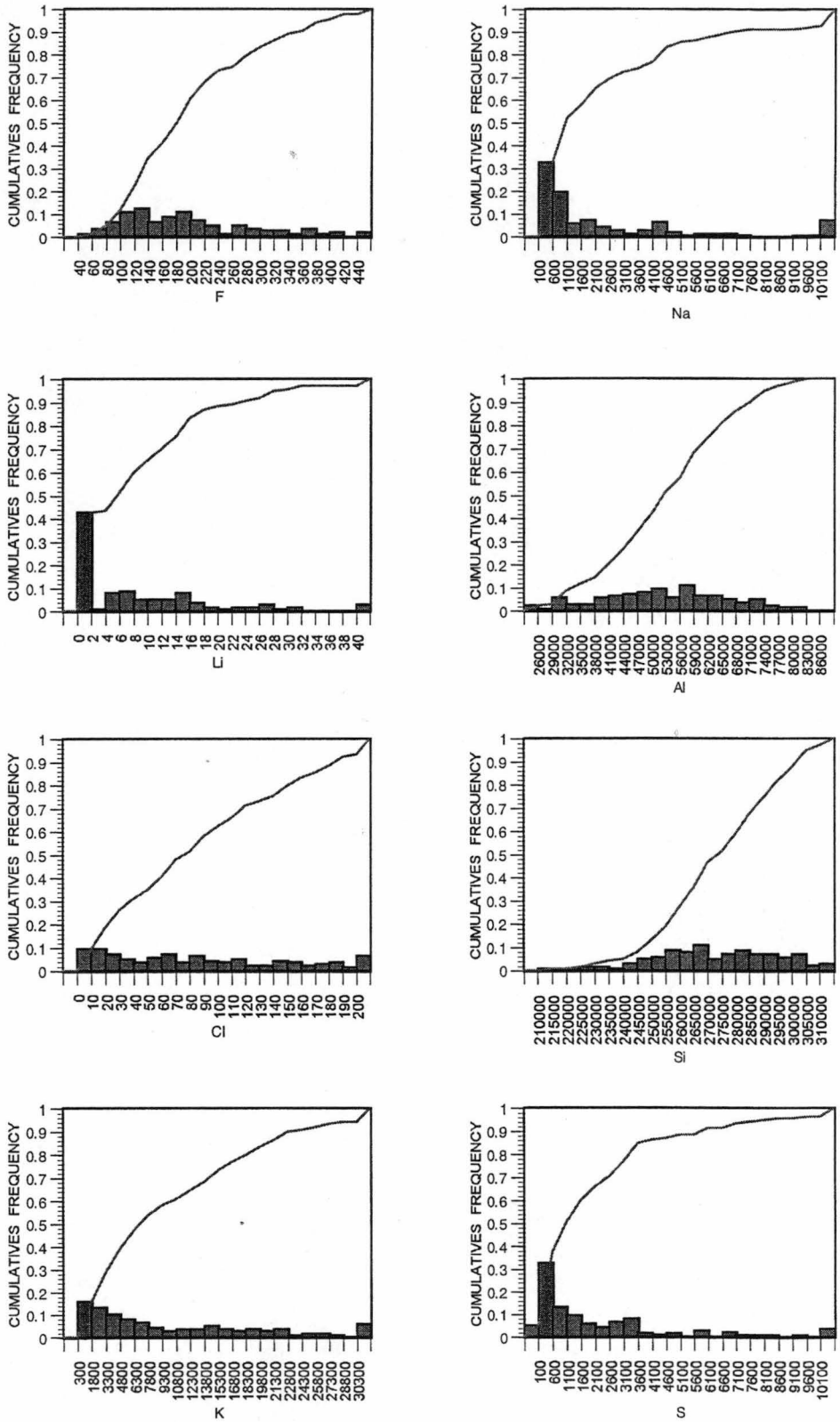

Figure 11-4. The histograms and cumulative frequency plots of F, Na, Li, Al, Cl, Si, K and S in ppm of the acid insoluble residue

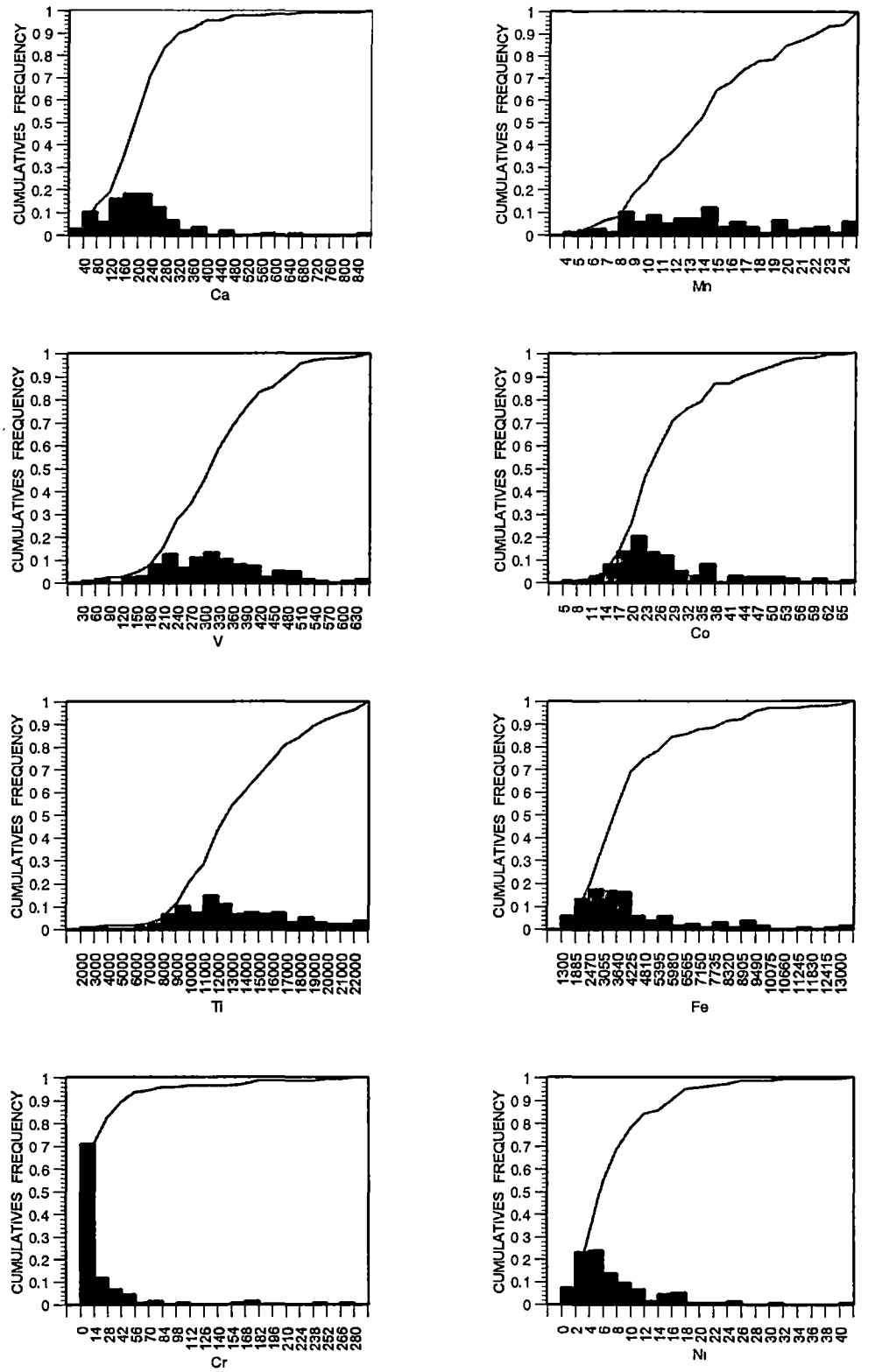

Figure 11-5. The histograms and cumulative frequency plots of Ca, Mn, V, Co, Ti, Fe, Cr and Ni in ppm of the acid insoluble residue

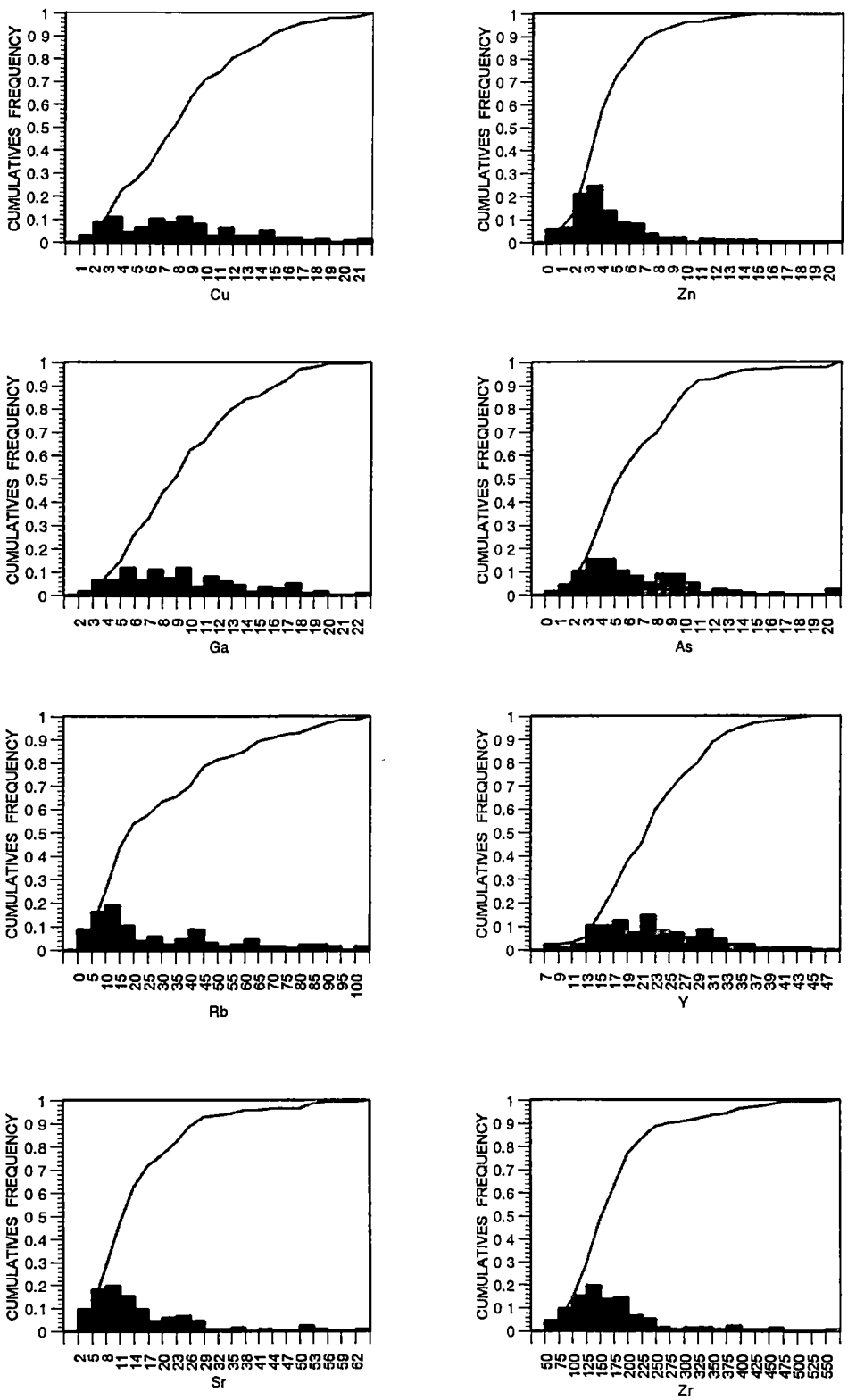

Figure 11-6. The histograms and cumulative frequency plots of Cu, Zn, Ga, As, Rb, Y, Sr and Zr in ppm of the acid insoluble residue

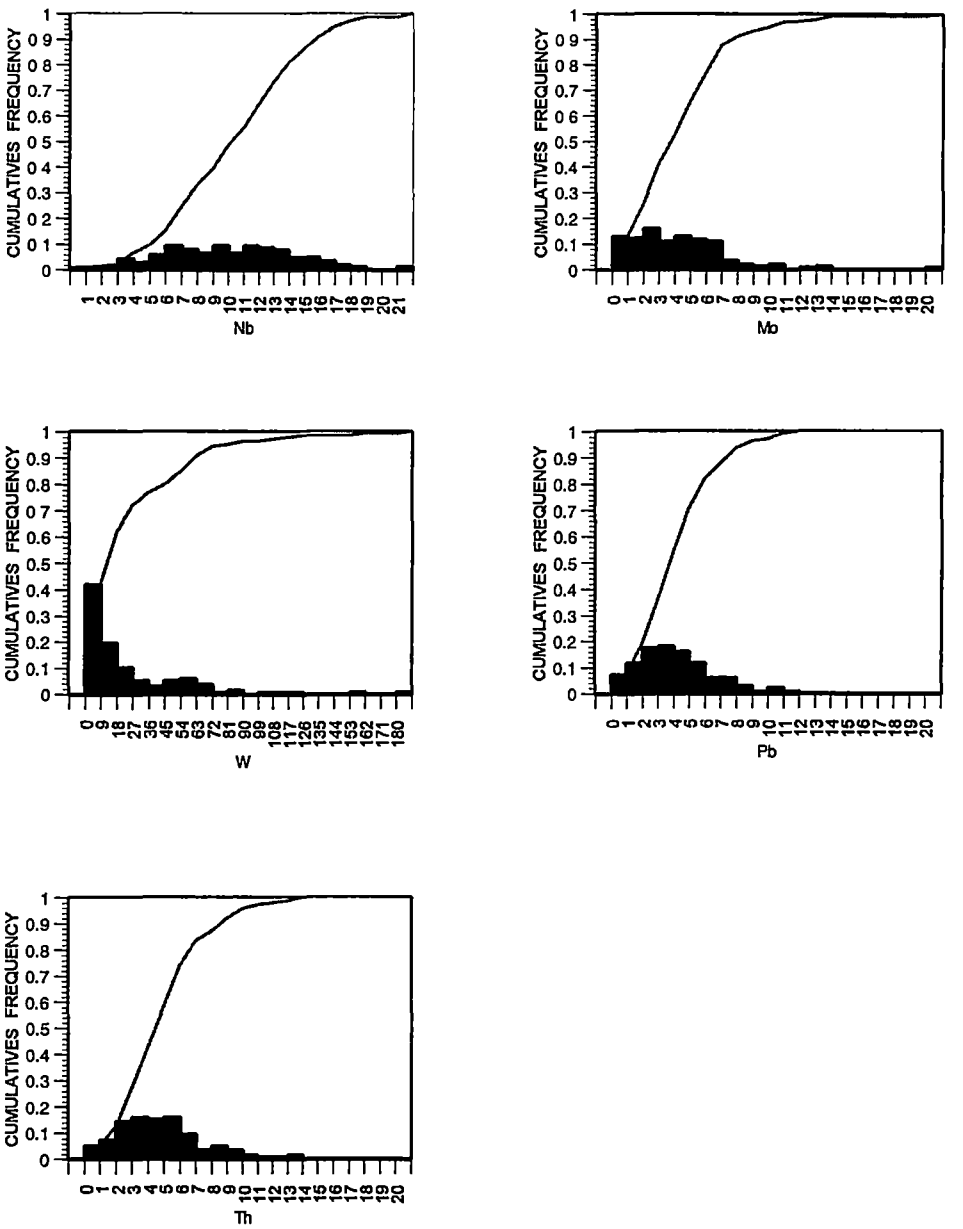

Figure 11-7. The histograms and cumulative frequency plots of Nb, Mo, W, Pb and Th in ppm of the acid insoluble residue

between the Au and the compared elements. Further investigation is necessary to determine whether these correlations result from a primary genetic relationship, represent an artifact of the weathering environment, or whether they are pure coincidences.

The element distributions are described in the same order as used in Mystery Zone (Chapter 5) and Rand Pit (Chapter 8). The principal features of elements with distribution patterns identified as having affinities with the Au mineralization at Jim's Find are as follows.

11.3.1 Major elements (Al, Fe)

Aluminum: Aluminium has a range of 29900 to 83000 ppm in the acid insoluble residue of the regolith. The distribution contour map is shown in Figure 11-8. Compared to surface and bedrock concentrations, Al is enriched throughout the regolith, especially in the saprolite horizon where it has a vertical character. A leaching zone is evident in the lateritic residuum, except from 9870E to 9890E, on the western side of the profile. An anomalous concentration of Al enriched samples is noted to the east of 9990E on line 10150N.

Iron: It has a range of 1312 to 3000 ppm and is strongly enriched at the two sides of the long section 10150N. The distribution contour map is shown in Figure 11-9. Compared to the surface and bedrock concentration Fe is enriched throughout the regolith. At the two sides in the mottled zone, higher Fe sits in the lower part rather than near the surface. Except for the occasional high concentration of Fe within the saprock zone, the lower Fe content of the saprock and bedrock (means 0.2-0.3%) compared to that of saprolite and mottled zone (> 3%) indicates the decline of Fe concentration with depth.

11.3.2 Alkaline earth elements (Ca and Sr)

Calcium: Because of acid attack, the Ca concentration is rather low, and the values change significantly from 40 to 1048 ppm. The distribution contour map is shown in Figure 11-10. Leaching of bedrock Ca in the acid insoluble residue is not noted above the weathering front unlike its behaviour in the general weathering profile. The depletion process is gradual. More visible changes in the calcium content occur

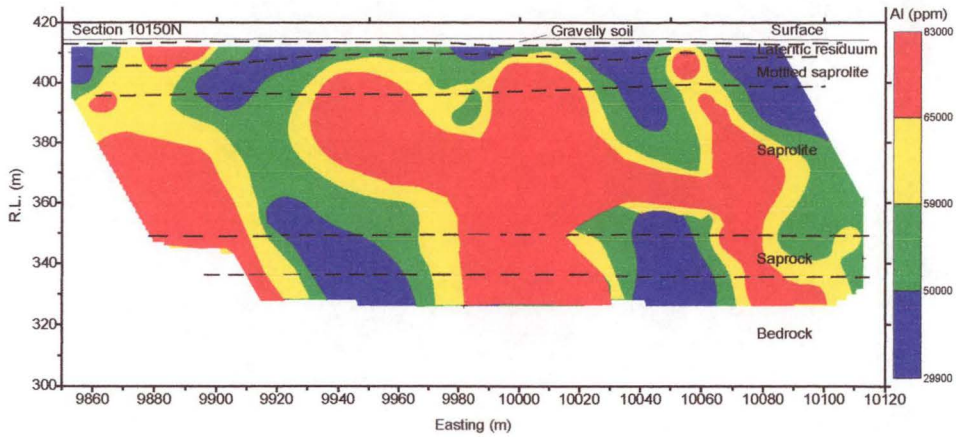

Figure 11-8. Al distribution of acid insoluble residue at 10150N in Jim's Find, N.T.

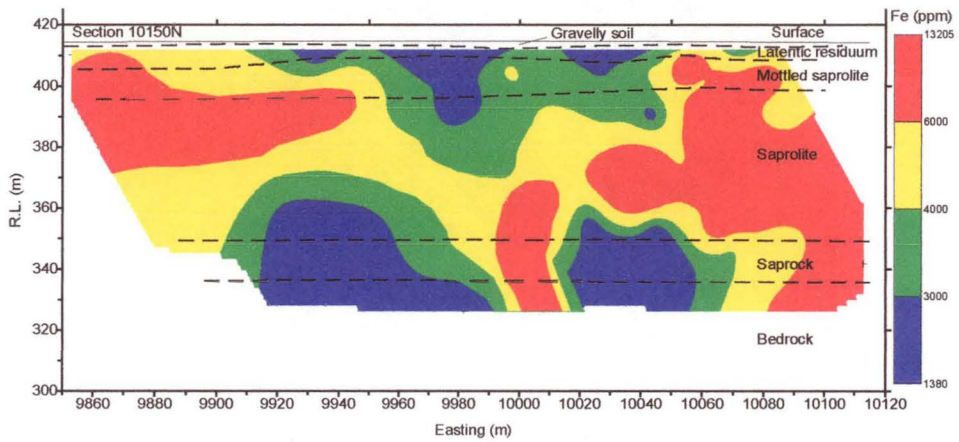

Figure 11-9. Fe distribution of acid insoluble residue at 10150N in Jim's Find, N.T.

in the middle part of the saprolite about R.L. 365. Calcium content near the surface averages 3–6 times lower than to the content found in bedrock and saprock.

Strontium: The concentration of Sr ranges from 2 to 70 ppm. The distribution contour map is shown in Figure 11-11. Sr throughout the regolith at Jim's Find is depleted in the upper part of the profile. Concentrations of about 5 ppm occur in the unmineralized mottled zone and upper saprolite, this is more than three times the concentration of the same lithology units within the mineralized zone.

11.3.3 Alkali metals (Na, K and Rb)

Sodium: Sodium ranges from 0.01% to 3.5%. The distribution contour map is shown in Figure 11-12. Leaching from the surface to the mottled zone produces a

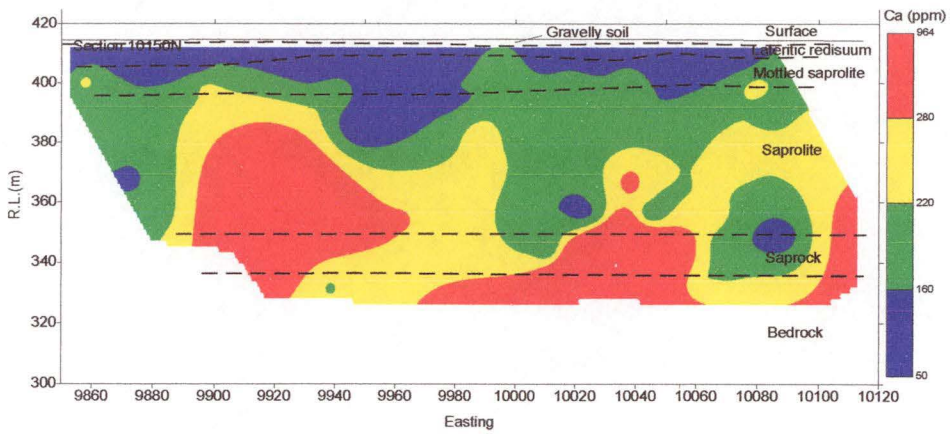

Figure 11-10. Ca distribution of acid insoluble residue at 10150N in Jim's Find, N.T.

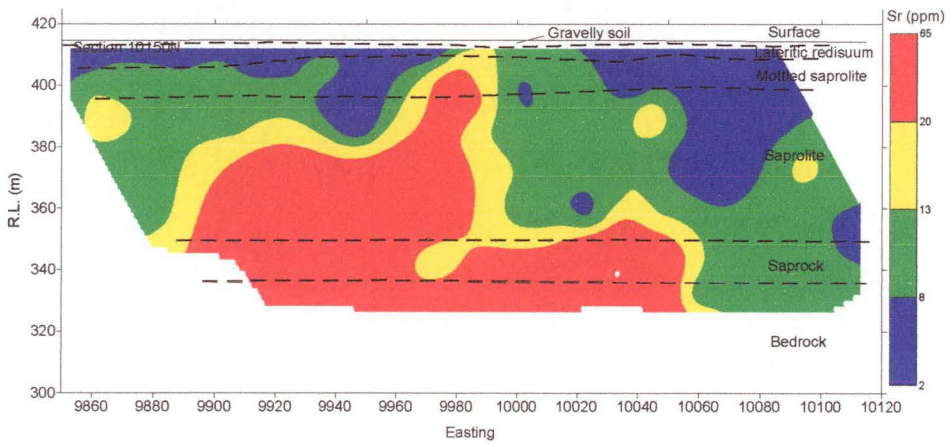

Figure 11-11. Sr distribution of acid insoluble residue at 10150N in Jim's Find, N

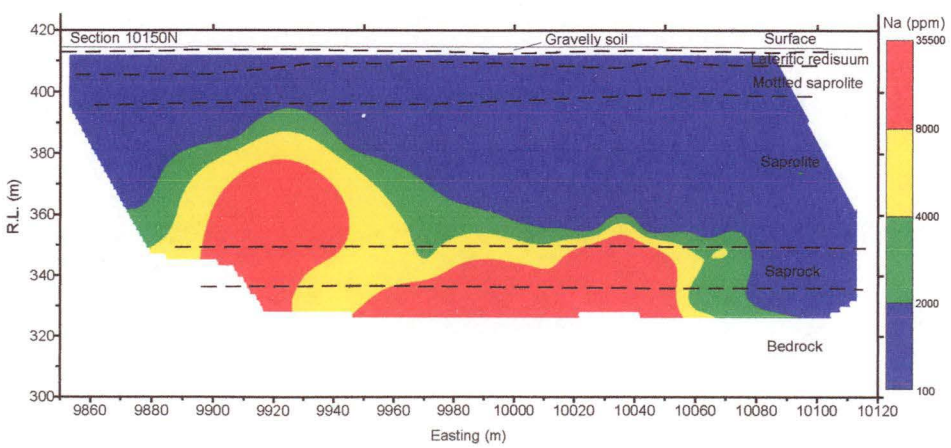

Figure 11-12. Na distribution of acid insoluble residue at 10150N in Jim's Find, N.T.

depletion zone in the lateritic residuum where Na concentrations are less than 0.1%. The distribution of Na in the regolith profile shows a strong leaching above the saprock zone. Less than 0.3% Na occurs in the mottled zone and saprolitic horizon, except for samples 130305, 130306 and 130199. There is an increasing trend from few hundred ppm to three thousand ppm in these two zones. There is low Na zone (<0.07%, except sample 130291) at the non-mineralized eastern side of the profile. Higher concentrations appear to show a positive relation to the lower mineralization system.

Potassium: Potassium varies from 0.03% to 3.5% in the regolith profile and averages greater than 0.1%. The distribution contour map is shown in Figure 11-13. The persistence of muscovite in the profile up to the mottled zone is indicated by concentrations of 0.3–2% K in the regolith to this level. However, the K content of the lateritic duricrust near the surface is in generally lower than 0.4%.

The K distribution in section 10250N and 10400N is similar to that in section 10150N (see Appendices 7 and 8). The high K contents in the middle saprolite (below R.L. 370) to saprock indicate strong enrichment associated with the projection of the primary Au mineralization.

Rubidium: The Rb distribution closely follows that of K, which is largely controlled by the distribution of micas. It ranges from 1 to 105 ppm. The distribution contour map is shown in Figure 11-14. There are two pronounced zones of Rb greater than 35 ppm at the eastern and western portions of the profile. The Rb content generally decreases towards the surface, especially in lateritic residuum where it is normally only a few ppm.

11.3.4 Base and transition metals (Cu, Pb, Zn, Co, Ni and Mn)

Copper: Copper has a range of 0 to 23 ppm. The distribution contour map is shown in Figure 11-15. It reveals a zone of greater than 10 ppm Cu in the upper part of the saprolite and the near surface lateritic residuum. Generally, the abundance of Cu below the lower saprolite is less than 4 ppm. This low Cu distribution zone includes the saprock and unweathered bedrock. Similar distribution of Cu occurs in the two other sections.

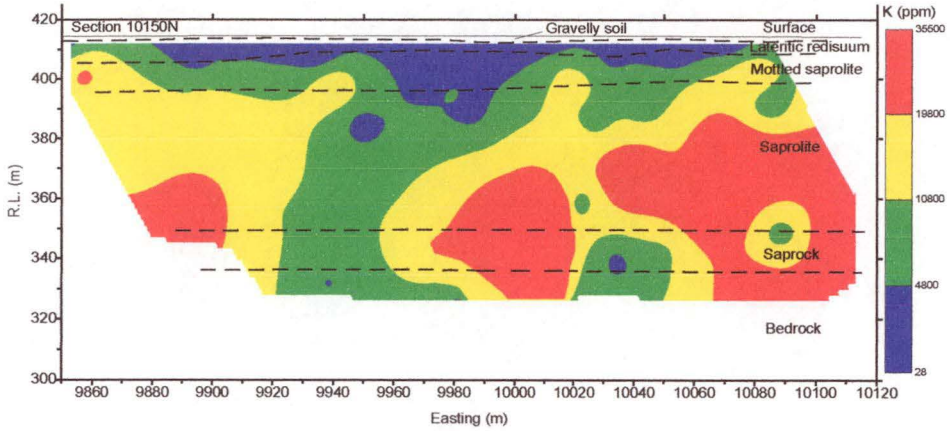

Figure 11-13. K distribution of acid insoluble residue at 10150N in Jim's Find, N.T.

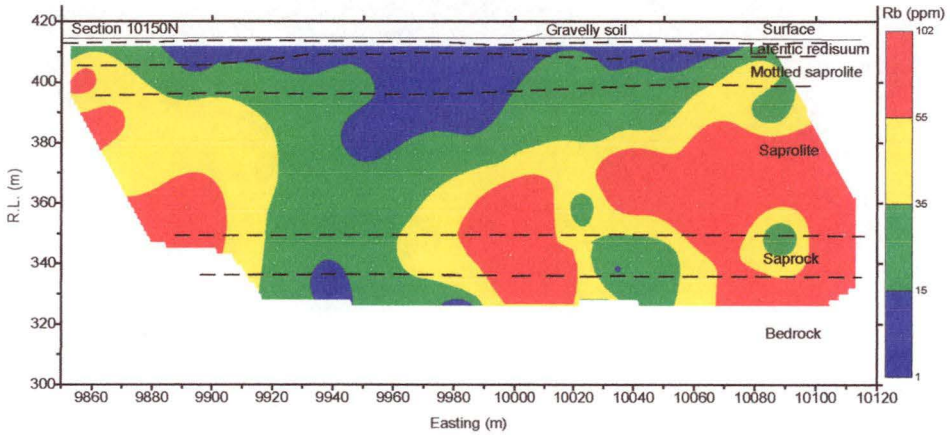

Figure 11-14. Rb distribution of acid insoluble residue at 10150N in Jim's Find, N.T.

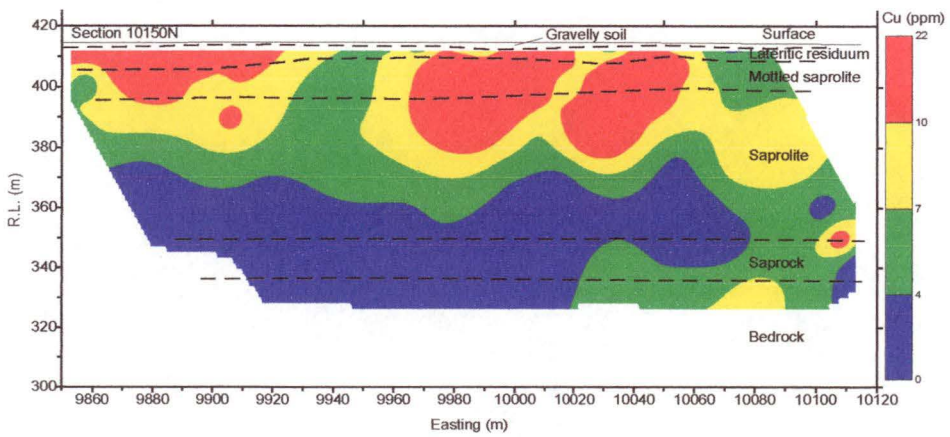

Figure 11-15. Cu distribution of acid insoluble residue at 10150N in Jim's Find, N.T.

Lead: The Pb abundance of the acid insoluble residue in both the unweathered bedrock and the regolith of the study area is from 0 to 8 ppm, but average content values are low (<3 ppm). The distribution contour map is shown in Figure 11-16. Zones of enrichment of greater than 4 ppm Pb occur sporadically in the profile.

Zinc: It has a range of 0 to 14 ppm. The distribution contour map is shown in Figure 11-17. The average concentration of Zn in the acid insoluble residue is less than 5 ppm. Because of its low abundance, the distribution pattern in the regolith is indistinct, particularly on Section 10150N.

Cobalt: The Co content has the range of from 5 to 67 ppm. The distribution contour map is shown in Figure 11-18. The distribution of Co is generally similar to that of Zn. A Co depletion zone occurs between 9850E and 9950E. Higher Co contents occur in the middle to lower saprolite between 10000E to 10060E and through the whole regolith further to the east. The reason for these zones of Co enrichment is not clear.

Nickel: Nickel has a similar distribution compared to Cu. Nickel varies from 0 to 55 ppm. The distribution contour map is shown in Figure 11-19. The higher Ni contents occur in the mottled and lateritic residuum zones and range from 7 to 55 ppm. Compared to the Cu distribution in the upper regolith profile, the enrichment in Ni is continuous and mainly limited into the lateritic residuum and mottled saprolite. Nickel concentration under the mottled saprolite is very low.

Manganese: The Mn content of the regolith in acid insoluble residue is very low. It ranges from 4 to 41 ppm. The distribution contour map is shown in Figure 11-20. Manganese has a very similar distribution pattern to that of Zn. Unlike the bulk geochemistry, there is no marked leaching of Mn occurring in the regolith. Instead Mn has a rather patchy distribution in the profile.

11.3.5 Lithophile transition elements (Cr, Ti and V)

Chromium: Chromium ranges from 0 to 277 ppm. The distribution contour map is shown in Figure 11-21. Chromium is enriched at both sides of the profile, especially at the western side from 9860E to 9910E. In the middle part of the profile, reasonably high Cr concentrations (> 16 ppm) occur at the base of the profile near the

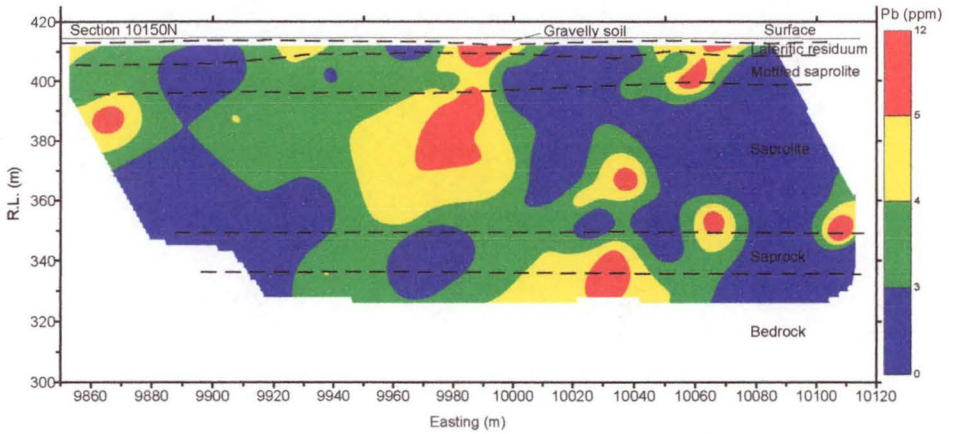

Figure 11-16. Pb distribution of acid insoluble residue at 10150N in Jim's Find, N.T.

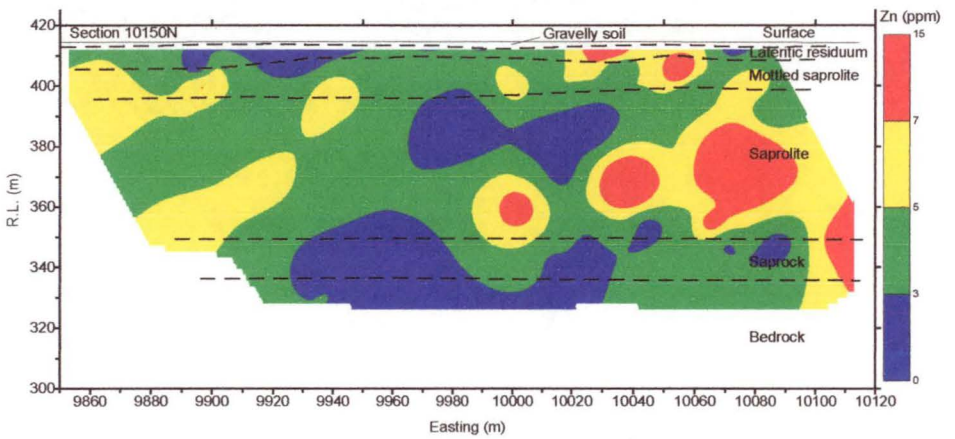

Figure 11-17. Zn distribution of acid insoluble residue at 10150N in Jim's Find, N.T.

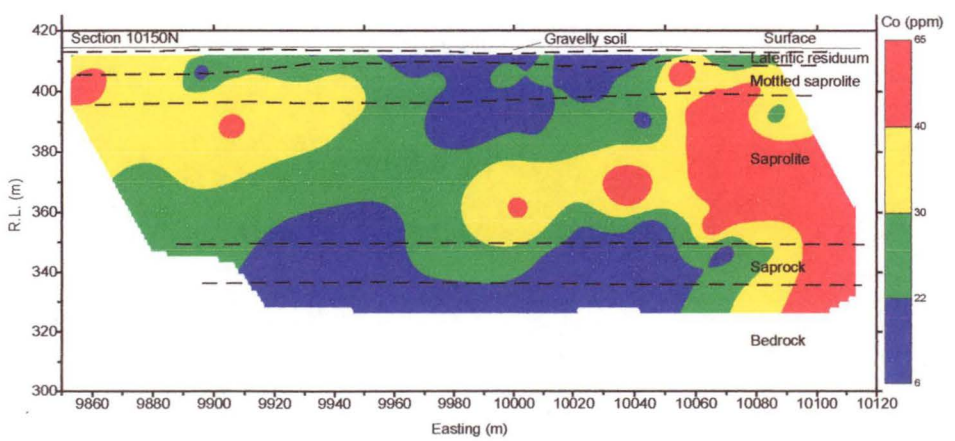

Figure 11-18. Co distribution of acid insoluble residue at 10150N in Jim's Find, N.T.

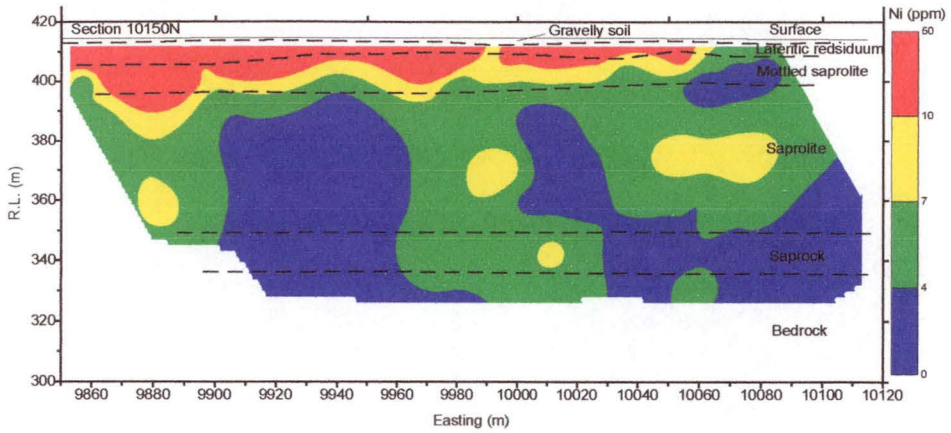

Figure 11-19. Ni distribution of acid insoluble residue at 10150N in Jim's Find, N.T.

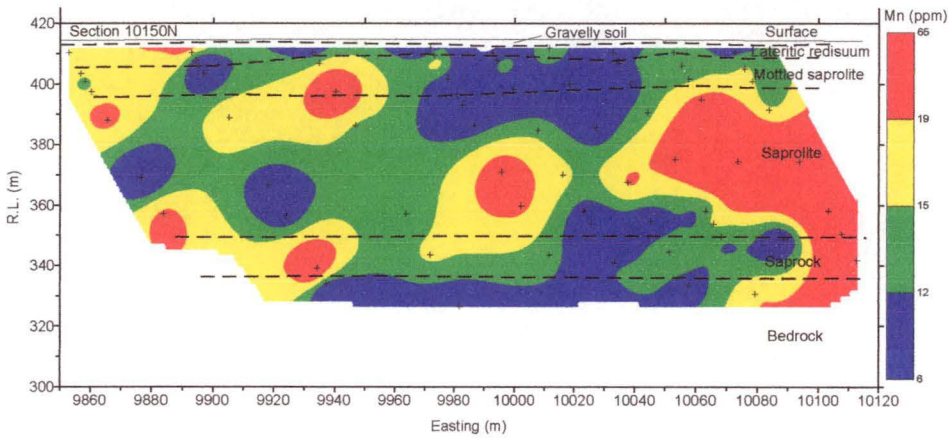

Figure 11-20. Mn distribution of acid insoluble residue at 10150N in Jim's Find, N.T.

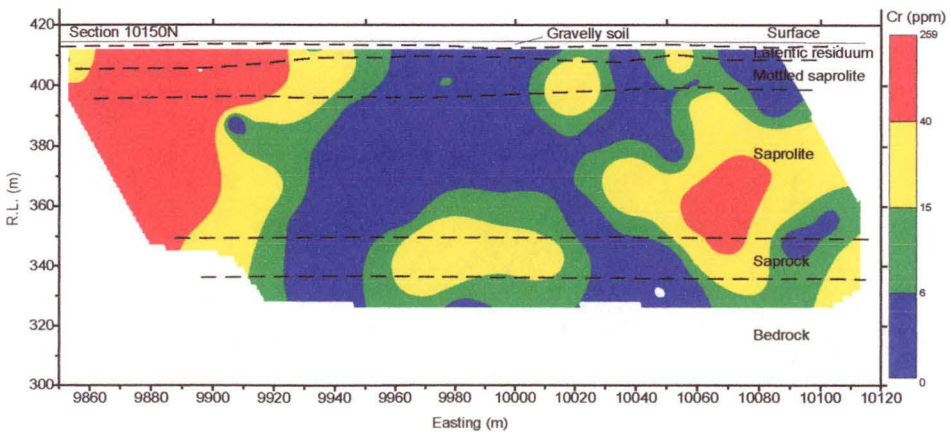

Figure 11-21. Cr distribution of acid insoluble residue at 10150N in Jim's Find, N.T.

mineralization.

Titanium: Titanium ranges from 0.29 to 2.6% in the regolith profile. The distribution contour map is shown in Figure 11-22. It exhibits at least two zones of concentration with westerly dipping trends. The zone of greatest concentration is flanked by two zones of lower concentration (< 11000 ppm and 11000 –13000 ppm) that probably define different lithologic units. The XRD data indicates that rutile is present in the acid insoluble residue. This suggests that Ti may be hosted by rutile and other ferromagnesian minerals.

Vanadium: The V content of the regolith has a range of 84 to 639 ppm. The distribution contour map is shown in Figure 11-23. Generally the V is concentrated in the lower part of mottled zone to the saprock. Lower V values (< 270 ppm) occur in the gravelly soil and lateritic residuum horizons, and extend into the mottled zone at depth (from R.L. 395 to R.L. 405).

11.3.6 Immobile elements (Zr, Nb and Th)

These elements generally exhibit little chemical mobility in the weathering environment. Zr, Nb and Th are all members of the second and third transition series and have very similar chemical characteristics. Zircon is probably the principal host mineral for each of these elements and hence the stability of zircon determines their distribution and dispersion in the regolith (Butt, 1991).

Zirconium: It varies from 51 to 451 ppm and increase upward through the regolith. The distribution contour map is shown in Figure 11-24. Pronounced Zr enrichment near the surface in the gravelly soil and lateritic residuum reflects its immobile character. Similar near surface expression can also be found in Sections 10250N and 10400N. In the deeper part of the profile, Zr enrichment occurs in a fork-shaped zone with a westerly dip. This is similar to the observed Ti distribution. These characters seem to reflect the primary variations in geochemistry.

Niobium: Niobium concentration in the regolith ranges from 0 to 25 ppm. The distribution contour map is shown in Figure 11-25. Its distribution is very similar to that of Zr, except for high values (> 10 ppm) in the saprolite on the eastern side of the profile. Strong westward dipping high values occur between 9930E and 10000E, similar to those of Ti and Zr, and probably reflect the primary distribution of minerals

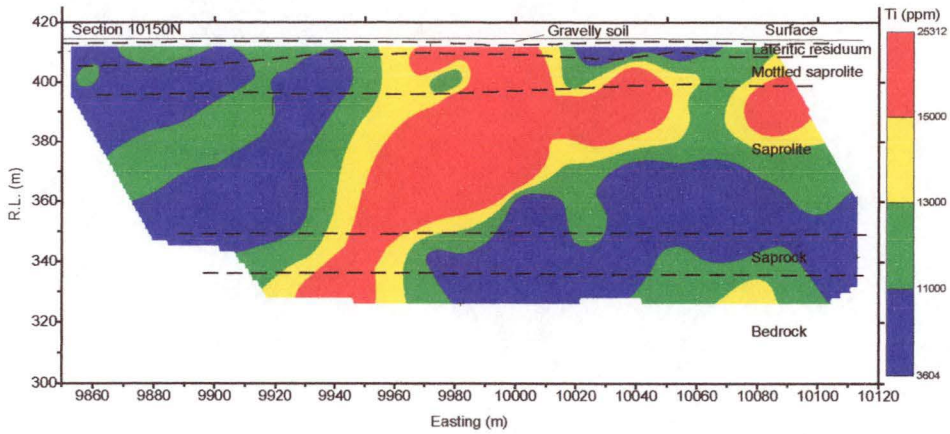

Figure 11-22. Ti distribution of acid insoluble residue at 10150N in Jim's Find, N.T.

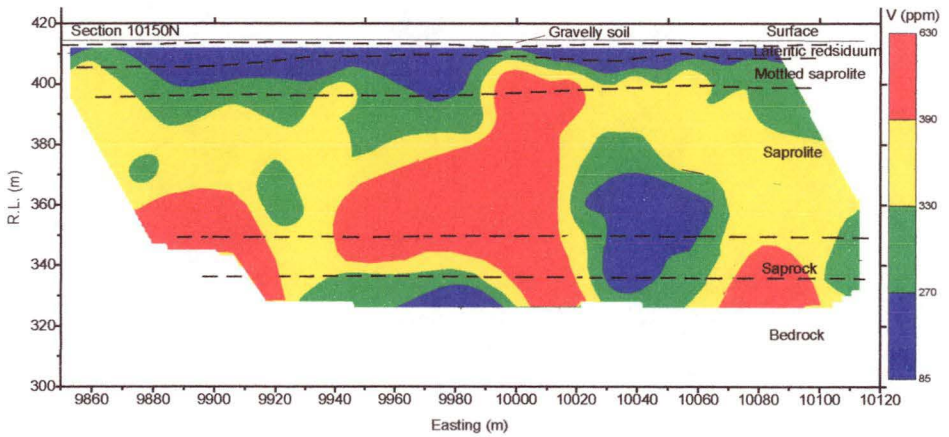

Figure 11-23. V distribution of acid insoluble residue at 10150N in Jim's Find, N.T.

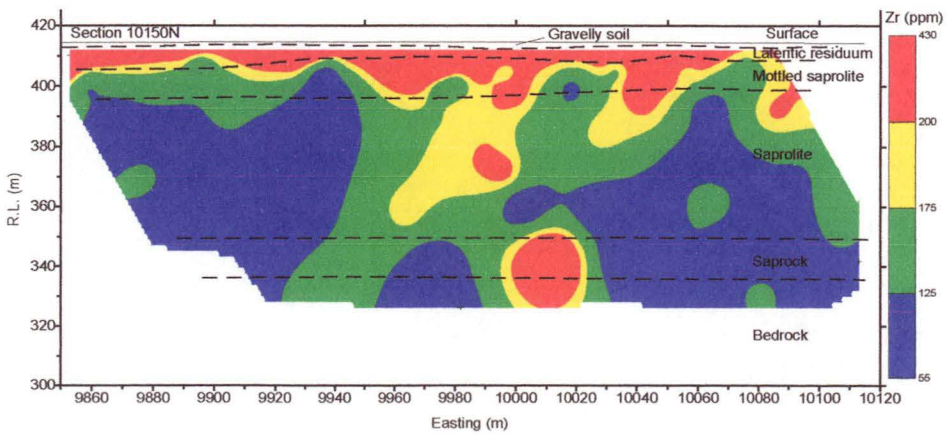

Figure 11-24. Zr distribution of acid insoluble residue at 10150N in Jim's Find, N.T.

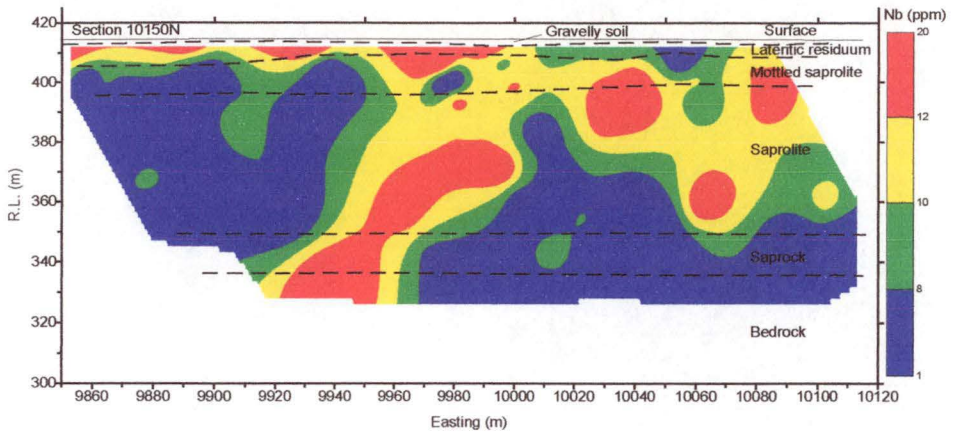

Figure 11-25. Nb distribution of acid insoluble residue at 10150N in Jim's Find, N.T.

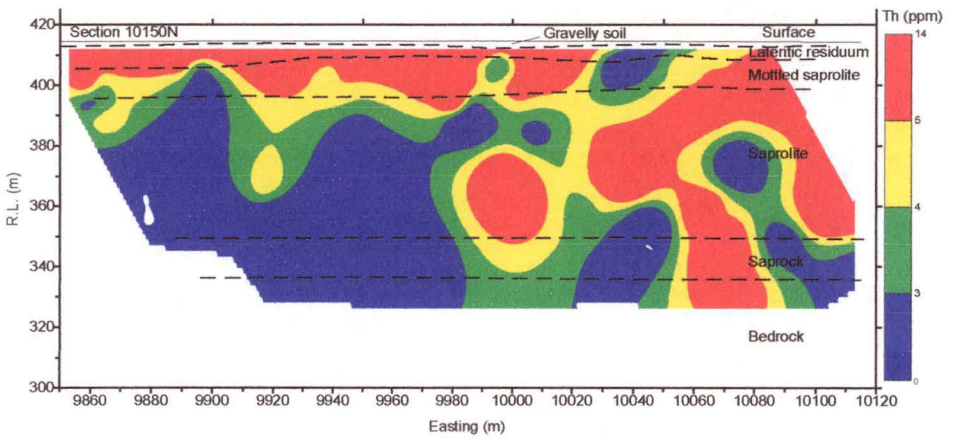

Figure 11-26. Th distribution of acid insoluble residue at 10150N in Jim's Find, N.T.

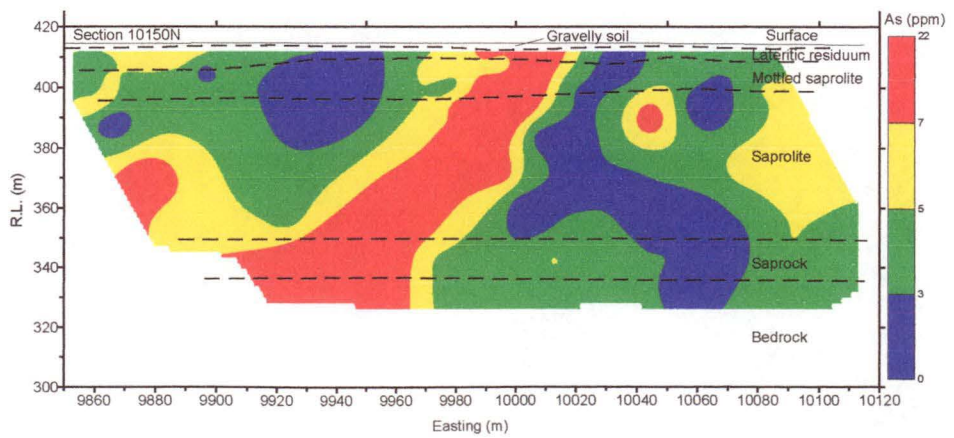

Figure 11-27. As distribution of acid insoluble residue at 10150N in Jim's Find, N.T.

and lithologies.

Thorium: Significant accumulations of Th are noted in the lateritic residuum and mottled zone. Its content in the profile varies from 0 to 12 ppm. The distribution contour map is shown in Figure 11-26. Thorium in the shallow part of the profile is almost double that in the deeper saprolite and saprock, especially on the western side of the profile. This reflects the immobile character of Th. Some erratic high values (>5 ppm) occur on the eastern side of the profile. As the concentration of Th in the saprolite and saprock horizon is close to the detection limit Th will not be a key element in this study.

11.3.7 Other elements (As, S, W, Ga, Mo, F, Cl and Y)

Arsenic: It has the range of 0 to 14 ppm. The distribution contour map is shown in Figure 11-27. The As content of the acid treated residue increases towards the surface, reaching values greater than the As content of the bulk rock. As concentration greater than 7 ppm is enriched in the unweathered bedrocks from 9890E to 9970E and displays a westward dip, similar to Zr and Ti. The As distribution appears to be related to the lithology.

Sulphur: Sulphur in the unweathered bedrock is likely to be present in pyrite. Its value in the acid insoluble residue change from 77 to 12000 ppm. The distribution contour map is shown in Figure 11-28. Zones of high S enrichment, over 2100 ppm, occur in the saprolite horizon. These zones are partly coincident with the center of the supergene enrichment of gold in the upper saprolite. They transgress to the surface and seem to shroud the underlying mineralization.

Tungsten: The W is consistently enriched throughout the primary mineralization in all three sections. Generally W varies from 0 to 185 ppm in the profile. The distribution contour map for section 10150N is shown in Figure 11-29. A similar distribution pattern can also be found in section 10250N and 10400N (see Appendices 7 and 8). The primary mineralization can be characterized by moderate enrichment in W, that is greater than 26 ppm. Near surface in areas where there is no underlying mineralization, the abundance of W is less than 10 ppm.

Gallium: The Ga content varies from 0 to 23 ppm. The distribution contour map is

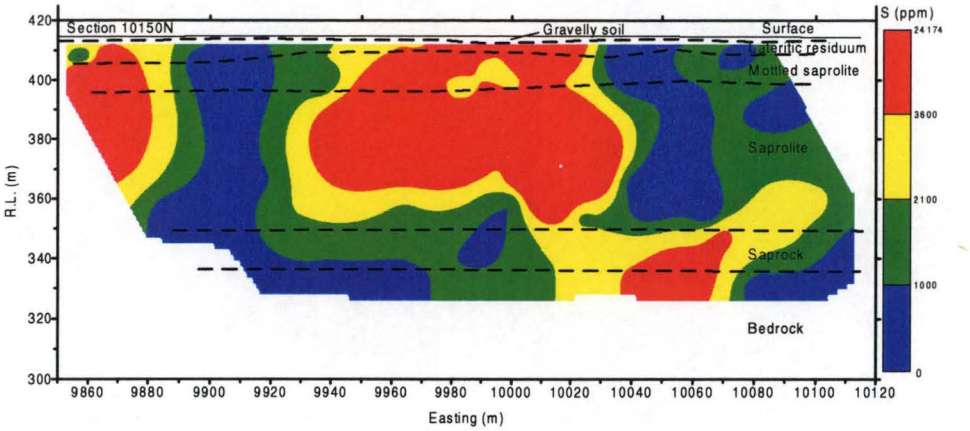

Figure 11-28. S distribution of acid insoluble residue at 10150N in Jim's Find, N.T.

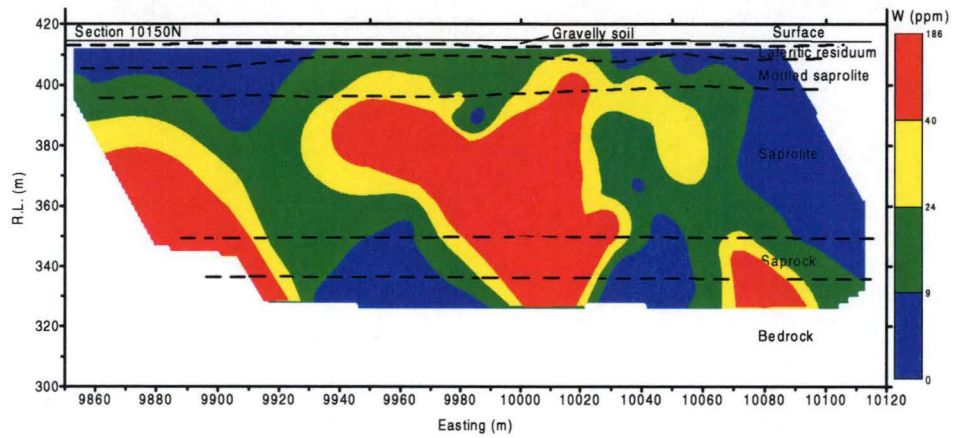

Figure 11-29. W distribution of acid insoluble residue at 10150N in Jim's Find, N.T.

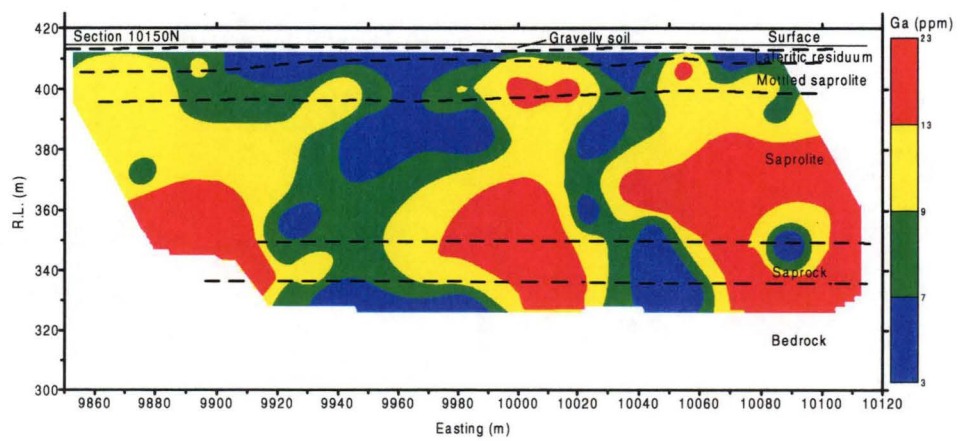

Figure 11-30. Ga distribution of acid insoluble residue at 10150N in Jim's Find, N.T.

shown in Figure 11-30. Its distribution generally follows that of Al, Rb and K in the regolith. This implies that Ga is concentrated in feldspars, sericite and muscovite, substituting for Al. Generally, high Ga concentrations occur in the middle to lower saprolite and saprock horizon. Leaching is evident in the lateritic residuum zone. The distribution of Ga is not homogeneous near surface, suggesting that little dispersion occurs during weathering.

Molybdenum: Molybdenum has a range of 0 to 22 ppm. The distribution contour map is shown in Figure 11-31. Generally Mo contents are very low in the profile (< 4 ppm). However Mo enrichment of more than 6 ppm occurs from 9910E to 10010E in both the saprock and bedrock horizons. This enrichment gradually decreases upwards to values of 4 ppm. An adjacent depletion zone occurs in the mottled saprolite. There is also some patchy zones of Mo enrichment in the lateritic residuum overlying the entire section.

Fluorine: The concentration of F ranges from 0 to 477 ppm. The distribution contour map is shown in Figure 11-32. Its distribution follows closely of Fe, Mn, Cr and Zn in the regolith very much. Generally the occurrence of F in the lateritic residuum is lower than 200 ppm. The highest values occur in the saprolite horizon.

Yttrium: The distribution of Y within the regolith on all three sections is very similar to the distribution of Zr and Nb. It shows the same westerly dip in the profile but the surface expression is not as high as those for Zr and Nb. Yttrium ranges from 0 to 45 ppm. The distribution contour map is shown in Figure 11-33.

Chlorine: Chlorine varies from 0 to 330 ppm. The distribution contour map is shown in Figure 11-34. Generally the abundance of Cl is much lower in the mineralized zone, less than 30 ppm. In contrast, the high Cl concentrations occur in the lateritic residuum and mottle zone.

11.4 DISCUSSION OF ELEMENT DISTRIBUTION

The element distributions in acid insoluble residue have been discussed extensively in Chapters 5 and 8, in which a series of elements that expressed the mineralization, lithology and relation to ferromagnesian minerals were defined. This section provides a discussion of the element distributions of the acid insoluble residue present in

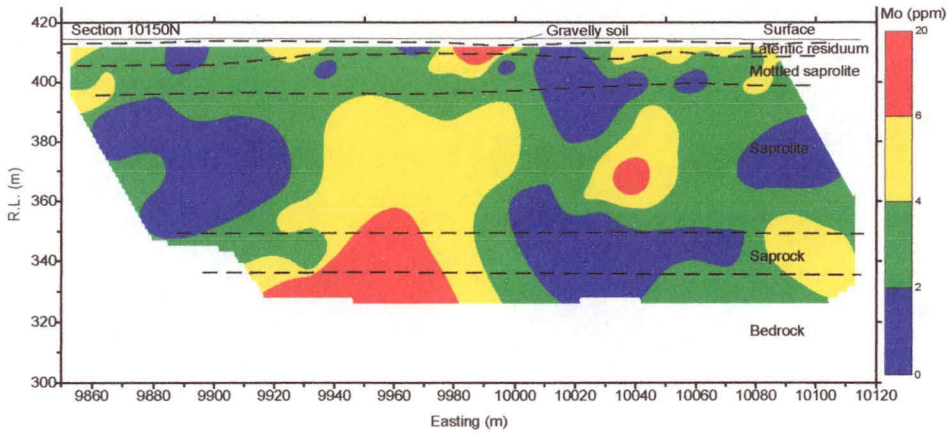

Figure 11-31. Mo distribution of acid insoluble residue at 10150N in Jim's Find, N.T.

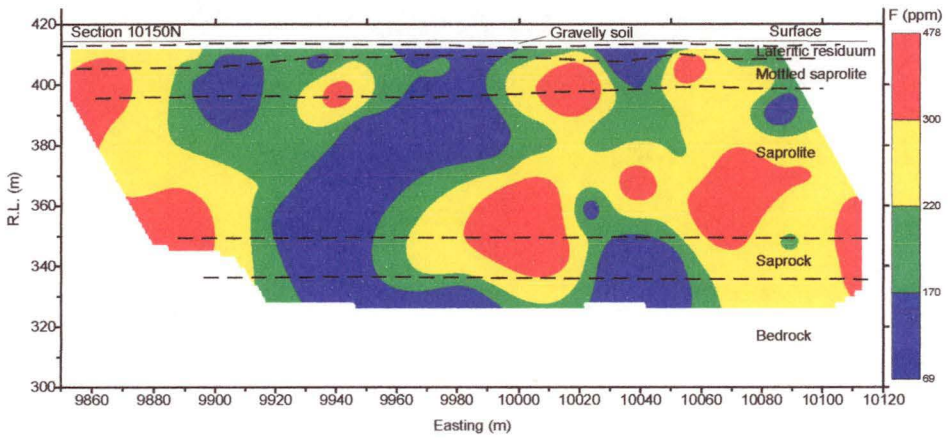

Figure 11-32. F distribution of acid insoluble residue at 10150N in Jim's Find, N.T.

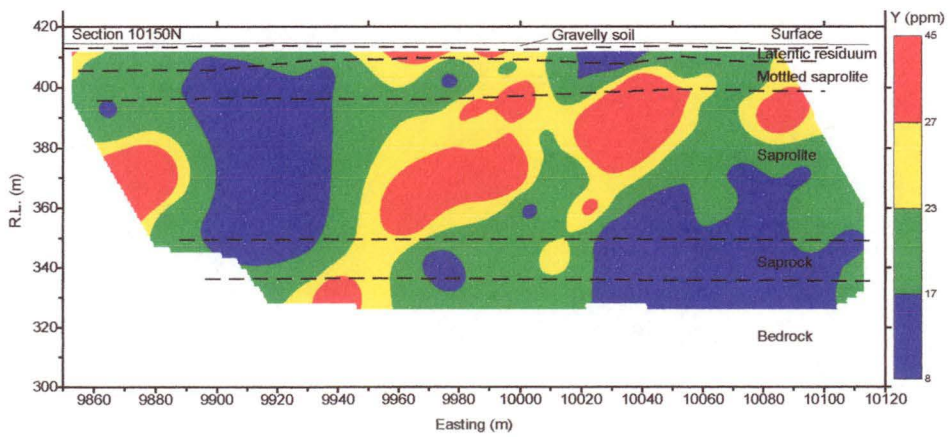

Figure 11-33. Y distribution of acid insoluble residue at 10150N in Jim's Find, N.T.

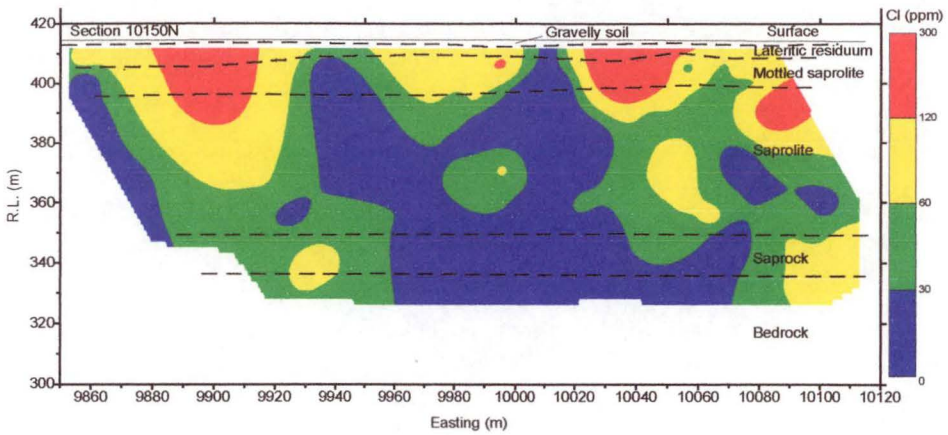

Figure 11-34. Cl distribution of acid insoluble residue at 10150N in Jim's Find, N.T.

section 11.3 and offers a further example to verify its use as a sample medium for gold exploration in deeply weathered terrain.

11.4.1 Statistical methods

As in the studies at Mystery Zone and Rand Pit in Western Australia presented in Chapters 5 and 8, Spearman ranking and two statistical methods, factor and cluster analyses have been applied.

One hundred and thirty-seven acid insoluble residue samples have been used in the statistical analyses. The means and standard deviation of the raw and $\log_{10}$ transformed data are given in Table 11-1. Considering the high variance of the raw data, all the statistical methods described below have been applied to $\log_{10}$ transformed data.

The Spearman correlation matrix is shown in Table 11-2. It can be seen that gold correlates well with Ga, K, F, Na, Nb, Rb, Sr, V, W, and possibly Al. Some of the correlation coefficients are low, but as a result of the large sample numbers they still indicate a strong positive correlation and have a very good confidence level (see Figure 6-6). These correlations derived from the acid insoluble residue are very similar to those of Rand Pit and Mystery Zone. The elements Ga, K, F, Na, Nb, Rb, Sr, W and Al are interpreted to be related to the mineralization on the alteration associated with mineralization.

Factor analysis has been carried out as in the Chapters 5 and 8. The number of

Table 11-1. Statistical data of the acidinsoluble residue, Jim's Find, N.T. (n=137)

	Raw data					log10 transformed data				
Variable	Mean	Std Dev	Variance	Min.	Max.	Mean	Std Dev	Variance	Min.	Max.
Aa	52655.5	13824.5	1.9_10^8	17178	82837	4.7	0.13	0.02	4.23	4.92
As	5.9	4	15.66	0	25	0.68	0.29	0.08	0	1.4
Au	34000	36705	1.3_109	3	34000	1.93	0.94	0.88	0.4	5.49
Ca	206.7	128.5	16511	11	1047	2.24	0.28	0.08	1.04	3.02
Cl	86.9	68.1	4635.36	0	311	1.71	0.58	0.34	0	2.49
Co	26.6	11.2	124.75	5	67	1.39	0.17	0.03	0.7	1.83
Cr	17.6	41.6	1734.01	0	277	0.59	0.73	0.54	0	2.44
Cu	7.8	4.8	23.46	1	30	0.8	0.3	0.09	0	1.48
F	199.2	98.2	9637.29	42	513	2.25	0.22	0.05	1.62	2.71
Fe	4239.1	2467	6086234	1312	14253	3.57	0.21	0.04	3.12	4.15
Ga	9	4.4	19.21	2	23	0.9	0.23	0.05	0.3	1.36
Ge	1	1	0.93	0	4	0.11	0.17	0.03	0	0.6
K	10343.9	9305.2	8.7_107	310	36346	3.78	0.52	0.27	2.49	4.56
Mn	14.3	7.9	62.79	4	74	1.11	0.2	0.04	0.6	1.87
Mo	3.7	3.2	10.1	0	21	0.46	0.34	0.11	0	1.32
Na	3150.5	5310.9	2.8_10^7	100	35479	3.11	0.58	0.33	2	4.55
Nb	9.8	4.3	18.43	0	25	0.94	0.23	0.05	0	1.4
Ni	7.2	6.9	47.35	0	55	0.72	0.35	0.12	0	1.74
Pb	3.6	2.4	5.54	0	11	0.48	0.29	0.08	0	1.04
Rb	28.9	25.6	655.47	1	105	1.27	0.45	0.2	0	2.02
S	2393.6	4031.7	1.6_10^7	37	27685	2.99	0.61	0.38	1.57	4.44
Si	273712	21466.3	4.6_10^8	214651	321655	5.44	0.03	0	5.33	5.51
Sr	14.4	11.3	126.5	2	70	1.05	0.3	0.09	0.3	1.85
Th	4.3	2.7	7.18	0	13	0.56	0.29	0.08	0	1.11
Ti	13469.7	4178.5	1.7_10^7	2850	25987	4.11	0.14	0.02	3.45	4.41
V	318.6	110.9	12308.6	32	639	2.47	0.18	0.03	1.51	2.81
W	23.8	31.4	984.38	0	199	1.03	0.59	0.35	0	2.3
Y	22	7.2	51.5	7	44	1.32	0.15	0.02	0.85	1.64
Zn	3.8	2.6	6.72	0	14	0.5	0.28	0.08	0	1.15
Zr	175.7	97.4	9489.75	51	802	2.2	0.19	0.04	1.71	2.9

factors has been chosen according to the eigenvalues larger than 1. The six-factor matrix obtained using the principal component factor analysis is shown in Table 11-3. Table 11-4 gives the final statistics indicating that the eigenvalues larger than 1 have more than 72 cumulative percentage. The factor analysis indicates that the factor 1 accounts for most of the variation in the elements Al, Ca, Co, Cr, F, Fe, Ga, K, Mn, Rb, V and W. Factor 2 is composed of As, Ca, Mn, Nb, Ti and Y. Factor 3 consists of Al, As, Nb, Ni, Pb, Th, Ti, V, Y and Zr.

The Oblique principal component cluster analysis is given in Table 11-5. Four clusters have been generated and the inter-cluster correlation is given in Table 11-6. The first

Table 11-2. Spearman correlation matrix for Jim's Find acid insoluble residue samples (base on log 10 transformed data, n=137)

	Al	As	Au	Ca	Cl	Co	Cr	Cu	F	Fe	Ga	Ge	K	Mn	Mo	Na	Nb	Ni	Pb	Rb	S	Sr	Th	Ti	V	W	
Al	1 00																										
As	-0 15	1 00																									
Au	0 10	-0 01	1 00																								
Ca	-0 07	0 10	0 00	1 00																							
Cl	-0 33	0 32	-0 09	-0 10	1.00																						
Co	0 38	-0 18	-0 19	0 22	-0 20	1 00																					
Cr	0 30	-0 26	-0.02	0 01	-0 07	0.36	1 00																				
Cu	0 04	0 14	-0 35	-0 27	0.26	-0 09	-0 13	1.00																			
F	0 60	-0.19	0 15	0 18	-0.26	0 64	0 50	-0.28	1 00																		
Fe	0 47	-0 24	-0 15	0 19	-0 25	0 89	0 45	-0 11	0 75	1 00																	
Ga	0 71	-0 11	0 15	0 24	-0 13	0.52	0 40	-0 16	0 78	0 63	1 00																
Ge	-0 11	0 16	-0 06	-0 10	0.13	0 03	-0 06	0 09	-0 18	-0 04	-0 15	1.00															
K	0 34	-0 15	0 21	0 52	-0 26	0 47	0 25	-0 46	0 68	0 56	0 61	-0 25	1 00														
Mn	0.27	-0 04	0 03	0 14	-0 11	0 52	0.10	-0 08	0 42	0.50	0.42	-0.01	0.40	1 00													
Mo	-0 27	0 25	-0 04	-0 14	0 06	-0 20	-0 15	0 10	-0 25	-0.18	-0 33	0 02	-0 19	-0 12	1 00												
Na	-0 17	0 16	0 17	-0 59	0 00	-0 24	-0 18	-0 29	-0 13	-0 29	0.03	-0 02	0 20	-0 06	-0.11	1 00											
Nb	-0 03	0 41	0 14	-0 19	0 12	-0 14	-0 31	0 12	-0 09	-0 14	-0 10	0 04	-0 14	-0 01	0 18	-0 11	1 00										
Ni	0 22	0 08	-0 07	-0 51	0 22	-0 09	0 20	0 44	-0 07	-0.10	-0.01	0 15	-0 44	-0 06	-0 04	-0 37	0 20	1.00									
Pb	-0 10	0 12	0 07	0 01	0 07	-0 07	-0.26	0 06	-0 04	-0 05	-0 14	-0 06	-0 05	0 10	0 11	0 05	0 18	-0 02	1 00								
Rb	0 38	-0 17	0 19	0 44	-0 26	0 51	0 30	-0 44	0.72	0.61	0.65	-0 22	0 97	0 43	-0 21	0 12	-0 12	-0.36	-0 09	1 00							
S	0 32	-0 23	-0 02	-0.13	-0 68	0 06	-0 07	0.00	0 04	0 08	-0.06	0.02	-0 14	-0 02	-0 04	-0 16	-0 02	0 07	0.01	-0 10	1 00						
Sr	-0 14	0 27	0 14	0 56	0.04	-0 25	-0 19	-0 20	-0 17	-0 28	-0 01	-0 02	0 13	-0 11	-0 06	0 81	-0 14	-0.31	0 14	0 05	-0 03	1.00					
Th	0 11	-0 25	0 04	-0 25	-0.04	0 15	0 07	0 09	0 22	0.15	0 21	-0 11	-0 01	0 12	-0 10	-0 27	0 15	0 20	0 15	0 06	0 10	-0 24	1 00				
Ti	0 02	0 50	0 05	0 14	0 01	-0 08	-0 55	0 21	-0 12	-0 15	-0 10	0 02	-0 06	0 04	0 16	0 11	0 58	0 02	0 25	0 10	0 14	0.14	0 00	1 00			
V	0 43	0 19	0 21	0 44	-0 17	0 34	-0 13	-0.11	0 52	0 33	0 53	-0 14	0 57	0.32	-0 09	0 23	0 19	-0 22	0 10	0.54	0 04	0 20	0 01	0 62	1 00		
W	0 27	-0 80	0 56	-0 01	-0 20	-0 07	0 00	-0 20	0 31	-0 03	0 22	-0 35	0 30	0 06	-0 02	0 01	0 06	-0 08	0 00	0.28	0 08	-0 01	0 09	0 21	0 43	1 (	
Y	0 01	0 46	0 08	-0 04	0 07	-0 03	-0 34	0 09	0.00	-0 06	-0 05	-0 01	-0 04	-0 01	0.19	-0 08	0 51	0 09	0 35	-0 07	0 04	-0.01	0 10	0 69	0 42	0 .	
Zn	0 18	-0 09	-0 13	0 29	-0 13	0 52	0 25	-0 23	0 47	0 61	0 37	-0 02	0 39	0 32	-0 20	-0 05	-0 11	-0 06	0 02	0.41	0 05	-0 07	0 05	-0.14	0 16	-0 (	
Zr	-0 09	0 36	-0 07	-0 50	0 27	-0 25	-0 21	0 36	-0 22	-0.23	-0 21	0 13	-0 45	-0 05	0 30	-0 36	0.57	0 47	0 24	-0 39	0 06	-0 29	0 24	0 40	-0 10	-0 (	

Table 11-3. The factor matrix of principal component factor analysis for the acid insoluble residue (n=137)

	Factor 1	Factor 2	Factor 3	Factor 4	Factor 5	Factor 6
Al	0.54873	0.40896	0.0094	-0.21839	0.48741	-0.09512
As	-0.27147	0.03365	0.60943	0.34137	0.12204	-0.23873
Au	0.14807	-0.1138	0.33385	-0.72753	-0.11379	0.04895
Ca	0.47334	-0.58169	0.31169	0.35004	0.06464	0.04298
Co	0.71676	0.32667	-0.17262	0.38157	-0.08431	-0.02845
Cu	-0.41268	0.41469	-0.05706	0.28287	0.43875	0.01361
F	0.85149	0.3041	0.00732	-0.10483	0.00398	-0.01269
Fe	0.78725	0.36226	-0.20163	0.30405	-0.10977	-0.04127
Ga	0.79874	0.22911	0.049	-0.09793	0.32403	0.01801
K	0.87179	-0.15813	0.18105	-0.05423	-0.16348	-0.08567
Mn	0.53241	0.24936	0.05665	0.20493	-0.09709	0.15383
Mo	-0.35665	0.06232	0.19476	0.12293	-0.46925	-0.35831
Na	0.09437	-0.75699	0.37859	0.04594	0.24544	0.2031
Nb	-0.25327	0.43207	0.56136	0.01439	-0.11336	-0.03187
Ni	-0.32546	0.58843	-0.15133	-0.09041	0.4243	0.07627
Pb	-0.108	0.10837	0.36061	0.1375	-0.27234	0.64754
Rb	0.8815	-0.0621	0.11996	-0.07028	-0.15549	-0.08077
Sr	0.02997	-0.70504	0.41102	0.1019	0.28465	0.24484
Th	0.08585	0.46708	-0.0717	-0.21167	-0.11276	0.58308
Ti	-0.14874	0.23488	0.83272	0.17586	0.09383	-0.05787
V	0.57854	0.10545	0.68041	0.018	0.1629	-0.08934
W	0.26629	0.08516	0.38422	-0.67947	-0.06649	-0.1213
Y	-0.13552	0.39007	0.73176	0.07032	-0.1273	0.00604
Zn	0.56825	0.1027	-0.13293	0.33733	-0.14548	0.11334
Zr	-0.51111	0.62665	0.30294	0.03083	-0.08283	0.05319

Table 11-4. The final statistics of factor analysis showing the eigenvalues (n=137)

Variable	Communality	Factor	Eigenvalue	Pct of Var	Cum Pct
Al	0.76275	1	6.46451	25.9	25.9
As	0.63465	2	3.63139	14.5	40.4
Au	0.69097	3	3.47898	13.9	54.3
Ca	0.78813	4	1.91688	7.7	62
Co	0.80376	5	1.37181	5.5	67.5
Cu	0.61823	6	1.14845	4.6	72
F	0.82873				
Fe	0.89786				
Ga	0.8078				
K	0.85481				
Mn	0.42394				
Mo	0.5327				
Na	0.82886				
Nb	0.58003				
Ni	0.6691				
Pb	0.66583				
Rb	0.83094				
Sr	0.81827				
Th	0.62817				
Ti	0.8138				
V	0.84363				
W	0.70661				
Y	0.72718				
Zn	0.49893				
Zr	0.75634				

cluster comprises the elements F, Al, K, V, Mn, Fe, Co, Zn, Ga and Rb and is essentially related to sericitic wall rock alteration. The second cluster consists of Na, Ca and Sr and is interpreted to comprise of elements in weatherable minerals such as feldspar, thus representing the weathering intensity. It also appears to depict wall rock alteration. The third cluster includes Ti, As, Y, Zr, Nb and Pb and is largely related to resistate minerals and primary lithology. The fourth cluster comprises F, Al, K, V, Ga, Rb, W and Au and is considered to be mineralization related. Because of the close relationship between cluster 1 and cluster 4 (Table 11-6) as well as their similar composition character, it can be inferred that the wall rock alteration is associated with mineralization.

The following description of acid insoluble residue regolith geochemistry has been divided into different groups according to their geochemical character as expressed by both factor and cluster analyses. The discussion is split up into sections relating to the mineralization, lithology and weathering related elements.

11.4.2 Deeper profile: ore and alteration related elements

The elements Au, F, Al, K, Mn, Fe, Co, Zn, Ga, Rb, Mo, W and V are considered to be related to ore and/or alteration.

Gold distribution patterns across sections 10250N and 10400N, define subvertical to vertical mineralized zones. The trend of these zones is persistent throughout the entire regolith profile. The mineralized zone is hereafter defined as the linear vertical zone that is mapped out by high gold concentration in the saprolite and presumably reflects the trend and location of the hypogene orebody. Anomalous gold values are closed off to both the east and the west on line 10400N. Line 10250N differs slightly in that the mineralization is closed off more so to the west for near surface levels changing to a tighter definition on both sides with increasing depth. The similarities in the gold concentration distributions across lines 10250 N and 10400N are not as obviously present along 10150N. Section 10150N exhibits a broad, somewhat slightly spread, vertical trend. A pronounced zone of gold enrichment has developed about the surface continuation of the identified subvertical to vertical hypogene mineralization zone. This surface to near surface mineralization is found on all sections. The depletion zone is most clearly developed on section 10150N where is coincides with the mottled saprolite. On line 10400N, the depletion zone is in the middle

Table 11-5. Oblique principal component cluster analysis - cluster structure

Cluster	1	2	3	4
F	0.860764	-0.006903	-0.15108	0.735719
Na	-0.153537	0.854184	-0.060994	0.146211
Al	0.564485	-0.184803	-0.060723	0.578216
K	0.653865	0.42044	-0.205447	0.869962
Ca	0.264734	0.805067	-0.115113	0.373001
Ti	-0.131033	0.069857	0.824265	0.166291
V	0.460317	0.313215	0.353166	0.774537
Mn	0.634357	0.002193	-0.00034	0.386209
Fe	0.920293	-0.090296	-0.198811	0.481533
Co	0.862878	-0.063813	-0.167367	0.398225
Ni	-0.075675	-0.673341	0.205454	-0.270162
Cu	-0.200341	-0.497472	0.234514	-0.370384
Zn	0.674158	0.087801	-0.153588	0.283776
Ga	0.791552	0.073288	-0.151849	0.699805
As	-0.202564	0.143166	0.668693	-0.091247
Rb	0.698267	0.320962	-0.2141	0.863217
Sr	-0.184254	0.811307	0.01116	0.09475
Y	-0.061427	-0.090439	0.838928	0.144033
Zr	-0.269597	-0.529417	0.723244	-0.300349
Nb	-0.137813	-0.213551	0.778531	0.001884
Mo	-0.350908	-0.079569	0.276635	-0.200288
W	0.097321	0.037836	0.115434	0.615796
Pb	-0.052337	0.031702	0.415555	-0.021055
Th	0.193997	-0.41922	0.085058	0.062551
Au	-0.025575	0.157779	0.060312	0.454061

Table 11-6. Oblique principal component cluster analysis - Inter-cluster correlation

Cluster	1	2	3	4
1	1	0.00061	-0.19763	0.62975
2	0.00061	1	-0.14639	0.28909
3	-0.19763	-0.14639	1	-0.00882
4	0.62975	0.28909	-0.00882	1

saprolite zone. For line 10250N, no depletion is recognized.

In general, the solubility of Al during weathering is low, this promotes the retention of Al in stable weathering products. In many studies of weathering, Al has been presumed to be entirely or almost entirely conserved in the residual rock and solid alteration products like kaolinite and gibbsite (Hem, 1968). The bulk geochemistry analyzed by XRF (Stott, 1994) at Jim's Find displays increased Al content upwards with enrichment in the lateritic residuum and mottled saprolite, this is caused by the accumulation of Al in clay minerals near surface. In comparison, Al in the acid insoluble residue increases from the bedrock and is maintained in the saprolites and further into the mottled zones and duricrust horizons. This trend reflects that presence of unweathered sericite and possibly feldspar and suggests that Al comes from high temperature fluid which is related to the sericitic alteration. This also corresponds with the primary mineralization.

Some of the earlier research on the K geochemistry of weathering was by Correns (1961; 1969). In the muscovite case of silicate weathering study, he found that the diffusion rate of the K ions is relatively greater than in feldspar. Butt (1991) demonstrated that the K content in the regolith is controlled by the availability of micas, principally chromian muscovite and biotite, and their relative resistance to weathering. In this work, the K content of the lateritic residuum is very low (<0.5%). In contrast, the higher K content occurring below the upper saprolite zone is either lithology or alteration related. It is impossible to distinguish between mineralization and K related alteration.

In general, the processes controlling Rb distribution in regolith are similar to those of other alkali elements. During weathering, Rb is closely linked to K. Absorption may play an important role in the concentration of Rb relative to K in the late stages of weathering. Goldschmidt (1954) found that Rb was held in adsorption positions more firmly than that stated by Butler (1957), where Rb concentration was related to K only when illite formed from weathered micas and feldspars. Harris and Adams (1969) found a continuous increase in the Rb/K ratio during weathering, probably as a result of a combination of ion exchange and adsorption. From surface to fresh bedrock the Rb concentration increases and order of magnitude, while the K increase is only about eight times. It is very interesting to notice that Rb/K in the acid insoluble

residue (Figure 11-35) is very similar to that of Rb/K in bulk geochemistry with the two zones of high values in the lateritic residuum. These two zones of high Rb/K probably reflect the two underlying mineralization zones. Because the clay minerals have been removed by the acid treatment, the high Rb/K ratio of the surface material can not be related to ion exchange and adsorption but is probably due to the presence of residual sericite. This may either express an enrichment of Rb in sericite as a result of weathering, or alternatively the presence of residual sericite as the only K/Rb-bearing mineral near surface.

It is interesting to note that the ratio of Rb and Al shows high values in both the bedrock and the upper level of the regolith profile (Figure 11-36). These two zones are connected by two depletion belts. The distribution of Rb/Al in the lower saprock and unweathered rock (below RL 340 m) in Section 10150N shows a strong increase associated with the projection of Au mineralization itself. This association is not distinguished higher in the regolith, possibly due to some remobilization of Al. So Al plus the character of Rb could be used to outline the mineralization zone. The data indicate that high Rb/Al ratio at the surface could well be used as an indicator of the mineralization at depth. The distribution of the Rb/Al ratio could be explained as follows: (1) at surface enrichment of Rb through weathering is residual mica; (2) below surface some Al in the altered feldspar is not reached by acid; (3) at depth a Rb rich mica is a feeder.

Due to the aqua regia attack, the PIXE distribution of Fe is quite different compared to the bulk geochemistry. Most of ferric oxides and hydroxides were washed away. Unlike the occurrence of Fe in typical weathering profile, there is no strong enrichment of iron in the lateritic horizon. This reflects the accumulation of discrete segregations including nodules and pisoliths that are known to consist dominantly of goethite, hematite and/or maghemite. Iron enrichment of the acid insoluble residue is very similar to F, K and Rb, indicating that it must be derived from sericite. Muscovite with appreciably high Fe contents has been reported (Deer et al., 1992). Iron minerals undergo weathering and disappear in the order shown by Goldich (1938): olivine first, followed by pyroxene, amphibole and biotite. Biotite is the most resistant mineral keeping iron, but it is soluble in H_2SO_4. At Jim's Find Prospect, the presence of muscovite is related to the mineralization. Thus, Fe can be used to indicate the spatial distribution of mineralization or sericitic alteration.

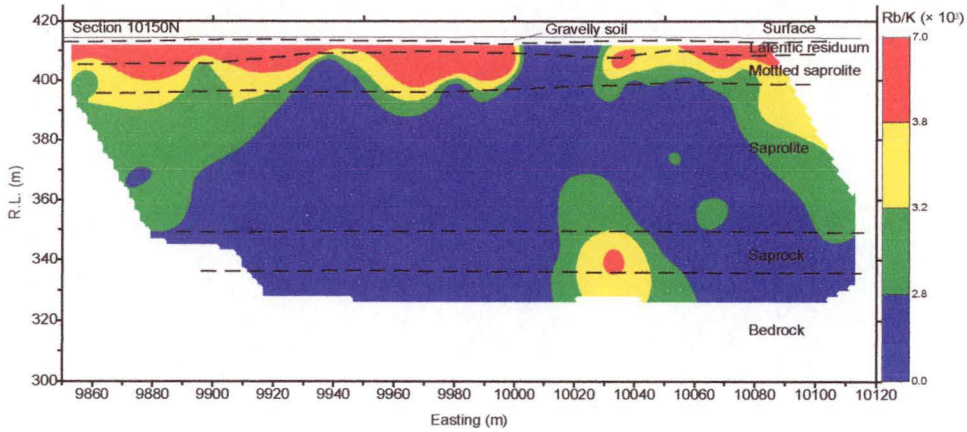

Figure 11-35. Rb/K distribution of acid insoluble residue at 10150N in Jim's find, N.T.

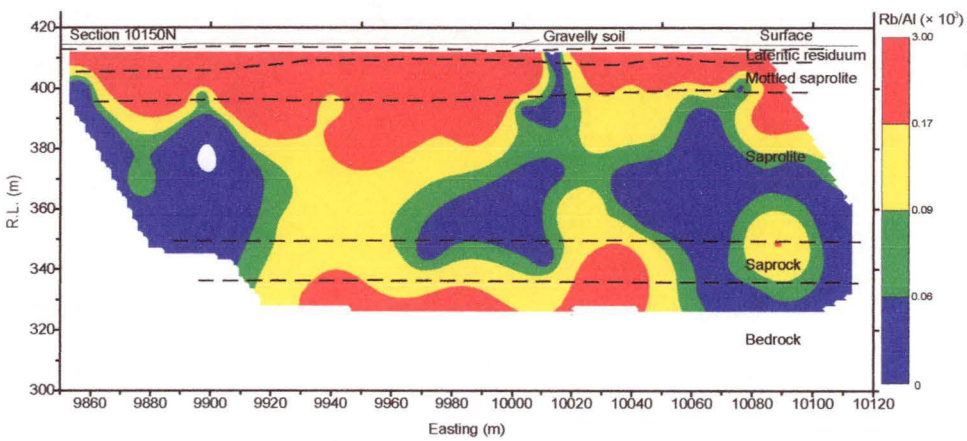

Figure 11-36. Rb/Al distribution of acid insoluble residue at 10150N in Jim's Find, N.T.

Vanadium is a major constituent and mineral-forming element. Early work (Butler, 1953) indicates that V remains in the residual rock-forming and iron-bearing minerals and/or enters minerals in the silt or clay fraction. In the clay fraction, V can be adsorbed and incorporated in clay mineral structures or in Fe oxide coating. In this work, however, V was leached from the lateritic residuum. It is noteworthy that in the saprolite horizon there is a zone with high values of V (> 330 ppm). A very large zone of V enrichment is found above the mineralization. The same distribution can be found in other two sections. V can probably be used as a pathfinder element for gold, and is likely to be associated with the occurrence of sericite.

The distribution of Mo is rather simple because of its low mobility and relatively low

constant background concentrations in regolith. Its concentration seems to correlate well with gold mineralization in Sections 10250N and 10400N. In Section 10150N, the concentration zone is much smaller than both the alteration and mineralization zone. There are some areas of minor enrichment near surface, above the mineralization zone. Manheim (1978) stated that under oxidizing surficial conditions, a slow oxidation to more soluble Mo will take place, and net leaching is to be expected. However, differential accumulation of Mo may be anticipated by uptake on iron, manganese, or aluminum oxides. Such elements, however, where destroyed by the acid treatment and the character of Mo enrichment and its relationship with mineralization in acid insoluble residue are more or less related to the alteration in which aluminum is very important factor.

Gallium, like Al, is normally enriched in the products of intense weathering. It is more mobile than Al. In bulk geochemistry, the general tendency of Ga to be concentrated in residual materials, although generally to a lesser degree than Al, is reflected in the many soil profiles where the concentration of Ga is positively correlated with the amount of clay present. The usual trend in soil profiles is an increase in Ga content with depth (Oertel and Giles, 1964). A pronounced opposite trend appears to have been found only in the gravel fraction of some gravelly laterites (Turton and Marsh, 1962). In acid insoluble residue, Ga is more enriched in the lower part of the profile with some vertical zonation. This is very similar to the distribution of K and Al. The main components in acid insoluble residue are rock-forming minerals. Among the common rock-forming minerals Ga is generally concentrated above its crustal abundance only in some feldspars and amphiboles, and less commonly in micas and magnetite. These features reflect the close coherence of Ga and Al, and possibly K, in most geochemical processes. So Ga can be used to outline the alteration related to the gold mineralization together with Al and K.

The primary mineralization at the Jim's Find is shown, by analysis of bedrock samples, to be enriched in W (Stott, 1994). The association between W concentration and the mineralized zone has been recognized from the saprock zone to the mottled saprolite horizon. The distribution of W in acid insoluble residue is very similar to that of the bulk geochemistry, but has more in similarities with the gold mineralization, especially on sections 10250N and 10400N (refer to Appendices 7 and 8). This may be explained by the immobility of W during lateritization and post lateritic

modification of the weathering profile. The continuation of a W trend throughout the regolith may result from the occurrence of W in residual scheelite (Butt, 1991). Tungsten could be the best indicator element for Au.

Manganese in the acid insoluble residue is low in both the regolith and unweathered bedrocks. Manganese is not retained in a specific zone, like the bulk geochemistry, but is strongly leached in the lateritic zone above R.L.400. There is a close similarity between the distribution of Mn and Fe implying that these metals are hosted by the same primary minerals, i.e. ferromagnesian minerals, and are released together on weathering. The Mn distribution in the whole profile is similar to that of the other transition metals, specifically Co and Zn. It has been strongly leached from the upper saprolite and clay-rich horizons of the regolith with some patchy reprecipitation lower in the profile.

Zinc and Co have very similar distribution patterns; the Zn distribution is more patchy in character. Zinc is probably hosted by ferromagnesian silicate minerals in the unweathered rocks. It primarily occurs in the structure of silicates and oxides, and is dissolved into solution during the chemical weathering of these minerals. The Co is easily solubilized during weathering and unlike Zn does not form silicate minerals. Co appears to have been strongly leached from the central part of the profile, and the higher concentrations are largely confined to the wings of the profile. It probably reflects the occurrence of Co in muscovite or ferromanganese minerals. Weathering of sulfides controlled by oxidation can support relatively high concentrations of Zn because of the high solubility of Zn sulphate. The high concentrations of Zn sulphate can be adsorbed by clay minerals, iron oxides and organic substances away from the occurrences of primary sphalerite. There is no statistical relationship between these two elements and gold mineralization, but the spatial correlation can be observed. Both of them correlate well with Fe and Mn. This is similar to the results give by Short (1961) from the residual soil and probably indicates that their distribution in the regolith profile is determined either the presence of muscovite or by the fate of iron and manganese oxide phase formation.

The distribution of F >220 ppm is similar to that of Fe, K and Rb, and occurs from east of 9960E and west of 9930E. Concentrations of F are sporadically distributed inside the profile. This is more or less related to the sericite alteration or reflects the

presence of biotite and micas, which are the F host minerals and are also related to gold mineralization. According to Gillberg (1964), biotite coexisting with muscovite contained more fluorine. In muscovite ($KAl_2(AlSi_3O_{10})(OH)_2$), F is usually present replacing OH (Berry and Mason, 1959). Coexisting amphibole and biotite generally have F contents of about the same magnitude. The behavior of F during weathering in a humid climate was investigated by Koritning (1951). It is widely known that F decreases in abundance towards the soil surface and micas are the major phases containing fluorine. The influence of weathering on the relationship between F and mica has been investigated by Rimsaite (Rimsaite, 1970) in detail. The study showed that if we compare the F content of clastic sediments, as well as from the weathering profile (where the F is nearly entirely leached), we see that the mica proportion is not the only control on the F content in clastic sediments. In this study, however, F in the clay minerals has been washed away by acid treatments. The leaching effect coming from weathering is consequently absent and the distribution of F is sericitic alteration related.

Figure 11-37 shows the binary plots between Fe and F, Co, Zn and Mn. A strong positive correlation can be observed. This indicates that these elements are hosted by the same primary minerals, most possibly by micas. Although biotite can be bleached in sulphuric acid, its solubility is lower in concentrated H_2SO_4. Considering the co-existence of biotite and muscovite and their concentration in muscovite, the occurrences of these elements must be either related to biotite or muscovite.

11.4.3 Lithology related elements

Similar to Mystery Zone and Rand Pit of Western Australia, Ti, Zr, Nb, Pb, V, Y and Th are considered to be lithology related elements, and As can also be added to the list at Jim's Find. They all exhibit very similar characters in the regolith profile at Jim's Find.

The distribution of Ti in acid insoluble residue at Jim's Find is interesting because it seem to locate different lithologies. Titanium in this case is not strongly concentrated in the lateritic duricrust like in ordinary regolith profiles. It appears to be concentrated or depleted along some presumed geological border and is likely to be related to the presence of rutile in the acid insoluble residue. The titanium oxides are very resistant to weathering. They occur undecomposed in soil and are transported into the

sediment. If Ti-bearing silicates (i.e. titanite) in the basalt are decomposed, the Ti will be dissolved but is soon transformed into Ti oxide-aquate, which is transformed to rutile or other titanium oxides in the sediments. As a result, in the weathering profiles we find an accumulation of Ti, and indeed Ti enrichment at the surface is observed above the west dipping Ti-rich lithology both in profile 10150N and 10400N.

The behaviour of Zr during weathering and transportation is well known. Generally, Zr accumulates in weathering profiles; soil/rock concentration ratios greater than ten have been reported. Since zircon accounts for most of the Zr present in most crustal rocks, and has a relatively high chemical stability, it follows that this mineral has a profound influence on the geochemistry of Zr during the weathering cycle. Many aspects of the weathering, transportation and diagenesis of zircon have been comprehensively reviewed and examined in detail by Marshall (1967). However, occasional strong concentrations of Zr may also occur in clay minerals such as kaolinite. Goldschmidt (1954) stated that Zr concentrates strongly in laterites. In this study, Zr is indeed highly concentrated in the lateritic residuum and extends into the mottled saprolite, again above the west dipping presumed geological formation in the 10150N.

Niobium is either released during the weathering cycle through the destruction of host species such as biotite, amphibole (and Ti minerals) of magmatic or metamorphic rocks or remains behind within resistate minerals such as Zr. Niobium is chemically unique as most of its compounds are almost insoluble in acid and alkaline media. In general, high enrichments of Nb are not to be expected in lateritic soils, and it is unusually to have high Nb contents of laterities and clay minerals. In the acid insoluble residue, some enrichments in Nb do occur in the lateritic residuum from 9860E to 9990E in Section 10150N (>12 ppm). A curious feature of the main accumulation in Nb is its downslope dispersion, which is very similar and at the same location to that of Ti. This probably implies the Ti oxide, i.e. rutile, and the Nb-bearing mineral phase occur together. Some sporadic high values are distributed in the saprolite, at the east of the downslope dispersion. The average value in this zone is also higher, greater than 10 ppm. This implies that the Nb is not as immobile as Zr and the mobility is not constant.

An important feature of the distribution of Y is its enrichment in the saprolite on the three sections. This enrichment does not occur in the whole profile, but westward extending into both the surface and unweathered rocks. The behavior of the Y in lateritic environment is not well understood. Nevertheless, the enrichment of Y in the acid insoluble residue is evidence that it is not immobile during weathering. The source and relative concentration of Y, and the location of the saprolite enrichment; are similar to Ti, Zr, Nb and other immobile elements. It is possible that these enrichments are due to the same processes in the evolution of the regolith. Yttrium distribution could be lithology related.

Figure 11-38 gives the binary plots of Ti vs Zr and As, Zr vs Nb and Y illustrating their similarities and concentration in the regolith. There is a limited dispersion of As in the lower regolith as the depth of weathering profile decreases in the bulk geochemistry (Stott, 1994). The distribution pattern of As in the acid insoluble residue is rather different. It has a similar distribution to that of Zr, Ti and Nb indicating that As also reflects different lithologies.

The Pb abundance is very low in the unweathered rocks and the regolith. Some isolated high values (from 5 ppm to 12 ppm) occur in the profile. Lead primarily occurs in the structure of K-feldspars and micas of magmatic and metamorphic rocks (Wedepohl, 1978). These minerals are fairly resistant against weathering but, because of the low concentration of Pb, the distribution pattern in the regolith is indistinct, particularly in the long section 10150N. There is no relationship between Pb and the mineralization.

Thorium expression near the surface horizon is very similar to Zr. It accumulated in the lateritic residuum and extends down to the mottled zone. It is also similar to that of Nb, but the distribution range is larger and extends down to the unweathered rocks. This probably means that the unweathered rocks contain host minerals for Th. The relatively immobile Th becomes concentrated in residual materials such as soil and weathered rocks. In bulk rock Th is partly in resistate minerals but in large part attached to the clay. After the acid treatment and washing out of the clays, Th is still left in the residue showing high values in the clay-rich zone.

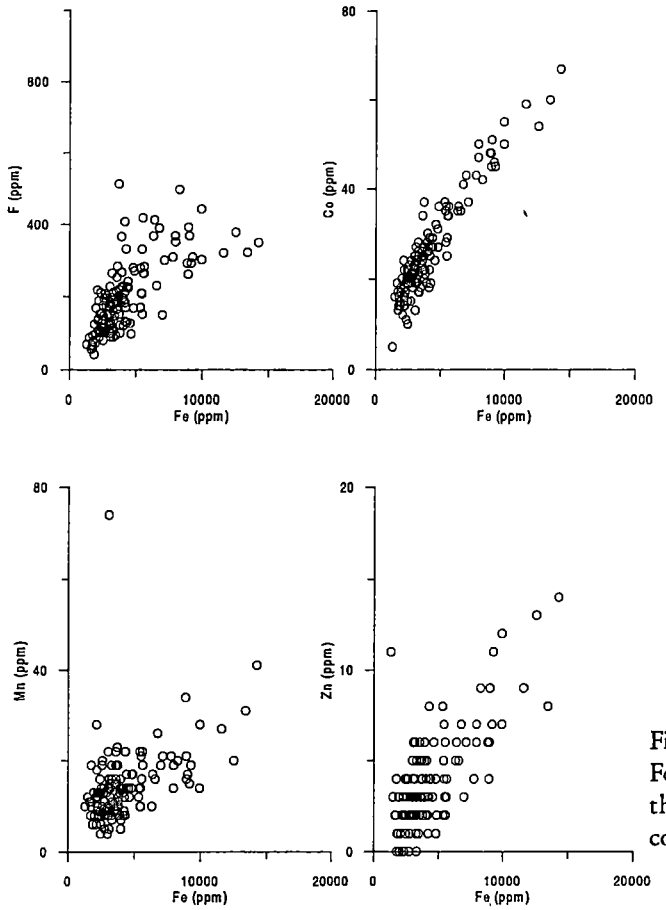

Figure 11-37 Binary plots between Fe and F, Co, Zn and Mn illustrating their close correlation and concentration in the regolith

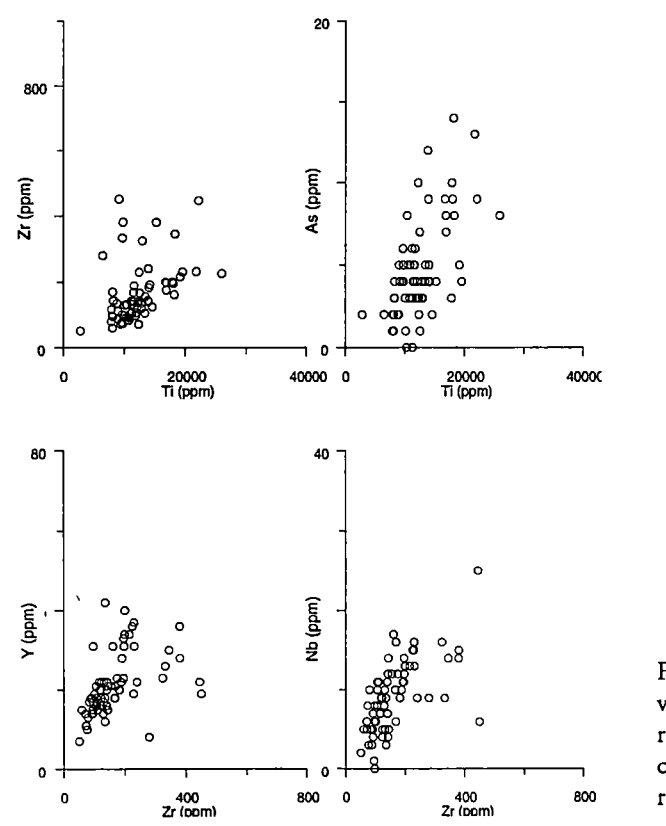

Figure 11-38. Ti vs Zr and As, Zr vs Nb and Y plots of acid insoluble residue illustrating their close correlation and concentration in the regolith

11.4.4 Weatherable mineral related elements

The two reported alkali earth elements, Ca and Sr, show similarities in their weathering behaviour. The common characteristic is marked depletions above the saprock horizon. Strontium shows some relation to the position of the alleged west dipping formation in the long profile 10150N. The carrier of the both elements is undoubtedly feldspar.

The distribution of Sr in the acid insoluble residue is quite different compared to the bulk geochemistry as discussed as Stott (1994). In the bulk geochemistry, Sr shows marked depletion above the saprock along with ordinary alkali earth elements in the regolith profile. But in this study, Sr does not show leaching from the middle part of the profile. It exhibits high values from the bedrock until the lateritic residuum. One possible explanation for the retention of Sr in the upper regolith profile is offered by its incorporation into a secondary mineral following leaching from the bedrock. The major primary host minerals of Sr are feldspars (Wedepohl, 1978). Feldspars are identified by XRD study in the acid insoluble residue. Strontium is usually less mobilized during weathering than Ca because it is held more tightly on clay minerals. This may explain why the depletion zone of Sr is not as clear as for Ca.

The stronger leaching of Ca is noted in the profile in comparison to Sr. The intensity of weathering at a constant amount of solution and constant temperature is controlled by the composition of the rocks. The most important Ca-minerals which decompose during weathering are plagioclase, amphibole, calcite, dolomite and gypsum in sedimentary rocks.

In a similar fashion to the alkaline earth elements, Na shows a marked leaching above the saprock (R.L. 350 m). The distribution of Na above the saprock shows a close affinity to that of Sr. Above R.L. 345 m to the base of the lateritic residuum, the Na content is variable from 0.01 to 0.2%, except in three samples, 130305, 130306 and 130199 at the bottom of the saprolite. Sodium is strongly leached from the lateritic residuum, where it is less than 0.05%. The decrease in Na results from the high solubility of Na during weathering. Sodium is more mobile during weathering than K (Short, 1961).

Unfortunately the minimum detection limit of Ba in this study was too high to establish any reliable distribution pattern.

11.4.5 Multi-element indices distribution

It has been established that better defined geochemical halos can be revealed around ore bodies if the contents of a group of indicator elements are combined. There are two types of composite halos: (1) additive, and (2) multiplicative.

Additive halos are constructed by the simple addition of the contents of the indicator elements normalized against their average background contents in the enclosing rocks. The halos are, in this case, delineated by using the value of the total minimum anomalous (threshold) content of the indicator elements, which are determined by comparison with samples obtained from background regions.

It is stated in earlier chapters that additive halos are larger and more distinct in comparison to mono-element halos. In addition, the effects of random errors are reduced to a minimum. Because of this, additive halos exhibit a closer relationship to the structural geological features associated with ore deposits. This in turn, contributes significantly to the reliability of their interpretation.

Similar results can be obtained if the contents of the indicator elements in each sample are multiplied (instead of being added). The multiplicative halo method is less time consuming compared to the additive method because it eliminates the necessity of their concentration in all the chosen samples.

In cases where the concentration of certain elements is not detected because of the lack of sensitivity of the analytical technique, the element concentration can arbitrarily be assigned a value equal to one half the limit of sensitivity of the analytical technique. In Chapter 5 and 8, some successful examples have been used with both types of composite halos.

These methods have been applied at Jim's Find according to the elemental distribution character of the acid insoluble residue. Although there is an indication that base metals Fe, Mn and Cr of the acid insoluble residue are enriched in the saprolite, and more or less in accordance with the Au occurrences, the enrichment zone is not continuous, especially for Mn and Cr because of their low content. With their additive indices Mn+Cr, their indication usage is very much enhanced because analytical error and other adverse factors are minimized or erased. Figure 11-39 gives the Mn+Cr

distribution, which shows a very much improved spatial correlation with gold distribution. Figure 11-40 shows the distribution of W+Mo+Ga. The mineralization zone could be outlined including the surface expression with the addition values over 30. Figure 11-41 is the multiplicative Al x K x Rb distribution of the acid insoluble residue. Similar to other complex indices distributions, it produces a better map of the sericitic alteration than any of the mono-elements respectively. At Jim's Find, the additive halos give better surface expression, but the multiplicative halo is superior at defining the alteration zone in the cross section of the regolith profile. These two halos could be used together as a tool to distinguish Au anomalies according to both their surface and depth expression.

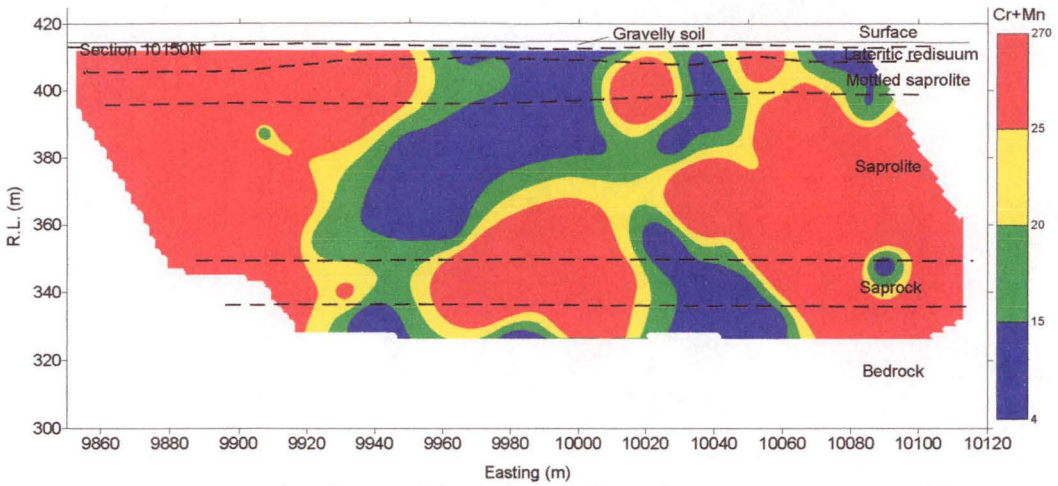

Figure 11-39. Cr+Mn distribution of the acid insoluble residue at 10150N, Jim's Find, Tanami, N.T.

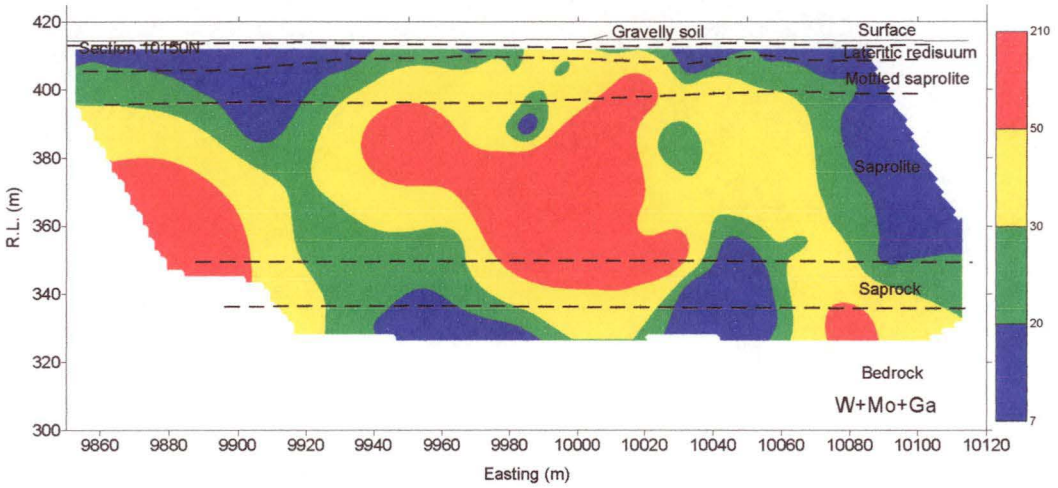

Figure 11-40. W+Mo+Ga distribution of the acid insoluble residue at 10150N, Jim's Find, Tanami, N.T.

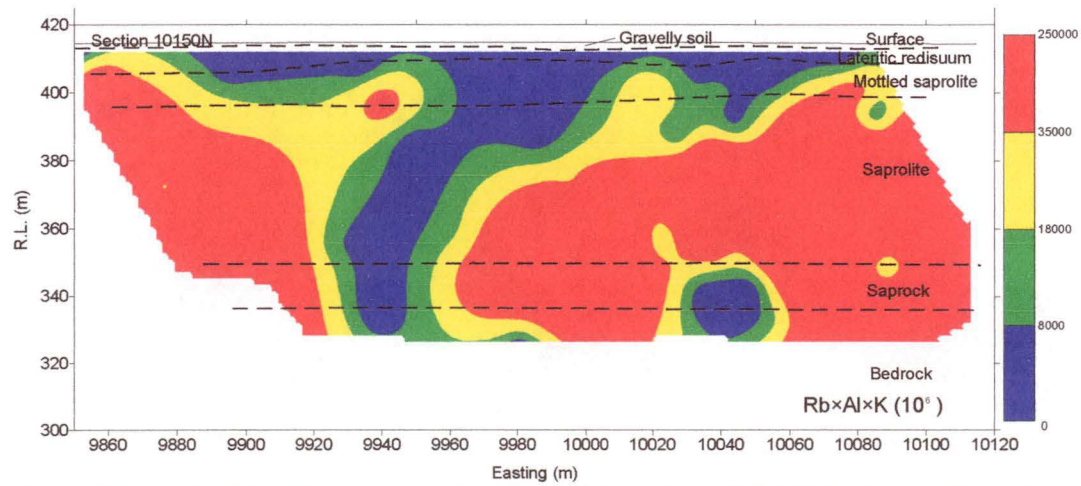

Figure 11-41. Al x Rb x K distribution of acid insoluble residue at 10150N, Jim's Find, Tanami, N.T.

Chapter 12

EPR CHARACTERIZATION AT JIM'S FIND

The EPR principles, instrumentation and the sample preparation have been introduced in Chapter3. This chapter gives the EPR signal observed at Jim's Find, presents their distribution and their relationship with Au and other elements.

12.1 EPR CHARACTER OF REGOLITH SAMPLE

Sixty-seven regolith and bedrock samples from the long section at 10150N at Jim's Find Prospect were analyzed by EPR in this study. These samples are the same as those used in Chapter 11 for the study of regolith geochemistry by PIXE/PIGE.

Two type of EPR X-band first derivative signals were found to be of practical use in Jim's Find:

- The large V-shaped signal at g ≈2 with a width of about 2 mT, often superimposed on a signal about 50 mT wide (Figure 12-1), which is best observed in the ± 5 mT sweep.
- The strong single signal, often not more than an off-set, is best observed in the ± 100 mT sweep (Figure 12-2).

The major center is likely to be the $[AlO_4]^\circ$ centre (Petrov et al., 1989; Russell and van Moort, 1997). The nature of the center, observable in the larger sweep is unknown. In some samples, the $[GeO^4/M^+]$, Fe^{3+}, E′ or oxygen hole centers can be observed (van Moort and Barth, 1992). These additional centers do not correlate in any way with the gold content.

The major signal in the ±5 mT sweeps of the samples from near the surface is rather flat. The spectra show a signal of greater peak to peak height for samples from greater depth (Figure 12-1). This central EPR line can be observed in all samples and the intensity changes not only with depth but also with increased mineralization. This change probably reflects teh variation of parameters controlling the quartz cristallography like teh temperature of crystalisation. The signal width of 2 mT does not changé and the individual peak-to-peak widths, B, of the central signal to E' does not change from a value of about 0.2 mT. In addition a small peak is observed

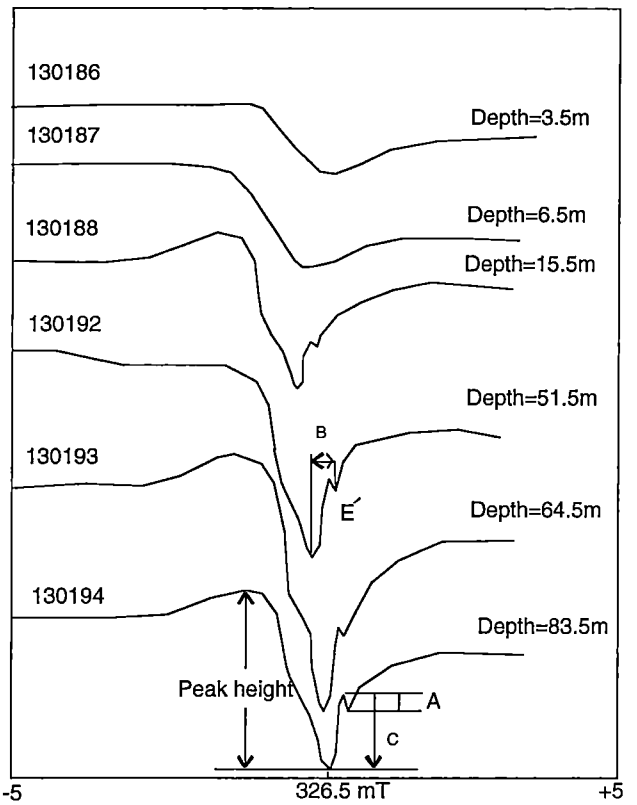

Figure 12-1. First derivative EPR X-band 326.5±5 mT spectrum at room temperature of powdered samples from drill hold JRC 031, Section 10150N (from Xu and Van Moort, 1997)

whose relative intensity changes with the depth and mineralization C/A from 1:1 to 8:1. For the deeper mineralized samples, the ratio of two peaks C/A is larger, and for the barren and near surface samples, the ratios are smaller. This additional peak is likely to be the E' defect structure in the SiO_2 lattice, which is the result of an electron trapped in the vacancy when a bridging oxygen is removed from the lattice (Yip and Fowler, 1975).

The difference in the intensity of the EPR signals and their detail as a function of depth may be caused by admixtures of wind blown sand near the surface or loss of primary quartz through recrystallization. Figures 12-3 and 12-4 show typical silica grains observed by the Scanning Electron Microscopy at the Central of Science Laboratory, University of Tasmania. The deeper sample 130195 represents primary quartz. The sample 130175 represents near surface material representing less defined quartz aggregates. Their scanning energy dispersive spectra also show clear differences. The main peaks of the surface sample 130175 are composed of O, Si, Al and K

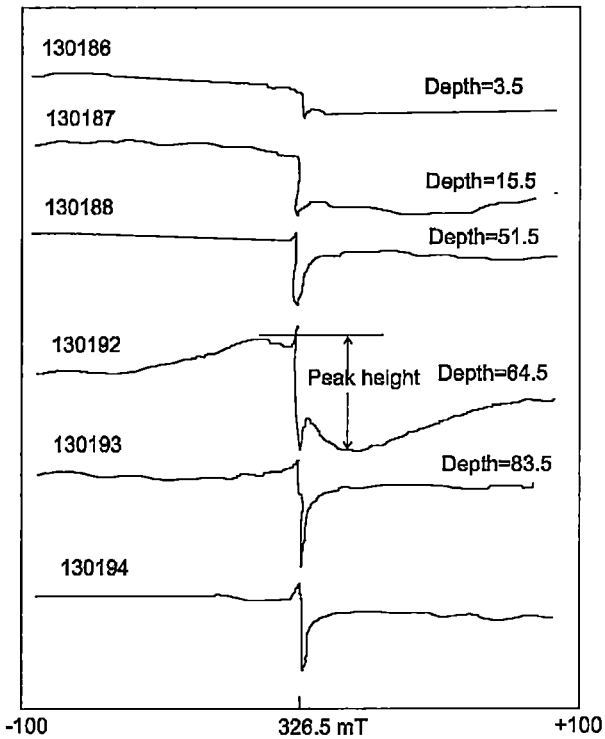

Figure 12-2. First derivative EPR X-band 326.5±100 mT spectrum at room temperature of powdered samples from drill hold JRC 031, Section 10150N (from Xu and Van Moort, 1997)

(Figure 12-5). The main peaks of the deeper sample 130195 are composed only of O and Si with minor Al, indicating its main component is quartz (Figure 12-6).

Van Moort and Russell (1987) found in their original EPR paper that there is a "shoulder" at $g \approx 2.005$ on the first derivative EPR curve of the quartz reef samples, and used the ratio of the sine of the angle to the peak height to discriminate between mineralized and barren samples and proposed that it may be used as a indicator of mineralization. This angle is, of course, very much dependent on instrument settings. The regolith sample from the Jim's Find also showed the shoulder appearing in some of the spectra of EPR ± 5 mT. This study investigates the deviation from a straight derivative line shape and the correlation of this deviation with mineralization.

Consider the trace 1, 2, 3, 4 and 5 of a typical EPR spectra of a regolith powder sample (Figure 12-7); the angular deviation of 2, 3 from the horizontal was previously identified by van Moort and Russell (1987), as α. Physically the shoulder is almost a right angle in this mineralized regolith. However, the recent study has found that

Figure 12-3. The deeper acid insoluble residue sample observed by Scaning Microscopy represent primary quartz (sample number 130195)

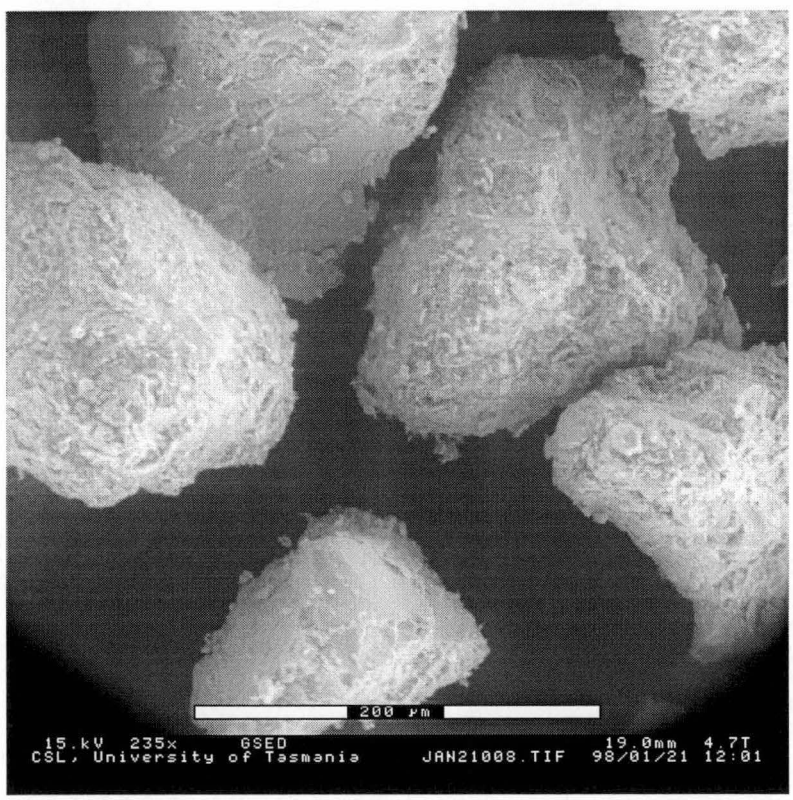

Figure 12-3. The surface acid insoluble residue sample observed by Scaning Microscopy represent primary quartz (sample number 130175)

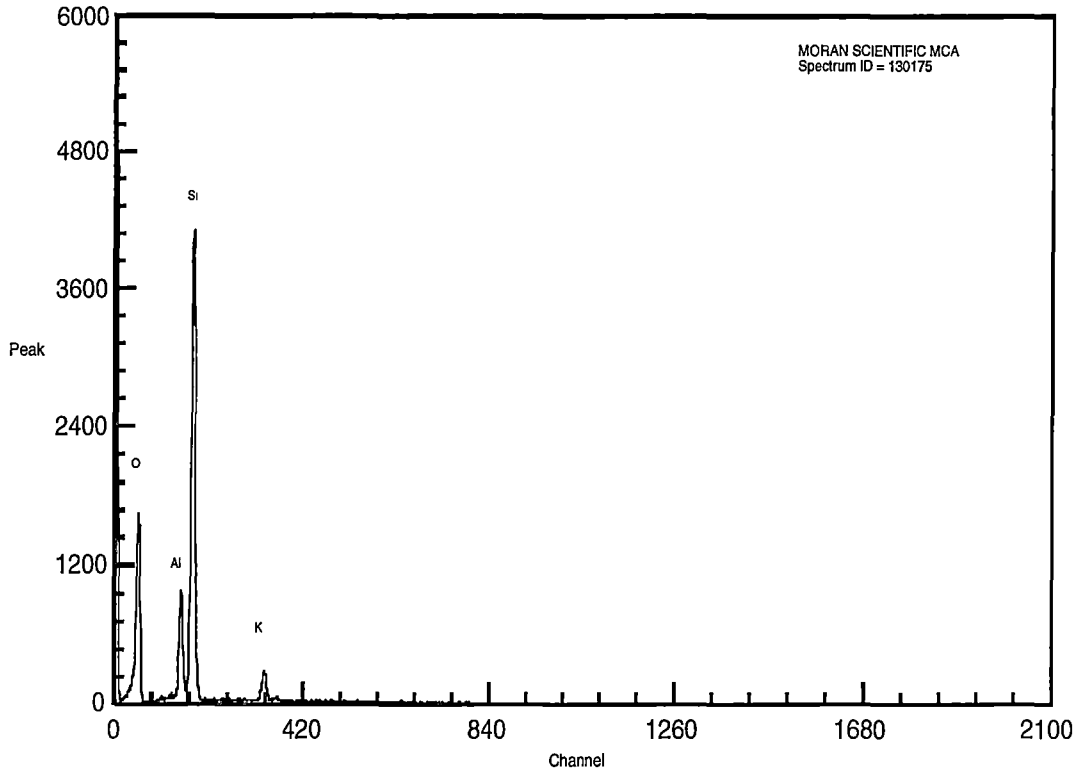

Figure 12-5. The main peaks of the surface sample 130175 (acid insoluble residue) consists of O, Si, Al and K, indicating its main component quartz

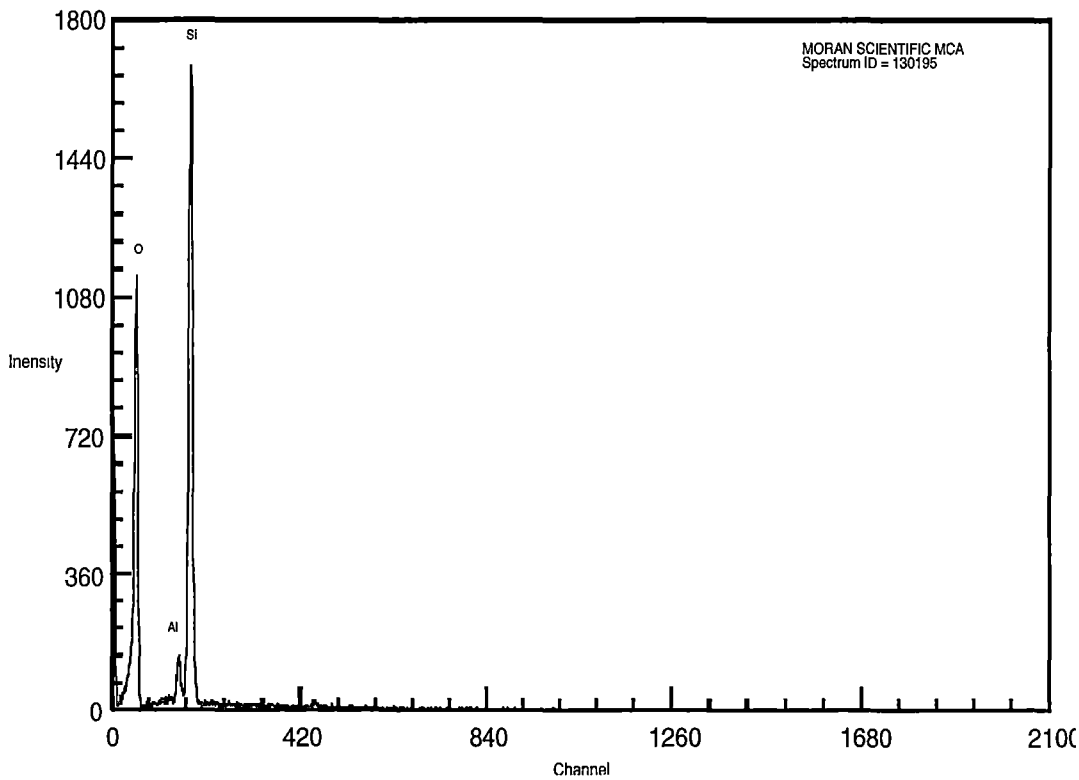

Figure 12-6. The main peaks of the surface sample 130195 (acid insoluble residue) consists of onlyO and Si, indicating its main component quartz

the angle α′ between the horizontal line through the point 4, which is the resonance centre g = 2.003 (g_{xx} of $[AlO_4]^\circ$ of the 4, 5 section of the trace, carries a more significant indication of mineralization. After the shoulder and at the resonance center g = 2.003, the curve has changed direction downward again. The angle α' (see Figure 12-7) is smaller when the gold content is relatively low and will be higher when the

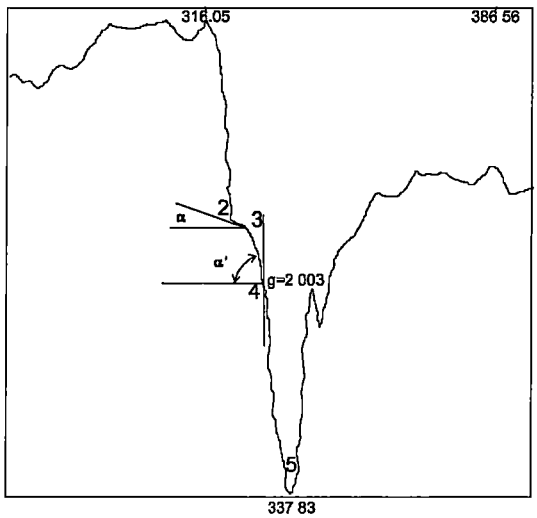

Figure 12-7. The diagram of EPR spectra related an angular deviation

gold content is higher.

According to the above, the mineralization has a certain relationship with the $[AlO_4]^\circ$ centre. This finding corroborates the work by Pwa (1996) that the EPR spectra of mineralized samples of VHMS deposits are characterized by similar large signals.

Table 12-1 shows the data from drill hole JRC 030 and other deeper samples with a

Table 12-1. Spearman rank correlation coefficient of Au (bulk geochemistry), EPR (acid insoluble residue) and degree of shoulders (n = 42)

	Au	±5 mT	±5 mT x 100 mT	α	±5 mTxα	±5 mT x 100mTxα
Au	1	0.423	0.533	0.575	0.613	0.613
±5 mT	0.423	1	0.485	0.303	0.921	0.453
±5 mT x 100 mT	0.533	0.485	1	0.486	0.561	0.969
a	0.575	0.303	0.486	1	0.595	0.623
±5 Mt x a	0.613	0.921	0.561	0.595	1	0.608
±5 mT x 100mT x a	0.613	0.453	0.969	0.623	0.608	1

"shoulder" in its spectra. There are only 42 samples with this character. For correlation calculation, the relative EPR intensity of the quartz samples and the Au content in parts per billion of the rock pulps have been used, with samples with more than 1000 ppb all being treated the same. Both indices, EPR ± 5mT x α' and EPR ± 5 mT x 100 mT x α', give a good correlation with the gold content. So, if the EPR spectra have an additional shoulder, α' degrees multiplied by EPR ± 5 mT and EPR ± 100 mT can be used as a promising indication of the mineralization.

12.2 EPR DISTRIBUTION

The frequency distribution of EPR intensities measured at magnetic flux density sweeps over 326.5 ± 5 mT and ± 100 mT under standard condition mentioned in Chapter 3 in the regolith is shown in Figure 12-8.

12.2.1 Distribution of EPR intensities at 326.5±5 mT

EPR intensity of the regolith measured at magnetic flux density sweeps over 326.5±5 mT has a range of 0–35 cm (Figure 12-8). The distribution contour map of EPR 326.5 ± 5 mT is shown as Figure 12-9. In contrast to the samples from near the surface and the barren zone, the washed acid insoluble samples from the hypogene mineralized zone show approximately three times stronger EPR ±5 mT signals. A

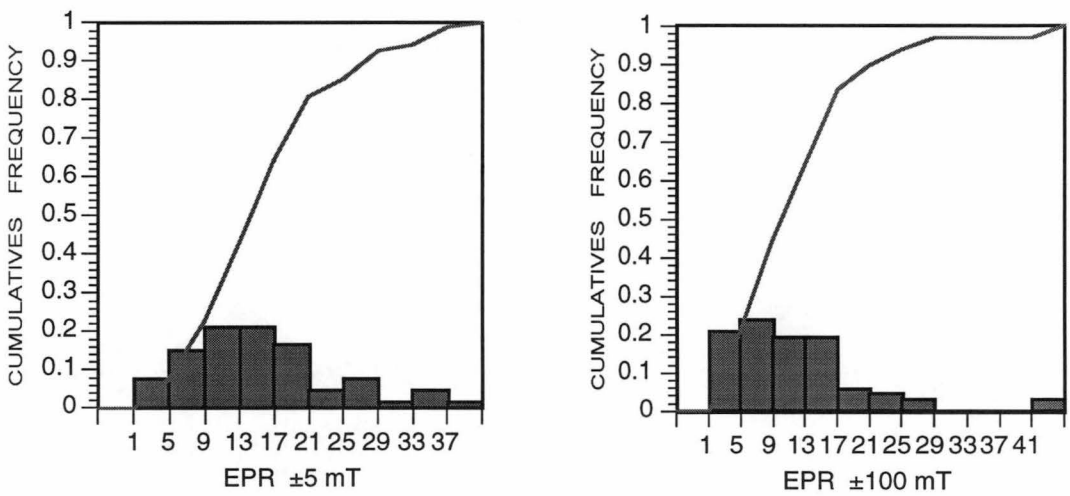

Figure 12-8. Cumulative frequency distribution on EPR intensities measured at 326.5±5 mT and ±100 mT

zone of EPR intensity greater than 13 cm (for the standard instrument setting specified above) trending from the west to the east, except the blank occurred along the 9910N to 9960N. The EPR intensity measured in 326.5±5 mT sweeps decreased toward the surface into the gravel soil in which there is no primary quartz.

12.2.2 EPR distribution at 326.5±100 mT

EPR intensity measured at magnetic flux density sweeps over 326.5 ± 100 mT in regolith powders varies from 0 to 27 cm (Figure 12-8). Figure 12-10 shows the profile distribution of EPR intensities measured at magnetic flux density sweeps over 326.5 ± 100 mT in the regolith. A well defined zone of more than 10 cm EPR intensities trending from the west to the east continuously outlines a belt which envelope the mineralized area. In the ester side of the profile, the background of EPR ± 100 mT is higher than the western side of 10030E.

12.3 EPR MULTIPLICATION

In this study, an EPR multiplication simply defined as the intensity of EPR 326.5 ± 5 mT x 326.5 ± 100 mT is used to enhance the places in the profile where both signal intensities are high.

This EPR multiplicative index in the regolith varies from 0 to 684. The distribution contour map of the index is shown as Figure 12-11. The high product values define the two gold mineralization zones very well.

An important practical aspect of the EPR multiplicative index is its continuity in the saprolite and saprock where the Au mineralization is present. The zone of high EPR index breaks through to the surface in the eastern part of the profile.

12.4 EPR AND GOLD MINERALIZATION

The heights of the major peak in the ±5 mT and ±100 mT sweeps of the samples correlate significantly with the Au content.

The distribution of EPR ±5mT intensity in section 10150N shows there are two halos separately overlain on the gold anomaly, which extend upward to the surface (Figure 12-9). The gold mineralization zone was wrapped by a big EPR ± 100 mT

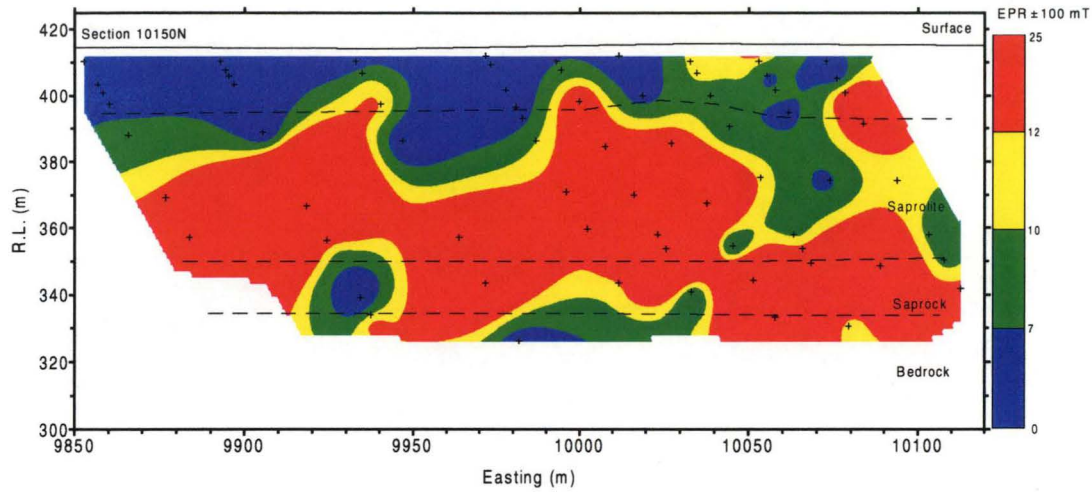

Figure 12-10. The distribution map of EPR ±5 mT of the acid insoluble residue in section 10150N at Jim's Find, N.T.

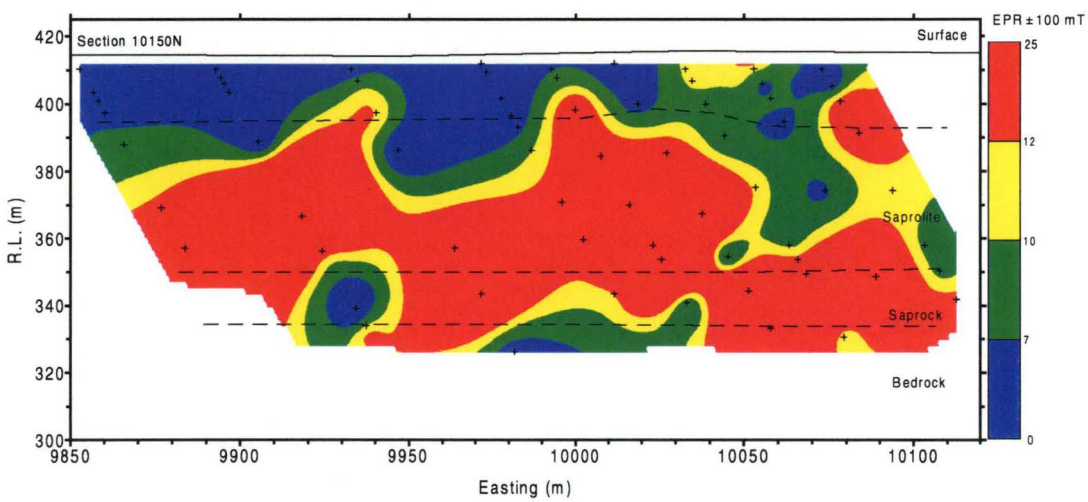

Figure 12-11. The distribution map of EPR ±100 mT of the acid insoluble residue in section 10150N at Jim's Find, N.T.

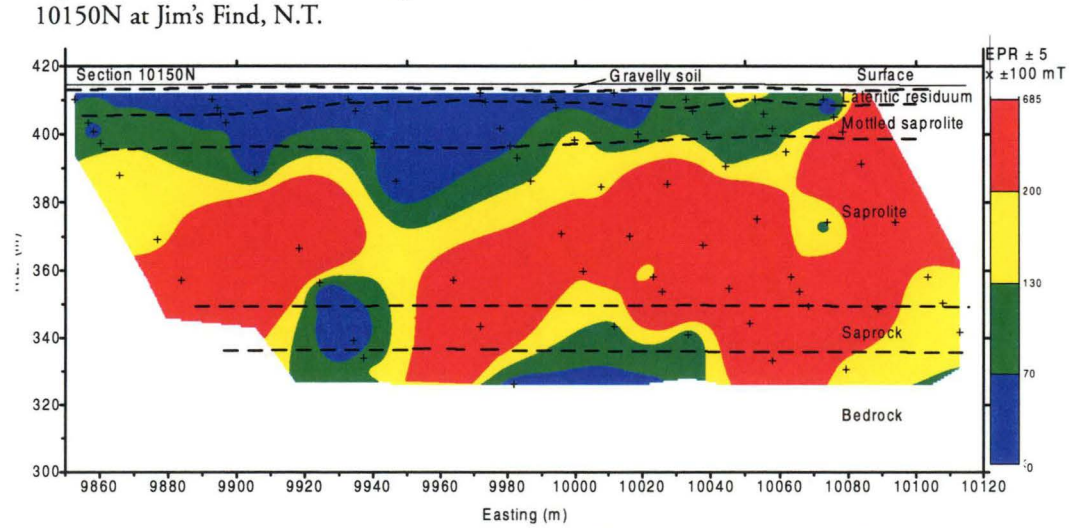

Figure 12-12. The distribution map of multiplication EPR ±5 mT and ±100 mT of the acid insoluble residue in section 10150N at Jim's Find, N.T.

halo (Figure 12-10). The products of EPR ±5 mT x ±100 mT signal intensities are found to agree more accurately with the primary gold mineralization. All of the EPR ±5 mT, EPR±100 mT and ±5mT x ±100 mT open to the east along the gold anomaly. This evidence suggests that such a horizontal anomaly may have existed toward the east as an extension of the gold mineralization, and provides a potential target for further attention. The EPR and the gold anomaly both end at the same bottom, except from holes 10040E to 10080E where the distribution of EPR and gold goes down to the bedrock, and upper part of the EPR anomaly is vertically larger than the gold anomaly.

12.5 THE RELATIONSHIP BETWEEN EPR AND TRACE ELEMENTS

The relationship between EPR and trace element concentration in the acid insoluble powder of the regolith from Jim's South Prospect has been investigated.

Table 12-2 shows the Spearman rank correlation coefficients between EPR intensities and concentration of some elements. The relation between EPR intensity measured at magnetic flux density sweeps 326.5 ± 5 mT and the elements Al, Ca and V exhibit weak to moderate positive correlation in the regolith profile. EPR intensity measured at magnetic flux density sweeps 326.5 ± 5 mT show a strong positive correlation with F, K, Mn, Fe, Co, Ga and Rb, especially K and Rb with the coefficient over 0.6. Those elements are related to sericite alteration and associated mineralization. EPR intensity measured at magnetic flux density sweeps 326.5 ± 5 mT display moderate negative correlation coefficients with Na, Ni, Cu, Sr and Zr which are depleted in

Table 12-2. Spearman rank correlation coefficients between EPR intensities and some elements of the acid insoluble residues (n=76)

	F	Na	Al	K	Ca	Ti	V	Mn	Fe
±5mT	0.45	-0.16	0.1	0.66	0.13	-0.22	0.17	0.3	0.51
±100 mT	0.28	-0.17	0.02	0.2	-0.02	-0.03	0.15	0.27	0.36
	Co	Ni	Cu	Zn	Ga	As	Rb	Sr	Zr
±5mT	0.45	-0.27	-0.25	0.31	0.42	-0.23	0.68	-0.13	-0.3
±100 mT	0.41	-0.01	0.16	0.16	0.22	-0.05	0.24	-0.15	-0.03

the regolith and also Ti, As and Zr.

The relationship between EPR intensity measured at magnetic flux sweeps 326.5 ± 100 mT has similar results to those of EPR ± 5 mT, but with less strong positive and negative correlations.

Figuré 12-12 gives the binary plots of EPR and the elements K, Fe, Co, Ga, Rb and Mn. A remarkable feature is that the contour map of EPR ±5 mT intensities is very similar to those of Rb and K, indicating the character of EPR signal is, more or less, alteration related.

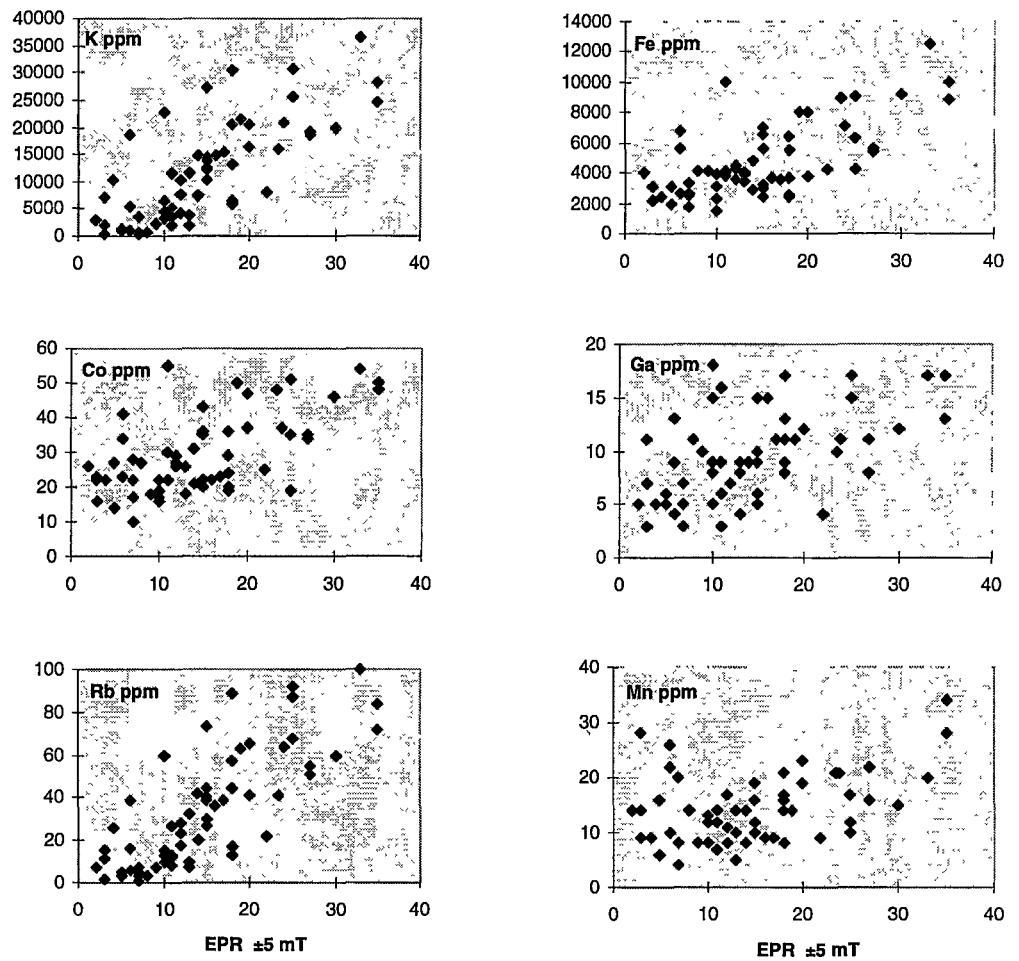

Figure 12-12. The binary plots of EPR and elements K, Fe, co, Ga, Rb and Mn

Chapter 13

DISCUSSION AND CONCLUSIONS

13.1 INTRODUCTION

Each of the three areas on which this thesis is focussed have undergone multiple cycles of subtropical to tropical weathering through the Mesozoic era to the Tertiary period (Mazzucchelli, 1997; Stott, 1994). The imprint of this weathering has survived the Recent arid climate. The common characteristic between the three study areas is the deep weathering that results in the complete alteration of the primary mineralogical, chemical and petrographic characteristics of bedrock and mineralization, and which is hosted within the bedrock. Nonetheless, the dispersion of ore-related elements in the bulk regolith can create larger, though commonly subtle, exploration targets, which is advantageous in Au exploration.

This chapter summarizes the geochemistry and EPR characteristics of acid the insoluble residue of the regolith. Discussion is given on the empirical effectiveness of this regolith geochemistry; and whether the methods, to a large extent generically, can be applied to the search for Au mineralization in weathered lateritic regolith terrains. In particular the acid insoluble residue geochemistry and EPR may provide advances towards identifying large concealed Au deposits.

The Mystery Zone at Kalgoorlie, Rand Pit near Meekatharra and Jim's Find in the Tanami Desert will be discussed separately, prior to a general conclusion.

13.2 ELEMENT AND EPR DISTRIBUTION AT MYSTERY ZONE

13.2.1 Acid insoluble geochemistry

At Mystery Zone, Au mineralization occurs throughout the porphyries, and also locally developed adjacent to these mineralized porphyries. The elements W, Al, K, Ca, Cr, V, Ga, and Rb in the acid insoluble residue have a similar spatial distribution to the primary Au mineralization. The Au distribution in the fuchsite altered ultramafic and porphyry is relatively patchy compared with the distribution of W, Al, K, Ca, Cr, V, Ga and Rb elements. Additionally, the chemical expressions of these elemental halos is somewhat larger than the Au mineralization. The gold and

associated elements are absent from the non-mineralized biotite-talc ultramafic unit. The Al distribution of non-acid treated samples is high throughout the whole regolith profile, particularly within the ultramafic rocks, whilst the acid insoluble Al content has much lower values in talc and biotite ultramafics that do not contain Au mineralization (Figure 5-6). The enrichment of Al, K and Cr is mostly related to fuchsite alteration. The Rb distribution in the acid insoluble residue is characterized by moderate to high values throughout the porphyry and fuchsitic rocks, with only minor changes from the base to the surface of the profile (Figure 5-14). In contrast high Rb values in the non-acid treated bulk analysis occur in saprolite and mottled clays between the 385 and 400 m level due to enrichment in the weathering products (Butt, 1991).

Zinc (Figure 5-17) is enriched in the fuchsite ultramafic rocks and spatially relates to wall rock alteration. Vanadium in the acid insoluble residue (Figure 5-21) has a very similar distribution to Au. Despite this similarity, the V concentration increases slightly towards the surface and lacks a subsurface depletion zone. The bulk geochemistry V contents of the major lithological units are similar (Butt, 1991), however, the distribution of V in the acid insoluble residue differs from that of bulk geochemistry. Vanadium in bulk rock geochemistry is concentrated relative to Ti and Zr, without any evidence to support the relation of this element to Au mineralization. The distribution of V at the Mystery Zone F is distinct (Figure 5-22) in zones of alteration, becoming wider above the primary Au mineralization. The behavior of V is likely caused by mineral redistribution related to the surface Au enrichment. Within the acid insoluble residue samples, V most likely resides in muscovite.

The distribution of Cr is similar to Al and Rb and is related to fuchsite alteration. Chromium (Figure 5-20) is concentrated in fuchsite altered ultramafic rocks, which confirms that chromian muscovite is the principal host for Cr in the weathered rocks. The unweathered porphyry, biotite and talc-chlorite ultramafic rocks have a significantly lower Cr content. Tungsten (Figure 5-28) and Ga (Figure 5-29) are consistently enriched throughout the primary mineralization, except for scattered high values in fuchsitic rock.

Additive halos such as Ga+Ge or As+W+Mo (Figures 5-47 and 5-48) and also the

multiplicative halo Al x K x Rb (Figure 5-46), yield larger and distinct enrichment zones when compared to their respective mono-element halos. The additive halos (Ga+Ge and As+W+Mo) have a close association to Au in both the primary and secondary surface enrichment zones. The addition (Figure 5-48 and 5-49) of two additive halos Ga+Ge and As+W+Mo further improves this enrichment correlation with in the primary and secondary Au mineralization. In contrast, although the multiplicative halo Al x K x Rb is better than its respective mono-elements in defining alteration related to primary mineralization, having a similar distribution to Rb/K ratios. This implies that the alteration is muscovite dominated. The vertical halo, expressed by the accumulation of Al, K and Rb, occurs within and above the primary mineralization.

Chemically, Zr, Nb, Th and Y (Figures 5-23 to 5-25) behave similarly and are lithology dependant in the deeper profile, with a largely immobile character in shallow part of the profile. These elements have the highest values near the surface due to concentration of resistate zircon.

Titanium (Figure 5-21) is concentrated in the talc-chlorite-carbonate altered ultramafic rocks during weathering processes. In the bulk, Ti is concentrated relative to Zr such that lithological discrimination based on Ti-Zr plots is not possible (Butt, 1991). In this study, although Ti is correlated to Zr, the Ti/Zr ratio remains relatively constant within different geological units, even in intensely chemical weathered zones, excepting talc-carbonate altered ultramafic rocks. Despite Butt's (1991) conclusion, Ti-Zr plots of the geochemistry of acid insoluble residue broadly reflect the different geological lithologies (Figure 5-43). Talc-chlorite-carbonate ultramafic, talc-carbonate ultramafic rocks, fuchsite-carbonate ultramafic rocks and porphyry can be identified on the basis of their Ti-V contents (Figure 5-44). This interpretation is supported by Figures 5-44 and 5-45. The plots of different element pairs, namely Zr vs V and V vs Ti, yield consistent information on lithological classifications (Figures 5-44and 5-45). Vanadium therefore has dual characteristics, relating as it relates to both Au mineralization (muscovite alteration) as well as to the occurrence of titanium minerals.

Copper, Pb (Figures 5-15and 5-16) and Mo (Figure 5-30) are present in the acid insoluble residue of laterite at the top of the profile in relatively small concentrations. Copper is not particularly useful in exploration at Mt Percy because of erratic high

levels related to porphyry and ultramafic lithologies. As Pb and Mo are close to the detection limit, their distributions do not correlate well with Au mineralization. Zn and Ni (Figures 5-17 and 5-18) are enriched in unweathered ultramafic rocks, but depleted in clay saprolite above the biotite-talc ultramafic unit and also have low values in porphyry. There is no evidence of Cu, Pb and Mo association within the primary Au mineralization at Mystery Zone.

13.2.2 EPR distribution character

The results of this work indicate that mineralized regolith samples generally have a pronounced EPR signal with a broad positive correlation between Au content and EPR ± 5 mT intensity. This corroborates the usefulness of EPR as an exploration tool for Au mineralization (Xu and van Moort, 1997b; Russell and van Moort, 1997). Most importantly, the EPR signal is present in the surface regolith and correlates to underlying primary Au mineralization. EPR intensities near the surface are slightly weaker than at depth, but still reflect the presence of the primary Au mineralization. EPR does not show secondary near surface Au enrichment away from mineralization.

The flat EPR ±5 mT signals in the talc and talc-chlorite altered ultramafic rocks confirm that those geological units are not related to Au mineralization. In contrast, EPR ±100 and ±250 mT have significant signals in talc-chlorite geological units. Therefore, EPR may also be used to distinguish between primary lithologies.

13.2.3 Discussion

The sample medium of acid insoluble residue consists of quartz with some muscovite, talc and minor amounts of resistate minerals. Secondary minerals such as Fe, Mn and Al oxides and hydroxides, clay minerals, sulphates and carbonates were efficiently removed by the acid treatment. The sample residue is relatively constant in composition. Nonetheless, near surface material contains a considerable amount of secondary chalcedony.

The results of multi-element dispersion patterns of the acid insoluble residue and the EPR characterization in this study have several implications for Au exploration. The distributions of elements and EPR intensity exhibit different characteristics in different regolith layers and lithologies, and were useful in constraining the expression of primary wall rock alteration and Au mineralization in weathered rocks, even within

extreme weathering near surface. In addition they provide ancillary data relevant to exploration for other commodities.

13.2.3.1 Implication for near surface exploration

Gold in the Mystery Zone forms a broad supergene anomaly in the soils and lateritic horizons. This anomaly formed during lateritic weathering associated with Fe oxides and/or during more recent arid weathering associated with pedogenic carbonates. The primary alteration zone is typically pyritic and, in addition to Au, is characterized by high abundances of S, Sb, Ag, Te and W. There is however, no close correlation between Au and these elements statistically in the bulk chemical composition within the primary alteration zone itself (Butt, 1991). Within this zone, some high As values are retained, particularly in Fe-rich materials based on the projection of primary mineralization at this level. Tungsten is consistently enriched throughout the primary mineralization (Butt, 1998).

From this study, it is apparent that Al, K, Rb, V, W and Ga in the acid insoluble residue yields a surface expression of Au-related alteration, providing wider targets areas than the deeper mineralization itself. The significant multiplication values of K, Al and Rb precisely outline the anomalous surface expression related to the underlying primary mineralization, but itself has no expression in the secondary Au enrichment at surface. The ratio of Rb/Al is also pronounced in the lateritic duricrust, but is absent from soils. The ratio of Rb/K is only high in the lateritic gravels and soil above the porphyries and fuchsite altered ultramafic rocks, and is closely related to the distribution of fuchsitic alteration. The multi-element composite halos As+W+Mo, As+W+Mo+Ga+Ge or AL x K x Rb in the acid insoluble residue are larger and more pronounced than Au and any other mono-element halos in the near surface expression.

EPR distribution in the lateritic duricrust and soil is similar to that of K and Rb, however, the EPR is somewhat lower near the surface due to the dilution of the primary quartz by secondary chalcedony.

Below the laterite zone, leaching has removed much of the Au over a thickness of 5–15 m and formed a "depleted zone". It is important to note that Cu, and, to a lesser extent, Zn, Ni, Cr, W and Ga are, however, anomalous through this depleted zone.

Similarly, the high concentrations of K, Al and Rb are maintained through the clay-rich horizons. This data has particular significance when applied to areas in which the lateritic regolith has been partially truncated. The elements W, V, Ga, Cr, K, Al and Rb are expected to be anomalous even if Au contents are depleted to very low values. The acid insoluble W, as an indicator for Au in the mottled and plasmic clay zones, is more significant than the W in the bulk geochemistry. The ratios of Rb/Al and Rb/K are similar to those of lateritic gravel and soil, but the Rb/Al ratio is less extensive. The additive composite halos Ga+Ge and As+W+Mo are enlarged in this zone, however, they are not consistent due to some extremely low values of As and Ge. However, the additive halo As+W+Mo+Ga+Ge improve this distribution pattern significantly and is highly concentrated in the mottled and plasmic clay zones.

EPR distributions in the mottled and plasmic clay zones are more pronounced than those in lateritic gravel and soil of the upper horizon, . This distribution follows the distribution of K, Rb and Ga, indicating their relation to ore-related alteration.

13.2.3.2 Implication for deeper profile exploration

High Au contents occur throughout the saprolite, but its distribution is patchy. The distribution of the other ore associated elements in the acid insoluble residue generally have greater consistency and wider anomalous zones. The wall rock alteration exceeds that of Au mineralization in size. Dispersions of Ga and Al are greatest in the middle to lower saprolite, but they do not permit an assessment of the extent of lateral dispersion within the saprolite. However, W, K, and Rb are dispersed in the mineralized porphyries and fuchsitic altered ultramafic rocks in the whole clay saprolite and saprolite profile, whereas Cr, Ni, Zr are highly concentrated in the mineralized fuchsitic ultramafic rocks. In the clay saprolite and saprolite zones, both high Rb/Al and Rb/K ratios form continuous zones within the porphyries and fuchsitic ultramafic rocks. The multi-elements indices Ga+Ge, As+W+Mo and As+W+Mo+Ga+Ge have consistently high values within the mineralized zone of the clay saprolite and saprolite horizons.

EPR distribution in the clay saprolite and saprolite horizon is similar to many ore- and alteration-related elements. Three EPR specifications, 326.5 ± 5 mT, 326.5 ± 100 mT and 326.5 ± 250 mT, can be used to outline the mineralized zone in both the clay saprolite and saprolite zones.

13.3 ELEMENT AND EPR DISTRIBUTION AT RAND PIT

The mineralization at Reedy is classified as a shear zone and quartz vein type within mafic/ultramafic rocks and is intruded by porphyries (Watkins et al., 1987). Although the mineralization type is different to the Mystery Zone at Mt. Percy, the acid insoluble residue geochemical and EPR data presented in this study are consistent with the general features established at the Mystery Zone.

13.3.1 Acid insoluble geochemistry

At the Reedy Mine, Au is concentrated in and around two sub-economic ore shoots on the south face of the Rand Pit, approximately conformable to two micaceous schist zones, hosted within the black shale and mafic schists M1 and M3. Gold is also surface enriched. The acid insoluble elements Al, K, Rb, Pb, W, Ga and Mo have a similar distribution to Au, particularly in the deeper part of the profile. To a lesser extent, Ti and V may also be included in this element array. The elements Ni, Ti, V, Y and Zr are closely related to lithological variation, as are Al and Ga. Aluminium and Ga have the dual characteristics and are both alteration and lithology controlled.

In the bulk geochemistry study at Rand Pit, the elements Ag, Au, As, Cu, Mo, Pb, W and Zn are related to mineralization. Comparatively, the elements Ga, Nb, Ti, V, Y and Zr are related to lithological variation. Aluminum and Ga differentiate the mafic and mica schist and the porphyry pods from the ultramafic rocks. Low Fe concentrations mark the mica schist, black shales and porphyries, although some high Fe concentrations occur at depth in the M3 mafic band. Iron is interpreted to reflect largely hydrothermal pyrite from the adjacent ore shoot. Useful pathfinder elements of the bulk geochemistry in the shallow weathered profile prove to be As, Ag, Sb, Cu (possibly Mo) and W (Robertson et. al., 1990).

Although the Al distribution in bulk geochemistry can accurately outline the border between mafic and ultramafic rocks at depth, there is no obvious connection with the distribution of Au mineralization. In the acid insoluble residue Al has not only the highest concentration in mafic rocks, but is also elevated in the M1 and M3 mafic schists where mineralization is present, and where the Al has a high surface

expression values (>7000 ppm). This surface expression is twice as high as the level of Al in mafic rocks (Figure 8-8). Similar distributions are observed for Rb and K, with the difference that Rb and K are necked at the upper part of the profile. Rubidium and K are only concentrated in M1 and M3 mafic rock and the nearby porphyry pods. Although there are some minor depletions at depths of 10–15 m, these depletions are not sufficient to affect the strong positive correlation between Rb, K and Au mineralization. Rubidium and K are either related to muscovite alteration or unweathered to partly weathered micas. The distribution of Ga in the acid insoluble residue follows that of Al indicating the replacement of Al^{3+} with Ga^{3+} during weathering processes. Gallium is typically a dispersed element with the majority of the Ga atoms in the Earth's crust dispersed into the structures of the Al-bearing minerals (Beus and Grigorian, 1977). Although Robertson et al. (1990) used Ga as a lithological discriminator for the mafic and mica schists and the porphyry pods from the ultramafic rocks, it is clearly an indicator of Au in the acid insoluble residue. Tungsten concentrations in the acid insoluble residue are similar to the bulk geochemistry in outlining the primary Au mineralization. However, acid insoluble W has a better surface expression because it does not have the high values, unlike total geochemistry in the near surface of barren UM2 ultramafic rocks.

The distribution of Mo may also be regarded as ore-related, however, due to its low abundance after acid digestion, its distribution is patchy. A few sporadic elevated values are distributed in the ultramafic rocks from the surface to a depth of 10–15 m, probably due to the mobility of Mo during weathering. Nevertheless, an appreciable enhancement of Mo halos in accordance with the primary Au mineralization.

Elemental anomalism (Al, K, Rb, Pb, W, Ga, Mo, and less commonly Ti and V) halos in the acid insoluble residue are more widely distributed than those in the bulk geochemistry. In other words, the pronounced surface expression of acid insoluble residue discriminate and outline the underlying mineralization.

The group of resistant mineral-related elements such as Ti, V, Zr, Nb and Y in the acid insoluble residue not only confirms their immobile characteristics due to gradual enrichment in the upper part of the weathering profile, but also reveals their use as

lithological indicators, some of which have ore-related characteristics.

The characteristics of base and transition metals in the weathering profile are complicated. Only Pb can be used as a useful pathfinder element in the shallow weathered profile. The other elements such as Cu, Zn, Ni and Mn were less useful because of intense leaching and/or erratic enrichment.

Low Fe concentrations are typical in mark the mica schist and black shales extending through the whole profile of M3. Scott (1998) pointed out that the Fe contents, of the micas are depleted close to mineralization. This implies that some high Fe concentrations occurring at depth in the M3 mafic band in bulk geochemistry, are caused by sulphate minerals related to the adjacent ore shoot.

Alkaline earth elements Ca and Sr are surprisingly enriched in the near surface zone of the profile. This is a different result from the bulk geochemistry.

Application of the Ga+Ge, W+Mo+Ga, As+W+Mo and Cu+Pb+Zn indices delineate additional anomalous fields based on combinations of elements that are often close to or below the minimum detection limit.

13.3.2 EPR distribution character

The distribution of EPR intensity near the metalliferous zones have a primary halo of EPR 326.5 ± 5 mT proximal to the Au ore shoots. The horizontal dimensions of this halo in the deeper part of the profile are not widespread, but extend beyond the ore body and narrow downwards along the ore shoots. In the shallow part of the profile, EPR 326.5 ± 5 mT intensity halos are larger and have higher intensities.

Another characteristic of these EPR halos is their considerable vertical extent. They are distributed through the whole regolith profile and are quite strong and broad at surface. The vertical zonality in the EPR distribution is best exemplified by the pair of EPR signals, EPR 326.5 ± 5 and EPR 326.5 ± 100 mT. The halos formed by both of these intensities are near identical.

13.3.3 Discussion

Using factor and cluster analysis, different inter-related groups of elements are recognized. The results at Rand Pit are similar to that of Mystery Zone. However, at Rand Pit the results relate to alteration (Al, Au, Ga, K, Na, Pb, Rb, Sr, W and possibly V and Ti), resistant mineral of immobile related character (Al, Cu, Ga, Ti, Pb, V, Zr) and ferromagnesian minerals (F, Fe, Mn, Ni, Zn).

Some elements in the deeper part of the regolith profile are also regarded as ore-related (Al, K, Rb, V, Ti, W, Ga and Mo), whilst some elements are lithology-related (Ti, V, Zr, Nb, Al). Similar characters are identified in EPR distributions. The group of elements Al, Ga, Rb, K, V, W and Mo and EPR 326.5 ± 5 mT define useful pathfinders to Au mineralization at surface.

13.3.3.1 Implication for near surface exploration

Primary and secondary Au mineralization at Rand Pit, Reedy Mine is indicated by a broad anomaly in the soils and lateritic horizon in the top 5–15 m of the profile. The anomaly extends along the trends of the ore bodies and is influenced by two factors: 1) lateral Au dispersion associated with secondary enrichment in the weathered ultramafic units, and 2) the relations of mafic schist host rocks to the primary Au mineralization. These Au anomalies are strong and extend from the ore shoots to the surface.

A anomalous Au near surface zone is indicated by high concentration in the acid insoluble residue of the mineralization, and relates to pathfinder elements Al, K, Rb, Cu, Cr, Pb, V, Ti, Zr, W, Ga and Mo in the surface horizon. The elements Al, Cu, Cr, Pb, V, Ti and Zr are distributed widely, whilst the other elements occur mainly within the rocks related to primary mineralization. Copper cannot be used as a pathfinder element because of its surface enrichment, which is not related mineralization. This supports the conclusion from bulk geochemistry that the deeper Cu enrichment is unrelated to Au mineralization. The multi-element composite halos W+Mo+Ga, Ga+Ge, Cu+Pb+V and As+W+Mo also provide good surface expressions of underlying mineralization. In this case Ga+Ge and Cu+Pb+V have broader anomalous near surface zone, whereas W+Mo+Ga and As+W+Mo reflect

the broad Au enrichment in the host rocks.

The Au anomaly zone is also marked by high EPR 326.5 ± 5 mT distribution in the near surface profile, indicating that both primary mineralization and some dispersion related to by primary quartz redistribution occurs.

13.3.3.2 Implication for exploration at depth

In the deeper parts of the saprolite, the mineralization at Rand Pit is characterized by acid insoluble enrichment of Al, K, Rb, Pb, W, Ga and possibly Ti and V. The primary halos of these elements delineate the area around the Au mineralization in shear zones, however the halos are wider than the zone of Au mineralization. Among these elements, Ti and V have low values near the ore shoots, and indicate that they were either depleted or are unrelated to mineralization.

The multi-element composite halos follow the pattern of Al, Ga, W, Rb, K and V, and are much larger than the primary mineralization. Based on this data, an idealized distribution pattern of the primary halos would closely overlap in plan and define the Au ore structure. The halo is expected to appear at the surface (along the black shale and mica schist within the mafic rocks), but either disappears or is attenuated rapidly away from the ore-enclosing structure and/or mineralization host rocks. This feature is particularly distinct in the structure of the composite additive anomalies (Figures 8-39 to 8-72).

EPR characteristics of zones of primary and dispersed mineralization are considered to be similar. Although the EPR intensity at depth is lower than that of its surface expression, there is a distinct zonality in the structure of EPR 326.5 ± 5 mT intensity around the ore shoots.

13.3.3.3 Implication for lithology discrimination

High Fe, Mn and Zn are useful indicators of ultramafic rocks in the acid insoluble residue. These abundances commonly persist to the surface. The meta-sedimentary rocks are distinguished by high mica abundances, which are related to high K and Rb. However the mica schist is chemically distinct from other lithologies. Using the ratio of Ti/Zr and Ti/V to distinguish different lithologies was not successful.

13.4 ELEMENT AND EPR DISTRIBUTION AT JIM'S FIND

At Jim's Find, deep regolith consists of weathered bedrock with a thin overlying cover of gravel soil and is widely distributed in the present arid climate of the Tanami area. Although this deeply weathered terrain now occurs in a climatic environment that is different to that of Rand Pit and Mystery Zone, Western Australia, they were formed under broadly similar conditions in the past, which resulted in their broadly similar petrographic, mineralogical and geochemical characteristics. As a consequence, many features of the surface expression of mineralization between these terrains are also similar, and extends not only to acid insoluble residue geochemistry, but also to the distribution of EPR intensities.

The effects of weathering on sulphides is clearly described by Butt and Smith (1992), both in terms of chemistry and mineralogy. They recorded a basal zone of supergene alteration involving sulphide dissolution and redeposition at depths of between 70 and 85 m. Above this zone is an oxide zone dominantly consisting of hematite, goethite, quartz and kaolinite, but also containing a large number of secondary ore minerals including oxides, carbonate, sulphates, halides and native metals. Leaching predominates in the upper 10–20 m where few base metal compounds are retained. The surface regolith was therefore characterized by high S values, whilst Cu, Zn As and Ni were also anomalous. It is likely that these elements are trapped in the hematite and goethite inclusions observed in the quartz/chalcedony concentrates.

Gold mineralization occurs as sheeted quartz-carbonate veins within interbedded sedimentary and basaltic packages. Tunks (1996) identified a bleached muscovite alteration halo surrounding auriferous quartz-carbonate veins, which are typical of many shear-zone-hosted Au deposits in sub-greenschist facies rocks (Mikucki and Groves, 1990), as well as Carlin style Au mineralization (van Moort et al., 1995). This muscovite alteration expresses itself by increased K content around the ore body, as observed in the results of PIXE/PIGE analyses (in Chapter 11). Gold enrichment in the upper levels of the regolith, as observed in the Tanami, is common and such enrichments are easily located in regional exploration programs. However, it is usually difficult to locate the primary Au mineralization at depth, as in most cases, the secondary enrichment has no obvious continuity at depth (e.g. in profile

10150N), due to displacement or erosion. The surface expressions of possible As halos around the gold mineralization tend to be poor in the bulk rock geochemistry from Jim's Find.

13.4.1 Acid insoluble regolith geochemistry

The composition of the acid insoluble residue represents quartz, feldspar and muscovite, along with some of resistate accessory minerals such as rutile and zircon. The primary Au mineralization at depth is expressed by high F, Al, K, V, Mn, Fe, Ga, Rb, Co and W values. These distributions are largely related to muscovite wall rock alteration.

The Rb/K ratio of the muscovite at Jim's Find are enhanced, in a similar trend to Carlin deposits (van Moort and Xu, 1995), porphyry copper deposits in Chile (Armbrust et al., 1977) and Sn-W greisen (Govett, 1983), as well as many other types of Au-rich ore deposits. The Rb/K ratio is highest in the regolith overlying the ore body, near the surface. This distribution likely represents the relative enrichment of muscovite in the near surface regolith due to the preservation of Rb in the muscovite. The use of Al x K x Rb, Cr x Mn and W+Mo+Ga as surface indicators of the gold mineralization is well defined, as all secondary minerals containing these elements appear to have been removed during the acid treatment.

Another expression of the sericitization is the Rb/K and Rb/Al ratios. The ore body has distinct halos of Rb/Al ratios both in primary and secondary mineralization. Rb/K and Rb/Al are also useful near-surface because they have significant high values in the upper regolith profile. Although residual kaolinite in the acid insoluble residue of the near-surface samples causes increased Al values, Rb/Al ratios remain constant and reflect deep buried mineralization, similar to that derived at Mystery Zone.

In the acid insoluble residue, lithology is expressed by variations in Ti, Zr, Nb, As and Y. The close correlation between As and these elements is lithology related and explains why As is a poor indicator of Au mineralization at Jim's Find. Surface enrichment of the same elements occurs due to their residence in sericite, zircon and other resistate minerals abundant near the surface.

13.4.2. EPR characteristics

EPR results indicate that the altered and/or mineralized samples are more paramagnetic than the barren samples. The samples from deeper profile have two peaks, in which small peaks are closer to the large peak in barren samples and further away from the large peak in mineralized samples. The spectra of the mineralized samples have a greater peak height of the main signal and also have an additional peak. These EPR features and the EPR intensity outline the primary Au mineralization. The EPR spectra with a shoulder should reveal the presence of Au mineralization using its degree value and multiplication indices with the EPR intensities. The EPR spectra of the near surface samples are comparatively flat compared to deeper samples in the regolith profile. Transmitted light microscopy and scanning electron microscopy reveal that near surface samples consist of chalcedonic material, free of inclusions, with relatively few grains of secondary quartz. The secondary weathering material has surprisingly, has retained many primary EPR characteristics.

EPR spectra of non-acid treated samples does not differentiate between barren and mineralized samples, due to multiple paramagnetic species in the samples, which results in a complex spectrum. Acid treatment of samples is essential to yield useful EPR spectra.

13.4.3 Discussion

The effective removal of the Fe and Mn oxides and hydroxides, carbonate, sulphates and remnants of primary sulphides from regolith material (and rock pulps in general) can be achieved by use of an aqua regia treatment. Biotite, kaolinite and Al oxides/ hydroxides may also be removed by subsequent sulfuric acid treatment. The remaining acid insoluble residue consists mainly of quartz with minor muscovite and some heavy minerals like rutile and zircon.

In the acid insoluble residue, elevated elemental concentrations of Rb, K, Al, V, W, Mo, Ga and in particular, Rb/Al outline primary Au mineralization. The elements Cu, S, Ni, Pb and the ratio Rb/K likely reflect relative enrichment of resistant minerals, which correspond to the Au-enriched lateritic gravels near the surface and/or the surface expression of the buried mineralization. Zirconium, Ti and Nb are similarly

enriched at the surface where Na, Ca and Sr are strongly depleted.

Meaningful EPR spectra is obtained from samples consisting dominantly of primary quartz. If the sample is mineralized, the EPR signal is more pronounced. The application of EPR analysis for Au exploration in highly weathered terrains is therefore feasible. The main useful characterization are EPR 326.5 ± 5 mT and their multiplication EPR ± 5 mT x ± 100 mT. Both of them are correlated well with the primary Au mineralization, with dispersive halos larger than the Au ore bodies. This indicates that the EPR intensity can be used effectively to outline the primary Au mineralization.

13.5 COMPARISON OF THE CASE STUDIES

In each of the three case studies, the characteristics of bulk geochemistry related to Au mineralization is different due to the complicated weathering processes. In contrast, the acid insoluble residue method yields constant results in all three areas, irrespective of how deep and how intense the weathering was. Table 13-1 shows the comparative results between bulk geochemistry and the acid insoluble residue methods detailed

Table 13-1. Comparison between the character of acid insoluble residue and bulk geochemistry

	Alteration/Mineralization Related Elements	
	Acid Insoluble Residue Geochemistry[1]	Bulk Geochemistry[2]
Mystery Zone	Al, Rb, K, W, Ga, V, Cr, Ca	Au, S, Sb, As, W, Ba, K, Rb, Ag, Te, Cs
Rand Pit	Al, Rb, K, W, Ga, Pb, Mo	Ag, Au, As, Cu, Mo, Pb, Sb, Se, Sn, Te, Tl, W, Zn(?), Rb
Jim's Find	Al, Rb, K, W, Ga, V, Mo	Au, S, W, K, Rb, As(?)
	Possibility of Lithology Discrimination (ratios)	
	Acid Insoluble Residue Geochemistry	Bulk Geochemistry
Mystery Zone	Ti/Zr*, Zr/V(?), Ti/V*	Ti/Zr(?), Zr/V(?), Ti/V(?)
Rand Pit	Ti/Zr(?), Ti/V(?)*	Ti/Zr(?), Ti/Cr(?)
Jim's Find	Ti/Zr*, Zr/V(?), Ti/V*	Ti/Zr (?)

Note: the underlined element were not analyzed in this study; the ratio with a * indicates it may be useful and with a question mark indicates it is weak or no utility

1. This study
2. From Butt (1991), Robertson et al., (1990) and Stott (1994)

in this thesis.

The results indicate that bulk geochemistry offer a different suite of elements to indicate alteration or mineralization in each of the three study areas. Bulk geochemistry pathfinder elements are limited to only As, W, Rb, and Au. Comparatively, the acid insoluble residual gives a wider range of indicator elements, viz. Al, Rb, K, W, Ga and possibly V and Mo.

Hallberg (1984) indicated that Ti and Zr are the most stable elements in the weathered environment and their ratio can be used to distinguish different lithologies. This is not always the case as silicates, notably amphibole and chlorite, also contain significant quantities of Ti (Correns, 1978) and these minerals are highly weatherable (Robertson and Butt, 1997). Ti/Zr and Ti/Cr ratios distinguish the major rocks in Rand Pit and Mystery Zone, but and their ability to discriminate between lithologies is weak (Robertson and Butt, 1997). At Jim's Find, Ti/Zr ratios can not be used (Stott, 1994). In contrast, the acid insoluble residue are better at distinguishing lithological variation using the Ti/V and Ti/Zr ratios both at Mystery Zone and Jim's Find, but less so at Rand Pit.

There is evidence in the above geochemical data that the acid insoluble residue relates not only to the wall rock alteration associated with the mineralization, but also to secondary dispersion. This can be demonstrated by the near surface enrichment of Al, Fe, Ca, Sr, Ni, Mn, Cr, Zr, Nb, Ti, Th, As, S, Cl and W at Mt Percy, Ca, Sr, Cu, Cr, Zr, Ti, Zr, W, Cl, Nb, Th and S at Reedy and Cu, Zn, Ni, Zr, Nb, Th, S, W, Y and Cl at Jim's Find. Of these elements, Ti, Zr, Nb, Y and Th are related to accumulation of resistate minerals. The other elements likely relate to inclusions of secondary minerals, such as like carbonates, iron or maganese oxides, sulphates and clay minerals. This material must be very fine indeed, as microscopic inspection of the acid insoluble residue does not reveal such minerals. Secondary chalcedony often contains inclusions of dark chalcedony. Inspection with ESEM and associated energy dispersive analysis identified the inlcusions of quartz, sericite, kaolinite and rutile and zircon in the secondary chalcedony, but not carbonates or sulphates.

The EPR of the quartz concentrates, on the other hand, does not indicate surface enrichment and expresses only the primary dispersion pattern of wall rock alteration.

The EPR signal survives in the regolith above the ore bodies, except at Jim's Find. Where a EPR signal is absent, likely due to the presence of secondary chalcedony, which lack lattice defects and hence EPR signal. However, Inclusions of primary quartz in secondary chalcedony are insufficiently abundant to explain the excellent preservation of the EPR signal in near surface material.

13.6 COMPARISON WITH ANOTHER AREA

Geochemical and EPR work in this thesis was supplemented by a study on the EPR and chemical characteristics of the regolith at the McKinnons Gold Mine near Cobar, NSW (van Moort et al., 1999). The study involved 101 drill core regolith samples from a mine section through the open pit and surface soil samples.

The geochemical halo associated with the McKinnons Au mineralization is characterized by enrichment in Cu, Zn, Pb, Ag, As, Sb, Ba and Bi and depletion of K, Al, Fe, Mg, Ca, Na, Ti, Cl, F, Ga, Rb, Zr, Y, V and Ti. Most of these depleted elements, except possibly Ti and V, are considered indicators of wall rock alteration involving muscovite destruction during the emplacement of Au mineralization.

EPR distributions in the mine drill core samples also reveal a significant EPR halo outlining the Au mineralization.

An interesting aspect of the McKinnon's study is that the mineralization is characterized by sericite destruction and depletion of all the elements K, Al, Fe, Mg, Ca, Na, Ti, Cl, F, Ga, Rb, Zr, Y, and V enriched in cases of sericitic wall rock alteration. Despite this the EPR signal at McKinnons is strongly developed over the mineralized zone, as is the case in three areas detailed in this thesis.

13.7 GENERAL DISCUSSION

13.7.1 Introduction

Extensive research and its application over the last two decades has significantly changed the explorationists' perspective of the regolith, having an important impact on mineral exploration. Lateritic residuum of regolith profiles is now seen as a valuable and useful asset . It is highly effective as a sample medium for exploration geochemistry and provides an imprint of bedrock relationships along with any

concealed mineral deposits which may be underlying (Smith and Anand, 1992; Anand, 1995). Although the regolith, especially laterite, geochemistry involves samples related to residual accumulation as well as mechanical and hydromophic dispersion, the weathering processes have tended to smooth much of the local chemical and mineralogical variation from changes in local bedrock type (Anand and Smith, 1997). This results in difficulties when interpreting regolith geochemical data because most of weathering products are not related to mineralization and 'false' anomalies. Using strong acid treatment, most of the weathering products, such as oxides, carbonates, sulphides and clay minerals, can be effectively removed from regolith samples. This treatment creates a new sample medium more suitable to reflect the original information in local bedrocks, including its original degree of wall rock alteration. It should be stressed that the acid insoluble concentrate consists essentially of quartz and chalcedony; a mineral with limited capacity to take up impurities.

13.7.2 Application of bulk geochemistry

The main advantages of regolith geochemistry, especially lateritic residuum, is that it reflects long periods weathering history (10 to 50 million years). The samples not only represent residual accumulation as well as mechanical and hydromorphic dispersion, but also reflect the local chemical and mineralogical variation arising from changes in local bedrocks. Although weathering processes have tended to smooth much of this variation (Anand and Smith, 1997), it should be still significant due to the long period of weathering and enrichment of the weathering products.

Provided it is properly carried out, bulk regolith geochemistry can provide an effective means of exploration wherever lateritic residuum is present. Different sampling programs can aid the regolith-landform control (Anand and Smith, 1997). An appropriate sampling strategy can not only direct explorationists to establish regolith landform models, which help to understand regolith stratigraphy and evolution, but also find mineral deposits as many of the geochemical characteristics of lateritic residuum are relatively stable to further weathering and the target associated elements suite are contained within resistate minerals or in Fe-oxyhydroxides.

13.7.3 Application of acid insoluble geochemistry and EPR

The chemical composition of the acid insoluble residue reflects the type of wall rock alteration in all three case studies where sericitization and feldspar destruction occur.

There is further evidence that the wall rock alteration is associated with the formation of a Rb- and V-rich sericite. Of further importance is the reliability of Rb/K ratios and Al abundances in acid insoluble residue as indicators of mineralization throughout the regolith, including the surface profile. The haloes of these elements are larger than the associated Au mineralization. In the case of the McKinnons deposit, Pb occurs at the upper level of the mineralization and Ni and Zn are enriched at the lower level. Similar distributions and relationships are generally obtained by total analyses of rock pulps.

Positive correlation between the intensities of the EPR signals and the occurrence of Au were observed in all three studies. The EPR of quartz is unaffected by the degree of weathering of the material in which the quartz is present. The present study indicates that EPR can detect surface indications of concealed Au deposits in highly weathered terrain and that it can be implemented to differentiate between barren and mineralized regolith at the surface (e.g., at Rand Pit and Mystery Zone). The partial failure of this study to detect an EPR surface expression of underlying Au mineralization at Jim's Find is attributed to admixtures of microcrystalline secondary chalcedony resulting from the hydrolysis of silicates during weathering. Such material does not have a strong EPR signal. Additionally some of the surficial material may also have a transported component.

13.7.4 Comparison of bulk and acid insoluble geochemistry

Effective exploration based on regolith geochemistry requires controls of regolith landform relationships and knowledge of regolith stratigraphy and syntheses of regolith evolution. Both bulk and acid insoluble regolith geochemistry require understanding the truncation of weathering profiles, appropriate clean sample preparation, sensitive multi-element analyses. If the lateritic residuum is preserved at depth beneath the sediment cover, both methods can detect buried geochemical haloes in laterite. Supergene Au haloes can occur within the saprolite zone of weathering profiles in inland Australia. Bulk geochemistry can enlarge the exploration target in the supergene hydromorphic dispersion (Butt, 1991). From this study, it can been seen that the acid insoluble geochemistry is also applicable to outline the supergene halos. Methods of data presentation and interpretation are however different. In bulk geochemistry, samples may consist of variety of minerals and

geochemical signatures, the later which is stronger than the acid insoluble geochemistry. These characteristics may also produce large anomaly which is probably residual accumulation or mechanical dispersion rather than alteration or mineralization related, so careful data interpretation is necessary.

There are normally two stages regarding the use of geochemistry in weathered terrains. At the reconnaissance stage of exploration, sampling of lateritic residuum is best directed at the pisolitic upper part of the residuum in order to take advantage of enhanced mechanical and hydrochemical dispersion and homogenisation. When following up to locate the of source of mineralization with a laterite geochemical anomaly, further sampling program may be direct to the basal part of the residuum.

Compared with the bulk geochemistry, the acid insoluble geochemistry is more direct in reflecting the local wall rock alteration and associated mineralization. After the effective removal of weathering products, regolith samples should, more or less, indicate information on primary wall rock alteration and/or mineralization without, or with less, obstacles caused by weathering products. Unfortunately, due to the complexity of the sample medium under different weathering process, there is no general rule in bulk geochemistry exploration that can be universally applied. In different weathering terrains, different suite of elements are used to define different exploration models. However, in the integrated acid insoluble residue geochemistry, EPR is used as a supplementary method and always yields vectors to locate the mineralized target.

Because EPR signal is mainly produced by quartz the sample preparation is vital. If the sample is not prepared properly, abundant clay minerals will remain in the sample medium and affect the EPR signal. For example, kaolinite absorbs incoming microwaves resulting in a flat response such that further data reduction and a interpretation is difficult. Moreover, other uncleaned weathering products can cause a large noise effect to the EPR signal. Although the acid insoluble residue is a better sample medium for geochemical and EPR analysis, the acid treatment process is time consuming.

13.7.5 Implication for exploration

Acid insoluble residue geochemistry is an efficient tool for Au exploration in regolith dominated terrains, particularly when it is considered that many traditional geophysical and geochemical techniques have limited application. The geomorphology and regolith profile of a region are the products of its weathering history and result from past and present processes of weathering and geochemical dispersion. Identifying these processes is fundamental to determining the geochemical expression of mineralization. The most important features of lateritic regoliths include the strong leaching of most ore elements, the restricted dispersion of most elements in the saprolite and the broad, multi-element haloes in the lateritic residuum. In contrast, the nature of the acid insoluble residue geochemical expression of mineralization, and the availability and usefulness of specific surface and subsurface acid insoluble residue elemental halos, reflect the alteration and mineralization more accurately because of the "pure" character of the sample medium after strong acid treatment.

Gold distribution in the three working areas of this study have typical characteristics of Au deposits formed in tropical environments (Butt and Smith, 1980; Mann, 1984; Freyssinet, 1990; Robertson et al., 1990; Butt, 1991; Colin and Vieillard, 1991; Freyssinet, 1993; Freyssinet and Itard, 1997), with broad supergene Au anomalies in the soils and lateritic horizons. However, at Rand Pit, Au is weakly depleted under the lateritic near surface enrichment zone. These observations are in accordance with the general occurrence of Au in lateritic profiles capped by ferruginous crusts (ferruginous duricrust, cuirass, ferricrete) overlying Au concentrations within the mineralized structures of the fresh parent rock or overlying saprolite. Commonly, Au is strongly dispersed in the upper ferruginous horizons, however Au anomalies are relatively weak in surficial zones (Freyssinet and Itard, 1997). Moreover the Au distribution pattern is highly heterogeneous at the mineralized structure scale, which is why the acid insoluble residue geochemistry needs to not only take into account the occurrence of the Au mineralization, but also its relationship to the wall rock alteration, as well as the dispersion haloes in the weathering horizons.

Explorers for in-situ Au mineralization in weathered terrains require a reliable indicator to underlying mineralization. Although in many cases, the uppermost part of the weathering profile has a Au response, if is not always the case due to intense chemical

and physical weathering. Moreover, Au can be leached from the immediate surface in high rain fall regions (Smith et al., 1997). Wall rock alteration and mineralization-related elements in the acid insoluble residue, such as Al, K, Rb, V, W and Ga, increase the effectiveness of anomaly recognition and allow the delineation of source anomalies. These indicator elements in the acid insoluble residue extend to surface through the entire saprolite and mottled zones of the regolith profile. Consequently, the distribution of Au in the regolith profile can be predicted by acid insoluble residue geochemistry. This method has been extensively used in the three areas presented in this thesis from the Northern Territory and Western Australia.

In this study, all three working areas indicate that Al, K, Rb, V, W and Ga give a surface expression of wall rock alteration, which is useful in defining buried Au mineralization. The multi-element composite halos Ga+Ge, As+W+Mo cumulatively emphasize the surface expression and make up for a lack of sensitivity of the analytical technique for each of the specific elements. In the mottled and saprolite zones, this group of elements is expected to be similar to their individual distribution near the surface. However, the composite anomaly halo is much wider than that of Au. EPR distributions in the mottled and saprolite zone are also more pronounced than that of Au, but their intensity is decreases to the near surface.

The case history information presented in this thesis indicate that the complex nature of the regolith in areas affected by tropical weathering is not necessarily an impediment to the use of surface geochemical techniques. The results of this work illustrate that acid insoluble geochemistry and EPR are highly effective in defining the surface expression of buried primary muscovite alteration and Au mineralization. These techniques are also readily applicable to deeply weathered terrains elsewhere, as indicated by the Cobar example (Section 13.6).

13.8 GENERAL DISCUSSIONS

De spite many complexities, it is possible to distinguish a series of chemical processes in the regolith that can be related to alteration and mineralization. Strong and broad halos formed by several elements were revealed in each of the three areas in this study. The acid insoluble residue geochemistry displays three distinct geochemical associations, which can be distinguished in terms of the element distribution.

1. Halos formed by acid insoluble Al, K, Rb, W, Ga, Mo and possibly V, outline

the wall rock alteration zone which is genetically related to the formation of mineralization/wall rock alteration zone.

2. Halos formed by Ti, V, Y, Zr, Al and Ga in acid insoluble residue are related to lithology and lesser to the surface accumulations of resistate elements. Ti/Zr and Ti/V ratio have the potential to be used as lithological differentiators.
3. The dispersion of Fe, Mn, Zn and Ni in acid insoluble residue reflect the occurrence of ferromagnesian minerals in the regolith profile.
4. The acid insoluble residue of near surface material also reflects secondary dispersion patterns of Ca, Sr, Cr, Cl and S presumably due to extrapment of submicroscopic inclusions.

The observed chemical changes in the acid insoluble residue are consistent with the distribution of alteration and weathering trends in the profile. Statistical methods successfully applied to the acid insoluble residue, classify the three groups of elements stated above. The main advantage of the statistical method used in this study is that it can outline alteration-related elements and also be used to define mineralization. Both factor and cluster statistical analysis define the three groups of elements classified above, but do not replace the interpretation of spatial distribution.

The results of geochemical sampling around ore bodies and their surrounding regolith in heavily weathered terrains have made it possible to determine the characteristics of acid insoluble residue halos, as well as assess the distribution of mineralization in the lower regolith. The halos of the indicator elements, Al, Rb, K, W, Ga and Mo in the regolith profile precisely outline ore-related alteration. In comparison to bulk geochemistry, the results of acid insoluble residue geochemistry have significant advantages in distinguishing wall rock alteration. The distribution pattern of Al, Ga, Rb, K, Pb in acid leached residues are more pronounced than those of bulk geochemistry, while similar distributions of V and W were observed.

The chemical expression of the acid insoluble residue of muscovite wall rock is K and Rb enrichment, increased Rb/K and Rb/Al ratios and, commonly, Al, Fe, F and V enrichment; except where wall rock alteration is characterized by muscovite destruction. Sodium, Ca and Sr depletion invariably occur and are caused by plagioclase destruction. Arsenic, Ga, V and W in the acid insoluble residue are considered good indicators of Au mineralization below the regolith.

Similar results were obtained for these and other potential pathfinder elements by total analysis of whole rock pulps. However, not all Au deposits have an associated suite of pathfinder elements, whereas research to date suggests that there is always an EPR signal, which suggests EPR is a more consistent and reliable technique.

Three measurements of EPR intensities were used in this study: EPR intensities measured at magnetic flux density sweeps (1) 326.5 ± 5 mT, (2) 326.5 ± 100 mT and (3) 326.5 ± 250 mT. The 326.5 ± 250 mT signals are generally the same as those of the 326.5 ± 100 mT sweeps.

There are significant differences in the intensities of the EPR signals between altered/ mineralized and barren regolith samples. The halo formed by EPR 326.5 ± 5 mT intensity mimics the haloes described by Al, K, Rb, Ga and W. In contrast, EPR 326.5 ± 100 mT intensity is more descriptive of Fe, Mn, Zn and Ni element distributions. This indicates that the areal distribution of the EPR intensity measured at a magnetic flux density sweep of EPR 326.5 ± 5 mT reflects alteration better than EPR 326.5 ± 100 mT.

The results of the EPR study in the Mystery Zone and Rand Pit of Western Australia, as well as Jim's Find of Northern Territory are sufficiently encouraging to apply the EPR method to deeply weathered terrains elsewhere. EPR could be used to define the extent of mineralization and associated wall rock alteration, as well as a technique to distinguishing between alteration related to Au mineralization versus background variation.

Problems with the application of geochemical methods are frequently due to using analytical methods with inadequate sensitivity. An analytical technique sufficiently sensitive to characterize the background population is a fundamental requirement for anomaly recognition. The PIXE/PIGE techniques seems to satisfy the basic demand for Au exploration in weathered terrains. Other methods may be needed to improve sensitivity for some useful elements, such as As, Mo, Ge and Ba, and would make the use of the acid insoluble residue as a sampling medium even more promising.

Finally, the results of this work at the regolith surface indicate that the geochemistry

of Al, Cr, Ga, K, Rb, V, W, Rb/K and Rb/Al plus the EPR intensity measured at 326.5 ± 5 mT in the acid insoluble regolith residue correctly define the location of underlying Au mineralization. The composite halos Al x K x Rb, Ga+Ge and As+W+Mo could help emphasize this expression and make up for a lack of sensitivity of the analytical technique for some mono-elements (i.e. As, Ge and Mo). If the analytical method detection limit can be improved, other trace elements, such as Ba and Zn could also be used. Overall mineralized regolith samples have a more pronounced EPR signal and with a general positive correlation between Au content and the intensity of the EPR ± 5 mT and other ore- and alteration-related elements. This corroborates the usefulness of EPR as an exploration tool for Au mineralization (Xu and van Moort, 1997, 1998; van Moort and Xu, 1997).

As the emphasis in exploration changes to more difficult and scientifically challenging terrains, the suitability of the relatively simple EPR technique will require widely application in order to test its viability and applicability to different geological areas. The EPR spectra, however, must be obtained on quartz concentrates using the acid insoluble residue method, as the spectra of untreated bulk rock pulps are less effective. The study results from Western Australia and Northern Territory suggest that EPR may have a significant role to play in the future search for deeply buried Au deposits.

REFERENCES

ALS, 1995. Exploration in the Australian Regolith, Mineral Division, Australia Laboratory Services News, 4: No.1, 4 pp.

Anand, R.R. and Smith, R.E., 1997. Laterite geochemistry. Exploration Geochemistry and Hydrothermal Geochemistry, Master of Economic Geology Course Work Manual 11, Part 1, Centre for Ore Deposit Research, University of Tasmania, 71-79.

Anand, R.R., 1995. Genesis and classification of ferruginous regolith materials in the Yilgarn Craton: implications for mineral exploration. Exploration and Mining Research News. CSIRO Australia, Division of Mineral Exploration, 3:3-5.

Anderson, A.J., Clark, A.H., Ma, X.P. and Palmer, G.R., 1989. Proton-induced X-ray and gamma ray emission analysis of unopened fluid inclusions, Economic Geology, 84: 924-933.

Andrew, J.C. and McQueen, K.G., 1994. Resistate and heavy mineral dispersion around the Paddy's river skarns: Implication for exploration in the regolith, 12th Australian Geological Convention, Perth, September, 1994. Geological Society of Australia Abstracts 37: p76.

Annegarn, H.J. and Bauman, S., 1990. Geological and mineralogical application of PIXE: a review. Nuclear Instrumental Methods in Physics Research, B49: 264-270.

Archibald, N.J., 1987. Geology of the Norseman-Kambalda area, Second Eastern Goldfields Geological Field Conference. Eastern Goldfield Discussion Group, Kalgoorlie, pp. 13-14.

Armbrust, G.A., Oyarzun, J. and Aria, J., 1977. Rubidium as a guide to ore in Chilean porphyry copper deposits. Economic Geology, 3: 347-357.

Ayres, L.D., 1983. Bimodal volcanism in Archaean greenstone belts exemplified by greywacke composition, Lake Superior Park, Ontario, Canadian Journal of Earth Sciences 20: 1168-1194

Barley, M.E. and Groves, D.I., 1988. Geological setting of gold mineralization in the Norseman-Wiluna Belt, Eastern Goldfields Province, Western Australia. In: D.I. Groves, M.E. Barley, S.E. Ho and G.M.F. Hopkins (Editors), Western Australia Gold Deposits. Geology Department Extension, University of Western Australia, pp. 18-46.

Barton, A.H., Johnston, S.R. and Head, D.L., 1987. The Mount Percy gold deposits, In: The Second Eastern goldfields Geological Field Conference, Kalgoorlie, 1987, Abstracts and Excursion Guide, pp. 127-130.

Bates, R.L. and Jackson, J.A., 1984. Dictionary of Geological Terms. Anchor Press,

Doubleday.

Blake, D.H., Hodgson, I.M. and Muhling, P.C., 1979. Geology of the Granites-Tanami region, Northern Territory and Western Australia. Bureau of Mineral Resources Geology and Geophysics, Bulletin: 197.

Berry, L.G. and Mason, B., 1959. Mineralogy, Concepts, Descriptions Determinations. W.H. Freeman and Company, 618 pp.

Bettanay, E. and Churchward, H.M., 1974. Morphology and stratigraphic relationships of the Wiluna Hardpan in arid Western Australia. J. Geol. Soc. Aust., 21: 73-80.

Beus, A.A. and Grigorian, S.V., 1977. Geochemical exploration methods for mineral deposits. Applied Publishing Ltd., Wilmette, Illinois. USA, 287 pp.

Bird, J.R., Duerden, P. and Wilson, D.J., 1983. Ion beam techniques in archaelogy and the arts. Nuclear Science Application. Harwood Academic Publishers, 1: 357-516.

Bird, J.R. and Williams, J.S., 1989. Ion Beams for Materials Analysis. Academic Press, Sydney, 719 pp.

Boni, C., Cereda, E., Braga Marcazzan, G.M. and De Tomasi, V., 1988. Prompt gamma emission excitation functions for PIGE analysis of Li, B, F, Mg, Al, Si and P in thin samples. Nuclear Instrumental Methods in Physics Research, B35: 80-86.

Bradshaw, P.M.D. (Editor), 1975. Conceptual models in Exploration Geochemistry - The Canadian cordillera and Canadian Shield. Journal of Geochemical Exploration, 4. Elsevier, Amsterdam, 1-213 pp.

Brissaud, I., de Chateau Thierry, A., Frontier, J.P. and Lagarde, G., 1986. Analysis of geological standards with PIXE and PIGE techniques; applications to volcanic rocks. Journal of Radioanalytical and Nuclear Chemistry, 102(1): 131-141.

Brissaud, I., Houdayer, A. and Hinrichsen, P.F., 1987. PIXE analysis of geostandards at the University of Montreal. Journal of Radioanalytical and Nuclear Chemistry, 117(2): 99-110.

Burkov, V.V. and Podporina, Y.K., 1967. Rare earths in granitoid residuum. Dokl Academy of Science, USSR, Earth Science Section., 177, 214-216.

Burns, D.T. and Flockhart, B.D., 1990. Application of quantitative EPR. Phil. Trans., 333: 37-48.

Butler, J.R., 1953. The geochemistry and mineralogy of rock weathering. I. The Lizard area, Cornwall. Geochimica et Cosmochima Acta, 4: 157.

Butt, C.R.M., 1998. Regolith Geochemistry, Mystery Zone, Mt. Percy Gold Mine. In: I.D.M. Robertson (Editor), Regolith 98 Field Guide. CRC-LEME Report 81, pp. 1-13.

Butt, C.R.M., 1991. Dispersion of gold and associated elements in the lateritic regolith

Mystery zone, Mt. Percy, Kalgoorlie, Western Australia. 156R, Division of Exploration Geoscience, CSIRO, Wembley, Western Australia, 60. pp.

Butt, C.R.M. and Smith, R.E., 1992. Characteristics of the Weathering Profile. In: G.J.S. Govett (Editor), Handbook of Exploration Geochemistry. Elsevier, pp. 299-330.

Butt, C.R.M., and Zeegers, H., (Editors), 1992. Regolith Exploration Geochemistry in Tropical and Subtropical Terrains. Handbook of Exploration Geochemistry, 4. Elsevier, Amsterdam, 607 pp.

Butt, C.R.M., 1995. Evolution of regoliths and landscapes in deeply weathered terrain: implications for geochemical exploration. 17th International Geochemical Exploration Symposium, Townsville, pp. 9-11.

Butt, C.R.M. and Smith, R.E. (Editors), 1980. Conceptual Models in Exploration Geochemistry. Journal of Geochemical Exploration, 12. Elsevier, Amsterdam, 89-365 pp.

Butt, C.R.M., Lintern, M.J. and Anand, R.R., 1997. Evolution of regoliths and landscapes in deeply weathered terrain - implications for geochemical exploration. In: A.G. Gubins (Editor), Proceedings of Exploration 97: Fourth Decennial International conference on Mineral Exploration. pp323-334.

Butt, C.R.M., 1998. Regolith Geochemistry, Mystery Zone, Mt. Percy Gold Mine. In: I.D.M. Robertson (Editor), Regolith 98 Field Guide. CRC-LEME Report 81, pp. 1-13.

Calas, G., 1988. Electron paramagnetic resonance. In: F.C. Hawthorne (Editor), Spectroscopy Methods in Mineralogy and Geology. Reviews in Mineralogy. Mineralogy Society of America, pp. 513-571.

Camanske, G.K., Kunilov, V.E. and Zientek, M.L., 1992. A proton-microprobe study of magmatic sulfide ores from the Noril'sk-Talnakh district. Siberia. Canadian Mineralogists, 30: 249-287.

Cameron, E.M., 1968. A geochemical profile of the Swan Hills Reef. Canadian Journal of Earth Sciences, 5: 287-309.

Campbell, J.D., 1953. The Triton gold mine, W.A. In: A.B. Edwards (Editor), Geology of Australian ore deposits, Fifth Empire Mining and Metallurgy in Australia and New Zealand Congresss, Vol.1 195-207.

Carlsonn, L.E. and Adeselsson, K.R., 1980. The application of PIXE/PIGE. Advanced X-ray Analysis, 24: 313.

Carlsson, L.E., 1984. Accuracy and precision in thick-target PIXE-PIGE analysis determined with geological standards. Nuclear Instruments and Methods in Physics Research, B3: 206-210.

Charman, P.E.V. and Murphy, B.W. (Editors), 1992. Soils: their properties and management. Sydney University Press, Sydney.

Clarke, J.D.A., 1994. Geomorphology of the Kambalda region, Western Australia. Australian Journal of Earth Sciences, 41: 229-239.

Clark, M.E., Archibald, N.J. and Hodgson, C.J., 1986. The structural and metamorphic setting of the Victory Gold Mine, Kambalda, Western Australia. In: A.J. Macdonald (Editor), Gold'86, An International Symposium on the Geology of Gold, Toronto, pp. 69-70.

Clayton, E., 1986. PIXAN: The Lucas Heights PIXE analysis computer package. AAEC/M113, Australian Atomic Engineering Commission, Sydney.

Clout, J.M.F., Cleghorn, J.H. and Watt, R.D., 1988. Geology of Kalgoorlie mining associates leases, Kalgoorlie. In: D.I. Groves, M.E. Barley, S.E. Ho and G.M.F. Hopkins (Editors), Western Australian Gold Deposits. The Geology Department and University Extension,University of Western Australia, Perth, pp. 70-77.

Commander, D.P., Kern, A.M., and Smith, R.A., 1992. Hydrogeology of the Tertiary palaeochannels in the Kalgoorlie Region (Roe Palaeodrainage), Western Australia Geology Survey, Record 1991/10.

Commander, L.K. et al., 1994. Chlorite-36 and carbon-14 measurements on hypersaline groundwater in Tertiary palaeochannels near Kalgoorlie, Western Australia No 34, Professional Papers, Western Australia Geological Survey, Perth.

Correns, C.W., 1961. The experimental chemical weathering of silicates. Clay Minerals Bulletin 4: 249-265.

Correns, C.W., 1969. Introduction to Mineralogy. Spinger, 484 pp.

Correns, C.W., 1978. Titanium. In. K.H. Wedepohl (Editor), Handbook of Geochemistry, Spinger, Vol II-2, 22-G-1 - 22-G-3

Dann, E.S. and Ford, W. E., 1966. A Text Book of Mineralogy, 851pp.

Davis, J., 1973. Statistics and Data Analysis in Geology. John Wiley & Sons, Inc, 550 pp.

Davis, T.C. and Bloxam, T.W., 1979. Heavy-metal distribution in laterites, southwest of Regent, Freetown Igneous Complete, Sierra Leone. Gcom. Geol., 74: 638-644.

Deer, W.A., Howie, R.A. and Zussman, J., 1992. The Rock Forming Minerals. Logman, 687 pp.

Domahidy, G., 1990. Hydrogeology of The Granites-Tanami region: Explanatory notes. Power and Water Authority N.S.W

Duda, R. and Reji, L, 1990. Minerals of the World, Arch Cape Press, 520pp.

Eisenlohr, B., 1987. Structural geology of the Kathleen Valley-Lawlers region, Western Australia, and some implications for Archaean gold mineralization. In: S. Ho and D.I. Groves (Editors), Recent Advances in Understanding Precambrian Gold Deposits. Geol. Dept & Univ. Extension, Univ. Wet. Australia, pp. 1775-1783.

Etheridge, M.A., Rutland, R.W.R. and Wyborn, L.I., 1987. Orogenesis and tectonic processes in the Early to Middle Proterozoic of Northern Australia. In: A. Kroner (Editor), Proterozoic Lithospheric Evolution. Geodynamic 17. American Geophysical Union and the Geological Society of America, Washington, D.C.

Eupene, G.S., Micholson, P.M. and Hickey, S.H., 1989. The Tanami gold project. In: A.J. Hosking and D.G. Jones (Editors), Northern Territory Gold Deposits. The Geology Department and University Extension, the University of Western Australia, Perth, pp. 64-69.

Feldtmann, F.R., 1916. Contributions to the study of the geology and ore deposits of Kalgoorlie, East Coolgardie Goldfield, Part III. Geol. Surv. West. Aust. Bull, 69.

Fletcher, R.J., 1985. Geochemical exploration for gold in the Red Sea Hills, Sudan, Prospecting in Areas of Desert Terrain. Institute of Mining and Metallurge, London, pp. 79-94.

Freyssinet, P., Lawrance, L.M. and Butt, C.R.M., 1990. Geochemistry and morphology of gold in lateritic profiles in savanna and semi-arid climates. Chemical Geology, 84(1-4): 61-63.

Freyssinet, P., 1993. Gold dispersion related to ferricrete pedogenesis in south Mali: application to geochemical exploration. Chronique de la Recherche Miniere, 510: 25-40.

Freyssinet, P., Zeegers, H. and Tardy, Y., 1989a. Morphology and geochemistry of gold grains in lateritic profiles of southern Mali. In: S.E. Jenness (Editor), Journal of Geochemical Exploration. Geochemical Exploration 1987, pp. 17-31.

Freyssinet, P., Lemon, P. and Edimo, A., 1989b. Dispersion of gold and base metals in the Mborguane lateritic profile, East Cameroun. Journal of Geochemical Exploration, 32: 99-116.

Freyssinet, P. and Itard, Y, 1997. Geochemical mass balance of gold under various tropical weathering conditions: application to exploration. In A.G. Gubins (Editor). Proceedings of Exploration 97: Fourth Decennial International conference on Mineral Exploration, pp 347-354.

Garrison, E.G., Rowlett, R.M., Cowan, D.L. and Holroyd, K.V., 1981. ESR dating of ancient flint. Nature, 290: 44-45.

Gatehouse, S. Russell, D.V. and van Moort, J.C., 1977. Sequencial soil analysis in exploration geochemistry, Journal of Geochemical Exploration, 8: 483-494.

Glasson, M. J., Lehne, R. W., Wellmer, F. W., 1988. Gold exploration in the Callion area, Eastern Goldfields, Western Australian, Journal of Geochemical Explo ration, 31: 1-19.

Gedeon, A.Z. and Butt, C.R.M., 1977. The applicability of some geochemical tech-

niques in determining "total" compositions of some lateritized rocks. Journal of Geochemical Exploration, 8: 283-304.

Gee, R.D., 1975. Regional geology of the Archeannuleii of the Western Australian Shield. In: C.L. Knight (Editor), Economic Geology of Australia and Papua New Guinea. I. Metals. Australian Inst. Min. Metall., Monography, pp. 43-55.

Gee, R.d., Baxter, J.L., Wilde, s.A. and Williams, I.R., 1981. Crustal development in the Yilgarn Block, Western Australia. In:J.E. Glover and d.I. Groves (Editors), Archaean geology, Second International Symposium, Perth 1980. Geological Society of Australia Special Publication 7: 43-56.

Gillberg, M., 1964. Halogenes and hydroxyl contents of micas and amphiboles in Swedish granitic rocks. Geochim. Cosmochim. Acta, 28: 495.

Goldfarb, M.S., 1981. Hydrothermal deposits, EPR 21 degrees N, The fourth annual meeting of the U.S-Japan-Canada Cooperative Research Project on the genesis of volcanogenic massive sulfide deposits. Pa. state University, University Park, PA, University Park, PA.

Goldich, S.S., 1938. A study in rock weathering. Journal of Geology, 46: 17.

Goldschmidt, V.M., 1954. Geochemistry. Oxford, Clarendon Press.

Govett, G.J.S., 1983. Rock Geochemistry in Mineral Exploration. Handbook of Exploration Geochemistry, Vol. 3 Amsterdam, Elsevier,

Gray, D.J., Butt, C.R.M. and L.M., L., 1992. The geochemistry of gold in lateritic terrains. In: Govett (Editor), Handbook of Exploration Geochemistry. Regolith Exploration Geochemistry in Tropical and Subtropical Terrains, pp. 461-481.

Greenwood, N.N. and Earnshaw, A., 1993. Chemistry of the Elements. Pergamon Press, 1542 pp.

Griffiths, J.H.E., Owen, J. and Ward, I.M., 1984. Paramagnetic resonance in neutron irradiated diamond and smoky quartz. Nature, 173: 439-442.

Griscom, D.I., 1980. Electron spin resonance in glasses. Journal of Non-Crystalline Solid, 40: 211-272.

Gustafson, J.K. and Miller, R.S., 1937. Kalgoorlie geology re-interpreted, Proceedings of Australas. Inst. Min. Metall. No 106:83-125.

Guttman, L., 1956. Best possible systematic estimates of communalities. Psychometrika, 21: 273-285.

Hall, G.E.M. and Bonhan-Carter, G.F (Editors), 1998. Selective Extraction, Special Issue of Journal of Exploration Geochemistry, pp232.

Halden, N.M., Campbell, J.L. and Teesdale, W.J., 1995. PIXE analysis in mineralogy and geochemistry. Canadian-Mineralogist, 33(2): 293-302.

Hallberg, J.A., 1984. A geochemical aid to igneous rock type identification in deeply

weathered terrain. Journal of Geochemical Exploration, 20(1): 1-8.

Haycraft, J.A., 1964. Ore bodies in the Mt Charlotte-Hannans North area, Kalgoorlie,. Proc. Australas. Inst. Min. Metall.(No 213): 49-64.

Henderson, R.G. and Hill, L.V., 1990. Reedy gold deposits, Meekatharra. In: F.E. Hughes (Editor), Geology of the Mineral Deposits of Australia and Papua New Guinea. The Australian Institute of Mining and metallurgy, Melbourne. pp. 205-209.

Hem, J.D., 1968. Graphical methods for studies of aueous aluminum hydroxide, floride and sulfate complexes. U.S. Geol. Surv. Water Supply Papers 1827-B, 33 pp.

Horowitz, P. and Grodzins, L., 1975. Scanning proton induced X-ray microspectrometry in an atmospheric environment. Science, 189: 795-797.

Hotz, P.E., 1964. Nickeliferous laerites in southwestern Oregon and northwestern California. Economic Geology., 59: 335.

Hunter, W.M., 1993. Geology of the granite-greenstone terrain of the Kalgoorlie and Yilmia 1:100 000 sheets, Western Australia, Geological Survey of Western Australia, Perth, 35.

Ikeya, M., Devine, s.d., Whitehead, N.E. and Hedenquist, J.W., 1986. detection of methane in geothermal quartz by ESR. Chemical Geology, 56: 185-192.

Ikeya, M., 1994. ESR (EPR) dating based on natural radiation effects. Nuclear Geophysics, 8(3): 201-224.

Ikeya, M., 1995. New Application of Electron Sping Resonance, Worlk Scientific, 485 pp.

Ireland, T.J., 1989. The geology of the Granites gold deposits, Northern Territory. In: D.G. Jones (Editor), Northern Territory gold deposits. Department of the Geology Department and University extension, the University of Western Australia, pp. 59.

IUPAC, 1989. Recommendations for EPR/ESR nomenclature and conventions for presenting experimental data in publications. Pure and Applied Chemistry, 61: 2195-2200.

Ivey, M.E., 1987. The geology of the Hannan South gold mine, Kalgoorlie, Second Eastern Goldfields Geological Field Conference. Abstracts and Excursion Guide. Geological Society of Australia (Western Australia Division), pp. 118-120.

Johannsen, a., 1958. A descriptive Petrography Vol II Quartz-bearing rocks, 428. University of Chicago Press, Chicago.

Johnston, S.F., Sauter, P.C.C., Hyland, S.J. and Bradley, T., 1990. Mount Percy Gold Deposits. In: F.E. Hughes (Editor), Geology of the Mineral Deposits of Australia and Papua New Guinea. The Australian Institute of Mining and Metallurgy,

Melbourne, pp. 433-437.

Kern, A.M. and Commander, D.P., 1993. Cainozoic stratigraphy in the Roe Palaeodrainage of the Kalgoorlie Region. Western Australia Geological Survey, Report 34, p p. 1-11,

Kaiser, H.F., 1958. The varimax criterion for analytic rotation in factor analysis. Psychometrika, 23: 187-200.

Koerber, B., Capp, S. and Harley, B., 1992. Annual report for exploration leases 1271, 1276 and 1277. No. 08.6098, Billiton Australia Report.

Koritning, S., 1951. Ein Beitra zur Geochemie des Flor. Geochimica el Cosmochima Acta, 1: 89.

Kullerud, G., Steffen, R.M., Simms, P.C. and Rickey, F.A., 1979. Proton-induced X-ray emission (PIXE) - a new tool in geochemistry. Chemical Geology, 25: 245-256.

Levinson, A.A., 1974. Introduction to exploration geochemistry, 2 edition, Applied Publishing, Calgary, Canada, 612 pp.

Lawrance, L.M., 1988. The morphology and geochemistry of supergene gold at Hannan South gold mine, Western Australia. In: A.D.T. Goode, E.L. Smyth, W.D. Birch and L.I. Bosma (Editors), Bicentennial Gold 88. Abstracts Series. Geological Society of Australia, Melbourne, pp. 360-364.

Lintern, M.J., 1989. Study of the distribution of gold in soils at Mt. Hope, Western Australia. restricted Report, 24R. CSIRO Australia, Division of Exploration Geoscience, Perth, 17 pp.

Lintern, M.J. and Butt, C.R.M., 1993. Pedogenic carbonate: an important sampling medium for gold exploration in semi-arid area. Exploration News, CSIRO Australia, Division of Exploration Geoscience, 7: 7-11.

Levinson, A.A., 1974. Introduction to Exploration Geochemistry, Applied Publishing Ltd., 611 pp.

Loughnan, F.C., 1969. Chemical Weathering of the Silicate Minerals. Elsevier, 154 pp.

MacAurthur, J.D., Ma, X.P., 1991. A review of particle induced X-ray emission, Int. PIXE, 1:311-338.

Macknize, B. and Woodall, R., 1987. Mineral Exploration Economics: The Search for Base Metals in Australia and Canada, Center for Resource Studies Wording Paper No. 40 (Queen's University: Kingston, Ontario).

Manheim, F.T., 1978. Mo behavior during weathering and rock alteration. In: K.H. Wedepohl (Editor), Handbook of Geochemistry. Spinger-Verlag, pp. 42-G-1.

Mann, A.W., 1984. Mobility of gold and silver in lateritic weathering profiles: some observations from Western Australia. Economic Geology, 79: 38-49.

Marshall, B., 1967. The present status of zircon. Sedimentology, 9: 965.

Maschmeyer, D. and Lehmann, G., 1983. New hole centers in natural quartz. Physics and Chemistry of Minerals, 10: 84-88.

Matyash, I.V., Brik, A.B., Monakov, V.I. and Derskii, L.I., 1982. Formation of native gold in quartz according to EPR data. Geokhimya: 1048-1051.

Mayer, T.E., 1990. The Granites goldfield. In: F.E. Hughes (Editor), Geology of the Mineral Deposits of Australia and Papua New Guinea, pp719-724.

Mazzucchelli, R.H. and James, C.H., 1966. Arsenic as a guide to gold mineralization in laterite covered areas of Western Australia. Institute of Mining and Metallurgy, B75: 286-294.

Mazzucchelli, R.H., 1997. Geochemical exploration in areas affected by tropical weathering - an industry perspective. In: A.G. Gubbins (Editor), Proceedings of Exploration 97: Fourth Decennial International conference on Mineral Exploration, pp.315-322.

McLaren, J.M. and Thompson, J.A., 1913. Geology of the Kalgoorlie goldfield, Min. Scient. Press., London, No 107.

McMorris, D.W., 1970. ESR detection of fossil alpha damage in quartz. Nature, 22: 146-148.

McQueen, K.G., 1996. Some new styles of gold mineralization in the Lachlan Oroger of Eastern Australia. In: Abstracts, Thirtieth International Geological Congress, 4-14 August 1996, Beijing, China. 2: p 759.

McQueen, K.G. and Gibson, D.L., 1996. Some landscape and regolith features of the Cobar region with implications of mineral exploration. In: Program and Abstracts, Regolith '96, Second Australian Conference on Landscape Evolution and Mineral Exploration, The State of the Regolith, 12-15 November 1996, Brisbane. Cooperative Research Center for Landscape Evolution and Mineral Exploration, Canberra, pp. 37.

McQueen, K.G. and Gibson, D.L., 1997. Landscape, regolith and ore deposit relationships in the Cobar area, NSW. In: New Developments in Research for Ore Deposit Exploration, Third National Conference of the Specialist Group in Economic Geology, Geological Society of Australia, Abstracts No. 44, Sydney, pp. 50.

Michel, D., 1987. Concentration of gold in situ laterites from Mato Grosso. Mineral Deposita, 22: 185-189.

Mikucki, E.J. and Groves, D.I.G., 1990. Mineralogical constraints. In: S.E. Ho, D.I. Groves and J.M. Bennett (Editors), Gold deposits of the Archaean Yilgarn Block: Western Australia: Natue, Genesis and Exploration Guides. Geology Department and University Extension, The University of Western Australia, Perth, pp. 212-220.

Miono, S. and Ono, H., 1992. PIXE analysis technique and its application to geology. Journal of the Geological Society of Sri Lanka, 4: 57-60.

Mueller, A.G. and Harris, L.B., 1987. An application of wrench tectonic models to mineralized structures in the Golden Mile district, Kalgoorlie, Western Australia. In: S. Ho and D.I. Groves (Editors), Recent Advances in Understanding Precambrian Gold Deposits. Geoogy. Department and University Extension, Univ.ersity of Western Australia, pp. 97-107.

Nand, A.S. and van Moort, J.C., 1995. Comparison between EPR spectra and composition of the aqua regia insoluble and aqua regia plus ammonium acetate insoluble residue of diamond drillhole pulp samples from section 30 and section 175 Broken Hill and additional information on the formation of metasomatic quartz formation. Geology Department, University of Tasmania. Report submitted to Pasminco Mining Broken Hill, March 1995, 50 pp.

Nelson, J.H. et al., 1982. Characterization of Carlin-type gold ore by Photoacoustic, Raman, and EPR spectroscopy. Applied Spectroscopy, 36(5): 574-576.

Nicholson, P.M., 1990. Tanami gold deposit. In: F.E. Hughes (Editor), Geology of the Mineral Deposits of Australia and Papua New Guinea. The Australian Institute of Mining and Metallurgy, Melbourne, pp. 715-718.

Oertel, A.C. and Giles, J.B., 1964. Trace element contents of some Queensland soils. Australian Journal of Soil Resources, 1: 215.

Page, R., Sum, S., Blake, D.H., Edgecombe, D.R. and Pearcey, D.P., 1995. Geochronology of an exposed late Archean basement terrane in the Granites-Tanami region: AGSO Research Newsletter, 22: 19-20.

Page, R. and Sun, S., 1994. Evolution of the Kimberley region, W.A. and adjacent Proterozoic Inliers - New geochronological constraints. Geological Society of Australia Abstracts, 37: 332-333.

Page, R., Sun, S., Bake, D.H., Edgecombe, D.R. and Pearcey, D.P., 1995. Geochronology of an exposed late Archean basement terrane in the Granites-Tanami region. AGSO Research Newsletter, 22: 19-20.

Page, R., Sun, S., Bake, D.H., Edgecombe, D.R. and Pearcey, D.P., 1996. Geochronology of an exposed late Archean basement terrane in the Granites-Tanami region, Northern Territory. Geological Society of Australia Abstracts, 41: 334.

Partington, G.A., 1987. The tectonic environments of gold deposition and intrusion of rare-metal pegmatites: implications for Au, Sn and Ta exploration in the Yilgarn Block, Western Australia. In: S.E. Ho and D.I. Groves (Editors), Recent Advances in Understanding Precambrian Gold Deposits. University of Western Australia Publication 11, 67-83

Petrov, I., Agel, A. and Hafner, S.S., 1989. Distinct defect centers at oxygen positions

in albite. American Mineralogist, 74: 1130-1141.

Petrov, I., Mineeva, R.M., Bershov, L.V. and Agel, A., 1993. EPR of $[Pb\text{-}Pb]^{3+}$ mixed valence pairs in amazonite-type microcline. American Mineralogist, 78: 500-501.

Pilbrow, J.R., 1990. Transition ion electron paramagnetic resonance. Oxford Sciences Publication, New York, 688 pp.

Platt, J.P., Allchurch, P.D. and Rutland, R.W., 1978. Archean tectonics in the Agnew supracrustal belt, Western Australia. Precambrian Research, 7: 3-30.

Plumb, K.A., 1990. Halls-Creek Province and the Granites-Tanami Inlier - Regional Geology and mineralization. In: F.E. Hughes (Editor), Geology of the Mineral Deposits of Australia and Papua New Guinea, The Australian Institute of Mining and Metallurgy, Melbourne, pp. 681-694.

Pwa, A., 1996. Application of rock geochemistry and electron paramagnetic resonance of rock in mineral exploration, Rosebery mine area, western Tasmania. unpublished Ph.D. Thesis, University of Tasmania, Hobart, 303 pp.

Reynolds, R.C., 1963. Potassium-rubidium ratios and polymorphism in illites and microclines. Geochmica et Cosmochimia Acta, 27: 1097-1112.

Rimsaite, J.H.Y., 1970. Structural formulae of oxidized and hydroxi-deficient micas and decomposition of the hydroxyl-group. Beitr. Mineral. Petrog., 25: 225.

Robertson, I.D.M., Chaffee, M.A. and Taylor, G.F., 1990. The petrography, mineralogy and geochemistry of a felsic, mafic, ultramafic and metasedimentary weathered profile at Rand pit, Reedy mine - Cue, W.A. 102R, Division of Exploration Geoscience, CSIRO, Wembley, WA, 68 pp.

Robertson, I.D.M., 1996. Ferruginous lag geochemistry on the Yilgarn Craton of Western Australia; practical aspects and limitations. Journal of Geochemical Exploration, 57: 139-151.

Robertson, I.D.M. and Butt, C.R.M., 1997. Atlas of Weathered Rocks, CRC LEME

Robins, G.V., Selley, N.J., McNeil, D.A.C. and Symon, M.C.R., 1981. Manganese (II) as an indicator of ancient heat treatment in flint. Archaemery, 23: 32-332.

Roquin, C., Freyssinet, P., Zeegers, H. and Tardy, Y., 1990. Element distribution patterns in laterites of southern Mali: consequence for geochemical prospecting and mineral exploration. Applied Geochemistry, 5(3): 305-315.

Rose, A.W., Hawkes, H.E. and Webb, J.S., 1979. Geochemistry in Mineral Exploration. Academic Press, London, 657 pp.

Rudowicz, C.Z., 1997. Modern Applications of EPR/ESR-From biophysics to Material Science. Springer, Singapore, pp666.

Russell, D.W., 1995. The characterization of quartz and gold in the Beaconsfield and Letroy areas, Northern Tasmania. Unpublished Ph.D. Thesis, University of

Tasmania, Hobart, 300 pp.

Russell, D.W. and van Moort, J.C., 1997. EPR as an exploration tool to access quartz reefs, Beaconsfiled Gold Mine, Tasmania, Australia. In: C.Z. Rudowicz (Editor), First Asia-Pacific EPR/ESR Symposium. Springer, Hong Kong, pp. 295-303.

Rutland, R.W.R., Etheridge, M.A. and Solomon, M., 1990. The stratigraphic and tectonic setting of the ore deposits of Australia, In: F.E. Hughes (Editor), Geology of the Mineral Deposits of Australia and Papua New Guinea: Melboune, The Australian Institute of Mining and Metallurgy, pp. 15-26.

Ruxton, P.A., 1994. Central desert joint venture geological resource estimate 2. Billiton Australia report No. 08.7024.

Sauter, P.C.C., Hyland, S.J. and Bradley, T., 1988. The Mount Percy gold mine. In: M.E. Groves, S.E. Ho and G.M.F. Hopkins (Editors), Western Australian Gold Deposits. Bicentennial Gold 88 Excursion Guidebook. Geology Department and University Extension, University of Western Australia, pp. 84-86.

Schnadt, R. and Räuber, A., 1971. Motional effects in the trapped-hole center in smoky quartz. Solid State Communication, 9: 159-161.

Shcherbakova, M.Y. et al., 1985. Investigation of EPR spectra of quartz from different types of granitoids. Soviet Geology and Geophysics, 26(9): 82-87.

Shimakowa, K., Imai, N. and Hirota, M., 1984. Dating of volcanic rock by electron spin resonance. Isotope Geoscience, 2: 365-373.

Short, N.M., 1961. Geochemical variations in four residual soils. Journal of Geochemical Exploration., 69: 534.

Shriaki, K., 1978. Chromium. In: K.H. Wedepohl (Editor), Handbook of Geochemistry. Springer-Verlag, II-3, 24-G-1.

Sie, S.H., 1993, Progress of quantitative micro-PIXE application in geology and mineralogy, Nuclear Instrument Method, Physocs Researcj, B75: 403-410.

Smith, R.E. and Anand, R.R., 1990. Geochemical exploration. In: S.E. Ho, D.I. Groves and J.M. Bennett (Editors), Gold Deposits of the Archaean Yilgarn Block, Western Australia: Nature, Genesis and Exploration Guides. Geology Department and University Extension, The University of Western Australia, Perth, pp. 331-336.

Smith, R.E., Anand, R.R. and Alley, N.E., 1997. Use and implications of paleoweathering surfaces in mineral exploration. In: A.G. Gubins (Editor), Exploration 97: Fouth Decennial International Conference on Mineral Exploration, pp. 335-346.

Smith, R.E. and Anand, R.R., 1992. Callion Au deposit, Western Australia. In: G.J.S. Govett (Editor), Handbook of Exploration Geochemistry. Regolith Exploration Geochemistry in Tropical and Subtropical Terrains. Elsevier, pp. 607.

Smith, R.E., Moeskops, P.G. and Nickel, E.H., 1979. Multi-element geochemistry at the Golden Grove Cu-Zn-Ag deposit. In: J.E. Glover, D.I. Groves and R.E. Smith (Editors), Pathfinder and Multi-element Geochemistry in Mineral Exploration. University of Western Australia, Geology Department. Extension Service, Publication 4, pp. 30-41.

Smith, R.E. and Perdrix, J.L., 1983. Pisolitic laterite geochemistry in the Golden rove massive sulphide district, Western Australia. Journal of Geochemical Exploration, 18: 131-164.

Smyth, E.L. and Button, A., 1989. Gold exploration in the Tertiary palaeodrainage systems of Western Australia. In: R.S. Bhappu and R.J. Harden (Editors), Gold Forum on Technology and Practices - World Gold'89. Society for Mining, Metallurgy and Exploration Inc., Littleton, Colorado, Reno, Nevada, pp. 1-11.

Spry, M and McQueen, K, 1997. An approach to understanding the regolith-landform features of the Cobar region. In: New Approaches to an Old Continent, Programs and Abstracts, Regolith'98, 3rd Australian Regolith conference, 2-9 May 1998, Kalgoorlie, pp. 60.

Stott, C., 1994. A regolith study of the Jim's South gold anomaly, Tanami Desert, Northern Territory. Unplublished Honours Thesis, University of Tasmania, Hobart, 137 pp.

Stott, C., Xu Li, butt, C.R.M., Bailey, G.M. and van Moort, J.C., 1998. Gold and associated elements in the lateritic regolith at Jim's Find South, Tanami Desert, Northern Territory, Australia. In. Xie Xuejing (Editor), Geochemistry, Proceedings of the 30th International Geological Congress.19: 241-256.

Sund, J.O., Schwabe, M.R., Hamlyn, D.A. and Bonsall, E.M., 1984. Gold mineralization at the north end of the Kalgoorlie field, Mount Percy-Kalgoorlie, Western Australia, Gold-Minig, Metallurgy and Geology, Regional Conference, Kalgoorlie, 1984. The Australian Institute of Mining and Metallurgy: Melbourne, pp. 397-404.

Swager, C.P., Griffin, T.J., Witt, W.K., Wyche, S., Ahmat, A.L., Hunter, W.M. and McGoldrick, 1990. Geology of the Archaean Kalgoorlie Terrane - an Explanatory Note, Geological Survey of Western Australia Report 48.

Taylor, G., 1997. Educating explorationists in a regolith dominated continent. Journal of Geochemical Exploration, 28(1): 29-36.

Travis, G.A., Woodall, R. and Bartram, G.D., 1971. The geology of the Kalgoorlie goldfield. In: J.E. Glover (Editor), Symposium on Archean Rocks. Special Publication 3, Geological Society of Australia, Sydney, pp. 175-190.

Tröger, W.E., 1979. Optical Determination of Rock-Forming Minerals. Part1 Determinative Tables. E. Schweizerbart'sche Verlagsbuchhandlung.

Tulhoat, A., Courel, P., Trocellier, P. and Gosset, J., 1993. Stability and distribution

of lithium and boron in minerals. Nuclear Instruments Methods in Physics Research, B77: 436-443.

Tunks, A.J., 1996. Geology of the Tanami Gold Mine, Northern Terrotory. Unpublished Ph.D. Thesis, University of Tasmania, Hobart, 214 pp.

Turekian, K.K., 1978. Ni behavior during weathering. In: K.H. Wedepohl (Editor), Handbook of Geochemistry. Springer-Verlag, pp. 38.

Turton, A.G. and Marsh, N.L., 1962. The chemistry and mineralogy of lateritic soils in the southwest of Western Australia. No. 8/61, Commonwealth Science and Industry Research Organization., Division of Soils.

Twidale, C.R., 1990. The origin and implication of some erosional landforms. Journal of Geology, 98(3): 343-364.

van Moort, J.C., 1986. Electron spin resonance spectra of quartz as guide to mineralization. In R. Lare (Editor), the Mount Read Volcanics and associate Ore Deposits, Geological Society of Australia. Tasmania division, 85pp.

van Moort, J.C., 1987. Electron Paramagnetic resonance powder spectra of natural vein quartz in Tasmania, especially related to mineralization., Pacific Rim Congress 87. Institute of Mineral and Metallurgy, Australia, pp. 437-444.

van Moort, J.C. and Russell, D.W., 1987. Electron spin resonance of auriferous and barren quartz at Beaconsfield, Northern Tasmania. Journal of Geochemical Exploration, 27: 227-237.

van Moort, J.C., 1989. The use of EPR powder spectra for the characterization of vein quartz, Advances in the study of the Sydney Basin, Sydney, pp. 271-278.

van Moort, J.C, Cohen, D.D., Russell, D.W. and Katsaros, A., 1990. Correlation between chemical compositions as determined by PIXE and the paramagnetism of auriferous vein quartz. Nuclear Instrument Methods, Physics. Research, B49: 323-327.

van Moort, J.C. and Barth, W.H., 1992. The application of electron paramagnetic defects to the characterization of vein quartz. In: T. Guanzhi, X. Keqin and Q. Yuzhao (Editors), Petrogenesis and Mineralization of Granitoids. Science Press, Beijing, pp. 1072-1086.

van Moort, J.C., Hotchkiss, M.A.C. and Aung Pwa, 1995. EPR spectra and lithogeochemistry of jasperoids at Carlin, Nevada: distinction between auriferous and barren rocks. Journal of Geochemical Exploration, 55: 227-237.

van Moort, J.C. and Xu Li, 1997. A PIXE/PIGE study of gold mineralization in lateritic terrain, Tanami desert, Australia, In. Conference Handbook, ANA97, Second conference on Nuclear Science and Engineering in Australia, 1997, 16-17 October 1997, Sydney.

van Moort, Xu Li, Aung Pwa, Bailey, G.M., Russell, D.w. and Butt, C.R.M., 1999. The use of acid insoluble residue of rock powders as a sample medium in the

recognition of primary wall rock alteration patterns of gold mineralization in regolith, In: Taylor, G and Pain, C.F. (Editors), The State of teh Regolith, Geol. Soc. Australian Special Pub. 20:69-78.

Vearncombe, J.R., Barley, M. E., Eisenlohr, B., Grigson, M.W., Groves, D.I., Houstoun, S.M., Partington, G.A. and Skwarnecki, M.S., 1988. Structural controls on gold mineralization: examples from the Archaean terranes of Western Australia and southern Africa. Bicentennial Gold 88, Extended Abstracts, Geological Society of Australia Abstract 22, 19-23.

Watkins, K.P., Tyler, I.M. and Hickman, A.H., 1987. Explanatory notes on the Cue 1:250,00 geological sheet Western Australia. Geological Survey of Western Australia, 31 pp.

Watkins, K.P. and Hickman, A.H., 1988. The Murchison Province: Stratigraphy, Structure and Mineralization. Geological Survey of Western Australia, Bulletin. 137 Plate 2.

Watkins, K.P. and Hickman, A.H., 1990a, Geology of the Murchison Province granite-greenstone terrain, Western Australia. In: S.E. Ho, J.E. Gloves, J.S. Myers and J.R. Muhling (Editors), Excursion Guidebook. Third International Archaean Symposium, Perth, 1990. Western University Publication No. 21, 147-201.

Watkins, K.P. and Hickman, A.H. 1990b. Geological Evolution and mineralization of the Murchison Province, Western Australia. Geological Survey of Western Australia, Bull. 137, 287pp.

Wedepohl, K.H., 1978. Lead Behavior during Weathering and Rock Alteration. In: K.H. Wedepohl (Editor), Handbook of Geochemistry. Springer-Verlag, pp. 82-G-1.

Weil, J.A., 1984. A review of electron spin spectroscopy and application to the study of paramagnetic defects in quartz. Physics and Chemistry of Minerals, 10(149-165).

Whitten, D.G.A. and Brooks, J.R.A., 1972. The Penguin Dictionary of Geology. Penguin Books, Harmondsworth, England.

Woodall, R., 1965. Structure of the Kalgoorlie Goldfield. In: J. McAndrew (Editor), Geology of Australian Ore Deposits. 8th Commonwealth Mining and Metallurgy Congress, Melbourne, pp. 71-79.

Woodall, R., 1995. Exploration: the life-blood of a mining company. The AusIMM Bulletin (No. 1, February): 62-67.

Wright, J.H., Eshurs, E. and Anand, R., 1998. Bronzewing-the role of regolith-landform control and regolith geochemistry in the discovery of a large gold deposit, Regolith'98 New Approach to an Old continent Program and Abstracts. CRC LEME, Kalgoorlie.

Xie, X. and Yan, M., 1989. Geochemical standard reference samples GSD9-12, GSS1-

8 and GSR1-6. Geostandards Newsletter, 13: 83-179.

Xu, Li. and Zhang, Y.G., 1987. Rapid XRF determination of 24 elements in geochemical samples, Physical Testing and Chemical Analysis, Part B, Chem. Anal., 23:100-116.

Xu, Li., 1989a. Background correction for the determination of 14 trace elements in soil. Rock and Mineral Analysis, 8: 46-51.

Xu, L.i, 1989b. Optimization of working conditions in X-ray fluorescence analysis of geochemical prospecting samples. Geoscience Exploration 2: 60-74.

Xu, Li., 1996. Application of PIXE/PIGME analysis in exploration geochemistry, 30th International Geological Congress, Beijing, pp. 64.

Xu Li and van Moort, J.C., 1997a. A PIXE/PIGE study of lateritic gold mineralization from the regolith of the Mystery Zone, Mt Percy, Western Australia, The 10th AINSE Conference on Nuclear Techniques of Analysis, Abstracts, November, 1997, Canberra, pp. 23-26.

Xu Li and van Moort, J.C., 1997b. EPR as a tool in gold exploration. Unpublished internal report, Geology Department, University of Tasmania, 15pp.

Xu Li, Butt, C.R.M. and van Moort, J.C., 1997. Electron paramagnetic resonance (EPR) as a tool in gold exploration. In. He Zhenhua (Editor), Engineering and Environmental Geophysics for the 21st Century, Sichuan Publishing House of Science and Technology, pp. 206-212.

Xu Li and van Moort, J.C., 1998a. The distribution of EPR data, gold and associated elements in weathered terrain, two case studies from the goldfields of Western Australia. Unpublished internal report, Geology Department, University of Tasmania, 32pp.

Xu, Li and van Moort, J.C., 1998b. EPR characterization of gold mineralization inweathered terrain, Jim's find South, Tanami Desert, N.T., Australia. In. C.A. Rudowica (Editor), Modern Application of EPR/ESR - from Biophysics to Materials Science, Springer, Singapore, pp. 141-148.

Yim, W.S., 1997. ESR measurement of alluvial zircons as an aid to provenance determination in geology. In: C.A. Rudowica (Editor), First Asia-Pacific EPR/ ESR Symposium. Springer, Hong Kong, pp. 128-134.

Yip, K.L. and Fowler, W.B., 1975. Electronic structure of E' centers in SiO_2. Physics Review, B11: 237-238.

Zeegers, H., Goni, J. and Wihelm, E., 1981. Geochemistry of lateritic profiles over a disseminated Cu-Mo mineralization in Upper Volta (West Africa) preliminary results. In: M.K. Roychowdhury, B.P. Radhakrishna, R. Vaidyanadhan, P.K. Banerjee and K. Ranganathan (Editors), Lateritisation Processes. Balkema Publishers, Rotterdam, pp. 359-368.

APPENDIX 1

SAMPLE ANYLYSES INFORMATION, MYSTERY ZONE MT. PERCY, W.A

SAMPLE	Unique sample identifier given to open pit samples
ROCK TYPE	General rock description. As=Talc chlorite ultra mafic, Af=Porphyry, Asf=Fuchsite ultramafic, Ast= Talc ultramafic
REGO TYPE	Ak=Calcareous soil, L=Laterite, Lk=Calcareous laterite, M=Mottled zone, Mc=Mottled clay, C=Plasmic clay, Sc= Clay saprolite
EASTING	Coordinated for sample locality
R.L.	Reduced level
AU (NAA)	Gold data analzed by NAA (from Butt, 1991)

Sample	Easting	RL	Unit	Rego	Au(NAA)	F	NA	AL	SI	S
MW 0001	445.0	400.0	Asf	Ak	1060	2931	813	16091	330532	64
MW 0006	440.0	400.3	Asf	Ak	1240	2582	1286	17612	301788	83
MW 0014	432.0	400.7	Asf	Ak	1520	2857	902	28995	299709	198
MW 0028	418.0	401.5	Asf	Ak	410	1636	907	20433	291724	499
MW 0041	405.0	402.3	Asf	Ak	2210	2233	1426	16180	312612	65
MW 0048	397.0	402.7	Asf	Lk	1320	1458	1195	35023	342271	167
MW 0115	432.0	400.0	Asf	Lk	1320	3823	1402	8566	337520	47
MW 0129	418.0	400.0	Asf	Lk	735	1380	100	49154	229780	520
MW 0142	405.0	400.0	Asf	Lk	460	1858	152	21180	323016	316
MW 0161	383.0	403.1	Asf	Lk	696	1612	1362	17241	298499	693
MW 0167	377.0	403.5	Asf	Lk	2120	2413	649	16099	323078	751
MW 0173	371.0	404.1	Asf	Lk	1540	2441	657	12597	292041	600
MW 0179	365.0	404.5	Asf	Lk	2060	1601	276	9603	308953	706
MW 0184	359.0	405.0	Af	L	450	1351	862	16193	229355	139
MW 0258	346.0	405.5	Asf	Lk	61	1502	196	30392	106191	405
MW 0266	338.0	405.8	Asf	Lk	150	1412	331	32581	82296	408
MW 0270	334.0	406.1	Asf	Lk	360	1771	252	31968	96256	738
MW 0276	328.0	406.4	Asf	Lk	90	1818	134	30253	93269	532
MW 0285	319.0	406.9	Asf	Lk	470	2071	653	19040	201378	397
MW 0407	352.0	402.4	Af	Lk	380	1600	380	33215	218168	1061
MW 0413	346.0	403.1	As	Lk	420	1509	115	16000	175126	525
MW 0417	342.0	403.3	As	Lk	621	2979	108	12648	168247	422
MW 0421	338.0	403.4	As	Lk	120	2105	241	7331	87411	451
MW 0431	328.0	403.8	As	Lk	230	1931	193	6840	116850	749
MW 0440	319.0	404.2	As	Lk	614	2643	202	8648	231577	729
MW 0445	314.0	404.4	As	Lk	190	1738	158	14824	182778	586
MW 0531	398.0	400.0	Asf	Mc	240	2213	384	75489	226569	232
MW 0537	392.0	400.0	Asf	Sc	100	2019	202	26056	320592	924
MW 0541	388.0	400.0	Asf	Sc	53	1749	168	25620	319401	960
MW 0545	384.0	400.0	Asf	Mc	340	2340	253	26298	313618	244
MW 0549	380.0	400.0	Asf	C	74	1846	27	8493	330164	66
MW 0553	376.0	400.0	Asf	C	58	3710	195	27591	302706	82
MW 0559	370.0	400.0	Asf	C	64	1664	248	26999	320903	192
MW 0565	364.0	400.0	Asf	C	24	2389	453	24464	336672	28
MW 0576	353.0	400.0	Af	C	16	2188	137	44887	308875	1071
MW 0701	319.0	397.0	As	M	160	1885	458	63776	260140	136
MW 0706	324.0	397.0	As	M	1600	1461	153	77608	278547	473
MW 0710	328.0	397.0	As	M	44	1314	124	97079	251616	289
MW 0720	338.0	397.0	Ast	Mc	9	1407	0	66324	287025	249
MW 0724	342.0	397.0	As	Mc	62	1641	0	71657	260503	3993
MW 0741	359.0	397.0	Af	Mc	38	1498	270	64072	266788	609
MW 0746	364.0	397.0	Af	C	39	1544	441	38410	304553	4655
MW 0752	370.0	397.0	Asf	M	41	1439	459	38116	311622	235
MW 0758	376.0	397.0	Asf	Sc	160	1573	285	30894	312553	586
MW 0762	380.0	397.0	Asf	Sc	41	1678	145	27470	314455	1176
MW 0766	384.0	397.0	Asf	Sc	360	1339	88	17048	340961	972
MW 0770	388.0	397.0	Asf	Sc	83	1508	120	21853	300231	1758
MW 0774	392.0	397.0	Asf	C	3	1693	126	51250	279028	1704
MW 0780	398.0	397.0	Asf	Mc	170	1641	378	52478	274647	164
MW 0807	425.0	397.0	Asf	Mc	58	1907	223	23304	285728	481
MW 0814	432.0	397.0	Asf	Mc	29	1350	120	20012	336490	1564
MW 0822	440.0	397.0	Asf	M	56	1300	119	19088	333450	1456
MW 0954	328.0	395.0	As	Sc	3	956	0	90234	229814	320
MW 0959	333.0	395.0	As	Sc	3	1499	0	76652	265725	9021
MW 0964	338.0	395.0	As	Sc	18	1979	0	54579	280847	625
MW 0968	342.0	395.0	As	Sc	17	1330	45	65365	220914	50387
MW 0972	346.0	395.0	As	Sc	18	1473	0	68349	257784	19099
MW 0978	352.0	395.0	As	Sc	16	1150	89	72600	274997	2346
MW 0984	358.0	395.0	Asf	Sc	400	971	258	47417	274296	2586
MW 0990	364.0	395.0	Af	Sc	69	2033	515	40342	286222	4574
MW 0996	370.0	395.0	Asf	Sc	25	1242	255	23550	321502	134
MW 1002	376.0	395.0	Asf	Sc	23	878	268	27735	310040	652
MW 1006	380.0	395.0	Asf	Sc	21	1587	142	23977	326567	975
MW 1010	384.0	395.0	Asf	Sc	67	1475	84	19429	337602	5775
MW 1018	392.0	395.0	Asf	Sc	360	1698	170	29819	315298	799
MW 1026	400.0	395.0	Asf	Sc	44	1241	111	17924	325597	2159
MW 1032	405.0	395.0	Asf	Mc	64	2030	64	85034	258259	398
MW 1038	412.0	395.0	Asf	Mc	130	1548	51	53556	299999	3760
MW 1044	418.0	395.0	Asf	Mc	28	2015	30	25274	311810	886

Sample	Easting	RL	Unit	Rego	Au(NAA)	F	NA	AL	SI	S
MW 1051	425.0	395.0	Asf	Sc	24	1354	119	19088	337290	1564
MW 1102	324.0	392.5	As	Sc	3	1536	49	90785	253267	430
MW 1106	332.0	392.5	As	Sc	3	1376	64	71442	275035	747
MW 1109	338.0	392.5	As	Sc	13	2131	41	79006	263142	471
MW 1116	352.0	392.5	As	Sc	13	917	60	63362	271746	353
MW 1118	356.0	392.5	Asf	Sc	78	922	60	33237	320458	210
MW 1122	364.0	392.5	Af	Sc	86	2195	438	36581	279882	15830
MW 1125	370.0	392.5	Asf	Sc	32	963	234	22558	323825	81
MW 1128	376.0	392.5	Asf	Sc	230	1564	159	13950	339631	4620
MW 1133	386.0	392.5	Asf	Sc	490	1584	142	25608	282290	513
MW 1136	392.0	392.5	Asf	Sc	390	1253	175	26230	321159	438
MW 1138	396.0	392.5	Asf	Sc	78	1962	271	47551	288371	4810
MW 1140	400.0	392.5	Asf	Sc	160	1707	0	2597	349521	2883
MW 1143	406.0	392.5	Asf	Sc	55	2338	49	5543	357082	7215
MW 1149	418.0	392.5	Asf	Sc	18	1942	79	2130	292508	12064
MW 1210	358.0	390.0	Af	Mc	44200	1335	166	9472	324182	1379
MW 1213	364.0	390.0	Af	S	682	253	23	0	358951	501
MW 1216	370.0	390.0	Asf	Sc	2420	872	210	17986	345762	549
MW 1223	384.0	390.0	Asf	Sc	25	1855	97	14316	325386	12191
MW 1276	328.0	387.5	Ast	Sc	3	1894	48	6127	313265	32647
MW 1285	346.0	387.5	As	S	3	1854	114	1950	339715	5257
MW 1287	350.0	387.5	As	S	100	1732	125	8242	324993	7187
MW 1288	352.0	387.5	Asf	S	52	1734	510	30965	322883	1645
MW 1290	356.0	387.5	Af	S	43	2121	359	23307	262945	43193
MW 1294	364.0	387.5	Asf	S	1370	829	438	13671	260569	55741
MW 1297	370.0	387.5	Asf	S	7100	1707	351	28416	307949	6025
MW 1300	376.0	387.5	Asf	S	450	1219	222	33624	304491	572
MW 1302	380.0	387.5	Asf	S	130	1523	148	16901	277471	17758
MW 1305	386.0	387.5	Asf	S	7330	1037	136	19639	332162	1154
MW 1307	390.0	387.5	Asf	S	961	770	148	24086	297022	1040
MW 1309	394.0	387.5	Asf	S	54	1430	158	23851	320358	4052
MW 1312	400.0	387.5	Asf	S	508	1792	124	19705	306907	6869
MW 1315	406.0	387.5	Asf	S	110	976	148	18175	288475	36112
MW 1318	412.0	387.5	Af	S	717	2631	331	40709	284664	16885
MW 1321	418.0	387.5	Af	S	210	2543	356	38042	262089	30086
MW 1449	346.0	382.5	Ast	S	3	2309	0	615	345268	1020
MW 1452	352.0	382.5	As	S	130	1229	159	12274	326132	8429
MW 1455	358.0	382.5	Ast	S	1260	1102	181	14429	336584	2461
MW 1460	368.0	382.5	Asf	S	2150	2163	274	27556	311942	2202
MW 1461	370.0	382.5	Asf	S	3230	944	484	40789	286811	1248
MW 1463	374.0	382.5	Asf	S	200	1229	400	24847	240045	53105
MW 1468	384.0	382.5	Asf	S	39	1019	176	23668	307384	11193
MW 1470	388.0	382.5	Asf	S	1020	1514	198	33273	289828	5251
MW 1471	390.0	382.5	Asf	S	260	1153	270	34560	293775	1838
MW 1473	394.0	382.5	Asf	S	260	1157	239	31325	296508	18904
MW 1476	400.0	382.5	Asf	S	71	2252	90	8073	327387	1159
MW 1479	406.0	382.5	Asf	Sc	87	614	97	2554	341959	5634
MW 1481	410.0	382.5	Asf	S	18	1793	83	5898	348162	1991
MW 1517	337.0	380.0	Ast	S	3	2185	0	1774	324472	8147
MW 1519	341.0	380.0	Ast	S	3	2472	55	12581	265122	16083
MW 1521	345.0	380.0	Ast	S	3	2321	0	3004	314029	8483
MW 1524	351.0	380.0	Ast	S	3	1186	101	1160	346543	6712
MW 1526	355.0	380.0	Asf	S	16	889	123	4977	346813	752
MW 1527	357.0	380.0	Af	S	795	1395	453	29362	320891	1198
MW 1530	363.0	380.0	Af	S	2270	2277	331	29759	314857	6090
MW 1533	369.0	380.0	Asf	S	1450	1604	299	25458	306209	1017
MW 1534	371.0	380.0	Asf	S	400	644	380	23004	294453	13413
MW 1536	375.0	380.0	Asf	S	3	1923	309	31052	300528	10257
MW 1537	377.0	380.0	Asf	S	140	1340	230	27008	295793	1931
MW 1539	381.0	380.0	Asf	S	140	1712	131	27755	313317	2229
MW 1542	387.0	380.0	Asf	S	150	1227	199	30024	320104	3606
MW 1545	393.0	380.0	Asf	S	280	1613	166	16830	298267	2936
MW 1548	399.0	380.0	Asf	S	2090	1663	141	21367	302693	577
MW 1586	343.0	375.0	Ast	S	12	2556	84	1835	266650	3097
MW 1590	351.0	375.0	Ast	S	3	1844	41	1651	310871	3616
MW 1592	355.0	375.0	Asf	S	14	1174	134	6647	337348	1170
MW 1596	363.0	375.0	Af	S	644	2077	363	38905	302614	1859
MW 1597	365.0	375.0	Af	S	3	1210	307	28730	268721	31372
MW 1599	369.0	375.0	Asf	S	290	1994	338	39489	302050	5370

Sample	Easting	RL	Unit	Rego	Au(NAA)	F	NA	AL	SI	S
MW 1600	371.0	375.0	Asf	S	390	466	555	24302	328949	135
MW 1603	377.0	375.0	Asf	S	1560	1270	324	28822	317380	4721
MW 1604	379.0	375.0	Asf	S	330	893	129	27336	246627	42809
MW 1605	381.0	375.0	Asf	S	2010	1674	291	40002	288183	456
MW 1608	387.0	375.0	Asf	S	230	1231	175	35187	302363	697
MW 1609	389.0	375.0	Asf	S	66	1414	142	22984	309559	2262
MW 1611	393.0	375.0	Asf	S	590	1433	135	25864	321281	5001
MW 1614	399.0	375.0	Asf	S	200	1781	123	13847	295045	1442
MW 1616	403.0	375.0	Asf	S	160	659	118	1678	332089	1443
MW 1617	347.0	370.0	Asf	S	3	3014	0	1797	285951	1705
MW 1619	351.0	370.0	Asf	S	23	174	1408	15597	287549	3202
MW 1621	355.0	370.0	Asf	S	390	2774	0	0	303602	366
MW 1623	359.0	370.0	Asf	S	597	525	438	36204	291853	7796
MW 1625	363.0	370.0	Af	S	79	558	407	56305	270766	5501
MW 1628	369.0	370.0	Af	S	23	617	307	65657	259184	7343
MW 1630	373.0	370.0	Af	S	6480	389	285	77074	237876	16691
MW 1632	377.0	370.0	Asf	S	34	149	190	18034	333077	3599
MW 1635	383.0	370.0	Asf	S	300	409	476	31037	281859	229
MW 1637	387.0	370.0	Asf	S	220	382	338	33702	293280	2857
MW 1640	393.0	370.0	Asf	S	460	285	205	29103	279093	17681
MW 1642	397.0	370.0	Asf	S	160	311	198	34647	289694	16584
MW 1692	354.0	365.0	As	S	30	245	107	727	320718	2885
MW 1693	356.0	365.0	Asf	S	23	239	2828	8058	313355	1024
MW 1703	376.0	365.0	Asf	S	12	134	456	36909	289383	31739
MW 1707	384.0	365.0	Asf	S	210	305	250	36926	255514	22195
MW 1711	392.0	365.0	Asf	S	15	351	529	50426	286048	749
MW 1714	398.0	365.0	Asf	S	28	293	182	43550	295220	1109
MW 1716	402.0	365.0	Asf	S	3880	285	164	31794	294690	9898
MW 1718	406.0	365.0	Asf	S	1760	266	163	30987	293676	9736
MW 1721	412.0	365.0	Af	S	502	520	31692	63122	241417	11234
MW 1722	364.0	360.0	Af	S	913	479	28613	60625	276595	4973
MW 1723	365.0	357.5	Af	S	1250	499	28581	59893	276590	1888
MW 1733	370.0	357.5	Af	S	300	419	26498	56546	287376	5298
MW 1734	370.0	360.0	Af	S	2090	575	19697	61708	272048	12466
MW 1745	376.0	357.5	Asf	S	520	196	12657	34929	285422	11821
MW 1758	384.0	360.0	Asf	S	100	278	416	29319	269728	24235
MW 1759	385.0	357.5	Asf	S	410	243	1199	32627	306292	7115
MW 1766	392.0	360.0	Asf	S	120	305	312	44090	296360	1965
MW 1767	393.0	357.5	Asf	S	200	296	468	39331	302513	1948
MW 1840	312.5	363.0	As	S	15	103	82	11915	298063	39221
MW 1841	318.5	355.0	As	S	9	108	75	1189	331764	694
MW 1866	371.0	350.0	Af	S	602	300	22364	57827	238591	21721
MW 1867	372.0	347.5	Asf	S	423	272	8542	33417	308621	245
MW 1870	373.0	350.0	Asf	S	927	184	2172	28599	318880	3303
MW 1871	374.0	347.5	Asf	S	429	102	5503	18487	310021	12762
MW 1874	375.0	350.0	Asf	S	422	170	15828	27684	324064	7638
MW 1875	376.0	347.5	Asf	S	652	183	17039	32020	309577	688
MW 1884	380.0	350.0	Asf	S	360	163	15312	28703	308913	869
MW 1885	381.0	347.5	Asf	S	269	167	12632	20639	332543	3199
MW 1894	385.0	350.0	Asf	S	516	271	9339	26954	293757	21291
MW 1895	386.0	347.5	Asf	S	1070	283	13848	38743	304121	2574
MW 1901	389.0	347.5	Asf	S	267	174	13133	39307	292204	799
MW 1937	388.0	347.5	Af	S	517	454	37395	58519	285561	3759
MW 1990	388.0	350.0	Asf	S	794	276	5577	33515	297524	960

Sample	CL	K	CA	TI	V	CR	MN	FE	NI	CU
MW 0001	516	7009	905	3994	42	78	40	2304	17	2
MW 0006	330	7047	819	5196	98	34	30	1949	12	3
MW 0014	280	11109	767	4600	135	870	32	2716	38	3
MW 0028	365	2683	344	31622	464	137	111	20427	32	4
MW 0041	422	2613	786	10274	151	572	78	3803	40	3
MW 0048	211	7584	669	14103	279	943	71	7354	111	3
MW 0115	674	2504	989	9193	91	189	36	2057	8	2
MW 0129	210	258	83	5290	14	1108	263	177834	607	26
MW 0142	279	4462	106	5383	74	1311	23	17065	153	6
MW 0161	263	2817	476	42999	794	361	169	53760	24	9
MW 0167	532	1789	1119	9791	204	281	79	3013	27	4
MW 0173	174	1471	453	32062	594	67	151	11635	16	3
MW 0179	216	2951	319	30402	567	304	64	5198	13	2
MW 0184	617	2008	182	102472	1535	0	516	69505	9	3
MW 0258	1138	185	83	200204	2717	0	666	219416	19	0
MW 0266	1019	305	50	241694	2592	0	708	193972	34	0
MW 0270	1276	118	56	271612	2263	0	858	148767	25	1
MW 0276	1112	112	46	250445	2106	0	894	150397	22	0
MW 0285	994	858	196	151096	1645	0	490	68425	30	0
MW 0407	737	433	1	135643	1803	0	1064	75388	113	14
MW 0413	926	359	74	171317	2185	0	1148	185856	40	6
MW 0417	648	72	64	129742	1689	0	560	128825	16	3
MW 0421	1237	170	34	272337	2108	0	854	155349	28	3
MW 0431	1149	98	100	240165	1920	0	1059	172249	20	7
MW 0440	1044	144	140	179533	1349	0	729	59447	9	5
MW 0445	887	123	98	167913	2040	0	927	197174	17	8
MW 0531	311	34328	220	8856	361	4998	47	17833	407	7
MW 0537	198	16880	166	3153	117	2818	14	5408	141	2
MW 0541	182	16666	210	3460	126	1859	8	4772	93	2
MW 0545	205	13367	201	5795	190	1706	33	4257	63	1
MW 0549	389	1516	56	4773	104	446	9	1077	34	0
MW 0553	437	12788	146	7663	288	874	12	4746	34	2
MW 0559	247	16281	158	2966	165	2857	18	4195	92	1
MW 0565	253	10329	113	4027	145	1381	0	694	12	2
MW 0576	288	529	7	53065	1045	125	325	15158	134	8
MW 0701	232	15006	157	19243	363	100	75	9258	43	4
MW 0706	268	191	11	11385	179	375	24	4180	133	6
MW 0710	148	303	41	13855	206	449	48	6361	160	8
MW 0720	590	177	65	17010	305	641	30	3375	172	6
MW 0724	243	236	16	19536	366	511	59	4994	150	3
MW 0741	256	9376	103	6797	174	1004	13	2558	62	4
MW 0746	85	19244	177	4211	131	330	10	2511	19	7
MW 0752	326	14532	132	5381	200	1521	27	2390	40	2
MW 0758	240	13731	123	4394	153	2489	24	3841	83	0
MW 0762	180	10767	100	5334	169	1854	25	4452	64	0
MW 0766	256	6328	100	2920	127	1284	8	1584	30	0
MW 0770	241	13940	129	2552	166	1702	2	4095	81	2
MW 0774	153	4476	66	9389	180	451	17	4574	43	1
MW 0780	154	27675	224	5226	217	3939	36	10312	293	0
MW 0807	298	8953	116	3247	110	1475	10	2356	99	2
MW 0814	67	5877	99	3254	37	1042	3	1533	58	2
MW 0822	77	5862	89	3344	39	1033	2	1503	55	3
MW 0954	255	93	28	9030	79	602	17	5309	61	4
MW 0959	61	197	10	9639	146	648	30	7058	88	8
MW 0964	372	240	7	9550	128	335	6	3241	92	4
MW 0968	0	303	31	7094	111	362	14	4883	145	5
MW 0972	0	547	4	9434	163	376	23	4004	163	6
MW 0978	70	537	17	8137	145	569	16	3521	146	1
MW 0984	21	11415	147	4574	174	1269	0	2350	44	3
MW 0990	175	21465	134	3722	92	160	7	3234	21	4
MW 0996	223	14248	142	3107	181	3072	12	3601	71	0
MW 1002	99	17532	121	2175	193	3881	15	2911	75	1
MW 1006	164	9706	112	4191	182	1046	0	3637	37	0
MW 1010	128	6568	94	3402	156	1447	3	1524	30	0
MW 1018	320	20444	167	3418	190	3088	15	7407	166	5
MW 1026	138	7643	88	2953	166	1286	24	2275	64	2
MW 1032	426	2090	39	7098	112	1253	20	3467	427	12
MW 1038	170	717	41	7956	88	656	1	2918	178	7
MW 1044	165	245	8	5034	39	277	6	3340	177	5

Sample	CL	K	CA	TI	V	CR	MN	FE	NI	CU
MW 1051	76	5878	98	3265	39	1058	2	1503	55	3
MW 1102	200	162	21	7619	94	705	6	5744	76	5
MW 1106	193	180	23	6927	122	558	17	3874	54	5
MW 1109	396	260	3	7896	106	1107	0	4049	98	3
MW 1116	222	363	34	5921	64	464	12	3916	65	4
MW 1118	176	1360	42	3936	58	407	10	1909	64	18
MW 1122	251	18690	177	3826	91	161	6	4406	26	4
MW 1125	137	13172	156	2598	132	2416	2	2441	44	2
MW 1128	221	6522	54	2905	107	2615	10	1680	35	2
MW 1133	246	12443	145	3770	185	1922	12	3354	57	1
MW 1136	170	18058	179	2816	188	2246	14	5741	119	2
MW 1138	85	32186	264	4687	327	5099	39	10942	312	5
MW 1140	490	1311	41	2955	63	317	19	1034	25	0
MW 1143	72	1219	10	8255	125	385	9	1188	28	0
MW 1149	392	129	29	2963	42	143	15	9067	521	7
MW 1210	450	5661	38	2445	24	64	7	493	4	5
MW 1213	96	84	1	235	0	2	4	59	5	1
MW 1216	101	11691	135	1721	85	1760	11	1232	30	1
MW 1223	391	7846	100	3381	126	1017	0	1794	14	2
MW 1276	0	112	66	7004	72	198	9	6276	29	5
MW 1285	232	528	39	4611	50	195	7	2214	10	1
MW 1287	384	4306	57	3496	61	373	5	956	9	3
MW 1288	367	17308	184	3732	152	2041	4	1293	15	3
MW 1290	291	11633	137	3623	97	85	10	1841	3	4
MW 1294	0	9889	106	2066	72	1208	25	17693	55	16
MW 1297	95	15008	157	4731	195	1542	12	3604	42	2
MW 1300	214	22042	183	2811	191	2389	30	5510	113	4
MW 1302	254	8549	51	3378	116	1813	3	3164	64	2
MW 1305	199	15204	151	2273	111	1902	14	5747	126	2
MW 1307	118	16218	128	2291	150	2681	5	6229	133	2
MW 1309	183	16183	161	3170	102	2525	0	6633	142	3
MW 1312	71	12418	149	2257	117	2510	0	6762	175	3
MW 1315	0	10720	101	1774	92	1576	95	20082	115	22
MW 1318	356	23061	183	7662	288	74	26	10361	34	9
MW 1321	325	19244	136	7675	251	21	23	7901	25	11
MW 1449	233	185	71	13621	208	97	8	754	11	2
MW 1452	52	6539	96	2393	50	740	17	3646	21	5
MW 1455	153	7964	53	2286	55	868	6	1012	13	3
MW 1460	441	14793	274	2949	127	1999	2	1946	38	0
MW 1461	119	23288	238	2885	140	2868	13	1576	46	2
MW 1463	0	20912	198	2534	112	2303	13	2917	52	9
MW 1468	151	11682	138	2728	126	1475	18	3254	46	3
MW 1470	110	21084	224	2782	128	3000	16	5656	145	3
MW 1471	75	19582	153	2678	182	2585	24	8288	179	3
MW 1473	57	19593	141	2831	167	2526	30	7893	172	4
MW 1476	448	4160	115	2846	31	1337	32	8399	554	7
MW 1479	9	134	19	2508	50	173	9	917	22	3
MW 1481	137	2915	16	3958	95	669	2	1414	15	2
MW 1517	155	62	33	3207	0	121	127	17994	579	5
MW 1519	116	133	44	3357	38	245	143	23066	589	6
MW 1521	151	108	44	7149	75	109	32	5998	116	4
MW 1524	196	270	23	4507	54	63	2	969	14	1
MW 1526	145	2431	33	2314	32	224	1	766	8	2
MW 1527	184	14734	164	4090	146	881	17	1225	21	3
MW 1530	290	15197	142	4257	139	166	4	1285	8	9
MW 1533	267	14386	178	3220	110	1529	4	1385	26	1
MW 1534	0	9683	108	2206	109	1379	6	1480	20	2
MW 1536	384	14922	130	2597	131	1556	0	2104	22	1
MW 1537	283	16402	138	2440	150	1895	6	2752	49	0
MW 1539	200	16858	153	3471	156	1932	14	3307	70	0
MW 1542	133	18436	218	2770	115	2691	25	4916	101	2
MW 1545	212	11141	146	2839	109	1374	16	4604	105	2
MW 1548	349	13247	162	2635	139	2205	2	5414	147	0
MW 1586	184	91	29	2948	10	570	118	21622	916	4
MW 1590	100	136	21	5491	78	146	28	9466	332	4
MW 1592	199	2592	57	3660	75	290	7	734	16	0
MW 1596	211	20901	182	3360	115	618	20	1797	17	2
MW 1597	93	14009	97	3385	72	119	0	1337	12	5
MW 1599	118	17650	187	2450	128	2445	16	1641	54	3

Sample	CL	K	CA	TI	V	CR	MN	FE	NI	CU
MW 1600	156	11302	132	3175	123	1426	44	4827	59	5
MW 1603	167	16891	168	2801	158	2882	9	3719	70	1
MW 1604	0	15214	174	2590	101	1820	63	22518	121	13
MW 1605	120	25133	225	3055	195	2847	13	9596	208	2
MW 1608	144	22123	161	3186	187	2851	10	8329	170	4
MW 1609	314	13849	154	3339	212	2533	0	5607	114	2
MW 1611	134	16520	174	2544	196	2451	14	6364	124	1
MW 1614	332	8468	83	2333	85	1531	4	4198	145	3
MW 1616	156	183	30	3943	60	263	21	6179	386	3
MW 1617	257	76	49	3434	10	173	97	21781	714	4
MW 1619	27	23	26	4127	27	126	56	16804	405	3
MW 1621	353	31	39	2696	14	142	32	13030	561	5
MW 1623	0	19027	186	2663	187	2210	0	1829	33	1
MW 1625	24	18663	178	3568	149	453	11	2691	35	2
MW 1628	23	16672	138	3925	114	182	12	3926	26	4
MW 1630	0	12243	109	12131	402	0	12	4316	36	8
MW 1632	13	2981	90	2694	71	459	6	568	51	2
MW 1635	163	16319	174	2990	142	1840	15	5877	248	1
MW 1637	28	18543	186	3103	181	2038	29	8046	239	1
MW 1640	0	16070	155	2775	164	2421	9	6831	202	2
MW 1642	40	18641	169	2724	149	2656	10	6649	149	1
MW 1692	4	66	19	3443	16	39	19	7310	355	3
MW 1693	20	2003	18	3246	24	111	9	5910	270	2
MW 1703	0	8705	89	2927	85	1114	0	1130	39	1
MW 1707	0	19956	192	2771	142	2479	15	4505	109	0
MW 1711	12	32887	177	3175	222	3752	17	12911	303	1
MW 1714	46	27573	224	2820	211	3018	12	11113	217	3
MW 1716	0	16394	165	2398	159	2570	18	7782	165	6
MW 1718	0	16235	135	2246	148	2487	16	7645	164	5
MW 1721	15	16661	230	4878	169	72	20	6734	31	3
MW 1722	0	13949	243	2520	92	138	14	2468	17	4
MW 1723	22	13650	217	2740	101	141	8	2286	11	2
MW 1733	48	13032	214	2576	84	115	10	1397	10	5
MW 1734	0	19371	225	4205	186	349	21	3142	15	8
MW 1745	0	11018	191	2549	170	2238	26	4090	50	3
MW 1758	0	16523	204	2342	119	2350	12	4601	123	2
MW 1759	0	16940	143	2527	190	3022	4	4569	131	0
MW 1766	25	25984	199	2662	220	3138	19	10551	221	3
MW 1767	17	23512	179	2599	171	2967	15	9253	195	5
MW 1840	0	399	0	2753	18	200	56	2687	43	7
MW 1841	110	80	54	2870	18	317	32	5421	304	1
MW 1866	0	15195	239	4126	196	773	12	2266	18	4
MW 1867	84	11237	152	3164	105	971	12	1571	21	4
MW 1870	0	13134	139	2493	158	1609	4	1085	18	1
MW 1871	39	7072	156	2623	93	801	15	1657	33	5
MW 1874	0	5067	140	2822	86	1126	0	1559	21	1
MW 1875	70	7233	152	2438	123	1805	0	2128	34	1
MW 1884	20	7886	221	2696	130	1462	12	2521	41	1
MW 1885	42	3840	120	2347	75	738	8	1753	28	0
MW 1894	0	8699	164	2609	118	991	0	2231	39	1
MW 1895	22	14728	230	2757	200	2574	5	5258	115	0
MW 1901	56	15837	161	2730	157	2499	16	5815	84	0
MW 1937	0	8302	189	2640	75	83	7	1410	10	1
MW 1990	23	16901	182	2416	132	2088	8	6531	124	3

Sample	ZN	GA	GE	AS	BR	RB	SR	Y	ZR	NB	MO	W	PB	TH	U
MW 0001	7	5	0	2	3	22	20	7	65	4	0	3	1	2	0
MW 0006	9	2	0	3	1	21	24	10	200	2	4	5	0	3	0
MW 0014	9	7	1	2	3	33	20	14	74	4	0	6	1	3	5
MW 0028	7	4	3	14	0	14	18	27	304	11	5	16	8	0	3
MW 0041	27	3	2	2	1	11	22	30	313	5	4	3	8	14	3
MW 0048	11	3	3	13	1	36	19	8	105	6	4	13	1	4	1
MW 0115	46	0	2	3	1	8	11	9	177	12	8	6	9	0	0
MW 0129	35	3	10	51	0	0	0	17	60	3	2	2	0	1	0
MW 0142	41	1	14	10	2	15	3	5	51	3	0	11	5	0	0
MW 0161	7	1	3	49	4	22	20	24	296	22	1	20	5	20	0
MW 0167	39	1	2	6	2	5	38	6	74	1	0	4	9	5	2
MW 0173	12	2	0	28	2	8	16	23	284	13	4	25	10	2	2
MW 0179	4	2	1	33	1	12	15	21	210	15	8	27	12	4	6
MW 0184	16	2	1	20	2	20	20	51	563	28	22	41	17	12	7
MW 0258	20	28	6	13	16	41	16	96	908	50	6	120	51	24	18
MW 0266	27	13	12	24	12	30	25	112	1033	62	17	116	31	25	26
MW 0270	19	11	7	66	4	9	16	130	1063	74	12	165	22	15	5
MW 0276	14	10	10	36	11	17	28	131	1127	84	25	133	26	17	22
MW 0285	14	2	3	23	5	10	16	65	763	41	0	62	12	10	8
MW 0407	37	9	5	54	1	9	8	53	681	51	13	56	13	2	3
MW 0413	21	7	8	59	5	20	18	71	760	41	3	65	18	20	26
MW 0417	8	3	8	41	8	18	10	67	642	35	11	69	16	16	19
MW 0421	19	0	3	61	9	11	13	113	1262	61	30	192	8	13	7
MW 0431	23	1	5	52	6	25	20	82	984	54	24	144	25	9	10
MW 0440	120	4	2	70	2	7	11	85	718	51	4	88	18	12	3
MW 0445	19	14	6	29	8	25	9	56	572	36	0	72	20	0	15
MW 0531	115	15	8	7	3	148	2	7	89	3	0	26	4	1	0
MW 0537	35	5	5	0	0	50	3	7	26	5	2	16	6	2	0
MW 0541	8	6	3	1	1	48	2	1	26	0	0	14	1	0	0
MW 0545	20	5	3	1	1	42	5	5	64	3	2	9	4	0	3
MW 0549	2	1	3	3	1	4	0	7	46	2	2	6	2	1	5
MW 0553	9	6	4	8	1	37	7	12	98	3	0	14	1	7	0
MW 0559	35	7	6	0	1	52	4	7	21	2	2	8	4	3	1
MW 0565	1	3	3	4	1	28	20	7	39	3	1	6	0	4	1
MW 0576	41	6	6	37	2	4	4	23	325	20	2	24	8	7	0
MW 0701	19	12	2	9	1	39	13	11	163	7	1	6	2	4	2
MW 0706	1	4	2	4	1	2	2	24	135	5	0	6	2	1	2
MW 0710	2	4	6	4	0	4	3	16	109	10	3	0	0	2	0
MW 0720	60	3	4	4	1	0	0	21	89	1	2	9	17	0	0
MW 0724	25	1	4	2	1	1	1	19	124	7	2	10	1	3	2
MW 0741	5	11	1	12	0	24	4	6	151	3	3	32	1	7	4
MW 0746	17	13	2	2	0	46	18	4	120	7	5	20	2	1	0
MW 0752	8	7	1	2	2	40	17	5	62	2	2	6	3	2	0
MW 0758	29	9	3	2	2	43	5	9	46	9	2	17	4	0	0
MW 0762	35	8	2	4	1	34	4	13	61	2	0	11	2	3	0
MW 0766	3	4	1	0	0	16	2	6	21	2	0	4	2	0	2
MW 0770	11	5	3	1	0	44	3	7	27	0	1	8	2	2	1
MW 0774	22	5	1	2	2	14	3	15	86	3	0	0	2	3	1
MW 0780	111	8	3	4	0	97	4	3	44	0	0	18	5	4	0
MW 0807	10	4	3	2	1	30	3	7	41	2	5	9	2	4	0
MW 0814	7	3	3	2	1	17	4	3	35	3	0	7	4	3	3
MW 0822	6	2	3	2	1	16	4	3	33	2	0	6	5	4	2
MW 0954	0	3	3	1	2	0	3	31	57	0	1	3	0	0	2
MW 0959	3	3	5	2	2	0	1	37	69	5	7	5	5	0	0
MW 0964	3	3	4	3	2	2	1	12	106	2	2	12	0	2	2
MW 0968	5	3	3	2	1	1	0	5	83	2	4	20	1	7	0
MW 0972	5	4	3	4	0	4	1	12	107	6	4	10	1	3	1
MW 0978	2	4	5	4	0	3	2	14	106	4	7	7	1	5	2
MW 0984	6	9	6	14	0	31	7	7	103	3	3	20	4	4	0
MW 0990	10	17	0	0	1	60	22	1	128	3	2	14	3	5	0
MW 0996	43	6	3	0	2	44	3	6	22	1	1	12	4	0	1
MW 1002	32	7	2	1	1	60	2	4	20	0	0	5	5	0	0
MW 1006	4	7	2	0	2	35	3	15	35	1	1	11	6	5	3
MW 1010	4	4	4	0	1	21	2	7	22	0	0	1	4	3	0
MW 1018	122	7	5	1	3	61	2	8	29	0	2	25	1	2	4
MW 1026	7	3	2	1	0	28	2	7	29	0	4	5	1	1	2
MW 1032	6	6	5	7	3	10	1	10	88	3	0	15	5	1	3
MW 1038	3	2	6	13	2	3	3	19	103	7	2	3	0	1	0
MW 1044	5	1	4	1	1	3	1	11	51	7	4	4	2	0	0

Sample	ZN	GA	GE	AS	BR	RB	SR	Y	ZR	NB	MO	W	PB	TH	U
MW 1051	6	2	3	2	1	16	4	3	33	2	0	6	4	3	2
MW 1102	1	2	2	1	1	1	2	25	92	5	0	1	4	2	0
MW 1106	5	4	4	0	1	0	0	11	71	1	0	9	2	5	6
MW 1109	5	3	4	0	2	1	0	7	74	3	1	16	6	5	1
MW 1116	5	2	3	2	0	2	1	7	58	1	0	0	1	2	1
MW 1118	1	2	3	7	1	8	1	9	47	1	0	4	2	1	0
MW 1122	12	17	1	0	0	47	14	8	143	0	0	19	2	2	8
MW 1125	29	6	1	3	0	42	6	3	21	0	0	16	1	0	0
MW 1128	50	3	0	2	1	26	3	7	24	1	0	14	3	4	0
MW 1133	16	7	3	1	0	47	4	3	33	1	2	10	5	0	0
MW 1136	15	5	3	0	0	53	3	1	26	1	0	10	3	6	0
MW 1138	205	13	7	0	0	97	2	2	28	2	3	64	4	6	0
MW 1140	9	0	2	0	1	6	2	9	25	0	0	7	3	5	2
MW 1143	6	0	4	1	0	6	1	14	94	1	9	13	3	1	2
MW 1149	20	1	1	0	0	3	0	9	27	1	3	11	4	2	0
MW 1210	3	5	2	0	0	12	4	3	50	2	3	19	1	1	1
MW 1213	2	1	2	1	0	1	0	0	7	1	0	5	0	2	2
MW 1216	18	5	2	0	0	26	6	2	9	2	0	7	1	1	0
MW 1223	2	4	2	1	1	22	6	7	30	3	0	6	4	0	1
MW 1276	9	0	0	0	1	0	3	9	46	4	0	0	2	1	3
MW 1285	9	1	1	1	1	1	1	16	42	0	0	6	0	3	0
MW 1287	2	1	3	0	1	8	3	9	34	3	0	6	2	1	0
MW 1288	3	9	3	0	2	33	8	6	25	0	0	12	5	6	1
MW 1290	6	8	3	2	0	31	15	0	95	6	3	19	1	5	2
MW 1294	20	3	0	10	0	33	10	8	13	2	2	15	18	2	0
MW 1297	6	7	2	0	0	45	13	3	73	5	3	12	0	3	1
MW 1300	32	9	4	2	0	59	5	14	23	3	2	13	1	3	0
MW 1302	39	5	3	1	0	26	2	4	28	3	0	10	0	0	0
MW 1305	17	6	10	0	0	40	1	0	18	2	0	16	1	2	0
MW 1307	47	6	6	2	2	50	2	4	18	0	0	22	1	2	0
MW 1309	20	7	6	2	0	47	1	6	17	2	0	17	0	0	1
MW 1312	39	7	7	4	1	40	2	3	15	1	7	11	4	3	0
MW 1315	54	6	2	6	0	29	2	1	17	3	0	6	5	0	0
MW 1318	26	16	1	0	0	62	16	13	161	6	2	22	4	3	0
MW 1321	18	16	0	0	3	55	11	6	130	5	0	26	3	5	0
MW 1449	4	0	1	1	1	0	2	13	67	4	3	1	0	0	2
MW 1452	4	4	2	2	0	17	2	3	19	2	0	7	2	0	0
MW 1455	9	5	0	2	0	19	6	3	32	2	0	12	2	2	0
MW 1460	43	7	2	0	2	41	10	5	31	3	0	12	4	5	3
MW 1461	16	6	1	0	0	63	12	0	17	0	0	13	5	2	0
MW 1463	13	4	3	1	1	59	8	3	22	5	0	7	1	6	3
MW 1468	8	5	4	7	1	30	3	2	29	1	3	9	1	5	0
MW 1470	17	9	2	0	0	69	3	6	26	0	0	16	0	0	0
MW 1471	37	9	2	0	0	72	4	5	23	4	1	16	5	2	0
MW 1473	27	8	5	2	1	56	7	8	19	4	3	16	2	7	0
MW 1476	33	1	3	0	3	15	2	4	22	4	4	7	5	3	0
MW 1479	9	1	3	1	1	1	1	5	13	2	0	7	3	2	2
MW 1481	9	1	5	2	1	10	1	7	29	1	0	5	0	3	0
MW 1517	24	0	1	0	1	3	0	37	27	4	0	0	2	2	0
MW 1519	37	2	2	2	1	3	1	10	24	1	0	0	0	0	0
MW 1521	26	1	3	0	2	1	1	16	54	2	4	0	2	5	3
MW 1524	2	1	2	1	2	2	1	9	36	2	0	2	2	1	0
MW 1526	1	2	1	1	1	6	1	8	15	1	0	4	1	2	0
MW 1527	4	5	3	9	1	32	15	5	63	1	0	24	3	3	4
MW 1530	4	15	4	2	1	35	14	7	110	4	0	26	5	2	0
MW 1533	7	6	3	0	1	40	13	7	35	1	0	13	4	2	3
MW 1534	6	4	3	4	0	25	12	4	15	0	0	2	4	3	3
MW 1536	2	5	3	1	1	42	6	12	28	0	1	3	3	4	0
MW 1537	4	3	2	0	2	56	4	8	18	0	1	4	1	3	0
MW 1539	7	5	3	8	1	56	6	18	30	2	0	11	0	1	1
MW 1542	27	5	2	5	0	58	7	9	20	1	3	10	0	2	0
MW 1545	29	8	5	2	2	36	3	8	32	0	0	12	3	8	0
MW 1548	46	4	5	1	0	36	1	6	20	0	2	11	0	3	3
MW 1586	41	0	2	1	2	6	3	26	17	3	2	0	1	0	0
MW 1590	18	0	1	0	2	1	1	15	34	0	2	0	6	0	0
MW 1592	2	2	3	2	1	4	1	8	26	0	0	2	2	2	1
MW 1596	6	13	1	1	0	55	17	3	54	1	1	21	5	5	2
MW 1597	4	9	1	3	0	26	14	5	76	5	2	24	9	1	0
MW 1599	15	6	0	1	0	45	10	4	15	0	0	9	2	0	0

Sample	ZN	GA	GE	AS	BR	RB	SR	Y	ZR	NB	MO	W	PB	TH	U
MW 1600	17	5	3	16	0	30	15	15	23	0	2	0	0	0	0
MW 1603	13	8	3	2	1	52	3	3	18	1	0	9	0	0	0
MW 1604	29	5	1	31	2	59	2	7	25	2	2	11	10	0	0
MW 1605	20	9	5	3	0	86	2	12	26	5	3	20	0	0	0
MW 1608	29	11	6	1	0	73	3	1	21	1	0	18	5	0	0
MW 1609	38	4	6	1	2	40	2	5	26	2	0	18	2	2	0
MW 1611	31	8	8	1	0	55	1	3	13	0	0	24	3	0	0
MW 1614	41	4	7	2	1	28	1	7	15	1	0	20	1	3	0
MW 1616	26	1	4	3	2	1	0	5	30	0	3	8	0	0	0
MW 1617	35	1	3	0	3	0	0	6	22	0	0	0	3	0	0
MW 1619	26	1	2	0	1	1	2	5	25	3	0	0	0	0	0
MW 1621	16	0	1	2	1	0	1	3	18	2	0	0	0	4	0
MW 1623	19	8	1	2	1	50	9	5	18	0	0	5	5	1	2
MW 1625	13	17	0	0	0	51	17	3	78	1	5	30	3	6	1
MW 1628	12	16	1	0	0	41	11	5	108	0	0	31	1	2	0
MW 1630	6	17	1	0	1	34	9	13	188	13	0	51	4	7	0
MW 1632	3	2	2	0	0	9	2	2	13	0	2	6	0	2	2
MW 1635	16	5	5	0	1	56	3	6	22	0	2	10	3	2	0
MW 1637	38	8	2	2	1	58	4	9	32	0	2	17	1	2	0
MW 1640	22	5	4	0	0	51	3	6	19	2	3	12	3	7	0
MW 1642	25	5	6	4	1	56	5	6	25	0	0	6	1	2	5
MW 1692	13	1	3	2	1	0	0	7	20	0	0	6	3	1	1
MW 1693	11	0	2	1	1	6	9	9	30	2	1	0	0	1	0
MW 1703	4	5	2	1	0	23	6	6	15	2	1	0	2	1	1
MW 1707	39	8	5	0	0	60	10	5	22	0	1	7	3	4	0
MW 1711	107	15	5	2	0	109	7	4	22	3	3	37	0	5	0
MW 1714	39	12	7	0	0	82	3	3	21	0	0	20	1	1	0
MW 1716	35	8	8	0	0	57	1	0	17	0	0	22	1	5	0
MW 1718	33	6	7	1	0	55	1	0	16	0	0	21	1	5	0
MW 1721	20	12	1	0	1	48	164	13	107	1	0	16	6	5	1
MW 1722	11	16	0	1	0	35	173	2	56	6	0	14	0	2	4
MW 1723	7	13	1	0	1	35	171	4	66	1	4	15	4	6	2
MW 1733	6	13	1	1	0	36	144	5	60	0	0	14	3	4	4
MW 1734	11	13	0	0	0	53	76	4	74	3	0	26	5	5	3
MW 1745	42	9	2	0	0	37	4	3	18	3	0	7	3	3	2
MW 1758	13	7	3	0	0	58	2	7	15	0	3	5	2	0	0
MW 1759	27	7	4	1	0	60	1	1	8	0	0	8	2	3	0
MW 1766	61	11	10	1	0	88	6	6	13	2	2	19	0	2	0
MW 1767	53	9	6	0	2	80	9	7	13	2	3	23	2	6	0
MW 1840	11	1	1	2	0	1	1	4	15	1	0	4	0	1	1
MW 1841	20	1	1	2	1	0	0	4	10	2	0	0	0	1	0
MW 1866	11	12	2	4	0	40	64	8	77	4	0	11	1	4	0
MW 1867	23	7	2	1	1	26	30	5	167	3	1	3	5	2	5
MW 1870	17	3	2	4	0	30	33	3	13	2	3	2	0	2	0
MW 1871	7	3	2	0	0	16	21	5	17	0	1	1	2	0	1
MW 1874	32	4	3	1	0	17	11	5	17	3	0	11	0	1	2
MW 1875	53	5	2	0	0	23	11	5	15	2	1	9	3	3	0
MW 1884	21	5	4	1	0	24	4	0	10	1	1	5	0	0	0
MW 1885	15	4	3	0	1	11	4	3	15	4	1	7	3	0	2
MW 1894	15	6	4	1	1	29	7	2	32	2	2	6	2	3	0
MW 1895	52	8	5	0	1	49	4	0	18	1	1	6	0	4	0
MW 1901	38	8	5	1	0	52	7	9	10	0	1	5	0	1	0
MW 1937	4	9	1	0	0	17	245	1	32	1	1	7	3	3	6
MW 1990	17	7	3	1	0	55	3	4	14	2	0	4	3	2	0

APPENDIX 2

EPR ANYLYSES INFORMATION, MYSTERY ZONE MT. PERCY, W.A

SAMPLE	Unique sample identifier given to open pit samples
ROCK TYPE	General rock description. As=Talc chlorite ultra mafic, Af=Porphyry, Asf=Fuchsite ultramafic, Ast= Talc ultramafic
REGO TYPE	Ak=Calcareous soil, L=Laterite, Lk=Calcareous laterite, M=Mottled zone, Mc=Mottled clay, C=Plasmic clay, Sc= Clay saprolite
EASTING	Coordinated for sample locality
R.L.	Recuced level

Sample	Easting	RL	Rock Type	Rego Type	EPR5	EPR100	EPR250
MW 0014	432.0	400.7	Asf	Ak	0	0	0
MW 0128	418.0	401.5	Asf	Ak	0	0	0
MW 0135	418.0	400	Asf	Lk	0	0	0
MW 0142	405.0	400	Asf	Lk	2.9	1.2	1.4
MW 0173	371.0	404.1	Asf	Lk	0	0	0
MW 0184	359.0	405	Af	L	0	0	0
MW 0280	346.0	405.5	Asf	Lk	0	0	0
MW 0435	338.0	405.8	Asf	Lk	0	0	0
MW 0450	334.0	406.1	Asf	Lk	0	0	0
MW 0531	398.0	400	Asf	Mc	0	0	0
MW 0537	392.0	400	Asf	Sc	6.4	2	2.1
MW 0541	388.0	400	Asf	Sc	7.9	2	2
MW 0545	384.0	400	Asf	Mc	3.6	1.4	1.7
MW 0549	380.0	400	Asf	C	2.4	0.9	1.2
MW 0553	376.0	400	Asf	C	2.2	1.4	1.5
MW 0559	370.0	400	Asf	C	5.4	1.6	1.7
MW 0565	364.0	400	Asf	C	3	1.3	1.3
MW 0576	353.0	400	Af	C	0	0	0
MW 0701	319.0	397	As	M	0	1.3	1.5
MW 0706	324.0	397	As	M	0	0	0
MW 0710	328.0	397	As	M	0	1.3	1.3
MW 0714	332.0	397	As	Mc	0	0	0
MW 0728	346.0	397	As	C	0	0	0
MW 0734	352.0	397	As	C	0	0	0
MW 0741	359.0	397	Af	Mc	6.3	2.3	2.6
MW 0746	364.0	397	Af	C	10.6	3.7	3.4
MW 0752	370.0	397	Asf	M	5.5	2.1	2.3
MW 0758	376.0	397	Asf	Sc	5.5	1.9	2.1
MW 0766	384.0	397	Asf	Sc	5	1.1	1.1
MW 0770	388.0	397	Asf	Sc	6.9	2.2	2.2
MW 0774	392.0	397	Asf	C	2.1	0.7	0.8
MW 0780	398.0	397	Asf	Mc	3.2	1.9	2
MW 0807	425.0	397	Asf	Mc	4.4	1.3	1.5
MW 0814	432.0	397	Asf	Mc	3.8	1.1	1.1
MW 0959	333.0	395	As	Sc	0	0	0
MW 0964	338.0	395	As	Sc	0	0	0
MW 0968	342.0	395	As	Sc	0	0	0
MW 0972	346.0	395	As	Sc	0	0	0
MW 0978	352.0	395	As	Sc	0	0	0
MW 0984	358.0	395	Asf	Sc	8	2.6	2.4
MW 0990	364.0	395	Af	Sc	8.7	3	3.2
MW 0996	370.0	395	Asf	Sc	5.8	1.6	1.7
MW 1002	376.0	395	Asf	Sc	9.3	1.4	1.5
MW 1006	380.0	395	Asf	Sc	5	1.3	1.6
MW 1010	384.0	395	Asf	Sc	5.1	0.8	0.8
MW 1013	392.0	395	Asf	Sc	6	2.3	2.5
MW 1018	400.0	395	Asf	Sc	7.5	1.9	1.1
MW 1022	405.0	395	Asf	Mc	7.7	2.2	2.3
MW 1026	412.0	395	Asf	Mc	5.8	1.8	2
MW 1032	418.0	395	Asf	Mc	0	0	0
MW 1051	425.0	395	Asf	Sc	5.5	1.5	1.5
MW 1044	324.0	392.5	As	Sc	1.2	0.7	0.6
MW 1102	332.0	392.5	As	Sc	0	0	0
MW 1106	338.0	392.5	As	Sc	0	0	0
MW 1116	352.0	392.5	As	Sc	0	0	0
MW 1118	356.0	392.5	Asf	Sc	3	1.9	2
MW 1122	364.0	392.5	Af	Sc	2.9	1.6	1.6
MW 1125	370.0	392.5	Asf	Sc	4.1	1	1
MW 1128	376.0	392.5	Asf	Sc	2.2	0.7	0.7
MW 1133	386.0	392.5	Asf	Sc	6.8	1.3	1.3
MW 1136	392.0	392.5	Asf	Sc	10.8	2.3	2.4
MW 1138	396.0	392.5	Asf	Sc	6.3	5.6	5
MW 1140	400.0	392.5	Asf	Sc	4.2	1.3	1.2
MW 1143	406.0	392.5	Asf	Sc	0	0	0
MW 1149	418.0	392.5	Asf	Sc	0	0	0

Sample	Easting	RL	Rock Type	Rego Type	EPR5	EPR100	EPR250
MW 1210	358.0	390	Af	Mc	4	1.2	1.3
MW 1213	364.0	390	Af	S	3	0.4	0.4
MW 1216	384.0	390	Asf	Sc	9.2	1.2	1.2
MW 1223	328.0	387.5	Ast	Sc	2.2	1.1	1
MW 1276	346.0	387.5	As	S	0	0	0
MW 1285	350.0	387.5	As	S	0	0	0
MW 1288	356.0	387.5	Af	S	4.5	1.3	1.5
MW 1290	364.0	387.5	Asf	S	2.4	1.1	1.2
MW 1297	370.0	387.5	Asf	S	4.8	0	0
MW 1302	380.0	387.5	Asf	S	5.8	4.4	4
MW 1305	386.0	387.5	Asf	S	5.7	2	2
MW 1307	390.0	387.5	Asf	S	8.7	2.7	2.5
MW 1309	394.0	387.5	Asf	S	8.2	3	3
MW 1312	400.0	387.5	Asf	S	0	0	0
MW 1315	406.0	387.5	Asf	S	0	0	0
MW 1318	412.0	387.5	Af	S	5.9	0	0
MW 1321	418.0	387.5	Af	S	5.8	2.3	2.3
MW 1449	346.0	382.5	Ast	S	1	0.7	0.7
MW 1455	358.0	382.5	Ast	S	8.4	3.2	3.2
MW 1460	368.0	382.5	Asf	S	4.6	2.2	2.3
MW 1461	370.0	382.5	Asf	S	6.6	1.8	1.9
MW 1463	374.0	382.5	Asf	S	1.9	1	1
MW 1466	380.0	382.5	Asf	S	7	2.3	2.5
MW 1468	384.0	382.5	Asf	S	3.5	2.3	2.5
MW 1470	388.0	382.5	Asf	S	5.7	2.5	2.7
MW 1471	390.0	382.5	Asf	S	10.8	4	4.4
MW 1473	394.0	382.5	Asf	S	7.6	2.5	--
MW 1476	400.0	382.5	Asf	S	1.7	0.8	1
MW 1479	406.0	382.5	Asf	Sc	3.7	1.2	1.4
MW 1481	410.0	382.5	Asf	S	3.3	1.3	1.3
MW 1517	337.0	380.0	Ast	S	0	0	0
MW 1519	341.0	380.0	Ast	S	0	0	0
MW 1521	345.0	380.0	Ast	S	0	0	0
MW 1524	351.0	380.0	Ast	S	2.2	1.1	1.4
MW 1526	355.0	380.0	Asf	S	3.3	1.1	1.2
MW 1527	357.0	380.0	Af	S	6	2.4	2.4
MW 1530	363.0	380.0	Af	S	7	3.6	3.6
MW 1533	369.0	380.0	Asf	S	6	1.7	1.9
MW 1534	371.0	380.0	Asf	S	5.2	4	4
MW 1536	375.0	380.0	Asf	S	1.7	2	2.2
MW 1537	377.0	380.0	Asf	S	6.1	1.4	1.4
MW 1539	381.0	380.0	Asf	S	4.5	1.7	2.1
MW 1542	387.0	380.0	Asf	S	5.1	3.4	3.6
MW 1545	393.0	380.0	Asf	S	7.3	3.4	4
MW 1548	399.0	380.0	Asf	S	7	2.3	2.3
MW 1586	343.0	375.0	Ast	S	0	7.9	8
MW 1588	347.0	375.0	Ast	S	0	0	0
MW 1590	351.0	375.0	Ast	S	0	0	0
MW 1592	355.0	375.0	Asf	S	2.4	1	1.2
MW 1594	359.0	375.0	Af	S	3.2	2.2	2.3
MW 1596	363.0	375.0	Af	S	7.6	2.6	2.7
MW 1597	365.0	375.0	Af	S	6.7	2.2	2.2
MW 1599	369.0	375.0	Asf	S	2.8	1.6	2
MW 1600	371.0	375.0	Asf	S	0	0	0
MW 1603	377.0	375.0	Asf	S	2.6	1.8	2
MW 1604	379.0	375.0	Asf	S	0	0	0
MW 1605	381.0	375.0	Asf	S	8.5	3	3.2
MW 1608	387.0	375.0	Asf	S	7	2	2.2
MW 1609	389.0	375.0	Asf	S	6	2.4	2.3
MW 1611	393.0	375.0	Asf	S	7	3.3	3.3
MW 1614	399.0	375.0	Asf	S	3	2.5	2.5
MW 1616	403.0	375.0	Asf	S	2	2	2
MW 1617	347.0	370.0	Ast	S	0	3.8	3.6
MW 1619	351.0	370.0	Asf	S	0	4	3.6
MW 1621	355.0	370.0	Asf	S	0	4	3.6

Sample	Easting	RL	Rock Type	Rego Type	EPR5	EPR100	EPR250
MW 1623	359.0	370.0	Asf	S	5.7	2.2	2.2
MW 1625	363.0	370.0	Af	S	6.2	1.2	1.5
MW 1628	369.0	370.0	Af	S	6.5	1	1
MW 1630	373.0	370.0	Af	S	4.4	1.7	2.1
MW 1632	377.0	370.0	Asf	S	1.9	0.6	0.7
MW 1635	383.0	370.0	Asf	S	3.8	2	1.9
MW 1637	387.0	370.0	Asf	S	6.3	2.3	2.4
MW 1640	393.0	370.0	Asf	S	5	0	0
MW 1642	397.0	370.0	Asf	S	4.5	3	3
MW 1690	350.0	365.0	As	S	0	0	0
MW 1692	354.0	365.0	As	S	0	0	0
MW 1693	356.0	365.0	Asf	S	1	0	0
MW1703	376.0	365.0	Asf	S	1.4	1.3	1.3
MW1707	384.0	365.0	Asf	S	4	2.5	0
MW1711	392.0	365.0	Asf	S	0	0	0
MW1714	398.0	365.0	Asf	S	10	3	3
MW1716	402.0	365.0	Asf	S	4.5	2.3	2.3
MW1721	412.0	365.0	Af	S	3.7	0	0
MW1722	364.0	360.0	Af	S	5.4	2.9	2.5
MW1723	365.0	357.5	Af	S	6.5	1.2	1.3
MW1733	370.0	357.5	Af	S	6	3	3
MW1734	370.0	360.0	Af	S	4.6	3	3.2
MW1745	376.0	357.5	Asf	S	2.1	1.3	0.6
MW1758	384.0	360.0	Asf	S	2.3	1.6	0
MW1759	385.0	357.5	Asf	S	3.1	1.1	1.6
MW1766	392.0	360.0	Asf	S	6.9	2.2	2.2
MW1767	393.0	357.0	Asf	S	6.9	2.2	2.3
MW1744	375.0	360.0	Asf	S	0	0	0
MW 1874	375.0	350.0	Asf	S	1.3	0.9	1.23
MW 1875	376.0	347.5	Asf	S	2.2	1.5	1.5
MW 1884	380.0	350.0	Asf	S	1.7	0.8	0.8
MW 1885	381.0	347.5	Asf	S	2.6	1.5	2
MW 1894	385.0	350.0	Asf	S	2.3	2	2
MW 1895	386.0	347.5	Asf	S	3.4	2.5	2.5
MW 1900	388.0	350.0	Asf	S	5	1.8	1.8
MW 1901	389.0	347.5	Asf	S	3.8	1.7	1.7
MW 1937	388.0	347.5	Af	S	4.6	2.5	2.5

APPENDIX 3

SAMPLE ANYLYSES INFORMATION, RAND PIT REEDY MINE, W.A

SAMPLE	Unique sample identifier given to open pit samples
ROCK TYPE	General rock description. Um=Ultra mafic, Py=Porphyry, Mf=Mafic, Ba=Black shale Sh=Mica schist
East	Coordinated at easting for sample locality
North	Coordinated at northing for sample locality
RL	Coordinated at altitude for sample locality
Ph East	Coordinated at X-axis for sample locality
Ph RL	Coordinated at Y-axis for sample locality
AU (NAA)	Gold data analzed by NAA (fromRobertson, 1990)

Sample	Ph-East	Ph-R.L.	Rock	Au (NAA)	F	NA	AL	SI	S	CL	K
RE 6	730	183	Py	0.007	132	36612	46218	292196	38	55	5894
RE 7	748	181	Py	0.005	108	42221	53737	278835	83	137	9328
RE 9	773	202	Mf	1.87	147	2092	30318	303680	834	47	39870
RE 11	796	183	Py	0.38	90	16707	45543	271851	899	80	30936
RE 12	830	185	Bs	1.09	413	734	69874	253201	1059	29	44557
RE 13	858	180	Mf	0.043	230	3962	44262	289725	4552	0	17638
RE 15	925	173	Um	0.004	269	79	400	286754	1167	50	47
RE 17	995	140	Um	0.015	222	6674	12183	275248	628	92	785
RE 18	917	47	Um	0.003	204	483	2798	253782	14370	0	35
RE 19	896	64	Um	0.009	260	37	793	238415	23817	0	38
RE 21	841	83	Mf	2.95	93	28835	49106	251512	3589	7	19925
RE 22	821	83	Mf	6.42	118	31444	51749	286367	10399	50	16772
RE 25	771	87	Py	0.025	108	32852	44650	302125	168	106	11966
RE 26	744	87	Um	0.019	642	87	1647	257869	2344	54	15
RE 29	625	93	Um	0.002	366	41	600	245716	2196	26	235
RE 30	485	80	Um	0.019	346	172	2076	286671	2534	18	44
RE 31	432	72	Um	0.003	227	552	3137	275398	2513	0	372
RE 32	227	670	Sh	0.12	262	263	39723	269214	6043	0	23487
RE 33	300	670	Mf	0.043	140	41	16026	333408	395	75	1779
RE 34	436	678	Um	0.02	254	71	6165	294985	254	85	42
RE 35	569	660	Um	0.004	349	61	8710	300674	6010	0	604
RE 36	622	667	Py	0.003	74	1922	41468	272591	4826	38	20426
RE 37	672	665	Um	0.013	263	52	2419	268416	2333	12	339
RE 38	724	666	Py	0.004	74	1265	47030	280981	510	134	58217
RE 41	917	663	Mf	0.089	119	50	26865	245598	41060	0	37
RE 42	940	667	Sh	18.4	445	637	72412	218289	26446	0	33034
RE 43	971	668	Mf	0.159	123	0	11566	329026	5770	5	58
RE 44	1104	667	Um	0.003	187	93	2359	266831	7575	0	36
RE 45	1149	667	Um	0.002	215	117	736	250966	1818	64	30
RE 46	1204	668	Um	0.003	85	2437	6625	308787	1847	57	1882
RE 47	1257	667	Mf	0.007	74	12829	30792	334395	952	69	8391
RE 48	1350	668	Mf	0.01	103	6609	19155	301371	18669	8	411
RE 49	1393	670	Um	0.007	182	1032	5055	290720	1806	67	121
RE 50	1453	660	Um	0.003	182	2684	7058	264698	932	20	124
RE 51	1486	651	Um	0.003	164	8746	13951	272743	1047	66	199
RE 53	1276	1198	Mf	0.004	113	0	34807	211090	75276	0	55
RE 54	1164	1178	Um	0.006	174	45	7980	276432	357	283	5
RE 55	1111	1172	Mf	0.105	176	226	71969	206197	26951	0	11561
RE 56	1019	1160	Mf	0.017	120	0	71408	240182	4458	27	33
RE 57	953	1161	Mf	2.06	205	0	104781	232610	11579	86	34
RE 58	922	1156	Mf	0.689	338	0	123841	211646	567	186	28
RE 59	894	1155	Um	0.009	143	0	63741	227777	14432	26	14
RE 60	834	1143	Um	0.007	243	151	26862	281383	369	169	46
RE 61	763	1133	Um	0.056	266	34	17700	278861	9369	5	34
RE 62	704	1132	Um	0.004	406	52	15520	245655	4186	25	45
RE 65	473	1117	Mf	0.011	125	39	39380	292761	15993	45	687
RE 66	430	1111	Sh	0.034	222	266	41860	300098	2509	14	16008
RE 67	398	1108	Sh	0.225	155	183	21151	316930	11484	0	10164
RE 68	368	1101	Mf	0.016	184	0	69363	255573	15421	0	163
RE 69	339	1098	Mf	0.016	164	0	56122	289165	8417	46	267
RE 70	286	1094	Py	0.005	190	0	67671	261923	10993	63	566
RE 71	222	1371	Mf	0.003	212	0	68806	266036	7989	95	201
RE 72	252	1374	Bs	0.003	289	94	55183	295894	721	130	2274
RE 73	268	1375	Mf	0.012	199	0	52886	294200	387	404	59
RE 74	287	1377	Mf	0.019	240	113	28641	320620	2253	30	3084
RE 75	312	1378	Mf	0.016	229	28	42590	299261	9629	54	358
RE 76	406	1377	Mf	0.022	147	61	73214	255148	4418	3	643
RE 77	542	1382	Mf	0.929	122	62	69501	263521	7325	7	416
RE 78	738	1387	Um	0.336	152	57	37392	261930	312	153	22
RE 79	826	1382	Um	0.026	346	0	60459	253672	683	67	42
RE 80	901	1382	Mf	0.062	131	38	48071	287056	5006	3	125
RE 81	964	1379	Mf	0.229	169	57	101436	240635	997	65	28
RE 83	1126	1388	Mf	0.018	154	102	108832	237966	592	141	54
RE 84	1172	1387	Um	0.009	168	81	99185	198582	45244	0	55
RE 85	1214	1385	Um	0.016	168	0	98961	237515	17391	0	47
RE 86	1390	1397	Um	0.008	62	106	57368	256113	1335	36	72
RE 87	1481	1380	Um	0.004	187	0	47928	293757	642	23	46
RE 88	1572	1380	Um	0.004	148	38	59701	262017	803	148	44
RE 89	1632	1380	Um	0.005	105	0	95815	232696	1480	137	24
RE 90	926	1388	Sh	0.018	152	309	123330	222282	363	57	14849

Sample	Ph-East	Ph-R.L.	Rock	Au (NAA)	F	NA	AL	SI	S	CL	K
RE 91	1345	1344	Bs	0.026	107	43	42748	293263	371	124	51
RE 92	1188	1442	Um	0.022	187	40	91287	251256	318	110	241
RE 93	1135	1451	Mf	0.044	230	75	76574	254538	424	166	164
RE 94	1097	1442	Mf	0.008	56	33	107774	237336	654	50	78
RE 95	1070	1438	Mf	0.022	152	127	95224	237602	124	85	5453
RE 96	916	1449	Mf	0.121	185	171	100503	234244	400	51	6171
RE 97	897	1433	Mf	0.04	121	26	50899	273061	724	164	97
RE 98	839	1454	Bs	0.021	161	48	77171	253029	545	54	363
RE 99	773	1447	Um	0.032	153	0	65072	267310	806	49	222
RE 100	668	1450	Um	0.034	233	50	60598	248967	631	47	30
RE 101	556	1451	Mf	0.058	88	0	52450	221225	21558	67	40
RE 102	404	1432	Mf	0.006	68	78	78765	253000	887	143	110
RE 103	307	1421	Mf	0.039	63	0	75432	261983	1538	71	162
RE 104	279	1418	Mf	0.019	105	26	62017	264410	604	92	1621
RE 105	252	1415	Mf	0.015	84	0	77318	251245	499	139	77
RE 106	225	1412	Mf	0.016	177	35	71498	270846	4154	27	2710
RE 107	199	1415	Mf	0.005	76	0	93533	220933	9551	63	66
RE 108	1552	1446	Um	0.011	184	39	35037	269378	1889	7	67
RE 109	1604	1446	Um	0.016	202	48	71565	267757	1374	127	51

Sample	CA	TI	V	CR	MN	FE	NI	CU	ZN	GA	GE
RE 6	628	1004	4	0	5	61	2	0	1	6	1
RE 7	808	1089	1	0	3	30	2	3	2	9	0
RE 9	232	1971	8	10	4	267	1	2	2	2	0
RE 11	495	4800	56	0	16	302	2	3	4	4	0
RE 12	229	3738	214	151	44	1061	0	0	3	15	2
RE 13	313	4366	67	14	15	1408	18	6	3	4	1
RE 15	474	815	11	95	124	15679	331	3	25	0	1
RE 17	42837	1341	95	393	729	24110	156	0	18	0	4
RE 18	34941	1519	86	446	687	23512	196	2	26	0	2
RE 19	239	577	19	161	182	21186	423	4	32	1	1
RE 21	1050	1976	7	0	7	316	2	0	1	3	0
RE 22	686	2949	18	0	5	521	2	0	1	7	1
RE 25	584	478	0	6	7	35	2	1	2	8	0
RE 26	239	2371	52	234	284	18203	166	4	96	1	2
RE 29	80	1101	12	150	179	18082	309	1	32	1	4
RE 30	9777	415	21	339	369	17810	299	3	28	1	2
RE 31	21129	302	54	422	610	22585	302	1	24	0	3
RE 32	228	3286	120	132	30	1934	1	1	5	9	0
RE 33	104	3900	56	13	7	988	5	1	2	3	2
RE 34	650	3089	44	299	125	16896	368	3	21	1	3
RE 35	16	3091	62	402	70	9427	199	2	11	1	0
RE 36	127	1217	13	1	8	217	9	2	3	7	0
RE 37	72	1988	21	140	177	16320	250	2	24	1	1
RE 38	355	1032	26	4	11	213	8	1	1	6	1
RE 41	45	4970	126	158	12	878	28	1	4	9	2
RE 42	230	4185	228	285	38	1376	7	1	5	16	0
RE 43	55	2759	58	70	20	979	16	1	4	2	0
RE 44	23	1465	10	167	190	21673	408	4	63	1	0
RE 45	20	1430	15	125	218	26944	899	7	43	0	1
RE 46	28963	1565	59	249	495	15914	80	3	15	0	3
RE 47	887	3352	78	0	11	754	6	1	2	2	1
RE 48	702	4394	91	16	11	1249	8	1	1	1	1
RE 49	43831	1276	93	628	699	24232	178	4	23	1	6
RE 50	47286	1647	92	676	720	25288	195	6	23	4	9
RE 51	44773	1594	101	651	781	26931	179	1	23	1	3
RE 53	39	4301	99	37	15	1663	24	3	3	4	0
RE 54	17	2632	53	472	93	11852	293	7	21	2	2
RE 55	173	5622	281	94	20	2797	15	2	5	14	0
RE 56	78	4439	251	755	2	225	54	6	5	13	2
RE 57	37	10028	322	945	9	1260	19	2	8	21	1
RE 58	31	10344	328	1251	12	1566	30	5	11	23	0
RE 59	39	3825	218	4748	80	9381	217	3	13	7	0
RE 60	61	4192	86	2174	131	15357	327	0	26	4	2
RE 61	24	3394	74	1107	138	16831	326	1	25	3	0
RE 62	29	2466	67	680	210	19251	267	0	35	3	2
RE 65	35	6342	140	30	12	2469	8	5	3	6	0
RE 66	149	3900	104	41	18	2417	5	6	4	9	0
RE 67	70	1861	74	60	23	1100	5	3	5	7	1
RE 68	53	6828	223	257	0	3051	20	8	6	11	3
RE 69	67	6615	176	200	9	2910	16	6	4	7	1
RE 70	37	10968	321	23	69	4945	46	10	12	12	3
RE 71	57	3880	123	84	0	2399	27	5	4	15	4
RE 72	90	4455	151	177	33	1575	12	3	4	9	2
RE 73	116	4528	142	355	9	1642	19	11	7	10	1
RE 74	62	3423	66	77	14	1816	20	5	6	5	1
RE 75	75	4954	123	93	8	2245	19	4	3	8	2
RE 76	37	5738	98	162	17	4343	31	3	4	14	1
RE 77	105	6213	222	101	0	1019	15	5	1	11	0
RE 78	70	2956	75	2032	156	18690	452	29	24	2	0
RE 79	144	5726	224	4467	90	9109	204	5	16	7	0
RE 80	141	1394	42	78	0	497	172	3	9	6	0
RE 81	681	7539	324	1086	0	714	156	17	4	18	1
RE 83	121	7303	127	188	11	1414	214	24	26	15	1
RE 84	31	6440	135	240	5	1717	205	14	17	11	0
RE 85	101	7425	226	383	5	1437	247	22	5	14	2
RE 86	66	9066	189	12	13	946	52	7	4	7	0
RE 87	33	4506	130	1357	52	11908	216	4	14	7	1
RE 88	80	16505	317	531	737	30761	520	21	48	2	1
RE 89	159	28639	498	686	1071	31156	76	30	17	2	0
RE 90	647	10812	413	103	28	1362	22	4	8	21	3

Sample	CA	TI	V	CR	MN	FE	NI	CU	ZN	GA	GE
RE 91	392	3271	78	13	52	1858	22	3	2	9	1
RE 92	377	6201	121	344	20	3026	209	17	3	12	2
RE 93	298	5007	87	175	34	3839	120	14	12	8	0
RE 94	294	6262	125	152	13	2150	127	10	15	8	1
RE 95	278	6385	280	133	15	1997	37	4	2	16	1
RE 96	275	5561	309	159	11	2338	41	5	4	21	1
RE 97	204	3531	167	564	5	379	73	3	3	8	0
RE 98	311	5580	296	859	14	2491	65	7	6	15	1
RE 99	314	2102	105	386	13	1842	36	5	5	10	1
RE 100	410	3169	199	4078	73	10918	210	6	16	10	0
RE 101	273	3409	102	2112	92	11016	240	15	22	7	0
RE 102	99	5940	249	577	5	1603	61	12	3	14	1
RE 103	75	6269	147	158	6	3509	31	5	5	13	1
RE 104	68	4853	147	232	3	2308	48	5	4	12	2
RE 105	98	5664	183	640	4	2552	64	8	5	10	1
RE 106	75	5190	154	301	31	2645	25	5	6	13	0
RE 107	34	8216	295	184	38	5354	53	3	9	16	2
RE 108	69	7112	101	952	158	23651	866	4	33	3	2
RE 109	164	17192	326	1682	434	22019	328	48	45	12	1

Sample	AS	BR	RB	SR	Y	ZR	NB	MO	W	PB	TH	U
RE 6	1	1	15	102	2	52	0	1	7	0	0	0
RE 7	0	1	24	176	3	56	0	1	7	1	0	7
RE 9	0	1	101	23	3	46	3	0	5	3	2	0
RE 11	0	0	80	76	4	38	1	3	33	25	0	0
RE 12	0	1	103	32	2	76	4	2	13	4	4	1
RE 13	0	1	53	28	2	71	3	2	16	2	0	2
RE 15	0	1	0	1	4	27	0	2	2	1	0	0
RE 17	0	2	2	19	6	23	1	0	3	2	0	3
RE 18	1	3	2	4	10	19	3	0	7	0	4	0
RE 19	1	1	0	0	3	15	1	0	2	0	0	0
RE 21	0	2	59	85	5	52	0	0	7	1	2	5
RE 22	1	0	45	42	0	43	1	3	15	3	5	3
RE 25	1	1	31	112	0	49	0	0	4	2	0	2
RE 26	1	1	0	0	2	35	2	0	0	5	2	1
RE 29	0	2	0	1	1	30	0	0	0	0	0	1
RE 30	0	0	0	2	5	18	0	1	0	0	0	1
RE 31	0	0	0	7	5	27	1	0	4	0	0	0
RE 32	0	0	52	4	4	49	6	0	3	4	3	1
RE 33	0	0	5	2	4	68	6	2	7	2	3	0
RE 34	0	1	1	0	2	33	5	2	0	3	0	1
RE 35	2	1	1	1	1	33	1	0	0	1	2	1
RE 36	0	1	54	51	4	80	2	3	12	2	3	0
RE 37	0	1	2	1	2	27	1	0	0	1	1	2
RE 38	0	1	152	107	3	113	6	5	4	2	1	0
RE 41	0	1	0	1	7	87	7	1	15	3	2	3
RE 42	1	0	67	36	7	88	9	2	13	1	4	3
RE 43	0	1	1	1	5	61	4	2	9	3	1	0
RE 44	0	1	0	0	1	15	0	0	0	0	0	1
RE 45	0	1	0	4	0	17	0	0	0	0	3	0
RE 46	0	1	5	8	12	33	0	0	0	1	2	4
RE 47	1	1	23	28	2	85	8	2	2	3	4	0
RE 48	2	0	2	23	1	53	3	0	2	0	2	0
RE 49	1	0	1	1	9	38	1	2	0	0	1	3
RE 50	2	2	1	9	5	55	3	0	6	0	1	0
RE 51	0	1	2	33	11	35	3	0	0	2	1	6
RE 53	1	1	1	0	2	73	6	7	5	4	4	2
RE 54	1	0	0	2	5	26	0	0	0	0	2	4
RE 55	1	1	22	2	6	86	7	1	3	5	1	0
RE 56	2	1	0	1	7	77	3	4	10	1	4	0
RE 57	1	0	1	0	10	164	10	6	11	7	2	1
RE 58	2	0	2	0	11	180	15	1	10	3	1	2
RE 59	0	1	0	2	4	87	4	0	0	3	5	1
RE 60	2	1	2	0	3	41	5	0	0	1	6	0
RE 61	1	1	0	1	3	36	2	0	5	0	0	0
RE 62	0	0	0	1	2	41	3	2	0	3	3	0
RE 65	0	1	3	1	5	101	6	1	7	4	2	1
RE 66	0	1	30	6	9	86	5	8	3	8	2	2
RE 67	0	0	20	2	4	58	3	0	6	9	5	0
RE 68	2	1	1	1	11	102	8	2	4	2	5	1
RE 69	0	3	2	1	7	112	6	3	4	8	1	1
RE 70	2	2	3	1	3	92	0	1	0	3	0	5
RE 71	1	1	2	1	5	150	4	3	0	5	4	2
RE 72	1	3	19	1	3	82	3	0	0	4	7	0
RE 73	1	1	2	3	2	89	3	0	16	3	4	0
RE 74	1	1	11	1	2	76	5	0	8	1	4	1
RE 75	0	0	2	2	3	112	6	5	7	3	3	1
RE 76	0	1	6	2	4	91	5	1	1	5	5	3
RE 77	3	0	0	3	8	134	3	0	7	5	1	5
RE 78	0	2	0	2	2	40	2	1	0	8	0	0
RE 79	0	1	0	3	6	71	2	3	0	2	5	3
RE 80	0	0	1	3	4	140	2	0	7	1	3	0
RE 81	0	1	1	15	11	132	5	2	0	5	5	2
RE 83	0	2	0	3	9	120	7	0	1	3	4	0
RE 84	0	0	1	1	3	106	5	0	0	1	2	0
RE 85	0	0	1	3	8	131	7	0	0	2	5	6
RE 86	0	0	1	5	27	469	16	0	0	4	14	3
RE 87	0	1	0	1	8	82	3	2	0	3	5	2
RE 88	0	2	6	0	0	131	8	5	0	1	3	0
RE 89	0	0	6	10	2	119	9	0	0	2	5	6
RE 90	0	0	31	22	15	74	1	0	24	2	3	1

Sample	AS	BR	RB	SR	Y	ZR	NB	MO	W	PB	TH	U
RE 91	1	0	1	10	17	233	12	7	0	3	20	2
RE 92	0	1	3	8	5	137	3	0	3	2	6	1
RE 93	0	1	2	10	5	92	4	1	0	3	0	1
RE 94	0	1	1	5	4	101	2	3	0	2	3	1
RE 95	0	0	25	4	6	109	10	2	11	0	3	0
RE 96	1	1	26	10	6	105	2	0	9	2	7	2
RE 97	0	2	1	5	2	48	5	3	7	4	3	1
RE 98	0	1	3	14	9	90	5	2	7	4	0	0
RE 99	0	1	1	7	3	83	3	0	4	1	3	2
RE 100	1	0	0	11	4	52	4	5	0	0	2	1
RE 101	0	1	1	7	21	48	2	0	1	6	6	1
RE 102	2	0	0	3	7	121	10	3	5	5	5	2
RE 103	0	1	1	3	11	220	4	12	2	1	4	1
RE 104	1	1	10	3	3	93	6	3	8	4	2	0
RE 105	0	1	1	1	4	85	3	3	0	5	2	0
RE 106	1	0	19	0	5	90	7	3	0	4	4	0
RE 107	0	0	1	2	0	83	3	0	0	6	1	2
RE 108	0	1	1	1	6	48	1	0	0	10	0	0
RE 109	0	0	2	6	4	106	5	0	0	3	3	1

APPENDIX 4

EPR ANYLYSES INFORMATION, MYSTERY ZONE MT. PERCY, W.A

SAMPLE	Unique sample identifier given to open pit samples
ROCK TYPE	General rock description. As=Talc chlorite ultra mafic, Af=Porphyry, Asf=Fuchsite ultramafic, Ast= Talc ultramafic
Ph East	Photo face coordinated for sample locality
Ph R.L.	Photo face coordinated for sample depth

Sample No	Ph-East	Ph-R.L.	Rock	EPR 5mT	EPR 100mT	EPR 250mT
RE1	373	153	Um	0	30	29
RE3	574	180	Um	0	12.8	12
RE4	650	180	Geo	0	13.7	13.7
RE6	730	183	Py	2	0.4	0.4
RE7	748	181	Py	1.2	0.3	0.3
RE9	773	202	Mf	3.8	0.6	0.5
RE11	796	183	Py	2.2	1	1
RE12	830	185	Bs	0	4.5	1.7
RE13	858	180	Mf	5.5	1	1
RE15	925	173	Um	0	12.6	12.3
RE17	995	140	Um	0	23	23
RE18	917	47	Um	0	12.5	12.5
RE19	896	64	Um	0	11.8	11.8
RE20	866	77	Um	0	11.8	11.8
RE21	841	83	Mf	1.5	0.5	0.5
RE22	821	83	Mf	1.3	0.7	0.7
RE23	796	87	Mf	2.6	0.7	0.9
RE25	771	87	Py	1.7	0.5	0.4
RE26	744	87	Um	0	32.4	18.2
RE28	682	93	Um	0	11	21.3
RE29	625	93	Um	0	20	21.8
RE30	485	80	Um	0	21.3	21.2
RE31	432	72	Um	0	24.9	24.5
RE32	227	670	Sh	7.8	2.4	2.3
RE33	300	670	Mf	2.8	0.4	0.6
RE35	569	660	Um	0	0	6
RE36	622	667	Um	11.3	0.5	0.7
RE37	672	665	Py	no	11.5	18.5
RE38	724	666	Um	3.5	0.7	0.6
RE40	804	663	Py	no	9	9
RE41	917	663	Mf	1.7	0.7	0.4
RE42	940	667	Sh	0	3.3	0
RE43	971	668	Mf	1	0.6	0.6
RE44	1104	667	Um	0	17.5	17
RE45	1149	667	Um	0	22	21.6
RE46	1204	668	Um	1.2	14.4	13.9
RE47	1257	667	Mf	1.8	0.6	0.7
RE48	1350	668	Mf	0.8	0.5	0.5
RE49	1393	670	Um	1.8	16.3	16.4
RE50	1453	660	Um	0	22.6	21.4
RE51	1486	651	Um	0	18.7	18.2
RE52	1386	1212	Um	1.5	0	0
RE53	1276	1198	Mf	2.2	1	1
RE55	1111	1172	Mf	19	3.7	3.7
RE56	1019	1160	Mf	15.8	1.5	1.5
RE57	953	1161	Mf	0	2	2
RE58	922	1156	Mf	0	2.4	2.4
RE59	894	1155	Um	0	19.7	19.7
RE60	834	1143	Um	0	17.3	3.1
RE61	763	1133	Um	0	19.1	18.5
RE62	704	1132	Um	0	19.8	20.2
RE63	629	1128	Um	0	15.2	16.2
RE64	541	1119	Mf	4.2	1.8	1.8
RE65	473	1117	Sh	2.8	1.8	1.8
RE66	430	1111	Sh	8.2	1.5	1.5
RE67	398	1108	Mf	6.9	2	2
RE68	368	1101	Mf	5.5	2	2

Sample No	Ph-East	Ph-R.L.	Rock	EPR 5mT	EPR 100mT	EPR 250mT
RE69	339	1098	Py	5.4	2	2
RE71	222	1371	Mf	10.5	1.3	1.3
RE72	252	1374	Bs	11	0	0
RE73	268	1375	Mf	12	1.2	1.2
RE74	287	1377	Mf	6.5	1.5	1.3
RE75	312	1378	Mf	4.8	1.8	1.8
RE76	406	1377	Mf	8.1	1.8	2.1
RE77	542	1382	Mf	11	2	2
RE78	738	1387	Um	0	25	23.5
RE79	826	1382	Um	0	15	14.1
RE80	901	1382	Mf	10.6	0.8	1
RE81	964	1379	Mf	17	0	0
RE83	1126	1388	Mf	13.8	1.3	1.3
RE84	1172	1387	Um	10.8	3.7	3.7
RE85	1214	1385	Um	11.3	1.4	1.4
RE86	1390	1397	Um	36	1.8	1.4
RE87	1481	1380	Um	0	5	5
RE90	926	1388	Sh	12.6	1.2	1.2
RE91	1345	1344	Bs	10	2.6	2.6
RE92	1188	1442	Um	12.5	1.3	1.3
RE93	1135	1451	Mf	6	1.7	1.8
RE94	1097	1442	Mf	20	1.5	1.5
RE95	1070	1438	Mf	23.5	1.2	1.6
RE96	916	1449	Mf	16.5	1.6	2
RE97	897	1433	Mf	12.8	1.2	1.2
RE98	839	1454	Bs	0	1.3	1.5
RE99	773	1447	Um	0	1.2	1.3
RE100	668	1450	Um	0	22.2	19.5
RE101	556	1451	Mf	0	15.2	14.9
RE102	404	1432	Mf	0	1	1.2
RE103	307	1421	Mf	11	2	2.2
RE104	279	1418	Mf	10.2	1.7	1.8
RE105	252	1415	Mf	11.4	1.8	1.9
RE106	225	1412	Mf	10.8	1.7	2
RE107	199	1415	Mf	0	2.3	2.4
RE109	1604	1446	Um	0	7.2	7.5

APPENDIX 5

SAMPLE ANYLYSES INFORMATION, JIM'S FIND TANAMI, N.T.

SAMPLE	Unique sample identifier given to open pit samples
Easting	Coordinated at easting for sample locality
Northing	Coordinated at northing for sample locality
Ph Easting	Coordinated at X-axis for sample locality
Ph R.L.	Coordinated at Y-axis for sample locality
AU (NAA)	Gold data analzed by NAA (from Stott, 1994)

Sample	Easting	Northing	Ph Easting	Ph R.L.	F	NA	AL	SI	S
130171	10010	10150	10011.75	412.00225	171	310	56714	262595	10985
130172	10010	10150	10018.75	400.01125	513	1840	66472	259379	3207
130173	10010	10150	10027.25	385.45075	171	238	61421	289964	5644
130174	10010	10150	10037.75	367.46425	379	606	71287	259014	1209
130175	10010	10150	10045.25	354.61675	208	829	40142	281329	478
130176	10010	10150	10051.25	344.33875	155	9573	41143	303194	3415
130177	10010	10150	10057.75	333.20425	176	2785	36682	299456	5854
130178	9990	10150	9992.75	410.28925	137	476	38157	302870	4898
130179	9990	10150	9994.25	407.71975	189	373	62625	257024	3136
130180	9990	10150	9999.75	398.29825	268	389	76830	258061	2746
130181	9990	10150	10007.75	384.59425	184	866	82837	257293	6788
130182	9990	10150	10016.25	370.03375	265	483	57368	229925	27685
130183	9990	10150	10023.25	358.04275	115	538	41361	303164	1721
130184	9990	10150	10025.75	353.76025	202	1790	56215	279154	2303
130185	9990	10150	10033.25	340.91275	88	35479	57237	289147	3222
130186	9970	10150	9971.75	412.00225	125	708	51610	287910	2835
130187	9970	10150	9973.25	409.43275	195	100	55923	294816	7726
130188	9970	10150	9977.75	401.72425	153	616	53327	293567	3190
130189	9970	10150	9980.75	396.58525	118	895	67105	262487	4454
130190	9970	10150	9982.75	393.15925	135	1938	50143	270039	952
130191	9970	10150	9986.75	386.30725	95	840	61909	236105	16583
130192	9970	10150	9995.75	370.89025	220	480	70703	250447	3478
130193	9970	10150	10002.25	359.75575	498	1357	66199	262836	1670
130194	9970	10150	10011.75	343.48225	366	6957	73896	226437	2241
130195	9930	10150	9932.75	410.28925	188	129	39465	300458	1642
130196	9930	10150	9934.75	406.86325	133	921	57300	275484	2141
130197	9930	10150	9940.25	397.44175	390	382	72599	265761	1225
130198	9930	10150	9946.75	386.30725	121	139	79829	243920	8548
130199	9930	10150	9963.75	357.18625	198	4102	57319	246507	1691
130200	9930	10150	9971.75	343.48225	284	4122	63102	231666	1162
130201	9930	10150	9981.75	326.35225	68	23498	39168	303436	1285
130202	10040	10250	10043.25	409.43275	94	286	29726	298025	2702
130203	10040	10250	10047.25	402.58075	112	524	58327	280875	7145
130204	10040	10250	10052.75	393.15925	169	980	66300	262230	3769
130205	10040	10250	10061.25	378.59875	170	234	66340	273929	2942
130206	10040	10250	10077.75	350.33425	98	4418	18157	314525	1220
130207	10020	10250	10022.75	410.28925	150	417	73258	282373	2150
130208	10020	10250	10023.75	408.57625	188	3100	70529	250313	6938
130209	10020	10250	10026.25	404.29375	195	598	55985	274759	828
130210	10020	10250	10033.75	391.44625	122	1749	52639	265540	5601
130211	10020	10250	10042.25	376.88575	182	2308	69269	257230	2987
130212	10020	10250	10059.25	347.76475	56	12088	17178	286231	1066
130213	10000	10250	10002.25	411.14575	162	590	62765	266419	3518
130214	10000	10250	10003.75	408.57625	132	511	64213	261444	2435
130215	10000	10250	10005.75	405.15025	90	936	56794	297545	2825
130216	10000	10250	10013.25	392.30275	152	1036	51754	280465	572
130217	10000	10250	10024.75	372.60325	227	3712	60943	263629	1338
130218	10000	10250	10033.75	357.18625	212	12316	45042	288074	613
130219	10000	10250	10044.25	339.19975	73	21701	29839	292830	1288
130220	10000	10250	10051.25	327.20875	100	16847	31351	301533	609
130221	9980	10250	9982.75	410.28925	208	153	32425	311649	1171
130222	9980	10250	9984.75	406.86325	127	624	57566	266976	842
130223	9980	10250	9998.75	382.88125	242	4429	74597	221995	27154
130224	9980	10250	10012.25	359.75575	104	1639	29442	304848	4951
130225	9980	10250	10017.25	351.19075	148	2658	46379	275528	167
130226	9980	10250	10026.25	335.77375	393	4474	57835	241944	3213
130227	10050	10400	10052.25	411.14575	99	434	32899	291862	119
130228	10050	10400	10053.75	408.57625	265	1156	46745	252780	110
130229	10050	10400	10058.75	400.01125	254	2041	51491	260718	381
130230	10050	10400	10070.25	380.31175	229	1461	47552	268641	126
130231	10050	10400	10081.25	361.46875	124	643	37190	294949	557
130232	10050	10400	10091.25	344.33875	61	20453	30724	305349	393
130233	10030	10400	10032.25	411.14575	78	355	42836	265948	502
130234	10030	10400	10035.25	406.00675	174	4207	52772	271420	418
130235	10030	10400	10038.25	400.86775	184	6499	53477	240215	138
130236	10030	10400	10041.75	394.87225	218	7078	60732	243781	557
130237	10030	10400	10049.25	382.02475	187	4414	48160	245870	75
130238	10030	10400	10062.75	358.89925	188	937	40368	281325	151
130239	10030	10400	10071.25	344.33875	271	1203	49770	267016	230
130240	10010	10400	10012.75	410.28925	113	543	47020	297884	730
130241	10010	10400	10015.75	405.15025	107	2007	56269	252619	891
130242	10010	10400	10020.75	396.58525	135	4537	47656	256218	37
130243	10010	10400	10030.25	380.31175	89	2918	39554	283025	102

Sample	Easting	Northing	Ph Easting	Ph R.L.	F	NA	AL	SI	S
130244	10010	10400	10042.75	358.89925	127	4378	45039	279106	835
130245	10010	10400	10051.25	344.33875	189	7527	55794	259737	219
130246	10010	10400	10059.75	329.77825	331	1911	58388	246649	133
130247	10010	10400	10066.75	317.78725	110	18110	39344	302198	224
130248	9990	10400	9992.75	410.28925	104	610	46448	298212	762
130249	9990	10400	9994.25	407.71975	177	2200	56156	249603	172
130250	9990	10400	9999.25	399.15475	228	5481	54023	245988	174
130251	9990	10400	10011.75	377.74225	89	4692	49457	272663	1106
130252	9990	10400	10020.75	362.32525	102	3403	37153	285341	204
130253	9990	10400	10030.25	346.05175	81	5657	29861	299109	572
130254	9990	10400	10037.75	333.20425	152	9719	32844	277083	189
130255	10080	10400	10082.25	411.14575	42	299	23709	277702	90
130256	10080	10400	10087.25	402.58075	105	1316	50399	269278	1536
130257	10080	10400	10097.75	384.59425	211	3748	50048	248361	79
130258	10080	10400	10108.25	366.60775	202	6360	55942	266180	266
130259	10080	10400	10121.25	344.33875	310	2119	44499	267823	272
130260	10100	10400	10101.75	412.00225	128	269	69308	232296	9388
130261	10100	10400	10102.75	410.28925	134	626	56693	252066	757
130262	10100	10400	10106.25	404.29375	279	2104	62945	214651	3031
130263	10100	10400	10115.75	388.02025	197	3825	51850	252875	506
130264	10100	10400	10137.25	351.19075	169	1004	33643	292415	311
130265	10300	10150	10302.75	410.28925	69	143	27845	264419	280
130267	10300	10150	10308.75	400.01125	165	377	44277	282507	77
130268	10300	10150	10314.25	390.58975	176	2121	43723	294209	1299
130269	10300	10150	10323.25	375.17275	210	393	49847	277087	245
130270	10300	10150	10333.25	358.04275	368	1064	63373	253527	196
130271	10300	10150	10335.75	353.76025	369	1044	59615	260641	94
130272	10300	10150	10338.25	349.47775	332	4725	73607	270287	4039
130273	10300	10150	10349.25	330.63475	283	1860	71107	255135	221
130274	10300	10150	9852.75	410.28925	224	272	43617	284190	3494
130275	10300	10150	9856.75	403.43725	352	672	47444	288679	351
130276	10300	10150	9858.25	400.86775	369	587	48237	268554	12817
130277	10300	10150	9860.25	397.44175	413	1005	67426	259086	6076
130278	10300	10150	9865.75	388.02025	301	1537	63805	258662	6794
130279	10300	10150	9876.75	369.17725	225	1460	70303	265549	3446
130280	10300	10150	9883.75	357.18625	418	3027	71365	258496	510
130281	10050	10150	10052.75	410.28925	192	612	64305	266547	846
130282	10050	10150	10055.25	406.00675	443	209	76091	268873	1118
130283	10050	10150	10057.75	401.72425	280	151	61471	280319	1054
130284	10050	10150	10061.75	394.87225	262	243	67920	279314	895
130285	10050	10150	10073.75	374.31625	350	467	79469	248435	1883
130286	10050	10150	10088.75	348.62125	197	364	53505	291635	2687
130287	10070	10150	10072.75	410.28925	173	227	30848	321655	1023
130288	10070	10150	10075.75	405.15025	231	402	41448	302224	340
130289	10070	10150	10078.25	400.86775	293	349	43674	295901	2686
130290	10070	10150	10083.75	391.44625	112	123	37748	304466	106
130291	10070	10150	10093.75	374.31625	303	2263	60075	287494	1677
130292	10070	10150	10103.25	358.04275	293	699	51821	284255	2239
130293	10070	10150	10107.75	350.33425	322	790	61698	276944	1255
130294	10070	10150	10112.75	341.76925	323	626	56840	306303	257
130295	10060	10150	10063.75	408.57625	148	1042	45996	283270	261
130296	10060	10150	10068.75	400.01125	408	1991	64984	250828	57
130297	10060	10150	10079.25	382.02475	121	3999	40101	267245	198
130298	10060	10150	10073.75	391.44625	106	1484	50703	274095	3145
130299	10060	10150	10066.75	403.43725	310	228	49653	281545	121
130300	9890	10150	9892.75	410.28925	264	319	82724	262508	1645
130301	9890	10150	9894.25	407.71975	106	216	43683	305653	812
130302	9890	10150	9895.25	406.00675	212	663	61206	286869	287
130303	9890	10150	9896.75	403.43725	130	262	42780	293353	359
130304	9890	10150	9905.25	388.87675	150	231	50948	288544	259
130305	9890	10150	9918.25	366.60775	213	14533	52398	276810	795
130306	9890	10150	9924.25	356.32975	127	20109	45769	297335	1967
130307	9890	10150	9934.25	339.19975	139	5652	44966	291467	1026
130308	9890	10150	9937.25	334.06075	153	4740	31883	310274	489

Sample	CL	K	CA	TI	V	CR	MN	FE	CO	NI	CU
130171	17	1925	86	13960	183	0	14	3128	23	15	14
130172	23	14712	201	11970	419	42	9	3719	22	7	8
130173	15	8018	164	17847	334	0	9	4235	25	6	17
130174	52	36346	312	7920	247	37	20	12540	54	6	5
130175	47	19675	180	2850	84	13	8	2724	15	4	2
130176	45	10243	460	12144	278	0	16	2437	20	2	3
130177	0	14300	230	12354	311	0	10	3018	22	5	6
130178	62	590	175	18298	250	0	4	2491	10	8	8
130179	156	500	215	14054	338	0	14	4101	27	11	16
130180	13	6551	179	21785	495	0	8	3946	19	6	13
130181	0	11641	178	14599	399	0	14	4182	22	1	7
130182	0	18423	190	12355	360	5	16	5571	34	1	3
130183	43	5422	144	11888	252	0	10	2620	23	3	2
130184	6	14702	166	13389	326	0	8	2829	21	4	2
130185	25	3164	1047	9421	228	2	12	1498	16	3	7
130186	121	1109	54	15254	197	0	6	1903	14	14	6
130187	81	574	40	22175	306	0	20	2599	22	24	14
130188	144	3068	141	8178	201	9	8	3042	22	7	10
130189	16	5760	169	16882	290	0	8	2396	20	4	18
130190	82	3331	132	16918	284	0	6	2502	15	7	14
130191	0	3918	240	18032	293	0	10	3491	18	5	14
130192	68	16442	225	25987	639	0	23	3731	37	10	5
130193	19	33277	204	8080	512	11	20	8287	42	3	2
130194	21	22665	194	9709	410	21	13	3920	19	8	1
130195	55	354	80	12970	231	8	9	2217	22	14	8
130196	15	1312	57	8003	175	47	16	3122	27	10	7
130197	6	18646	231	10257	398	12	26	6779	41	4	4
130198	5	2942	76	12844	285	0	14	4069	26	2	7
130199	30	12145	283	17920	459	0	12	3248	22	4	3
130200	9	20595	264	10503	382	40	16	3642	24	7	4
130201	23	3664	305	10800	179	0	8	1722	17	3	3
130202	26	2105	50	12459	207	0	19	1780	14	7	7
130203	10	704	87	17058	324	0	12	3204	20	5	13
130204	30	4938	122	18933	495	0	17	4832	27	4	11
130205	82	6693	137	16710	407	0	12	5348	37	7	6
130206	73	518	218	18020	208	0	12	4661	32	2	9
130207	19	1159	23	14187	248	0	9	2880	18	22	9
130208	18	3432	142	10809	196	11	19	3621	26	16	8
130209	140	3084	149	14734	315	0	11	3782	27	3	7
130210	30	6128	155	20140	341	0	10	3831	21	2	10
130211	68	13309	205	23714	633	0	16	3322	25	7	6
130212	27	338	366	13187	212	0	11	1658	19	2	5
130213	19	1905	62	15010	235	2	15	3297	26	19	8
130214	103	554	105	7712	128	20	13	4202	29	16	11
130215	79	761	123	9774	193	14	5	3112	20	9	6
130216	99	9430	126	11281	281	0	10	3748	25	3	6
130217	59	21822	330	22479	621	0	22	4335	29	4	2
130218	117	12249	236	19238	457	0	7	3328	17	3	4
130219	115	2006	364	14624	173	0	13	1947	18	3	3
130220	87	5059	384	16124	308	0	8	3071	25	6	6
130221	94	4122	150	11046	196	7	10	5453	28	5	8
130222	136	2351	56	9265	187	6	22	3042	22	17	6
130223	0	17530	214	15414	502	0	14	4412	27	4	3
130224	26	5815	312	21753	272	0	13	2667	20	4	3
130225	172	17268	257	20120	352	0	19	2578	20	9	2
130226	9	26058	244	17652	498	24	16	8968	45	5	2
130227	143	1867	58	9999	141	17	13	1962	17	8	8
130228	143	14603	223	11218	279	34	14	3213	24	11	9
130229	162	16420	288	13236	436	50	15	3587	25	7	7
130230	175	17834	305	14129	482	41	16	3978	28	4	4
130231	114	8565	353	20732	348	0	15	3143	24	4	5
130232	154	1185	670	16183	253	0	10	1760	13	4	16
130233	177	852	11	13880	216	0	11	1803	16	17	11
130234	117	1927	175	10605	338	0	9	2777	24	11	12
130235	185	4696	162	15110	495	0	15	3695	27	5	8
130236	108	6845	163	16392	455	0	12	2104	12	4	6
130237	151	12851	158	14656	479	0	9	3074	13	4	6
130238	111	14680	186	12432	339	2	11	2769	19	2	9
130239	61	22692	386	16952	518	17	17	4890	36	4	5
130240	189	1281	73	21119	331	0	13	2500	22	21	12
130241	137	1404	195	12072	226	0	4	2993	22	16	10
130242	135	3272	261	14912	321	0	6	2166	24	5	11
130243	253	4719	477	24316	340	0	19	3311	25	31	30

Sample	CL	K	CA	TI	V	CR	MN	FE	CO	NI	CU
130244	118	5406	398	19751	349	0	13	2939	21	4	8
130245	180	9176	228	13147	395	0	22	3640	34	4	5
130246	81	23930	223	9409	432	29	14	5477	36	3	4
130247	77	5757	317	9773	246	0	12	2245	18	3	4
130248	182	2066	37	12982	200	0	10	2242	16	14	8
130249	154	3635	139	14252	312	0	12	3206	19	10	9
130250	170	7383	194	11273	295	0	74	3074	19	3	8
130251	119	4075	255	15364	335	0	13	2240	14	11	20
130252	237	5274	176	11375	239	0	13	2358	19	3	14
130253	104	4922	243	15426	236	0	8	2565	22	1	5
130254	31	10928	204	9946	238	0	10	5503	25	1	7
130255	311	497	29	3776	32	6	6	1880	15	6	6
130256	125	6714	167	11272	295	7	5	2781	20	3	15
130257	99	15163	230	11896	346	18	8	2366	11	2	6
130258	108	8602	249	18282	472	0	19	3751	20	4	2
130259	90	19050	222	11360	381	0	21	7788	43	3	7
130260	72	1616	77	15638	264	7	14	4578	24	25	14
130261	206	2791	101	12568	276	9	11	3323	21	15	9
130262	107	15456	277	16100	467	0	14	5391	35	8	13
130263	162	14108	268	15979	451	0	14	2726	21	3	11
130264	146	9084	135	11333	301	9	8	2029	20	3	3
130265	235	2115	60	6480	88	5	10	1312	5	13	6
130267	227	10242	204	19566	380	0	11	3587	26	5	18
130268	52	6370	157	16756	330	0	14	2524	19	5	11
130269	84	19283	218	12001	371	0	22	5423	35	9	3
130270	63	30802	231	8101	251	78	10	6339	35	3	2
130271	67	30562	283	8947	285	37	17	9032	51	8	3
130272	0	25631	175	7890	224	60	12	4258	19	3	1
130273	54	27178	262	13963	486	15	19	5662	36	3	9
130274	54	4122	71	9792	230	16	17	4428	29	17	12
130275	65	20477	195	11339	409	16	19	7987	47	9	7
130276	0	21569	233	11279	366	49	14	7978	50	6	5
130277	24	13241	181	10375	363	181	17	6419	36	8	8
130278	26	20685	181	10117	391	36	21	7172	37	6	8
130279	23	11541	156	12205	306	170	5	3990	26	7	2
130280	32	30479	194	9653	446	55	21	5529	29	8	2
130281	193	1952	61	9119	164	20	14	3924	26	12	10
130282	39	3582	105	11511	326	20	14	9951	55	10	12
130283	89	7387	129	14182	371	0	14	4812	31	3	9
130284	30	16108	184	11268	322	24	21	8951	48	3	8
130285	0	35696	242	11187	369	47	41	14253	67	9	9
130286	63	5191	121	10850	237	0	7	4022	30	3	5
130287	50	1567	104	11604	210	0	10	3000	21	4	3
130288	96	12625	153	11140	315	1	16	6583	35	4	8
130289	40	19932	239	13439	326	4	15	9193	46	2	3
130290	190	3801	202	19179	309	0	14	3017	25	6	9
130291	44	28201	240	11698	344	40	28	9964	50	6	9
130292	17	24710	272	11609	382	3	34	8862	48	1	2
130293	72	33498	306	8234	283	10	27	11598	59	1	13
130294	69	35599	340	8977	286	29	31	13413	60	0	1
130295	284	1796	189	10124	223	17	11	3407	17	9	14
130296	187	22728	269	15314	548	72	13	4155	29	4	7
130297	154	8157	124	18478	401	0	14	3015	23	3	11
130298	10	3998	165	16115	322	0	18	2192	15	4	11
130299	90	17445	206	9365	210	22	19	9286	45	4	6
130300	168	990	49	12464	192	104	22	5628	34	55	23
130301	81	310	151	8792	144	156	8	3300	28	17	15
130302	148	2164	119	10061	218	277	8	4162	18	14	16
130303	204	7796	211	8233	244	238	8	4299	27	10	7
130304	126	13771	255	12904	361	0	19	7011	43	4	11
130305	60	15517	463	9776	315	23	9	3563	23	3	3
130306	18	10157	575	9583	315	6	9	2451	22	1	3
130307	87	7126	272	13857	394	0	28	2168	16	1	3
130308	56	4332	214	18188	297	0	8	2320	17	1	1

Sample	ZN	GA	GE	AS	RB	SR	Y	ZR	NB	MO	W	PB	TH
130171	3	7	1	9	11	9	22	240	9	1	19	3	9
130172	5	15	0	3	36	13	17	107	11	0	52	2	5
130173	1	4	1	3	22	8	40	200	13	1	12	3	5
130174	13	17	0	2	100	13	22	116	7	8	6	6	8
130175	2	6	2	2	49	16	7	51	2	3	6	2	0
130176	4	6	1	3	27	27	18	123	4	1	5	2	3
130177	5	5	0	2	40	11	14	71	6	4	8	4	5
130178	3	5	1	8	3	14	30	345	14	13	22	8	6
130179	5	11	0	5	3	12	20	182	9	1	15	4	2
130180	6	15	1	13	15	7	31	231	13	4	23	2	6
130181	2	9	1	2	27	8	22	124	5	3	59	3	2
130182	2	8	0	3	51	10	16	141	7	2	52	1	4
130183	4	4	1	3	16	7	31	97	8	4	25	5	3
130184	3	9	0	4	42	13	16	105	8	0	82	1	4
130185	3	8	2	4	13	70	11	72	5	0	1	6	2
130186	3	5	2	4	5	4	36	380	14	0	9	2	5
130187	3	5	2	9	5	5	22	446	25	6	26	4	10
130188	4	9	1	3	10	28	14	95	1	3	13	4	4
130189	2	9	1	8	13	23	23	175	12	3	33	3	10
130190	2	6	2	7	9	28	31	197	12	2	10	8	2
130191	1	4	1	9	10	14	23	195	11	6	4	5	1
130192	5	12	0	8	41	15	36	225	15	5	199	5	8
130193	9	23	0	1	89	8	15	60	5	1	53	3	7
130194	3	18	0	5	60	26	26	333	9	1	35	4	4
130195	0	3	2	3	2	3	23	324	16	6	10	5	12
130196	3	6	2	2	3	14	15	96	6	1	12	3	4
130197	7	13	0	0	39	3	18	92	4	3	23	3	5
130198	4	5	1	3	7	2	20	119	9	6	65	4	2
130199	3	10	2	10	30	50	33	196	14	6	9	5	2
130200	2	13	2	5	57	10	14	92	7	6	13	1	1
130201	2	3	0	3	7	41	18	90	5	6	3	4	3
130202	0	4	1	2	10	8	44	802	9	21	29	5	13
130203	3	8	0	6	4	9	29	146	15	2	121	1	2
130204	1	9	0	1	14	11	26	145	11	6	78	7	3
130205	8	11	3	8	15	7	28	188	12	0	2	11	1
130206	6	2	3	10	1	15	22	188	9	10	0	10	2
130207	2	7	2	3	7	5	20	255	12	4	8	1	1
130208	3	7	0	2	13	10	14	167	6	2	7	5	7
130209	3	7	1	6	9	15	18	171	12	3	7	4	5
130210	2	5	0	9	16	21	26	207	11	12	28	7	1
130211	3	13	0	4	34	19	29	201	13	3	153	2	5
130212	2	3	2	5	2	22	15	150	6	3	5	1	2
130213	3	7	2	5	10	5	18	269	16	3	9	4	8
130214	3	9	2	2	4	5	13	133	3	1	4	2	6
130215	2	7	2	5	5	13	16	118	6	6	1	1	7
130216	5	6	3	3	25	10	13	78	7	1	10	0	2
130217	4	16	0	12	56	20	29	192	14	9	51	5	3
130218	5	8	1	3	29	21	27	169	12	2	67	4	4
130219	3	3	0	6	6	35	13	119	10	4	2	1	1
130220	6	5	2	7	13	50	26	130	13	1	3	3	4
130221	7	4	0	6	13	7	24	181	12	8	11	7	6
130222	2	5	2	3	10	8	14	192	13	6	2	2	3
130223	4	12	2	3	45	23	21	106	6	2	20	2	9
130224	4	2	2	10	13	17	35	200	10	5	5	9	2
130225	4	8	0	8	46	12	24	124	16	2	105	2	4
130226	6	13	0	2	76	19	26	196	18	1	64	8	13
130227	0	3	1	9	9	5	20	380	12	6	11	2	3
130228	4	12	0	10	40	9	22	130	7	5	63	2	5
130229	5	10	1	8	43	16	29	149	15	0	40	3	4
130230	3	10	0	9	44	19	21	147	4	0	55	6	4
130231	2	5	1	11	19	10	29	179	13	2	5	4	2
130232	4	3	2	6	5	23	20	157	11	5	3	3	0
130233	1	4	1	8	5	4	21	226	15	6	5	4	9
130234	2	12	1	7	4	19	24	169	6	2	24	2	7
130235	4	11	0	6	13	23	29	199	12	5	52	3	2
130236	1	15	0	9	15	31	32	194	13	9	60	3	4
130237	2	9	0	4	29	24	22	138	8	6	48	6	5
130238	0	7	3	7	40	11	24	145	7	2	44	4	4
130239	2	12	1	6	61	7	20	170	11	7	16	3	4
130240	1	6	4	13	4	5	28	360	22	7	11	8	4
130241	3	11	1	9	6	11	25	202	9	0	3	2	3
130242	2	8	1	16	9	32	29	171	13	10	1	7	6
130243	2	5	2	25	14	24	29	235	14	10	2	5	2

Sample	ZN	GA	GE	AS	RB	SR	Y	ZR	NB	MO	W	PB	TH
130244	3	6	2	20	13	20	32	217	18	4	9	6	1
130245	3	11	2	9	26	21	24	105	6	1	8	2	3
130246	4	16	2	9	81	8	18	119	5	5	61	2	3
130247	3	4	1	3	12	28	15	66	7	0	29	5	3
130248	2	5	2	8	10	6	29	412	17	2	3	4	5
130249	6	8	1	10	15	8	27	312	11	5	18	5	5
130250	2	14	1	8	19	53	24	153	9	1	5	7	5
130251	3	7	1	8	10	14	30	190	8	7	7	3	1
130252	2	5	1	4	11	9	14	99	3	4	2	2	3
130253	3	4	2	6	17	25	30	130	11	2	4	2	3
130254	3	8	2	4	36	21	18	113	8	5	1	5	7
130255	1	4	1	2	2	6	8	213	6	5	3	2	2
130256	1	6	0	3	21	15	13	138	14	4	0	1	5
130257	0	9	0	9	38	8	16	132	7	3	57	0	3
130258	4	12	1	20	19	26	25	170	10	0	0	10	2
130259	4	9	2	4	62	13	23	119	3	1	12	7	3
130260	3	9	4	10	10	11	25	466	13	3	5	0	11
130261	0	9	2	5	9	9	22	177	10	4	0	4	4
130262	2	19	2	1	40	7	14	176	12	2	7	1	5
130263	0	14	1	4	41	12	13	150	11	0	3	3	3
130264	0	5	0	4	24	9	26	120	8	4	83	3	3
130265	11	3	0	2	7	4	8	280	9	4	5	3	4
130267	5	7	0	4	28	4	37	230	16	0	37	4	3
130268	3	8	0	9	17	18	34	199	13	5	25	2	5
130269	5	11	0	4	55	6	18	107	10	4	37	1	5
130270	5	17	0	2	87	9	21	169	16	2	19	4	8
130271	9	15	0	2	92	10	15	111	11	0	9	6	4
130272	3	17	0	1	68	10	13	80	10	0	31	5	9
130273	4	15	1	4	73	11	16	140	7	2	45	1	6
130274	4	7	2	5	18	3	28	381	15	6	3	5	5
130275	6	12	1	4	65	7	20	141	7	2	11	3	6
130276	7	11	0	3	63	11	22	132	5	2	9	3	6
130277	6	11	0	8	44	13	17	131	10	8	10	3	2
130278	6	11	0	1	64	15	17	97	0	0	26	6	5
130279	3	8	0	10	32	8	42	136	9	3	59	2	0
130280	6	17	1	6	89	12	19	101	6	1	66	0	0
130281	5	9	1	4	7	7	19	451	6	5	8	5	3
130282	12	16	3	5	12	4	18	168	6	4	1	3	5
130283	4	9	0	4	20	4	28	191	11	0	19	7	4
130284	4	10	1	0	41	4	21	106	8	3	21	3	8
130285	14	19	1	6	94	5	16	107	11	2	4	0	0
130286	2	3	0	5	13	13	17	84	5	6	10	1	1
130287	2	3	1	4	9	5	22	188	10	5	7	5	4
130288	5	9	1	3	39	3	22	142	12	2	4	2	6
130289	7	12	1	5	60	5	21	155	12	5	9	0	6
130290	3	7	2	5	13	4	34	215	13	3	0	3	6
130291	7	17	1	6	84	15	16	122	9	0	0	2	5
130292	6	13	1	5	72	8	22	140	11	3	0	3	9
130293	9	17	0	4	105	7	15	144	5	4	0	7	5
130294	8	17	3	5	82	8	18	88	3	4	4	0	2
130295	3	7	0	12	7	20	18	147	7	4	27	4	4
130296	2	16	1	7	48	15	24	157	6	7	60	2	1
130297	3	5	0	8	17	13	22	161	15	5	59	6	4
130298	2	7	0	3	12	11	28	154	9	7	111	10	8
130299	11	13	2	7	53	5	25	218	17	4	12	0	6
130300	3	9	2	7	6	6	19	229	15	1	4	3	8
130301	1	7	0	2	1	5	18	135	3	1	2	1	6
130302	2	10	0	3	7	9	14	129	8	2	0	1	3
130303	8	7	2	3	23	12	15	142	4	4	5	1	2
130304	3	9	1	4	44	9	12	135	9	2	3	4	3
130305	6	11	0	4	39	36	11	74	8	0	17	4	5
130306	4	5	2	4	26	52	10	77	3	5	11	0	0
130307	2	11	2	12	15	25	21	143	14	2	15	4	3
130308	3	5	1	14	10	24	31	161	17	13	3	4	2

APPENDIX 6

EPR ANYLYSES INFORMATION, JIM'S FIND TANAMI, N.T.

SAMPLE	Unique sample identifier given to open pit samples
Easting	Coordinated at easting for sample locality
Northing	Coordinated at northing for sample locality
Ph Easting	Coordinated at X-axis for sample locality
Ph R.L.	Coordinated at Y-axis for sample locality
AU (NAA)	Gold data analzed by NAA (from Stott, 1994)

Sample	Easting	Northing	Ph Easting	Ph R.L.	5mT	100 mT
130171	10010	10150	10011.75	412.00	3	1.0
130172	10010	10150	10018.75	400.01	22	4.4
130173	10010	10150	10027.25	385.45	33	2.2
130174	10010	10150	10037.75	367.46	40	1.8
130175	10010	10150	10045.25	354.62	38	0.6
130176	10010	10150	10051.25	344.34	15	0.6
130177	10010	10150	10057.75	333.20	15	0.6
130178	9990	10150	9992.75	410.29	7	1.0
130179	9990	10150	9994.25	407.72	8	1.0
130180	9990	10150	9999.75	398.30	10	0.6
130181	9990	10150	10007.75	384.59	11	0.8
130182	9990	10150	10016.25	370.03	27	1.4
130183	9990	10150	10023.25	358.04	6	0.5
130184	9990	10150	10025.75	353.76	14	0.3
130185	9990	10150	10033.25	340.91	10	1.7
130186	9970	10150	9971.75	412.00	5	2.0
130187	9970	10150	9973.25	409.43	7	2.4
130188	9970	10150	9977.75	401.72	10	2.9
130189	9970	10150	9980.75	396.59	18	4.9
130191	9970	10150	9986.75	386.31	13	1.3
130192	9970	10150	9995.75	370.89	20	1.5
130193	9970	10150	10002.25	359.76	16	1.2
130194	9970	10150	10011.75	343.48	10	0.8
130195	9930	10150	9932.75	410.29	3	0.9
130196	9930	10150	9934.75	406.86	5	0.5
130197	9930	10150	9940.25	397.44	6	0.5
130198	9930	10150	9946.75	386.31	2	0.8
130199	9930	10150	9963.75	357.19	15	0.8
130200	9930	10150	9971.75	343.48	18	0.8
130201	9930	10150	9981.75	326.35	7	1.8
130265	10300	10150	10302.75	410.29	11	1.0
130267	10300	10150	10308.75	400.01	12	1.3
130268	10300	10150	10314.25	390.59	18	2.6
130269	10300	10150	10323.25	375.17	27	2.3
130270	10300	10150	10333.25	358.04	25	2.8
130271	10300	10150	10335.75	353.76	25	1.9
130272	10300	10150	10338.25	349.48	25	1.3
130273	10300	10150	10349.25	330.63	15	1.5
130274	10300	10150	9852.75	410.29	12	2.4
130275	10300	10150	9856.75	403.44	20	3.6
130276	10300	10150	9858.25	400.87	19	6.3
130277	10300	10150	9860.25	397.44	18	3.0
130278	10300	10150	9865.75	388.02	24	3.0
130279	10300	10150	9876.75	369.18	13	1.0
130280	10300	10150	9883.75	357.19	18	1.0
130281	10050	10150	10052.75	410.29	13	1.0
130282	10050	10150	10055.25	406.01	11	1.8
130283	10050	10150	10057.75	401.72	14	1.8
130284	10050	10150	10061.75	394.87	23.5	3.9
130285	10050	10150	10073.75	374.32	16	2.7
130286	10050	10150	10088.75	348.62	11	0.5
130288	10070	10150	10075.75	405.15	15	3.0
130289	10070	10150	10078.25	400.87	30	2.0
130291	10070	10150	10093.75	374.32	35	2.3
130292	10070	10150	10103.25	358.04	35	3.2
130293	10070	10150	10107.75	350.33	18	2.0
130294	10070	10150	10112.75	341.77	18	2.0
130298	10060	10150	10073.75	391.45	11	0.8
130300	9890	10150	9892.75	410.29	6	1.3

Sample	Easting	Northing	Ph Easting	Ph R.L.	5mT	100 mT
130301	9890	10150	9894.25	407.72	7	1.6
130302	9890	10150	9895.25	406.01	9	2.0
130303	9890	10150	9896.75	403.44	12	2.0
130304	9890	10150	9905.25	388.88	15	4.5
130305	9890	10150	9918.25	366.61	17	0.0
130306	9890	10150	9924.25	356.33	4	0.3
130307	9890	10150	9934.25	339.20	3	3.0
130308	9890	10150	9937.25	334.06	10	0.8

APPENDIX 7

ELEMENT DISTRIBUTION PLOTS, SECTION 10250N

JIM'S FIND, N.T.

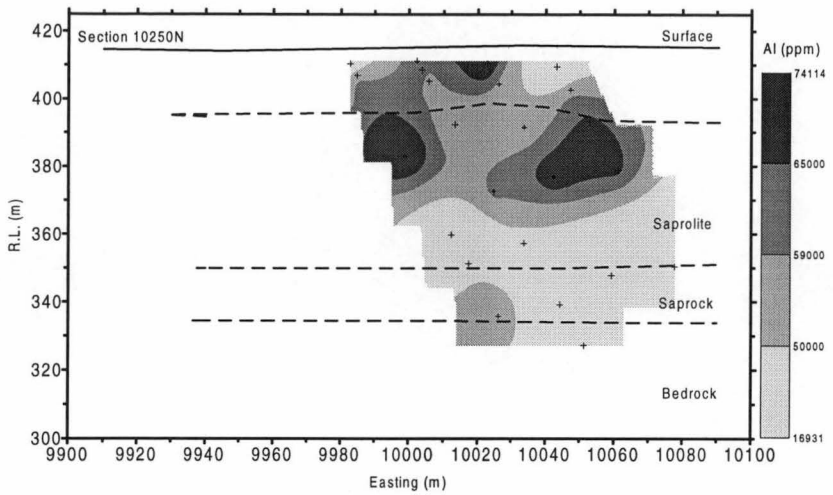
Section 10250N
Surface
Al (ppm)
74114
65000
59000
50000
16931
Saprolite
Saprock
Bedrock
R.L. (m)
420
400
380
360
340
320
300
9900 9920 9940 9960 9980 10000 10020 10040 10060 10080 10100
Easting (m)

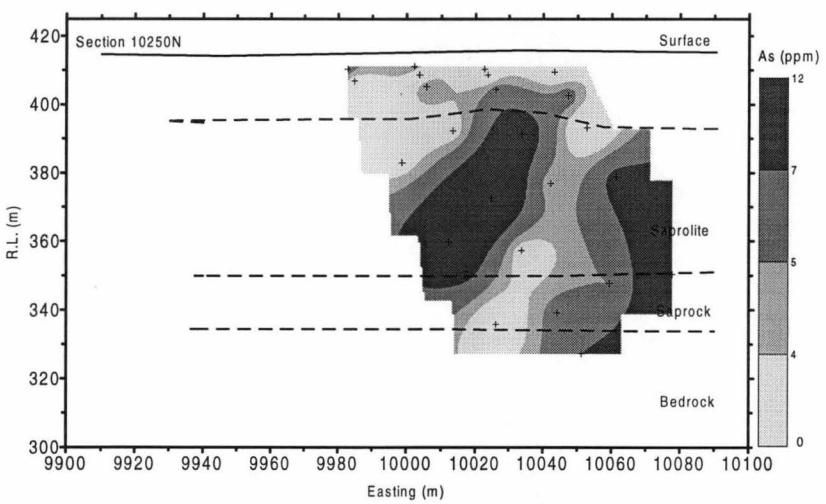
Section 10250N
Surface
As (ppm)
12
7
5
4
0
Saprolite
Saprock
Bedrock
R.L. (m)
420
400
380
360
340
320
300
9900 9920 9940 9960 9980 10000 10020 10040 10060 10080 10100
Easting (m)

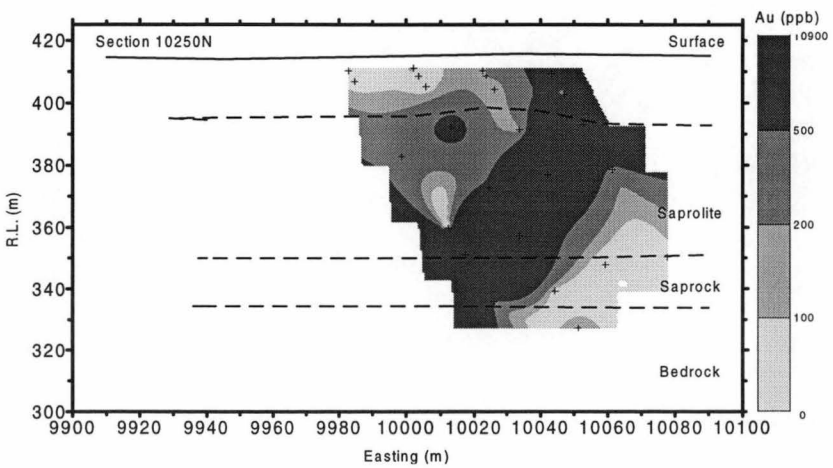
Section 10250N
Surface
Au (ppb)
10900
500
200
100
0
Saprolite
Saprock
Bedrock
R.L. (m)
420
400
380
360
340
320
300
9900 9920 9940 9960 9980 10000 10020 10040 10060 10080 10100
Easting (m)

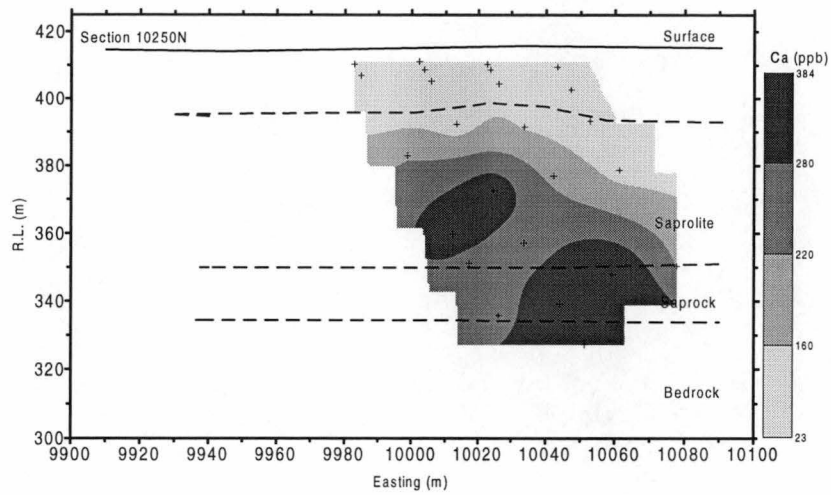
Section 10250N
Surface
Saprolite
Saprock
Bedrock
R.L. (m)
Easting (m)
Ca (ppb)
384
280
220
160
23

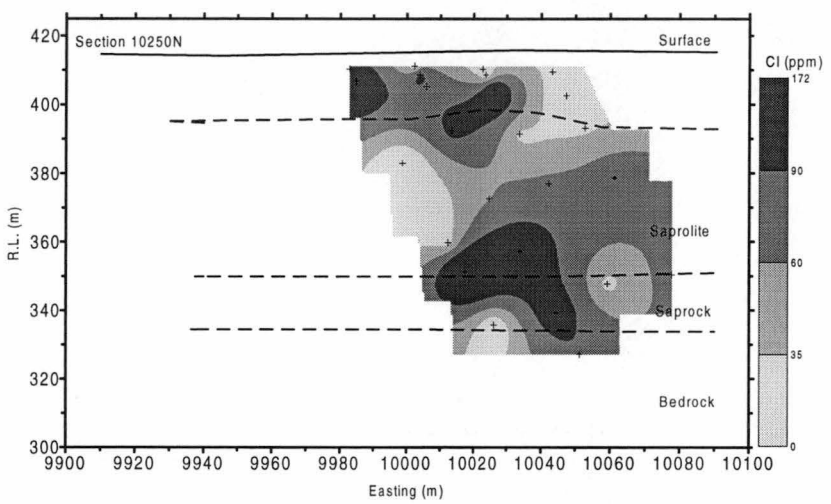
Section 10250N
Surface
Saprolite
Saprock
Bedrock
R.L. (m)
Easting (m)
Cl (ppm)
172
90
60
35
0

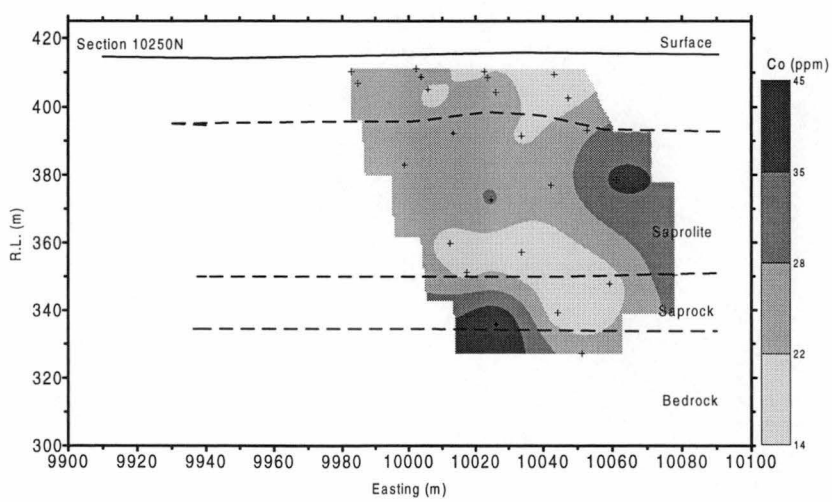
Section 10250N
Surface
Saprolite
Saprock
Bedrock
R.L. (m)
Easting (m)
Co (ppm)
45
35
28
22
14

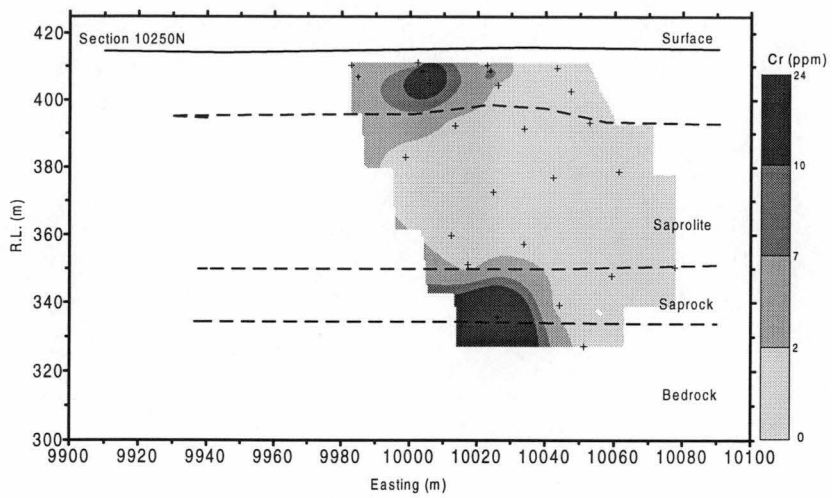
Section 10250N
Surface
Cr (ppm)
24
10
7
2
0
Saprolite
Saprock
Bedrock
R.L. (m)
420
400
380
360
340
320
300
9900
9920
9940
9960
9980
10000
10020
10040
10060
10080
10100
Easting (m)

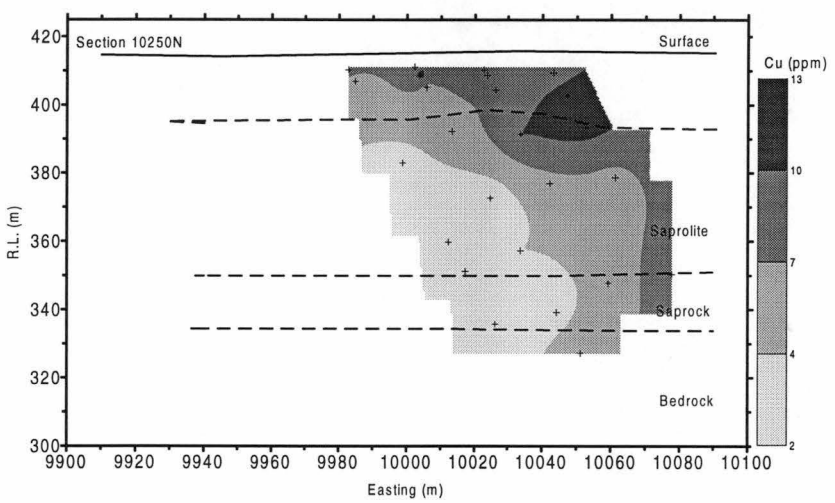
Section 10250N
Surface
Cu (ppm)
13
10
7
4
2
Saprolite
Saprock
Bedrock
R.L. (m)
420
400
380
360
340
320
300
9900
9920
9940
9960
9980
10000
10020
10040
10060
10080
10100
Easting (m)

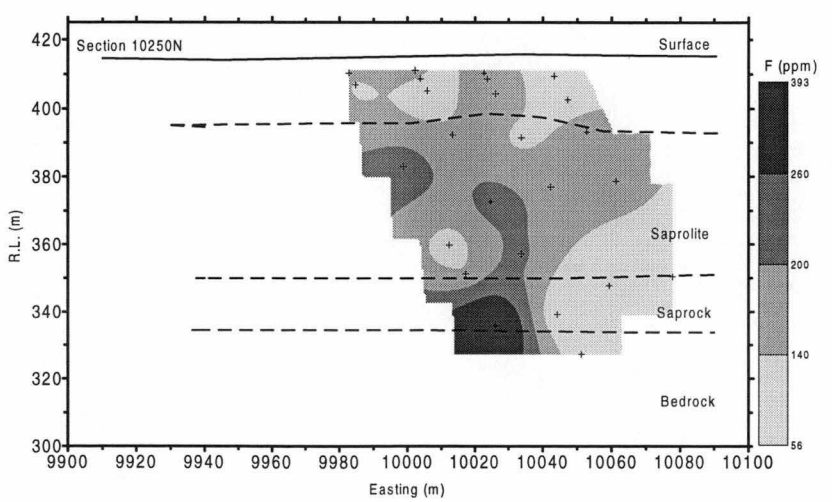
Section 10250N
Surface
F (ppm)
393
260
200
140
56
Saprolite
Saprock
Bedrock
R.L. (m)
420
400
380
360
340
320
300
9900
9920
9940
9960
9980
10000
10020
10040
10060
10080
10100
Easting (m)

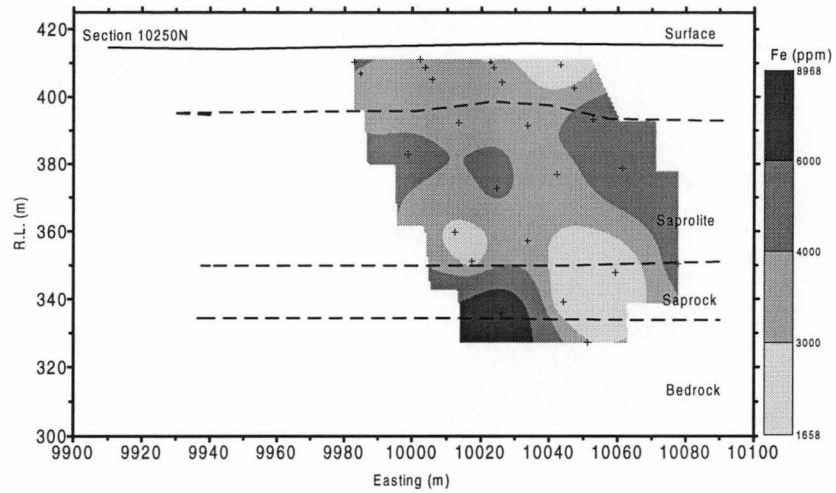
Section 10250N
Surface
Fe (ppm)
8968
6000
4000
3000
1658
Saprolite
Saprock
Bedrock
R.L. (m)
420
400
380
360
340
320
300
9900
9920
9940
9960
9980
10000
10020
10040
10060
10080
10100
Easting (m)

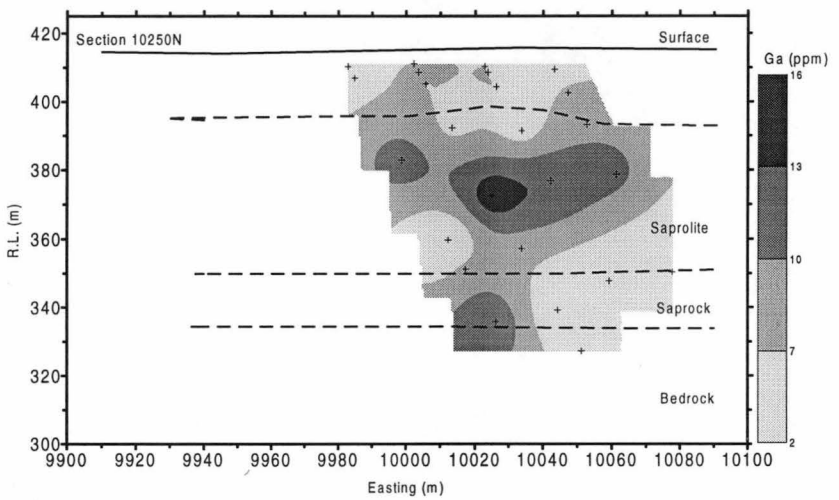
Section 10250N
Surface
Ga (ppm)
16
13
10
7
2
Saprolite
Saprock
Bedrock
R.L. (m)
420
400
380
360
340
320
300
9900
9920
9940
9960
9980
10000
10020
10040
10060
10080
10100
Easting (m)

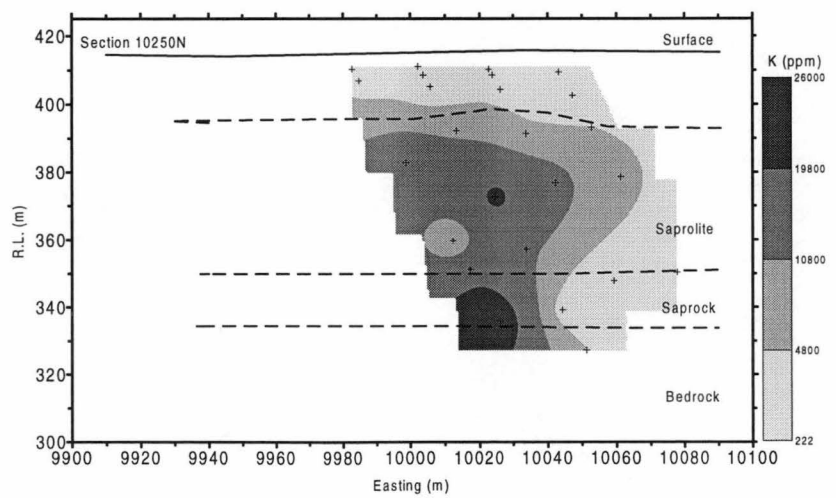
Section 10250N
Surface
K (ppm)
26000
19800
10800
4800
222
Saprolite
Saprock
Bedrock
R.L. (m)
420
400
380
360
340
320
300
9900
9920
9940
9960
9980
10000
10020
10040
10060
10080
10100
Easting (m)

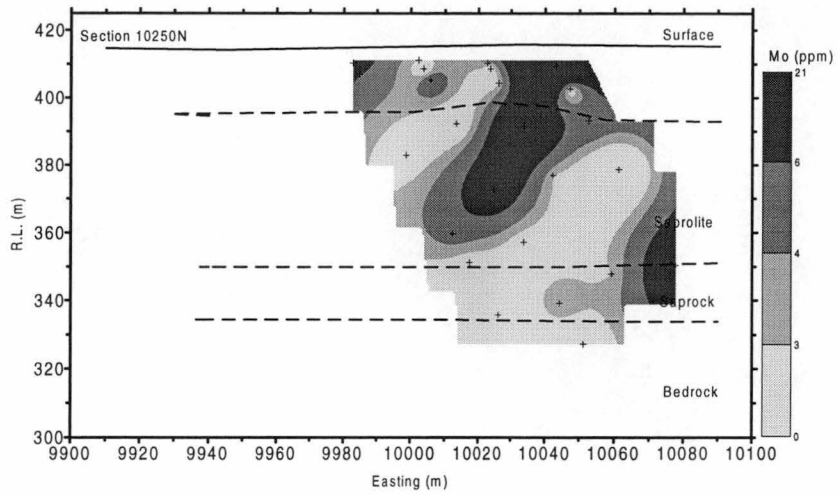
Section 10250N
Surface
Saprolite
Saprock
Bedrock
R.L. (m)
Easting (m)
Mo (ppm)
21
6
4
3
0

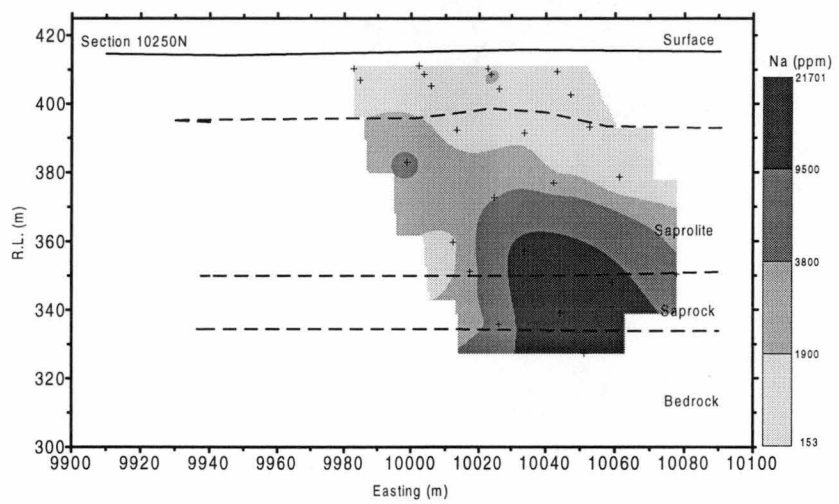
Section 10250N
Surface
Saprolite
Saprock
Bedrock
R.L. (m)
Easting (m)
Na (ppm)
21701
9500
3800
1900
153

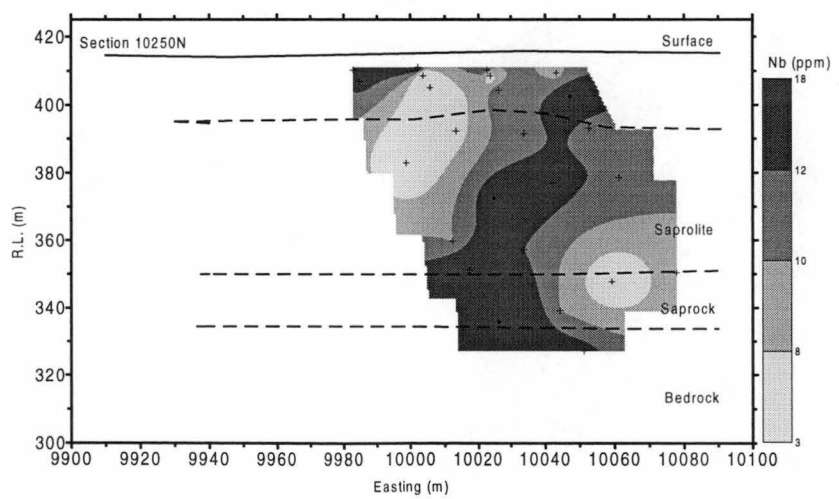
Section 10250N
Surface
Saprolite
Saprock
Bedrock
R.L. (m)
Easting (m)
Nb (ppm)
18
12
10
8
3

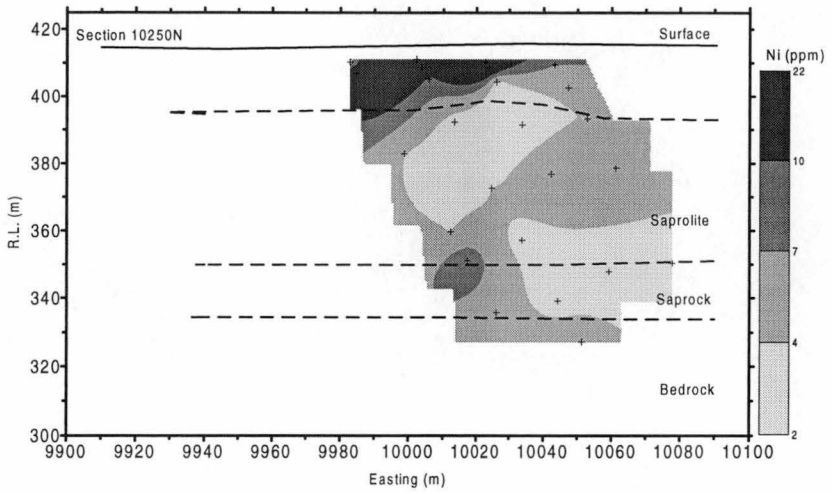
Section 10250N
Surface
Ni (ppm)
22
10
7
4
2
Saprolite
Saprock
Bedrock
R.L. (m)
420
400
380
360
340
320
300
9900 9920 9940 9960 9980 10000 10020 10040 10060 10080 10100
Easting (m)

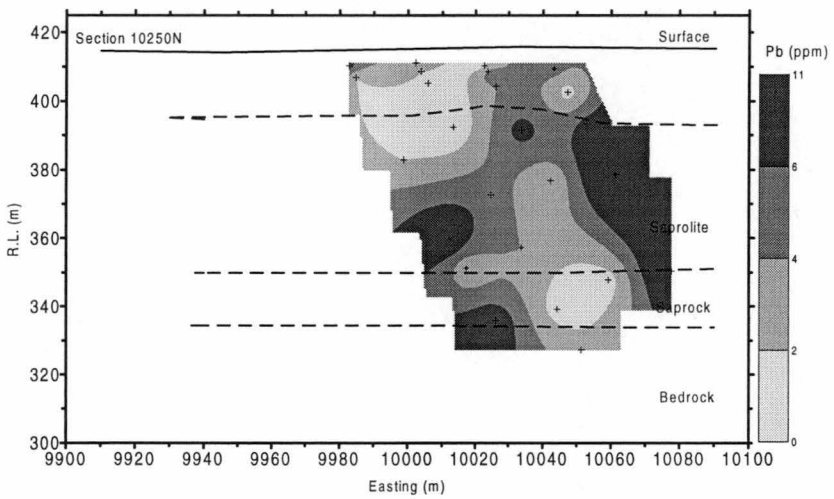
Section 10250N
Surface
Pb (ppm)
11
6
4
2
0
Saprolite
Saprock
Bedrock
R.L. (m)
420
400
380
360
340
320
300
9900 9920 9940 9960 9980 10000 10020 10040 10060 10080 10100
Easting (m)

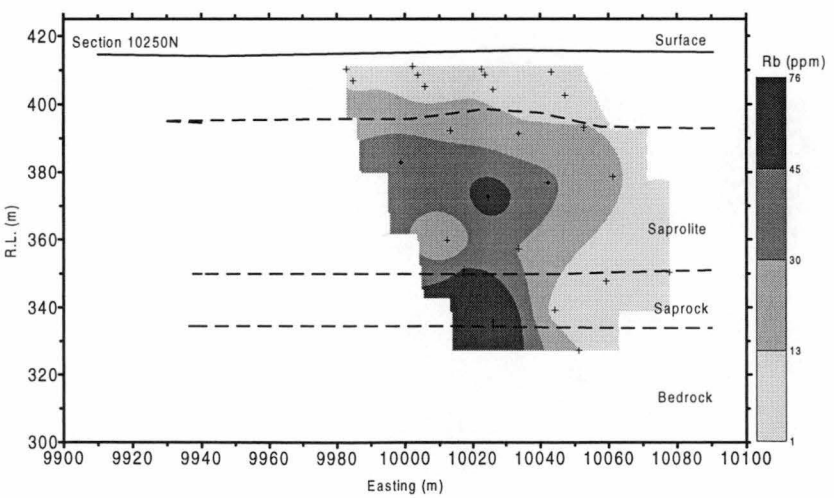
Section 10250N
Surface
Rb (ppm)
76
45
30
13
1
Saprolite
Saprock
Bedrock
R.L. (m)
420
400
380
360
340
320
300
9900 9920 9940 9960 9980 10000 10020 10040 10060 10080 10100
Easting (m)

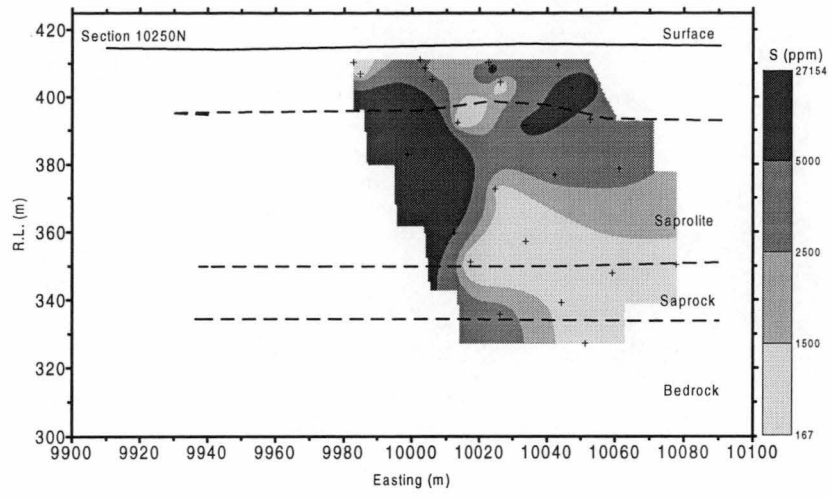
Section 10250N
Surface
S (ppm)
27154
5000
2500
1500
167
Saprolite
Saprock
Bedrock
R.L. (m)
420
400
380
360
340
320
300
9900
9920
9940
9960
9980
10000
10020
10040
10060
10080
10100
Easting (m)

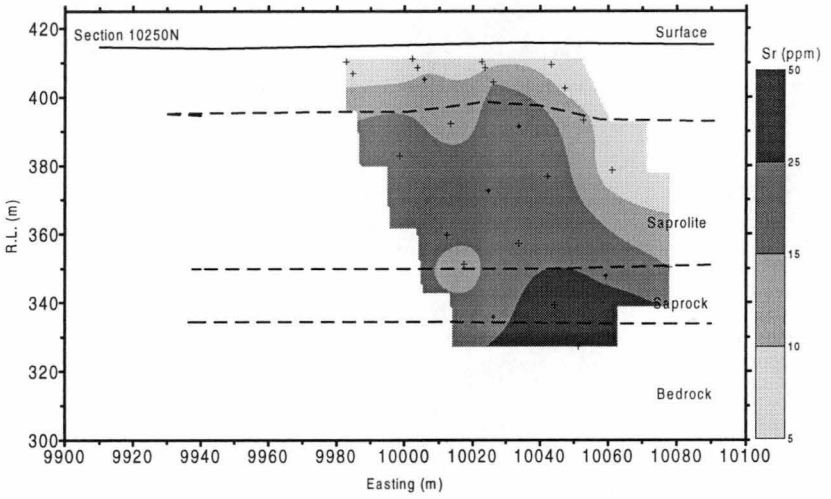
Section 10250N
Surface
Sr (ppm)
50
25
15
10
5
Saprolite
Saprock
Bedrock
R.L. (m)
420
400
380
360
340
320
300
9900
9920
9940
9960
9980
10000
10020
10040
10060
10080
10100
Easting (m)

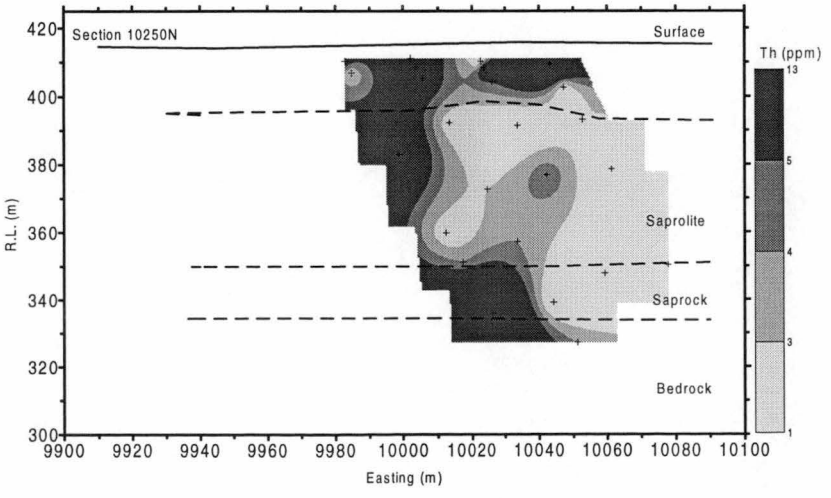
Section 10250N
Surface
Th (ppm)
13
5
4
3
1
Saprolite
Saprock
Bedrock
R.L. (m)
420
400
380
360
340
320
300
9900
9920
9940
9960
9980
10000
10020
10040
10060
10080
10100
Easting (m)

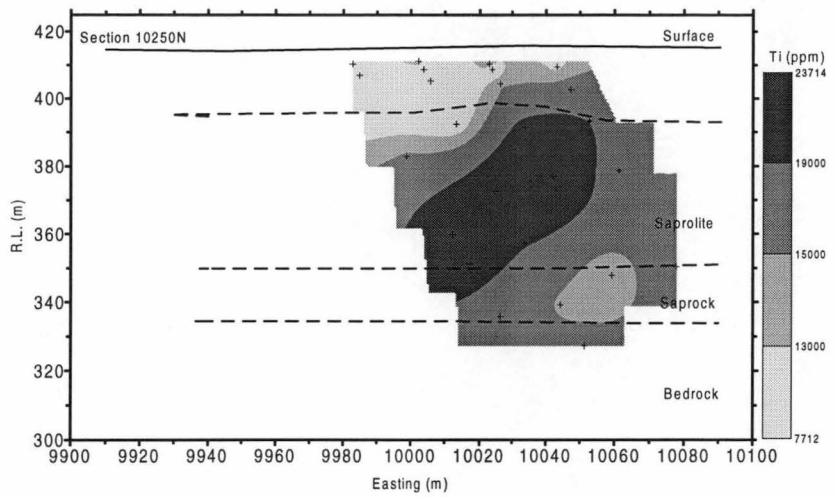
Section 10250N
Surface
Saprolite
Saprock
Bedrock
Ti (ppm)
23714
19000
15000
13000
7712
R.L. (m)
420
400
380
360
340
320
300
9900 9920 9940 9960 9980 10000 10020 10040 10060 10080 10100
Easting (m)

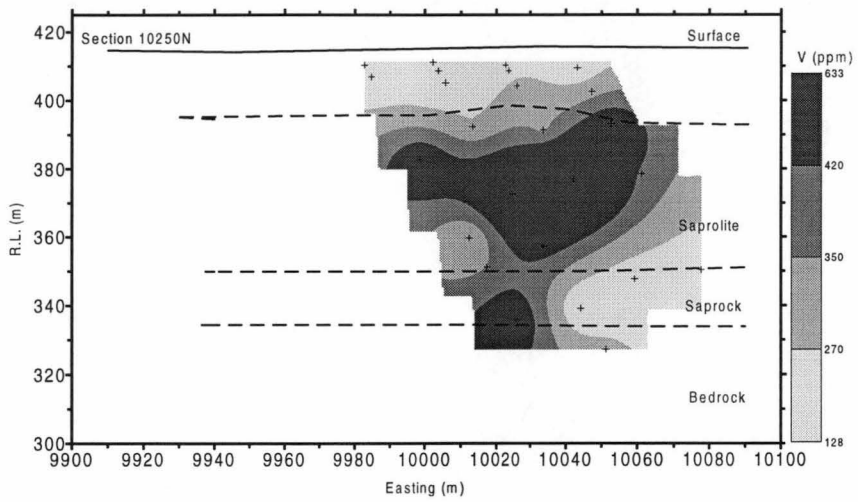
Section 10250N
Surface
Saprolite
Saprock
Bedrock
V (ppm)
633
420
350
270
128
R.L. (m)
420
400
380
360
340
320
300
9900 9920 9940 9960 9980 10000 10020 10040 10060 10080 10100
Easting (m)

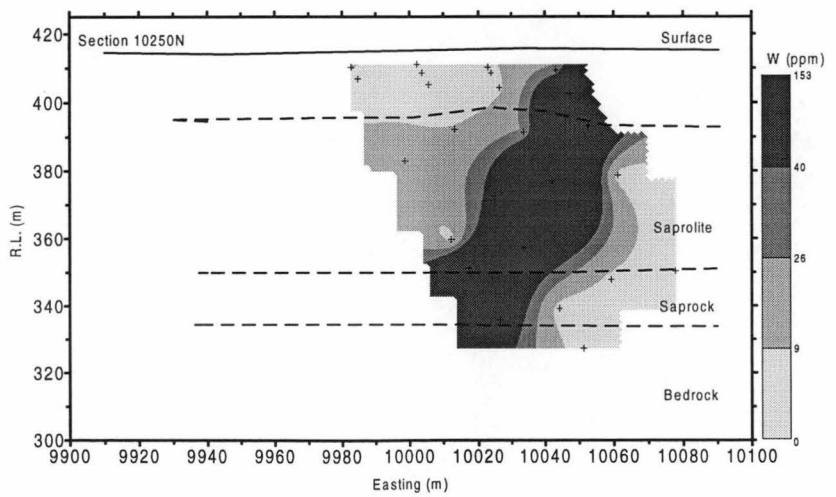
Section 10250N
Surface
Saprolite
Saprock
Bedrock
W (ppm)
153
40
26
9
0
R.L. (m)
420
400
380
360
340
320
300
9900 9920 9940 9960 9980 10000 10020 10040 10060 10080 10100
Easting (m)

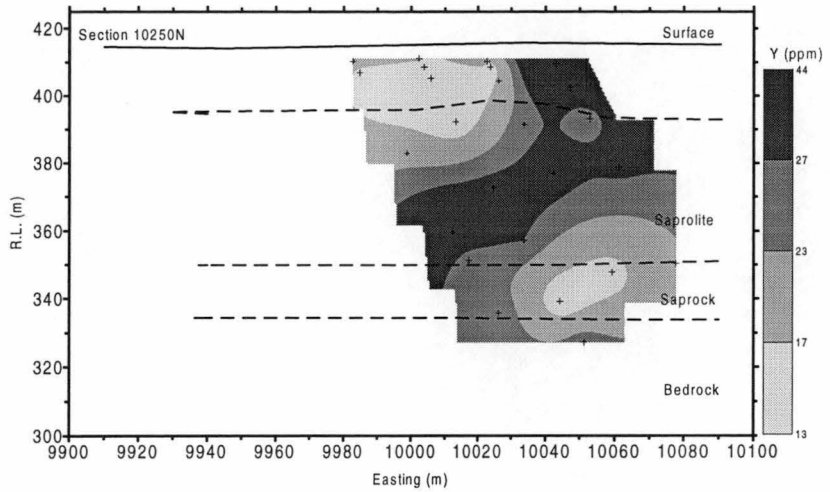
Section 10250N
Surface
Saprolite
Saprock
Bedrock
R.L. (m)
Easting (m)
Y (ppm)
44
27
23
17
13

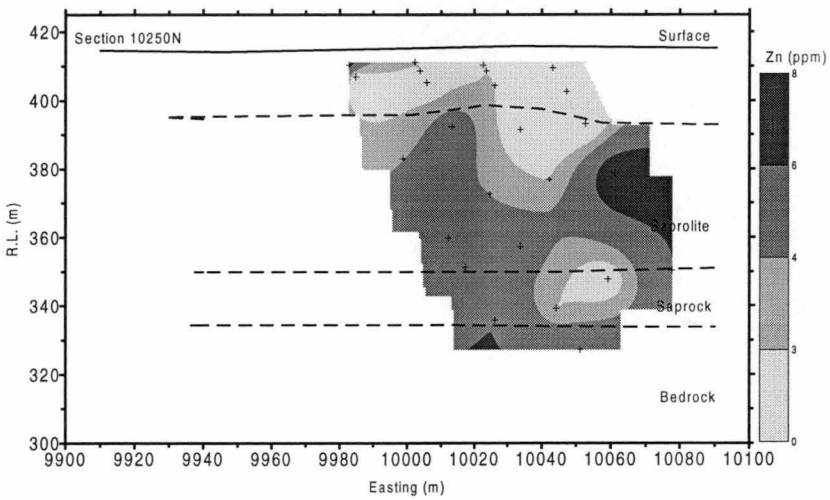
Section 10250N
Surface
Saprolite
Saprock
Bedrock
R.L. (m)
Easting (m)
Zn (ppm)
8
6
4
3
0

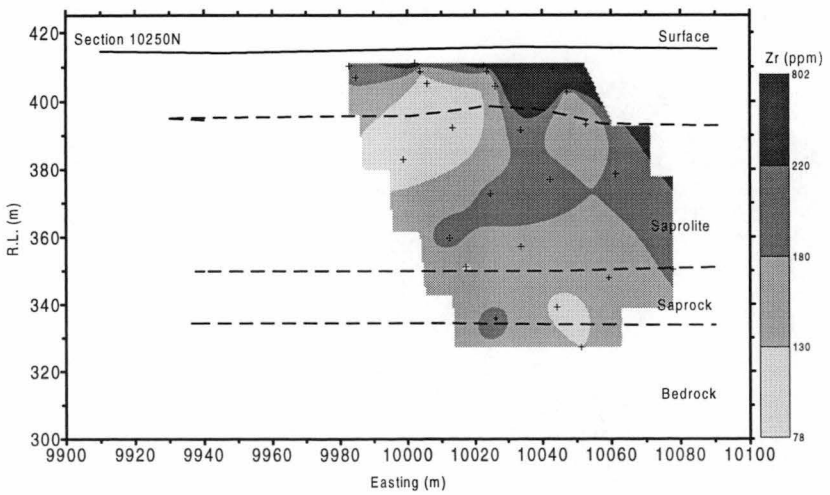
Section 10250N
Surface
Saprolite
Saprock
Bedrock
R.L. (m)
Easting (m)
Zr (ppm)
802
220
180
130
78

APPENDIX 8

ELEMENT DISTRIBUTION PLOTS, SECTION 10400N

JIM'S FIND

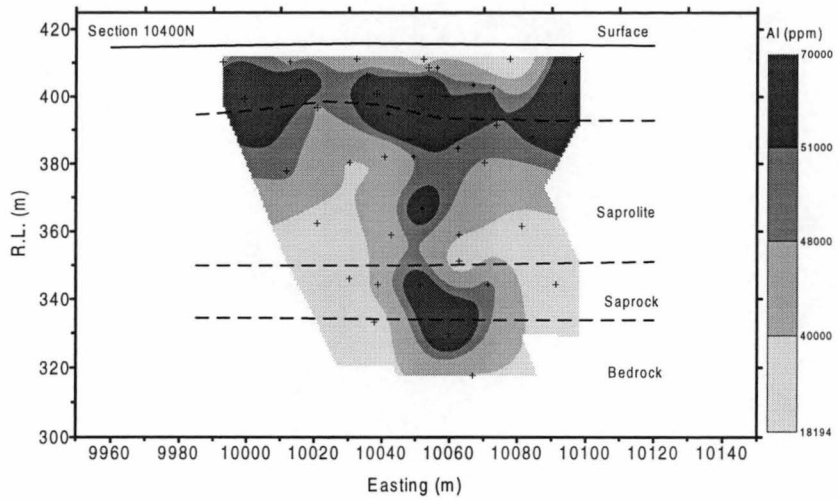
Section 10400N
Surface
Al (ppm)
70000
51000
48000
40000
18194
Saprolite
Saprock
Bedrock
R.L. (m)
420
400
380
360
340
320
300
9960
9980
10000
10020
10040
10060
10080
10100
10120
10140
Easting (m)

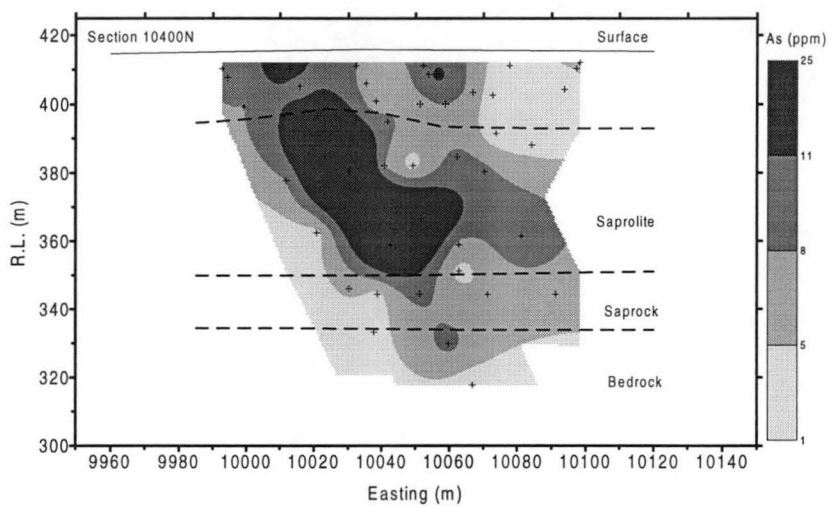
Section 10400N
Surface
As (ppm)
25
11
8
5
1
Saprolite
Saprock
Bedrock
R.L. (m)
420
400
380
360
340
320
300
9960
9980
10000
10020
10040
10060
10080
10100
10120
10140
Easting (m)

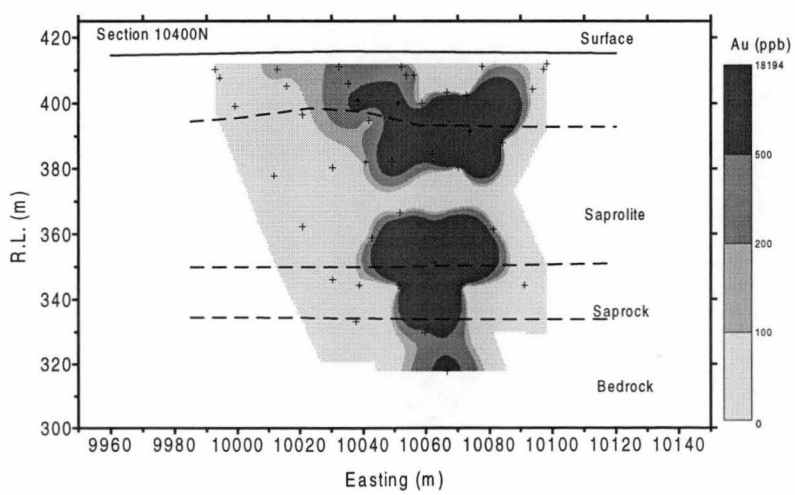
Section 10400N
Surface
Au (ppb)
18194
500
200
100
0
Saprolite
Saprock
Bedrock
R.L. (m)
420
400
380
360
340
320
300
9960
9980
10000
10020
10040
10060
10080
10100
10120
10140
Easting (m)

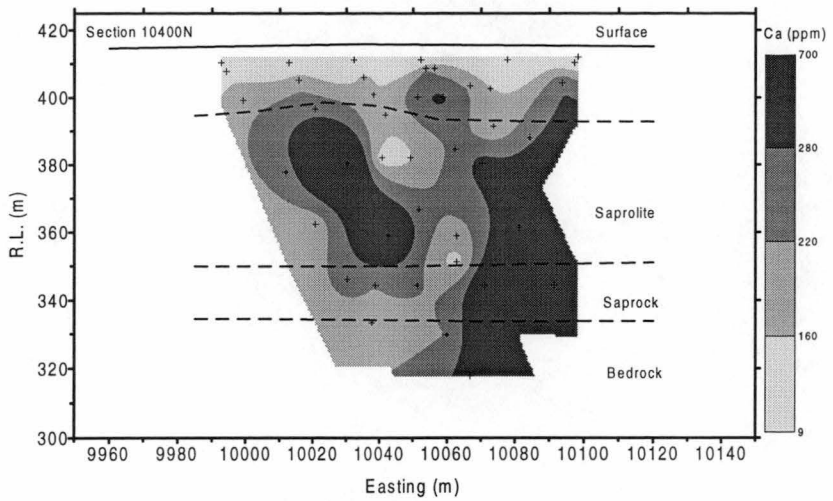
Section 10400N
Surface
Saprolite
Saprock
Bedrock
R.L. (m)
Easting (m)
Ca (ppm)
700
280
220
160
9

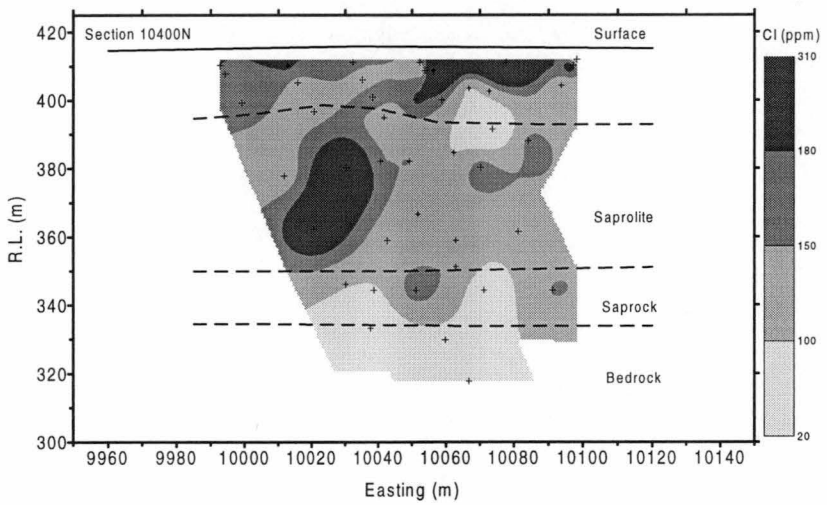
Section 10400N
Surface
Saprolite
Saprock
Bedrock
R.L. (m)
Easting (m)
Cl (ppm)
310
180
150
100
20

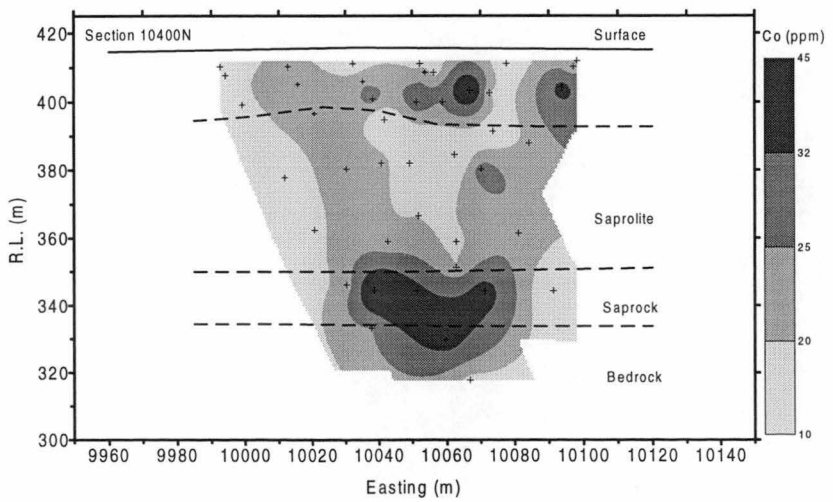
Section 10400N
Surface
Saprolite
Saprock
Bedrock
R.L. (m)
Easting (m)
Co (ppm)
45
32
25
20
10

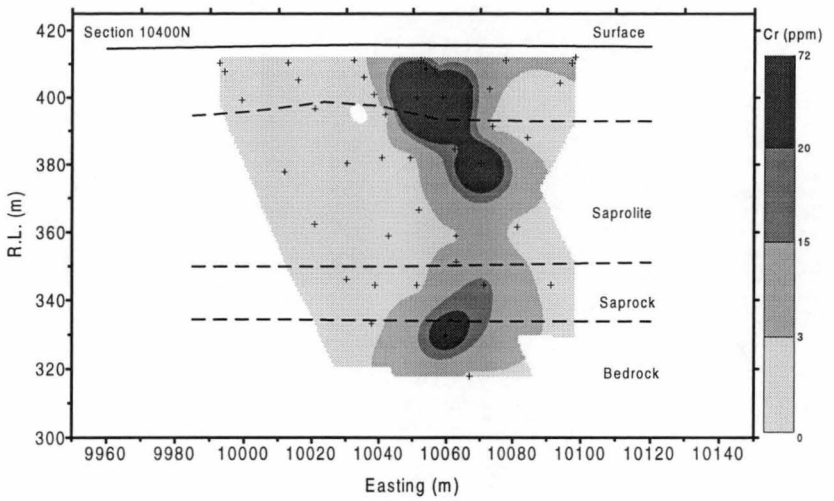
Section 10400N
Surface
Cr (ppm)
72
20
15
3
0
Saprolite
Saprock
Bedrock
R.L. (m)
420
400
380
360
340
320
300
9960
9980
10000
10020
10040
10060
10080
10100
10120
10140
Easting (m)

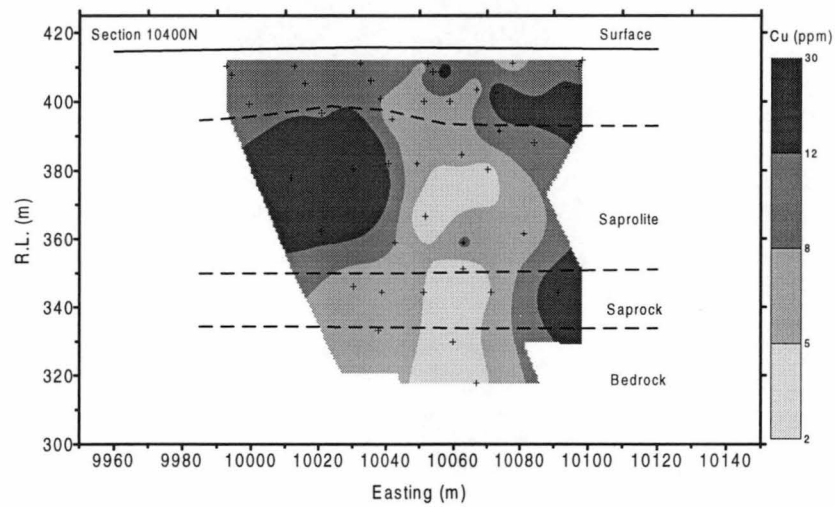
Section 10400N
Surface
Cu (ppm)
30
12
8
5
2
Saprolite
Saprock
Bedrock
R.L. (m)
420
400
380
360
340
320
300
9960
9980
10000
10020
10040
10060
10080
10100
10120
10140
Easting (m)

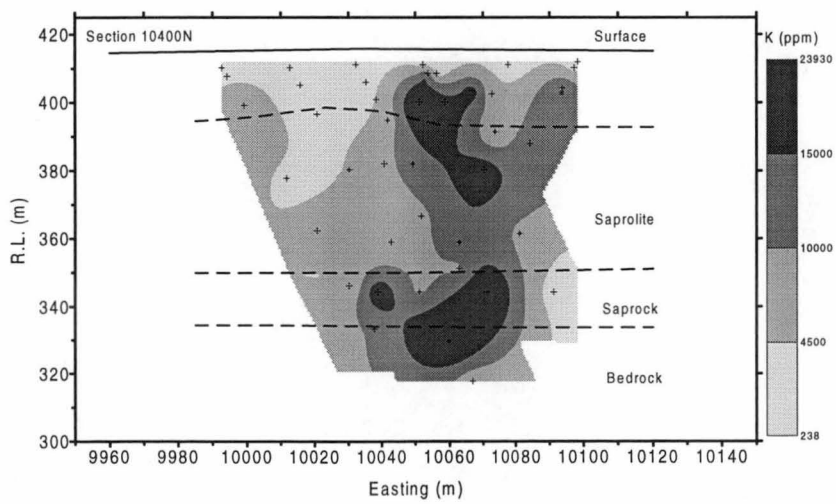
Section 10400N
Surface
K (ppm)
23930
15000
10000
4500
238
Saprolite
Saprock
Bedrock
R.L. (m)
420
400
380
360
340
320
300
9960
9980
10000
10020
10040
10060
10080
10100
10120
10140
Easting (m)

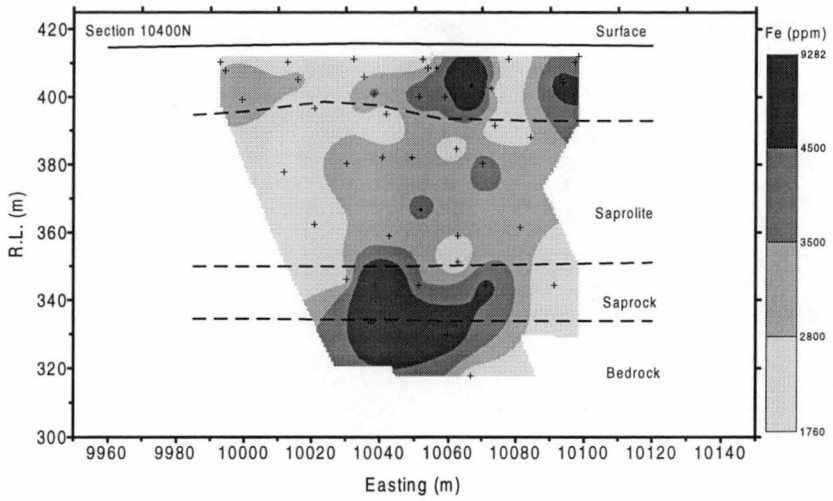
Section 10400N
Surface
Fe (ppm)
9282
4500
3500
2800
1760
Saprolite
Saprock
Bedrock
R.L. (m)
420
400
380
360
340
320
300
9960
9980
10000
10020
10040
10060
10080
10100
10120
10140
Easting (m)

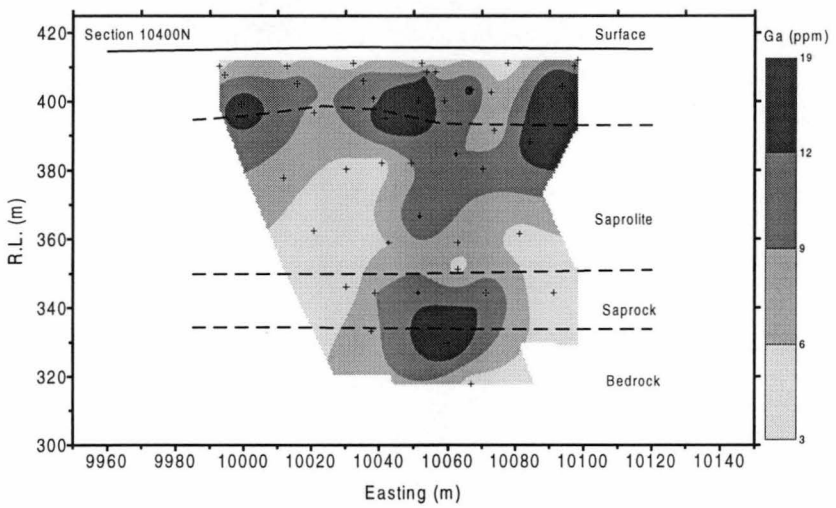
Section 10400N
Surface
Ga (ppm)
19
12
9
6
3
Saprolite
Saprock
Bedrock
R.L. (m)
420
400
380
360
340
320
300
9960
9980
10000
10020
10040
10060
10080
10100
10120
10140
Easting (m)

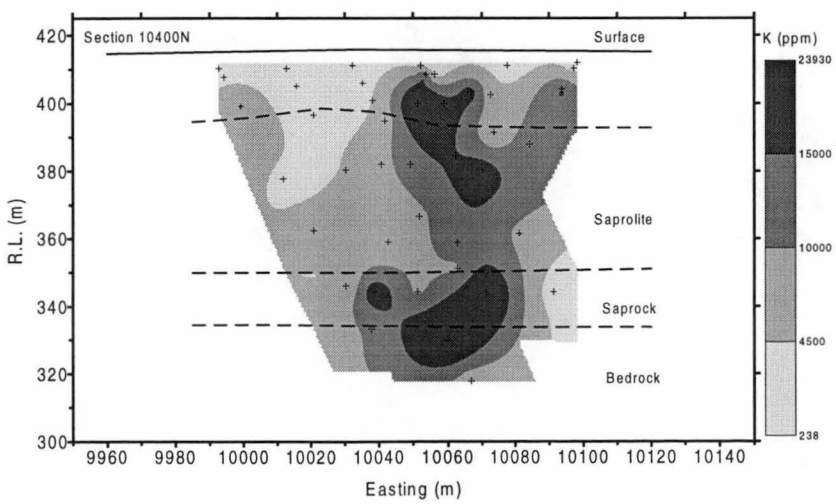
Section 10400N
Surface
K (ppm)
23930
15000
10000
4500
238
Saprolite
Saprock
Bedrock
R.L. (m)
420
400
380
360
340
320
300
9960
9980
10000
10020
10040
10060
10080
10100
10120
10140
Easting (m)

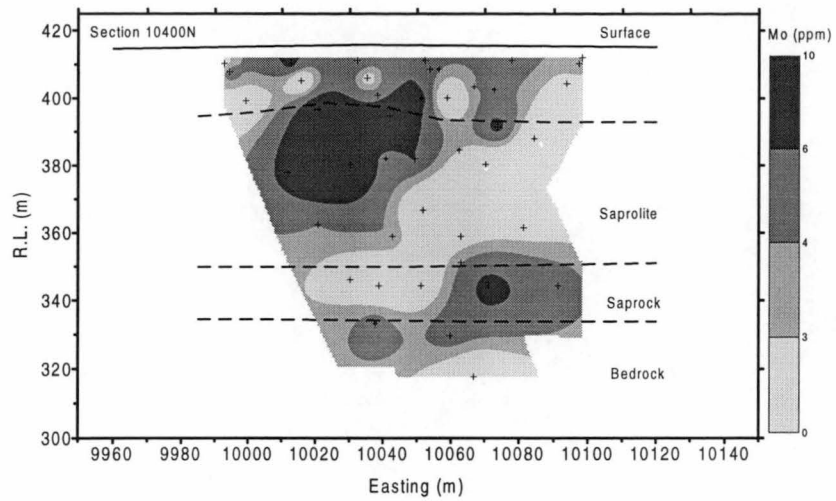
Section 10400N
Surface
Saprolite
Saprock
Bedrock
R.L. (m)
Easting (m)
Mo (ppm)
10
6
4
3
0
420
400
380
360
340
320
300
9960
9980
10000
10020
10040
10060
10080
10100
10120
10140

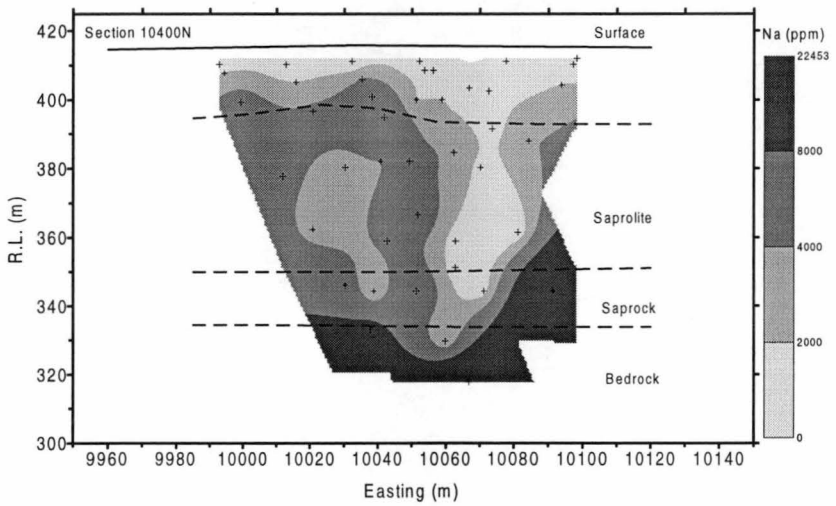
Section 10400N
Surface
Saprolite
Saprock
Bedrock
R.L. (m)
Easting (m)
Na (ppm)
22453
8000
4000
2000
0
420
400
380
360
340
320
300
9960
9980
10000
10020
10040
10060
10080
10100
10120
10140

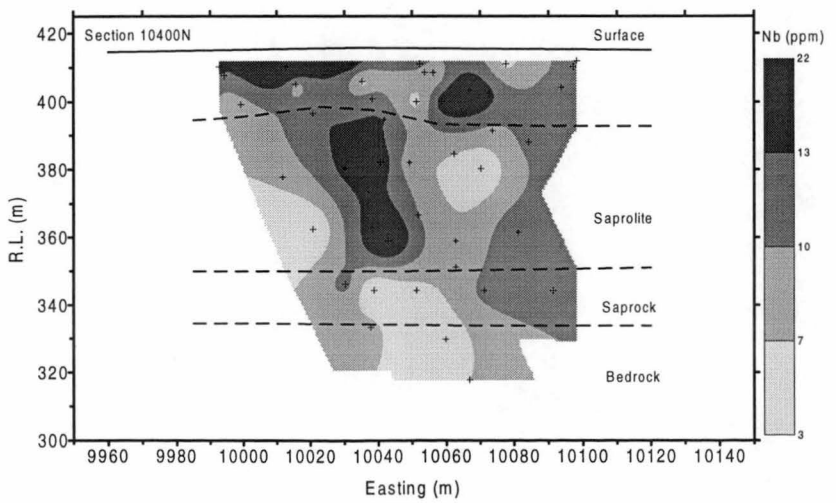
Section 10400N
Surface
Saprolite
Saprock
Bedrock
R.L. (m)
Easting (m)
Nb (ppm)
22
13
10
7
3
420
400
380
360
340
320
300
9960
9980
10000
10020
10040
10060
10080
10100
10120
10140

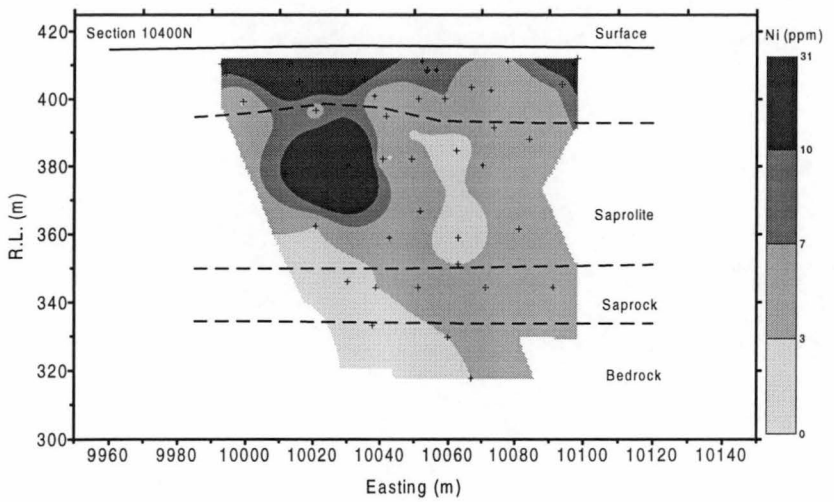
Section 10400N
Surface
Ni (ppm)
31
10
7
3
0
Saprolite
Saprock
Bedrock
R.L. (m)
420
400
380
360
340
320
300
9960
9980
10000
10020
10040
10060
10080
10100
10120
10140
Easting (m)

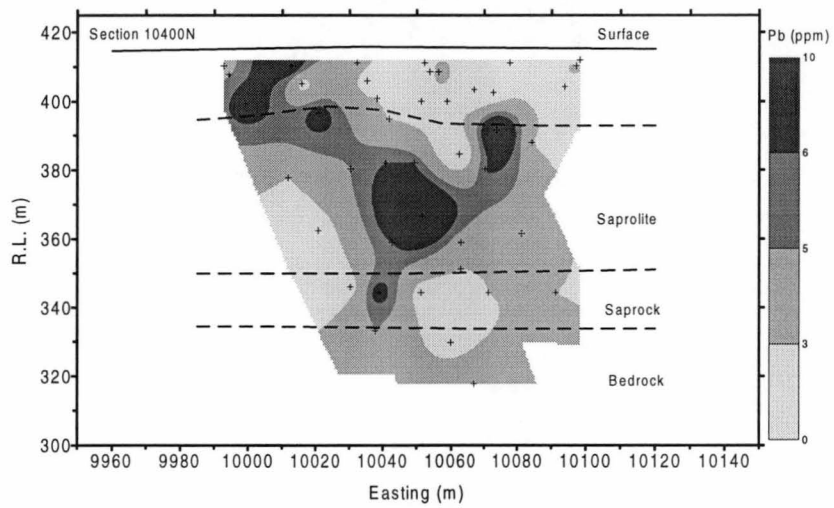
Section 10400N
Surface
Pb (ppm)
10
6
5
3
0
Saprolite
Saprock
Bedrock
R.L. (m)
420
400
380
360
340
320
300
9960
9980
10000
10020
10040
10060
10080
10100
10120
10140
Easting (m)

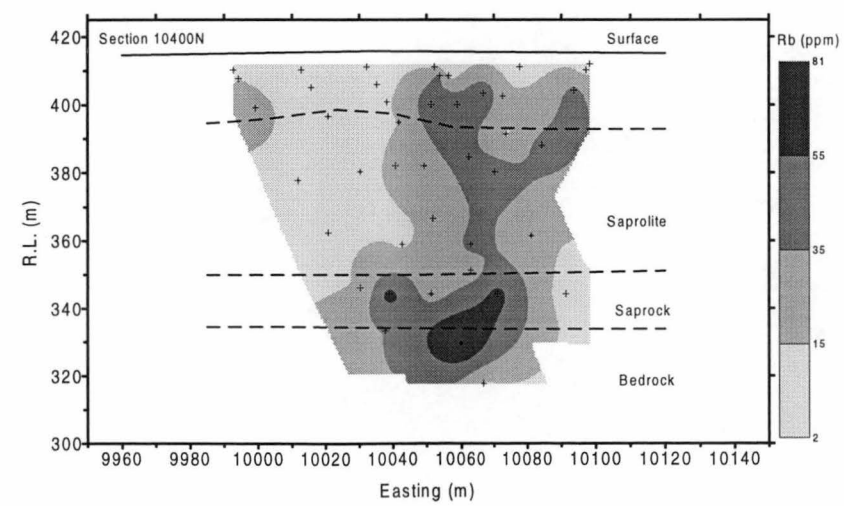
Section 10400N
Surface
Rb (ppm)
81
55
35
15
2
Saprolite
Saprock
Bedrock
R.L. (m)
420
400
380
360
340
320
300
9960
9980
10000
10020
10040
10060
10080
10100
10120
10140
Easting (m)

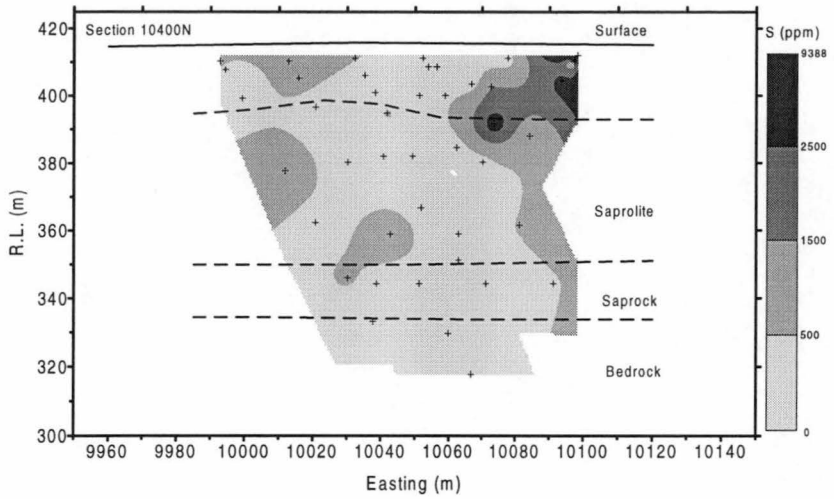
Section 10400N
Surface
S (ppm)
9388
2500
1500
500
0
Saprolite
Saprock
Bedrock
R.L. (m)
420
400
380
360
340
320
300
9960
9980
10000
10020
10040
10060
10080
10100
10120
10140
Easting (m)

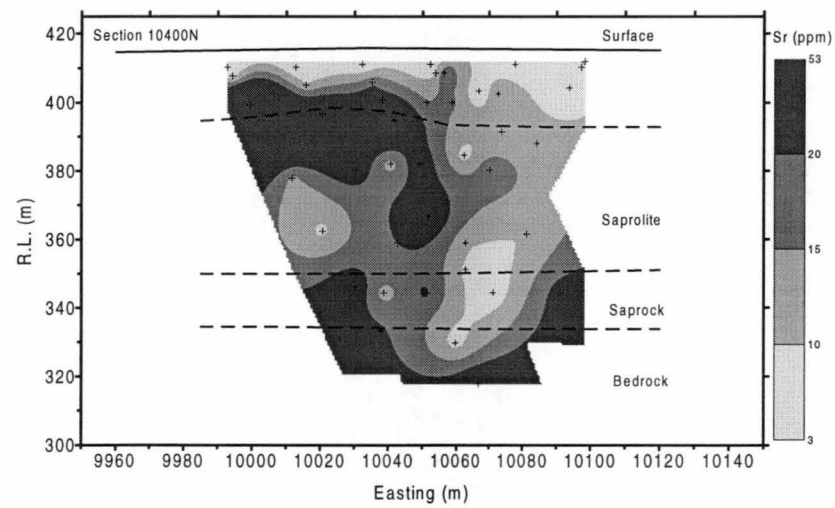
Section 10400N
Surface
Sr (ppm)
53
20
15
10
3
Saprolite
Saprock
Bedrock
R.L. (m)
420
400
380
360
340
320
300
9960
9980
10000
10020
10040
10060
10080
10100
10120
10140
Easting (m)

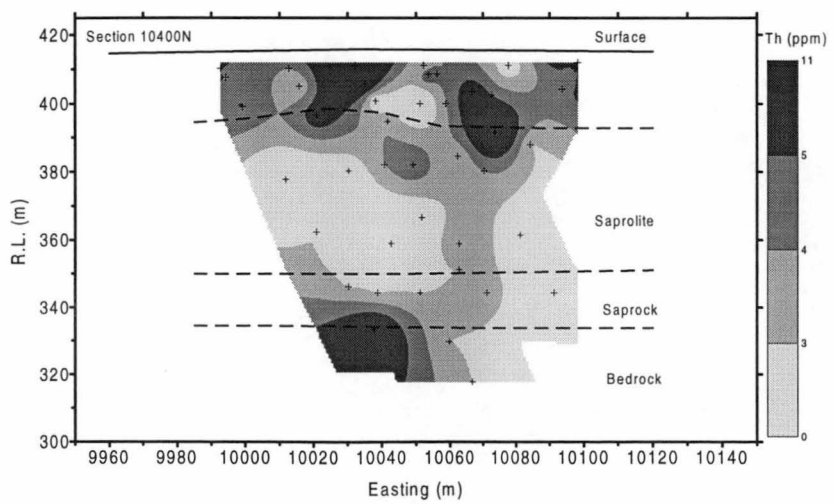
Section 10400N
Surface
Th (ppm)
11
5
4
3
0
Saprolite
Saprock
Bedrock
R.L. (m)
420
400
380
360
340
320
300
9960
9980
10000
10020
10040
10060
10080
10100
10120
10140
Easting (m)

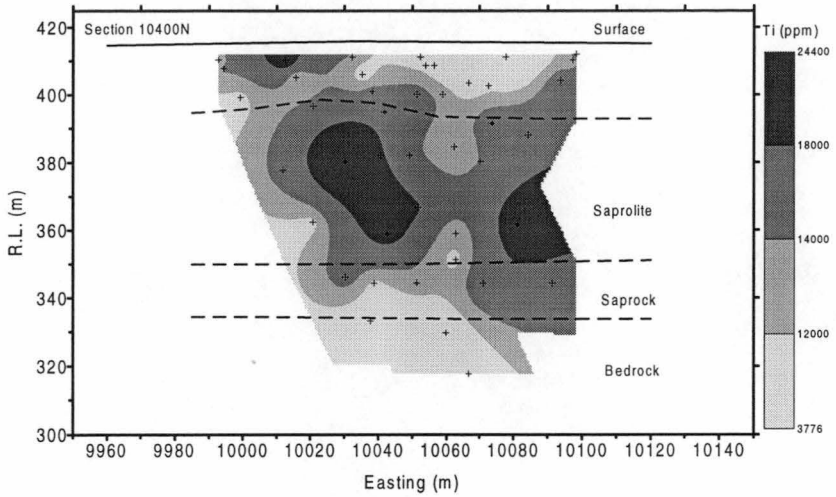
Section 10400N
Surface
Saprolite
Saprock
Bedrock
Ti (ppm)
24400
18000
14000
12000
3776
R.L. (m)
420
400
380
360
340
320
300
9960 9980 10000 10020 10040 10060 10080 10100 10120 10140
Easting (m)

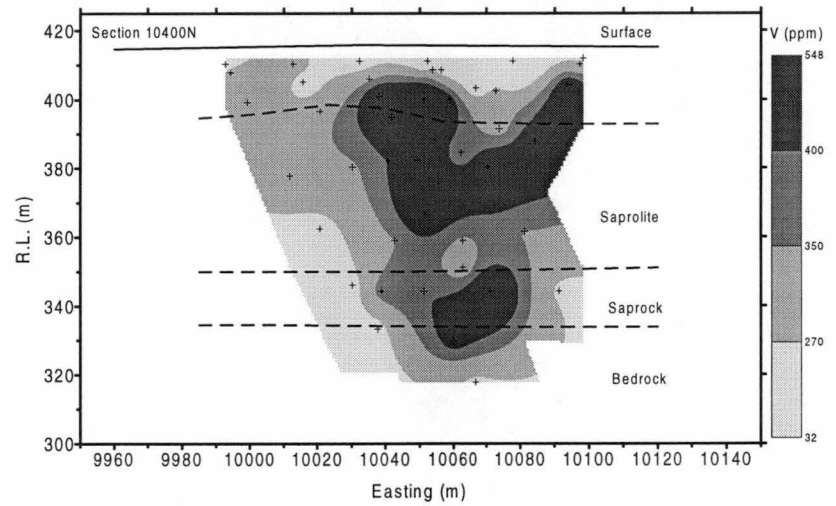
Section 10400N
Surface
Saprolite
Saprock
Bedrock
V (ppm)
548
400
350
270
32
R.L. (m)
420
400
380
360
340
320
300
9960 9980 10000 10020 10040 10060 10080 10100 10120 10140
Easting (m)

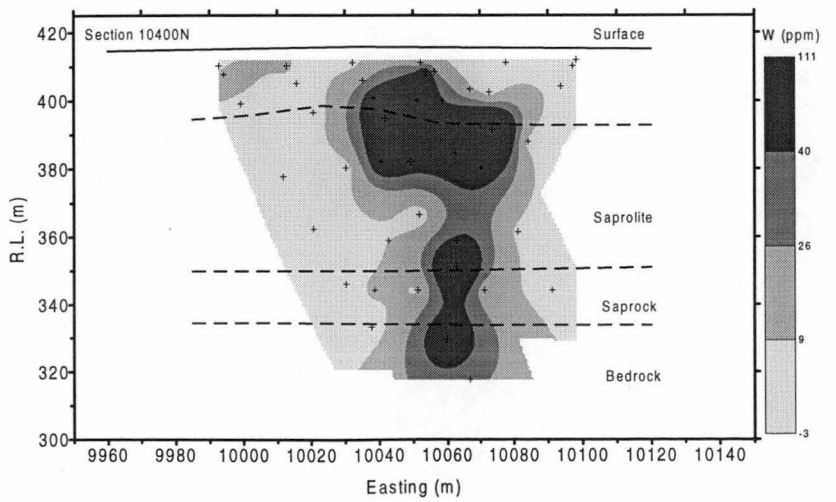
Section 10400N
Surface
Saprolite
Saprock
Bedrock
W (ppm)
111
40
26
9
-3
R.L. (m)
420
400
380
360
340
320
300
9960 9980 10000 10020 10040 10060 10080 10100 10120 10140
Easting (m)

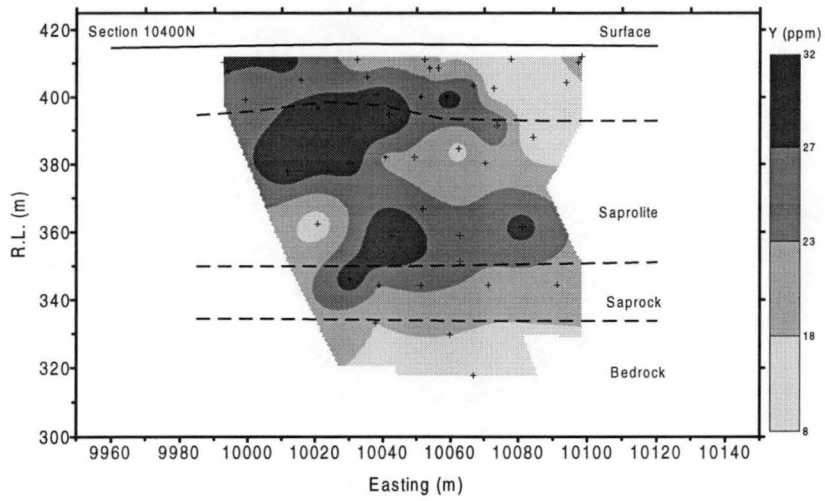
Section 10400N
Surface
Y (ppm)
32
27
23
18
8
Saprolite
Saprock
Bedrock
R.L. (m)
420
400
380
360
340
320
300
9960
9980
10000
10020
10040
10060
10080
10100
10120
10140
Easting (m)

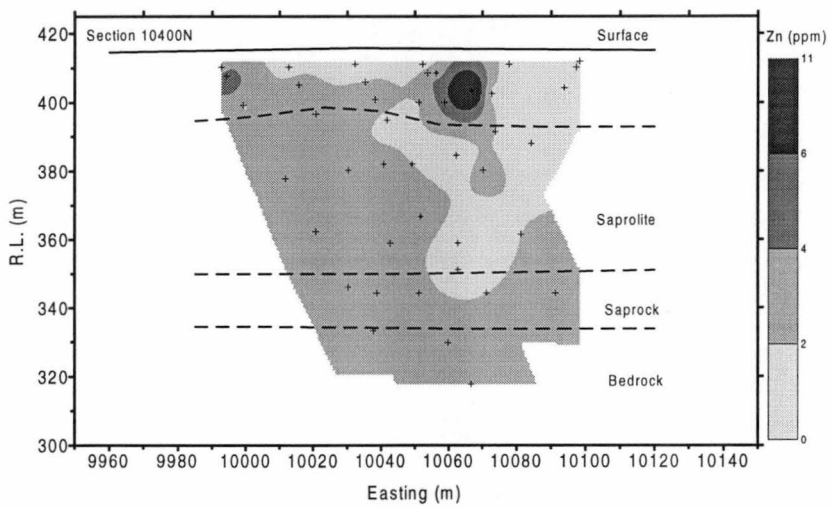
Section 10400N
Surface
Zn (ppm)
11
6
4
2
0
Saprolite
Saprock
Bedrock
R.L. (m)
420
400
380
360
340
320
300
9960
9980
10000
10020
10040
10060
10080
10100
10120
10140
Easting (m)

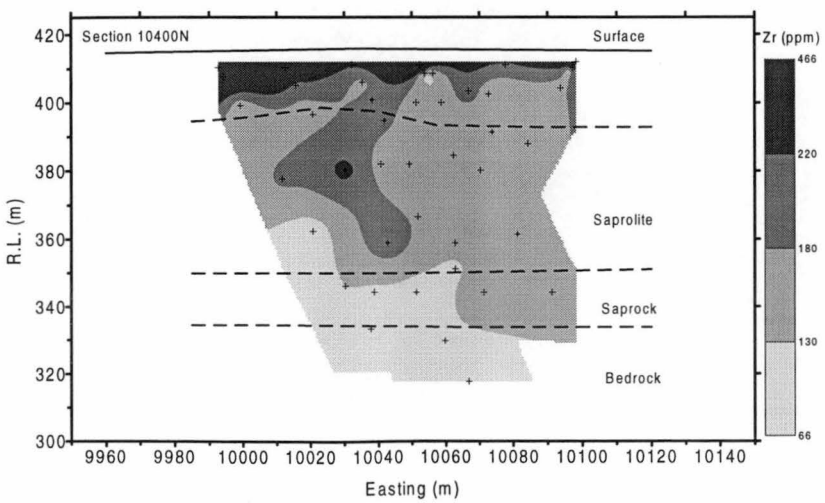
Section 10400N
Surface
Zr (ppm)
466
220
180
130
66
Saprolite
Saprock
Bedrock
R.L. (m)
420
400
380
360
340
320
300
9960
9980
10000
10020
10040
10060
10080
10100
10120
10140
Easting (m)